ANL-6640

Argonne National Laboratory

PROCEEDINGS OF THE AMU-ANL SUMMER STUDY PROGRAM

June 19 - July 14, 1961

ANL-6640
Reactor Technology
(TID-4500, 18th Ed.)
AEC Research and
Development Report

ARGONNE NATIONAL LABORATORY
9700 South Cass Avenue
Argonne, Illinois

PROCEEDINGS OF THE AMU-ANL SUMMER STUDY PROGRAM

(June 19 - July 14, 1961)

Amended Notes Edited by C. V. Pearson
from Original Notes
Compiled by G. E. Schweitzer,
Resident Research Associate

November 1962

Operated by The University of Chicago
under
Contract W-31-109-eng-38
with the
U. S. Atomic Energy Commission

PREFACE

During the summer of 1961, Argonne National Laboratory in conjunction with the Associated Midwest Universities presented an eight-week study program to familiarize representatives of the university community with the development and operation of the Experimental Boiling Water Reactor (EBWR). This manuscript is a revised and amended version of G. E. Schweitzer's first draft of the proceedings of the first four weeks of the study program. During that period, members of the Reactor Engineering Division, the Metallurgy Division, and the International Institute of Nuclear Science and Engineering presented lectures and conducted tours to acquaint the program participants with the EBWR system. Since the brevity of the familiarization period limited detailed discussion of many facets of the system, this document reflects primarily the high points of EBWR development. However, when used together with the cited references, it should give the reader a comprehensive picture of the problems encountered in the design and operation of a boiling water reactor. The repetitive discussions of certain development problems should not detract from the document's utility since representatives of different engineering disciplines often view the same problems from different vantage points.

C. V. Pearson

TABLE OF CONTENTS

TABLE OF CONTENTS

TABLE OF CONTENTS

TABLE OF CONTENTS

TABLE OF CONTENTS

LIST OF FIGURES

LIST OF FIGURES

LIST OF FIGURES

LIST OF FIGURES

LIST OF FIGURES

LIST OF FIGURES

LIST OF FIGURES

LIST OF TABLES

SECTION I

INTRODUCTION

B. Spinrad

NOTES AND EDITED DATA FROM LECTURE - June 19, 1961

SECTION I

INTRODUCTION

As early as 1939, the New York Times prognosticated on the front page that fission of uranium submerged in water could conceivably cause boiling of the water. The escaping steam could then be harnessed as a source of power. During the war, the possibility of nuclear reactor power production was often discussed by those scientists primarily concerned with producing an atomic bomb. By 1945, controlled production of nuclear power had been enthusiastically recognized as a realizable goal. Within a year, however, enthusiasm had turned to gloom. The technological problems uncovered, when serious thought was devoted to the program, loomed as insurmountable obstacles. In fact, only due to the insistence of the Navy and Admiral Rickover's ability to obtain funds, was the Oak Ridge Pile Project kept alive. In 1948, the AEC decided to focus reactor activity at Argonne. Development subsequently centered around the CP-5, a heavy water research reactor, and CP-4, a fast breeder reactor. Gradually, with advancement in metallurgy, heat transfer, and the other associated disciplines, the pessimism of the late 1940's disappeared. Two significant stimuli to further power reactor development were the successes of the submarine power reactor program and of the breeder reactor EBR-I.

In the early 1950's, a series of studies of power reactors were undertaken at Oak Ridge and elsewhere by individual groups. Project Hannah, a 1952 evaluation of the Hanford and Savannah River reactors as power sources, and Project Dynamo, a 1953 MIT report on the future of power reactors, gave further impetus to the surge in the power-reactor program. In 1954, the AEC presented the "five-year plan" for power reactor development, briefly outlined in Table I-1. The program proceeded and other reactors were added as a result of the incentives indicated in the outline.

Table I-1

FIVE-YEAR PLAN FOR DEVELOPMENT OF NUCLEAR POWER (1954)

Origin	Reactor Experiment	Experimental Reactor	Prototype
Materials Testing Reactor	Submarine Thermal Reactor	PWR	Yankee Indian Point
Los Alamos "Water Boiler"	Homogeneous Reactor Experiment-I	HRE-II	
ANL Breeder	Experimental Breeder Reactor-I	EBR-II	Fermi
Na-Thermal (Knolls Atomic Power Laboratory)	Sodium Reactor Experiment		Hallam Nuclear Power Station

Other Reactors Added to Program

Origin	Incentive	Reactor Experiment	Experimental Reactor
One man's bright idea	High temperature	Liquid Metal Fuel Reactor (BNL)	
NEPA (Nuclear Energy Propulsion for Aircraft)	High temperature	Aircraft Reactor Experiment Molten Salt Reactor Experiment	
Development of D_2O Technology	Assist countries without access to enriched uranium	Halden (Norway) NRU (Canada)	CANDU (Canada) HWCTR - Savannah River Plutonium Recycle Reactor-Hanford
X10, BNL (British)	Not to be caught short if idea successful	Gas-cooled Reactor Experiment (ORNL)	High-temperature Gas-cooled Reactor, Peach Bottom, Pa.
ANL, BNL, Calif. Research and Develop. Corp. interests	High temperature without pressure or corrosion	Organic-moderated Reactor Experiment (AI)	Experimental Organic-cooled Reactor

Note: This chart should not be intepreted as a complete listing of planned power reactors. For example, see 5th Nuclear Power Report, Electrical World (May 16, 1960) p. 63.

Originally, the suggestion of a boiling reactor was rank heresy. It was believed by physicists that (1) the ensuing film boiling would result in coolant starvation, with subsequent burnout of the fuel, and (2) the bubbles which would form would collapse immediately, with a resulting increase in reactivity and reactor explosion. The early beliefs of the physicists were proved incorrect, and experiments have subsequently shown that a boiling reactor can operate stably.

At Argonne, boiling heat transfer experiments demonstrated the feasibility of a boiling reactor. It was not until the Los Alamos "Water Boiler" was allowed to boil and a scaled-down model of the Materials Testing Reactor was also allowed to boil at Oak Ridge that the demonstration at Argonne was permitted to proceed through the BORAX-I, -II, and -III Experiments which comprised this demonstration. The feasibility of boiling reactors as a reliable source of power was firmly established, and the EBWR was added to the list of "five-year plan" reactors.

SECTION II

HISTORY AND DEVELOPMENT OF THE EXPERIMENTAL BOILING WATER REACTOR

N. Balai
C. Breden
L. Fromm
H. Iskenderian
V. Kolba
L. Link
W. Lipinski
P. Lottes
D. Roy

NOTES AND EDITED DATA FROM LECTURES - June 21, 23, and 24, 1961

SECTION II

HISTORY AND DEVELOPMENT OF THE EXPERIMENTAL BOILING WATER REACTOR

I. History of Boiling Water Reactor Development*

Some of the first reactors ever constructed and operated were water-cooled-and-moderated reactors. Six such reactors were brought to criticality in the period 1944-1951. All but one of these early units were of the low-power research type and employed heavy water. The exception, NRX in Canada, employed heavy water as moderator with light water as coolant, and attained a power of 40 Mw. These pioneer efforts provided the basic physics knowledge and understanding of operating characteristics which have been essential in the more recent development of water reactors for materials testing, marine propulsion, and power generation.

Although NRX, the Hanford graphite-moderated plutonium-production reactors, and some solution-fueled experimental units employed light water as coolants, the development of light-water-moderated reactors was delayed because of early unavailability of enriched uranium for use as reactor fuels. A light-water reactor cannot be made critical with natural uranium fuel primarily because of physics considerations, such as the relatively high cross section for absorption of neutrons by ordinary hydrogen.

The first light-water-moderated-and-cooled heterogeneous reactor to be operated was the Low Intensity Testing Reactor (LITR), built in 1950 at Oak Ridge National Laboratory. The operating power level was 3 Mw. Actually, LITR was originally constructed as a full-scale flow test mockup for the Materials Testing Reactor (MTR), then in design. After the unit was used for this purpose, shielding, actual instead of dummy fuel elements, controls, and other necessary equipment were added in order to convert the facility to a testing reactor.

The second light-water reactor was the MTR, completed at the Idaho National Reactor Testing Station in 1952. This reactor operated at 30 Mw initially and is now running at 40 Mw. Also developed during this period was the pressurized water power plant for the submarine NAUTILUS. The land-based prototype, also at the Idaho site, began operation in 1953.

The possibility of permitting boiling to occur in water-moderated reactors has been subject to speculation since the early days of reactor development. Applications considered ranged from employment of surface boiling in pressurized reactors in order to improve heat transfer rates, to the design of bulk boiling reactors generating usable steam directly. It was recognized that the latter concept could effect considerable cost savings by simplifying reactor design, minimizing the hazard problem, and increasing net efficiency.

*L. W. Fromm

Figure II-1 illustrates a basic, simplified comparison of a boiling-water cycle with a pressurized-water cycle. Both systems are pictured as generating 4800 kw of electrical power and utilizing 600 psig saturated steam. In the boiling case, steam is generated directly in the reactor. The reactor vessel is designed for an operating pressure of 600 psig. The only pumping power required is 100 kw for the return of condensate to the reactor. In the pressurized case, the 600-psig turbine steam is generated in the secondary side of a heat exchanger whose primary side contains water heated by the reactor. Because of the necessary temperature difference across the heat exchanger to provide driving head, the primary system must operate at a considerably higher pressure and temperature. Therefore, in the boiling system, the cost of the intermediate heat exchanger, the increased cost of a reactor vessel and primary system

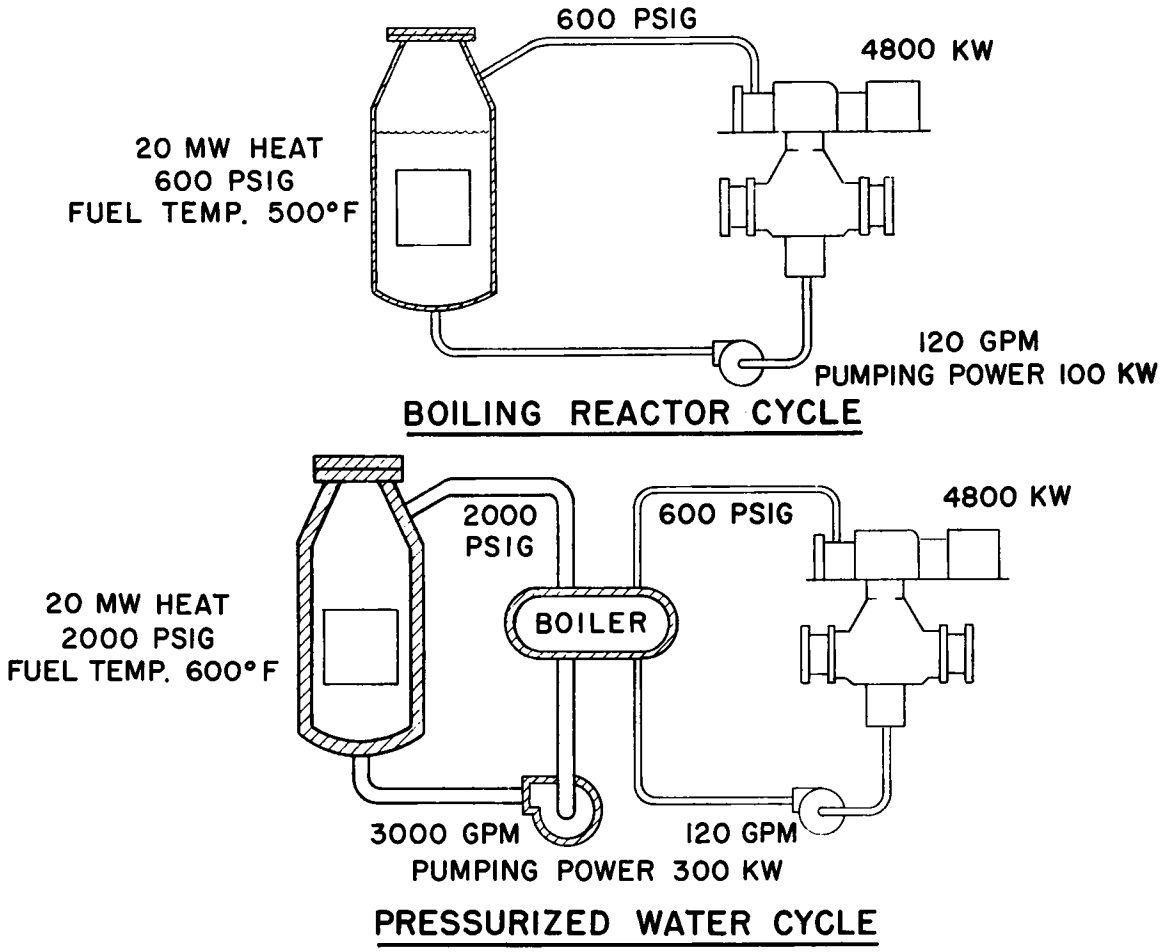

Fig. II-1

Water Reactor Cycles
111-5012

of higher pressure rating, and the cost of primary circulating pumps are eliminated. The absence of circulating pumps reduces plant internal power consumption so that an increase in net efficiency results.

This is a grossly oversimplified comparison. Some of the gains mentioned are compensated by other factors, such as more stringent sealing requirements on the turbine shaft. Nevertheless the figure is representative of theoretically possible advantages.

The principal question was whether power fluctuations, resulting from variation of moderator density with steam formation, would be so large as to preclude stable operation. The issue was clouded to some extent by the experience in Hanford reactors with positive void coefficients (increase in reactivity upon formation of steam voids). In Hanford reactors, the formation of steam in cooling water channels increased the reactivity (because of removal of absorber) so that heat generation rose in the immediate area. The steam formation increased the resistance to coolant flow in the tube. Since tubes were supplied in parallel from headers, the tube became starved of coolant. The combination of increased power and decreased coolant flow usually resulted in fuel burnout. This phenomenon was known as "boiling disease." The effect could spread progressively to adjacent tubes if the reactor was not shut down in time.

By 1952, calculations had shown that boiling water-moderated-and-cooled reactors could be designed to have negative void coefficients of reactivity (formation of steam and displacement of water cause a net reactivity decrease through increased neutron leakage and, in reactors containing U^{238}, resonance absorption). It was determined that all practical heavy-water designs and all small light-water designs would have negative void coefficients. Large light-water cores could be designed to have negative coefficients by adjustment of lattice constants, such as the metal-water ratio. The remaining question was whether, in the event of power disturbances, steam formation would occur fast enough to limit reactor power to safe limits or whether the reactor would "run away," with attendant effects of fuel melting, violent chemical reactions, etc.

The BORAX-I reactor was designed and constructed at the Idaho testing station to investigate those questions experimentally. The design was kept to an absolute minimum of cost because of the temporary nature of the experiment. The reactor was located in a hole in the ground with the core a few feet below grade. A plastic-lined carbon-steel reactor vessel, designed for 125-psig operating pressure, was placed within a shield tank. The shield tank could be filled with water, to provide additional shielding while personnel were working near the reactor (between operating test runs), and emptied during runs. Shielding for personnel located at the control trailer one-half mile away from the reactor took the form of about 11 ft of sand and gravel piled against the shield tank.

Pumps for emptying and filling the shield tank and reactor vessel, an electric reactor water preheating system, and other auxiliaries were located in a pit adjacent to the shield tank.

The reactor was controlled by a set of four ganged shim blades which would be positioned in the normal manner and injected rapidly for quick shutdown, and one central rod which could be rapidly ejected from the core for experimental, quick additions of reactivity.

The results of the BORAX-I experiments, conducted in the summers of 1953 and 1954, showed that reactivity additions with periods as short as 0.005 sec could be made without runaway. In the 0.005-sec-period test, a peak power of 2600 Mw was reached 0.1 sec after the reactivity addition. It decayed almost instantaneously. Thus, the fuel-plate temperatures did not exceed 640°F (338°C). With low reactivity additions, the excursion settled down to steady boiling at a power of about 500 kw, whereas with higher additions, the excursion was followed by power oscillations with a frequency of about 1 sec, known as "chugging."

Steady boiling was achieved at 130-psig pressure and at power levels up to 1200 kw, at which steam voids represented about 2% reactivity. Above this level, the "chugging" oscillations were encountered. Probably the most significant observation from the BORAX-I series of tests was the fact that, as anticipated, the reactor steam power was self-regulating.

In a final experiment, about 4% reactivity was added to the core on a period of 0.0026 sec. The peak power in this case was about 13,000 Mw. Most of the fuel elements melted, and pressure failure of the reactor vessel occurred. The reaction had the character of a steam explosion.

It must be emphasized that this last experiment was run primarily for the purpose of determining the effects of a reactor explosion. The explosion was expected, and the reactivity additions at periods of 0.005 sec and 0.0026 sec were considerably greater than those originally expected to damage the reactor.

To verify observations made with BORAX-I that higher power densities were stably attainable at higher pressures (130 psig vs atmospheric pressure) and to increase understanding of the boiling reactor principle, BORAX-II was constructed in late 1954. This facility was somewhat more refined than BORAX-I, but retained much of its simplicity and low cost. The reactor, in a 300-psig pressure vessel, was housed in a sheet-metal building to permit all-year-round experimentation. Control of the reactor was still carried out from the remotely located trailer of BORAX-I. Connecting control cables were merely strung on the ground.

Operation at 300 psig was found to be more stable than former tests, and a power density of 21 kw/liter of core was reached. In 1955, BORAX-II was converted to BORAX-III by addition of a turbogenerator set. Fuel elements and control rods were also changed. A demonstration of commercial possibilities of boiling water reactors was carried out by supplying the full power demand of the town of Arco, Idaho, for a significant period of time. The town's normal electrical supply was disconnected during this period.

The Experimental Boiling Water Reactor (EBWR) was constructed at the Argonne (Argonne, Illinois) site. It attained criticality and operation at the design power of 20 Mwt (5 Mwe) in 1956. Continuing the trend of increasing pressure, the plant was built for a 600-psig operating pressure. EBWR was designed as an integrated power plant to demonstrate the feasibility of such a direct-cycle plant. Slightly enriched fuel was used to demonstrate a commercially more attractive fuel and to investigate the effect of a greater time constant between heat generation within the fuel and release of that heat to the coolant.

Stability at 600 psig was found to be so high that short-term operation at thermal power levels up to 61.7 Mwt was carried out. Transfer-function measurements indicated stability up to 65 Mwt, with the original 4-ft-diameter and 4-ft-high core. Predictions based upon the 5-ft-diameter core, which presently is to be installed, indicate stable operation at up to 100 Mwt. The plant is being revised to dissipate that amount of power. Additional heat will be removed as process steam to be distributed in the Laboratory's regular system of steam supply.

The economics of EBWR at its 20-Mwt rating showed a power cost of about 52 mill/kw/hr. This figure is not unreasonably high for a plant intended to be no more than a demonstration model, but is certainly not in the same range as fossil-produced power. At a power of 100 Mwt, even with several millions of dollars added to the initial plant cost to cover the additional turbine-generator condenser and other equipment necessary to utilize this thermal power, costs begin to approach those obtained from coal-fired plants of comparable size. Therefore, the revised plant is now considered to be an actual prototype of a small commercial plant which could be competitive with non-nuclear power in some locations.

In 1956, the BORAX-III plant was converted to BORAX-IV by the installation of an oxide core. The new fuel was in the form of UO_2-ThO_2 pellets contained in extruded tube plates (tubes connected by longitudinal webs) of aluminum-nickel alloy. The concentration of the UO_2 in the ThO_2 was about 6%. The uranium was enriched to 93% U^{235}.

The BORAX-IV experiment was primarily a fuel-element test, with particular emphasis on investigating the effects of the longer heat release time constant on stability and self-limiting characteristics. The

tests showed that stable operation was possible with very high reactivity in steam voids (6.9%) and at a very high power density (45 kw/liter of core). Self-limiting characteristics were somewhat inhibited in comparison with earlier experiments with thin metallic-plate cores, but not to the extent that reactor safety was compromised. These effects are attributed to the higher time constant of the fuel, calculated to be 0.8 sec.

The Argonne Low Power Reactor (ALPR) is a combination power-generating and space-heating reactor designed primarily for low-cost, simple construction, and easy transportability of components, with a view toward installation in remote areas. The facility was constructed at the Idaho testing station and began operation in 1958.

Considerable development work has been carried out on boiling water reactors at sites other than Argonne. The SPERT-I (Special Power Excursion Reactor Test) Facility in Idaho is a reactor very similar to BORAX-I. It has been used to demonstrate that reactor pressure and steam-void reactivity are not the only factors affecting stability, but that hydrodynamics also plays a part. Whereas operation at 1.5% steam-void reactivity was stable with 2 ft of water over the core, it became decidedly unstable with 4 ft of water over the core. This is attributed to the fact that at 4 ft a more difficult core exit passage is produced, and a larger mass for oscillation is present. At a water height of 9 ft above the core, operation again became more stable because of the rise in pressure in the core.

The Vallecitos Boiling Water Reactor (VBWR) was built by the General Electric Company, with support from the Pacific Gas and Electric Company, at Pleasanton, California. It began operation in 1957. The principal functions of the plant were to gain knowledge and experience for General Electric personnel and to serve as a pilot plant for developing design information needed for the Dresden Nuclear Power Station, a 180-Mwe plant. A significant fact about both VBWR and Dresden is that both plants have been built completely with private capital. The reactor is about the same size as EBWR, but operates at up to 1000 psig, thus adding another point to the pressure vs stability curve.

The currently expanding activity in boiling water reactors is illustrated in Fig. II-2.

II. Developments in Reactor Analysis*

A. Reactor Physics

Methods of calculation of critical mass, temperature coefficient, void coefficient, etc., are now considered to be fairly well established for presently favored core geometries. Experimental measurements check within the predicted error of the calculations. For example, in EBWR initial

*H. P. Iskenderian, W. C. Lipinski, and P. A. Lottes

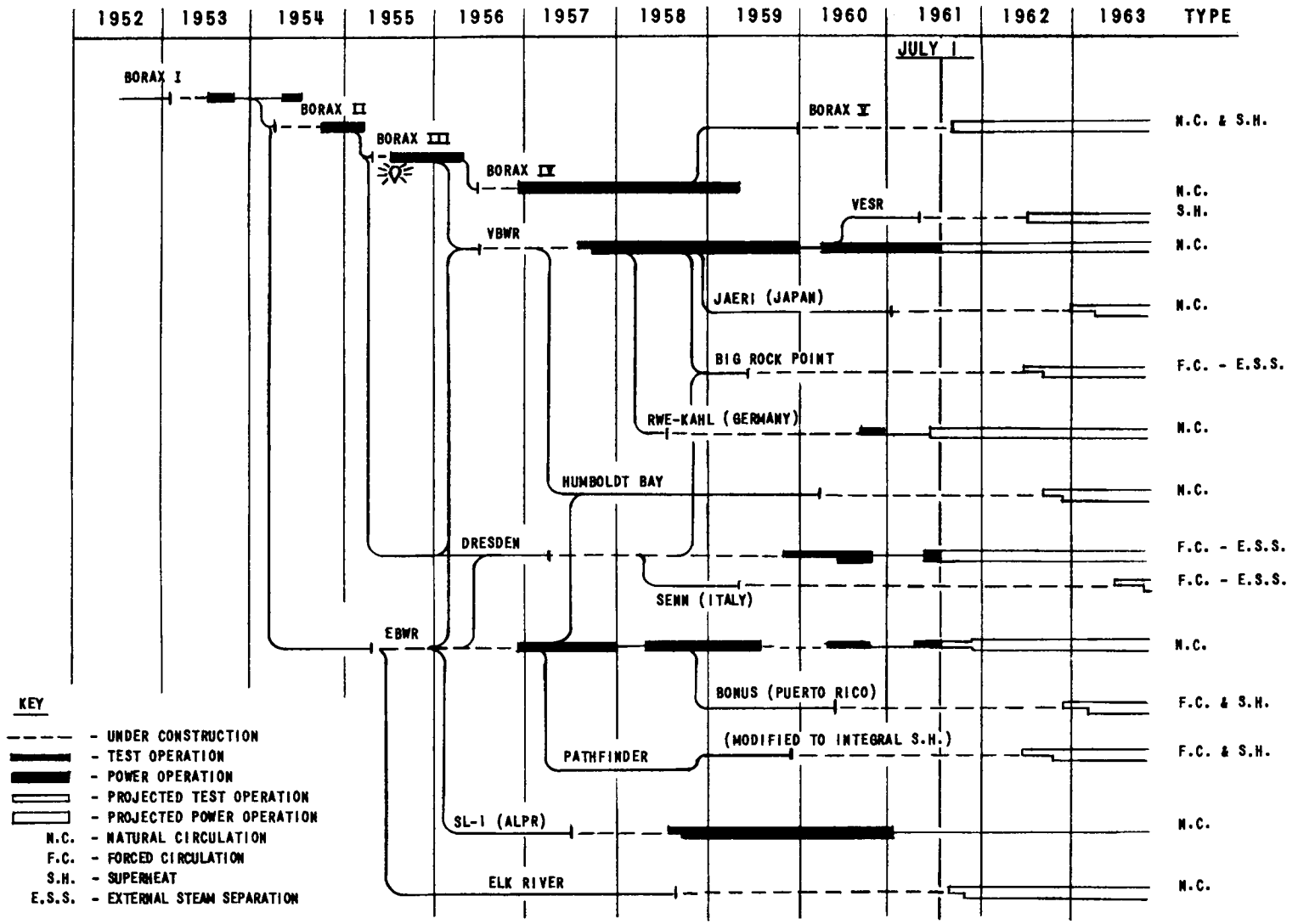

Fig. II-2

Boiling Water Reactor Development Chart (Under Construction or in Operation as of July 1, 1961)
112-1402

cold criticality approaches without voids, the two-group calculation overestimated reactivity by 3.39%. However, the root-mean-square error predicted on the basis of uncertainties in constants is ±3.56%.

This is certainly a rather large amount of reactivity, and advanced multigroup calculations might improve the accuracy. However, an accepted principle of reactor physics is that theory need be no more than one order of magnitude more accurate than the constants used. It is believed that real improvements can be made only by improvement of accuracy in constants.

Experimental flux plots in EBWR have been compared with theoretical homogenized-core calculations and have in general agreed, allowing for the presence of natural uranium power-depressing fuel elements in the center of the core and the effects of control rods partially inserted during operation at 20 Mwt.

The use of burnable poison has been seen as a means toward extending core life and reducing the frequency of fuel processing. The incorporation of burnable poison in a core permits a substantial increase in the amount of fissionable material which can be included for burnup without increasing control rod requirements. The theory is that the burnable poison, usually boron (natural or enriched in B^{10}), is burned up at a rate of the same order of magnitude as the rate of burnup of fuel. The only burnup reactivity which the control rods must control is the difference between the rates of burnup of fuel and poison. If the initial amount of poison is about equal in reactivity to the allowance of fuel burnup, the reactivity difference to be handled by control rods reaches a maximum somewhere near the middle of the core life period.

The removal of the requirement for control rods to control all of the burnup reactivity constitutes a double advantage. Firstly, simplicity in design operation and maintenance can be achieved by utilizing a small number of rods and rod-drive mechanisms, and leakage is kept to a minimum in cases where drives incorporating pressure seals are used. Secondly, the even distribution of burnable poison throughout the core permits the reactor to be operated through most of its life with control rods withdrawn almost completely. In this way, lower maximum-to-average neutron and heat flux ratios can be maintained. Specific power can be raised somewhat without reducing the burnout heat flux safety factor.

Considerable experimentation has been carried out to develop methods of incorporating burnable poisons directly in the fuel material of a core. The general experience has been that the achievement of sufficient uniformity of concentration of the poison is very difficult. The main concern here is that hot spots would develop in operation in local areas where poison concentration is low. Consequently, in the Argonne Low Power Reactor (ALPR), burnable poison had been incorporated in the form of strips

containing boron which were welded to the outsides of each fuel assembly. The welding was not done until after critical measurements were made. Critical experiments were carried out with and without the poison strips, and with different amounts of poison, confirm calculations of the amount required. The core life of ALPR was calculated to be 3 yr.

The possibility of improving the long-term economy of nuclear-power production by increasing the conversion ratio has received considerable attention. An increased conversion ratio can be used to prolong core life (since the core operates during the latter part of its life partially on self-generated feed); to reduce the amount of initial allowance of fuel burnup required for a given core life (lower initial enrichment); and to permit higher specific power through reduced distortions of the control rod flux.

Higher conversion ratios can be achieved by reducing neutron losses by leakage and absorption. Therefore, the physical design changes in the core to improve conversion ratio can be generally stated as increase of core size, reduction of the coolant-to-fuel ratio, and increase of fuel density by use of metal rather than oxide fuel. Current studies are directed at optimizing the extent to which these adjustments in core parameters should be made in view of conflicting economic effects, such as tightening lattices requiring forced circulation or higher risers, and pressure vessels to remove heat from the core.

A great deal of experimental and analytical work has been carried out by Argonne National Laboratory and the General Electric Company on the dynamics of boiling reactor systems. This work has been directed toward understanding the stability-instability phenomenon in boiling reactors, and the core and system parameters affecting this phenomenon. The ultimate goal of these studies is the ability to predict with accuracy the stability and operational limits of given reactors and to permit design to those limits. Existing boiling reactors have all demonstrated capability of higher rates of power generation than contemplated in the original designs. Therefore, the reactors are in effect oversized for their design capacities, and expensive expansions are necessary in order to permit full utilization of reactor capacity.

The technique of transfer-function measurement and feedback analysis has been developed wherein reactivity gain and phase shift are measured with the insertion of reactivity disturbances of various known frequencies and amplitudes at various pressures and power levels. The data obtained may be used to predict stability at higher power levels. In the EBWR, stable operation at power levels up to 65 Mwt were predicted from measurements made at lower powers. Operation at 61.7 Mwt confirmed this prediction. (Operation at this power was limited by the external system for heat dissipation, and not by instability, although indications were that instability might be encountered at slightly higher levels, i.e., the predicted 65 Mwt.)

The conclusion which can be drawn from these studies is that the stability limit of power in a given reactor can be predicted accurately from transfer-function measurements at lower powers in that reactor. Stability limits can be estimated for a new design by estimating time constants for the various parameters affecting reactivity. However, these estimates are very sensitive to the parameter values used, and extreme care must be exercised when a new design deviates very far from existing designs upon which measurements have been made.

A very large increase in the time constant of heat transfer from the fuel to the coolant, (as in the BORAX IV core design), may improve the stability, depending on the other gains and time constants. A long-time delay would reduce the inherent self-limiting ability during a transient.

It has been found that the amount of reactivity held in voids is not a singular criterion of stability, but enters the system as one of several contributing parameters. Incremental change in void reactivity with power is also an important stability consideration. Observations indicate that making the second derivative of the power vs reactivity curve zero or positive in the high-power region will promote stability.

The approach of a boiling reactor to instability can be detected as a recognizable flux pattern with the insertion of a reactivity disturbance. This pattern can be expected to repeat in different experiments under similar conditions. However, it is advisable to obtain a firm basis for such observations by examination of flux signals before and after instability begins, possibly in low-pressure tests.

The area of reactor dynamics in which only qualitative information is presently known is that of flux-tilt instability resulting from xenon and void shifts within a core. This effect is not observed in cores of EBWR size and smaller. It is expected to exist in larger cores which contain several critical masses that may tend to behave somewhat independently of each other. Such tilting has been observed in a limited way in the PWR at Shippingport, Pennsylvania (Westinghouse-Duquesne Light Company) and in the Dresden Nuclear Power Station near Kankakee, Illinois (General Electric Commonwealth-Edison Company). The instability results from a shifting of flux between various parts of the core as a result of variations in xenon and void concentrations in these parts.

Experiments conducted in the Dresden reactor have provided valuable information about this problem. Investigation into the effects of high core voids, stability at various pressures, coolant flow rates, power density, and xenon oscillation have indicated that the reactor has been conservatively designed.

The low magnitudes of xenon oscillation and the resulting flux tilting indicate that there is no danger to the reactor from this phenomenon. Likewise, the high-power density experiments have demonstrated Dresden's ability to operate safely at much higher powers than its present rating. Needless to say, the successful demonstration of the Dresden plant's capabilities has done much to develop confidence in the design of large boiling water reactor power plants.

A more fundamental approach to the detailed understanding of the dynamics of boiling-water reactors is being made as a part of the OEEC Halden Reactor Project. A major goal of this program is the quantitative determination, through in-core and overall transfer-function measurements, of the parameters affecting the stability of the Halden boiling heavy water reactor and to develop an analytical model which would be valid in predicting the characteristics of other such reactors. A subsequent project, now in the proposal stage, would extend these efforts to cover the entire range of boiling light and heavy water reactors, by employing the spectral-shift principle to vary power coefficients of reactivity in a redesigned experimental reactor facility.

B. Heat Transfer and Hydrodynamics

Exhaustive laboratory tests on boiling heat transfer, pressure drop in channels, and flow of steam-water mixtures have been correlated sufficiently to compute the performance of natural-circulation boiling-water reactors. Several major uncertainties still exist in the prediction of overall performance. The most important of these is the question of entrainment or "carryunder" of steam in the downcomer water. Such entrainment reduces the effective density of the downcomer water, and thereby reduces the driving head for natural circulation. Entrainment can also adversely affect nuclear parameters, since the downcomer in most designs also serves as the radial reflector for the core.

No positive method of calculating the entrainment to be expected in a given design has been developed. Accurate measurement of this effect in an operating reactor is most difficult, if not impossible. A method which has been employed for EBWR has been to determine the actual recirculation rate, by temperature difference between the recirculating water at the top of the downcomer and the water at the bottom of the downcomer, after a known flow of feedwater at a known temperature has been added. This difference is then compared with the theoretical recirculation rate calculated from laboratory test data. Any differences are attributed to steam entrainment. This method is very rough, as it depends upon measurements of small temperature differences under high radiation conditions.

Laboratory studies have shown that at low operating pressures the extractable power of a boiling-water reactor is probably limited by hydrodynamic and kinetic feedback instability, whereas at high pressures, the limit is probably burnout heat flux. Methods of calculating burnout heat flux in boiling systems have been developed.

III. Developments in Component Design*

A. Fuel Elements

Despite the fact that current fashion in fuel-element design for water-cooled reactors very strongly favors oxide elements, most of the experience in operating reactors, particularly those of the boiling type, has been with elements having the uranium in metallic form. In the cases of BORAX-I and -II, curved, thin-plate aluminum-clad, highly enriched uranium-aluminum alloy elements (in most respects identical with MTR elements) were used. This was primarily because of easy availability. In early reactors these elements served their purpose well. In BORAX-III, a similar element, but incorporating flat plates, was employed. In these reactors the only aim was to obtain elements which would perform reliably in the experimental program. No effort was made to use an element which would have practical economic interest for larger reactors later on.

For EBWR, low enrichment was employed in order to provide fertile material for conversion and to demonstrate a more commercially practical fuel cycle. It was recognized early that metallic fuel elements in which uranium was the major constituent would present a severe corrosion problem in the event of cladding failure, as well as a problem of radiation-induced dimensional instability which did not exist with highly enriched elements. A very exhaustive program of research was carried out to determine the properties of uranium alloys containing additions of other elements acceptable from the physics standpoint. This program led to the development of the uranium-5 w/o zirconium-1.5 w/o niobium alloy which was used in EBWR.

No alloy was found which would satisfy simultaneously the two needs of resistance to corrosion and dimensional stability under irradiation. The U-Zr-Nb alloy used could actually satisfy either need, but not both at the same time. This is because different heat treatments are necessary to obtain the different properties. Quenching the alloy from 850°C (1560°F) results in a gamma structure which is resistant to corrosion, while a 24-hr soak at 650°C (1200°F) is necessary to produce the alpha-plus-gamma structure which is dimensionally stable under irradiation.

---

*N. Balai, C. Breden, V. Kolba, and D. Roy

In the case of EBWR, the decision was made to heat treat for dimensional stability and to rely upon the Zircaloy-2 cladding for corrosion resistance, assuring the latter by means of very careful acceptance testing of all fuel plates. The latter acceptance testing essentially took the form of ultrasonic bond testing of fuel plates both before and after a 2-week corrosion test in 288°C (550°F) water, with a thorough visual inspection. Only three of the 984 plates tested failed in corrosion, and these within 36 hr of the start of the test. The final, completed fuel assemblies, of six plates each, spot-welded to Zircaloy-2 side plates, were also corrosion tested under the same conditions, with no failures.

As of November 1958, the most highly irradiated EBWR fuel plates had undergone burnup to the extent of about 3000 Mwd/metric ton. The average for the central 36 assemblies was about 2500 Mwd/t. Small model fuel plates, fabricated by methods duplicating as closely as possible those used for the EBWR plates, have been irradiated to about 8000 Mwd/t in the Argonne high-temperature water loop in the MTR. There have been no failures or indications of incipient failure in any of these plates to date.

A total of 1120 fuel plates were fabricated for EBWR. Of these, about 150 plates, which were either rejected because of defects detected ultrasonically or visually, or not used in EBWR for other reasons, have been subjected to 20-month life tests in 288°C (550°F) water. Only one of these plates has failed during these tests; eight others have developed blisters and were removed from test before failure. All of these nine plates had been rejected for use in EBWR because of ultrasonically detected bond defects.

Samples of Zircaloy-2 from production ingots and sample coupons from fuel plates have been subjected to accelerated life tests in 400°C (750°F), 1500 psi (100 atm) steam for 13,000 hr. These samples are coated with light oxide but have not disintegrated. This test is estimated to be equivalent to a 20-yr exposure in 288°C (550°F) water.

Based upon this experience, both in the EBWR and in auxiliary tests, it can be said that fuel elements of the EBWR type and Zircaloy-2 cladding, in general, are satisfactory for use under boiling water conditions at 252°C (486°F) and are probably satisfactory to 288-300°C (550-570°F). This has been corroborated by pressurized water reactor experience as well.

The current trend toward uranium oxide (UO_2) fuel for water reactors results mainly from continued concern over the rapid and extensive release of fission products and other active material possible upon rupture of a metallic fuel element, such as those in EBWR. Although the latter have functioned well to date, there has as yet been no statistical determination of the safe limit of operation of such elements from the

standpoint of corrosion failure. It is also anticipated that oxide elements are inherently more resistant to radiation damage. Exposure of oxide would be possible to higher burnup values than in metallic elements. Although there have been a few tests made wherein oxide samples have been subjected successfully to burnup as high as 30,000 Mwd/t, there has again been no statistical determination of achievable burnup in oxide. The EBWR elements have, to date, shown no indication of approaching their limit in this respect. Early anticipation that oxide elements would be less expensive to fabricate has not been supported by experience. Fabrication costs now appear to be about the same for oxide or metal, at least in the case of Zircaloy-2 cladding.

Along with the advantage of resistance to corrosion failure, several disadvantages of oxide elements must be considered. Conversion ratios obtainable with oxide elements are inherently lower than with metal elements. Because of the necessarily lower density of uranium atoms, less fertile material is available for conversion.

The rod shape, which is probably the most practical for oxide elements, makes it more difficult to approach higher conversion ratio by reducing the water-to-fuel ratio. In rods of diameters considered practical for fabrication at the present time, the very poor thermal conductivity of UO_2 creates extremely high central temperatures in the fuel.

Attainable power densities in oxide-fueled cores are apt to be limited neither by stability nor by cladding burnout, but by the approach of the central UO_2 to its melting point. The solution to this problem may lie in the use of thinner oxide fuel rods. Problems in structural stability, with respect to vibration and strength, may limit any major improvement in this direction. Another possible solution is the incorporation of thin fibers of metals of high melting point into the oxide. This may prove to be a successful approach if the thermal conductivity can be increased significantly without introducing too much neutron poison into the fuel material. Development work on this is in progress.

Oxide fuel elements containing thorium oxide and highly enriched UO_2 have been used successfully in BORAX-IV. These elements were aluminum-nickel clad, and employed lead as a bonding agent between the oxide and clad. It has been determined that the actual failure of BORAX-IV fuel elements was the result of mechanical weakness of the tube plate used to contain the oxide pellets, and had nothing to do with either the use of thorium oxide in the pellets, the lead bonding, or the corrosion properties of the aluminum-nickel alloy used as cladding. A similar element sample has been successfully exposed to 4000 Mwd/t in the Argonne high-temperature water loop in MTR under comparable water conditions. Post-irradiation examination showed only slight pellet cracking, with no gross physical changes in the sample.

The corrosion properties of aluminum and its alloys have been under study for many years. The low neutron-absorbing properties (in comparison with stainless steel) and low material and fabrication costs (in comparison with Zircaloy) of aluminum, offer very significant advantages in considerations of fuel-cycle economy, provided corrosion resistance at economically attractive reactor temperatures can be brought up to acceptable standards. The presently developed aluminum-1% nickel alloy (X8001) is currently believed to have an operating temperature limit of 418°F (215°C), which is equivalent to 300 psi (20 atm) in a saturated boiling system. However, even this will require longer tests for confirmation. The Argonne Low Power Reactor (ALPR, now redesignated as SL-1) was operating at these conditions with aluminum-nickel-clad fuel.

There are indications that the corrosion resistance of aluminum alloy at higher temperatures can be improved significantly by reducing the pH of the water, such as by adding phosphoric acid. However, pH values as low as 3.5, which are most beneficial to the aluminum, may cause intergranular attack of Type 304 stainless steel, which is the popular structural and cladding material for components of the reactor primary system. It has also been found in some tests at low pH that, although the overall corrosion rate of the aluminum alloy is much reduced, a pitting type of attack may occur which would be highly undesirable in a fuel element clad. Other tests at low pH have shown accelerated attack of aluminum-nickel alloy which is in contact with Type 304 stainless steel. In a test in the BORAX-IV reactor, net rates of water dissociation and activity in the direct-cycle-generated steam were found to increase markedly upon addition of phosphoric acid to the reactor water.

Much of the experimentation on corrosion of aluminum alloys has been clouded by recent evidence that the corrosion rate is influenced by the ratio of aluminum alloy surface area to water volume, the higher ratios being associated with lower corrosion rates. The mechanism has not been fully explained, although some investigators believe this effect to be caused by dissolved corrosion product acting as an inhibitor to further attack. If this is correct, corrosion rates will to a considerable extent vary with the operating characteristics of purification systems attached to the reactor or corrosion-test facility.

Erosion and mechanical strength are also problems with aluminum alloys. Some alloys with relatively high strengths have been produced, but these have not been corrosion resistant. Consideration is being given to the use of a duplex clad of two different alloys, the inner one being selected for strength and the outer one for corrosion resistance. There is also indication that the use of aluminum in a reactor brings on a corrosion product (crud) problem. EBWR water contains an undesirable amount of solid particles of corrosion product which originate largely from the corrosion of aluminum-1% nickel "dummy" elements used to fill the

peripheral spaces in the core not occupied by fuel assemblies. This has resulted in the buildup of deposits on the surfaces of the Zircaloy-clad fuel plate as thick as 0.003 in. (0.075 mm), with a weight of 6.5 mg/cm^2. The deposits consist of 67% aluminum (in the form of Boehmite), 25% nickel, and 8% iron. They were found to flake off the fuel plates at points of highest heat flux while remaining tenacious in other areas. The aluminum dummy elements have been replaced by stainless steel dummy elements.

It is not believed that the "one best choice" of fuel and cladding materials can be made at this time, based upon experimental evidence. Economic studies have in many cases been based upon "eventually anticipated" fabrication costs, rather than actual present-day selling prices.

Achievable burnups used have been based upon very limited in-reactor tests. It has been said that the degree of optimism expressed in such cost studies appears to be directly proportional to the estimator's distance from the engineering and fabrication department. It is probable that the determining factors in optimum choice of fuel element will be relative reprocessing costs, the statistical frequency of fuel failures, the seriousness of those failures and cost of subsequent decontamination, the effect of clad metals on other system components, the concurrent requirements for system water purity, and future process improvements - none of which can be evaluated with any degree of accuracy and realism until much more operating experience with the various fuel types has been obtained.

B. Control Elements

The important properties of materials which must be considered in the selection of a control element material for a water-cooled reactor are high thermal and preferably epithermal neutron-absorption cross section, structural stability, ability to retain neutron absorptivity, structural stability under irradiation, and corrosion resistance. To date, cadmium, boron, and hafnium have been used as control materials in reactors.

The BORAX-I reactor used cadmium blades, nickel plated and clad with aluminum. The choice of these rods was essentially made on the same basis as the choice of BORAX-I fuel, i.e. ready availability and short life requirement. Cadmium rods were again used in BORAX-II, but for BORAX-III and -IV, hafnium and boron in the form of Boral (physical mixture of 35 w/o B_4C in aluminum) were used.

In EBWR, hafnium and boron were again used. For this reactor, a "sheet-metal" fabrication technique was developed for both materials in order to manufacture the required cross-shaped elements. Sheets of hafnium ($\frac{1}{16}$ in. thick) and Type 304 stainless steel containing 2 w/o natural boron ($\frac{1}{8}$ in. thick) were bent in a standard sheet-metal press to form

angular shapes. They were then surface spot-welded to form the crosses. Five hafnium and four boron-stainless steel rods were made and initially put in use in EBWR. (The new rods are discussed later.)

The sheet-metal spot-welding technique offered a considerable saving in fabrication cost over heliarc or arc-welded and machined rods manufactured from plate, and offered a very large saving in both material and fabrication over rods completely machined from the billet form. The method also appeared less expensive than extrusion or precision casting, and was resistant to catastrophic failures of solid metal rods. The sheet-metal construction developed and used produced a flexible rod compatible with the strength of the core shrouds. Solid-plate control rods having plate thickness of $\frac{1}{4}$ or $\frac{1}{8}$ in. would have been too solid for the EBWR shrouds in the event the control rods stuck. Consequently, the more flexible rod was selected so that in the event the rods did stick it would be possible to wiggle them free without destroying the core geometry.

Hafnium rods are basically better than boron rods because the hafnium does not lose its effectiveness under prolonged irradiation and has higher epithermal capture. Because of the destruction of boron by (n,α) reaction, boron loses its effectiveness. It has been calculated that after one year of operation, 14.5% of the boron should burn up. Effectiveness of the boron-stainless steel rods should decrease slightly from 109 to 104%. The material cost advantage of boron-stainless steel indicates that such rods could be replaced several times during reactor life and still retain lower overall cost. If a method were developed whereby the Zircaloy follower pieces (which represented major fraction of the cost of the boron-stainless steel rods) could be re-used, the overall cost difference would be very large.

Examination of the hafnium and boron-stainless steel control rods, after 3 yr of use in EBWR, showed no occurrence of gross warpage, bending, or other dimensional irregularities.

In the course of development of the Shippingport Pressurized Water Reactor by Westinghouse, a control rod alloy consisting of 80% silver, 15% indium, and 5% cadmium (w/o), nickel plated, was formulated and found to be a highly effective control medium. This is because the cadmium supplies blackness to thermal neutrons while the silver and indium exhibit moderately strong thermal capture as well as strong epithermal resonance capture. The alloy is relatively cheap, has nearly the effectiveness of hafnium, and has a low corrosion rate (0.00018 in/yr) in 600°F (316°C) water. This material has been used for PWR control elements and should be equally useful in boiling water reactors (if prolonged in-pile irradiation characteristics are satisfactory).

Considerable research and development has been carried out in recent years on the use of rare earth elements (which are not very rare) as control materials. Such elements as samarium, europium, and gadolinium offer high cross sections and appear to offer possibilities for selecting mixtures of materials, each chosen to cover specific ranges of neutron energy for absorption. The principal problems here are concerned with placing the absorbing material in suitable form or containing it in a satisfactory manner for use in the reactor. Several methods, one of which involves the dispersion of rare earth oxide in stainless steel, appear promising. None of these has, as yet, been used in boiling water reactors.

C. Control Rod Drive Mechanisms

Both top- and bottom-mounted control rod drive mechanisms have been utilized to date with boiling water reactors. Each type has its advantages and disadvantages. For example, with bottom-mounted drive mechanisms, the top closure lid of the reactor and the space above the reactor core are unobstructed, so that access is very convenient for removal, replacement, and rearrangement of fuel assemblies. Drive mechanisms need not be disturbed when the reactor vessel is to be opened. The removable shielding over the top of the reactor is quite simplified. The control rod drive thimble is always flooded, so that cooling and sealing of the drives are somewhat easier.

On the other hand, since corrosion products tend to accumulate in bottom-mounted control drive thimbles, special steps must be taken to prevent such accumulation or to prevent its interference with control rod operation. For bottom drives, more building height is usually necessary below the reactor, whereas in top-mounted drives, the drive mechanism space is the same as that required above the reactor for fuel handling.

Relative advantages and disadvantages of top and bottom drives tend to balance out. The proper choice usually results from other factors, such as building configuration and anticipated frequency of opening of the reactor vessel.

A linear seal drive mechanism employing an external lead screw and nut carriage, bottom mounted, was employed for the initial operation of EBWR. This drive has the advantage of accessibility to working parts for normal lubrication and maintenance. The reactor pressure, operating on the shaft where the latter passes through its linear pressure breakdown seal, provides an additional force for rapid rod insertion in emergencies. Considerable difficulty has been experienced with active corrosion product accumulation in seal housings of the control roddings, with the result that some rather high radiation levels exist in the subreactor room directly below the reactor. The design of the seal housings and thimbles is not well adapted to flushing out these corrosion products.

This difficulty, and the fact that column loadings on the sealed shaft limit this type of mechanism to a stroke of 4 ft or less, has led to replacement with a rack-and-pinion type of mechanism for future operation of EBWR with a 5-ft core height. The latter mechanism employs a rotary pressure breakdown seal on the pinion shaft, with an external clutch release for rapid insertion. Both pinion and rack operate in water-lubricated "Graphitar" bearings. The mechanism housing has been designed for clearances between moving parts and housing of about $\frac{1}{8}$ in. throughout. By opening a flushing valve at the lower end of the housing, relatively high water velocities will be obtained past all surfaces, and accumulated corrosion products will be adequately removed.

A somewhat similar rack-and-pinion design, but mounted above the reactor, had been employed in the ALPR (now SL-1).

Considerable effort has been expended by personnel at Argonne, Westinghouse, and Atomics International in the development of a totally enclosed type of drive known as the magnetic jack. In the magnetic jack, a bundle of steel rods within the enclosure can is moved stepwise in the axial direction by actuation of various combinations, in sequence, of four magnetic coils around the outside of the can. Emergency insertion is obtained by de-energizing all coils. This type of drive has been tested in both top- and bottom-mounted versions, in out-of-reactor tests, and it is being considered for use in the Halden Boiling Heavy Water Reactor.

D. Water Chemistry

The dissociation of water by reactor radiation into its component hydrogen and oxygen has been a matter of concern since the earliest consideration of water reactors. Relatively high rates of gas generation were observed in early low-power, low-temperature research reactors and in early capsule experiments. For a time, it was thought that high-power water-cooled reactors might be completely impractical for this reason.

It is generally agreed that the observed net decomposition of water represents the difference between a gross decomposition reaction, which is principally a function of neutron or heavy particle bombardment of H_2O (or D_2O) molecules and a reverse or "back" reaction, which is a function of temperature, impurity concentration, concentration of reactants and free radicals, etc. For the H_2O case, much simplified, the main gross decomposition reactions are

$$H_2O \rightarrow [H] + [OH] \qquad (1)$$

and

$$2H_2O \rightarrow H_2 + H_2O_2 \quad . \qquad (2)$$

In a secondary reaction,

$$2H_2O_2 \rightarrow 2H_2O + O_2 \quad . \tag{3}$$

The reverse of "back" reactions may be summarized as

$$H_2O_2 + [H] \rightarrow H_2O + [OH] \tag{4}$$

and

$$H_2 + [OH] \rightarrow H_2O + [H] \quad . \tag{5}$$

The net reaction is

$$H_2O_2 + H_2 \rightarrow 2H_2O \quad . \tag{6}$$

Temperature has little or no effect on the forward or decomposition reaction, but an increase in temperature increases the rate of the "back" reaction.

In the case of pure water above 300°F, containing a small amount of dissolved hydrogen to promote reaction (6), the net decomposition is very nearly zero. If the water contains ionic impurities, the free radicals [H] and [OH] are destroyed by oxidation-reduction reactions. They are, therefore, unavailable to take part in reactions (4) and (5). As a result, the H_2O_2 dissociates to free oxygen by reaction (3) instead of participating in reaction (4), and the H_2 and O_2 are liberated.

In pressurized water reactors, wherein a small partial pressure of hydrogen has been maintained, little or no net decomposition of water has been observed, in corroboration of the above discussion. However, in boiling water reactors, significant dissociation has been observed. In EBWR, the gas evolution rate is roughly linear with power up to 40 Mwt. Pressure has an inverse effect (i.e., increased pressure resulting in lower net decomposition).

Boiling water reactors show a greater net decomposition than pressurized water reactors. The reason for this is believed to be that the boiling process affords an escape for the decomposition gases before they can recombine. In the pressurized water reactor no phase change occurs. A small excess of hydrogen is maintained in solution, which tends to inhibit the decomposition process. Even if hydrogen was not added, the corrosion reaction between the water and the steel would tend to keep hydrogen in the water. Since the temperature of the primary water does not vary a great deal as the water circulates, the solubility of the hydrogen is relatively unaffected, and the hydrogen concentration is essentially constant throughout the system.

In a boiling water reactor, the coolant leaves the reactor in the vapor phase, so that the hydrogen and oxygen are no longer, strictly speaking, in solution. In passing through the turbine and condenser, the temperature of the steam is reduced so that the condensate temperature in the condenser hotwell is in the 100-150°F range. At these temperatures, for a given partial pressure of hydrogen and oxygen, the solubility is much lower than at reactor temperature. The radiolytic gases cannot return to the reactor at the rate at which they are removed from the reactor, and the excess is drawn off through the condenser air-ejector system.

If this theory is correct, net water dissociation should not be as high in indirect-cycle boiling reactors employing high-temperature steam condensation and high-temperature feedwater return. Some proportion of the freed radiolytic gases should redissolve in the condensate and return to the reactor, and an equilibrium approaching that experienced in pressurized water reactors should be attained. Since no such reactors have been operated as yet, the validity of the theory remains to be tested. Operation of the Halden Boiling Water Reactor, the German RWE-Kahl Reactor, and the Allis-Chalmers Rural Cooperative Power Administration reactor at Elk River, Minnesota, should provide valuable data on this subject.

Attempts have been made to reduce net water dissociation in existing direct-cycle boiling reactors by injection of hydrogen into the cold feedwater. In all cases, the amount of net dissociation (measured as volume of oxygen evolved per unit volume of steam condensed) was reduced.

It is interesting to note that the addition of hydrogen in these reactors resulted in a marked increase in the N^{16} activity in the evolved steam. As indicated by subsequent tests, in which hydrazine and ammonia were added to the reactor, this is probably the result of ammonia production in the reactor with the N^{16} combining with the added hydrogen and transferring from the liquid to the vapor phase at a higher rate. Under normal equilibrium conditions, the N^{16} activity in the reactor water is many times that in the steam phase.

The major short-lived activities which have been found in the operation of boiling water reactors to date are N^{16}, Na^{24}, and Mn^{56}. Almost 100% of the activity in the steam system during reactor operation comes from N^{16}. Since this isotope has a 7.4-sec half-life, this activity disappears within minutes after reactor shutdown and is of no concern with respect to plant maintenance. The Mn^{56} is an activated corrosion product of the steel, and the Na^{24} activity is formed from the aluminum in the systems (fuel cladding in BORAX and ALPR, fuel dummies in EBWR). The decontamination factor between reactor water and steam for this isotope has been measured to be in the order of 1000 for all three reactors mentioned. Therefore, Na^{24} activity in the steam system is negligible. The Na^{24} is effectively removed from reactor water by bypass ion exchange systems and decays within a few days after reactor shutdown.

The major long-lived activities are Co^{58} and Co^{60}, formed from the nickel and cobalt in the system. The only area where these materials affect shutdown maintenance is in the control rod drive mechanism room of EBWR, as mentioned earlier.

Activity buildup in the direct-cycle turbine of EBWR has been negligible. The plant was shut down for annual turbine inspection after one year of intermittent operation (2840 hr of actual operation). The general activity level found inside the turbine was 0.2 mr/hr at a 2-in. distance, increasing to the order of 2 to 5 mr/hr at steam admission nozzles and valves. Readings were taken 10 days after reactor shutdown.

The condition of the turbine interior from the corrosion and erosion standpoint was excellent. Blade deposit was estimated to be 0.1 mg/cm^2, and scrapings showed mostly Co^{58}. No loose materials were found anywhere in the turbine.

Although a considerable number of experiments have been carried out attempting to simulate by intentional defects the effects of oxide fuel-element ruptures, probably the most important experiment on fuel defects carried out thus far is the actual failure of a number of elements in the BORAX-IV reactor. The reason for these failures has been discussed earlier.

Several very interesting observations were made during this phase of BORAX-IV operation. The most important of these is probably the fact that gross activity in the reactor water showed no substantial increase over normal operating conditions. This indicates that only a very small fraction of the fuel material is in direct contact with the water and in a position to contribute direct contamination. The latter conclusion has been corroborated by the study of evolved fission gases. The theoretical ratio of Xe^{138} to Kr^{88} release would be 15 to 1. The actual observed ratio is only about 5 to 1. This indicates that the gases are sufficiently delayed in transfer from the fuel material to the reactor water (from which they are immediately involved), that the shorter half-life Xe^{138} has time to decay before emerging.

Similar effects have been observed in artificial defect tests in EBWR.

It is also interesting to note that it was possible to operate BORAX-IV at 4.5 Mwt on a short-term basis, even after fuel ruptures occurred. During such operation, the condenser hotwell activity rose to 5000 mr/hr, 10 times its normal value. All activity in the external system dropped to essentially zero within 17 hr after shutdown, except for the hotwell, where a 1.5-mr/hr residual remained. This shows that even with oxide fuel rupture, long-lived contamination of system components does not seem to be a serious problem.

E. Reactor Components

Experience in the design and fabrication of pressure vessels and other components for use in the primary systems of water reactors, both boiling and pressurized, has demonstrated the need for supplemental requirements in addition to the normal provisions of the ASME Boiler and Pressure Vessel Code in order to assume integrity of construction and dimensional accuracy. Important among these additional requirements are 100% radiographic examination of all circumferential and longitudinal vessel welds and of all nozzle-connecting welds, metallurgical control of materials (particularly low-temperature impact-strength properties and grain size), demonstration of cladding integrity, helium leak testing, and frequent inspection of fabrication processes.

Gasket tests on EBWR have demonstrated the superiority of Teflon-filled spiral-wound stainless steel and zinc-plated carbon-steel gaskets over similar asbestos-filled gaskets. These tests also showed that restraint strips inserted inside and outside the gaskets, within the gasket grooves, aided a great deal in preventing structural buckling of the gaskets. Despite the manufacturing simplicity of thick, flat closure heads and the shielding value offered by such designs, experience has shown this closure type to be less satisfactory than dome-type closures - primarily because a flat closure cannot expand with the bolting flange upon application of pressure, and severe gasket rubbing results.

Development work with structural materials has shown the adaptability of a number of alloys for use in pressure vessels, bolting, and piping. Procedures have been developed for welding quenched and tempered $2\frac{1}{4}$% chromium-1% molybdenum steel in 6-in. thickness, in a manner which retains both the excellent tensile and low-temperature impact properties of the base material (105,000 psi ultimate tensile strength, 15 ft-lb impact strength at -50°F at the half-thickness point). This alloy has shown very good resistance to creep at temperatures up to 800°F. Similar excellent properties are known to exist in another alloy, designated HY-80 (15 ft-lb impact strength at -100°F at the center of a 20-in.-thick slab). The welding and other properties of this material in 6-in. rolled plate are currently under study.

A number of hot die or tool steels have been investigated for creep strength with a view toward their use as high-temperature vessel-bolting materials. One of these alloys, known as Vasco Jet 1000 (Vanadium Alloy Steel Company), has a tensile strength of 200,000 psi at 700°F and is creep resistant at this temperature (1% creep in 100,000 hr at 100,000-psi stress). It has been found that hardness and bolt profile have a marked effect on the performance of this alloy. Rockwell "C" 50 has been found to be approximately the optimum hardness. At Rockwell "C" 40 the creep strength is reduced, whereas at Rockwell "C" 60 creep strength is no

better than at 50, but ductility at failure suffers considerably. The alloy has been shown to be notch sensitive at 800 and 900°F after 2000 hr at temperature. This difficulty can probably be avoided by the use of rounded thread-root profiles.

The advantages to be gained by utilizing such plate and bolt steels in reactor pressure vessels are significant. On the one hand, vessels of larger diameter may be fabricated with plate-forming equipment with a 6-in. thickness limit, or smaller vessels may be manufactured less expensively by virtue of the lighter walls and consequently greater ease of handling. Bolt steels of higher strength will bring larger closures into the realm of feasibility or will permit smaller closures to be built, with either a lesser number of bolts or smaller bolt diameter (or both). Thus, vessel opening for fuel charging is a simpler and less costly operation.

Material developments in the reactor vessel field are also applicable to other components, such as heat exchanger shells and pressurizer tanks for pressurized water reactors.

The question of materials for large-diameter stainless steel piping for reactor systems has also received attention of late. It has been found that essentially austenitic stainless steel piping can be manufactured by centrifugal casting, at strength levels superior to those obtainable in wrought seamless piping. Very favorable properties have been obtained in a basic Type 304L composition (CF8) by intentionally holding the chromium on the high side and the nickel on the low side of the Type 304 analysis range. A slightly unbalanced alloy results, containing about 90%-95% austenite and 10%-5% ferrite. The ferrite significantly increases strength without a corresponding drop in corrosion resistance. Weldability and creep strength are under detailed study at present. Preliminary results are highly promising.

Marked improvements in both cost and system reliability are obtainable by utilizing such materials in reactor piping. Centrifugal casting is a much less expensive method of fabrication. The resulting thinner walls make the piping system more flexible from the standpoint of absorbing the stresses resulting from thermal expansion of the system with reactor startup and shutdown.

IV. EBWR Costs and Nuclear Reactor Economics*

In view of the limited operational experience with nuclear power systems, it is difficult to estimate the cost of constructing and operating such a system. For speculative purposes only, Table II-1 attempts to compare the cost of electricity generated by a large nuclear plant (several hundred electrical Mw) in the not-too-distant future with electricity

*L. Link

generated by a fossil-fuel plant. Also, Fig. II-3 shows estimated construction costs of nuclear plants built or being built compared with the construction costs of coal-fired plants.

Table II-1

COMPARATIVE COSTS OF POWER PLANTS
(Mills/kw-hr)

	Fossil Fuel	Nuclear Fuel
Capital Investment	2.5-4.0	4.0- 5.5
Operation and Maintenance	0.5-1.0	0.7- 1.5*
Fuel	2.5-3.5	1.7- 4.0**
Total	5.5-8.5	6.4-11.0

*If D_2O is used as the moderator, makeup of D_2O would add 0.2-0.7 to costs. If an organic substance is used, makeup costs would add 0.5-1.2.

**Thermal reactors with relatively low enrichment of uranium.

At the present time, it appears that the capital costs of nuclear power plants will be higher than those of fossil-fuel plants. The nuclear plants have excellent potentialities for lower fuel costs than do the average fossil-fuel plants. In order to realize these potentialities, the reactor fuels must achieve a significant heat release in each fuel cycle. In thermal reactors, the minimum goal is 10,000 Mwd/t of fuel. For highly enriched systems, such as fast reactors, perhaps 50,000 Mwd/t is a minimum goal. Figure II-4 is a simplified illustration of a fuel cycle. In the present fuel cycles using wet chemistry processing, the out-of-reactor inventory is of the order of 12 months of feed rate. In the EBR-II pyrometallurgical cycle, the comparable inventory is of the order of a one-month feed rate. The higher burnup plus improved processing and fabrication procedures should bring the total nuclear power costs competitive with all but the lowest production cost in fossil-fuel plants.

The foregoing generalizations about the economics of power systems and the following comments about the EBWR power costs, specifically, are only an introduction to the subject, which is covered in detail in the AEC Technical Information Division, report series 8500.

EBWR was one of the first nuclear power plants in the United States to produce electricity under conditions that would satisfy commercial requirements. Special interest has centered on the cost of the power it produces. Detailed records of the basis for a cost analysis show a high present cost that can be reduced to more attractive levels by future improvements.

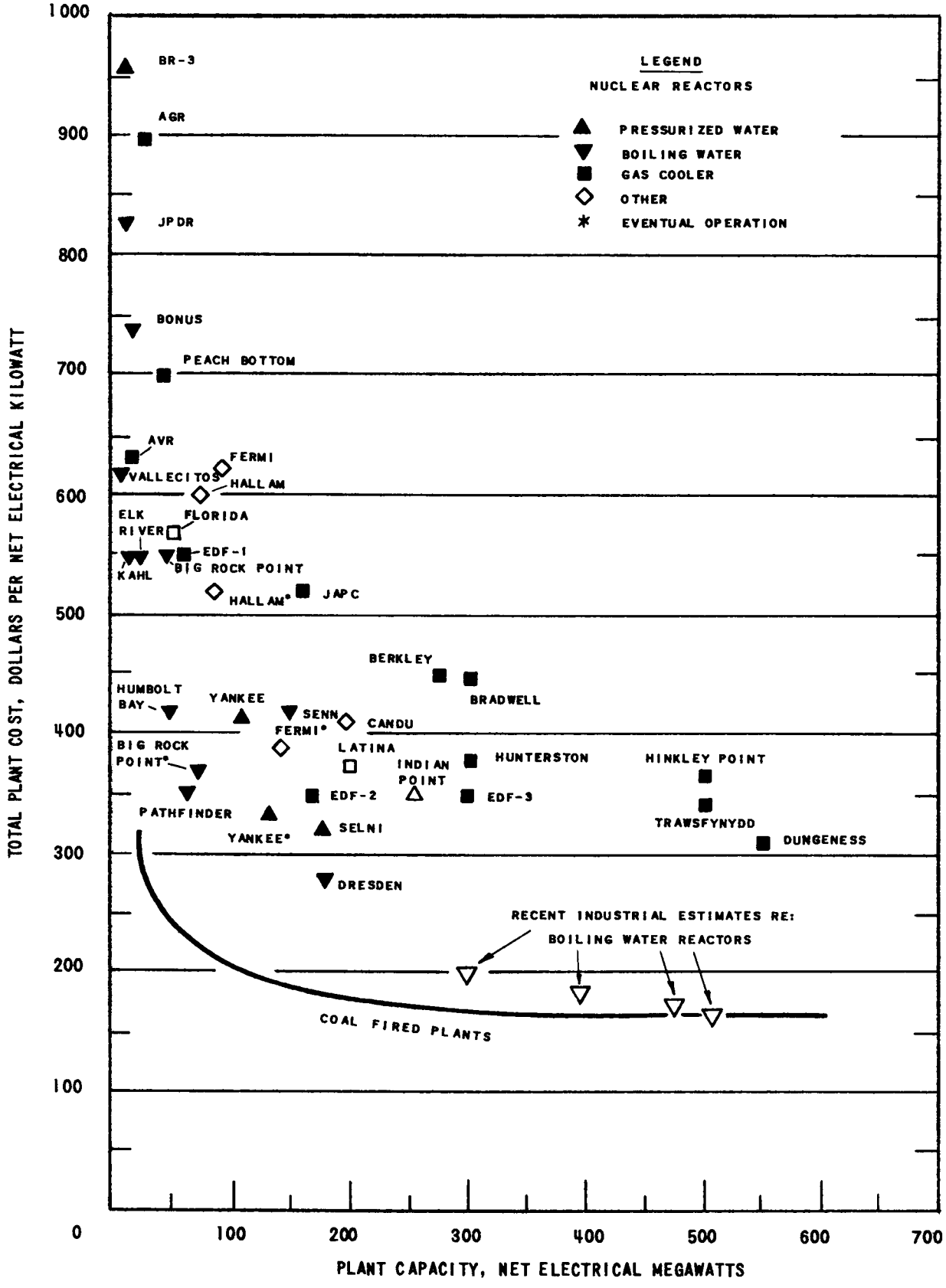

Fig. II-3

Power Plant Costs

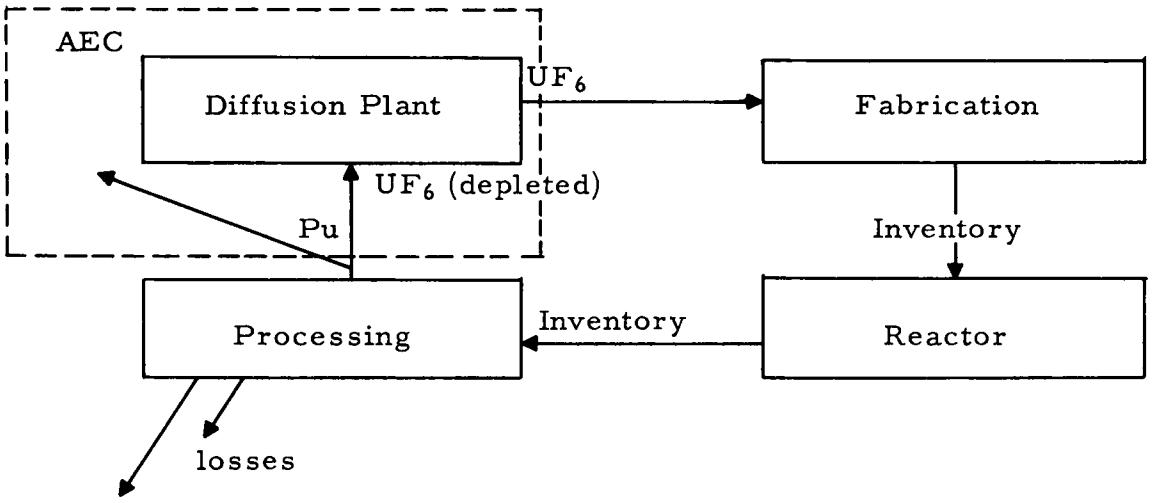

Fig. II-4

Uranium Utilization Cycle

A summary of the EBWR cost figures is given in Tables II-2, II-3, and II-4. The costs are intended to apply to the construction and operation of the EBWR as a 5-Mw(electric), light water, natural-circulation reactor plant. Those capital costs that could be attributed directly to plans for eventually operating the reactor with forced circulation and D_2O moderator-coolant were neglected. (The total amount omitted for these reasons was $220,100.) Note also that research and development costs given in Table II-3 are not included in determining the capital costs, the philosophy being that these are one-time costs and should not be capitalized. Under these ground rules, the total cost of power for the EBWR as it is now operating comes to 52 mills/kwh.

Table II-2

TOTAL EBWR COSTS

Item	Annual Charge ($\$10^3$)	Contribution to Power Cost* (mills/kwh)
Capital - $4,628,100 at 15%	694	22
Operation and maintenance	240	8
Fuel Costs		
Initial fabrication - $793,100 at 15%	119	4
Initial U rental - $730,000 at 4%	29	1
Annual burnup at 2,000 Mwd/ton	182	6
Annual fabrication	362	11
Total	1,626	52

*Assuming 3.15×10^7 kwh/yr at 80% plant factor; includes credit for Pu and residual U.

Table II-3

EBWR RESEARCH AND DEVELOPMENT COSTS (10^3)

Item	Total	Reactor System	Generation System	Fuel and Materials	Heat Transfer Study
Salaries	726	245	95	262	122
Staff time (man-years)	(54.5)	(21.9)	(7.9)	(17.1)	(7.6)
Tech. time (man-years)	(40.6)	(9.0)	(4.2)	(17.8)	(4.6)
Special materials (Zr, Nb, boron-stainless steel, etc.)	136			133	3
Materials and supplies - all others	132	12	7	99	14
Irradiation services	92			92	
Uranium processing	15			15	
Computing services	20	15		5	
Chemical analysis	33	0.4	0.2	32.4	
Hot-lab use	27			27	
Subcontracts (development and design)	31			30.8	0.2
Shop fabrication	297	94	2	176	25
Engineering and drafting (ANL shops)	45	30	3	9	3
Services - all others	83	21	9	45	8
Allocated administrative and service costs	1,402	552	192	471	188
Total	3,039	970	308	1,397	364

Table II-4

EBWR CAPITAL COSTS

Item	Investment (10^3)	Item	Investment (10^3)
Buildings		Turbogenerator	
Office and control building		Foundations	71
General construction	139	Turbogenerator	408
Heating, ventilation, air conditioning, plumbing, lighting, electricity, inspection	39	Condensers and water lines	127
		Air-dryer system	20
		Control	16
	178		642
Power Plants		Electrical	
Excavating and backfill	87	Motor controls, switch gear	123
Steel shell	288	Emergency power	8
Shell coatings and thermal insulation	54	Transformers and bus	164
Concrete inside shell	177	Miscellaneous	68
Inside steel	124		363
Utilities, air conditioning ducts, painting, etc.	147	Outside Facilities	
Miscellaneous equipment	89	Roads, walks, parking, site preparation	22
	966	Sewers	17
Reactor System		Water lines	11
Foundations	107	Cooling tower, basin, water lines, water treatment	56
Vessel external structure	164	Steam	35
Vessel	202		141
Vessel internal structure	148		
Shielding - total internal and external	398	Architect-Engineering	386
Control and instrumentation	139		
Control rods and drives	182	Grand Total	4,629
Boric acid system	58		
Fuel handling and storage equipment	68		
Feed-water system	147		
Water purification	60		
Steam system	134		
Miscellaneous equipment	146		
	1,953		

Several factors could reduce this power cost in the future. For one thing, EBWR could be run at a higher power level. If this were done, all costs per kilowatt hour (except fuel cost) would be reduced. Fuel costs were based on the 2,000-Mwd/t burnup which was calculated as the life of the original metal fuel core. If the burnup is increased to 10,000 Mwd/t and the electric power output to 10 Mw, the power cost should drop to about 23 mills/kwh. This figure of 23 mills/kwh is still large compared with the cost of power produced from fossil fuel in this country. A reactor of the same type, if built today, could do better.

The EBWR has to do two jobs. Firstly, it serves as an experimental facility as well as a producer of commercial electric power. This means that the EBWR capital investment cost includes money for experimental features that would not be present in a single-purpose power reactor. For instance, the experimental program calls for operating the reactor with a number of different core configurations. To allow for these changes, the designers had to provide extra accessories and a highly flexible core, both of which cost money.

Secondly, even as a power reactor, the EBWR is overpriced. The philosophy behind the original design was intentionally conservative. Experience has already shown that many things included in the system "to make sure" could be left out of the next design. For example, a forced-convection cooling system had been installed for the control rod thimbles. The operating temperatures of the thimbles without cooling are lower than expected so that the forced-convection system is not used.

Finally, and probably most importantly, the capacity of the EBWR as a power reactor is too small to give an optimum investment cost per kilowatt hour. A reactor in the 100-Mw class or larger could expect to realize a significant decrease in power cost over the EBWR.

SECTION III

EXPERIMENTAL AND SUPPORT STUDY FACILITIES AT ANL

C. Breden
L. Link
P. Lottes
C. Redman
E. Sowa

NOTES AND EDITED DATA FROM LECTURES - June 21, 1961

SECTION III

EXPERIMENTAL AND SUPPORT STUDY FACILITIES AT ANL

I. Technology Provenance*

A. Introduction

The experimental and developmental engineering work at Argonne has been quite varied in the 15 years of Argonne's existence. The early work with the critical facilities has evolved into two major engineering design programs for the Reactor Engineering Division at ANL. The one program, the boiling water reactor program, developed more quickly and has come to fruition much faster than the parallel developmental program in the sodium-cooled breeding-reactor program. Each of these major programs has offered challenges to the physicists and engineers. Through the close cooperation of personnel within the Reactor Engineering Division and between the various Laboratory Divisions, major advancements in theory and technology have been realized. However, on occasion, outside assistance has been solicited and formidable problems solved through the use of talent available outside of the Laboratory.

B. Project System

As each new project has been set up, man power has been assigned based on the anticipated requirements and specializations needed to pursue the proposed investigation to completion. In most cases this is accomplished by the selection of a relatively small group of qualified individuals who are charged with the responsibility of conducting initial investigations, making requests as to the nature and quantity of required experimental facilities, and obtaining services of other specialized groups at the Laboratory. They also make recommendations as to anticipated cost for the project and are responsible for making recommendations for the overall program following these initial investigations. As more individuals or services of the various departments are drawn into the project, the program is expanded to cope with the development work required. Recommendations for further expansion or requests for equipment involving large capital expenditures are made. The mandatory procedures for review of each request for action assures proper perspective and appropriate effort not only for the subproject, but for the total project as well.

Once the particular activity has developed into a large-scale project, a project manager is assigned and the project designated as a major budgetary item. All expenditures of man power, services, and equipment are budgeted and cost-accounted against the project. These projects, as well as all activities at the Laboratory, are budgeted on an annual basis starting with the first of July each year and are usually planned approximately six to nine months before the beginning of that budget year. Typical

* L. Link

examples of this type of evolvement of engineering effort are illustrated in the EBR-I and EBR-II projects, the BORAX and EBWR series of experiments and projects, and the S1W submarine reactor development activities.

As various aspects of the research and development program of the Reactor Engineering Division have been completed, the equipment has been dismantled. To date, much of the original equipment used in the development of boiling nuclear systems, heat transfer, corrosion, hydraulics, mechanisms development, and materials compatability investigations, has been dismantled or shut down and rendered inoperative prior to transfer to storage, or has been declared as surplus and is awaiting transfer to other institutions. The boiling water out-of-pile equipment in Building 11, which has been made available to the Universities, is a case in point.

II. The Role of Critical Facilities*,**

A. Introduction

Today's nuclear technology depends on critical facilities for information in four important areas: reactor design, weapons-systems design, criticality limits on processing operations, and basic physics data.

The largest number of critical facilities in the U. S. are devoted to reactor design. In these, the experimenter seeks to achieve a delicate balance between neutron production and loss over the full range of reactor operating conditions.

A complete knowledge of all the pertinent neutron cross sections and yield as a function of energy would enable the reactor designer to calculate the neutron distribution in space and energy - thereby specifying the reactor configuration in detail. In practice, the large gaps in our knowledge of the nuclear interaction parameters and the limited accuracy of much of the existing data, makes the use of refined theories and improved calculational techniques of questionable value in reactor design.

For example, theoretical calculations predicted a reference design loading for EBWR of 42 fuel assemblies with a probable error of 3% in k. As such calculations go, this one would appear reasonably accurate. However, in terms of fuel loading +3% corresponds to almost a factor of two in fuel load - some 40 extra fuel assemblies. In EBWR the observed loading fell just within the probable error, requiring a total of 81 assemblies. A much more accurate estimate for the loading could have been given by a critical experiment. In fact, this is what the first EBWR runs were supposed to do.

---

* W. C. Redman

** Reprinted from W. C. Redman, Nucleonics, 16 (12), 40-41, McGraw-Hill Publishing Co., Inc., Copyright 1958.

A critical experiment can be compared with a computer in which a Monte Carlo-type of calculation is performed. The appropriate neutron cross sections are inherent in the system being studied. The life histories of a tremendous quantity of neutrons are "calculated" simultaneously. Thus, critical experiments afford a means of obtaining required answers without a knowledge of the neutron cross sections. Analysis of the results of critical experiments enables the reactor theorist to arrive at better parameter values for use in reactor design calculations.

B. Experimental Objectives

Critical experiments serve primarily to yield information on the nuclear performance of the heart of the reactor system - namely, the reactor core and reflector.

Working within the limits set by heat transfer, metallurgical, and nuclear considerations, the critical experimenter seeks an optimum design. Variables typically at his disposal include quantity and enrichment of fuel, amount of moderator, dimensions of the reactor, lattice spacing of fuel channels, arrangement of fuel in the channel, area of coolant channel around fuel, physical properties and pressure of coolant, and parasitic absorber present as cladding and structure.

Changes in design that improve heat transfer, such as decrease in coolant channel flow length, increase in size of channel, flux flattening, decrease in moderator fuel ratio, and subdivision of the fuel for increased heat transfer surface usually affect the neutron economy adversely. Consequently, a combination of heat transfer and critical experiments is desirable to achieve a reliable core design.

C. Typical Program

The duration of the critical experiments depends upon several factors including the novelty of the reactor design, the importance of reliability in operation, the amount of pertinent data otherwise accumulated prior to startup, and pressure to achieve early operation of the reactor.

1. Exponential Experiments

If time permits and if materials that make possible a reasonable simulation of the proposed design are available, a series of exponential experiments may first be initiated to explore nuclear characteristics of assemblies having a range of values for lattice spacing, clustering, fuel concentration, enrichment, etc. Exponential experiments involve a thermal-neutron source plus an assembly containing only a fraction of the material required for a critical assembly with its self-sustaining chain reaction. Generally, an exponential program includes only a measurement of

buckling of a particular system. The availability of a high-intensity neutron source, such as a thermal column of a power reactor, makes possible the measurement of lattice parameters and neutron spectra. The main advantage of an exponential assembly is that the system is operated well below criticality and consequently requires no elaborate instrumentation, control, and shielding systems. The disadvantage is that the accuracy of information observed is limited. Results of measurements of nonuniform systems require extensive analysis and involve uncertainties in interpretation.

2. Critical Experiments

Once a tentative configuration and size for the core have been chosen, either by calculation or by exponential experiments, detailed knowledge of the nuclear characteristics of the proposed design is determined through a series of critical experiments.

The initial phase of a typical program will include:

a) determining the cold, clean critical mass by step-wise addition of the selected materials;

b) determining reflector savings from measurements of radial and axial flux distributions;

c) evaluating the factors comprising k_∞ from observed fission, capture, and flux patterns, in a representative lattice cell; and

d) measuring the migration area by adding distributed nuclear poisons or making dimensional changes in the core.

The program might then turn to an investigation of reactivity coefficients. Experimental evaluation of the temperature effects on reactivity generally involves a combination of actual heating of the entire assembly over a limited range and heating of a sample of fuel to an appreciably higher temperature. Some indirect effects, such as density changes, can be simulated by substitution of materials. For example, Styrofoam or organic materials can be used to mock up the reduced density of water at high temperature. The magnitude of other reactivity effects occurring during operation of a power reactor, such as fuel burnup, fission-product production, and formation of various plutonium isotopes, is normally calculated.

Next, the critical experimenter's attention may turn to evaluating control rod effectiveness. The cold, clean critical is loaded with rods of the proper composition, number, size, shape, and location to give the required reactivity margin. The rods are generally added individually or in symmetric groups and the system restored to criticality after each addition.

The selection of rods is also influenced by considerations of heat removal, so that the determination of power-production patterns is an important part of this stage of the program.

3. Zero-power Experiments

The measurement of detailed flux-distribution patterns for various rod configurations expected throughout the core life is carried out in the zero-power system. Since zero-power experiments may use assemblies of the actual fuel elements and control rods or perhaps the actual core itself, they are well suited for locating possible hot spots. Distributed neutron absorbers are introduced to permit the various rod positions anticipated in actual power operation. Differential calibration curves for the rods are obtained during the course of the flux-mapping program. Flux flattening by nonuniform distribution of fuel can also be investigated at this time.

Other important information that can be obtained from critical assembly measurements includes:

a) the interrelation between the location and strength of the startup source, and the location and sensitivity of the instruments for control;

b) measurement of neutron- and gamma-radiation intensities to determine the effectiveness and heating of the shield; and

c) neutron economy (conversion or breeding ratio).

The extensive manipulation of the components in a critical assembly requires that the induced activity be kept low. The materials and design generally preclude operation at very high temperatures. Consequently, critical experiments are not used for investigation of effects requiring high neutron fluxes and/or high temperatures. Thus, a program of critical experiments gives no information on heat transfer, radiation damage, or kinetic behavior at high-power density.

Since 1949, the zero-power reactors indicated in Table III-1 have been constructed by ANL.

Table III-1

ANL ZERO-POWER REACTORS

Name	Motivation
ZPR-I	Submarine Thermal Reactor Program
ZPR-II	Savannah River Reactor Design Studies
ZPR-III	Fast Reactor Program
ZPR-IV	Fast Exponential Studies
ZPR-IV'	Thermal Neutron Source Reactor
ZPR-V	Internal Fast Exponential
ZPR-VI	Fast Reactor Program
ZPR-VII	Water Reactor System Studies, including EBWR
ZPR-VIII	Fast Neutron Source Reactor
ZPR-IX	Coupled Reactor System (future)

III. Water Reactor Program Support Study Facilities*

A. Introduction

The active developmental activities with regard to boiling heat transfer hydraulics, water chemistry, corrosion, and fuel fabrication has centered mostly around out-of-pile test facilities. As these various activities have progressed into more refined technology, the bulk of the work has shifted from the out-of-pile facilities to in-pile experiments in the EBWR.

At the time the idea of the EBWR was conceived, it was recognized that, since the EBWR was the first of the prototype boiling water reactor power plants, a considerable amount of data would have be be obtained experimentally before a reasonable design could be ascertained. It was recognized that considerable information had been obtained in the BORAX-I and BORAX-II experiments. Technology and data on heat transfer, hydraulics, and high-temperature corrosion-resistant materials having low cross sections was almost nonexistent. In the course of the design of the EBWR, it was recognized that the time factor would prohibit extensive experimental activity prior to the finalizing of the design of the EBWR. It was believed that with conservative design the EBWR could be constructed and out-of-pile tests used to establish parameters of operation of the EBWR, with subsequent experimental work corroborating the information gained in the course of initial operation of the EBWR. This initial approach to the problem proved to be realistic.

B. Heat Transfer and Hydraulics

The development of applied technology in the field of heat transfer and hydraulics played an important part in the development of boiling water reactor technology. Although a great deal has been learned in the past six years, it is believed that there is still a great deal that is not thoroughly understood and that more work should be conducted.

In the original investigations, mockup designs were studied to determine dynamic behavior. Once sufficient data had been collected, new formulas were derived to permit prediction of dynamic behavior of the given design, but under different conditions. When this prediction had been verified, the formulas were applied to general theory and ultimately developed for accurate prediction of boiling heat transfer and hydraulics application to various designs and operating conditions. A review of the sequence of events in the investigations in this area will probably give the best illumination as to how this was accomplished. Details of the actual work will be presented during later sessions.

Chronologically, then, the heat transfer and hydraulics development activities progressed as follows. BORAX-I was primarily a physics

---

* P. Lottes and C. Breden

experiment in which the stability of boiling had to be demonstrated as to its mechanical and nuclear aspects. Once the inherent shutdown mechanism of boiling on the fission process had been demonstrated and the principles judged sound, the development of a new species of power reactor began. The BORAX-I reactor was operated at different power levels and at varying pressures up to 130 psi for short periods of time. The ability of the boiling reactor to cope with externally applied conditions, such as the quick closing and opening of the steam line, fairly rapid change in power level by control rods, sustained operation at relatively high-power densities, and behavior of the nuclear pile under varying feedwater inlet temperatures and mixing, made it quite apparent that further investigation at higher pressures would have to be conducted. Consequently, the BORAX-II reactor came into being and plans were underway for the higher-pressure (300-psi) facility before the BORAX-I final destructive experiment was conducted.

With the decision to construct a second boiling water reactor facility came the decision also to conduct basic investigations into the problem of boiling heat transfer. Similar action was taken in other fields, and the necessary investigations into corrosion, water, chemistry, fuel-fabrication techniques, high-integrity piping, equipment construction, and other associated techniques were also begun. These areas had to be developed and understood before the physicists and engineers could be satisfied that boiling water reactor was a sound engineering device. BORAX-II was operated from October 1954 to March 1955. BORAX-III, based on the very fine results of the BORAX-II experiment, was initiated. The BORAX-III reactor merely added a 3.5-Mwe turbine-generator system that permitted a more thorough investigation of the boiling water reactor as a power-generating device.

At about this same time, the Reactor Engineering Division had embarked on their boiling heat transfer studies and were conducting investigations up to 600 psi on multiplate heat transfer surfaces. Much of this work was conducted in line with the design activities on the EBWR which was begun in 1954.

It had been decided by both the physicists and the Metallurgy Division that the uranium-metal, zirconium-clad fuel plate was to be the type of fuel used in the EBWR. Work had to be conducted by the Metallurgy Division to develop materials and fabrication techniques for the proposed fuel. Time was a great factor, and it soon became apparent that the manufacture and delivery of the necessary heat engineering equipment would involve almost as much time as that needed for the development and manufacture of the actual core components.

The fuel for the EBWR was manufactured during the same time that the 600-psi boiling density studies were being conducted. These out-of-pile tests on an electrically heated multiplate mockup provided basic information to determine the two-phase pressure drop and the ultimate power densities available on this multiplate heat transfer geometry. Subsequent

work on steam volume fraction and vapor-to-liquid slip ratios for the steam-water mixtures (from 150 to 600 psi for natural circulation) enabled the engineers to anticipate the behavior of the EBWR and to attempt to correlate the information gained from the 300-psi BORAX experiments to what might be expected in the 600-psi EBWR. Some six to ten months before the EBWR was actually put into operation, the analytical method for predicting the steady-state performance of natural-circulation reactors was developed. Needless to say, the various experimenters, though quite sure about their data, were apprehensive as to the ultimate substantiation of the predicted behavior of the EBWR based on the out-of-pile Laboratory information.

By the time the EBWR was in operation in December of 1956, a great deal of information had been learned from the natural-circulation boiling tests. Since the EBWR was also to be used for forced circulation in later modifications, forced-circulation tests up to 600 psi were begun.

It was also decided that a high-pressure facility should be designed to provide for the study of full-sized reactor channels in order to investigate burnout and high-power density operation up to 2000 psi for natural and forced circulation.

By mid-1957, the outstanding performance of the EBWR substantiated the predicted performance of the EBWR with minor modifications. With this comforting reassurance behind them, the heat engineering section embarked on further investigations to enhance the natural-circulation operation of EBWR. By the beginning of 1958, it was quite apparent that the tests conducted in the 600-psi facility and the 2000-psi facility verified the theory that with proper design of chimneys, downcomers, and steam-separation devices, very high power densities could be obtained with natural circulation - yet provide the desired margin of stability (both nuclear and thermal). It became evident that the forced-circulation pumps originally planned for the future modification of EBWR were not capable of producing as high a coolant flow rate in the core as that possible with an optimized design of natural-circulation reactor internal structures. Consequently, the decision was made to drop the forced-circulation experiment and concentrate on natural circulation.

At about this same time, thought was being given to the program required for the ARBOR project (i.e., 200-Mwt, 2000-psi reactor facility proposed for construction at the Idaho test site) being designed to investigate and determine the best operating characteristics for large boiling water reactor systems.

A nuclear superheat concept was being considered for investigation: first, as a loop to be inserted in the EBWR and, second, as a separate nuclear, steam-cooled, reactor facility to be constructed adjacent to the EBWR facility, or a proposed BORAX-V coupled boiling superheated steam reactor complex to be constructed at the Idaho site.

In June of 1959, the BORAX-V reactor had been designated as an active project, and the ARBOR and the superheated steam experiment for EBWR had been set aside. The heat transfer and hydraulics investigations were intensified to gather the much-needed information which had been only briefly investigated in the parametric studies of the previous years. Investigations of maximum heat transfer rate on curved heat transfer surfaces were conducted at pressures up to 2000 psi. Work on film boiling and critical heat flux at the critical pressures (3206 psia) were considered and later subcontracted to the University of Purdue. Extensive data were obtained on circular heat transfer surfaces for steam volume fraction and slip ratios over a pressure range from 600 to 2000 psi in order to better understand the factors leading up to boiling instability, chugging, and the safe prediction of same. Several types of steam risers were used in the small-scale investigations to determine again the parameters for unstable operation for high boiling densities. During this same time, in-pile heat transfer hydraulics measuring devices, procedures, and methods were developed in the anticipation of more thorough investigation of the in-pile behavior of the EBWR fuel.

By 1959, the favorable operation of the EBWR up to 60 Mwt and the satisfactory operation of the out-of-pile loops had all demonstrated that the predicted safe operation of EBWR had been entirely accurate. Attention was then turned to the acquisition of new information for use in the solution of other problems. These constituted a formidable set of reactor problems which had to be investigated before all facets of heat transfer and hydraulics could be considered as being thoroughly understood. Work was then begun on the problem of steam-water separation, hydrodynamic instability at the very high power densities, burnout, extension of two-phase flow technology to the medium high-pressure ranges, heat transfer in the very high-pressure ranges (subcritical through the supercritical ranges), and also investigations of superheated steam heat transfer.

From this it can be seen that the heat engineering activities, which started out as a relatively small man-power activity, have developed into a major investigation. Other laboratories are also conducting investigations. As each new piece of information is learned in the EBWR, in the ANL heat engineering laboratory, or in the laboratories outside of Argonne, the data are compiled, and an ever-expanding technology of the heat transfer and hydraulics of boiling water reactors is emerging.

Most of the ANL boiling water heat transfer and hydraulics work is pretty well summed up in four documents. The early work on heat transfer and hydraulics conducted back in 1955, 1956, and 1957 at pressures around 300, 600, and 2000 psi are reported in ANL-5522, ANL-5735, and ANL-6063. The 1959 and 1960 out-of-pile investigations on superheated steam and saturated steam heat transfer are covered in ANL-6213.

The superheated steam work was terminated after the necessary verification of data about steam heat transfer had been completed. This work provided the necessary backup information for the BORAX-V reactor, which is due to go critical this year.

Each of the investigations has been terminated. The equipment has either been disassembled or set aside as surplus and offered to the universities to conduct work in the areas where ANL has chosen not to investigate. The man power of the heat engineering section has thus been released to work in boiling sodium heat transfer work and other programs of a more advanced nature.

Confirmation and investigation-type studies will continue with the EBWR to permit further optimization of the EBWR core, especially for the 100-Mw core loading. This work will culminate the out-of-pile and in-pile investigations of the last 5 years, and will utilize the techniques, instrumentation, and principles developed over the course of the boiling water reactor development program at Argonne.

C. Fuel-corrosion Studies

1. In-reactor Corrosion of Prototype Fuel Samples

Development of fuel elements for water-cooled power reactors requires information on the corrosion behavior of the fuel and its cladding under reactor operating conditions. The final proof is the behavior of the full-sized core in the reactor at power. Before the final selection of material and design can be made, a great many tests have to be conducted in order to evaluate the effects of possible variables and to screen out unpromising materials. A large amount of information has been obtained about the corrosion behavior of fuel and cladding materials in out-of-pile static autoclaves and flowing-water loops. Some out-of-pile corrosion testing has been done with fuel materials that have been previously irradiated. What was needed was a facility where corrosion behavior could be studied during irradiation, preferably with boiling occurring on the sample. The ANL-2 loop in the MTR in-pile loop was available. The operating policy on that loop, at the time, was to keep it as free from fission products as possible. Only prototype elements, with defect-free cladding as shown by preliminary autoclave testing, were exposed in this loop. The type of irradiation facility required was one in which screening tests could be made with unclad fuel materials as well as with elements with deliberately added cladding defects. Another factor of importance was that a reactor was available at the Laboratory. The physical dimensions of the test facilities of this reactor, CP-5, dictated the limiting factors in the design of this facility.

The selected solution to this problem was a small pressurized in-pile autoclave to hold a small specimen, preferably a pin or rod, about $\frac{1}{8}$ in. in diameter and 1 in. long, containing fuel enriched with U^{235} to achieve

increased rate of burnup. At a thermal neutron flux of about 1 x 10^{13} nvt, available in the reactor, a burnup rate of about 0.2% total core atoms in 1000 hr was expected, along with surface heat fluxes of 200,000 Btu/ft^2-hr. The burnup rate could be increased by higher neutron fluxes, but not by enrichment. Self-shielding affects the flux distribution within samples of this thickness if enrichment is greater than 20%. The use of a small sample would reduce total heat generation and would also reduce the amount of radioactive material to be dealt with during sample removal and examination.

The location of the autoclave in CP-5 was in an air-cooled thimble in the region just outside the fuel elements, where the highest neutron flux existed.

The autoclave is designed on the basis of local boiling at the surface of the pin sample. Ultimate heat removal is by the CP-5 thimble cooling air from the surface of the autoclave. Temperature gradients due to local boiling are relatively independent of heat flux over wide ranges. The temperature of the sample, and hence the temperature of the boiling process, can be accurately controlled by regulation of external helium pressure to the surge tank.

The water level extends half way into the surge tank. During normal operation the water in the surge tank and connecting tube remains relatively cold. The liquid level in the surge tank is measured by two heated thermocouple probes, which give different readings due to the higher conductivity of water as compared with gas.

Pressure was maintained at 690 psig and the temperature at about 550° F. Excessive temperature and high or low pressure results in reactor scrams. A rupture disc was provided as a backup safety device in event of excessively high pressure (possibly due to water dissociation gases in the presence of a disintegrated high uranium sample, or production of hydrogen gas by sample corrosion, or a combination of both).

Problems of autoclave fabrication, removal and sample examination encountered in this first model led to development of a second model. In addition to other modifications, it has increased heat-removal capacity to take three specimens instead of one.

2. Irradiation of Samples for Out-of-pile Corrosion Studies

Occasionally, it is desired to conduct out-of-pile corrosion studies with fuel elements. These studies may be directed at determining the effect of burnup and the presence of fission products on the corrosion behavior of the element, or it may be desired to use tracer techniques to follow the course of corrosion and deposition of corrosion products in circulating coolant systems. In the first case, the element must be irradiated

in the same manner as a fuel irradiation prototype to achieve the desired level of burnup. The element is removed from the facility, its activity permitted to decay for a period of time, and then placed into the equipment for corrosion study. For the radiotracer studies, a much simpler approach is possible. The element can simply be prepared by packaging in an aluminum protective container. In this way it can be placed in a low-flux region of the reactor and irradiated for a period of time sufficient to activate the element, which can now be used for the purpose of corrosion studies. In this way, the progress of corrosion or deposition can be followed in opaque systems such as liquid metal corrosion loops.

3. Fuel-failure Detection in Water Systems

A considerable amount of interest was generated some time ago and directed toward the detection of fuel-element failures in water-cooled reactors. For the purpose of studying the problems involved, a water loop was constructed. It is recognized that when a fuel element containing metallic fuel fails and the fuel comes in contact with high-temperature water, the corrosion products consist of finely divided particulate uranium oxide and hydride. A significant portion of the fission products are released to the water.

In the loop, water was circulated rapidly into the test section of the reactor, and finely divided UO_2 was inserted into the system at the test section. The water was continuously recirculated and monitored for the presence of fission product activity present either in the water, in the solution, or carried along with the finely divided uranium particles carried by the water. The decay coils (see Fig. III-1) provided a delay time for the decay of a large portion of the water activity before the gamma probe was reached. The instrumentation for this loop consisted primarily of (1) a rotameter for flow rate measurement, (2) a conductivity meter for water quality, (3) the gamma probe, and (4) pH meters (see Fig. III-1).

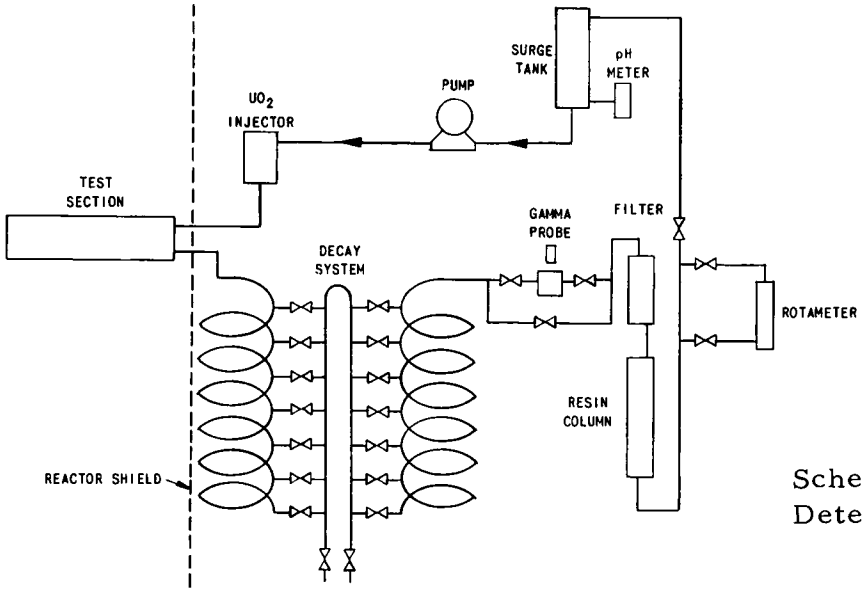

Fig. III-1

Schematic of Failed Fuel Detection Experiment

112-1010

IV. Fast Reactor Program Support Study Facilities*

A. Introduction

Much of the more recent experimental effort in the Reactor Engineering Division has been oriented toward the EBR-II project and specifically toward the problems of sodium technology. The problem of handling large quantities of sodium is a formidable one. For example, evaluations of gears, bearings, and bellows suitable for use in sodium are presented in ANL-5657. One factor which enters into the design of a containment vessel for EBR-II is the magnitude of the pressure buildup within the vessel due to a reaction between sodium and air in the remote event that a nuclear incident should result in ejection of primary tank sodium into the containment vessel. Experiments directed toward determination of such pressure transients are reported in ANL-5657. It was there reported that varying quantities of sodium at 750° F were expelled from a reservoir into a reaction vessel by detonation of a hydrogen-oxygen gas mixture. Boiler, pump, and valve designs have been examined, sodium vapor pressures at high temperatures (1300° C) and the oxygen content in the circulating moderator are being studied. However, for the purpose of this review, only the current in-pile investigations will be described.

B. Fuel-irradiation Experiments

1. MTR-ETR Capsule Fuel Irradiation

Specimens of cylindrical fuel elements of the EBR-II Mark I variety were irradiated in the MTR and ETR by taking advantage of the construction of the in-reactor test sites. Under these conditions, the cooling-water channel was utilized as part of the test loop.

The irradiation-test capsule was simply comprised of a fuel element surrounded by nickel-cobalt wire foil, installed within and sodium bonded to a Type 347 stainless steel tube (23.625 in. long, 0.500-in. OD, 0.085-in. wall thickness) with welded end plug closures. The sodium bond extended 1.6 in. above the top of the fuel element. The height of the sodium level provided sufficient space for expansion at temperature.

The capsule was positioned vertically in the reactor test facility at a position where the neutron flux was predetermined as sufficient to generate the desired heat flux and to establish the temperature in the fuel specimen. The heat was removed by flow of the reactor cooling water along the outer surface of the capsule in the annulus formed between the capsule and the inner wall of the facility tube. The nickel-cobalt wires were used to determine the total integrated flux sustained by the element. The flux pattern was used in conjunction with the fuel enrichment to calculate the average operating temperature. The construction of the reactor test facility precluded

---

* E. Sowa

the installation of thermocouples to monitor the fuel-element temperature during irradiation. Calculations were used to determine this parameter.

2. CP-5 Gas-cooled Loop for EBR-II Fuel Irradiation

This facility was installed in one of the central aluminum thimbles in CP-5. The thimble was modified to provide for the passage of air down through the inner aluminum tube assembly, around the test section, up through the annulus between the aluminum tube and the thimble walls, and out to the existing reactor air-filter-and-exhaust system. A suction pressure of 355 mm of mercury was maintained across the system by a Roots-Connersville blower to produce the air flow required to cool a fuel element generating approximately 5 kw of heat. Figure III-2 shows a cross section of the facility.

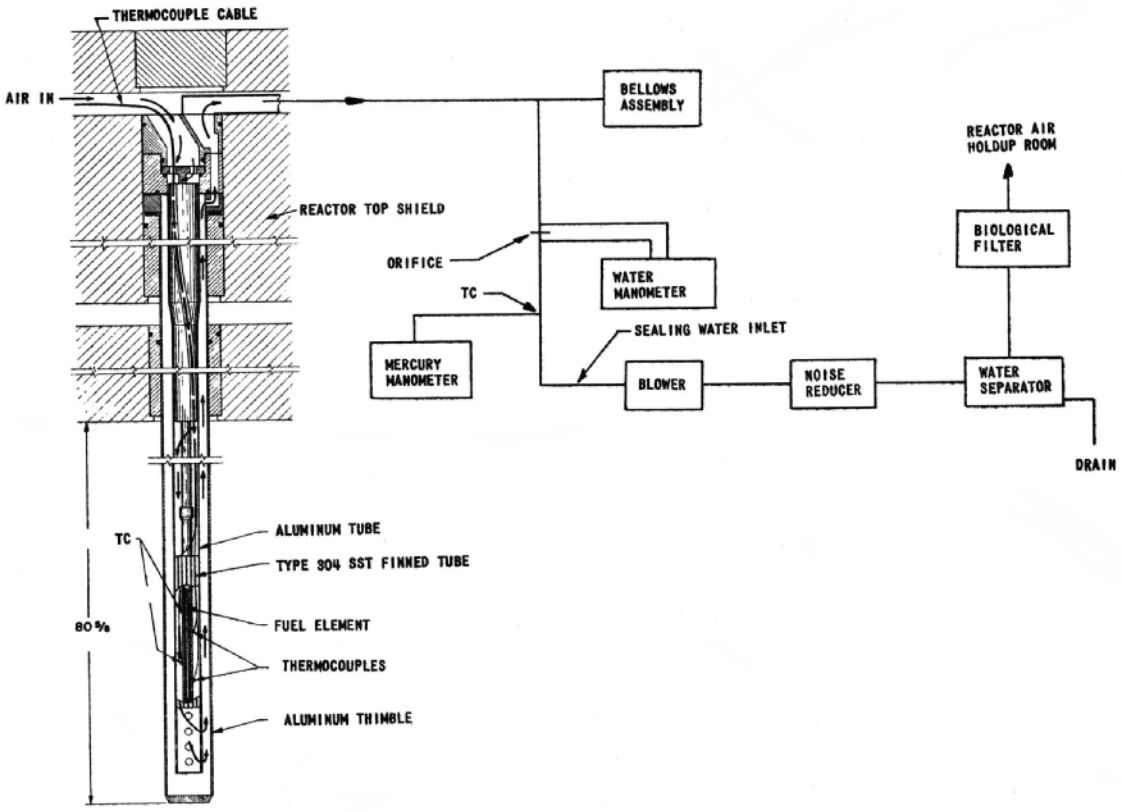

Fig. III-2

Air-cooled Facility for CP-5 Irradiation of Prototype EBR-II Fuel Elements.
112-882

The test section, as shown in Fig. III-3, was comprised of a fuel element encapsulated within and sodium bonded to a Type 304 stainless steel finned tube. The temperature gradient along the fuel element was monitored by thermocouples which were spot welded at the fin root and

distributed over eight positions along the length of the fuel element. The temperatures were recorded on the continuous strip chart of a multipoint recorder.

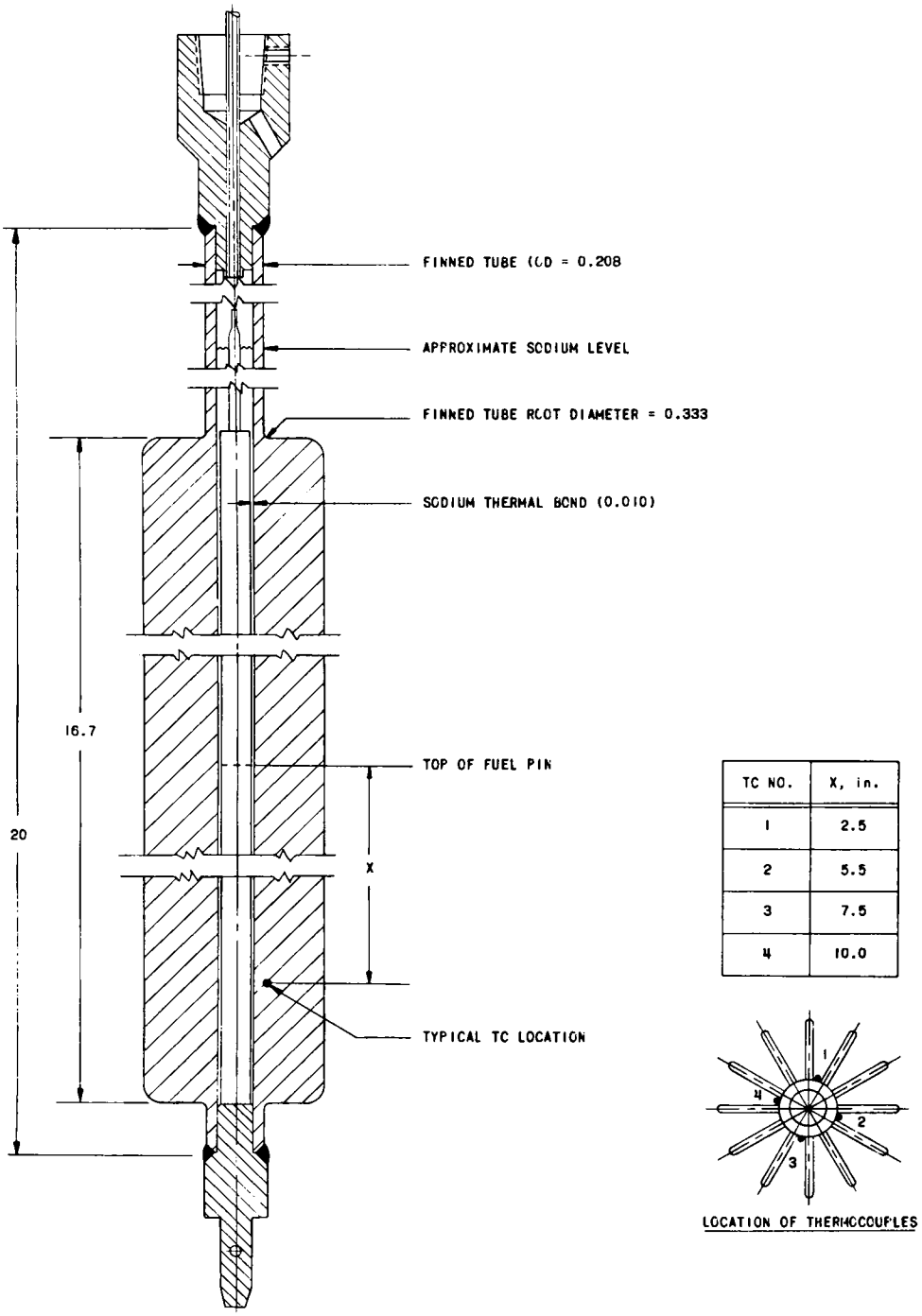

Fig. III-3

CP-5 Irradiation Test Assembly of EBR-II Pin-type Fuel Element within Finned Tube. (dimensions in in.)

112-881

In addition to the measurement of the fin-root temperatures, other parameters were also measured. These parameters consisted of test section inlet and outlet air temperature, air mass flow, and pressure differential across the system. In this manner the power generation of the fuel element was determined. The data collected were used to determine the operating central metal temperature of the fuel element and the accumulated burnup of fissionable material. For each fuel element irradiated, the only expendable items used in the facility consisted of the finned capsule and the aluminum hanger tube. When the element reached the desired burnup, the facility was unloaded by drawing the shielding plug with its attached tube and capsule vertically into a shielded cask. The aluminum tube was severed in two, and the cask containing the finned capsule and element was transported to the cave area where post-irradiation examinations were conducted.

3. CP-5 Pressurized Water Facility for EBR-II and Fermi Fuel Irradiation

One difficulty which affected the operation of the air-cooled facility was the appearance of argon-41 activity in the effluent air when this coolant was drawn through the test section. This activity was the result of argon-40 interaction with the neutron flux in the core and had to be discharged via the stack in the reactor building. Since the discharge rate to the stack was in the vicinity of 2 m^3/min, the output of activity from three such facilities (operating simultaneously in the reactor) soon became excessive. As a result, a new facility was designed as a substitute for the air-cooled unit. This facility utilized pressurized water as the medium for heat removal from the fuel element. This facility was initially designed for the irradiation of the EBR-II fuel element; a later modification was adapted for the irradiation of the Fermi-plant fuel elements.

Two types of possibilities were designed for operation in CP-5. One unit was to operate in the experimental thimble (see Fig. III-4), whereas the other was designed for installation within the center cavity of the tubular reactor fuel element, as shown in Fig. III-5. In these facilities, the encapsulated fuel element is bonded to the interior wall of the capsule. This capsule is suspended vertically by a stainless steel tube within a pressure vessel partially filled with heavy water. The capsule, in position, is immersed a considerable distance below the surface of the water. The tube containing the fuel element is fitted with four longitudinal fins running the entire length opposite the fuel-containing portion, as shown in Fig. III-6. These fins, in turn, are welded to cylindrical segments which are so arranged as to form a cylindrical vessel when appropriate end caps are fastened to the vessel. The intervening space between the finned tube and vessel wall is gas filled and thus presents a relatively high-resistance path for heat conduction. The path for heat flow is from the fuel element, through the radial fins, and to the outer surface of the cylindrical vessel. The vessel is immersed in the heavy water in the pressure vessel. Local boiling is

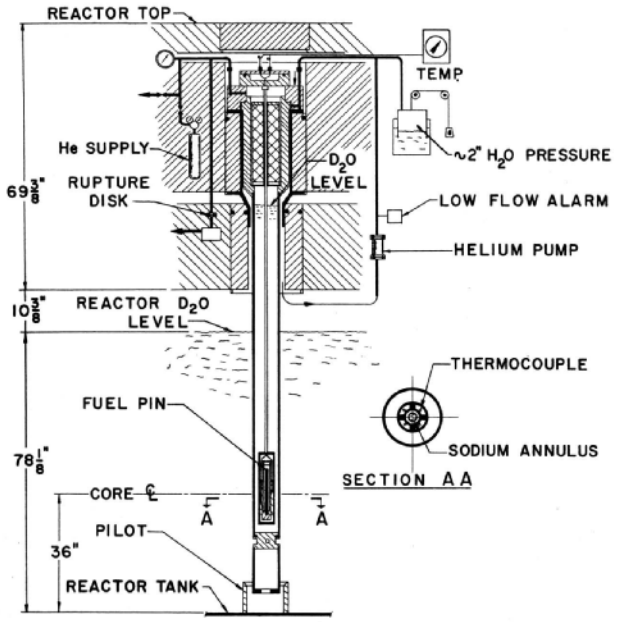

Fig. III-4

Fuel-irradiation Facility for EBR-II (Thimble Installation)
111-5790

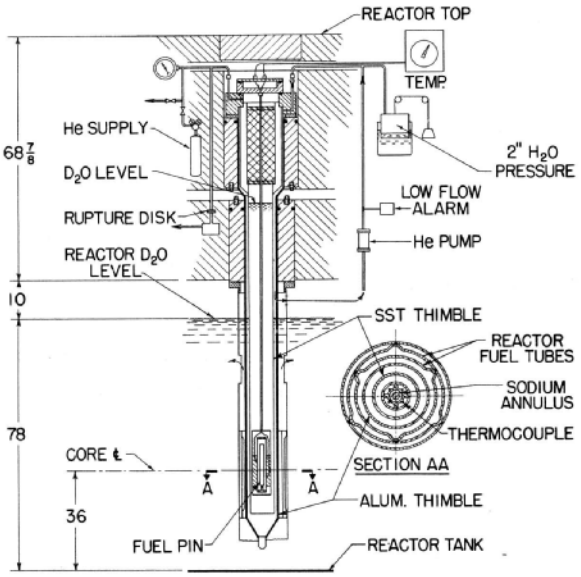

Fig. III-5

Fuel-irradiation Facility for EBR-II (Fuel-element Installation) (dimensions in in.)
111-5789

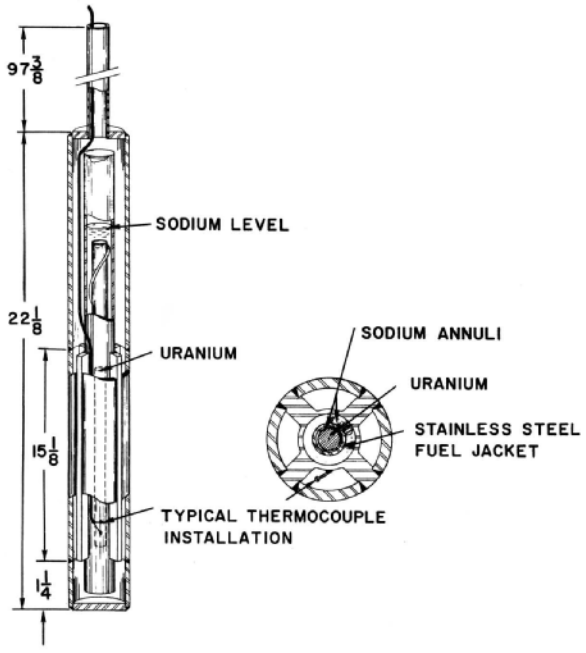

Fig. III-6

Fuel Capsule (dimensions in in.)
111-5793

thus initiated at the outer periphery of the cylindrical vessel. The degree of local boiling (hence, the fuel temperature) is controlled within limits by pressurizing the heavy water in the pressure vessel. The reactor heavy water moderator, in which the pressure vessel is suspended, provides the final heat sink for the heat generated by the fuel element during irradiation. The pressure vessel is a stainless steel tube (1.25 in. or 1.5 in. in OD; 0.060-in. wall) welded to a modified thimble shielding plug and designed for 1100 psia at 318°C (600°F). The operating pressure ranges from 150 psig to 810 psig, permitting a variation of central metal temperature over a range of 60°C (140°F). A rupture disk set at approximately

300 psi below the design pressure of the vessel isolates the interior from a shielded container, which serves as a reservoir for the containment of the condensate in the event of excessive pressure generated in the facility with consequent rupture of the disk. The pressure vessel is pressurized with helium from a helium-supply bottle situated along the outer face of the reactor. The facility can operate with the fuel element generating 10 kw of heat energy at a central metal temperature of 650° C (1200° F). In the experimental thimble facility, the final transfer of heat is made to the pool of reactor water surrounding the pressure vessel. The facility located in the fuel element has its heat removed by the flowing coolant supplied to the element. The design of the in-element facility greatly increased the available number of irradiation locations in the reactor.

The fuel specimen is unloaded very simply by opening the upper flanged connection and removing the fittings, flange, and shield plug. A cable connected to the exposed tube is wound about a drum located in a special cask. When the drum is rotated, the cable is followed by a wrapping of the stainless steel hanger tube about the drum, resulting in positioning of the fuel element vessel in the cask. Following this, the lower door to the cask is closed and the entire assemblage shipped to the caves for examination. Figure III-7 shows the details of the transfer coffin.

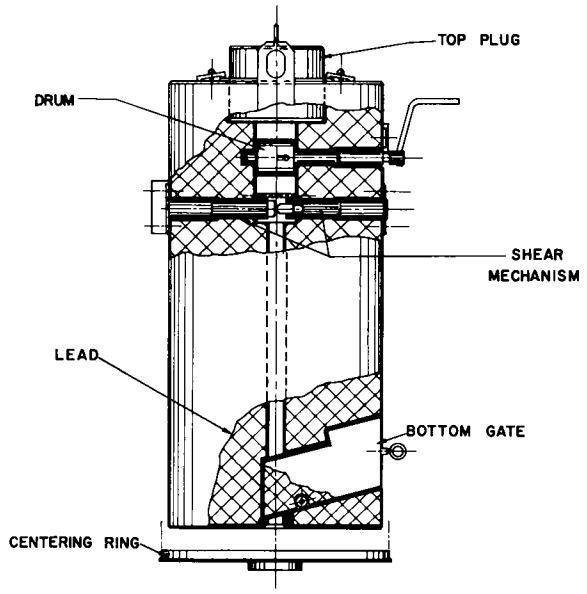

Fig. III-7

Removal Coffin
111-5792

Instrumentation consists simply of a circular chart pressure recorder and a multipoint temperature recorder.

The finned tubes, calibrated before assembly by the condensing-steam technique, have shown extremely good agreement with analog calculations; consequently, the power generated by the fuel element is accurately known. The approximate operating temperature of the element is set by sizing the thickness of the fins before assembly of the unit. Fine adjustment can then be made by setting the operating pressure of the facility.

4. Fast Reactor Fuel-element-failure Studies in TREAT

TREAT is a low-power, pulsed test reactor located at the Argonne National Laboratory, Idaho Division. Slightly over a year ago a

program was initiated for experiments to be conducted in this reactor and directed toward the study of meltdown failure of reactor fuel elements. The experiments involved the rapid destruction of fuel elements under rapid transient conditions, with and without coolant present. The series of experiments required the development of special equipment for their execution.

A dry, opaque, meltdown capsule was used for the failure studies of single uncooled elements. The sample fuel element is contained in a graphite crucible which serves to protect the stainless steel capsule wall from molten meltdown product and provides a heat sink for the freezing of such products. The stainless steel capsule encloses the entire assemblage and is suspended in the experimental TREAT fuel element by means of a long steel hanger tube. Thermocouple and pressure-transducer leads leave the capsule via the hanger tube and connect to external circuitry through a sealed electrical plug located at the top of the hanger tube. Figure III-8 shows details of the original design.

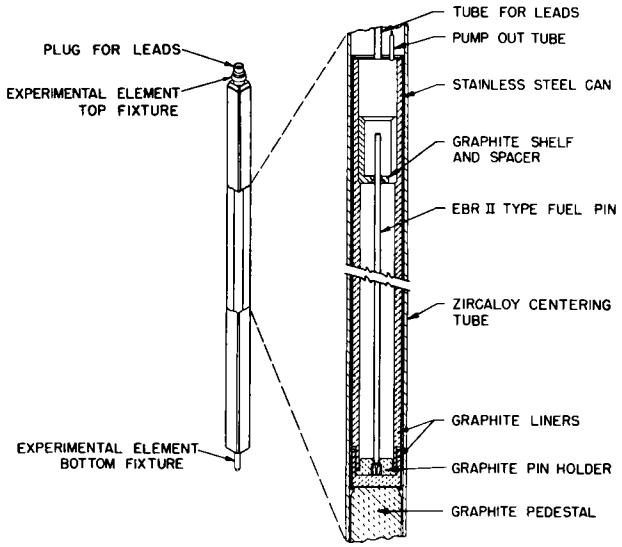

Fig. III-8

Dry, Opaque, Single-element Capsule
111-9567

In a modification of the dry opaque capsule, the meltdown element as shown in Fig. III-9 is held in a stagnant sodium bath. This element is contained in an inner sealed tubular chamber. The chamber, in turn, is surrounded by graphite in a region which also incorporates a pair of tubular electric heaters. The heaters permit raising of the capsule to a pre-determined temperature before initiation of the transient. The entire assembly is contained in a secondary stainless steel capsule which serves to contain and isolate the system. A high-pressure fitting and backup device is used to seal and isolate the interior of the chamber from the external capsule in the event of failure of the pressure transducer during the experiment.

A flowing sodium system of the type shown in Fig. III-10 was considered next. This packaged sodium loop fits inside an experimental TREAT fuel element. This loop was used for the meltdown of single elements, both irradiated and nonirradiated, under flowing sodium. The fuel element is inserted into the loop in a fitting which is attached to the

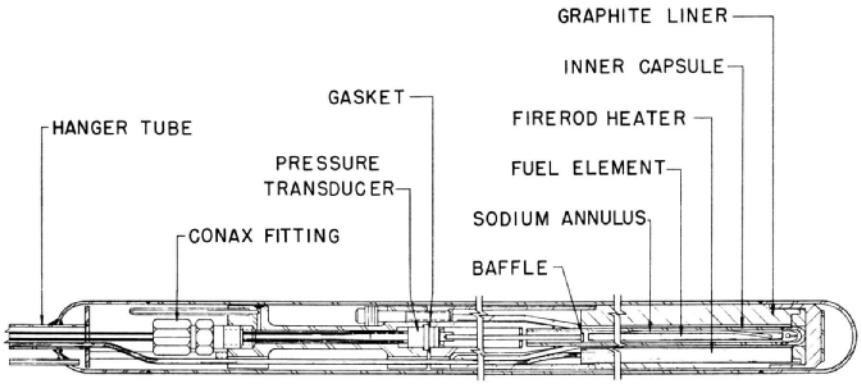

Fig. III-9

Single-element Stagnant Sodium Capsule
112-64

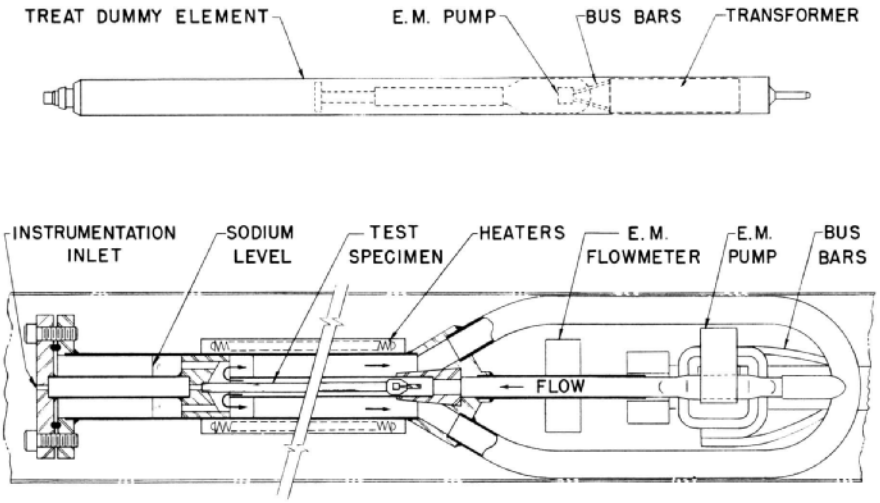

Fig. III-10

TREAT Single-element Package Sodium Loop
112-65

upper flange. The lower end of this fitting plugs into a vent in the mid-section of the loop to form a continuous channel for sodium flow. An electro-magnetic pump drives the sodium upward over the fuel element. Then it enters the upper chamber where the flow direction is reversed to move downward to re-enter the pump. A special transformer situated below the loop supplies low voltage and high current to the pump via bus bars. The electrical leads for heater supply and sensing elements, such as thermo-couples, pressure transducers, and flowmeters, are led from the chamber through a multiconnection plug mounted at the top of the experimental ele-ment above the top flange of the loop.

The purpose of the large TREAT sodium loop (see Fig. III-11) which is presently being designed is to provide a semipermanent facility for the meltdown of fuel clusters, under flowing sodium, in TREAT. The unit is being designed to provide a flow of sodium from a reservoir in the subreactor room to the top of the test section containing the test cluster. After passing through the cluster and test section, the sodium returns to the subreactor room. The sodium enters the test section at the top and flows downward in a concentric channel surrounding the fuel-bearing region. At the base of the test section, the flow reverses 180° to pass upward through the inner channel to exit at the top of the test section. The purpose of this arrangement is to interpose a stream of cooler sodium between the rapidly heated inner section and the outer test section wall. In this manner, severe high-temperature thermal shocks are prevented at the wall. A vapor-expansion chamber is located above the test section to accommodate any sudden expansion caused by rapidly vaporizing sodium. Special flanges are used to connect the test section to the loop, since it must be possible to remove the section from the reactor when experimentation is not in progress. Air-operated ball valves serve to isolate the in-reactor portion of the loop from the rest of the circuitry. In this way, the remainder of the loop can still be operated for test purposes. The test section containing the element will be capable of being drawn upward into a specially designed shielded cask for transport to another facility for inspection.

The instrumentation for such a facility inevitably must be fairly complicated. Basically, it will consist of:

1) sodium liquid-level detectors in the tanks;

2) flowmeters located at strategic positions throughout the loop;

3) pressure-sensing devices in the loop piping and tanks;

4) high-speed pressure-sensing devices in the test-section region;

5) thermocouples located throughout the loop for temperature control and measurement of sodium temperature. The loop will be heated electrically to obtain a preset temperature level before initiation of a transient;

6) ammeters to indicate the current to the loop heaters; and indicating devices for signalling valve positions, liquid-level positions, liquid metal leakage, etc.; and

7) an elaborate system of interlocked circuits to prevent transient initiation or to shut down the system in the event of malfunction. The controls for the loop will permit operation either from the reactor room or from the remotely located control room.

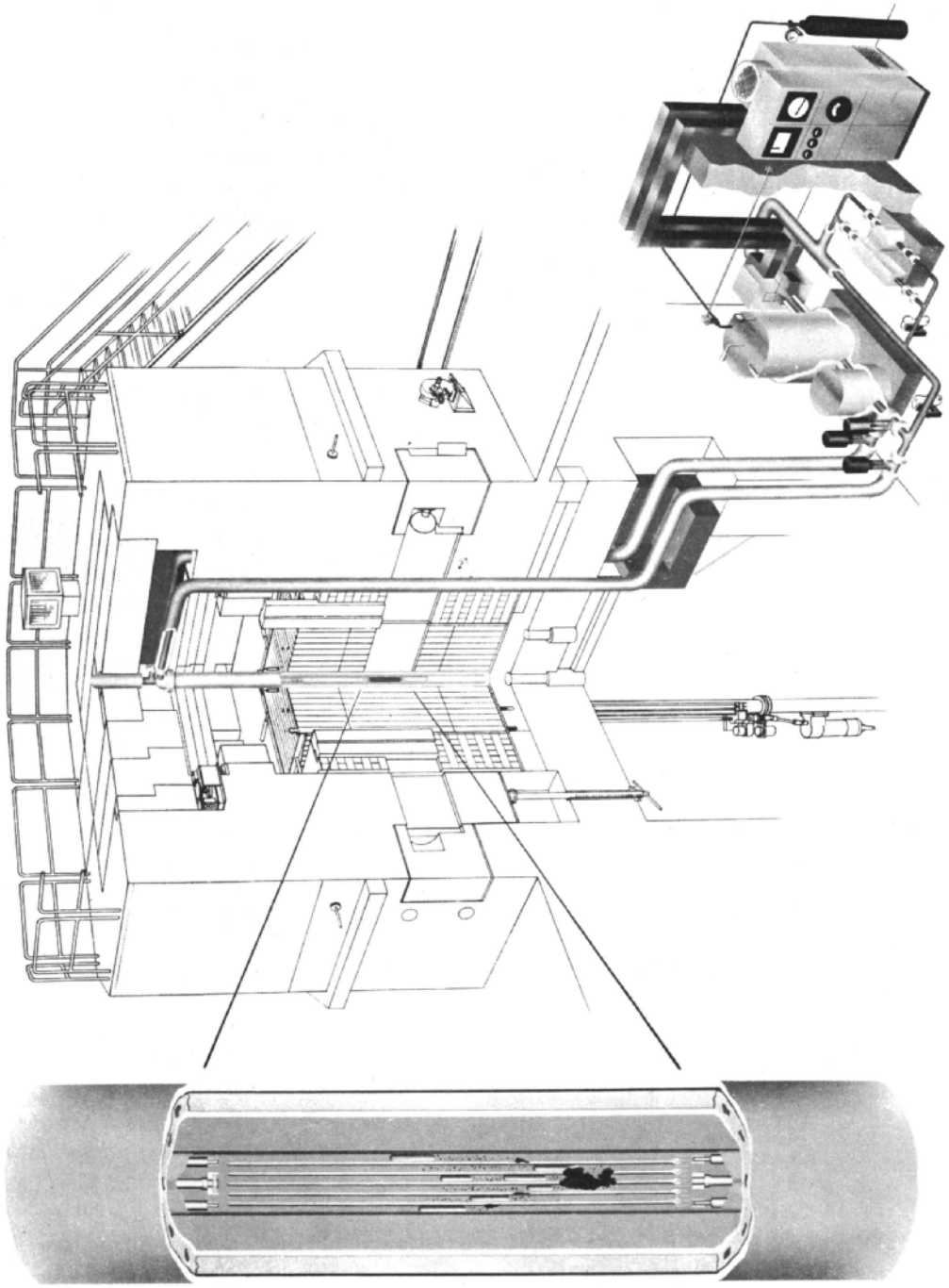

Fig. III-11
EBR-II Subassembly Meltdown TREAT Sodium Loop
111-8834

C. Special In-reactor Studies (UO_2-NaK Slurry Loops)

Three in-pile UO_2-NaK slurry loops were designed and operated at the Argonne National Laboratory for the purpose of studying the characteristics and behavior of this material and its potential as a fuel. The loops (shown in Fig. III-12) were designed to be inserted as complete units into the irradiation zone of the reactor. The UO_2-NaK slurry was circulated through the loop with motive power supplied by a small electromagnetic pump located in the piping just below the expansion tank. The electrical power to drive the pump was conducted via two parallel bus bars leading from the pump to the transformer situated at the top of the facility. Later versions were constructed with a special radiation-resistant transformer mounted at the base of the unit. Cooling was accomplished by means of a forced gas coolant loop which directed the coolant into the reactor. The coolant removed heat from the loop on contact, then carried it away by emerging from the system. In the later, higher-power versions, the coolant was a recirculating liquid which eventually disposed of its heat to a water-cooled heat exchanger.

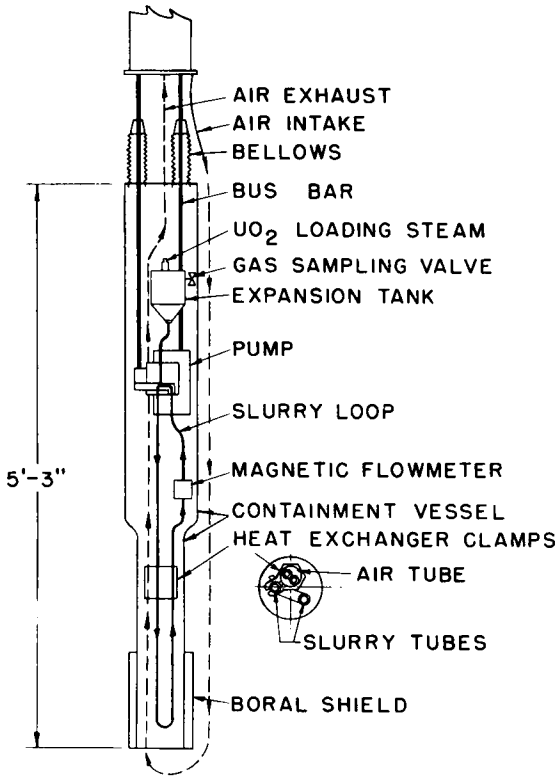

Fig. III-12

Typical In-Pile UO_2-NaK Slurry Loop

111-8195

The units were designed to pump slurries ranging up to 15 v/o UO_2 in the NaK and to operate at power levels from 2.5 to 6 kw at temperatures from 350 to 600° C (662 - 1112° F).

At the lower extremity of the loop, a small encircling boral shield was positioned to act as a neutron absorber to reduce the thermal-neutron flux by a factor of 100. This shielding was necessary to prevent excessive local heat generation when the UO_2 in the slurry was settled.

The instrumentation for these loops consisted of the following:

1) multipoint recording of temperatures sensed by thermocouples located along the tubing of the loop;

2) flowrate measurement and recording;

3) pressure measurement at the upstream and downstream ends of both legs; and

4) measurement of coolant flowrate and inlet and outlet temperatures to determine the power generation rate for the loop.

The flow and temperature devices were interlocked with the reactor controls to provide automatic shutdown of the reactor in the event of loop malfunction.

The post-irradiation examination, the entire loop was drawn upward and out of the reactor into a shielded cask in the same manner as described previously for the irradiated fuel elements.

D. Sample Preparation and Techniques for Remote Examination

It was mentioned previously that samples of fuel were prepared by pre-irradiation for various types of tests, such as corrosion and meltdown studies. In many instances, the samples achieved a considerable burnup and were consequently very radioactive. These samples had to be prepared for subsequent tests by utilizing remote-handling methods in a shielded facility. The same condition is true for post-experimental examination of the various samples considered.

The primary facility used to perform these operations was a 10,000-c cave, several of which are located at the Argonne National Laboratory. These caves are equipped with ANL model 8 master-slave manipulators. Excellent vision of the interior is provided by zinc bromide solution-filled shielding windows located about the periphery of the cave walls.

The common link between the reactor and the cave, serving as a medium of transportation of samples, was the shielded cask. In many instances the cask was specially designed to permit removal of the samples by vertical withdrawal from the reactor directly into the cask. This is accomplished by providing a bottom closure which can be closed after the sample is drawn into the interior. Finally, the cask is unloaded in the cave by either top withdrawal or by placing the cask on its side with its central cavity forming a common channel with a loading port penetrating the cave wall.

It is of paramount importance that all of the units which are to be unloaded remotely be designed with the remote procedure in mind. It is desirable that the opening of capsules and facilities be accomplished with a

minimum of difficulty and hazard to personnel involved. However, the unit must not compromise the in-reactor safety and reliability. The approach used was to use a weld-sealed capsule which was simple in external structure, preferably cylindrical in shape or having portions of its structure cylindrical. Simple pipe-cutting tools could be used to dissect the capsule into as many segments as desired.

Aside from the usual complement of tools associated with cave operations, a remotely operated milling machine proved to be extremely useful. This machine was used for more difficult operations involving the opening of finned-tube capsules containing failed fuel elements. Under these conditions, the finned tube was slotted longitudinally with a carbide-tipped cutter to allow access to the interior.

SECTION IV

EBWR COMPONENTS AND MATERIALS DESIGN

N. Balai
T. Kettles
E. Martinec
J. Matousek
D. Roy
B. Spinrad

NOTES AND EDITED DATA FROM LECTURES -
June 20, 23, 26, and 27, 1961

SECTION IV

EBWR COMPONENTS AND MATERIALS DESIGN

I. Design Features of the 20-Mwt EBWR*

A. Introduction

Once the possibility of stable operation of a boiling reactor system had been verified and it had been decided to construct the EBWR, several basic decisions about the design of the EBWR were made.

In 1954, the choice of fuel materials was quite limited. Ultimately, a Zircaloy-2-clad, ternary uranium alloy plate manufactured in two thicknesses and in two enrichments (natural uranium and 1.44 per cent enriched uranium) was developed. Since Zircaloy was not manufactured in tubing form and Argonne did not have experience in fabricating rods of this material, plates were selected rather than rods. The fuel characteristics made plates attractive. Arrangement of the plates was dictated primarily by heat transfer considerations, with a great deal of conservatism built in to accommodate possible "hot spots."

There was a sharp difference of opinion at Argonne whether to boil light water, which would necessitate using enriched uranium, or heavy water, which would require a leakproof system. It was decided to build a system scaled for light water, but with the option of later converting it to a D_2O system. The possibility of operating a light water system at higher power levels than originally anticipated has further reduced the incentive for a D_2O system. It is doubtful that the D_2O option will be exercised.

The system was intended to operate initially as a natural-convection system, but there was a provision for converting to a forced-circulation system at a later date. The BORAX-V and Vallecitos reactors are currently engaged in comparing natural- and forced-convection systems. The demand for a forced-convection system at Argonne has subsided, and the idea has been shelved for the time being. Conversion of the EBWR to a forced-circulation system could be accomplished only with the installation of new, large pumps. Forced circulation with the original pumping system would be less effective than natural convection and, in fact, might not carry off sufficient heat to allow reactor operation at power levels already achieved.

Once these basic decisions had been taken, the reactor system shown in Fig. IV-1 and described in the following paragraphs was developed.

---

*N. Balai, E. Martinec, J. Matousek, D. Roy, and B. Spinrad.

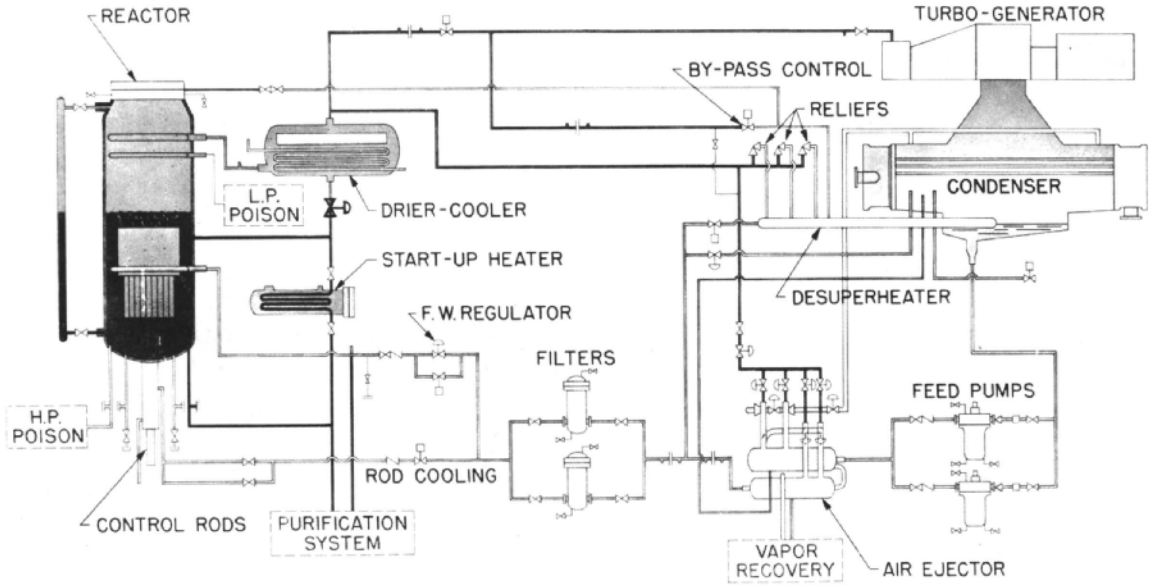

Fig. IV-1

EBWR Flow Diagram
111-3576

Summarized in this section are some of the outstanding features of the major components of the EBWR. A more complete description of these components is included in ANL-5607, as amended. The latter portion of this section describes some of the modifications of the system necessitated by the decision to increase heat-removal capability to 100 Mwt.

B. General Description

In the EBWR 20-Mwt power plant, saturated steam at 600 psig pressure and 255°C (489°F) is generated within the core and is passed from the reactor vessel through a steam dryer directly to a turbine. The steam dryer is equipped with cooling coils and is so placed as to permit its operation as an emergency cooler. The turbine discharges to a condenser. In response to generator-load fluctuations and consequent variations in turbine-steam demand, excess steam is bypassed around the turbine through a desuperheater and directly into the condenser, in order to maintain constant pressure in the reactor. Three steam-system relief valves also discharge into the desuperheater and thence to the condenser. An air-ejector system fed by steam from the dryer maintains the desired vacuum in the condenser.

Condensate collecting in the condenser hotwell is pumped by the reactor feed pumps through the air-ejector after-coolers and through a filter system, back to the reactor through a distribution ring near the top of the annular downcomer space surrounding the core. A small portion is passed into the vessel through the thimbles of the bottom-entry control rod drive mechanisms in order to maintain low mechanism temperatures.

A bypass water-purification system, consisting of ion exchangers and filters, is provided to maintain desired water purity. This system removes water (by pumping) from the bottom of the reactor vessel and returns it through the feedwater-distribution ring. In order to prevent discharge of active liquids up the stack and to avoid loss of working fluid if the plant is converted at a later date (to the use of D_2O as coolant moderator), a vapor-recovery system collects any water vapor carried over by the air ejectors and any leakage through turbine, pump, and valve seals. The water is then returned to the condenser. A startup heater fed by Laboratory steam is provided to permit heating of the reactor water prior to critical operation. Figure IV-2 shows a cutaway of the 20-Mwt power plant.

The core is made up of fuel assemblies arranged in a 4-in. square pattern within a core shroud structure and sealed in a support plate, which is bolted through legs to the bottom of the reactor vessel. The fuel assemblies each contain 6 plate-type elements of uranium-5 w/o zirconium-1.5 w/o niobium clad with Zircaloy-2. The reference core, about 4 ft in diameter, consists of 76 such assemblies containing uranium enriched to 1.44 percent U^{235} and 35 assemblies containing natural uranium, evenly distributed. Half the assemblies of each enrichment contain plates slightly thinner than those of the other half in order to permit experimental variation of metal-water ratio.

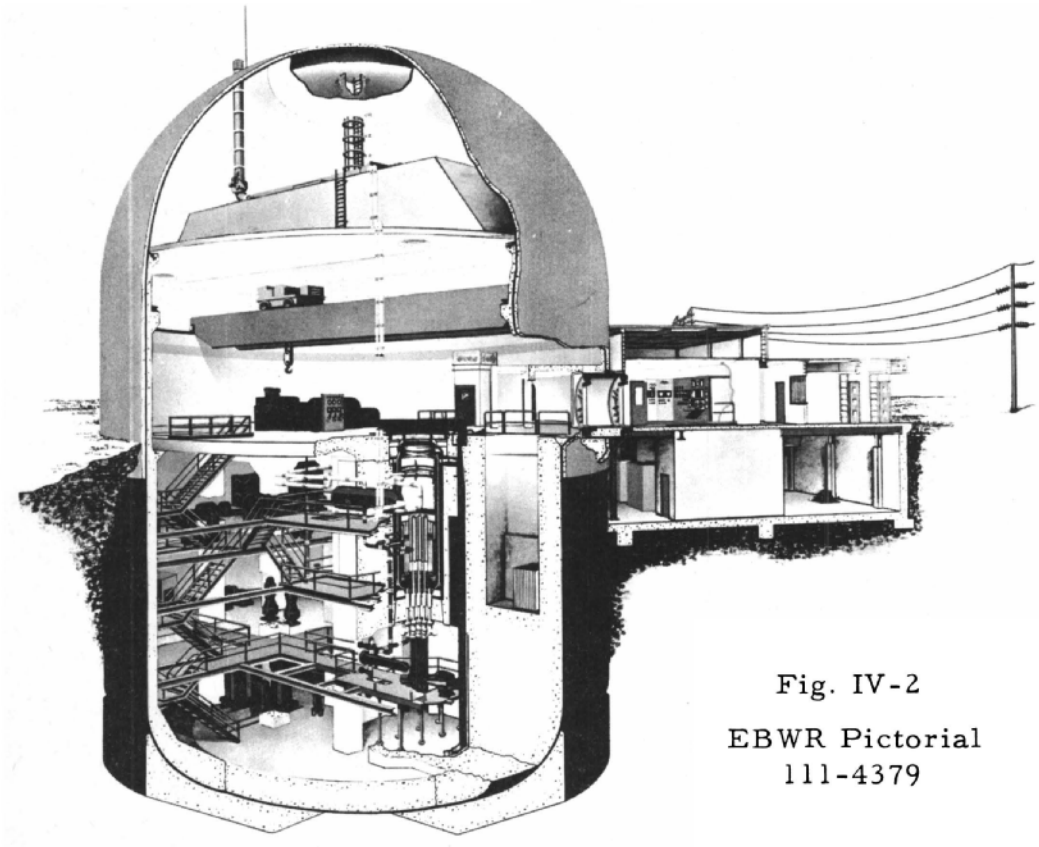

Fig. IV-2

EBWR Pictorial
111-4379

The core support plate and shroud structure are designed to accommodate up to 148 fuel assemblies in order to allow experimental variation of core diameter up to 5 ft. An addititional 36 enriched (1.44 per cent) assemblies, 18 of each plate thickness, are provided for these tests. During tests with core diameter smaller than the maximum, the outer fuel positions are occupied by dummy assemblies. Figure IV-3 provides a cutaway pictorial view of the 20-Mwt reactor.

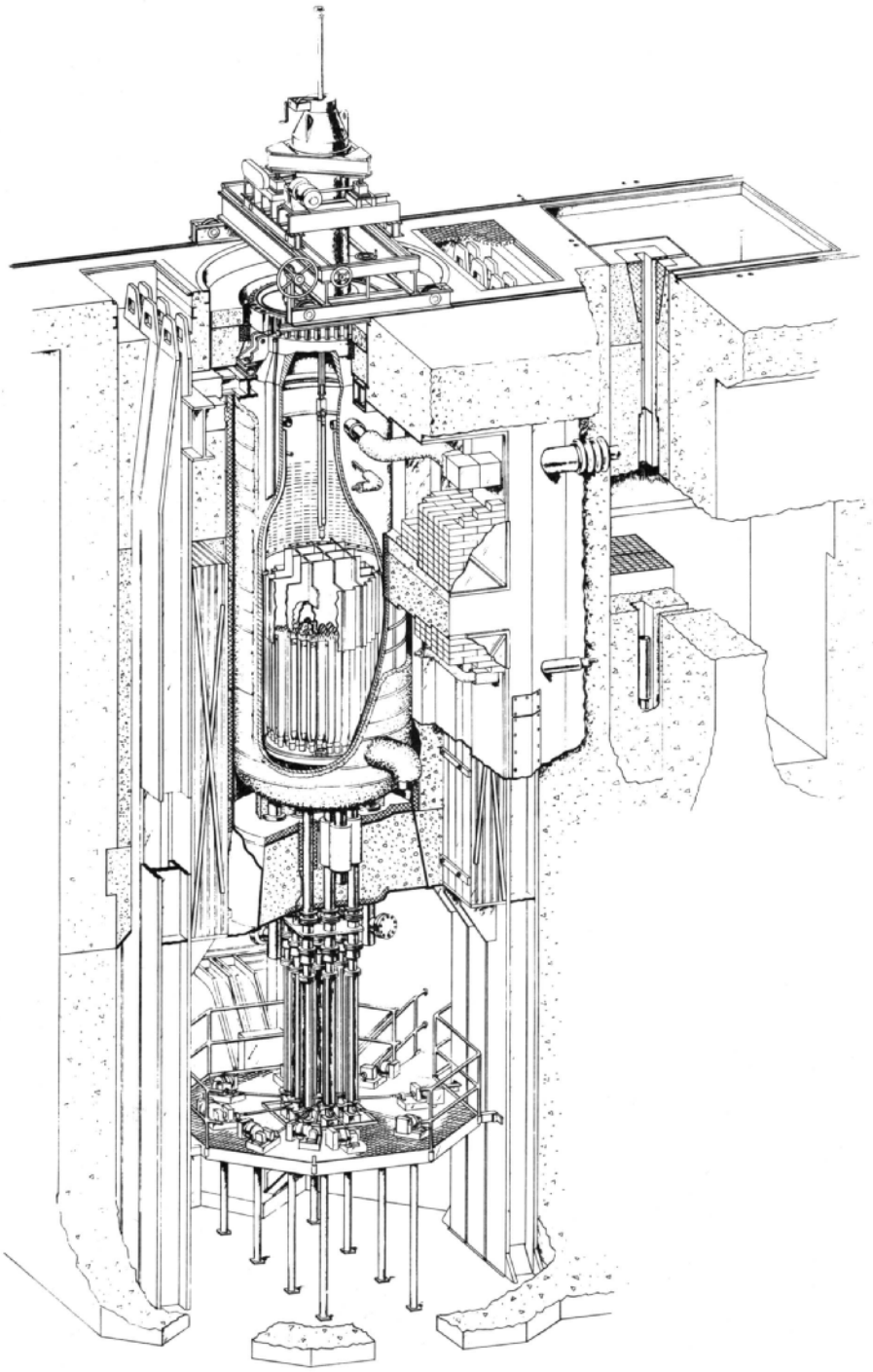

Fig. IV-3

Cutaway Pictorial of EBWR Reactor and Components
111-4395

The core shroud structure serves the triple purpose of positioning the upper ends of the fuel assemblies, providing additional riser height above the assemblies to enhance natural circulation, and acting as a guide for the 5 hafnium and 4 boron-stainless steel control rods moving within the core.

The control rod drive mechanisms, situated below the reactor, are of the external lead screw and nut type - employing a linear labyrinth pressure breakdown seal.

Auxiliary emergency shutdown control is provided in the form of a high-pressure and a low-pressure boric acid-injection system. In the high-pressure system, 160 gal of saturated boric acid solution are maintained under 1,600 psig air pressure in a tank and are injected into the bottom of the reactor vessel in the event of failure of control rods to scram. The low-pressure system is used only when reactor pressure is reduced to a value less than 20 psig, and water level is lowered to a point 6 in. above the fuel assemblies. Boric acid solution is introduced into the top of the vessel at a distribution ring equipped with spray nozzles (arranged to insure impingement of solution on all exposed parts of the core) for the purpose of removing decay heat. The boric acid is present here only to maintain subcriticality with water addition.

The reactor vessel has a 7-ft inside diameter and a 23-ft internal height, and is fabricated of SA-212 grade-B carbon steel with a Type-304 stainless steel lining. The vessel wall is protected from excessive heat generation by a boron-stainless steel thermal shield. The vessel is supported at its upper end by lugs resting on C-shaped compression springs, which, in turn, rest upon a Carilloy T-1 steel framework attached to columns that extend downward and are embedded in the concrete basement floor. The springs and framework are designed to absorb dynamic loadings which might result from the accidental dropping of heavy objects, such as the vessel cover plate, on top of the vessel.

The reactor is located below the main floor in an octagonal concrete shell extending to the basement floor level. The vessel is surrounded with a 3-in. thickness of stainless steel wool insulation, 3 in. of airspace, and a carbon-steel cylindrical tank which serves as an inner form for shielding. This tank is equipped with cooling coils on its outer side to remove heat generated within the shielding and transferred to the shielding from the reactor. It is covered with lead brick and with a plaster containing ferroboron as part of the fine aggregate. The remainder of the space between the plaster and the wall of the octagonal shell is filled with either magnetite concrete with steel punchings added, magnetite concrete, or ordinary concrete, depending upon the radiation intensity at the point concerned. The total thickness of radial shielding is 8 ft $3\frac{1}{2}$ in.

Shielding below the reactor vessel is essentially concrete containing magnetite-steel punchings. Perforations for the nine control rod drive nozzles and four forced-circulation discharge nozzles are stepped to prevent direct radiation streaming. Additional layers of lead and ferroboron plaster are provided in critical areas.

At the top of the reactor, shielding is provided by a stainless steel indexing plug assembly within the vessel, the top cover of the vessel, and a portable water tank which effects the top seal of the air envelope surrounding the reactor. Spaces surrounding the vessel support lugs and top closure are filled with specially shaped blocks of concrete containing magnetite-steel punchings, steel plates, and a container filled with lead pellets.

Removal of spent fuel is accomplished by a lead-shielded transfer coffin which travels between the reactor and the adjacent fuel-storage pit on a positioning carriage. After removal of top shielding components and the vessel cover, a plug carrier assembly containing bearings and drive gears is placed on top of the vessel, attached to the internal indexing plugs, and positioned over the assembly to be removed. The coffin is located above the discharge opening in the plugs. The telescoping fuel grapple is lowered and engaged, and the assembly is lifted into the coffin. The coffin is moved to a position over the discharge chute in the fuel-storage pit, and the assembly is lowered into the receiving tube and released. Subsequent movement of the assembly to a position in the boron-stainless steel storage rack for cooling, as well as ultimate removal of end fittings and shipment to a processing plant, is accomplished within the pit by use of special tools.

The entire power plant as described thus far is housed within a cylindrical steel tank having an ellipsoidal bottom head and a hemispherical top head, designed to withstand an internal pressure of 15 psig. The tank is 80 ft in diameter and 119 ft high, with about one-half the height below ground level. The purpose of the shell is to contain any radioactive materials which might be released as the result of accidental rupture of any part of the system during operation. In order to prevent excessive pressure buildup in the building because of steam release, a spray system has been provided to spray water into all parts of the building and condense any steam released. This system is supplied from a 15,000-gal emergency water-storage tank located just inside the top of the building dome.

During reactor operation, access to the power plant building may be gained only through one of two air locks, one connecting with the adjacent service building and the other communicating with the outside. The latter is designed primarily as an emergency escape feature. A gasketed and bolted freight door may be opened during reactor-shutdown

periods to permit movement of large components in and out of the shell. A 20-ton bridge crane operating on a circular track serves the main floor area and may be used to handle items between floors through a large hatchway extending to the basement.

Special provisions have been made to prevent puncturing of the steel building shell by missiles which might result from such accidents as reactor turbine or pipe ruptures. The entire shell is lined with concrete except for the upper hemispherical dome. The latter is protected by a steel plate and concrete ceiling over the main floor.

The reactor structural arrangement includes features to prevent a catastrophe in the event of an explosive zirconium-water reaction within the core. The shock pressures developed would cause the bottom head of the vessel to be blown, together with the bottom shielding, into the basement. The vessel itself would tend to act as projectile. The large upward force developed would be restrained by 3 heavy beams located across the top of the reactor and pinned by wedges to 6 columns whose bases are firmly anchored in the large mass of concrete forming the basement floor of the building. Laminated blast shields of compressible material and steel are interposed between the reactor and the columns (in the vicinity of the core) to protect the latter from side shear.

The service building adjacent to the power plant building houses the plant control and electrical switchgear, a laboratory, service, office, reception lobby, and sanitary facilities. The entire control of the plant is accomplished from the control room in the service building. Thus, the presence of personnel in the power plant building during reactor operation may be limited to occasional maintenance and inspection tours.

C. Pressure Vessel and Materials Studies

In addition to functional requirements, reactor vessels as they are currently designed are further burdened by:

1) corrosion-resistance requirements,
2) large closure requirements, and
3) interpretations of irradiation effects.

A nuclear reactor may be conveniently viewed in another way as a self-energized heat exchanger. On such a basis, all mechanical equipment designs (such as the pressure vessel, pumps, turbines, piping, and other auxiliaries) are subordinated to the requirements for the efficient removal of heat from the nuclear core. Under the conditions of high transfer rates (above 200,000 Btu/hr-ft^2), heat transfer surfaces (fuel elements) and the rest of the system require materials of the highest corrosion resistance.

Large size is a frequent reason for the problems of nuclear pressure vessels and the sources of many major difficulties are traceable to the design requirements for large high-pressure closures. Crowded closure geometry, coupled with limitations imposed by materials, have rightly focused attention on the behavior of metallic structures in a complex stress system - an area which is least understood. Integrity of any large high-pressure closure can be questioned for lack of the most rudimentary data, in at least the following instances:

1) structural performance of a flange geometry when bolt spacing seldom exceeds two bolt diameters, that is, the bolt hole ligament efficiency is less than 50 per cent;

2) structural performance of a flange geometry under the influence of transient stresses, such as occur in bolting up, startup, and depressurizing operations - particularly when metallurgically different structures are incorporated into a finished vessel;

3) structural performance of heavy-wall sections with non-uniform internal nuclear heat generation. Internal heat generation in the pressure vessel is not uniform. In the section of the vessel immediately surrounding the core and which is in contact with the reactor coolant, heating by neutrons and gammas is usually at its maximum and generally falls off rapidly. Above the coolant level, as in boiling reactors, heat generation in the wall may require additional design provisions to reduce metal temperatures - as was done for the upper section of the EBWR vessel. Other vessel sections which require at least a review consideration are the heads of the vessels (as in pressurized water reactors);

4) structural performance of wall sections (thin as well as thick) whose prior mechanical properties are progressively changing, as a result of nuclear bombardment and at a nonuniform rate.

A temporary solution to the sealing of the EBWR closure (which hindsight reveals as a difficult gasket geometry) has been effected. In the rugged experimental conditions under which these gaskets are forced to perform, their performance has been phenomenal. However, they are experimental gaskets. The importance of fabrication supervision, inspection departments, and inspectors of the work in progress has not received the attention it merits. The translation of an ideological abstraction outlined on paper into desired metallic configurations cannot be efficiently effected without their understanding of the problems involved and their explanation in shop language.

The EBWR pressure vessel consists of an upper ring forging, a 2-course rolled plate shell and spun plate lower head. A flat cover plate is held in place against the 2 sealing gaskets by 44-alloy bolt studs screwed

into the ring forging. The nominal inside diameter is 84 in. The length is 30 ft 11$\frac{1}{2}$ in. and the dry weight is approximately 60 tons. Pressure parts are fabricated from carbon steel. Surfaces in contact with reactor water or steam are clad with stainless steel. (Type 304 sheets or with weld metal deposited from stainless steel Type 312 and 308L electrodes.) Stainless steel Type 304 cladding sheets are $\frac{7}{64}$-in. in thickness and are spot welded to the base material in the shell and lower head. Because of its irregular geometry and the heat transfer requirements for rapid heating in startup and shutdown operations, the ring forging is clad with stainless steel Type 312 and 308L weld metal. The weld metal deposit has a minimum thickness of $\frac{3}{16}$ in. The carbon content (0.08 per cent maximum) is controlled to a minimum depth of 0.100 in. below the surface. The vessel design meets the requirements of Section I of the ASME Boiler and Pressure Vessel Code (1952 revision) with exceptions. The exceptions are in the direction of increased reactor vessel integrity and operational safety. Figure IV-4 shows a cross section of the EBWR reactor vessel.

Eight support brackets, paired symmetrically and radially about the principal axes of the vessel, are welded to the ring forging for mounting of the pressure vessel. The bearing plates are oriented for mounting on a rectangular structural frame and are machined to give a common mounting plane. Base plates and vertical side plates were fabricated from 1$\frac{1}{2}$-in. gage, SA-212, Grade B boiler plate. Vertical sway braces are placed symmetrically around the circumference of the shell and are oriented 30° clockwise from the principal vessel axes. Their purpose is to prevent "rocking" of the vessel in operation. Radial restraint is effected by a parallel-plate yoke mechanism welded to and extending inward from the lead shield form. Vertical travel is unimpeded to permit thermal expansion of the vessel. The maximum displacement provided for is 3 in. At the maximum displacement, radiation shielding around the control rod thimbles will "bottom" on the steps of the "heavy" concrete biological shielding beneath the pressure vessel.

Thermocouple blocks, containing 2 chromel-alumel thermocouples per block, were added to the exterior of the lower head, shell, and ring forging at approximately 2-ft intervals. The thermocouples were soldered into the blocks with a high-temperature cadmium-silver solder. The thermocouples are designed to indicate the extent and distribution of the internal heat generation in the steel wall and rates during the startup heating.

The top shield plugs are supported from the ledge of the ring forging. Continuous contact of the plug system with the ledge is prevented by 1-in. square bars welded to the radiation-blocking step of the plug to provide a controlled port for the admission of steam to the upper section of the ring forging, cover plate, and the plugs. The shield plug assembly is utilized for refueling and other operations with heavy water reactor modifications which preclude the use of water for shielding.

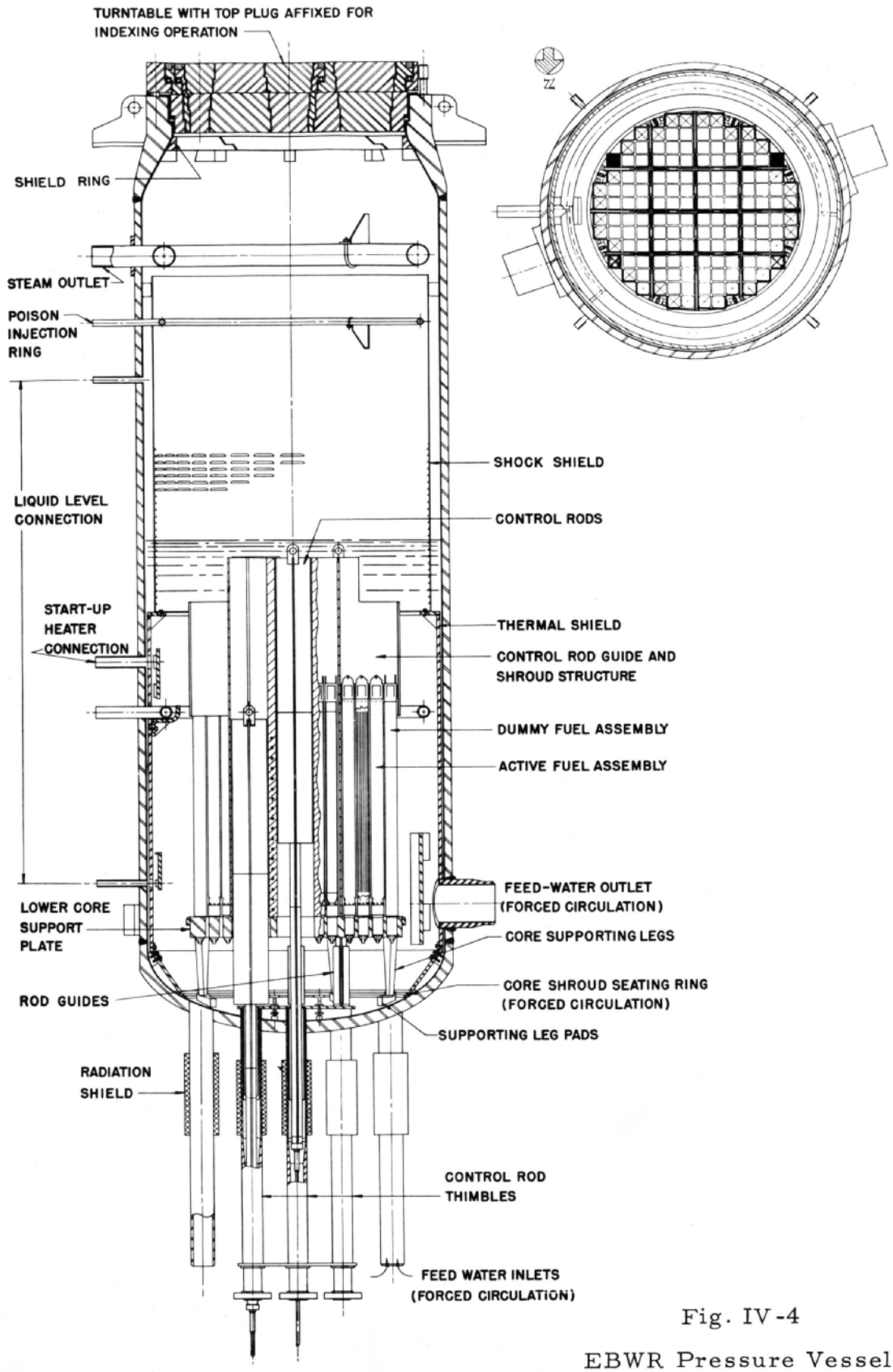

Fig. IV-4

EBWR Pressure Vessel
111-4547

In addition to the nozzle attachments and distribution rings, the shell houses:

1) an upper segmented (and bolted) 4-piece shock shield which is bolted to the upper ring of the thermal shield. The primary function of the shock shield is to prevent the accidental chilling of the hot steel walls by the admission of cold water through the poison line distribution ring;

2) a lower segmented (and bolted) 10-piece thermal shield supported on lugs welded to the lower head. Thermal shielding is not required in the light water version since thermal stresses are at low levels;

3) a Type 304 stainless steel, circular grid or core support plate (62-in. diameter x $5\frac{3}{4}$ in. thick). The grid plate is bolted to eight legs which, in turn, are bolted to machined and threaded bosses welded to the lower head.

The closure consists of a flat cover plate forging (6 ft $8\frac{7}{8}$ in. OD x $8\frac{13}{16}$ in. thick) bolted to the forged cylindroconical ring section of the pressure vessel. Two concentric gaskets, each with a $\frac{5}{8}$-in. face width, are used to maintain a pressure-tight joint. In-leakage of air (and water vapor) across the face of the outer gasket and out-leakage of steam across the face of the inner gasket (which may develop under service conditions) are collected in an annulus between the two gaskets. Gas from an external source may be admitted to the intergasket leakoff annulus to verify the integrity of each of the gaskets. Holes in the cover plate and ring forging were drilled to insure an accurate alignment of stud bolts; the maximum radial clearance in the holes of the cover plate is $\frac{1}{8}$ in. Bending loads on the bolting under service conditions are minimized by the use of male and female spherical washers placed between the cover plate and bolt stud nut. The cover plate is fabricated from a carbon steel made to fine-grain practice by treatment with aluminum to insure a fine-grained steel possessing high-impact properties at low temperatures. The steam side of the cover plate is clad with stainless steel weld metal deposited by the submerged arc process for corrosion resistance and is $\frac{3}{16}$ in. in thickness after machining. Like the cover plate, the SA-105, Grade II ring forging is clad (after machining) with a $\frac{3}{16}$-in.-thick stainless steel weld metal deposit for corrosion resistance. A submerged arc deposit weld metal ring ($72\frac{1}{2}$-in. OD x 68-in. ID x $\frac{5}{16}$ in. thick) and continuous with the ring forging cladding, contains two gasket grooves concentric with the closure opening.

The vessel shell and lower head are fabricated from SA-212 Grade B carbon steel made to fine-grain practice by the addition of aluminum to obtain low-temperature, impact-resistant metals (15 ft/lb Charpy at -50°F minimum). The ferritic carbon steel vessel is clad with

stainless steel Type-304 for the necessary corrosion resistance. Two types of cladding are used:

1) The cylindrical body and lower head plates are clad with a $\frac{7}{64}$-in. sheet of stainless steel Type-304 prior to rolling and spinning operations. The austenitic sheet is welded intermittently to the carbon steel plate by pressure-resistant welds which are approximately 1 in. long by $\frac{1}{2}$-in. wide and spaced on $\frac{1}{2}$-in. centers.

2) The irregular geometry of the upper ring forging does not lend itself to cladding by the resistance process. Here, the submerged arc cladding is $\frac{3}{16}$ in. thick. An integrally bonded cladding was needed for purposes of heat transfer (i.e., a 3-hr startup cycle was required). A heavier cladding was required to ensure a 0.100-in. (minimum) thickness of alloy conforming to the chemistry of stainless steel Type-304 (0.08-per cent carbon maximum).

The vertical location of the support structure for the pressure vessel, with respect to the EBWR building floor, is dictated by the water-level requirements of the turbine and condenser. The top of the pressure vessel closure flange was fixed at 24 in. below the main floor level. The establishment of this dimension, in turn, established the criterion for a number of possible impact loadings on the vessel and its support structure. The maximum free fall (assuming a drop height of the object when suspended with 6-in. clearance above the main floor level) and the masses involved are as follows:

	Weight, ton	Maximum fall, in.
Unloading coffin	15.0	30
Vessel cover	8.5	30
Top shield indexing plugs	6.0	42
Indexing plugs carrier	10.0	30

The pressure vessel is supported on eight lugs welded to the necked-down portion at the top of the vessel. Mounting at this point allows for downward thermal expansion of the vessel. Alloy and structural steel framing is provided to transmit the various loads, the weight of the vessel and impact loads imposed by accidental dropping of heavy equipment on the top of the vessel, horizontally to the holddown columns and thence downward to the concrete in the control rod room floor.

A study was made to determine the magnitude of the forces that the structure would have to withstand, and the loading sequence.* Armour Research Institute, under subcontract, determined that the top of the

*In this study it was assumed that there would be a reaction between 25% of the core metal and the water leading to a TNT-type explosion.

pressure vessel would not fail. The lower section of the pressure vessel would fail under reflected shock wave pressure, and the concrete biological shield surrounding the lower part of the vessel would be reduced to rubble by transmission of shock waves.

Since the power plant building shell is most vulnerable to missiles launched in the vertical direction, the first concern was to hold down the remaining top portion of the pressure vessel. This was accomplished by placing three parallel, horizontal hold-down beams across the top of the pressure vessel. In the D_2O option, a biological shield is required above the pressure vessel. A convenient design was evolved using a steel ring and a structural steel backup plate to transmit the upward force from the pressure vessel cover, through the ring and the plate, to the bottom flanges of the hold-down beams, as shown in Fig. IV-5.

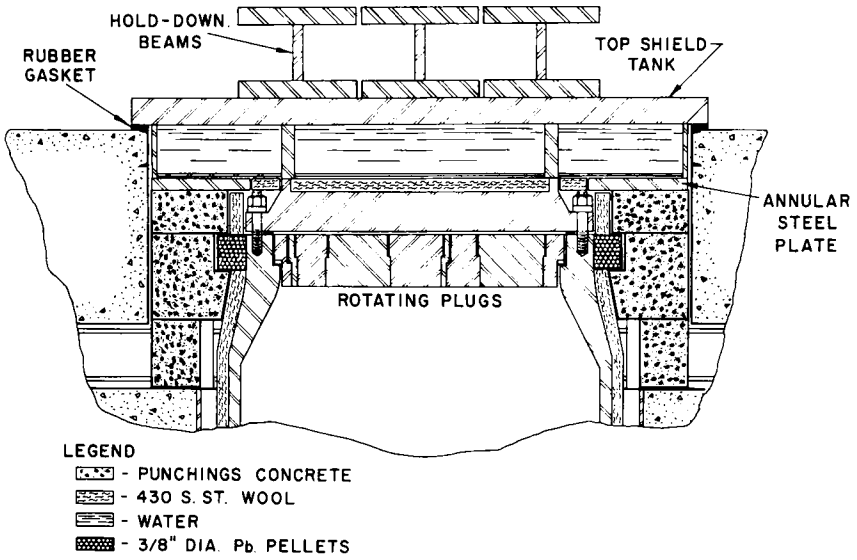

Fig. IV-5

Reactor Top Shielding
111-4114

From the earliest calculations it was apparent that the conventional structural steel design was inadequate. The calculated section sizes (with the conventional factor safety of 3) were extremely heavy and bulky. Accordingly, conventional design criteria were abandoned along with conventional steel (ASTM A-7) materials. A design, taking into account the inherent increase in strength of metals as a function of strain rate, was evolved, which was based on a high-strength quenched and tempered alloy steel (U.S. Steel Corp. Carilloy T-1). Beam and column sections were determined, using the static ultimate tensile strength of the alloy as the allowable stress with blast loads reduced by the dynamic load factors obtained from Armour. The sections required are much larger than any listed conventional rolled sections and were fabricated from plate.

One of the areas in which information is desperately needed is the effect of high-level irradiation on reactor vessels and the materials surrounding the reactor vessel. From ORNL's irradiation-effect data on SA-212B, it has been assumed that exposure levels up to 1×10^{20} nvt (<1 Mev) were safe. However, contradictory results from the ANL-26 irradiations of remnants from the lower head plate, which were prepared into irradiation specimens, indicated total embrittlement at exposure levels from 1×10^{20} to 1×10^{21} (<1 Mev). Subsequently, irradiation facilities have been installed in EBWR.

Investigations are being conducted to provide a better understanding of the irradiation mechanisms. Tensile strength, yield point, elongation, hardness, and impact strength will be investigated along with changes in magnetic properties. Also, attempts will be made to devise nondestructive test methods to trace the course of irradiation damage. During the past year there has been an awakening of the industry to the significance of this previously neglected field.

In a general investigation of irradiation effects of pressure vessel materials, a quenched-and-tempered T-1 steel plate in a 3-in. gage was cold sectioned into subsized tensile and impact specimens. After filling with NaK, the stainless steel Type 304 containers containing these specimens were irradiated in a high fast-neutron-flux region of the MTR for a total exposure of 13.5×10^{20} nvt fast and 73.2×10^{20} nvt thermal. The canned samples were located in 80°F process water during the entire irradiation. Post-irradiation measurements were performed in the high-level caves located at ANL. The measured changes in the mechanical properties of the base metal, heat-affected zone, and weld metal attributable to irradiation damage are summarized as follows:

1) a 55 per cent increase in the ultimate tensile strength;
2) an 80 per cent increase in the 0.1 per cent yield strength;
3) a 43 per cent decrease in the reduction of area;
4) an increase in hardness - 8 points Rockwell hardness D scale;
5) a marked increase of the fracture transition temperature; and
6) a reduction, by a factor of 3, of the impact resistance to fracture at the fracture transition temperature.

Although the original purposes of this irradiation were met, which were to extend the data on irradiation damage and to test the validity

of the promising beneficial effects of a tough micro-structure, the only valid conclusions which a vessel designer could draw were:

1) Structural damage to the ferritic steels, which are by far the most common materials entering into the construction of reactor vessels, occurs at an unknown and unpredictable rate.

2) Irradiation effects may also be influenced by the composition of the alloys, as is the case for the Carilloy T-1 analysis. Boron is utilized as an alloying agent to improve the hardenability of the T-1. Damage effects may be masked by the in situ bombardment by energetic alpha particles (later helium gas) as the boron-10 isotope burns out and is replaced by lithium-7.

3) Additional data on high-level irradiation-damage effects are badly needed, together with supporting studies of ways and means to either limit damage (through development of alloys) or to restore damaged metallic structures.

4) The embrittlement of steels by neutrons requires design refinements in the direction of reduced stress concentration factors to reduce the probability of brittle fracture failures. Figures IV-6 and IV-7 illustrate the effects of irradiation on T-1 steel.

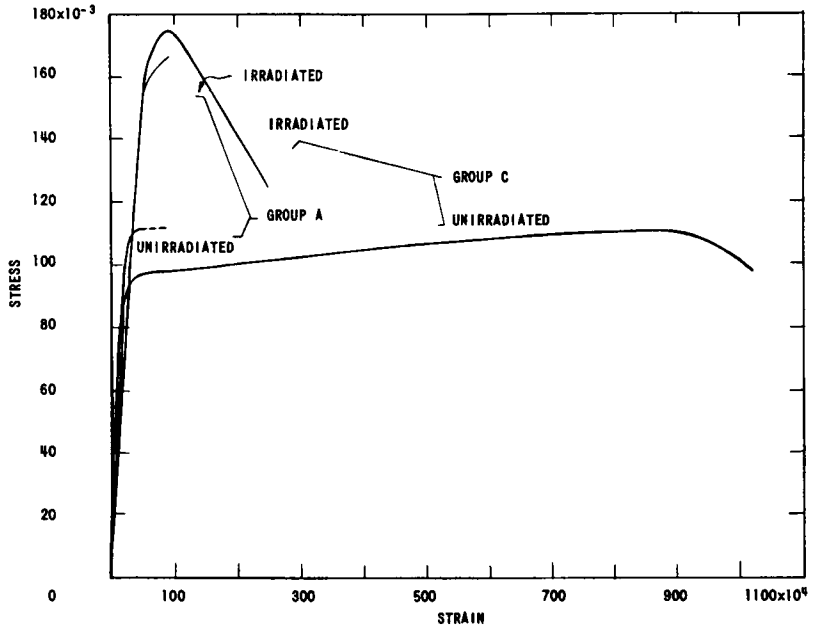

Fig. IV-6

Irradiation Effects on Tensile Strength of T-1

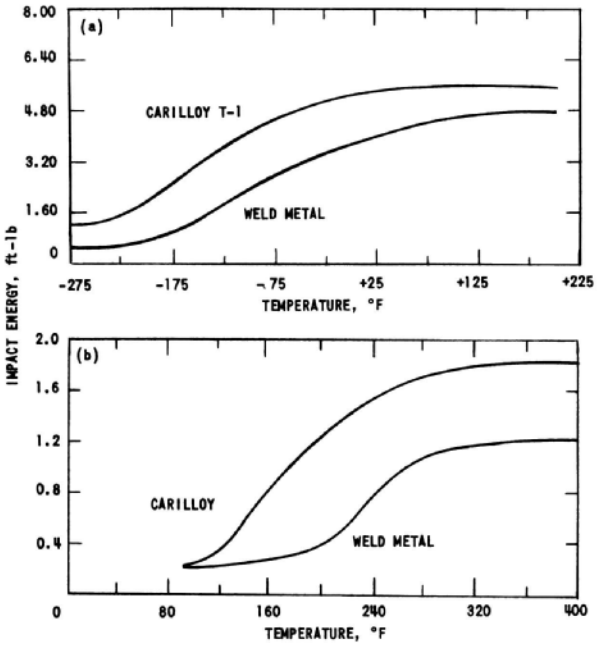

Fig. IV-7

Changes in Impact Resistance of T-1 Base Material (Long Rolling Direction) and in E12016 Weld Material. (a) Unirradiated Material; (b) Irradiated Material.

D. Steam Turbine-generator

The turbine-generator unit is composed of a multistage impulse turbine solidly coupled to a generator with a directly connected exciter (see Fig. IV-8). The turbine casing consists of a steam chest cast integrally with the steam-end casing and an exhaust end welded to the steam-end casing. To allow for thermal expansion, the turbine casing is flexibly supported at the steam end and rigidly supported at the exhaust end. Transverse keys at the exhaust and steam ends, plus structural supports at both ends, maintain correct alignment under all operating conditions. The turbine rotor is a forged steel shaft with keyed and shrunk-on forged steel wheels and an integral coupling flange.

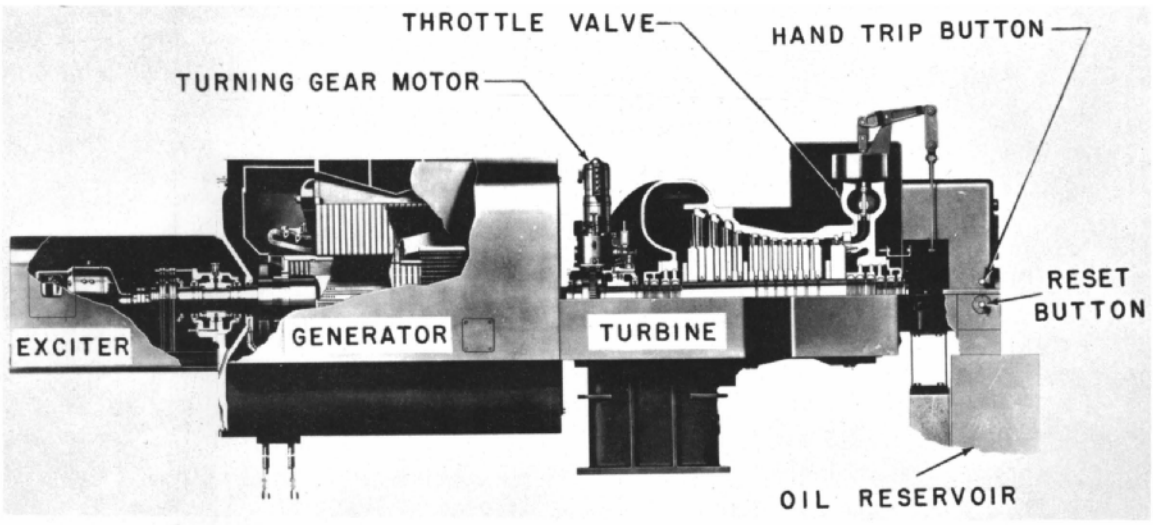

Fig. IV-8

EBWR 5000-kw Turbine-generator
111-5336

Contained in the turbine oil-reservoir assembly are the motor-driven auxiliary oil pump, auxiliary oil-pump control, pressure-reducing and relief valves, screens, internal piping, and an oil-level gage. Oil for lubricating and cooling the turbine generator and exciter bearings during normal operation is delivered by a helical-gear positive-displacement pump submerged in the oil reservoir. All oil returning from the bearings and governing system passes through fine mesh screens before entering the oil reservoir. The governing system, which receives oil directly from the main oil pump, supplies the hydraulic force necesary to lift the governing valves and actuate the trip cylinder on the throttle valve.

The turbine-governing mechanism consists of a speed governor with its oil relay, which multiplies governor power, a power cylinder with its oil relay, and suitable mechanical connections to the bar which lifts the governing valves. Steam control to the first-stage nozzles is governed by six spherical-seated plug valves. These valves are lifted in sequence from their seats by a single bar and a lever connected to the oil-operated and spring-loaded power cylinder. The trip and throttle valve, which is welded directly to the steam inlet of the turbine, has two functions to perform: one is to control, by throttling, the steam admitted to the turbine when bringing it up to speed; the other is to act as a quick-closing or emergency trip valve. A labyrinth seal at each end of the casing, through which the turbine shaft extends, prevents the escape of steam into the room and air leakage into the casing.

In addition to the conventional complement of seals, the turbine shaft, horizontal joint flange, steam-chest joint flange, governing-valve lift rods, throttle-valve cover joint flange, and the throttle valve stem are provided with a special sealing arrangement. It consists of a dry-air barrier, a vacuum leakoff, and a steam seal. Effective sealing is obtained by means of steam-seal regulators, manifold, and interconnecting piping together with dry air and vacuum connections to the Air Drying and Fluid Recovery System. The casing drain, leakoff pipe drain, and the gland-relief valve discharge are connected to the main condenser. These drains, as well as the throttle valve above and below seat drains, are arranged to be self-draining.

Dry air under a pressure of +6 in. H_2O is supplied to the outer chamber of the shaft-seal assemblies, the outer connection of the throttle valve and the governing valve lift rod stem packings, the welded enclosures around the casing horizontal joint, the throttle valve cover joint, and the valve chest cover joint. A vacuum of -6 in. H_2O is applied to the second chamber of the shaft-seal assemblies, the middle connection of the throttle valve and governing valve lift rod stem packings, the leakoff grooves in the horizontal joint and governing and throttle valve cover joints, and the welded enclosure surrounding the gland steam-regulator valve bodies. Steam under

a pressure of $\frac{1}{2}$ to 2 psig is supplied to the third chamber of the shaft-seal assemblies from the main gland steam manifold. Under normal operating conditions, the manifold is supplied with leakage steam from the governing-valve balance, lift rods, and the throttle-valve stem packing. Steam in the manifold is supplemented or relieved, as required, by the gland steam makeup or relief valve. The relief valve discharges excess steam from the manifold into the drain system.

On May 1, 1958, a turbine blade broke with no serious consequences. When the blade broke, the turbine-generator was tripped off the line by an operator. Originally, the turbine-generator had a vibration of about 0.6 mil and an alarm setting of 1.75 mils; the sudden vibration greater than 10 mils gave the alarm. Prior to the start of excessive vibration, all operating parameters were normal. The turbine went through its 2600-rpm resonant point. Approximately 5 min later, the vibration could be felt in the control room located in the service building adjacent to the containment building. Fearing possible piping damage, the reactor was shut down and isolated from the turbine. The turbine-generator rolled or coasted about 40 min before coming to a complete stop. On the following day, an Allis-Chalmers service engineer inspected the turbine by entering the condenser manhole and concluded that a blade had broken.

The upper turbine casing was removed on May 5 to confirm this observation. The turbine was then completely dismantled. The rotor and stationary blading diaphragms were removed. The maximum detectable radioactivity was 2 mr/hr at 2 in. A blade and an outer shroud had been torn free from the adjacent four blades. They were found lying between the last two rows of diaphragms at the low-pressure end of the turbine. Initial inspection indicated that the blade fracture probably resulted from fatigue of the root metal. The failure was progressive and occurred in stages across the root to the leading edge of the blade (see Fig. IV-9).

Following a microscopic examination of ten blades which had been attached to two shrouds, Allis-Chalmers decided to remove and replace all the blades (a total of 158) and two spacer blocks in the next-to-the-last stage of the rotor. The reason for replacing the entire ring of blades was that each of the ten blade roots inspected contained an unexplained groove or scratch in the fillet between the neck and outlet hook of the root. These blades were removed from the wheel at Argonne. The rotor was then shipped to Allis-Chalmers for reblading and balancing. At the time the failure occurred, the blades had been in service approximately $1\frac{1}{2}$ yr with a total of 4000 operating hours.

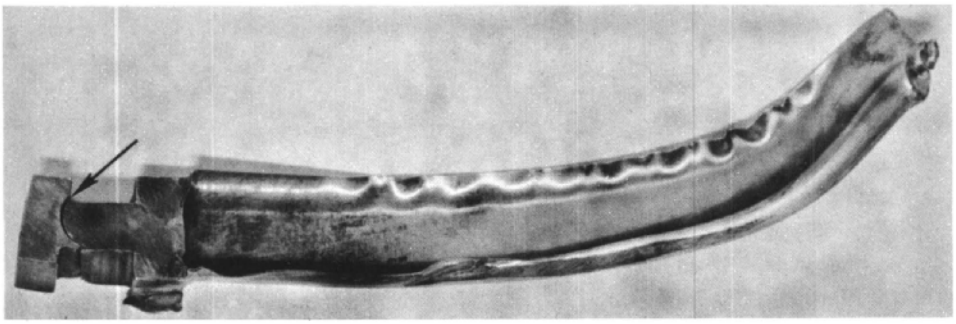

Failed blade showing the location of failure through the neck of the single "T" root. The fatigue failure began in the fillet between the hook and the neck on the outlet side of the blade and had progressed almost entirely across the neck before the blade root failed in tension.

Magnification: Approximately 1/2 x.

Fig. IV-9

EBWR Failed Turbine Blade

After a detailed metallurgical investigation, the Allis-Chalmers laboratory reported that the groove in the root metal was responsible for creating a stress concentration at that point. This stress would be in excess of the endurance limit of the material and could cause the root of the blade to fail. The groove was made in each root fillet by a holding fixture used during the manufacture of these blades.

Before replacing the blades, Allis-Chalmers deepened the blade-root groove in the wheel so that a soft iron caulking piece could be driven under the blade root to maintain a tight fit. Vibration would be minimized or eliminated by this expedient. All replacement blades were shot peened at the roots to improve fatigue strength. After vibration-frequency checks were made and the rotor was balanced, the unit was shipped back to Argonne. The turbine was in operation again on June 4. Total outage time was 35 days.

E. Main Condenser

The main surface condenser (see Fig. IV-10), located in a horizontal position directly below and parallel to the turbine, is a divided water-box type with a single-pass cooling-water circuit. It incorporates an air-cooling section at each end of the condenser and a deaerating hot-well. Under normal conditions, the condenser weight is carried by the turbine exhaust flange which is joined by a structural weld to the condenser neck. Since the condenser-turbine joint weld is deposited from the inside,

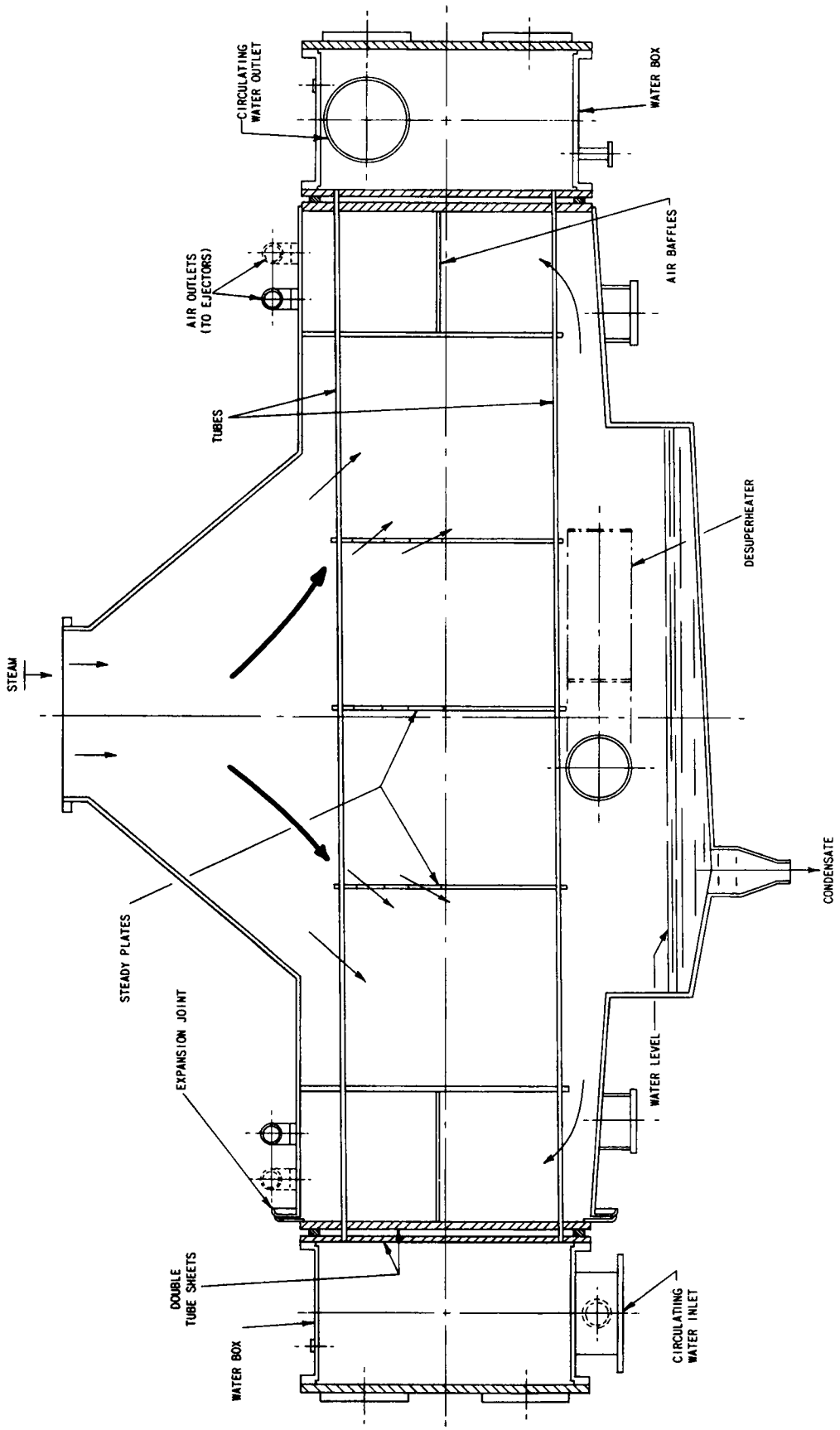

Fig. IV-10

EBWR Condenser (Courtesy Allis-Chalmers Mfg. Co.)

a personnel access hole is provided in the neck of the condenser. Similar access holes are located in the sides of the hotwell, inasmuch as there is a vertical partition which longitudinally divides the hotwell.

The condenser has been designed for an internal pressure of 20 psig. Pressure above 20 psig causes a relief diaphragm to rupture, and steam is discharged to the power-plant atmosphere. In view of the seriousness of a circulating water leak into the steam cycle, double-tube sheets are used to secure each end of the condenser tubes. A sight glass mounted on the drain tank monitors any leakage.

Aluminum has been used for the condenser tubes in place of conventional copper bearing alloys, as it reduces the radioactivity level in the reactor circuits. Regions in the condenser where the tubes are directly exposed to water particles from the turbine exhaust steam are protected by stainless steel shields snapped on over the vulnerable surface of the tubes.

The condenser hotwell and the water boxes have been longitudinally divided to permit plant operation even in the event of a tube rupture. By means of a change in reading of the conductivity cells in the condensate lines, a tube rupture would promptly be detected. Upon discovery of a tube rupture, the inlet and outlet motor-operated circulating water valves (isolating the half of the condenser containing the ruptured tube) must be closed by the operator.

When plant operation calls for reactor steam to bypass the turbine, the steam passes through the bypass valve directly to the 14-in.-diameter desuperheater pipe and into the hotwell. With normal circulating water flow available, the desuperheater is capable of passing full reactor steam flow without danger to the condenser. If condenser circulating water supply should fail, the two desuperheating sprays located in the 14-in.-diameter desuperheater pipe must be manually placed into operation. If any of the 20-in. motorized butterfly circulating water valves should be closed, the limit switch on the valve will automatically open the desuperheater spray line.

To inhibit corrosion in the vertically divided condenser water boxes, the face of the tube sheets has been sprayed with metallic aluminum. The balance of the interior surface of the water boxes has been covered with a layer of neoprene.

Pressure testing of the steam space was performed with compressed air at 20 psig. The first pressure test was applied after the tubes were rolled into the inner tube sheet to permit a separated check for leak-tightness. The rolling and flaring operations were then completed and the

pressure tests continued. Small amounts of Freon were introduced for purposes of leak detection. In lieu of the gas test, the conventional shop hydrostatic test was eliminated to assure a rust-free condenser shell before going into service. In interest of minimizing rusting during the storage period before plant startup, bags of silica-gel and a vapor-phase inhibitor were placed in the shell before sealing it for the gas tests.

II. Modifications for 100-Mw Operation*

A. Pressure Vessel Modification

The modification of the EBWR pressure vessel for the intended operation at 100 Mwt involved major alterations to the original design of the pressure vessel. Figure IV-11 shows the location and denotes the items added, namely, the replacement of the 6-in. steam-line nozzle with a 10-in. nozzle, 3-in. condensate return-line nozzle with a 6-in. condensate return line, the installation of two new $1\frac{1}{2}$-in. gage-line nozzles at a location somewhat higher in the pressure vessel than were the old gage nozzles, and the installation of a new (third) 3-in. instrumentation nozzle (when thermal sleeve is installed the actual instrumentation connection is only 2 in.). The machining and subsequent welding of this modification for the 100-Mw operation of the EBWR had been preceded some six months earlier by the installation of two instrumentation nozzles at the neck of the reactor. Many of the techniques used in the installation of the two 3-in. nominal pipe-sized nozzles through the stud ring forging (i.e., neck of the vessel) in February and March of 1959 were used in the more rigorous modification later on. In both cases, the work was done from within the vessel and completed with no detrimental effect upon the personnel performing this operation. In both alterations, a complete practice run was conducted in a full-scale mockup of the anticipated job. Techniques were perfected in the practice, pilot drilling and boring, and welding of a clad, curved plate of similar size and composition as that encountered in the wall of the EBWR pressure vessel. This careful practice exercise permitted the perfection of techniques and equipment, as well as providing training of the personnel so that the actual modification to the EBWR vessel required only 55 days.

Strict adherence to safety procedures prevented workmen from receiving more than 300 mr/week or more than 100 mr in any one day. Each new major step in the modification process involved an assay of the radiation field, then decontamination by scrubbing and scraping to reduce the radiation field (by removing loose radioactive material), followed by the installation of the necessary radiation shielding for the machinists. Once the necessary platforms and shielding had been installed, the personnel began each new process, such as new machining, torch cutting, welding, grinding and the subsequent cleanup operation, attired in an air-breathing mask. Oddly enough, the highest air-borne activity was measured in the

*N. Balai, T. Kettles, E. Martinec, and J. Matousek

final cleanup sanding of the vessel. The readings during this maximum hazard condition were 20% of the permissible β-γ dose rate for Co^{60} at the sander and 5% just outside the vessel. Analysis of this β-γ activity during all operations indicated that the major activities were due to Co^{58} and Co^{60}. Activity, both at the sander and outside the vessel, was less than the permissible value for unknown isotopes.

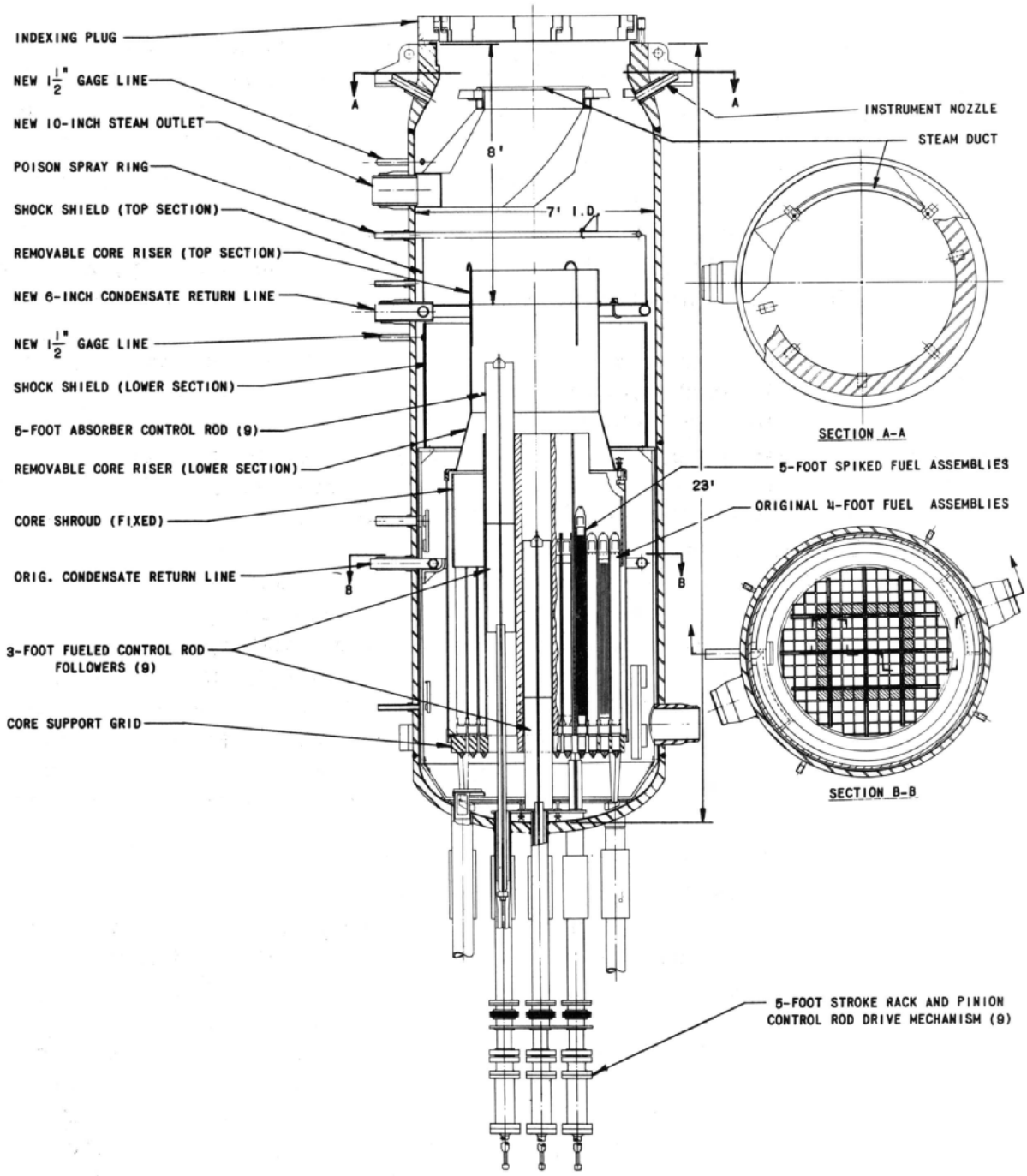

Fig. IV-11

EBWR 100-Mw Pressure Vessel Modifications

Referring to Figs. IV-4, IV-11, and IV-12, the step-by-step operation used was as follows:

1) Remove fuel and control rods from the reactor. (This again involved a major operation in that the control rods had to be cut into three sections and removed as approximately 5-ft long segments in the fuel-handling coffin before further machining operations could be done.)

2) Dismantle the removable shielding from the upper pipe tunnel in the 8-ft-thick concrete shielding. (This involved the dismantling of the composite shielding which consisted of concrete blocks that formed the 8-ft-thick concrete shielding, $\frac{1}{2}$ in. of ferroboron plaster, 2 in. of lead shield bricks, and two 6 x 3.5-ft pieces from the $\frac{3}{4}$-in. carbon steel cylinder that forms the inner surface of the shield.)

3) Cut piping leading to the reactor vessel, namely, the steam outlet line, the poison injection line, and the liquid-level gage lines.

4) Dismantle the $\frac{1}{8}$-in.-thick, 6.5-ft-diameter stainless steel shock shield that lines the vessel in the vicinity where the machining was to take place. Before this shield could be removed, surface decontamination scrubbings had to be conducted. The original average activity of 1 r/hr at 2 in. at the shock shield inner surface was reduced some 10% on vertical surfaces and 67% on horizontal surfaces. The men conducting the washing and dismantling of the shock shield conducted their work on a bucket-type platform which was lowered into the vessel by the overhead crane. Exposure to radiation was considerably reduced by raising the water level to 2 ft below the actual work area, thus making it possible to conduct the necessary work on the top of the shield without being subjected to the full radiation of the entire shock shield. By lowering the water level and the platform in intervals, it was possible to conduct each of the necessary shearing of the fastener bolts down the full height of the shock shield. When completed, the four sections of the shock shield were removed and disposed of in the burial grounds.

5) Remove the old steam ring by grinding off the lugs which supported the 6-in.-diameter steam-collector ring and sawing this circular pipe section into two pieces, sealing the two pieces and removing them from the vessel.

6) With the necessary reactor vessel components removed, decontamination procedures were conducted on the vessel walls. Operation in the reactor vessel was conducted as shown in Fig. IV-12. With the working platform in position for the lowest hole (the new $1\frac{1}{2}$-in. water nozzle), the workers were exposed to the highest working radiation background of the entire operation, namely, 15 mr/hr. The maximum radiation 2 in. from the vessel wall was 80 mr/hr. In this position the shielded platform, consisting of 3 in. of lead plus $\frac{3}{4}$ in. of steel, was positioned just above the core shroud with the reactor water level just 2 in. above the shroud.

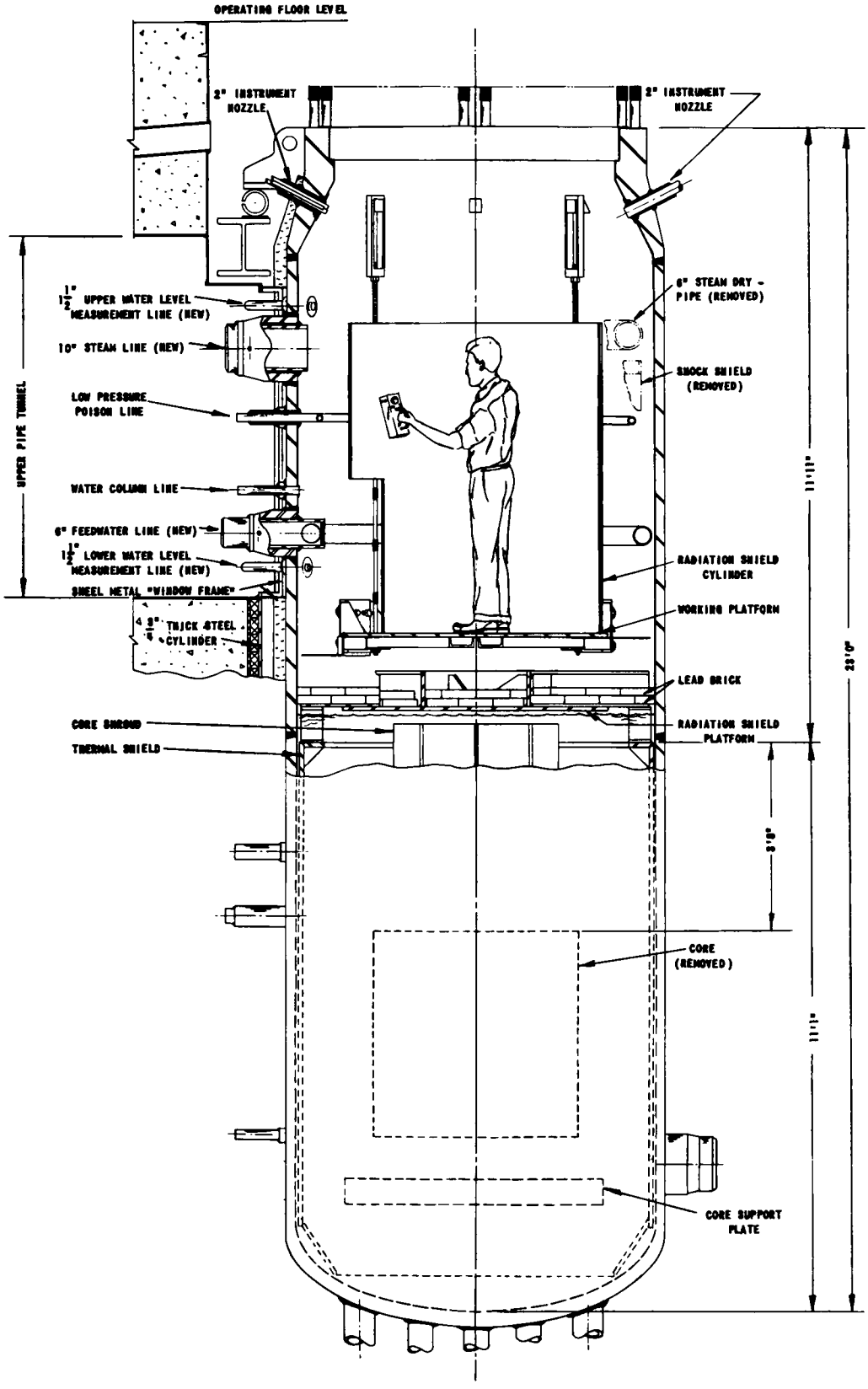

Fig. IV-12

Pressure Vessel Modification Construction Apparatus
111-9335-A

7) New and/or enlarged holes were cut into the pressure vessel. In the case of the enlarged steam-line nozzle and feedwater-line nozzle, $16\frac{5}{8}$-in. and $11\frac{5}{8}$-in.-diameter holes, respectively, were cut with an oxyacetylene torch and then ground-finished to obtain the desired 10° side taper. The two new $1\frac{1}{2}$-in. nozzle penetrations and the 3-in. instrument nozzle penetration were cut with a portable air-operated drill. Preparation of the five holes required $6\frac{1}{2}$ days (24 working hours per day).

8) New nozzles of carbon steel SA-105 Grade-II bar or SA-106-C hollow rounds were welded to the vessel with E-7015 electrodes and stress-relief peened on each weld layer. Welds were gas-heat preheated and held at a 300°F interpass temperature. The new nozzles are carbon-steel, lined with stainless steel (but not bonded). Prior to installation in the vessel, all nozzles were X-rayed, hydrostatically tested, and leak tested with helium.

9) Stainless steel liners were inserted in the nozzles and welded to the outer ends of the stubs of the nozzles, and the liner diaphragm plate was welded to the vessel cladding. This practice, used in the earlier construction, allows differential expansion between the dissimilar metals with minimum restraint. The carbon steel nozzle welds were radiographed with a 13-c iridium source to assure a sound and defect-free weld. The stainless steel diaphragm welds were then leak checked with 200-600 psi nitrogen through the $\frac{1}{4}$-in. pipe in the clad-base metal leak-detection monitor system, installed on all steam, feedwater, and instrument nozzles.

10) Upon completion of the installation of the nozzles, the reactor vessel internal structures were reassembled in the reverse manner from disassembly.

a. Two halves of the feedwater-distribution ring inserted and welded together and welded to the feedwater nozzle, and ring support lugs on the inside of the vessel.

b. Install new shock shield. The new shock shield, although consisting of multiple segments, now also consists of a top and bottom section as opposed to a one-piece bolted section used in the earlier vessel design.

c. Reinstall the liquid poison-injection ring.

d. Attach the new steam duct to the new 10-in. steam-outlet nozzle.

11) Upon completion of the work inside the vessel, new pipes were arc-welded from the nozzles to terminals outside the reactor shell. The pipe and fittings were matched before assembly and supported rigidly to assure close alignment. Consumable rings and shielded tungsten arcs were used for the root passes, with helium serving as the blanketing gas within the pipes. Observation of 90% of the back welds was possible by using careful assembly sequence and mirror arrangements. Dye penetrant was used to inspect root passes from the inside of the welds. Pipe welds outside the shield were ground to $\frac{3}{32}$-in. maximum reinforcement and examined with dye penetrant but were not radiographed.

12) Finally, the pipe tunnel was repacked with the necessary thermal- and radiation-shielding materials, and sealed.

B. System Modification

In the modified operating scheme, the 100 Mw of thermal power generated in the reactor is dissipated by two systems: 20 Mwt is utilized by the turbine-generator system, and 80 Mwt is absorbed by the new heat-dissipating system. The heat-dissipating equipment supplies steam to the Laboratory heat-distribution system or to the air-cooled heat exchangers. An intermediate loop is incorporated to prevent any possibility of contaminated steam escaping into the heating system. Primary steam condensed in the primary reboiler generates steam in the intermediate loop. Intermediate steam is condensed in the secondary reboiler and/or in the air-cooled condenser. Secondary steam is generated in the secondary reboiler and directed to the Laboratory system. In the revised plant, the turbine-generator system is unchanged and is used to generate up to 5 Mw of electrical power in the same manner as in the past. There are no significant mechanical or equipment changes in the turbine-generator system, except for an operating change in the turbine by-pass valve. The flow diagram for the 100-Mw system is shown in Fig. IV-13.

During operation of the reactor at 100 Mwt, the additional heat-removal equipment is capable of transferring approximately 67 Mw (227,000 lb/hr at 200 psig) to the Laboratory system. At 100-Mwt reactor output, about 10 Mwt of the remaining 13 Mwt is dissipated to the air-cooled equipment and 2 Mwt is lost to both the primary deaerator and intermediate flash tank systems. If desired, the amount of heat distributed between the secondary reboiler and air-cooled heat exchangers can be proportioned in accordance with need. During the winter, sufficient steam is generated to supply all Laboratory heating requirements. Any excess heat not required by the Laboratory heating system during the winter is absorbed in the air-cooled equipment. In an emergency the air-cooled heat exchangers can sustain the entire load of 77 Mw, providing the ambient air temperature is below 65°F. Hence, in winter, continuous operation of the EBWR facility is assured whether or not the secondary heat

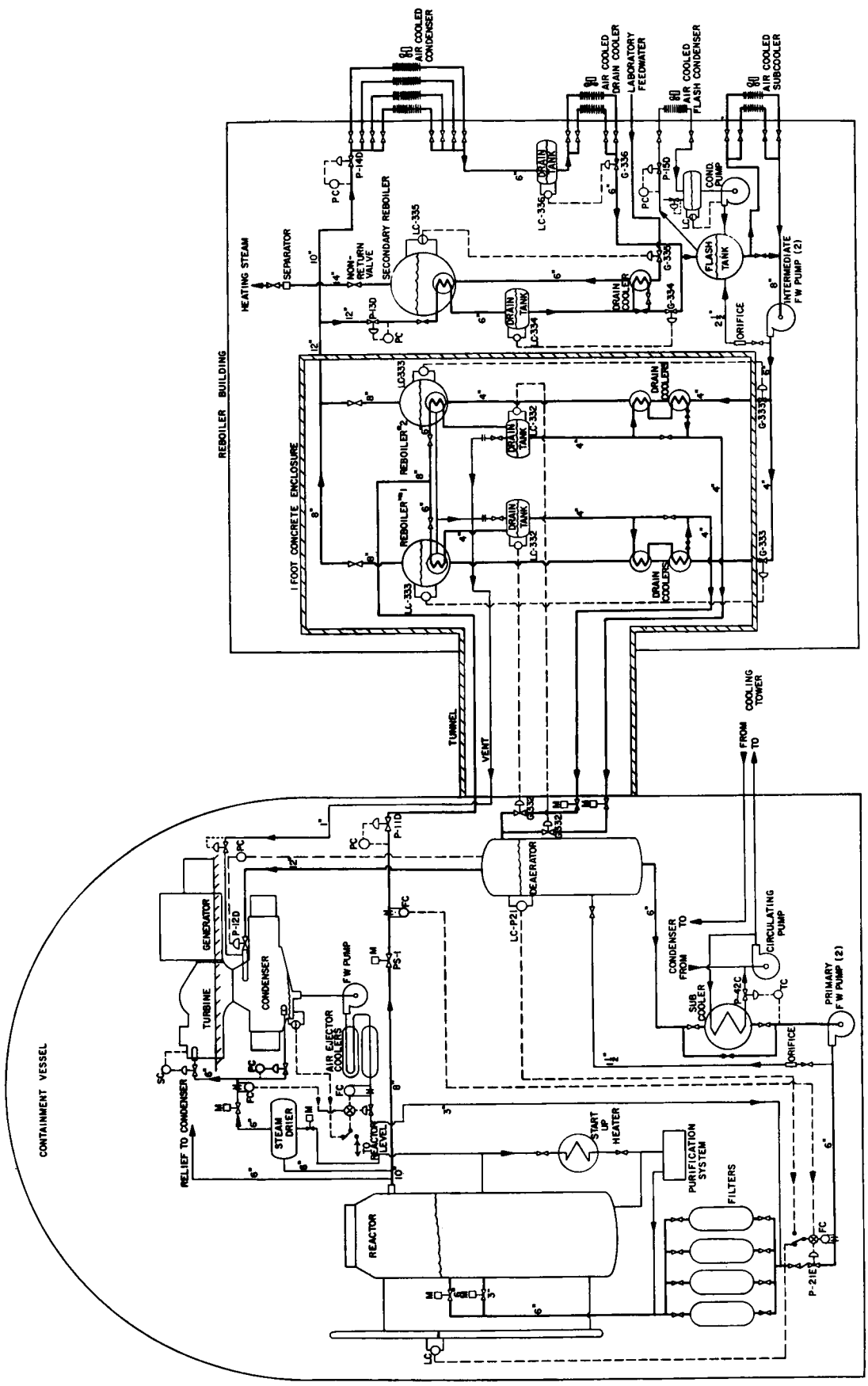

Fig. IV-13

EBWR - 100-Mwt Flow Diagram

111-9480

exchangers are operative. Combined heat exchanger capacity is available to operate the reactor at 100 Mw during the summer. The air-cooled equipment is not designed to accept singularly the entire 77-Mw load. At an ambient air temperature of 95°F, the air-cooled exchangers remove a maximum of 67 Mw; at lower air temperatures capacity increases. Normally, the secondary exchangers are supplied with 10 Mw during summer, which, when coupled with the 67 Mw of the air-cooled exchangers, accounts for 77 Mw. If the secondary exchangers are inoperative during the summer, reactor power must be correspondingly reduced commensurate with ambient air temperature.

Based on a heat-balance analysis, the maximum capacities of the modification equipment are listed as follows:

Primary reboiler	65.1 Mw
Primary drain cooler	20.7 Mw
Deaerator	3.23 Mw @10 psia
Primary subcooler	5.1 Mw
Secondary reboiler	56.6 Mw
Secondary drain cooler	10.1 Mw
Air-cooled condenser	57.6 Mw
Air-cooled drain cooler	10.1 Mw
Air-cooled flash condenser	1.36 Mw @34.5 psia
Air-cooled subcooler	7.12 Mw

The new heat-dissipating system is divided into three parts; the primary system, intermediate system, and secondary system. The primary system is operated at 560 psig saturated, the intermediate at 350 psig saturated, and the secondary at 200 psig saturated - which is the pressure of the existing Laboratory steam system. It was necessary to locate most of the new items of equipment outside the containment shell because of internal space limitations. The primary feedwater pumps, deaerator, subcooler, two new filters, and associated appurtenances are located in the containment shell. The primary heat exchangers, secondary heat exchangers, flash tank, blowdown tank, drain tanks, and intermediate pumps are all housed in the reboiler building. The air-cooled intermediate heat exchangers are located out-of-doors next to the reboiler building. For safety, the primary heat exchangers and primary piping, connecting the exchangers with the reactor system, are housed within a relatively gas-tight concrete enclosure inside the reboiler building. All electrical cables and pipes leading from the containment vessel are sealed against an internal building test pressure of 15 psig. There are five penetrations through the shell to accommodate the primary system piping to the adjacent reboiler building.

Previously, a trip of the activity monitor of the vent stack of the containment vessel closed the inlet and exhaust air ducts in addition to shutting down the reactor. This system has been modified to include automatic closure of the air-operated steam-control valve (and bypass) in the trip circuitry of the stack monitor of the containment vessel. Provisions are incorporated in the circuit to override manually the latter feature should the operator decide to dissipate heat to the reboilers in spite of high activity in the containment vessel. The activity-monitoring system has been expanded to include the primary reboiler enclosure and connecting tunnel. Effluent air discharged from the enclosure is monitored before being vented through the stack in the reboiler building. If activity is detected in the reboiler building enclosure, one air-operated valve in all lines (except the vent line) and the steam-control-valve bypass are automatically closed and the reactor is shut down.

About 80 Mwt is directed from the reactor to the primary reboilers via a steam back-pressure control valve, resulting in a reduction of steam pressure from 600 psig to approximately 560 psig. During actual operation of the turbine-generator and new steam plant, should the load drop out on the steam plant, the turbine bypass valve can dump excess steam to the condenser until such time as either the reactor overpressure interlock initiates reactor shutdown at 640 psig or some other affected device shuts down the reactor. Also, should the turbine load be dropped out, any excess steam that cannot be condensed by the reboilers without a pressure rise will be dumped to the condenser by the turbine bypass valve.

Primary steam is condensed in two primary reboilers, as shown in Fig. IV-14, operating in parallel. Primary steam condensed on the tube side of the reboilers regenerates steam in the shell side for the intermediate system. The two primary reboilers are each designed to condense 150,000 lb/hr of steam at 560 psig and 482°F. The quality of the intermediate steam leaving the reboiler shell is about 98 per cent, this being accomplished by the incorporation of a dry pipe within the reboiler shell.

Since the intermediate steam pressure is normally set at 350 psig and the shell water level is constant, the condensing pressure in the reboiler tubes is a function of the primary steam flow. The amount of heat transferred is directly related to the steam admitted to the reboilers. The temperature differential between the two fluids is inherently self-adjusting and fixed for any specific steam flow. Increase in the primary steam flow results in higher condensing pressure, which increases the heat transfer rate. Therefore, at partial loads the reboilers are self-adjusting to meet the conditions. Primary steam-condensing pressures can vary, according to load, from slightly over 350 psig to approximately 560 psig, if necessary.

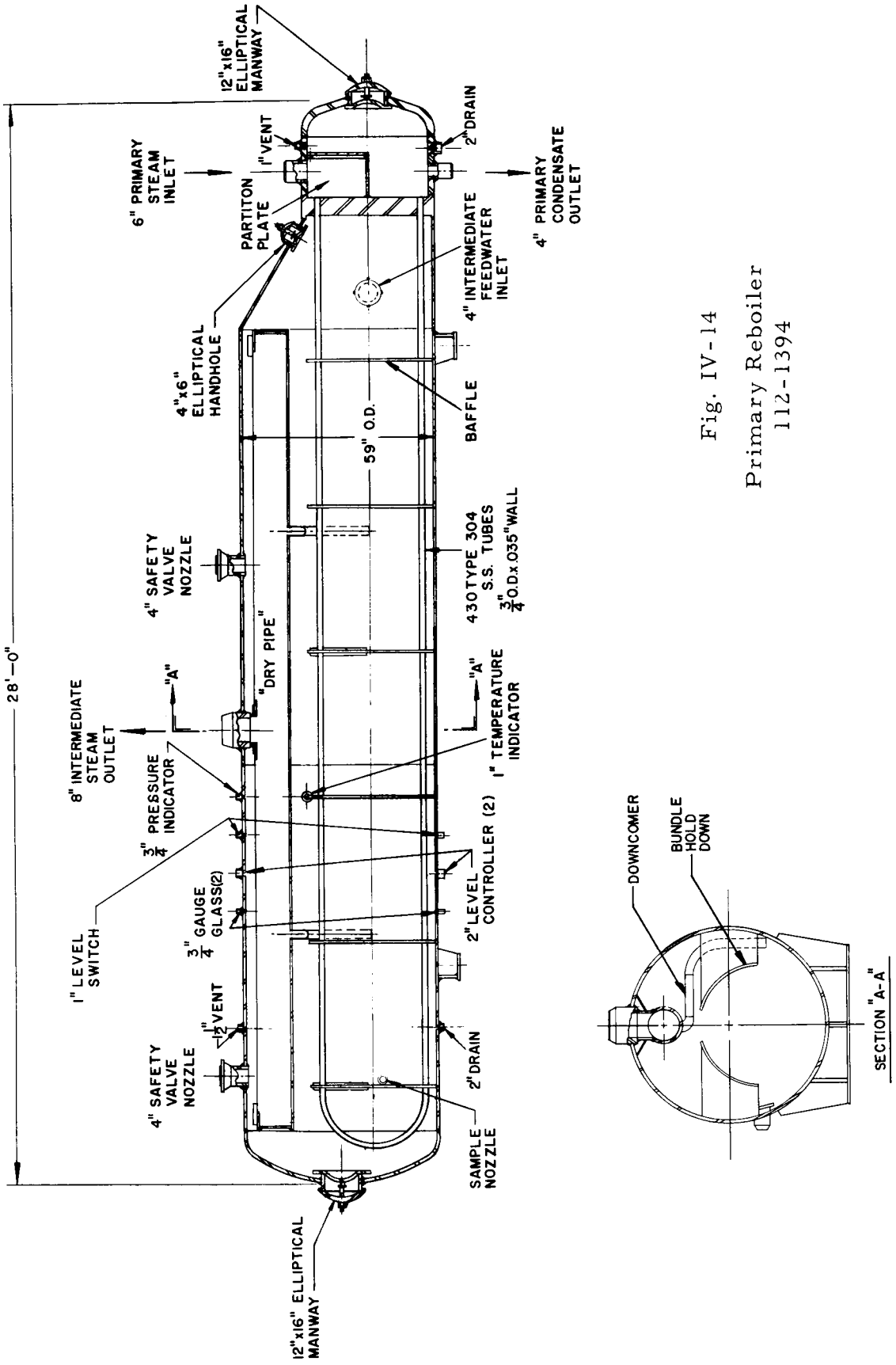

Fig. IV-14
Primary Reboiler
112-1394

The tube side of the primary reboilers is designed for 800 psig and 520°F, while the shell side is designed for 400 psig and 448°F. Each primary reboiler shell is provided with a chemical feed inlet nozzle for the addition of:

1) trisodium phosphate to maintain the desired pH and to prevent scale formation; and

2) sodium sulfite to scavenge dissolved oxygen.

Piping is arranged for independent chemical treatment of either reboiler by utilizing the pressure drop over the associated feedwater valve for the introduction of the chemical solutions. The blowdown connection is located approximately 6 in. below the normally maintained water level in the shell, since solids concentration is generally greatest near the top.

Each of the two primary drain tanks has a total capacity of 300 gal and is designed for 800 psig and 520°F. The primary steam condensed in the tubes of the primary reboilers is accumulated in the primary reboiler drain tanks and then flows through the primary drain coolers to the deaerator. The level of the condensate accumulated in the drain tank is maintained by controlling the flow to the deaerator. Liquid level is maintained independently in each vessel during operation by its respective level controller and associated air-operated control valve. Drain tank effluent is directed via a 4-in. line to two primary drain coolers connected in series (see Fig. IV-15). The effluent from each of the drain coolers is then conducted to the deaerator. Each drain tank and reboiler exit heater are provided with bleed orifices to vent a portion of the noncondensable gases and prevent any accumulation. The combined capacity of the drain coolers is sufficient to subcool 264,000 lb/hr of primary condensate from 482°F to 231°F, and raise the temperature of 247,000 lb/hr of intermediate feedwater from 160°F to 435.7°F. At these flow rates and temperatures, 20.68 Mw of heat are exchanged.

Radiolytic dissociation of water in the reactor results in the formation of hydrogen and oxygen. Separation of these gases at the liquid interface is followed by carryover in the effluent steam. The rate of the combined gases thus generated amounts to about one SCFM per 20-Mwt reactor power. Therefore, at 100-Mwt operation about 5 SCFM of hydrogen and oxygen are liberated. The distribution of these gases is directly proportional to the division of steam to the turbine and reboiler.

Discharge to the primary deaerator is regulated by the two air-operated control valves. Condensate leaves the primary drain coolers at a pressure of approximately 525 psig and at temperatures varying from 321°F to 340°F, depending upon the mode of operation. Flashing of condensate to the low pressure in the deaerator results in further cooling and

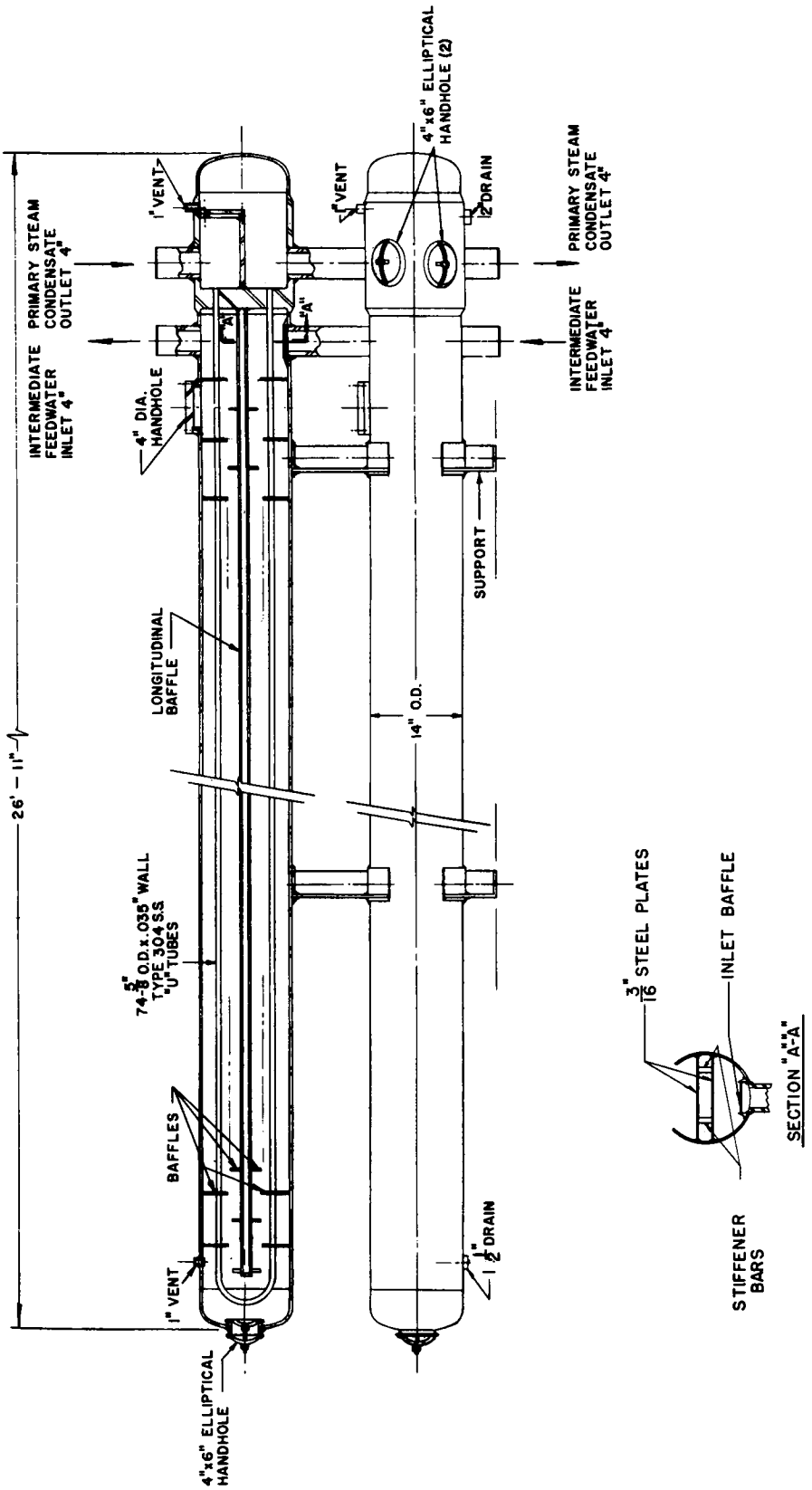

Fig. IV-15

Primary Drain Cooler

112-1395

the removal of noncondensable gases. Flashed steam and noncondensate gases are piped to the condenser via a 12-in. carbon steel line. Noncondensable gases are removed from the condenser by the air ejector and radioactive gas-disposal system.

Design of the deaerator is based on a maximum flow of 301,000 lb/hr flashing from a condensate temperature of 339°F to a deaerator pressure of 90 psia. At these conditions, 6570 lb/hr of condensate are flashed which, along with the extracted noncondensables, are sent to the condenser. Normally, the temperature of the condensate is between 230°F and 235°F, and the deaerator is operated at 10 psia. At this condition, about 10,450 lb/hr of vapor are formed. Deaerator pressure is varied in accordance with mode of operation throughout a range of 10 psia to 90 psia. Depending upon operation, the amount of condensate flashed varies from two to four per cent. Figure IV-16 shows details of construction of the deaerator.

Further cooling of the condensate after the deaerator is accomplished in the primary subcooler as shown in Fig. IV-17. The cooling water tower located 150 ft south of the containment vessel is used as the heat sink for the removal of heat from the subcooler. Condenser exit cooling water at a temperature of 95°F is used for cooling and is obtained from the discharge side of the circulating pumps. Cooling water return from the subcooler is directed back to the suction side of the pumps. Approximately 25 psig water pressure is available to circulate cooling water through the subcooler. Primary condensate is directed through or bypassed around the subcooler in accordance with mode of operation. The subcooler is designed to remove a maximum of 5.1 Mw with a condensate flow of 235,570 lb/hr. At this flow rate the temperature of the condensate is decreased from 193.2°F to 120°F. Approximately 1000 of the 13,000 gal/min of the cooling water circulated through the condenser is used at the design condition.

Two reactor feedwater pumps, one of which serves as a standby, are installed in the primary circuit immediately following the subcooler. The drive unit of each pump is a 3550-rpm, 350-hp electric motor. The pump is designed to give sufficient head to assure adequate flow of feedwater to the reactor even in the event of overpressure in the vessel. The differential shut-off head of the pump is 2220 ft of the water being pumped which, under the worst condition of 320°F feedwater temperature, is equivalent to 873 psi. At a feedwater temperature of 120°F, the 2220-ft head is equivalent to 952 psi. This shut-off head permits pumping of feedwater well past the opening pressure of the last relief valve, which is set at 775 psig. Both pumps are provided with a strainer, warm-up orifice, and minimum flow orifice. Minimum flow for each pump is 20 gpm. This amount is maintained by the minimum flow orifice in order to prevent damage to the pump should flow be interrupted. The minimum flow orifice discharges to the deaerator.

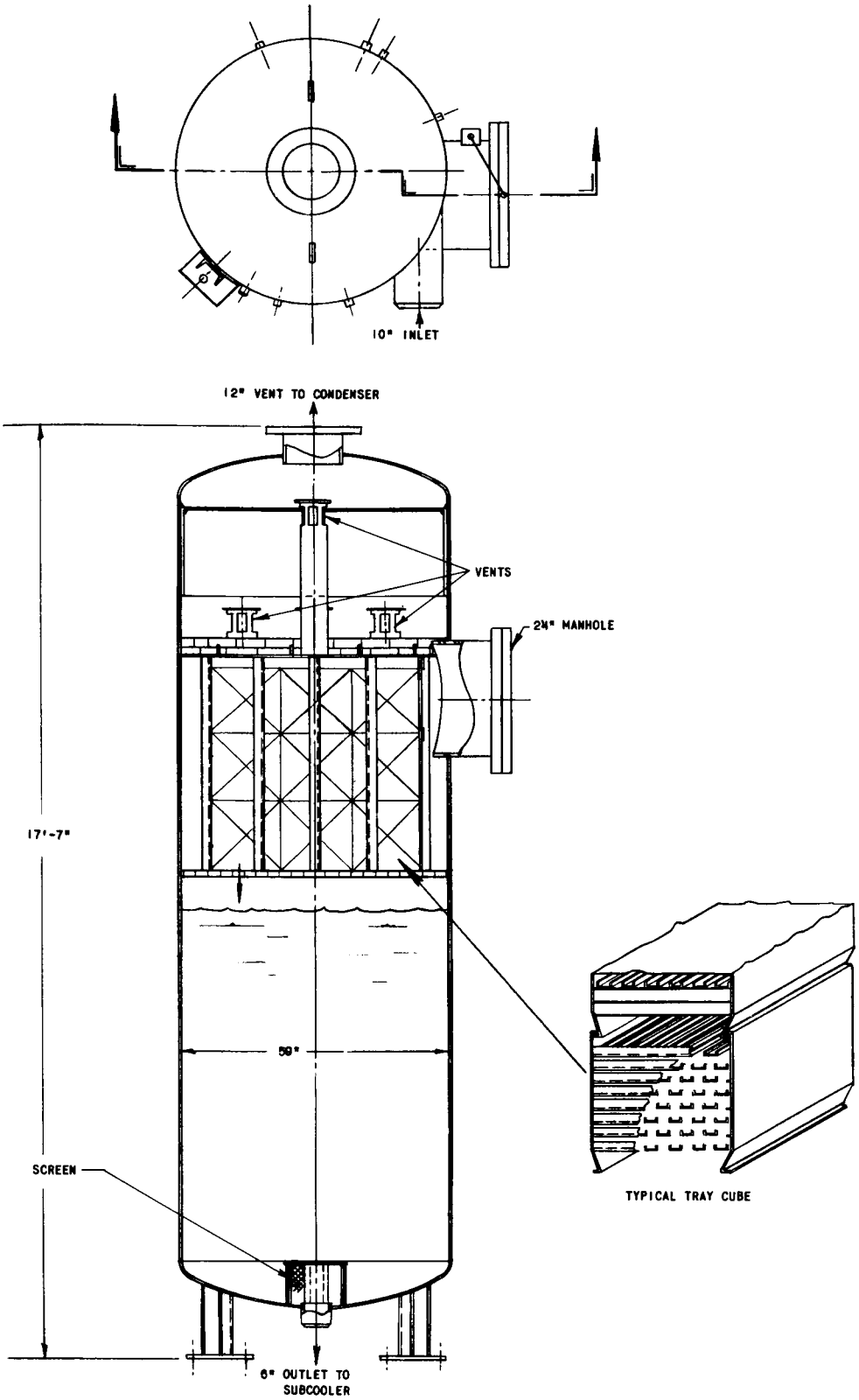

Fig. IV-16

Deaerator
112-1397

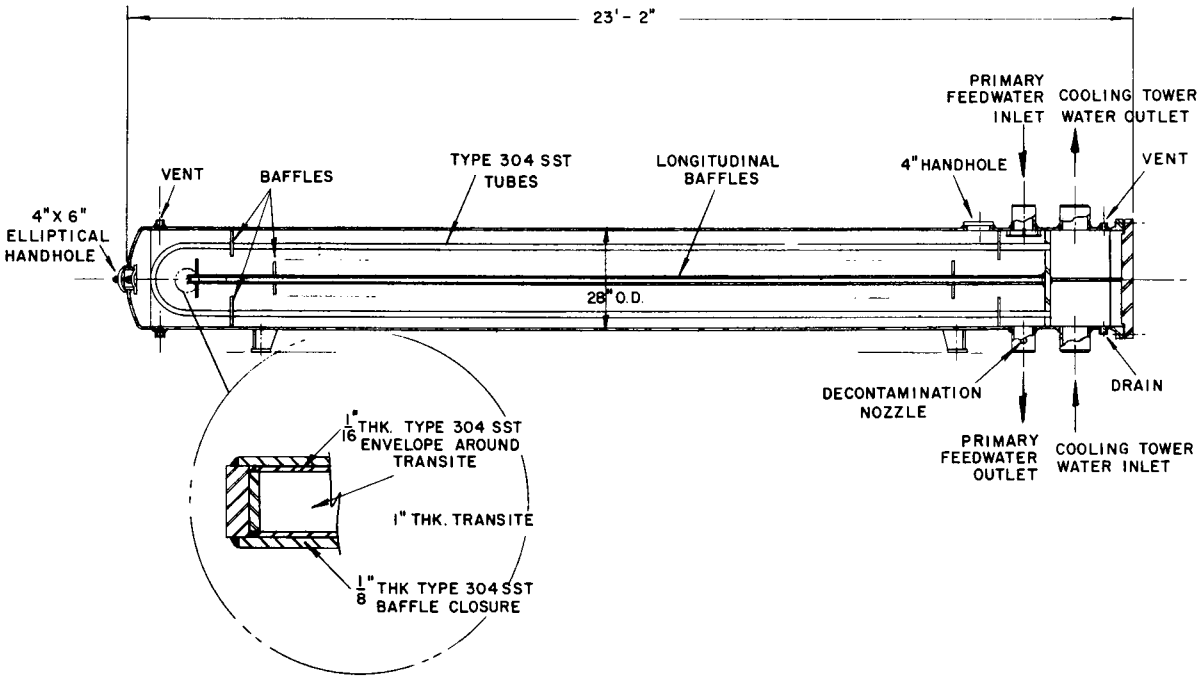

Fig. IV-17

Primary Subcooler
112-1396

Reactor water level is maintained by the new 4-in., electrically operated feedwater control valve. Feedwater flow from the turbine-generator plant is controlled by hotwell level, feedwater flow, and turbine steam flow. Regulation is obtained by the feedwater regulator.

Discharge from the new feedwater pumps is mixed with discharge from the original pumps prior to passage through the filters. Two additional filters have been added to the primary circuit to supplement the two filters in the original plant. The new filters have the same flow capacity as the old filters; each filter is designed for 180 gpm at 120°F. The new filters are of the vertical type with a removable, cotton filter cartridge. The cotton filter material is capable of removing particles in sizes of 2 μ or larger.

The first and most important method of preventing excessive overpressure is the automatic insertion of control rods when reactor pressure exceeds 640 psig. In the event of malfunction of the normal heat-removing equipment and failure of the reactor shutdown mechanism and/or emergency shutdown, a system of pressure relief is provided to protect the primary system. This system consists of one steam-powered pressure-regulator valve and four pop-safety valves located on the reactor steam line. Opening of any safety valve will initiate shutdown of the reactor. The

control rods are backed up by the boric acid system. Injection of the high-pressure boric acid is completed in about 20 sec after manual initiation, thereby guaranteeing permanent shutdown before the temporary relief afforded by the expulsion of steam has ended. The intermediate piping connecting each reboiler to its corresponding drain coolers contains no valves which can isolate the latter vessels from the reboiler. Hence, the system can be assumed as one unit, and safety valves on the reboiler are sufficient. These safety valves can handle any incident in the drain coolers providing the connecting lines are free of isolating devices. In the event of internal tube failure in the drain cooler, it is impossible for the vessel to become overpressured by the primary system since the steam space in the reboiler offers protection as a buffer.

The decay heat which must be removed from the reactor decreases from a maximum of 6% of operating power immediately after shutdown to about 1% after 7 hr. During normal shutdown, the reactor is cooled by removing the decay heat by boiling. The steam generated is rejected to the condenser through the steam bypass valve until the reactor temperature reaches about 260°F. Thereafter, the secondary coolers of the purification system are used for further cooling. The circulating pumps are kept in operation to supply cooling water to the main condenser to condense any steam that enters the condenser from the steam traps in the steam lines.

In the event of a shutdown caused by loss of electrical power, the emergency shutdown cooler is used to remove decay heat. Operation of the emergency cooler is initiated manually from the control room or automatically upon loss of instrument air or 125-v (DC) power. (The cooler is designed to remove 1000 kw at a steam pressure of 600 psig. During emergency shutdown caused by power failure, reactor pressure will rise until 610 psig is reached; thereafter, steam will be discharged through the turbine bypass valve to the condenser until such time as the emergency cooler capacity equals the steam formation at 610 psig. If the turbine bypass valve is unable to handle the steam load, the relief valve will limit the reactor pressure to 650 psig.) Even though the condenser is not supplied by the circulating water pumps at this time, sufficient cooling is available by natural circulation in the condenser to absorb the steam discharged.

Emergency shutdown cooling relies upon natural-circulation flow of water from the 15,000-gal storage tank located in the overhead dome of the containment vessel. Reactor steam is condensed outside of the cooling coils, and the condensate flows back to the reactor by gravity. The steam-water mixture formed within the tubes is directed back to the storage tank. The difference in density between the cooling-water supply and steam-water mixture establishes natural circulation between the

emergency cooler and storage tank. The main steam valves in the line to the reboilers are closed during operation of the cooler to reduce the loss of reactor water.

The system for high-pressure injection of boric acid is a standby system designed to reduce the reactor core reactivity below criticality should the control rods fail to operate properly under shutdown conditions. The original feature of automatic injection has been eliminated in favor of manual operation for the 100-Mw system. The volume of concentrated boric acid solution is able to handle more than 13% reactivity.

With minor exceptions, all additional equipment and piping for the primary heat-dissipating equipment is stainless steel. The stainless steel surface in contact with the primary fluid imposes only a minor additional burden on the water-purification system. Therefore, more capacity has not been added to the reactor water-purification system, since it is adequate for the 100-Mw operation.

The intermediate steam generated in the primary reboilers is directed either to the secondary reboiler (see Fig. IV-18) or the air-cooled condenser (see Fig. IV-19), or both, depending upon mode of operation. Once the condensing pressure is selected, shell pressure being maintained at 200 psig, the amount of intermediate steam admitted to the tubes is fixed by its dependence on heat transfer area and the coefficient of heat transfer. In short, the secondary reboiler essentially generates a constant supply of steam to the Laboratory. Since the generation of secondary reboiler steam is fixed by operator choice, the intermediate system must be provided with at least a single degree of freedom to allow for normal pressure control in the event of fluctuations in the primary or Laboratory system. Consequently, intermediate steam pressure must be, and is, regulated by a 10-in., electrically driven control valve which admits steam to the air-cooled condenser. In this respect the arrangement is analogous to the pressure control for the primary system.

Intermediate condensate formed in the secondary reboiler is discharged into the secondary drain tanks from whence it is directed to the tubes of the secondary drain cooler (see Fig. IV-20) where further cooling is accomplished. The intermediate condensate is flashed to the lower pressure maintained in the flash tank. Steam formed by flashing is routed to the air-cooled flash condenser where it is condensed, collected in the condensate tank, and returned to the flash tank by the condensate pump. Steam admitted to the air-cooled condenser is condensed and flows to the drain tank where liquid interface is maintained. Effluent from the drain tank is further cooled in the air-cooled drain cooler from whence it is directed to the flash tank. The intermediate condensate in the flash tank is pumped to the primary drain cooler shell by the intermediate pump, and thence to the reboiler shell where its cycle is completed.

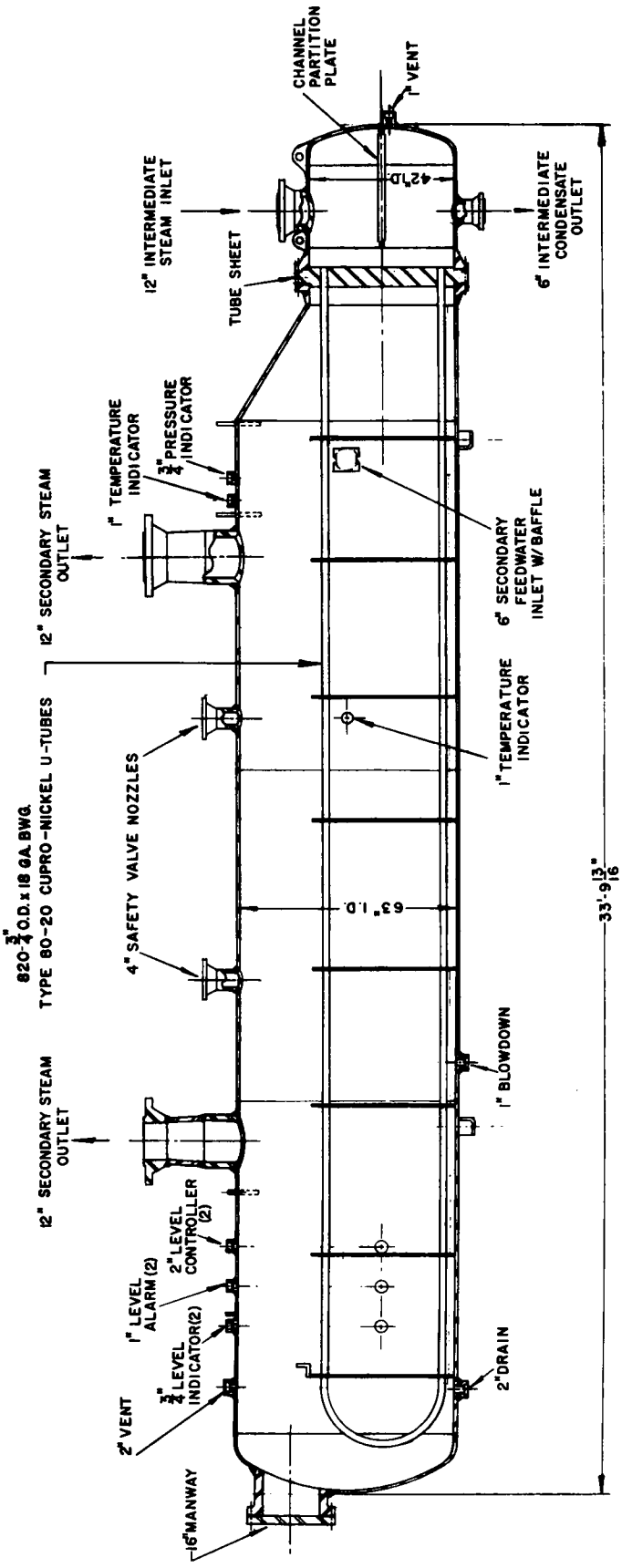

Fig. IV-18

Secondary Reboiler
112-1392

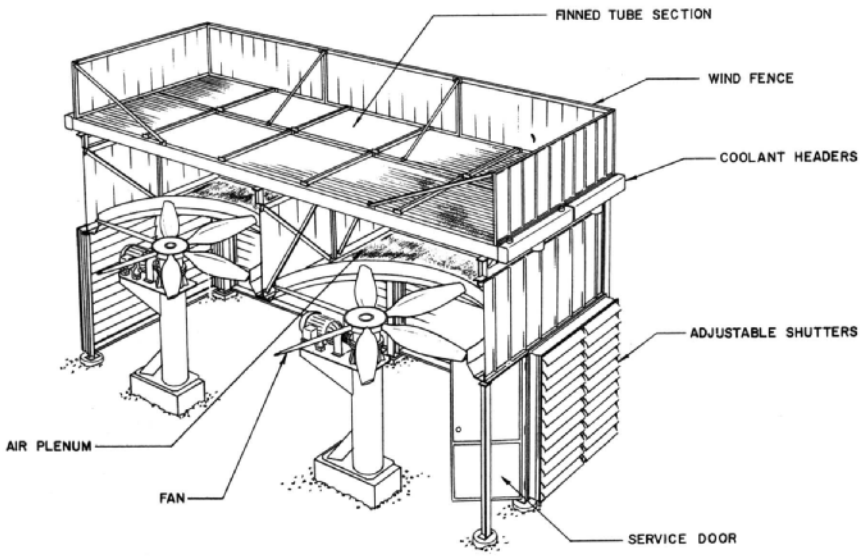

Fig. IV-19

Typical Air-Cooled Heat Exchanger Arrangement
112-1398

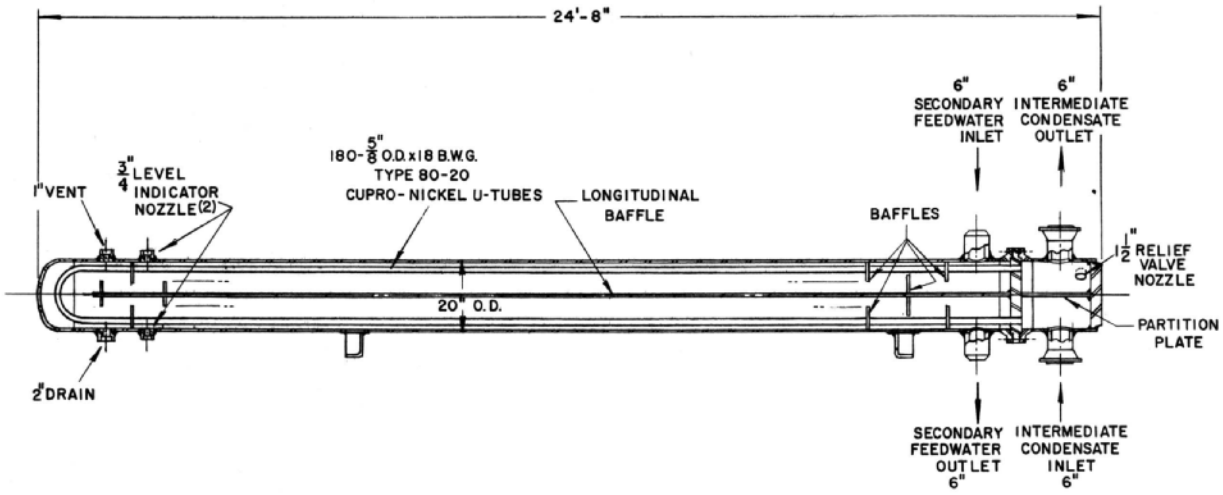

Fig. IV-20

Secondary Drain Cooler
112-1393

As mentioned previously, Laboratory changes in demand are prevented from being reflected back to the reactor. Although changes in Laboratory demands will affect the operation of the secondary reboiler to some extent, reasonable variations are damped completely by the operation of the flash tank and air-cooled flash condenser.

The secondary reboiler is designed to condense a maximum of 241,000 lb/hr of steam at 310 psig and 424.7°F at a mean temperature differential (corrected) of 36.7°F. In so doing, 227,000 lb/hr of saturated steam are generated at a shell pressure of 200 psig. The steam as provided to the Laboratory has a quality of 99.75 per cent, this being accomplished by passing the steam through two horizontal, line-type separators. The tube side of the secondary reboiler is designed for 400 psig and 448°F, whereas the shell side is designed for 250 psig and 406°F. The secondary reboiler shell is provided with a chemical feed-inlet nozzle for the addition of trisodium phosphate to obtain the desired pH to prevent scale deposition, and sodium sulfite to scavenge dissolved oxygen. A blowdown connection is located at the bottom of the reboiler shell, since it is expected that sludge will form.

The secondary drain cooler is designed to subcool 241,000 lb/hr of intermediate condensate from 424.7°F to 289.8°F, and raise the temperature of 227,000 lb/hr of Laboratory feedwater from 230°F to 376.5°F. Normally, the temperature of the Laboratory feedwater leaving the secondary drain cooler is 388°F, which corresponds to the saturation temperature of the secondary reboiler shell. The tube side of the drain cooler is designed for 400 psig and 448°F, and the shell side is designed for 250 psig and 406°F.

Because of the limited water supply at the Laboratory, dissipation of heat during summer operation is provided by air-cooled heat exchangers. Although this form of heat sink is capable of performing its intended function, it leaves much to be desired during winter operation. Actually, the installation of this type of unit for the function desired is unique for this section of the country, because of freezing difficulties that can be encountered. However, protective features have been incorporated in the installation which reduce the probability of freezing. The air-cooled exchangers are of standard design for this type of equipment, incorporating finned tubes and motor-driven fans. Each unit consists of vertical shaft fans which force air upward across the horizontal tube bundles.

The air-cooled condenser unit consists of eight, equally sized, horizontal, single-pass heat exchanger sections arranged for parallel flow. The entire unit is capable of condensing 245,000 lb/hr of steam at 310 psig with an ambient air temperature of 95°F, this being equivalent to 57.6 Mw of heat. The air flow at this rate of heat transfer is 3.4×10^6 lb/hr. Its exit temperature is 336°F. Four fans are mounted below the unit to furnish the air flow, and each 12-ft-diameter fan consists of six blades. The condenser is designed for 400 psig and 448°F.

The air-cooled drain cooler unit is composed of two horizontal, four-pass, heat exchanger sections. The entire unit is capable of cooling 245,000 lb/hr of intermediate condensate from 424.7°F to 291.7°F

with an ambient air temperature of 95°F, this being equivalent to 10.1 Mw of heat. The air flow maintained to accomplish the heat transfer is 0.72×10^6 lb/hr, and its exit temperature is 295°F. Three fans are used, and each 7-ft-diameter fan consists of six blades. The drain cooler is designed for 400 psig and 448°F.

The flash condenser consists of one horizontal, single-pass, heat exchanger section. A condensing rate of 4930 lb/hr at 19.8 psig is obtainable in the unit at an ambient air temperature of 95°F, this being equivalent to 1.36 Mw of heat. Approximately 0.6×10^6 lb/hr of air are required at this condensing rate for an effluent air temperature of 127°F. Three fans are available, and each 7-ft-diameter fan consists of four blades.

The air-cooled subcooler unit consists of two, equally sized, horizontal, four-pass, heat exchanger sections. The entire unit is capable of subcooling 246,600 lb/hr of condensate from 258.5°F to 160°F at an ambient air temperature of 95°F. For this heat dissipation of approximately 7.12 Mw, an air flow of 1.2×10^6 lb/hr is required for an exit temperature of 180°F. Two fans are installed below the heat exchanger deck, and each 12-ft-diameter fan consists of four blades.

Two intermediate feedwater pumps, one a standby, feed the flash-tank condensate to the primary drain cooler on the shell side. Each pump is capable of delivering 600 gpm of water with a differential head of 1040 ft across the inlet and outlet connections of the pump. Both pumps, which are of conventional design for this type of service, are of the horizontal, centrifugal, split-case type.

SECTION V

SHIELDING

M. Grotenhuis

NOTES AND EDITED DATA FROM LECTURES - June 28, 1961

SECTION V

SHIELDING

Shielding may be defined as "the study of radiation distribution in matter." This, of course, suggests an overlap with many other aspects of a reactor system although it is often relatively easy to guess quickly the approximate amount of shielding necessary for a given system, it is frequently necessary to use quite refined techniques to obtain a detailed knowledge about the radiation distribution in the system. The field of shielding provides an excellent example of how industry, the national laboratories, and the universities can cooperate in the advancement of a technology. The universities, by means of staff research and thesis work, are in a position to investigate many of the problems associated with shielding. The national laboratories are in a position to do the research requiring larger equipment and greater capital costs. Coordination of this information may be best accomplished by a national laboratory. This combination, with the aid of the American Nuclear Society as a professional clearing ground, should be able to supply the primary user (industrial firms) with the necessary theory and data with which to solve design problems.

The field of shielding may be split according to the reactor type, i.e., mobile or stationary. The approach to shielding problems is quite dependent upon the reactor type of concern. In the case of shielding for a mobile reactor, weight is a crucial factor, and, depending on the importance of the reactor, it may of necessity virtually be shielded with pure money. In practical terms, this means the use of exotic materials or at least of more or less exotic arrangements of ordinary materials. Money must not be a major concern in the design of the shield for the mobile reactor, or the project is not likely to continue. In contrast, stationary reactors may be shielded with ordinary materials, usually ordinary concrete. In specific instances a heavy concrete may be economically advisable; for example, beam holes in research reactors may be more easily utilized if they are kept as short as possible. Further, the costs may be reduced by shortening penetrations and by reducing the size of the containing building. Speaking of costs, it should be noted that there are commercial enterprises based on the construction of reactors. Therefore, it is not enough that "an extra measure of concrete may remove doubts;" it may also remove too much money.

The design of a shield for a reactor includes many complex problems concerning the distribution of the associated radiation. There are many fine theoretical analyses indicating what radiation will do in more or less ideal situations. For example, the distribution of neutrons in water from a monoenergetic source is well known both theoretically and experimentally. The application of these methods to a laminated shield of water and iron becomes less exact. For more complicated, though common, combinations of iron, water, concrete, and boron, the problem is solved only

by quite doubtful methods. The moments method can solve the problem of the distribution of gamma rays in a shield composed of a single material quite accurately; however, a shield composed of more than one material may still be solved only by approximations. No universal method for computing buildup through multilayer shields exists, although some progress is being made in this direction. Solving all these problems in a solid unperturbed shield still does not answer all the questions, since there will be a multitude of penetrations and voids that will change the radiation distributions in ways that at best may be only estimated. As a result, shield designers have to be educated guessers to a large extent and must depend quite strongly on experimental data and semi-empirical approaches. Although high-speed computing machines are becoming more useful all the time, they still cannot be used to solve a complete shield problem, even disregarding the void and penetration problems that inevitably appear.

In addition to the simple hand-computing procedure, there are other approaches--none of which are really independent. These include comparison methods, utilizing data from bulk shield facilities, specific experimental determinations, and, of course, computing-machine methods. The latter are of great value for particular parts of the shield design problem or for the more ideal problems that will aid the thinking done prior to making an educated guess. The choice of method, as well as being a somewhat personal choice of the designer, depends on the type of shield desired, the accuracy required, and the time and money available. Since virtually every approach contains approximations, this fact must be kept in mind so that the method used in designing one shield is not used on the next design without reconsideration of the basic assumptions. In shields that must be optimized to a very high degree, for example, those of mobile reactors, the detailed calculations must be verified with experimental mockups. Since a full-scale mockup is the only real test, a facility that is essentially the total shield must be built, or else a degree of uncertainty will exist until the actual plant is operated. A practical approach that may be utilized at times is to leave a portion of the shield flexible until full-power operation indicates the final answer.

The choice of the basic shield material or materials is one that must be evaluated in terms of the reactor involved. For a power reactor with few shield penetrations, the basic material may well be ordinary concrete. If the reactor is for research and will contain many beam holes, a thinner shield will no doubt be worth consideration. Concrete which is made more dense by the use of metal punchings and/or a heavy aggregate is then desirable, as the penetrations will be shorter and less expensive. When a dense concrete is utilized, the building itself will be smaller and a saving may be realized in construction costs. This is particularly true if the building is gas-tight. For extremely efficient shields, such as for a mobile reactor, more exotic materials, such as heavy metal hydrides or, at least, more expensive arrangements of ordinary materials, may be necessary.

Neutrons will be found in the reactor core as a direct result of the fission process. There are, on the average, 2.5 neutrons produced per fission of uranium-235, with an energy distribution according to the well-known fission spectrum. There will be delayed neutrons from fission, usually not significant in shielding problems, and neutrons from photoneutron reactions in materials such as beryllium or deuterium that may be utilized for their neutron-reflecting and moderating properties. The latter source of neutrons may be significant in cases where the reactor is in a shutdown condition. The specific activity of N^{17}, formed from the $O^{17}(n,p)\ N^{17}$ reaction, includes a neutron that may well be of importance in determining the access to the coolant pipes in the case of a water-cooled reactor.

Gamma rays may originate essentially anywhere in the reactor system that neutrons are found. The reactor core is a copious source of gamma rays that have their origin in the fission process, the decay of fission products, the inelastic scattering of neutrons, or the capture of neutrons in structural or coolant materials located in the core. The latter gamma rays may be further classified as the immediate result of neutron capture, "capture gamma rays," or of the decay of the unstable nuclei created by neutron capture, "radioactive decay gamma rays." The gamma rays born in the core are deep within the shield and usually of lower effective energy, so that they rarely determine the shield thickness. However, they are an important source of heat generation within the inner shield layers and may also figure prominently in instrumentation problems.

Gamma rays that originate outside the core are essentially all due to neutron capture or inelastic scattering in the structural and shield materials. The capture gamma rays are of higher effective energy and in greater quantity than those resulting from the fission process, decay of radioactive nuclei, or inelastic scattering, and, in addition, are created nearer the outer extremity of the shield. These facts explain why capture gamma rays are very often the controlling influence in determining the shield thickness and may never be disregarded in shield-design problems. It is to control the generation of capture gamma rays that materials of high cross section, such as boron, are incorporated into a shield. In such a material the capture gamma ray is of low energy, the remaining portion of the energy being given off as an alpha particle. Coupled with the importance of the capture gamma ray is the difficulty of predicting the location at which it will be created. This problem is essentially the heart of the reactor shield-design problem.

Shielding a reactor consists primarily of moderation and then absorption at thermal or near-thermal energy of the fast neutrons produced in the reactor core, plus the attenuation of the secondary products involved, chiefly gamma rays. Other radiation from the core usually produces local effects, such as gamma-ray heating in materials in or near the core. There are no extremely efficient materials for stopping fast neutrons that can compare with boron in the case of thermal neutrons. Fast neutrons must be reduced in energy by elastic or inelastic scattering. Probably the most

efficient way to reduce the neutron energy is by a combination of inelastic and elastic scattering. This may be considered convenient from the standpoint of including structural materials and gamma-ray shield materials, both of which will be needed and both of which require the heavy material necessary for efficient inelastic scattering. The elastic scattering will be provided by lighter materials, preferably by a hydrogenous nature.

In general, an efficient shield should have a neutron attenuation that is nearly the same as the gamma-ray attenuation. Since neutrons are attenuated by a reduction in energy, followed by absorption, they require a material of low mass. Gamma rays are more rapidly attenuated by a material of high mass or high atomic number (Z). These materials are conveniently efficient for fast-neutron attenuation also, by virtue of their inelastic scattering ability, if they are followed by hydrogenous material. In order to follow the above attenuation requirements this means that a homogeneous mixture of, perhaps, uranium and water would be an ideal shield, except for the additional complication of having fissions in the shield. Including reasonable cost, as well as structural requirements, the heavy material usually turns out to be lead and/or steel. Since a homogeneous compound such as a metal hydride is expensive, not always stable, and does not necessarily contain the most efficient proportion of metal to hydrogen, this is not a solution at the present time. A laminated structure, the next approximation to homogeneous, is nice, but quite expensive. This is exemplified by water-filled metal honeycomb structures, by laminated water and metal, or masonite and metal. The next best homogeneous material is concrete, and it turns out to be quite well balanced if the density is increased by including heavy aggregate, metal punchings, or both. The heavy concrete is more expensive, but the extra expense may well be justified in reduction of building costs or an increase in accessibility. Concrete is somewhat in question because of lack of detailed knowledge on the amount of water retained or the absolute minimum amount that must be contained for adequate moderation of the fast neutrons. This lack of knowledge is paid for in terms of the extra thickness of concrete required to guarantee results.

Portions of a reactor shield may not be chosen on the option of a shield designer alone. For example, the pressure vessel may be a few inches of steel and, thereby, an appreciable part of the shield. Likewise, the reflector may be a material that affords a considerable amount of shielding value. Neither of these materials are subject to alteration for strictly shielding considerations, since the primary function is containment and neutron reflection, respectively.

The procedure generally followed in determining the radiation distributions in the shield is to calculate the neutron fluxes and the gamma-ray fluxes. Shield design does not follow the design of the other parts of the reactor, but must progress with it. These calculations must be done more than once, each time progressing a little more toward the final design. As

an example, before the vessel containing the reactor can be designed, shielding calculations must be made to determine radiation heating. The vessel may have to be substantially altered or a thermal shield may have to be incorporated into the design, which, in turn, renders the preliminary calculations obsolete. Similarly, before a thickness of concrete can be established, the heating must again be considered. A common result is that 3 or 4 in. of lead may be required to reduce gamma-ray heating in the concrete. Calculations will again have to be revised. After the total shield thickness has been decided, a look at the largest contributions to the leakage from the shield may indicate a particular source of capture gamma rays could be reduced with proper location of boron.

In 1952, about the time that the first thoughts of the EBWR shield design were being generated, the problems in shielding were known but the methods were unknown, or at least untested. Both fast-neutron and gamma-ray attenuation were assumed to follow the basic point kernel:

$$\frac{C e^{-\sigma R}}{4\pi R^2} \quad .$$

If σ is the total cross section, the net result is the uncollided flux - a quantity which is not directly useful. The basic point kernel had to be adjusted in order to represent the radiation distribution.

The adjustment of the point kernel to suit fast-neutron attenuation was accomplished on an experimental basis by employing the removal cross section. Although this approach is known to have limitations, such as applying in hydrogenous media only, and does not supply enough information for problems of radiation damage, it still merits attention today.

In order to adjust the point kernel to problems of gamma-ray attenuation, it was multiplied by a buildup factor. At the time of the EBWR shield design there was quite a bit of data on buildup available. None of it applied directly to shields of more than one material, and thus the linear form

$$B(\mu R) = 1 + \mu R$$

was used. There are still times when this may reasonably be used today, although additional data permit adjustment.

The fast-neutron flux was then obtained by integrating the following expression:

$$\Phi_f(a) = \int_V dV \frac{Q}{4\pi R^2} \exp(-\sigma R) \; n/cm^2 sec \quad ,$$

over the proper source geometry. Similarly, the gamma-ray flux was obtained by integrating

$$\Phi_\gamma(a) = \int_V dV \frac{Q}{4\pi R^2} \exp(-\mu R)\, B(\mu R)$$

over the proper source geometry.

It was known that the capture gamma rays generated in the shield would be an important part of the radiation escaping the shield. It was further known that they were arising predominantly from the absorption of thermal neutrons. It was not known how to compute the thermal-neutron flux far out in the shield. A suggested method was to make the thermal-neutron source term depend on the fast-neutron current. The fast-neutron current, computed by removal theory, would then provide an approximate source far out in the shield. This approach was used in the EBWR shield design, mostly because no other better solution existed. Further work has indicated that this method still has utilitarian value.

Briefly, this method for computing thermal-neutron flux is the ordinary one-group diffusion problem with a source term:

$$D_s \nabla^2 \Phi_s - \sigma_{as} \Phi_s + Q_s = 0 \quad ,$$

with

$$Q_s = -\text{Div } J_f \approx \nabla \Phi_f \quad .$$

This approach can be adapted to two groups or more, with the derived value of Q (above) being inserted as the source term in the highest-energy group equation considered. The British have been experimentally confirming a six-group analysis. It should be remembered that in the foregoing the assumption was made that, in the initial collision, the neutron energy is reduced to the energy of the highest-energy diffusion equation considered.

The EBWR, as originally planned (see Fig. V-1), was to be a 20-Mw light water-moderated, ordinary concrete-shielded reactor. The procedure followed to obtain radiation-flux distributions necessary to arrive at a fixed shield design was to compute, in the following sequence, the fast-neutron flux, thermal-neutron flux, and gamma-ray flux. This was first done for a preliminary arrangement of moderator and reactor vessel in order to estimate the magnitude of the nuclear heating in the vessel wall and to determine the amount of thermal shielding necessary. The thickness of thermal shield was determined to be 1 in. of steel. When the arrangement of reactor vessel and thermal shield were completed, the fluxes were extended, and the heating in the concrete was established. The radiation heating in the concrete was reduced by adding lead until the heating was at a satisfactory level. As increasing the thickness of the lead also decreases the

total concrete thickness to some extent, the total amount of lead (3 in.) chose was the result of a combination of these two factors. Final selection of the concrete thickness naturally included some factor of safety. Pessimism injected into the calculations served this purpose, as well as rounding off the concrete thickness to an even number of feet. The result was 8 ft of ordinary concrete.

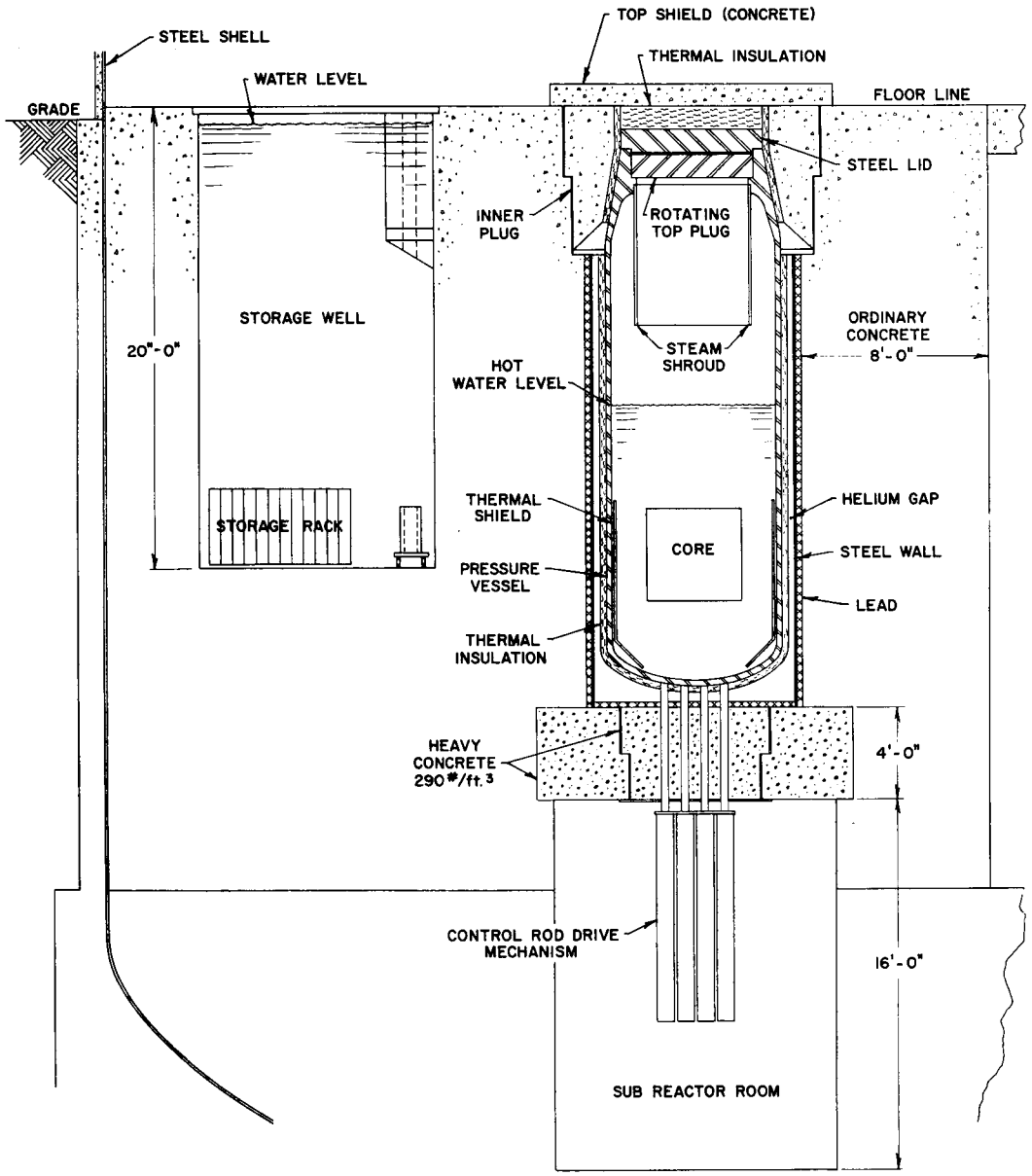

Fig. V-1

Vertical Section of the Light Water-Moderated EBWR Vessel and Shield
139-815

A similar procedure was followed to determine the shield thickness above and below the reactor core; however, there was considerably less available space in these directions. Shield design was thus somewhat limited to what material could best be placed in the available space. The shield design below the core consisted of the selection of materials that could best be utilized in the 4-ft space available. Four feet were selected as a reasonable minimum shield thickness consistent with keeping the control rod extensions in this region as short as possible. Under the circumstances, heavy concrete with steel punchings seemed the obvious choice. The design procedure was very much the same as for the radial shield. The final result included 3 in. of lead, as did the radial shield. The heavy concrete was made of magnetite ore rather than of the preferred limonite, because of availability.

Above the core there were 12 in. of space available for material which was to be selected solely on the basis of its shielding value. The remainder of the shield material in this region was selected primarily for purposes other than shielding. The result was an inordinate amount of iron in the shield. From a shielding standpoint, this does not appear to be a very efficient selection of materials. It presents very little problem in the light water-moderated reactor, as the neutron fluxes are not excessive. Doubts do arise because of the lack of moderating material. In such a shield, the predominant effect on the fast neutrons is that of inelastic scattering. This reduces the neutron energy, but not to thermal levels. Therefore, it is not consistent with the theory of attenuation involved; thus, the results cannot be considered completely accurate. To make up partially for this lack of moderator, ordinary concrete was selected as the most convenient material to locate in the available 12 in. of space.

During the preceding design process, a decision was made to incorporate the changes necessary in order to include operation as a 40-Mw heavy water-moderated reactor. Operation as a heavy water-moderated reactor results in an increase in neutron fluxes and, consequently, a change in shield design. Furthermore, the changes were required by economical and time considerations to be incorporated into the same space allocation as the existing light water-moderated design.

There were three modifications in the radial shield. The steel thermal shield was changed to a 1% borated steel thermal shield, a layer of ferroboron plaster was placed between the lead and the concrete, and the inner 5 ft of ordinary concrete was changed to 220 lb/ft^3 magnetite concrete. Figure V-2 shows the final shielding design of EBWR.

The lack of moderation in the shield above the reactor core became more critical as the neutron intensity was increased. It was then decided to use light water as the moderating material in place of the ordinary concrete. Heavy concrete is, in general, a more effective shield and, by this type of calculation, looks more efficient than water. It must be remembered that

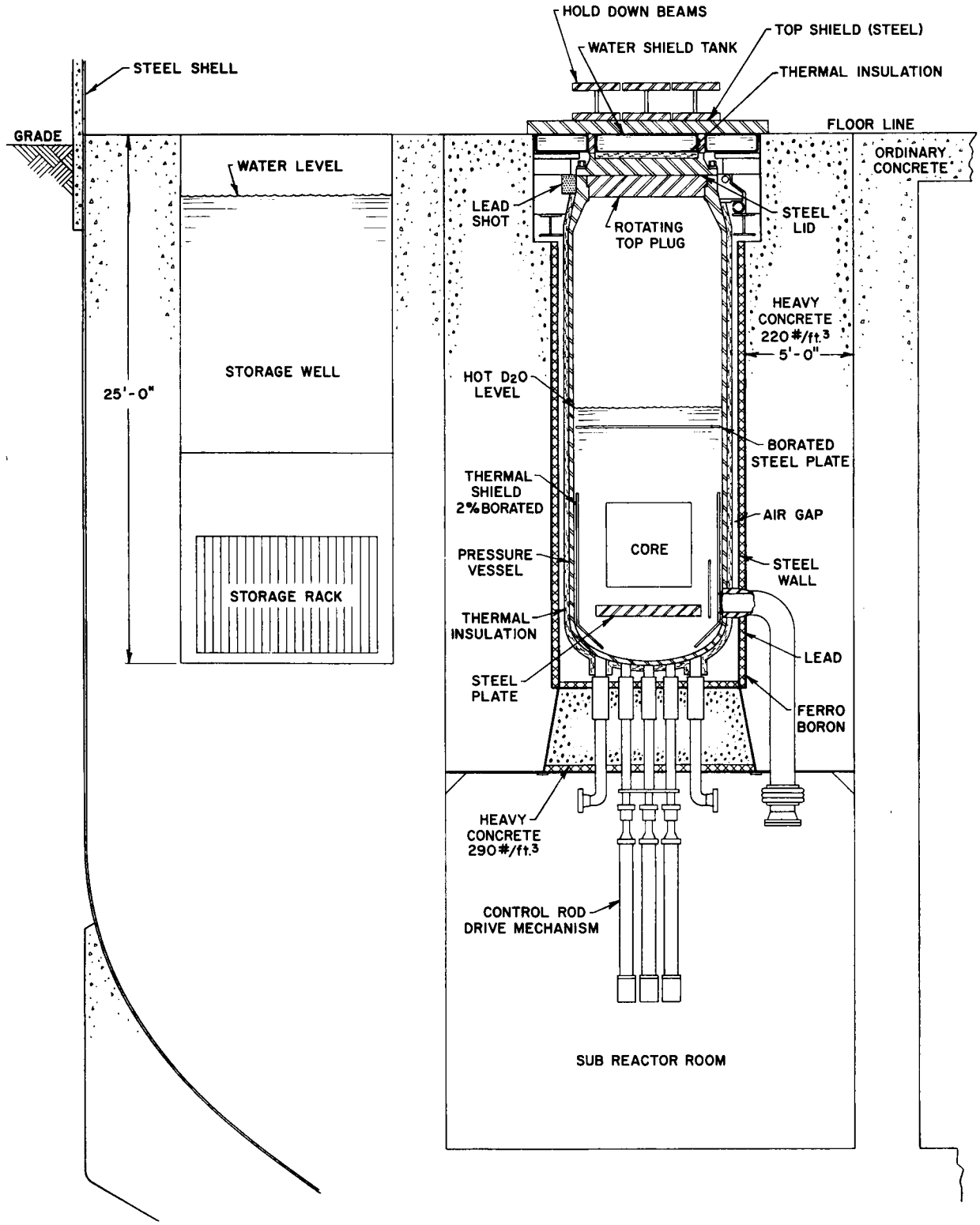

Fig. V-2

Vertical Section of the EBWR Vessel and Shield as Altered to Include Operation as a Heavy Water-Moderated Reactor
139-816

inconsistencies with the theory serve to make the calculation subject to greater suspicion. It is doubtful whether any calculations can accurately evaluate the situation; however, measurements during operation as a light water-moderated reactor may yield information that could shed some light on this problem. Due to the fact that other steel structures above the reactor shield will reduce the radiation level from that which was calculated and that streaming from voids and cracks will increase the radiation level from that which was calculated, it may be difficult to decide even then what the best material for the shield should have been. After some study of the vessel heating above the core and reflector region during heavy water-moderated operation, it was decided to include a 1% borated steel plate above the core but just below the water level. This steel plate replaces the portion of the borated steel thermal shield that extends above the water level. It should aid in reducing capture gamma rays from the steel above the core as well as in protecting the vessel itself. In addition, the problem of cooling a thermal shield extending above the water level is avoided. This plate would be put in place only at such time as the reactor was operated with heavy water.

Hope of attaining radiation levels that personnel might endure in the subpile room during operation seemed rather slim because of the numerous penetrations. A primary consideration was that of equipment activation and, at least in the light water-moderated version, this did not appear to be a problem. The radiation level after shutdown was also of concern, although this could be reduced to permissible levels by placing lead below the penetrations through which the forced circulation pipes pass. The maximum thickness of this lead was estimated to be 8 in. It was recommended that this be determined empirically after operational experience had been accumulated. Three inches of heavy concrete have been replaced by lead at the outer diameter of this shield. This represents a portion of the estimated 8 in. that could have been required.

Other shielding problems include those of compensating for voids caused by piping or structural considerations. This was accomplished by filling the openings around the piping with heavy concrete block backed up by lead brick in places where it seemed advisable, and filling voids around the vessel closure with removable blocks of heavy concrete and lead shot. The procedure used was to keep a constant shield density on a line of sight from core to shield exterior. While this has but little theoretical justification, it will suffice if care is taken that no unreasonable shield arrangements occur. For instance, reducing the shield to lead in any given direction would not be economical, nor would it be likely to produce an adequate shield.

Shield survey measurements while operating at 20 Mw with light water moderator showed no local hot spots in areas of concern. Since the light water-moderated version requires the least amount of shield thickness, this is not an unexpected result. Further, the shield does not have a large enough portion sufficiently free of penetrations in order than meaningful shield measurements may be made.

Useful experiments leading to increased knowledge of the shielding effectiveness and to a better appreciation of the methods applied may be done on the EBWR. These measurements are listed below.

1) Radiation traverses in the radial tubes

The measurements here should include traverses of fast-neutron flux, intermediate-neutron flux, thermal-neutron flux, and gamma-ray flux. Care must be taken to note irregularities in the shield surrounding the tubes.

2) Top plug measurements

The measurements of primary interest in this location are those of fast- and intermediate-energy neutrons. Measurements in this area would involve the problems incurred in operating instruments in high temperatures.

3) Activation measurements

The measurement of N^{16} has been investigated. Much remains to be done in order to really be able to calculate this activity. A similar problem exists with regard to the activation of crud in the cooling water. The activation of argon in the air around the vessel would also be a worthwhile problem to work on.

4) Fuel transfer measurements

Surveys of the fuel transfer have been made to indicate how fuel may be safely handled. This should be related to calculational procedures. It is likely that more measurements should be made, particularly if fuel with a known and simple operating history is available.

SECTION VI

CONTROL RODS AND CONTROL ROD DRIVES

N. Balai
W. Kann
V. Kolba
D. Roy

NOTES AND EDITED DATA FROM LECTURES - June 26, 1961

SECTION VI

CONTROL RODS AND CONTROL ROD DRIVES

I. Control Rods*

A. Original 20-Mwt Core Control Rods

The EBWR control rods are rectangular crosses, 10 in. across the arms. The development of wrought, corrosion-resistant 2 w/o natural boron modification of stainless steel Type 304 resulted in a mixed control rod material installation, although an all-hafnium rod cluster was intended initially. In the selected control rod geometry, the physics calculations indicated that the reactor would remain subcritical with the malfunctioning of any two control rods. A third rod type, a rare earth oxide compact clad with stainless steel Type 304, failed in the screening autoclave tests at temperature and pressure.

The construction of the EBWR afforded an opportunity of reducing the costs of control rods by incorporating a newly developed stainless steel alloy containing high concentrations of natural boron in the original core (Core 1). Numerous out-of-pile performance tests at pressure and temperature established the suitability of the boron-containing stainless steels. The control rods are placed in 3 x 3 square geometry and are actuated externally through pressure seals affixed to the control rod thimbles welded to the lower head of the pressure vessel.

The original hafnium control rods (see Fig. VI-1) were placed in the center and the side positions, while the natural boron-stainless rods (see Fig. VI-2) were located in the corners of the square pattern. The original control rods contained three major functional sections:

1. an upper poison section, either of hafnium or of stainless steel Type 304 containing 2 w/o natural boron;

2. a center Zircaloy-2 follower section to displace the water in the control rod channel, reducing neutron-flux peaking in the water hole; and

3. a lower extension shaft of reduced section and fabricated from Zircaloy-2 (in the region of high neutron flux) and stainless steel Type 304.

A bottom drive was selected to permit the loading and unloading of fuel elements, control rods, and core support structures from the top of the vessel for the future forced-circulation and heavy water reactor modifications. Permanent external biological shielding around the bottom

*N. Balai and V. Kolba

of the reactor vessel and removable stainless steel Type 304 control rod thimble shielding reduce the radiation levels to permit prolonged routine operational surveillance and shutdown maintenance of mechanical and electrical equipment. In the original design, a seat-and-plug arrangement was incorporated into the pressure seal housings to permit the removal of either the control rod drive assembly or of the control rod without draining of the reactor vessel.

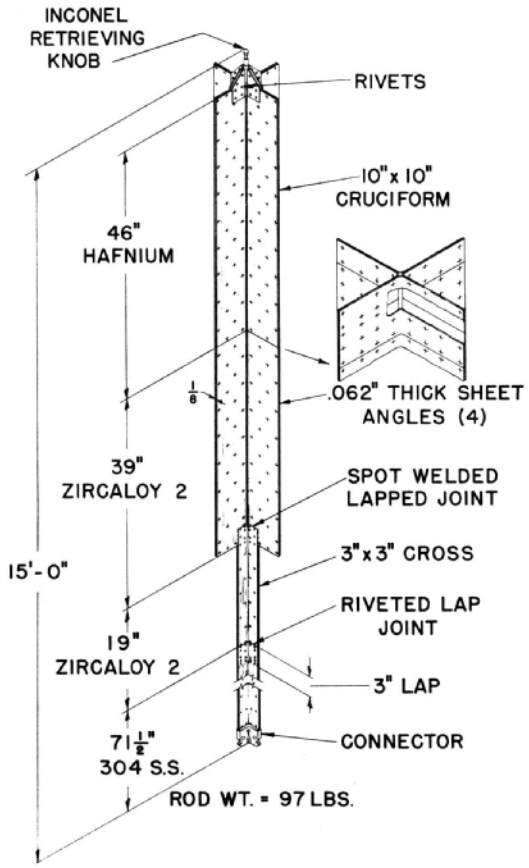

Fig. VI-1

Hafnium Control Rod
111-5517

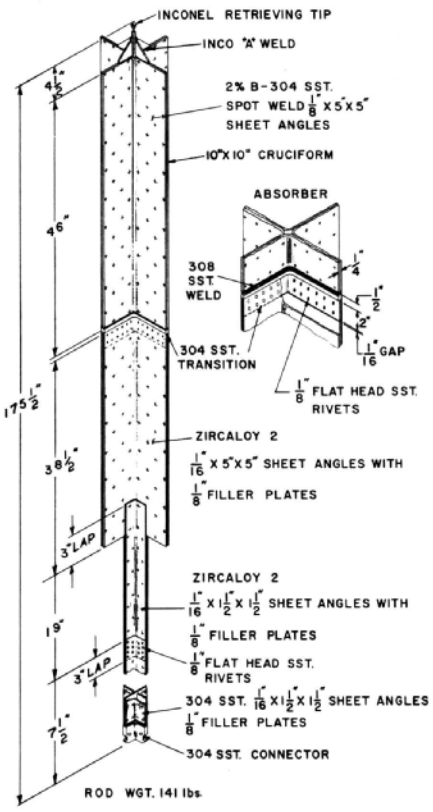

Fig. VI-2

Boron-Stainless Steel
Control Rod
111-5518

Thermal- and fast-neutron effects on hafnium are well known. Since the canned, rare earth-compacted powder control rods failed, only the effects on the boron-stainless steel alloy are presented herein. Irradiation damage to the high boron-stainless steels are theoretically more serious because of the n-α transformation. Four slugs of wrought boron-containing stainless steel containing 1 and 2 w/o natural boron were prepared from 1-in. plate material as 1-in. OD rounds x 5 in. long and irradiated in the MTR for an engineering check of effects.

The results obtained from the cold irradiation were heartening. The following data were significant:

1) no cracking - as shown by dye checking;

2) small increases in hardness and strength - comparable to that sustained by the austenitic stainless steels irradiated to comparable levels; and

3) minor changes in density and dimensions.

Numerous control rod experiments were made after the initial core-loading operations were completed. Only a few of these are summarized.

1) Any of the center rows of the hafnium control rods could be withdrawn without attaining a critical reactor.

2) The four corner boron-stainless steel rods could be withdrawn without attaining a critical reactor.

3) Any three side hafnium rods could be withdrawn without attaining a critical reactor; withdrawal of the fourth side hafnium rod to approximately the halfway point resulted in a critical reactor. The four hafnium side rods have a stronger effect than the four corner boron rods, which are at a greater distance from the center of the core.

4) Any corner boron rod could be traded for any other rod in the core except for an adjacent hafnium rod.

5) The complete withdrawal of either a hafnium or a boron rod coupled with a partial withdrawal of an adjacent rod resulted in a critical reactor. The effect was reproduced at all four corner positions of the control rod geometry.

The original control rods are currently being closely examined to determine irradiation effects. Thus far two defects have been detected:

1) The rivets used to connect dissimilar sections of the rods had begun to fail.

2) There are cracks around the spot welds on the 2% boron poison sections on the first row out from the center.

B. 100-Mwt Core Control Rods

The control rods for 100-Mw EBWR operation (Core 1A) incorporate several features which are an improvement on the previous rods. Improvements lie in the areas of potential increased rod worth, easier

post-irradiation handling, and material cost reduction. The reactivity (rod worth) advantage is gained by substituting a fueled follower cross for the inert Zircaloy-2 follower. In this system, as the poison is removed from the core, fuel is being inserted into the core. Figure VI-3 shows the type of control rods used in Core 1A.

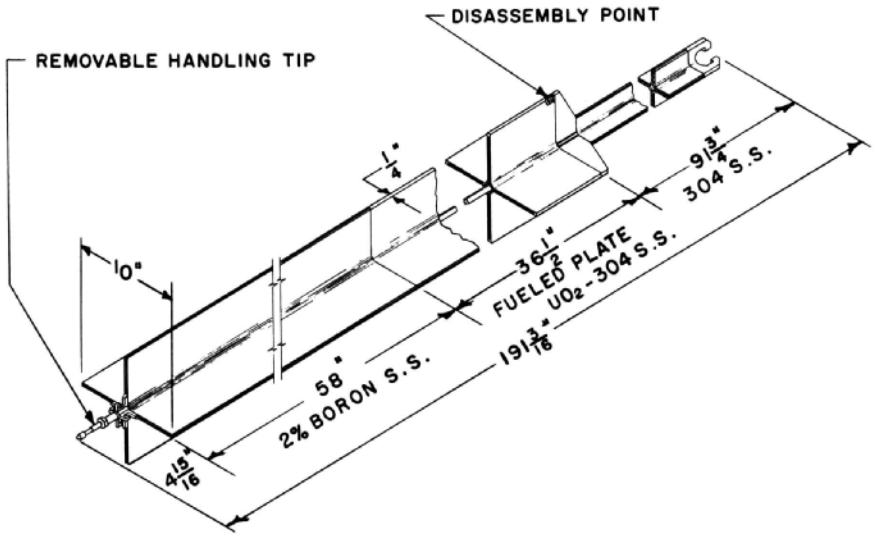

Fig. VI-3

EBWR 5 ft Control Rod with Fueled Follower
111-7960

Post-irradiation handling of the new rod is facilitated by incorporating a disassembly method into the design. This provides for removal of the 10-in. poison and fuel cross from the balance of the rod and handling of this portion in the present coffin for removal to the storage pit. The remaining portion of the rod is then handled by the handling tool, crane, and a small clamp-on shield can.

Cost reduction is accomplished by use of 2% boron-stainless steel instead of hafnium. The reduction arises because of the savings in costs of materials, availability of materials, and the ease of fabrication. The use of fuel in the control rod follower was chosen to add additional reactivity and control capability to the reactor. The amount of fuel used in the plates (~2.6-2.8 w/o UO_2 in 304 stainless steel) approximated the requirements of the fuel-to-surface-area ratio of the present EBWR thin, enriched fuel elements, modified to conform to heat-dissipation capacity and hydraulics of the control rod channels.

The control rod is composed of the following major areas: the poison section, the fueled section, and the 3-in. cross section. The poison section is composed of nominally 2% boron-Type 304 stainless steel. The sheet material was received in 0.125-in. $^{+0.010}_{-0.000}$ thickness stock, 10 in. wide

and approximately 70 in. long. These sheets were hot formed to 90° angles with a $\frac{1}{2}$-in. internal radius. Previous boron sheet had been cold formed; however, this material exhibited a gross tendency to cracking on cold forming, so the warm (hot) forming was attempted and found to be adequate. All remaining sheets were successfully hot formed at approximately 1650°F. Four of these angles were spot welded together to form a cross 10 x 10 in. with blades approximately $\frac{1}{4}$ in. thick.

The fuel section is composed of four plates having 50 g U^{235} per plate in the form of UO_2 dispersed in Type 304 stainless steel and clad with Type 304 stainless steel. These plates were fabricated by the picture-frame technique. The fuel plates are machined to size, a slot is then milled in one edge, and the ears are formed. Four plates are then assembled, and a longitudinal fusion weld made where the ears mate in the radius. This forms the fueled cross.

The poison cross is welded to the fueled plate cross to form one integral unit and machined to length. Holes are machined in the blades of the fueled plates to receive the $\frac{1}{8}$-in. locating dowel pins in the transition piece. The disassembly point is at the junction of the fueled plate and the transition piece. A lifting lug is also welded to the poison section to permit handling into the coffin.

The connection, 3-in. cross, transition section, and $\frac{1}{2}$ x $\frac{1}{2}$-in. bar are made of Type 304 stainless steel and welded together to form an assembly approximately 190 in. long. The connector is machined from a piece of Type 304 stainless steel. The 3-in. cross is made of four $\frac{1}{8}$-in.-thick sheets of Type 304 stainless steel formed to a 90° angle and spot welded together to form the 3-in. cross with $\frac{1}{4}$-in.-thick blades.

Assembly is accomplished by sliding the poison and fuel section over the $\frac{1}{2}$-in. bar and locating it on the transition section by means of the $\frac{1}{8}$-in. dowel pins at each arm extremity. The removable handling tip is then screwed on the $\frac{1}{2}$-in. bar and, when tightened, is back welded to the poison and fuel section-lifting lug. This tack weld is to insure against loosening during operation, but may be broken for disassembly purposes. The rod is then loaded into the reactor for locking to the drive mechanism for use.

A sample rod was constructed and tested in the control rod drive test rig in Building D-208. This unit, except for the fuel plate and poison section is an exact mockup of the design. Stainless steel was used to simulate the poison and fuel section. This rod was cycled in increments of 5000 scrams and examined after each 5000 scrams. The test unit was at pressure but not at temperature. The rig contained water at room temperature and at a pressure of 600 psi maintained by nitrogen overpressure.

Upon examination, there was no indication of failure at the end of a total of 15,000 scrams. A few slightly shiny areas were noted along several of the blade radii where the blade had rubbed the shroud. The amount of wear was negligible and not deemed detrimental to the operation of the unit. With the same rod, the disassembly and handling techniques were also tested. The present handling tool was modified by an adapter. The tack weld was broken between the handling tip and the lifting lug, and the handling tip unscrewed and removed. The simulated poison and fuel section was then removed from the balance of the control rod; the handling tip was then replaced on the bar and the balance of the control rod handled.

Another type of fuel rod is currently under development for Core 2. The major difference between the new rod and the rods for Core 1A is that the UO_2-Type 304 stainless steel fuel follower plate will be replaced by a Zircaloy-2 section. This change has been dictated by hydraulic considerations resulting from the effect of the UO_2-Type 304 stainless steel rod insertion on steam voids in the control rod channels.

II. Control Rod Drive Mechanism*

A. Original 20-Mwt Core Drive Mechanisms

The control rod drive mechanisms installed on the Argonne Experimental Boiling Water Reactor were of an externally operated lead screw-and-nut type in which the control rod extension shafts were driven through pressure breakdown, collected leakage seals. The mechanisms, located below the reactor, were fabricated from conventional industrial materials, such as carbon steel, brass, cast iron, and nylon, and lubricated with grease. They could be serviced during reactor operation and removed from the reactor without the necessity of draining the reactor vessel.

The decision to locate the original control rod drive at the bottom of the reactor was made after due consideration of the operating and design requirements. Since EBWR is primarily an experimental reactor, the fuel might be changed frequently. This was one very strong argument in favor of a bottom drive. After establishing the location of the drives, it became necessary to select a drive that would fulfill the design and operating requirements. Some of the main types considered were:

Sealed Types:

1) completely "canned" drive in which all components are sealed in the reactor housing and the only external connections are electrical;

*W. Kann and D. Roy.

2) hydraulic drive, which uses reactor fluid under pressure to actuate a piston in a cylinder;

3) an electromagnetic jack-type drive which derives its driving force from an external magnetic field.

External Types:

1) rotary seal drive, which has drive mechanism outside reactor (rack and pinion);

2) reciprocating seal type, which also has drive mechanism outside reactor.

Any of the types mentioned, except the hydraulic, can be adapted to the top or bottom of the reactor. The hydraulic unit requires a flooded cylinder, which would prove impractical on top of the reactor.

The decision to locate the drive mechanism on the bottom of the reactor simplified the fuel-handling problem, but it also interjected a very serious problem with respect to operation, namely, dirt. Corrosion products and any other particles will tend to settle on the working parts of a bottom-mounted mechanism. The hydraulic and magnetic jack drives could probably overcome the dirt problem fairly easily, but it appeared that they had design difficulties which might require a long-range development program. A completely canned drive meant that all parts, gears, bearings, etc., would be susceptible to the dirt. An external drive operating through a seal leaves the problem of handling the dirt in the seal elements. In a rotary seal drive, the rack and pinion still operate in the dirty water, which might affect the operation.

After weighing the possibilities, the decision was made to use a linear seal drive and in that way keep all the working parts external to the reactor and limit the problem to the seal. Figure VI-4 shows the actuating mechanisms as installed.

The choice of a reciprocating seal made available a considerable background in shaft seal development accumulated during the STR design, for what was considered the major design problem. Also, it was possible to design the majority of the drive parts from conventional industrial materials, such as carbon steel, brass, bronze, and cast iron, and to use grease and oil for lubrication.

The four main components of the installed EBWR drive as shown in Fig. VI-5 were:

1) connector and seal assembly;
2) main housing and roller latch carriage, with lead screw and extension rod;
3) position-indicator assembly; and
4) gear motor and drive shaft.

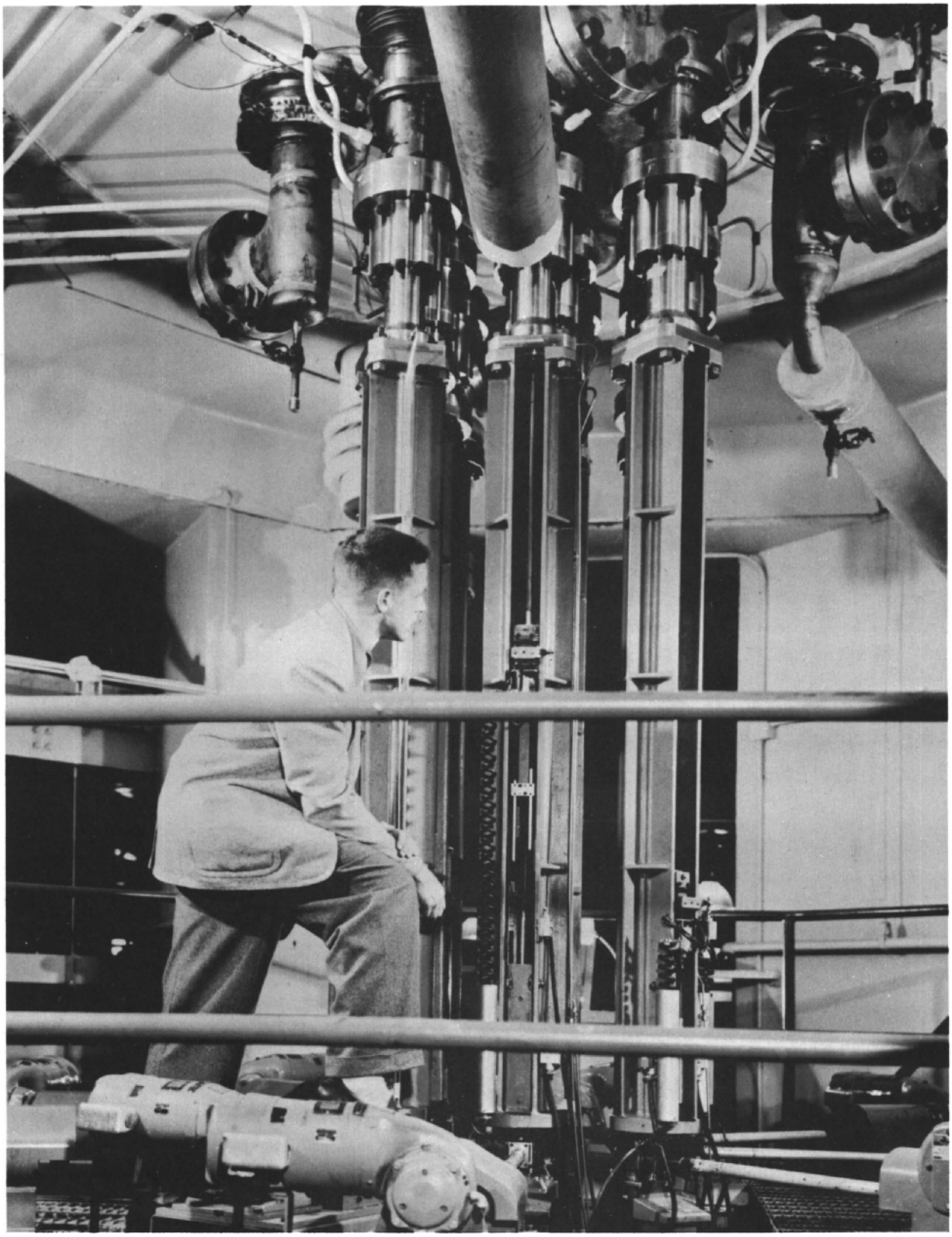

Fig. VI-4

View of Drive Mechanisms
201-1593

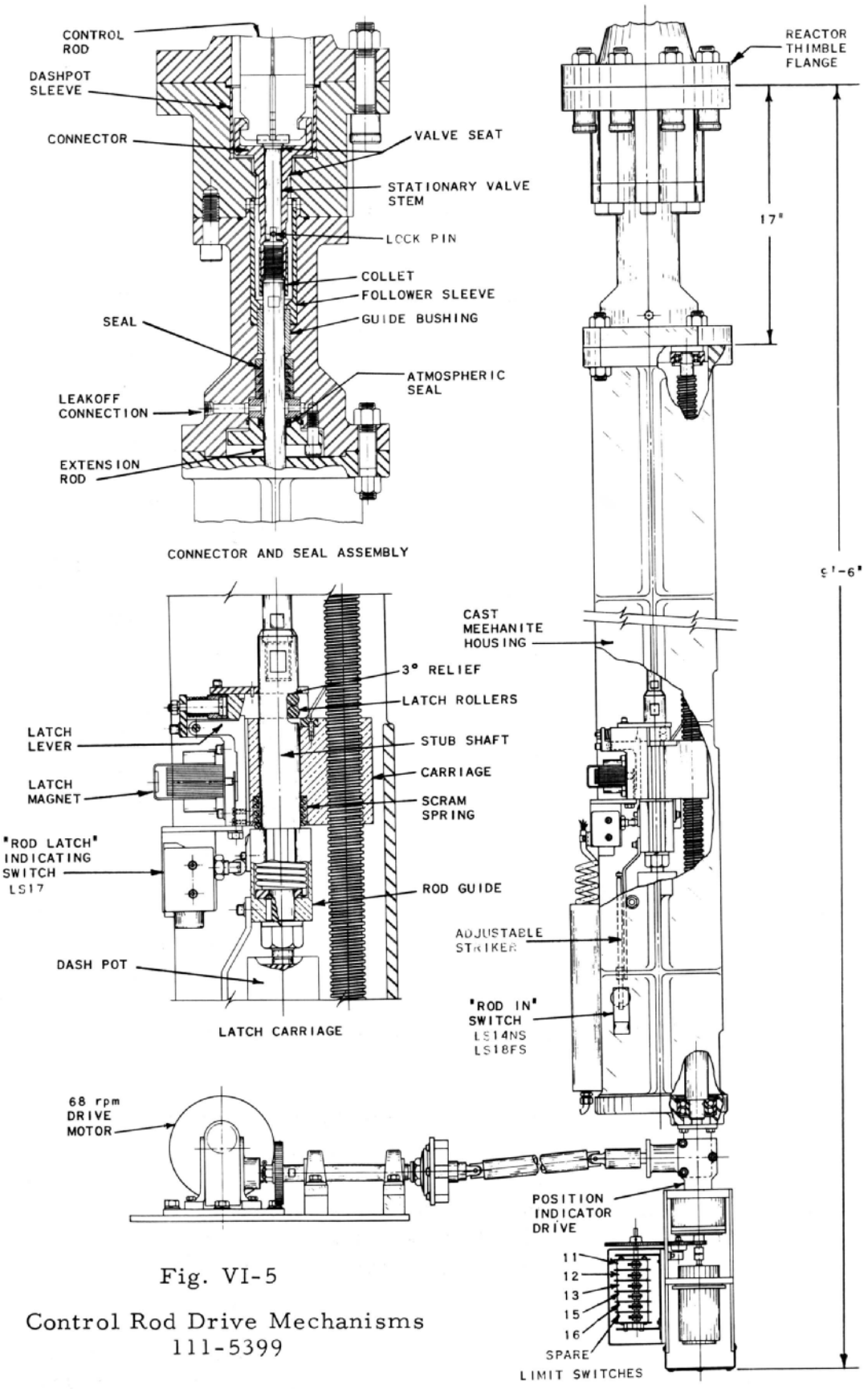

Fig. VI-5

Control Rod Drive Mechanisms
111-5399

The control rod locked into the connector by means of a cross-shaped, bayonet-type joint. The valve faces on the connector and the stationary stem were inlaid Stellite #6 and were lapped into their respective seats. This provided the shut-off valve for the reactor when the mechanism was removed for maintenance.

Because of sludge in the guide bushing, the control rod drives were removed from the reactor several times for servicing after the initial reactor startup in December, 1956. The shut-off valve feature proved that the drives could be maintained without draining the reactor vessel. In both instances, the amount of water that leaked out while the drives were removed was less than one gallon an hour per drive. An additional feature of the connector was that it served as the piston for the internal dashpot.

The seal assembly consisted of the nylon guide bushing and the 5 element labryinth-type pressure breakdown seal. The nylon guide bushing insured the alignment of the extension rod through the seal elements. The seal had 5 stationary rings and 5 floating rings. Leakage was collected in the lantern ring and returned to the reactor vapor-recovery system. A garter-type shaft seal assured that no leakage was lost to the atmosphere. The seals, during testing and operation, performed very satisfactorily, with leakage of less than 750 cc/min in all instances.

Originally, a Haynes Stellite #3 guide bushing was used. In the full-scale test, the misalignment over the 48-in. travel caused the extension rod to whip during a scram. This caused the extension rod to bear on opposite edges of the bushing bore, scraping chrome flakes from the shaft. The chrome particles were then carried downward into the seal rings, where they lodged, and caused further scoring of the shaft and internal diameter of the seal rings. The substitution of a nylon bushing solved the problem very well. During reactor operation, it was found that the diametral clearance between the extension rod and the nylon guide bushing had to be increased from 0.001 in. to 0.007 in. Considerable sludge (primarily iron oxide) was trapped in the small clearance annulus, and the resulting wedging action caused the rods to scram unsatisfactorily when the reactor was at atmospheric pressure.

The extension rod, operating through the seal, was the connecting link between the control rod and the drive mechanism. The top end of the extension rod was rigidly connected to the connector. The bottom was notched and attached to the carriage by means of a roller latch. The roller latch or scram latch, was a solenoid-operated device used to rapidly disconnect the extension rod from the carriage and allow the control rod to drop (scram).

Reactor pressure was the primary control rod expellant, but a spring attached to the extension rod overcame the inertia at low pressures.

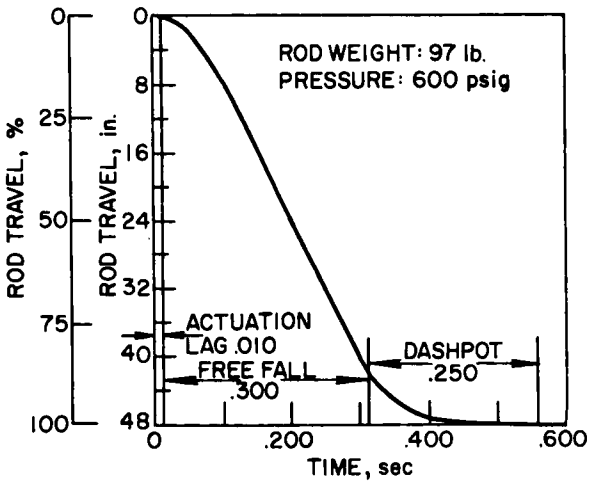

Fig. VI-6

EBWR Control Rod Scram Time with Original Rods

A typical scram-time curve is shown in Fig. VI-6. The average scram time for the 9 operating drives installed in EBWR was 0.35 sec for 42 in. of travel at 600 psig.

The carriage was driven by the Acme thread lead screw. The lead screw was in turn coupled, by means of a bevel gear arrangement, to the drive shaft and gear motor. A slip clutch, mounted as part of the drive shaft, was provided to prevent any damage to the lead screw and carriage in the event of an override past the upper and lower limit switches. The gear motor was supplied with a magnetic disk brake. The brake provided the operator with excellent "no coast" control and permitted very accurate positioning of the control rods.

The fabrication of the EBWR control drive components was for the most part conventional. The seal and connector housings, since they were in contact with reactor water, were of stainless steel. It was decided to machine them rather than use a casting, since the cost for nine items would be very nearly the same in either case. The lead screws required a special fixture because of the 0.2 pitch. For a future design, a 0.25-pitch lead screw could be purchased from a lathe manufacturer. It was also found that for the extension rod, good heat treating and chrome plating were essential. If surface preparation and hardness is not controlled, the chrome plating is always poor.

B. 100-Mwt Core Drive Mechanisms

The control rod drive mechanisms originally installed on the EBWR have now been replaced with units of a different design. Replacement has been made to obtain: (1) increased stroke length, and (2) performance experience. The change of core length from 4 to 5 ft requires increased control rod travel. The original 4-ft stroke unit could not conveniently be converted because of increased column-loading requirements and need for other major alterations. The original units were subject to sticking which was attributed to settlement of crud into the seal rings and shaft guide bushing. Due to design limitations, it was not possible to remove the crud by flushing. The new rack-and-pinion type units are flushable, and the worth of this feature has been demonstrated. In addition, the original connector dashpot part used for connecting the control rod to the drive shaft was a natural reservoir for collecting radioactive crud which could not be readily recovered.

The new control rod drive mechanism, as shown in Fig. VI-7, is a conventional rack-and-pinion design which drives through a rotating shaft fitted with a pressure breakdown seal. The original unit, with 4-ft strokes, was considered as a backup design for the EBWR reference drives. It was adapted from the original APPR model to meet EBWR operating requirements. Development work was continued over the interim period, which resulted in overcoming original objectionable features and reduction of cost from about $12,000 to less than $4000 per unit. The principal area

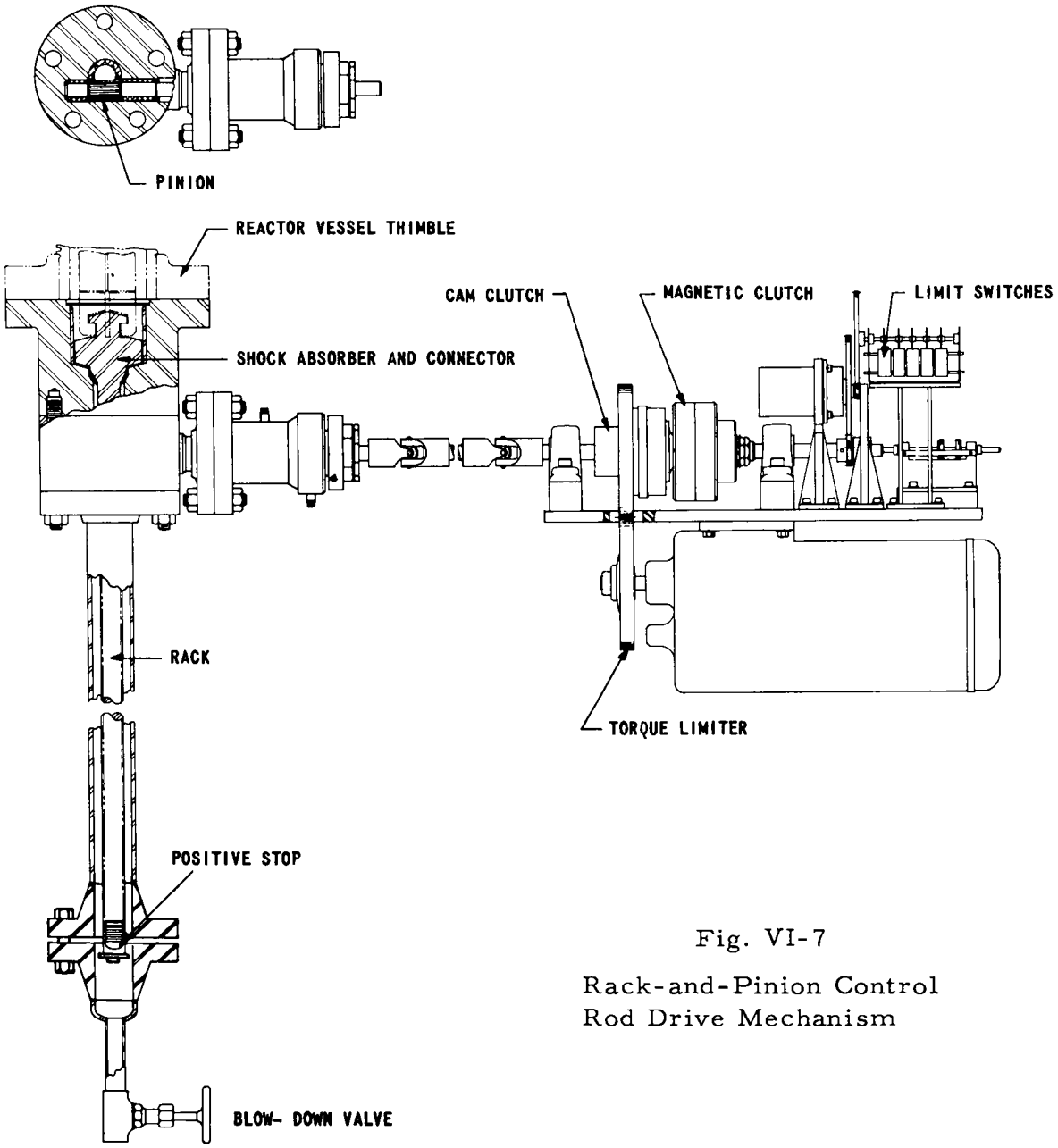

Fig. VI-7

Rack-and-Pinion Control Rod Drive Mechanism

of improvement has been around the pinion shaft support area via substitution of graphite bushings and sleeves for anti-friction bearings made of Stellite. The housing has been changed from a weldment to a more compact and less expensive casting. Crud-collecting pockets have been eliminated, and provisions for flushing incorporated.

Previously established reactor operation requirements and evaluation of test information have resulted in the design criteria listed in Table VI-1.

Table VI-1

CORE 1A - CONTROL ROD AND DRIVE MECHANISMS SPECIFICATIONS

Operating pressure	600 psig
Operating temperature of seal	110°F
Number of control rods	9
Rod travel	60 in.
Control rod spacing	$12\frac{3}{4} \times 12\frac{3}{4}$ in.
Rod speed in reactivity; Min.	1×10^{-5} k per sec
Max.	4×10^{-5} k per sec
Maximum rate of linear travel	28 in./min
Positionability	±0.025 in.
Scram speed at 200 psi	56 in. in 1.35 sec
Deceleration distance	4 in.
Maximum leakage rate per rod	200 cc/min
Complete "fail safe" characteristics	
Removal of each control rod and drive unit to be accomplished without draining the reactor vessel.	
Flushable during operation	

The control rod drive mechanism consists of a drive unit and a power unit connected to each other by a shaft with two universal joints for alignment. The main components of the drive unit are:

1) dashpot housing assembly;
2) pinion housing assembly;
3) seal housing assembly; and
4) lower housing assembly.

The dashpot housing is made of Type 304 stainless steel and contains a flash chrome-plated Type 304 stainless steel removable dashpot sleeve that is tapered for proper dashpot action. The combination dashpot piston and cross connector is made of Type 304 stainless steel

with a Stellite inlay which is ground to the contour of the seat in the bottom of the dashpot housing. This feature enables removal of the portions of the drive below the seat with the reactor vessel full of water.

Although the valve seats do not normally leak, a tool is used to prevent loss of water from the thimble while the mechanism is removed from the operating position. This tool also prevents inadvertent lifting of the connector when the control rod is removed from the core.

The control rod is connected to the rack by the combination connector dashpot piston with a bayonet lock-type joint. The rack cannot be disconnected from the control rod during operation. The rack is made from 17-4 PH stainless steel, heat treated to 45 Rockwell "C" hardness and flash chrome plated for resistance to galling. The end containing the connector pin hole is annealed to improve impact resistance.

The pinion housing is made from Type 304 stainless steel casting, and the combination pinion and pinion shaft is made from 17-4 PH stainless steel heat treated to 45 Rockwell "C" hardness and flash chrome plated. The splined end of the shaft is annealed to increase impact resistance. The "graphitar" sleeve bearings and guide bushings are held in place by a shrink fit. Bearing bores are machined for size to size shaft fits. Rotating shafts are allowed to seek natural centers during preliminary run-in.

The seal housing, which is a Type 304 stainless steel casting, contains a standard ANL-type 5-stage pressure-breakdown seal unit. The seal shaft, which extends through the seal, is made from 17-4 PH stainless steel with the same physical properties as the rack-and-pinion parts. It is suspended between a graphitar bushing on the pressure end and a combination radial-thrust ball bearing on the atmospheric end. A "Sirvene" synthetic rubber lip seal is inserted between the ball bearing and the leak-off connection.

The rack housing tube is made of Type 304 stainless steel pipe and flanges, and provides space for rack travel to the fully inserted position. The flanged joint in the lower portion of the tube is necessary for installation of the mechanical stop on the rack end, which is required to limit upward travel. The main components of the power unit are:

1) gear motor;
2) torque limiter;
3) magnetic clutch;
4) synchro-transmitter;
5) limit switch;
6) indicating light limit switches; and
7) "one-way" clutch.

The units are mounted as a package on wall brackets adjacent to the control rod drive mechanism-access platform.

Normal operation of the power unit consists of energizing the magnetic clutch and driving the output shaft with the gear motor through the torque limiter (set at $2\frac{1}{2}$-times the torque required to raise the rod) and magnetic clutch. Position indication is achieved through the synchro-transmitter and receiver, the transmitter being driven by a gear on the output shaft.

The five-unit, rotary adjustable, cam-operated microswitch assembly is also driven off the output shaft. A switch actuates the "Rod Out" light on the position indicator dial which should read in the 59-60-in. range at this time. Another switch actuates the "Rod In" light on the indicator dial when the rod is in the 0-4-in. range. Two additional limit switches are provided for "Rod In" and "Rod Out" limits. These switches are mounted on an ARCH limit device connected to the output shaft. The ARCH limit may be adjusted to a limit of $\pm 1/20$ in.

Rapid insertion of the control rods is effected by de-energizing the magnetic clutch and allowing the rod and rack to fall by gravity to the full in-position. Safety requirements prevent re-energizing the magnetic clutches until all 9 rods are down, as indicated by signal lights connected to the "Rod In" limit switches. Since the motor circuit is active and causes the motor to run for downward travel, a one-way clutch is provided which can be used to apply downward force only. This feature provides additional thrust in event a rod does not fall in by gravitational force. An adjustable torque-limiting clutch is provided in this train to prevent excessive thrust being applied which might result in damage to the mechanism.

The prototype model successfully demonstrated the feasibility of flushing out corrosion products in the test facility. Shortly after installation on EBWR, it was discovered that activity was increasing around the blowdown valve. When the level reached 1 r at the pipe surface, the unit was "blown down" to a level of 20 mr. The effectiveness can be determined only after prolonged operation.

In addition to checking the flushability of the drive, extensive tests were conducted to determine the minimum rapid insertion time and life expectancy of the complete mechanism attached to a control rod. The minimum insertion time for a full 56.0-in. stroke (the 4-in. dashpot was not included) was found to be 1.25 sec. This rapid insertion time was recorded after the mechanism had been through 9000 cycles at 28-in./min rack speed and 3000 rapid insertions. Inspection of all the wear surfaces after the above tests indicated negligible wear except in the graphitar

pinion bearings - the bore of the bearings having increased by 0.013 in. However, this wear did not affect the performance of the mechanism. The pinion bearings were replaced. The replacement bearings were originally sized to create an interference fit with mating parts and run-in in water until free (approx. 40 cycles run-in). Inspection of the bearings after run-in revealed a "glazed" contact surface which adds to wear resistance. The mechanism was reassembled and the rapid insertion time for a 56.0-in. stroke, as determined with a Brush Recorder, was found to be 1.35 sec.

Design drawings and specifications were submitted to vendors to cover purchase of nine complete drive packages, excluding seal rings, diaphragms, lanterns, synchro-transmitter and gear motors. The cost of each complete mechanism including the parts furnished by ANL was less than $4400. As the drive mechanisms arrived at ANL, each unit was assembled and checked out in the test facility. The check-out consisted of assembling the drive mechanism and cycling until a rapid insertion (56 in.) is accomplished in less than 1.35 sec. A tabulation of run-in data is in Table VI-2.

Table VI-2

DRIVE MECHANISM OPERATION DATA

Drive Mechanism	Cycles Required for Run-In	Rapid Insertion Time, sec	Seal Leakage Rate at 600 psi-cc/min
#1	20	1.24	75
#2	245	1.26	175
#3	256	1.32	80
#4	195	1.24	123
#5	35	1.32	55
#6	281	1.28	48
#7	13	1.16	75
#8	20	1.32	48
#9	24	1.28	40

SECTION VII

FUEL DESIGN AND BEHAVIOR

C. Bean
J. Kittel
V. Kolba
F. McCuaig
C. Reinke

NOTES AND EDITED DATA FROM LECTURES - July 6, 1961

SECTION VII

EBWR FUEL DESIGN AND BEHAVIOR

I. Fuel Element Design Philosophy and Performance*

Parameters for a given fuel element and core design are defined by the hydraulic, physics, and metallurgical requirements to achieve a desired goal. The design of a fuel element and core is an optimized balance between heat transfer, nuclear physics, and materials considerations, i.e., the metallurgical and chemical properties, and the mechanical design and fabrication. Heat transfer and flow aspects of a fuel element include the heat dissipation rate, surface area, coolant volume, required flow rate, pressure drop, equivalent diameter, boiling length, void volume, and other related items. Nuclear physics aspects to consider are the amount and type of fuel required (whether it be for a burning or for a conversion system), the type of moderator, the poisons in the core (including the control rod clad and matrix materials or burnable poisons for control requirements), and the lattice spacings of the fuel units. Within the area of materials are the metallurgical aspects which comprise the intercompatability problems of the fuel to the matrix and to the clad and bond materials. Also to be considered are the fabrication of fuel by standard state-of-the-art techniques, the type of clad desired, the form of an element and the fabricability of the unit, the worthiness of an element by test, and its irradiation stability. Chemical aspects include the corrosion problems of the "meat," clad, and bond material, and the reprocessing of the elements. Transfer effects include the electrochemical or crud deposition within the operating environment of the fuel element. From the mechanical standpoint, basically, one desires to select the simplest fuel unit design which will accommodate the integrated data from the previously listed areas and yet remain consistent with the performance standards and requirements. Suitable structural strength at operating conditions, ease of insertion and removal of the fuel unit from the core, reactor vessel, and handling equipment, proper locating and lifting end fittings for safe handling, adaptability to the present handling system, and a circumvention of any thermal-expansion problems are further considered. It is desirable in the fabrication of fuel units to attempt to use conventional fabrication techniques for low cost, consistent with the integrity and high quality desired in the fuel element to meet the specifications which have been placed upon it by the environment.

Areas of uncertainty or requiring control are tolerances on the clad and eccentricity of the "meat," proper fuel dispersion, coolant passage tolerances, warpage of fuel units, prediction of neutron-flux patterns, unequal flow distribution (especially in forced-circulation systems), variations in the heat transfer film coefficient, variations in the thermal conductivities of the clad, "meat" or bond, buildup of scale or crud and its associated heat transfer variations, errors in power measurements, mechanical distortion due to structural loads and thermal stress, and finally

*V. Kolba

the hot spot factor. Another necessary value to consider is the overall maximum-to-average flux value which will permit the design of the optimum core. This value is composed of the axial and radial values of nuclear flux, local peaking factors, engineering factors of tolerance and dimension, and thermal hot spot factors. Average design values for boiling water systems vacillate in the range of 3 to 4.5 with the higher maximum-to-average values being used more often at present. The heat transfer characteristics of the given type of fuel used will vary the approach to the design of the fuel unit. In the case of metal fuels and metallurgical bonds, the burnout heat flux is generally the limiting value. There may be instances when the clad-fuel diffusion may present an internal fuel element temperature limit. In the case of oxide or ceramic fuels with only a gas or a mechanical bond, the limiting value is generally the fuel centerline temperature, which usually reaches its peak prior to the attainment of surface burnout heat flux values. Fuel-element surface-flux burnout is considered to correspond to heat transfer rates greater than 500,000 Btu/hr-ft^2, depending of course on the geometry of the system, while for centerline temperature a maximum temperature limit of approximately 4500°F for ceramic fuels is generally used. This value is in the recrystallization range of UO_2 and about 500°F below the melting point. With metal fuels one may assume a maximum-to-average heat-flux value and, based on the burnout value, assign a limiting requirement for surface area. The surface area is then apportioned to the fuel consistent with the water-to-metal ratio desired for the core.

The majority of present designs for boiling water reactor (BWR) cores incorporate the UO_2 ceramic pellet Zircaloy-2-clad fuel unit in the rod configuration. This has several advantages. It is compatible with present fabrication techniques, the design is a simplified one, and it provides a structurally sound unit. In general, fuel elements contain the following items: an end fitting for support and for guiding into a grid plate, a shroud for water channeling, individual fuel units which provide the source of heat, support grids which support and guide these fuel units, and a handling end fitting to provide for handling in the core and in the storage pit.

The design of the locating end fitting is governed by the choice of the core support plate as well as structural properties necessary and water-flow area required. This unit is usually a finished machine casting, but may be a welded assembly. Materials for it are generally from the 300 series stainless steels, possibly Type 304. The shroud for the fuel element is usually a full length axial box surrounding the fuel and joining the locating end tip to the handling end fitting. The material is generally less than $\frac{1}{16}$ in. thick and may be one of several materials of low-absorption cross section. In power reactor cores, Zircaloy-2 is used for the equilibrium cycle. Zircaloy-2 may also be used for the startup cycle; however, the poisoning effects of stainless steel may be desired to limit reactivity. In the case of low-temperature boiling water units, an aluminum alloy, S-8001, may be used. Nominally, the strength required of the shroud is low, since the Δp it sees is low. Support grids are generally fabricated from

300 series stainless steel in the areas external to the active fuel section and from Zircaloy-2 or aluminum alloy in the active portion of the core. Methods of fuel spacing include the use of tubular spacers, wires, egg crate-type spacers, or support beams. These units, however, should be designed to provide the maximum open flow area compatible with structural support and spacing requirements since the effect of pressure drop induced by these units in a natural-circulation reactor can be a decisive criteria. Handling end fittings to accomplish the movement of the fuel within the core, as well as the loading and unloading of the fuel, are generally fabricated from a 300 series stainless steel, usually Type 304. Since these units are out of the active zone, no enrichment penalty is paid for the material used.

As previously mentioned, an important factor in the core design is the water-to-metal ratio which determines the core nuclear characteristics. High values of this ratio may result in a positive void coefficient while low values may result in a void coefficient which is too negative and a possible instability at elevated powers. On the basis of studies, it appears that an average water-to-uranium volume ratio of approximately 3.5 at room temperature would result in a zero void coefficient. The mixture of thin and thick elements chosen for the EBWR core provides for obtaining this ratio and also for a negative void coefficient of a reasonable magnitude at operating conditions. It is readily seen that calculation uncertainties in both void coefficient and reactivity are allowed for by the existence of 4 types of fuel elements. With these 4 types of fuel elements, the reactor can be loaded in a variety of ways; however, the optimum loading could not be determined initially without recourse to experiment. Initial calculations were based on a uniform mixture of 18 thin-plate natural elements, 18 thick-plate natural elements, 38 thin-plate enriched elements, and 38 thick-plate enriched elements. Fig. VII-1 shows a cross section of the EBWR Core-1 fuel assembly.

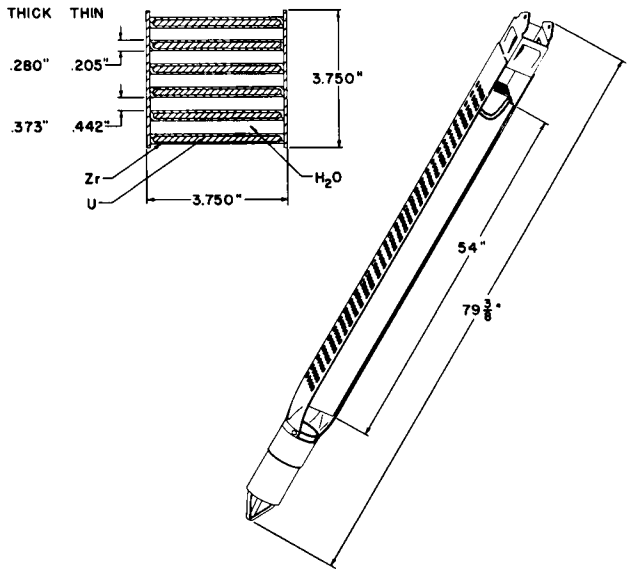

Fig. VII-1

EBWR Core-1 Fuel Assembly
111-4371

Two early design specifications for fuel elements for the EBWR were a long life-time (i.e., sufficient to reach ~1% burnup of core atoms), and attainment of irradiation stability and integrity with a minimum of absorbing material in the core clad and in structural materials. To meet these requirements it appeared that the fuel should be largely uranium with a minimum

amount of alloying elements for strength, corrosion resistance and irradiation stability, and a minimum degree of enrichment for reactivity. A corrosion-resistant cladding was considered necessary. Requirements for high-temperature corrosion resistance, combined with low neutron cross sections, are satisfactorily met by Zircaloy-2, which was selected as a reference cladding material. A corrosion-resistant core alloy was originally specified. When it was subsequently found that heat treatments of the reference alloy for corrosion resistance and irradiation stability were incompatible, the heat treatment for irradiation stability was selected and specifications on corrosion resistance were dropped.

Since going critical in December 1956, the EBWR Core 1 has operated a total of 11,164 hr which represents 211,509 Mw-hr. The average power level has been approximately 18.9 Mwt. A great portion of the initial operation was at a relatively low power; however, a sustained 40-Mwt run was made. The core contained nominally 5,508 kg of uranium during operation from 1956 to 1959. A peak output of approximately 62 Mwt was obtained, and the average burnup of the Core 1 is approximately 1600 Mw-days per metric ton. Several examinations of the core were conducted. In January 1958, a rather intensive investigation of the core was made by gamma probes and ferrous sulfate dosimetry. This work revealed that the center 36 fuel elements were producing approximately 50% of the power and that the fuel element in the center of the cell of 9 had the highest gamma flux and probably resided in the highest neutron flux. It was also noted that on several fuel elements there was considerable crud deposit. In one element this crud flaked off and was measured to be approximately 3 mils in thickness. Two fuel elements have been removed from the core and examined to date by the Metallurgy Division.

The successful operation of the EBWR at a 60-Mwt level pointed the way to the possible use of the reactor with modifications to produce 100 Mwt. The first approach to such a modification was to design an entirely new core, enlarged to 5 ft in diameter, which would have high integrity and capability of operation for approximately 3 yr. This first design incorporated 25 rods which were 5 ft long and 0.45-in.-OD stainless steel clad with UO_2 ceramic fuel and an isostatic-pressed mechanical clad-to-fuel contact. After serious considerations of the costs involved in replacing the complete core and considering the good performance of Core 1, the decision was made to place spikes in Core 1 and realize the maximum utilization and burnup of its fuel elements.

The similarity of the 25-rod fuel elements to several units which other facilities are testing led to the abandonment of that design. The decision to use the present 4-ft core in connection with the spikes presented several new design problems, such as the use of reversible fuel and the reuse of fuel end fittings. The possibility of using a symmetrical fuel element with fittings on both ends was investigated, but the requirement for springs for top spacing at both ends presented a problem of hooking and interlocking upon fuel removal.

The major advantage of the rod configuration selected for the spiked fuel elements is the higher surface area and flow area for equivalent fuel volume and, consequently, lower surface heat flux for equal heat output from the fuel element. The one area in which the spikes are not equal to the present core elements is in the equivalent diameter, which is lower than for either of the present fuel elements; however, there appears to be no major disadvantage to this with respect to the balance of the core. The choice of Zircaloy-2 clad, as opposed to aluminum or stainless steel, was made because of operating temperatures and to match the balance of the core materials, thereby permitting water-chemistry testing. Additionally, timely delivery of high-quality Zircaloy-2 tubing was purported to be no problem area. The fixed parameters given were the length of the active fuel and a power level of 100 Mwt. Selection of a rod geometry was based on the ease of fabrication, proper structural capabilities for the selected fuel and clad, and a ready adaptability to selections of a variety of fuel and clad materials. A cross-sectional view of the spike fuel element is shown in Fig. VII-2. Figure VII-3 shows the proposed 100-Mw EBWR core loading.

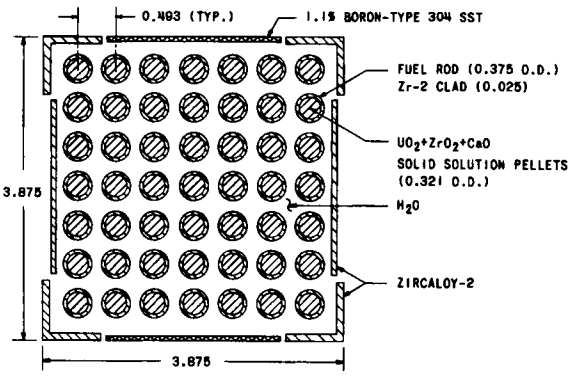

Fig. VII-2

Cross Section of EBWR Fuel Spike
(dimensions in in.)
111-9340

Fuel elements for boiling water reactors are not yet developed to produce electric power at a competitive cost in low-cost fuel areas. To date, no one material or design has demonstrated significantly superior characteristics; thus, the continued development of several fuel types is warranted. Current contract prices for fuel fabrication are considerably higher than the estimated cost used in arriving at the favorable fuel-cycle figures frequently published. The basic objective of the fuel element-development program is to produce engineering information and data which will reduce this gap.

Specific objectives of the overall Argonne fuel-development program are to secure elements having the following characteristics: corrosion resistance at elevated water, saturated, and superheated steam temperatures in a radiation environment; maximum structural strength for fission product retention; minimum neutron absorption in the cladding; mutual compatibility of the materials; resistance to changes of physical properties due to absorption of the internally contained gases or to coolant dissociation; resistance to physical change due to radiation damage and thermal cycling; adequate thermal conductivity, both of clad and fuel materials; good fabricating characteristics permitting low-cost manufacturing and testing procedures; and availability of clad materials at low cost.

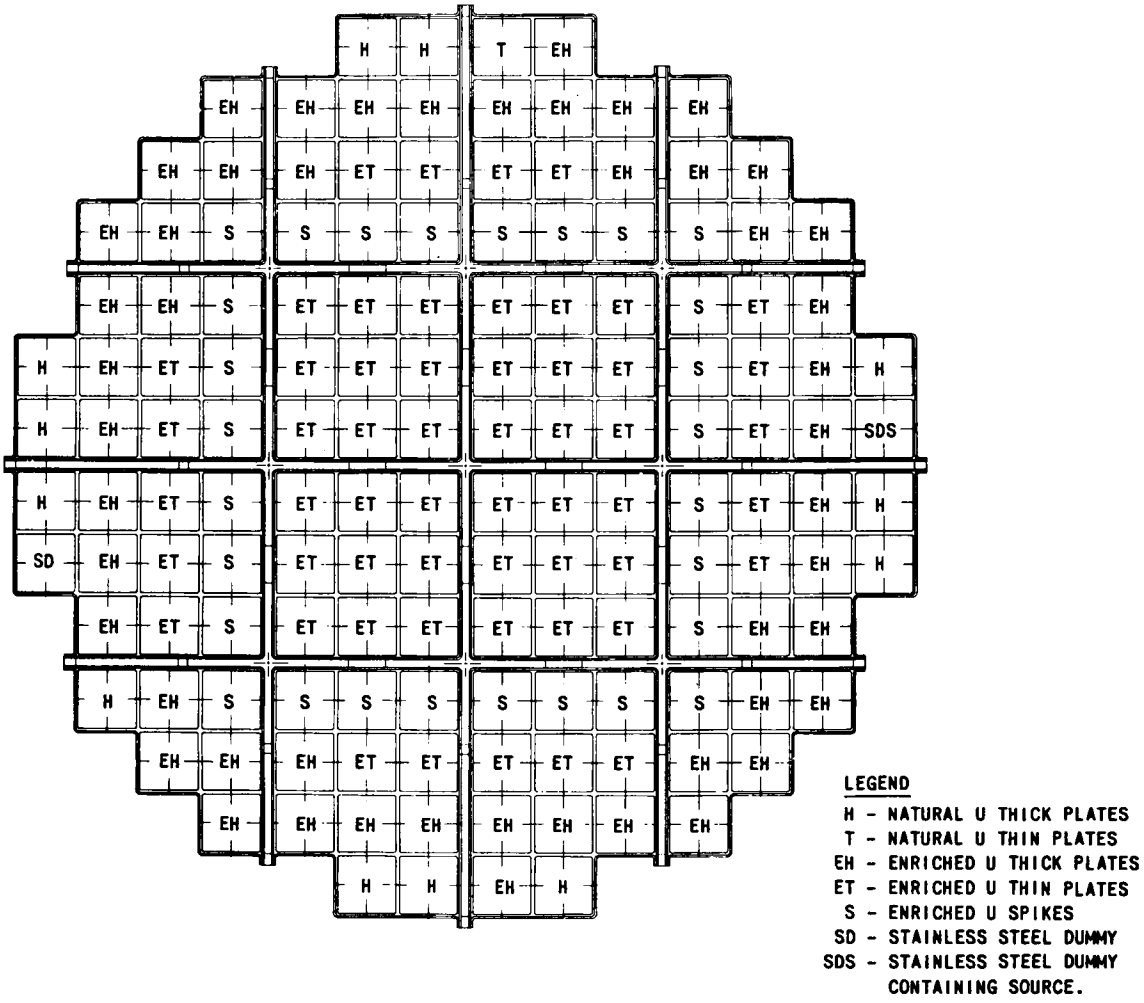

Fig. VII-3

Core 1A - EBWR Fuel-assembly Loading Pattern
111-9355

Fuel materials can be divided into two major groups: the fissile (U^{235}, U^{233}, and Pu) and the fertile (Th and U^{238}). These materials can then be further described by the form in which they are used, either metal or alloy, ceramics or combinations thereof. In general, the uranium alloys to date have not exhibited the desired characteristics as stated above. However, the performance of the metal fuel-element loading in EBWR has been quite encouraging. Central-zone fuel elements have received burnup exposure to a maximum value of 3900 Mw-days per metric ton. Continued exposure to 6000 Mw-days per metric ton will be attempted. Metallic fuel has enough desirable features, when weighed against the disadvantages, to warrant continued intensive development. Saturated steam at 500° F is economically attractive if the metallic fuel-cycle cost can be reduced sufficiently in connection with improved integrity. Uranium and alloy combinations have been investigated more thoroughly than plutonium and thorium. Development of ceramics has followed a similar pattern.

Advantages of metal alloys are a high uranium content and fair-to-good thermal conductivity. Disadvantages are instability to radiation damage, thermal-cycle growth, poor corrosion resistance, and low maximum operating temperature due to compatibility problems. The major advantages of ceramics are good radiation stability, good-to-excellent corrosion resistance, no appreciable thermal-cycle growth, and generally good compatibility with other materials. Disadvantages are low uranium content, poor thermal conductivity, and susceptibility to thermal fractures. A survey of the literature indicates that from the standpoint of corrosion, chemical reaction, and strength, the metal alloys must be clad to operate in reactors. To a limited degree, ceramic units such as UO_2 can be used temporarily without effective cladding, as was demonstrated in BORAX-IV when several fuel elements developed leaks.

Bonding of metal fuels to the clad is generally accomplished metallurgically in the fabrication process. In the case of ceramics this is not possible. The bonding problem is particularly acute in the case of oxide fuels. Gas bonding leads to a high thermal resistance between the ceramic and clad, which increases if fission product gases escape into the system. In some cases, this additional thermal resistance can cause a sufficient increase in the central fuel temperatures to result in melting of the element. To alleviate this problem, a definite effort to measure and correlate center fuel temperature should be made. An evaluation of other bonding media should be attempted, and the compatibility of the bond media with the fuel and clad material must be studied at reactor operating conditions.

II. Fabrication of Fuel*

A. Fabrication of Core 1 Fuel Plates

Core 1 was designed to accommodate 148 fuel assemblies (888 plates), making its diameter 60 in. An operational loading of fuel, however, consisted of 112 assemblies (672 plates) arranged in a 50-in.-diameter core. The fuel plates were made in two isotopic concentrations: 0.7% U^{235} (natural) and 1.44% U^{235} (slightly enriched), and in two overall thicknesses; 0.210 in. and 0.273 in., with corresponding core thicknesses of 0.170 in. and 0.233 in. The core was placed symmetrically within the Zircaloy-2 cladding, leaving nominal cladding thicknesses of 0.020 in. on each face, 0.155 in. on each side, and $1\frac{1}{2}$ in. on each end. The width and length of all plates were $3\frac{5}{8}$ and 54 in., respectively. An alloy of uranium containing 5 w/o Zr and 1.5 w/o Nb was selected as the fuel. In addition to the loss of corrosion resistance under irradiation, the dimensional stability of the alloy in the supersaturated alpha condition was very poor. Heat treatments are available which greatly improve stability of this wrought alloy. This heat treatment, like irradiation, destroys most of the corrosion resistance of the alloy. Duplex heat treatments, which were intended to superimpose the

*C. Bean and F. McCuaig

optimum for corrosion resistance on the optimum for stability, failed to produce an irradiation-stable and corrosion-resistant structure. The 5 w/o Zr-1.5 w/o Nb alloy, designated the reference alloy, was retained as the fuel for the EBWR, because of the close match in its rolling characteristics with those of the Zircaloy-2 cladding components. When compared with unalloyed uranium, this alloy greatly improves the uniformity of cladding, makes rolled end closures possible, and eliminates the extrusion of the core into the bonding interfaces of the cladding components. The ease with which rolled end closures could be produced was vastly improved by the alloy additions to the uranium core. Unalloyed uranium at the rolling temperature deformed so readily that it built up significant pressure within the cladding to the extent that the core extruded a great distance between the cladding components (end plug-cover plate and side plate-cover plate interfaces) before bonding of the cladding components could be effected. In severe cases, the extrusion of uranium extended to the outer surfaces of the cladding. The alloying additions improve the rolling characteristics of the core so as to eliminate this extrusion effect.

Zircaloy-2 was selected as the cladding material for the EBWR Core 1 fuel because of its low thermal-neutron cross section, its high corrosion resistance to water, and because of the absence of intermetallic compounds in the zirconium-uranium system. The need for a low-cross-section cladding material in a reactor competing with coal in the generation of power was obvious. Corrosion resistance of the cladding was of utmost importance, since the survival of the fuel plate was absolutely dependent upon the ability of the cladding to exclude water from the uranium core. Access of water to the uranium core alloy, heat treated for dimensional stability, caused complete conversion of the metal to oxide in less than 2 weeks, even in the absence of irradiation. This vital corrosion resistance of cladding material was available in very high-purity zirconium-crystal bar; but its relatively high cost, its erratic behavior in high-temperature water, and its low hardness level made crystal bar unattractive for this application. Zircaloy-2, on the other hand, costs considerably less in ingot form than crystal bar, does not vary in high-temperature water corrosion resistance from ingot to ingot, and is sufficiently harder than pure zirconium so that the roll-cladding operation is made easier. Ingot from zirconium sponge was unacceptable because of its high and erratic corrosion rate. The absence of high-melting-point intermetallic compounds in the uranium-zirconium system noted above makes zirconium very attractive as a cladding for uranium. The presence of compounds such as exist in the uranium-aluminum system makes the mechanics of developing and maintaining a metallurgical bond extremely difficult by comparison. A flow diagram showing EBWR Fuel Plate Manufacture is shown in Fig. VII-4.

The design of the cladding billet was arrived at after consideration of many factors, viz., the magnitude of reduction necessary to establish satisfactory bonds, limitations of equipment, cross section of core attractive

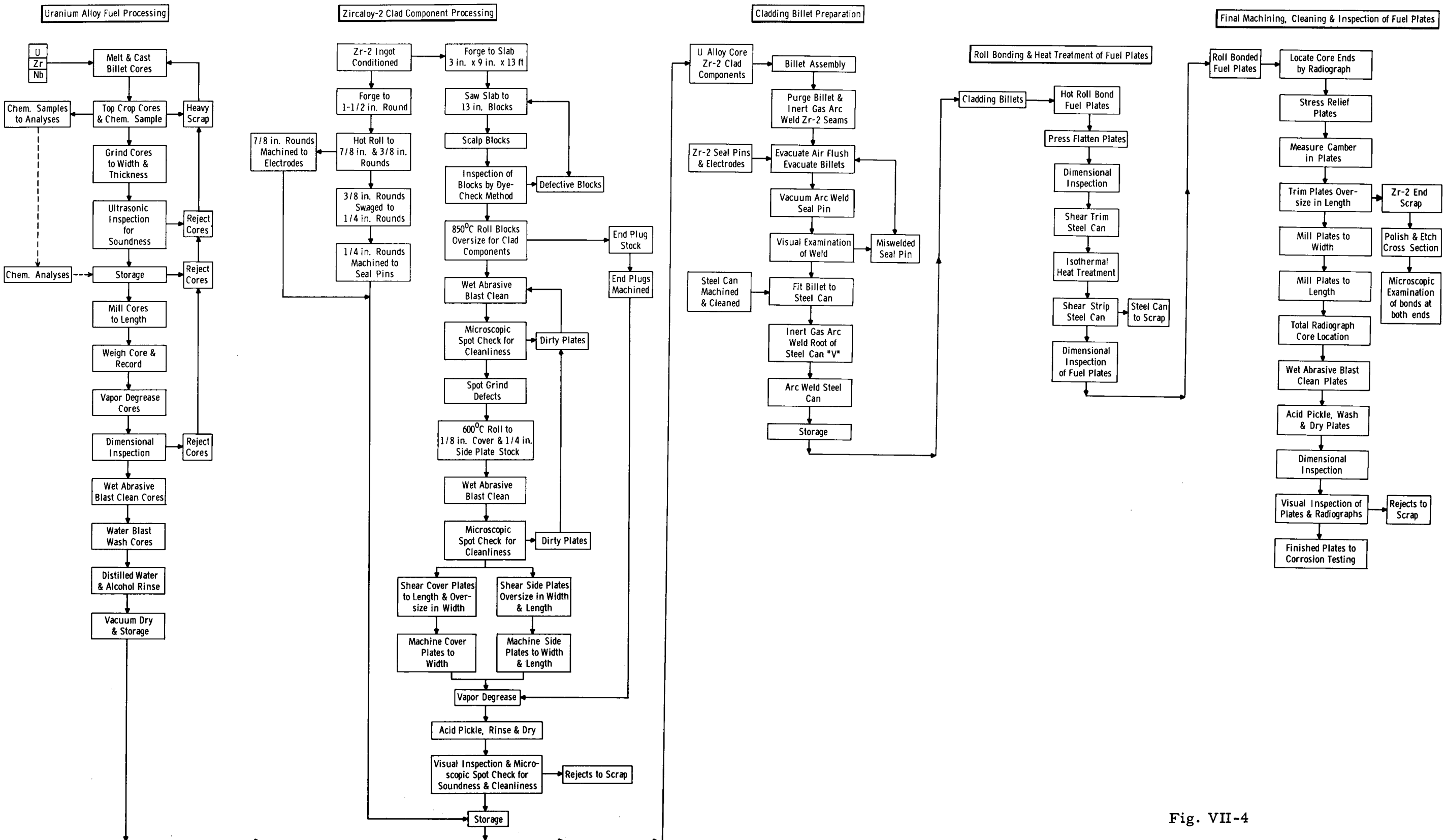

Fig. VII-4

Operations Comprising EBWR Fuel Plate Manufacture

for casting, ease and economy in fabricating cladding-component stock, and economy in machining cores and jackets. The primary factor was the reduction required for bonding. The thickness of the cladding billet was limited on the minimum side by the reduction necessary to produce bonding and on the maximum side by the capacity of the mill available for the roll-bonding operation. Between these two limits, the other factors listed influenced the final design. The problems involved in the casting of the core exerted the maximum influence on these intermediate factors. The greater the separation of the width and thickness dimensions, the more difficult it was to obtain a sound casting; furthermore, the greater the length of casting, the more difficult it was to cast sound metal. For these reasons, a core size suitable for a 5:1 reduction in rolling was selected. Fabrication, cleaning and machining cost of the cladding components, and machining cost of the core (both in time and metal loss) decrease with increasing billet thickness, because of the increase in volume-surface ratio of the billet components. In addition, the thickness variation in the face cladding of finished rolled plate decreased with increasing reduction.

The uranium alloy for fuel plate cores was produced by the dissolution of the alloying elements, zirconium and niobium, in molten uranium. The rough dimensions of the cladding billet cores were generated by casting into multiple cavity molds; the final dimensions were developed by grinding and machining. Cladding billet cores were made in two isotopic concentrations and in two sizes for the fabrication of fuel plates in the two thicknesses required for flexibility in reactor loading. The cores were produced with a 90° included angle taper. The method of casting cores directly to a size suitable for machining to finished dimensions was preferred to the procedure of casting large billets and rolling these billets into bar suitable for machining cores for two primary reasons. First, the losses incurred during rolling and machining to size were very high; and second, the high hardness developed in this age-hardening alloy by air cooling from the high rolling temperature made machining extremely difficult.

Melting, alloying, and casting of the cladding billet cores were carried out in two similar vacuum-induction furnaces.

The multiple-cavity mold was made up of wedge-shaped graphite segments which, when assembled, formed a cylindrical tube, $12\frac{3}{8}$ in. in diameter, standing 18 in. high, with a $3\frac{1}{2}$-in.-diameter hole running down the center. A groove the width and thickness of the desired casting (plus shrinkage) was cut into one side of each segment. The casting cavities were formed by these grooves in one side of each segment closed by the plane face of the adjacent segment. The two different billet core sizes required for the production of fuel plates in two thicknesses made two types of molds necessary. These mold types differed only in size and number of cavities. The billet cores for the thin fuel plates were cast into twelve-section, twelve-cavity molds, and the billet cores for thick plates were made in ten-section, ten-cavity molds. The molds were protected from attack by the metal by a duplex-ceramic coating consisting of a base coat of $MgO \cdot ZrO_2$ covered with a thoria wash.

The method of charging the uranium and alloying elements and the operation of the vacuum furnaces played important roles in dissolution of the alloying elements because of the high reactivity of the alloying elements with atmospheric constituents, the high stability of these reaction products of zirconium with respect to those of uranium, and the great difference in density of alloying elements and uranium. The wide difference between melting points of the zirconium, niobium, and uranium, and the absence of eutectics or peritectics in the uranium-alloying element system, meant that the mechanism of dissolution was diffusion between solid alloying elements and molten uranium at reasonable operating temperatures. For this reason, restriction of contamination to the alloying elements was very important. Since dissolution took place by a diffusion mechanism, intimate contact between molten uranium and alloying additions was necessary. The chief difficulty in establishing intimate contact, aside from restricting surface contamination, was the great difference in density. If the zirconium and niobium were charged on top of the uranium, they stayed there after melting and became mixed with skull which prevented or greatly retarded dissolution. If charged beneath uranium, it was necessary to hold these alloying additions there until completely wet by uranium. This was done by charging the 12-in.-diameter uranium biscuit on top of the alloying additions and causing the uranium to melt from the top down. In this way the additions were held down by the higher-density solid uranium while being wetted by the molten uranium.

Two types of charges were used. The bulk of heats were charged principally with virgin materials; the remainder of the heats were charged exclusively with remelt material. All heats were bottom-poured by means of a stopper rod into multicavity molds. Soundness of the castings was obtained by establishing a high thermal gradient (1200°C at top to 600°C at bottom) by an appropriate mold, crucible, and induction-coil arrangement. The top of the mold was heated both by conduction from the crucible, which rested directly on the mold, and by power induced from the induction coil. Magnesium vaporized from the melt was not allowed to condense in the mold cavities by having the mold above condensation temperature (400°C in vacuum employed). If magnesium was permitted to condense in the mold, it acted as any vapor or gas in producing blowholes when revaporized by the hot metal poured against it.

The castings were stripped from the molds and, after washing to remove ceramic coating, two castings from each heat were sampled top and bottom for analyses of zirconium, niobium, carbon, nitrogen, and minor impurities. The castings were then cut to rough length and ground to width and thickness. The length and 90° included angle end-tapers were produced by milling.

The alloy composition of the billet cores used for fuel plates averaged 4.87 w/o Zr and 1.55 w/o Nb. The range in zirconium content was 5.60-3.71 w/o and the range of niobium was 1.91-1.23 w/o. The carbon and

nitrogen contents of the billet cores were at low levels, averaging 22 ppm and 14 ppm, respectively. The alloy content of the heats was determined by a spectrographic technique which was very rapid and accurate to within 5% of the amount present. The carbon was determined by a combustion manometric method and the nitrogen by the Kjeldahl method.

The billet core castings were inspected for soundness by a through-transmission ultrasonic test. In brief, the method consisted of introducing the object to be tested into ultrasonic radiation generated by pulsing a piezoelectric crystal (quartz) at its resonating frequency and receiving radiation transmitted through the object by means of another matching crystal located on the opposite side of the object. The output of the receiving crystal was amplified, rectified, and impressed on a Helix recorder. The recorder darkened an electrosensitive paper in proportion to the amount of current flowing through it. Billet core castings which were acceptable for use were prepared for assembly, first, by removing tarnish, then washing, drying, and storing in vacuum. The tarnish resulting from grinding and standing in air was removed by a wet abrasive blasting operation using 400 mesh Al_2O_3 in special equipment. Following the water blasting, the cores were rinsed in distilled water, then in absolute alcohol to facilitate drying. The billet cores were dried and stored under vacuum to prevent tarnish until assembled.

The Zircaloy-2 cladding-component stock was purchased from commercial producers in the form of consumable electrode, double arc-melted ingots. These ingots were converted into stock from which cladding components were made by a sequence of forging, scalping, hot rolling, warm-finish rolling, wet-abrasive blast cleaning, and pickling operations. This sequence of operations was developed to eliminate surface machining which was previously considered necessary to obtain satisfactory bonding between the Zircaloy-2 cladding components. The primary objective was the elimination of a vast amount of useless and hazardous machine turning.

The 12-in.-diameter, 1000-lb Zircaloy-2 ingots were forged to 3 x 9-in. cross-sectional slab in preparation for the hot rolling which followed. Heating to 925°C for forging was done in an automatically controlled gas-fired furnace. Forging was performed with a 4000-lb steam hammer. Success in eliminating the final surface-machining operation was dependent upon complete removal of surface defects before the finish-rolling operation. Removal of forging and ingot surface defects was done after the forging operation, because of the minimum area to be machined at this point. Approximately $\frac{1}{16}$ in. was removed from each of the two major faces of the blocks. Surface contamination was removed by two wet abrasive-blasting operations, first with 100 mesh alumina for fast removal of the bulk of atmospheric contamination, then with fine 400 mesh alumina, which would reach down into the narrow crevices for complete removal of contamination.

The cleaned strip was finally rolled to 0.003-0.005 in. over the finished thickness of the cladding side and cover plates. Rolling was done at approximately 600°C to remove surface asperities by heavier total reductions than was possible by cold rolling. After cleaning, the surface finish of the 600°C rolled strip could not be distinguished from a cold-rolled surface similarly cleaned. The finished-rolled strip was again cleaned by two wet abrasive-blasting operations. The plates were finally prepared for billet assembly by pickling in boiling concentrated nitric acid containing $\frac{1}{2}$-1% concentrated hydrofluoric acid by volume, water rinsing, and drying.

When the billet core and cladding components (see Fig. VII-5) had been prepared, the cladding billets were assembled, welded, evacuated, and sealed. The cladding billet contained the uranium alloy core and the Zircaloy-2 components. The cladding components consisted of end plugs, side plates, cover plates, and seal pin.

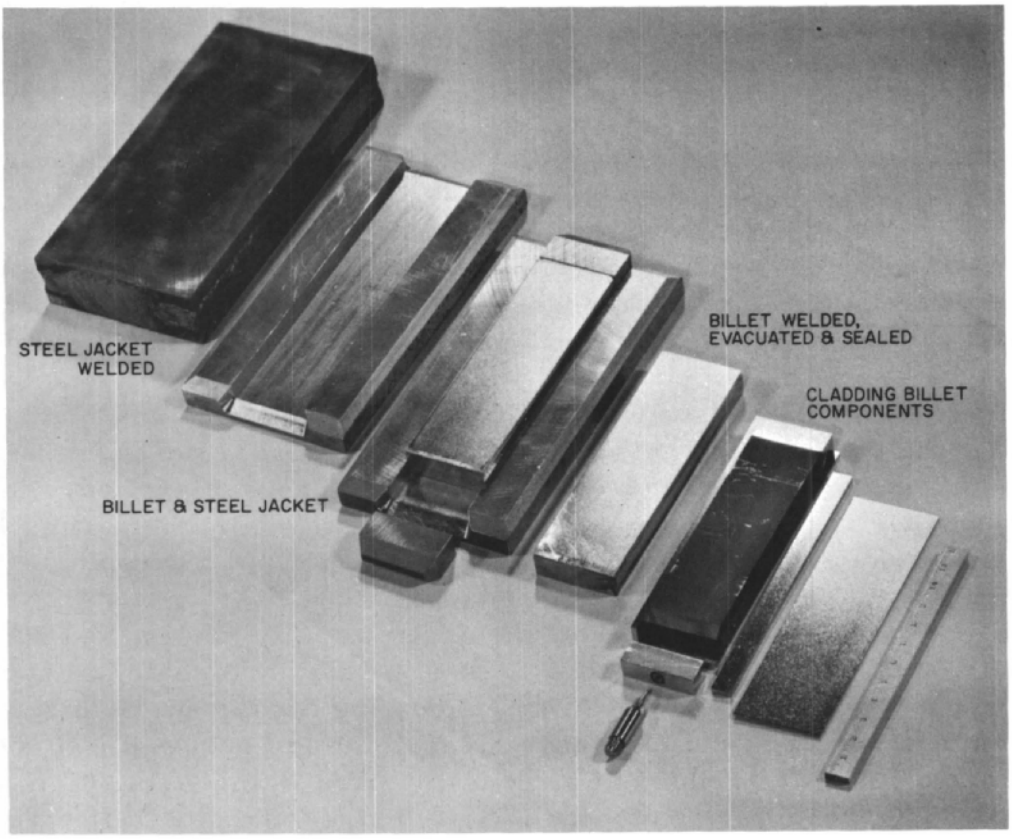

Fig. VII-5

Cladding and Rolling Billets at Various Stages of Preparation
106-2446

The rolled end closure, superior to a welded closure, was made possible by providing a 90° included angle taper at the ends of the core and

a matching female taper in the end plugs. This taper afforded a rolling transition zone between end plug and core to reduce the effect of the slight change in rolling characteristics between the uranium alloy core and Zircaloy-2 end plug. Upon examination of the cladding-billet dimensions, it will become apparent that a gap exists between the core and the surrounding cladding components. This gap was intentionally provided to compensate for the positive differential expansion of the core with respect to the clad of 0.020 in./in. taking place during heating from room temperature to the rolling temperature of 850°C. If this expansion gap were not provided, pre-rolling welds were subjected to triaxial stress during heating for rolling, which in some instances caused weld failure. A failure in the weld admitted contaminating gases which caused unbonded areas or bond-line inclusions. The opening machined in one end plug was for the purposes of introducing argon purge gas before and during welding of the Zircaloy-2 components.

Advantage was taken of the anisotropy in the rolling characteristics which existed in the plate stock from which end plugs were machined. The end plugs were oriented in the rolled plate stock so that maximum spread was obtained in subsequent roll bonding. This spread provided the necessary contact between end plug and side plate to effect bonding.

The cladding billet components were assembled then transferred to the press-welder and pressed between water-cooled, copper-alloy chills. The components were pressed together hydraulically in both the vertical and horizontal directions, thus making an "autodry" box of the cladding billet. The air entrapped within the billet was removed by an argon purge introduced through the purge opening in one end plug. During purging, the billets were held together by low pressure to permit escape of air and purge gas. After purging, full pressure was applied, which normally stopped flow of purge gas. All seams formed by the mating Zircaloy-2 components were closed by inert gas-shielded tungsten arc-welding torches motor driven along the work at 16 in./min.

The assembled plates were evacuated and sealed in groups of twelve in a vacuum chamber. After evacuating the billets in this chamber, a Zircaloy-2 seal pin and electrode extension were screwed into a copper electrode. This electrode seal pin was inserted in the $\frac{1}{4}$-in.-diameter tapered opening in the end of each billet. The electrodes projected into the vacuum chamber by means of sliding "O"-ring seals. The seal pin and weld area in the end plug was preheated by a current of 900 amp for 15 sec. The power was then raised to approximately 1300 amp, which melted the section of seal pin between the billet end plug and electrode, thus establishing the arc. The arc was allowed to exist for a predetermined 3-sec interval during which time the seal pin was fused to the filler end plug. The weld penetration was increased by consumption of a portion of the Zircaloy-2 electrode. Satisfactory and unsatisfactory pin welds are shown in Fig. VII-6.

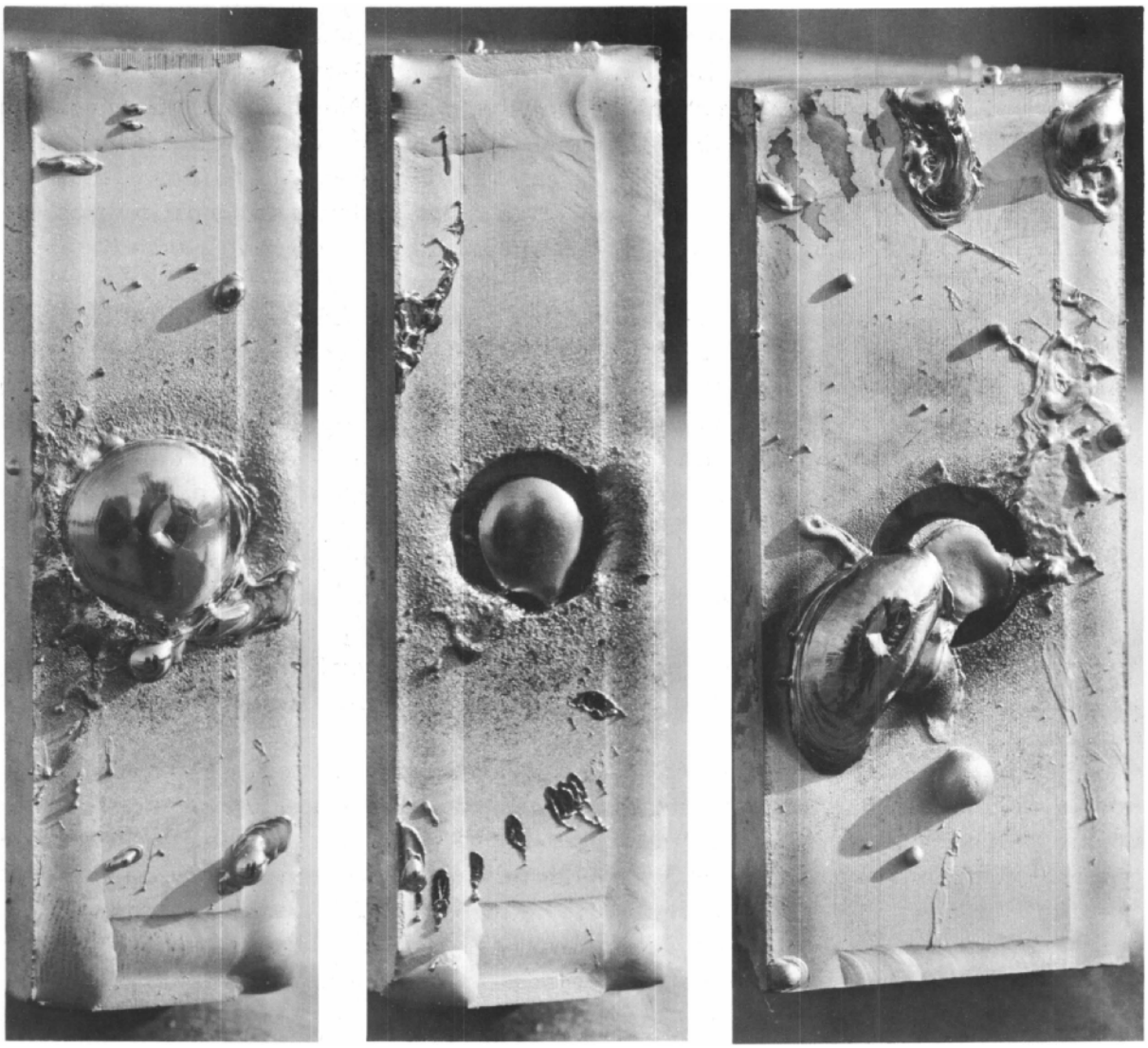

106-2797
Satisfactory Weld

106-2796
Unsatisfactory Weld
Incomplete Penetration

106-2794
Unsatisfactory Weld
Incomplete Sealing

Fig. VII-6

Vacuum-Arc Seal-Pin Welds, Satisfactory and Unsatisfactory

At this point the cladding billet was completely sealed. The internal surfaces (bonding interfaces) were practically free of contamination and were not subject to contamination during heating for rolling by air entrapped within the steel jacket used nor outgassing therefrom. This method was considered superior to the more common practice of evacuating an outer steel jacket in the preservation of clean bonding surfaces for early diffusion to take place.

Following removal from the evacuation-sealing equipment, the cladding billets were fitted into four-piece, channel-type steel cans of SAE 1020 steel, which were in turn closed by welding. No attempt was made to evacuate the steel jacket, since the bonding surfaces of the cladding billet were sealed already. The purpose of the steel jacket was to restrict atmospheric contamination of the cladding during heating and rolling and to provide restraint of the cladding billet, particularly against spread.

The bonding of the components which made up the cladding billet and the development of plate dimensions was accomplished by a flat-rolling process. The bond between all mating components was accomplished by diffusion and brought to reasonable rates by an elevated temperature, during intimate contact established by rolling. In addition, attenuation of residual contamination on the mating surfaces by deformation greatly aided in establishing the metallic intimacy necessary for initiation of diffusion. The bonding and developing of plate dimensions necessary for the finishing operations was accomplished by a total reduction in thickness of 80% at a nominal rolling temperature of 850°C. After rolling, the fuel plates were heat treated for irradiation dimensional stability while still in their steel jackets, which provided protection of the plates from atmospheric and lead contamination and mechanical damage during heat treatment. This practice was not objectionable, since the cooling rate was not a major variable in the heat treatment. The heat treatment consisted of heating the plates into the gamma phase of the core alloy at 800 -825°C, followed by an isothermal quench and 24-hr soak in lead held between 620 and 640°C. The plates were air cooled following removal from the lead bath. The gamma-solution treatment was performed in air in a box furnace. After heat treatment, the steel jackets were removed by, first, shearing the steel from the ends of the plate, then either shearing or planing the steel from the sides of the plate, followed by stripping the jacket from the plate faces. The stripped fuel plates were given a low-temperature (400°C) heat treatment for stress relief. For reference in machining the excess cladding from the end of the plates, the core ends were located by X-ray radiography.

The fuel plates were milled only to width and length (3.625 and 54 in., respectively). Corrosion-resistant surfaces were developed by wet-abrasive blasting with 400 mesh Al_2O_3 to promote uniform attack by the pickling which followed in a bath containing, by volume, 35% concentrated HNO_3 and 5% concentrated HF operated between 36°C and 40°C. Approximately 0.003 in. of cladding were removed from each surface by the blasting and pickling operations. Transverse sections of completed fuel plates are shown in Fig. VII-7.

The fuel assembly consisted of six fuel plates, two Zircaloy-2 side plates, and stainless steel bottom and top locating fittings (see Fig. VII-8). The fuel plates were arranged in parallel, spaced nominally $\frac{3}{8}$ in. apart, and welded to two perforated Zircaloy-2 side plates. Welding of the side plates to the fuel plates was done by means of a technique termed tungsten-arc spot welding.

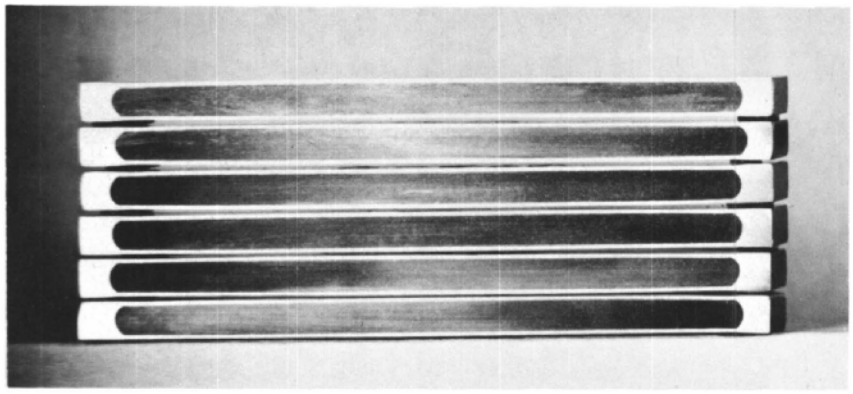

Thin (0.210-in.) Fuel Plate

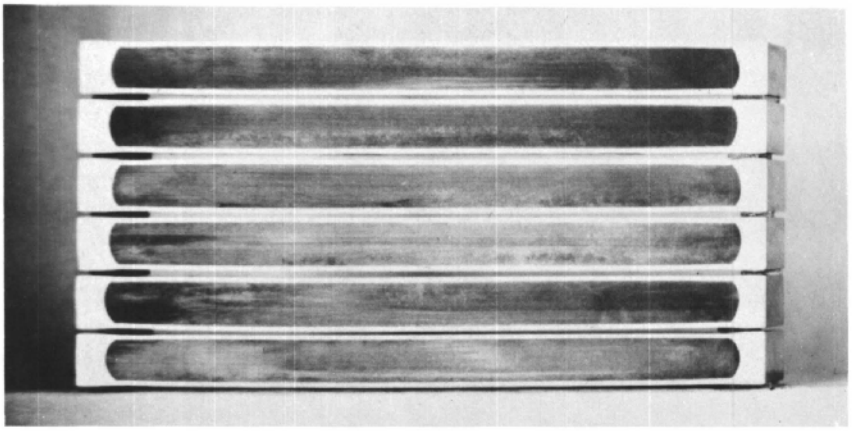

Thick (0.273-in.) Fuel Plate

Fig. VII-7

Transverse Sections of Fuel Plates at Six Equally Spaced Intervals along Length of Plates

The basic elements of the arc spot welding gun, designed and built by ANL, are illustrated in Fig. VII-9. The major components are the tungsten electrode and chill-retainer. The water-cooled chill-retainer functions as a cooling chill to remove heat preferentially from the thin side plate, thereby preventing excess melting from occurring before the fuel plate reaches a sufficiently high temperature to cause complete penetration. The chill-retainer also functions as a gas cup to channel inert gas around the electrode and arc. Inert gas flows downward around the electrode and is exhausted through vents in the chill-retainer at the surface of the side plate.

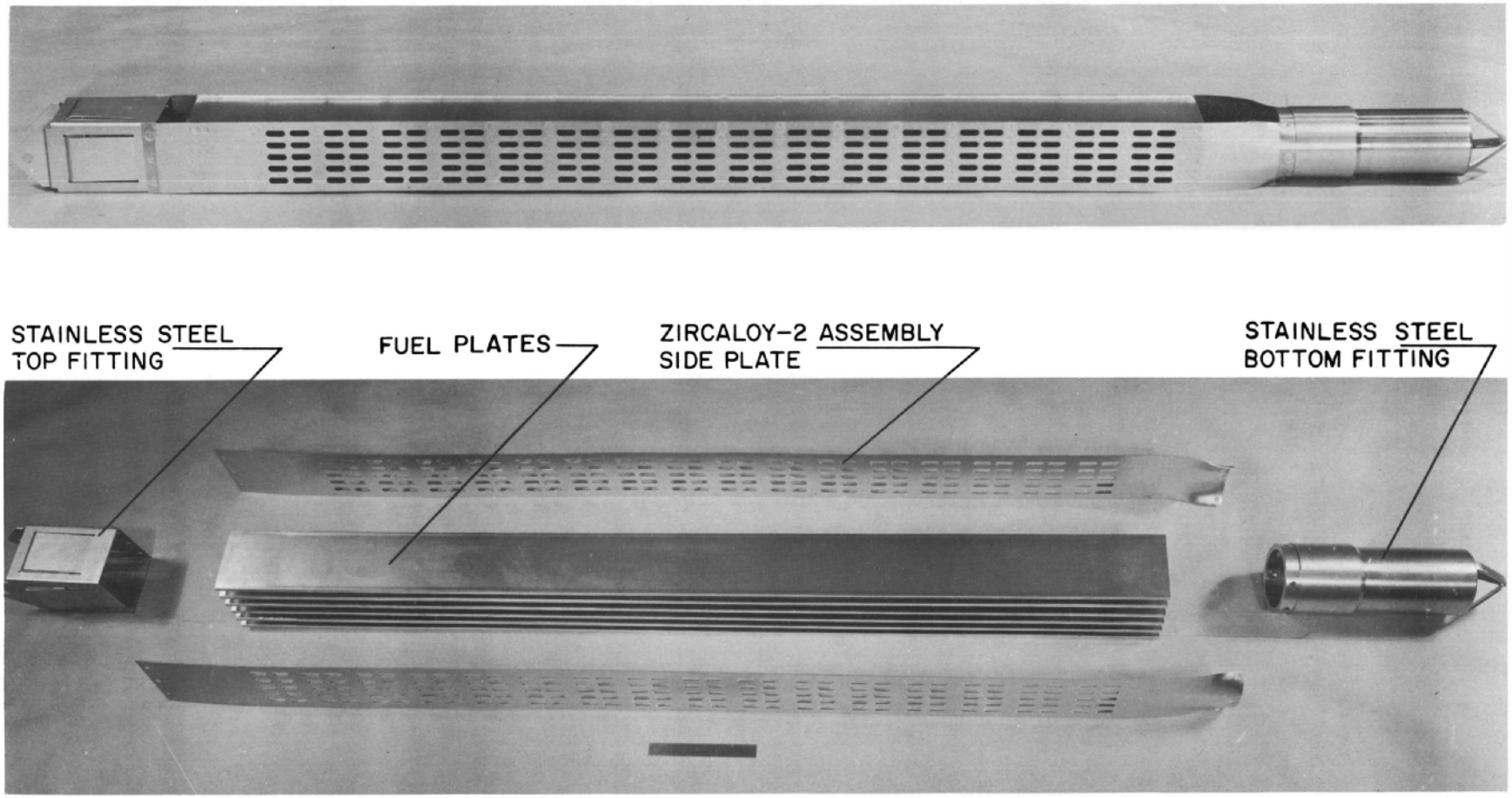

Fig. VII-8

EBWR Fuel Assembly and Fuel Assembly Components
Fuel Plates Are $3\frac{5}{8}$ Wide x 54 in. Long

111-2930

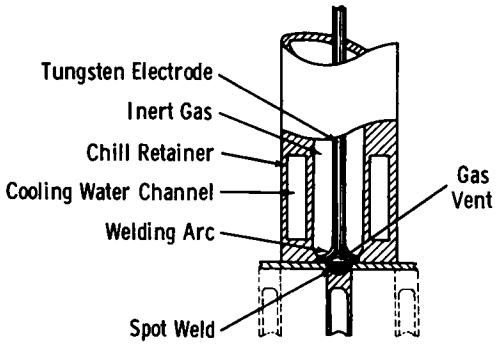

Fig. VII-9

Schematic of Arc Spot-welding Gun
106-2466

The spot weld is accomplished by an electric arc which melts through the side plate into the fuel plate. The arc is initiated by a high-frequency oscillator. An important phase of the process is the incorporation into the welding cycle of a preheating stage which compensates for the thermal mismatch between the thin ($\frac{1}{16}$ in.) side plate and the heavy, thick fuel plate. The effectiveness of the preheat is illustrated schematically in Figure VII-10. After the arc has been established, the welding current is reduced to such a value that the heat supplied to the side plate is in equilibrium with that removed by the chill-retainer, and additional melting of the side plate ceases. Since the fuel plate is in contact with the hot portion of the side plate, heat is transmitted into the fuel plate to raise its temperature to allow full penetration to take place. The final step in the operation is the weld stage, in which the welding current is increased to a relatively high value for a short period of time, producing a weld nugget (melt) that extends through the side plate into the hot zone of the fuel plate.

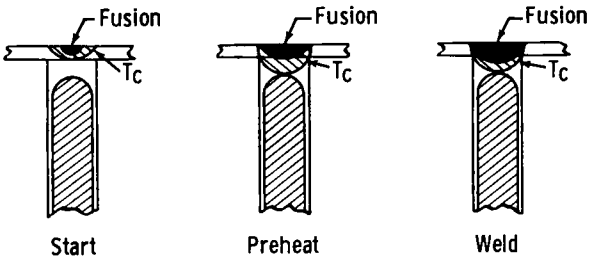

Fig. VII-10

Effectiveness of Preheat
106-2468

Commercially available inert gas spot-welding equipment was used for preliminary development work, but was found to be inadequate for the particular application. The equipment was modified and redesigned to give more extensive control, greater chill capacity, and shielding provisions, which contribute to the production of welds with good corrosion resistance and physical properties.

External shielding was found to be necessary and is provided by conducting the entire welding operation within a controlled-atmosphere dry box.

Each subassembly contains 264 spot welds which must be reproduced to a high degree of accuracy. The welds are spaced at 3-in. intervals, except for the welds at both ends of each fuel plate. Because the plate ends are the points of maximum anticipated stress, 3 welds spaced $\frac{1}{2}$ in. apart are placed at this location on every plate. To insure the reproduction of high-quality welds, the entire welding process is automated and incorporated into the controlled dry box.

The subassembly is mounted in a fixture which is positioned in yokes on a rolling carriage. The plate spacing is maintained by spacer fingers which operate through and locate from the precision-punched side-plate holes. Two fixtures are employed so that one can be loaded while the other is completing the weld cycle.

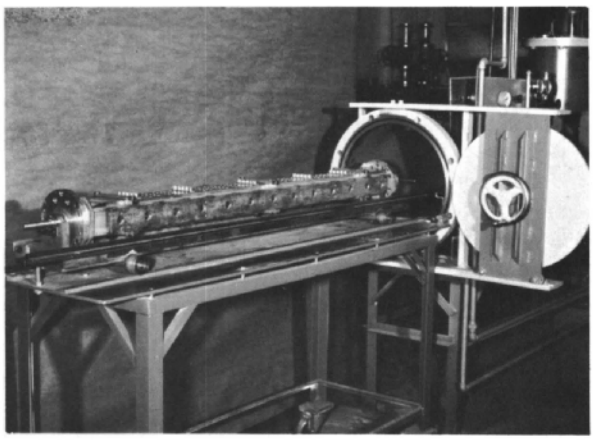

Fig. VII-11

Carriage and Positioning Fixture
106-2454

The carriage with the loaded welding fixture in place is manually rolled into the welding chamber (Fig. VII-11). Within the chamber, the subassembly is automatically moved longitudinally under the welding head by a motor-driven pinion which engages a rack fastened to the carriage. Motion of the carriage is not continuous; the carriage is stopped at each longitudinal weld position for a time sufficient to allow a row of six spot welds to be made before it is driven to the next welding position. After all the welds have been made on one side (132 welds), the subassembly is manually rotated 180° without opening the chamber and the unwelded side is then welded automatically. The direction of carriage travel is away from the loading door during the welding of the first side; and toward the door when the second side is being welded, so that the subassembly is located adjacent to the chamber exit when all welding is completed.

Figure VII-12 is a view of the specially designed welding head which employs three welding guns. The guns are shown positioned over the side plate with the gun in contact with the work being in firing position. Six welds were made successively by positioning each gun over alternate fuel plates (1, 3, 5), shifting the head, and then positioning in sequence over the remaining three fuel plates (2, 4, 6). The individual guns are spring loaded and are brought into contact one at a time by means of rotating cams located above the guns (not shown in Fig. VII-12). Only one gun may be in a position to fire at any given time. The complete head floats on ball bushings, which allows a cam at the rear to shift the gun group so alternate groups of three welds may be made. Individual torch gas flow may be used if desired. This is controlled by the sliding gun-support shafts, which are drilled to act as sliding valves.

The head drive mechanism may be seen at the top of welding chamber (see Fig. VII-13). All head motion is accomplished by the one drive, which enters the chamber through cheveron seals. All motors or

gaseous materials have been excluded from the inside chamber, where contamination of the shielding gas would be a serious problem. All flexible lines within the chamber are "tygon" tubing.

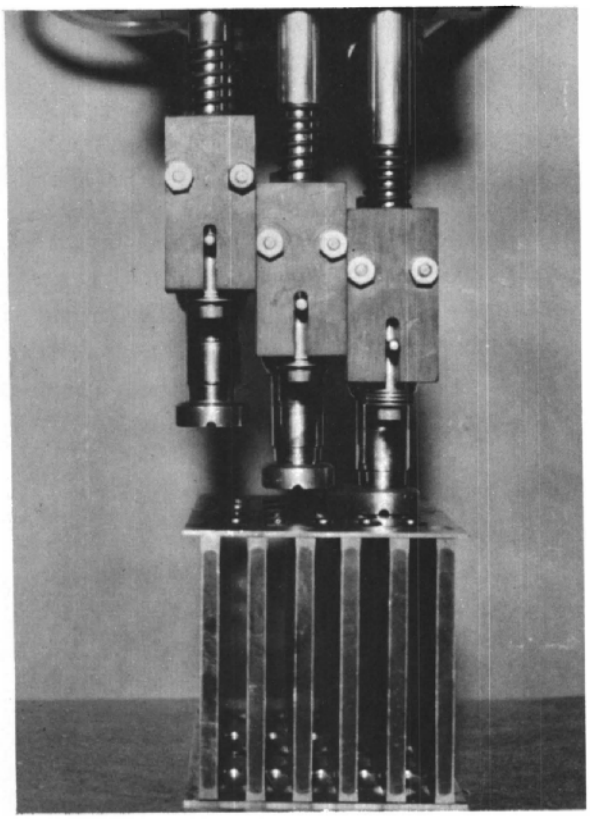

Fig. VII-12

Arc Spot-welding Guns
106-2227

The welding chamber (see Figs. VII-13 and 14), is 12 $\frac{1}{2}$ ft long and has a volume of 28 cu ft. Valves for controlling gas and water flow are located on a panel at the right of the loading door. Excessive pressure buildup within the chamber is prevented by a mercury bubbling system which is vented to the outside. Gas, water, control, and power lines enter at the top of the chamber near the head drive motor. The main control panel is located at the far end of the chamber. All weld timing, sequence selection, method of operation, and automatic control are accomplished with the main control panel. An operation of manual, semi-automatic, or fully automatic may be selected by the operator. In general, fully automatic operation is used, except for the welding of special test pieces having a geometry that does not coincide with a regular assembly. No further adjustment at the main control panel is needed after a weld sequence has been established. Controls which need the periodic attention of the operator are located within a portable control box, which may be seen directly above the view ports.

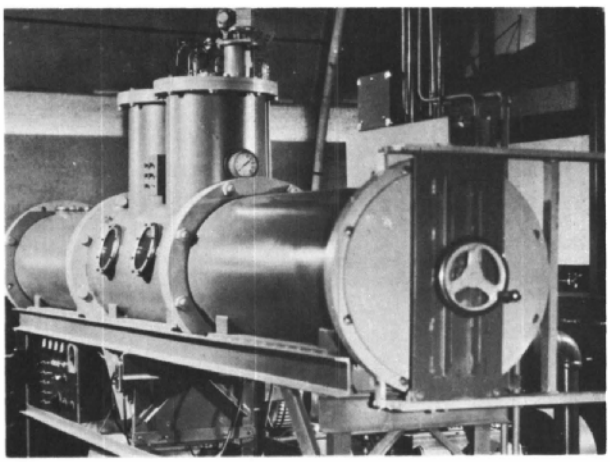

Fig. VII-13

Front View of Welding Chamber
106-2456

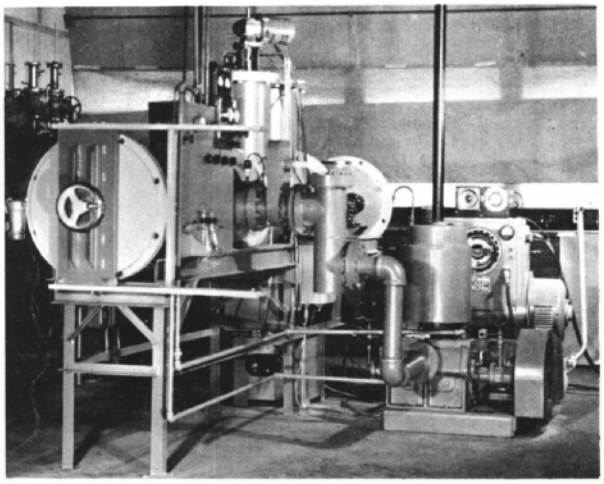

Fig. VII-14

Rear View of Welding Chamber
106-2453

Preparation of the welding atmosphere is begun by removing the air from the chamber by means of a single-stage vacuum pump (Kenney, Model KDH 130), which is shown in the lower right side of Fig. VII-14. Starting from atmospheric, pressure of 10μ may be attained in 5 min or less. Pumping rates are increased and the ultimate vacuum improved by the use of a liquid nitrogen cold trap located between the chamber and the the pump. The standard procedure after the chamber has been open to the air is to purge three times, as follows:

1. Evacuate to 20μ or less.
2. Fill to atmospheric pressure with bottled helium.
3. Evacuate as in step one.
4. Fill as in step two.
5. Evacuate as in steps one and three.
6. Fill to slightly above atmospheric pressure with mixture of 80% helium, 20% welding grade argon.
7. Weld.

After the first evacuation, and prior to the first helium filling, the chamber is isolated from the pump, and the rate of pressure increase is noted. If the pressure increase rate is over 0.1μ/sec, pumping is continued and/or the system is tested for leaks. Outgassing has been found to be responsible for rates of pressure increase above the maximum allowed value. During welding the pressure is maintained slightly above atmospheric.

The welding current supply, located behind the vacuum pump (see Fig. VII-14) may be either a standard 300-amp motor-generator unit with the field circuit modified to allow for automatic current adjustment during start, preheat, and weld cycles, or a 200-amp rectified transformer. Straight polarity (electrode negative) is used with the arc started by a superimposed high-frequency circuit. Retract starting is not considered because of the possibility of tungsten contamination in the weld.

The following is a brief summary of typical welding conditions:

Chamber Gas (during welding)	80% helium-20% argon
Number of Purges	3
Welding Current	Direct Current; Straight Polarity
Starting Current	1 sec at 100 amp
Preheat Current	4 sec at 50 amp
Welding Current	1 sec at 100 amp
Total Heating Time per Weld	6 sec

Consistent production rates of 6 subassemblies per 8-hr day per man have been achieved. This rate includes 15 min of purging and 45 min for welding. Only one operator is required; he performs the dual tasks of assembling the subassembly in the welding fixture and operating the near-automatic welding process.

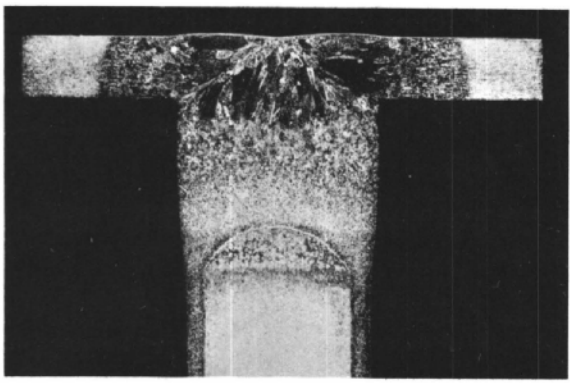

Fig. VII-15

Transverse Cross Section of Spot Weld
106-2472

Figure VII-15 is a cross-sectional view of a spot weld. The side plate thickness is $\frac{1}{16}$ in. The amount of penetration is evident by the large-grained cast structure which extends well into the Zircaloy-II edge on the fuel plate. The uranium alloy core may be seen at the far extremities of the heat-affected zone. No melting and very slight heat effect is present in the uranium core. Physical strengths of the welds are considered adequate. The weld metal is ductile and the $\frac{3}{16}$-in. nuggets will exhibit shear strengths in excess of 2000 lb per weld. A hardness traverse taken in the weld area indicated hardnesses that are near those of the parent metal, in accordance with the procedure described have been shown to be corrosion resistant to distilled water at 550°F.

Testing was done in the "as welded" condition without pickling or other preparation. None of the assemblies produced failed in the corrosion test. After testing and acceptance, the top and bottom stainless steel fittings were attached to the Zircaloy-2 assembly side plates by means of stainless steel rivets.

A total of 1120 fuel plates were produced. Of this total, 930 were acceptable for reactor use - making the recovery 83.0%. The bonds between core and cladding were satisfactory in 98% of the plates. The Zircaloy bonds based on metallographic examination of plate end sections were satisfactory

in 96.4% of the plates. Of the 1120 plates produced, three failed in corrosion testing - a 99.7% recovery. The plates which failed did so almost immediately, indicating that water reached the core through a defect present in the cladding before testing. Metallographic examination of the bond lines in the failed fuel plates did not reveal water channels in the bonds.

B. Fabrication of Spiked Core-1A Fuel Elements

In modifying the EBWR to allow for a heat-dissipation capacity of 100 Mwt, 28 of the original slightly enriched solid metal fuel elements were replaced with elements containing highly enriched fuel. The material in these "spike" elements was a solid solution ceramic composed of 82.21 w/o ZrO_2, 9.13 w/o CaO, 8.16 w/o UO_2, and 0.5 w/o impurities, in the form of cylindrical pellets, 0.322 in. in diameter and $\frac{1}{2}$ in. long. The fuel rods consisted of these ceramic pellets clad by nominal 0.375 in.-OD-0.325-in.-ID x 49-in.-long Zircaloy-2 tubing sealed at each end by 0.375-in.-diameter x $1\frac{1}{2}$-in.- long Zircaloy-2 end plugs. Element assemblies are 49 rods held in 3.6 x 3.6-in. bundles and these bundles, inserted in $3\frac{7}{8}$- x $3\frac{7}{8}$-in. frame assemblies, complete the fuel elements (see Fig. VII-16).

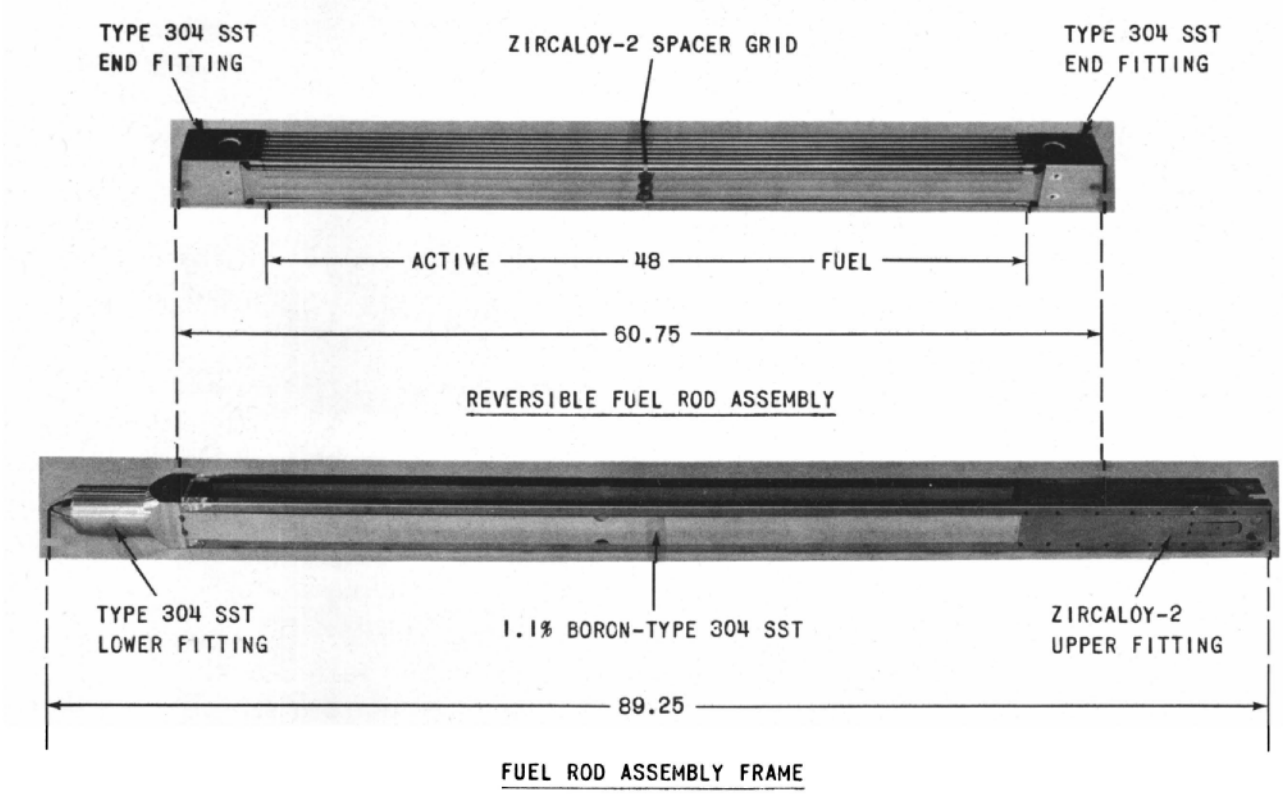

Fig. VII-16

EBWR Spike Fuel Rod Assembly and Frame
(All Dimensions in in.)
111-9385

Commercially fabricated Zircaloy-2 tubing, used for cladding the fuel, was given a small-area, pulsed-field, electromagnetic inspection for internal wall defects. Restriction of allowable crack depth to 0.004 in. resulted in rejection of approximately 43% of the tubing inspected. Zircaloy-2 rod stock for end plugs was given an ultrasonic through-transmission inspection for internal defects. Final machining of the end plugs was done after development of the arc-welding method had fixed the design of the end closures. After the acceptable tubes had been cut and faced to final length, end plugs were welded under an inert gas shield into one end of each tube. The ceramic fuel pellets were manually loaded into each tube; the loaded tubes were then evacuated and back filled with an atmosphere of 98 v/o helium, 1 v/o nitrogen, and 1 v/o hydrogen. The second end plug was welded into the open end of the fuel rods. The helium atmosphere enabled the checking of the end closure welds with a mass spectrometer helium leak detector, and served as a more efficient medium for heat transfer across the 0.003 to 0.004-in. annulus between the ceramic fuel and the Zircaloy cladding.

Completed fuel rods were wet-abrasive blasted at 50-60 psi with 400 mesh Al_2O_3 grit and pickled in a 35 v/o HNO_3-5 v/o HF solution maintained at a temperature of 35-40°C to ensure a corrosion-resistant surface finish. A total of 1,568 fuel rods of this type, enough for 32 elements containing 49 rods each, were fabricated.

The 51-in.-long fuel rods were held in element assemblies by fitting slots in each end plug onto stainless steel positioning grids at both ends. The rods were also held at their centers by a $\frac{1}{4}$-in.-thick Zircaloy-2 center spacer containing openings for 49 rods. The fuel rod assemblies were completed by riveting 0.064-in.-thick Zircaloy-2 strips on two opposing sides to stainless steel grid holders at each end and spot welding the Zircaloy-2 side strips to the center spacer. Stainless steel lifting lugs welded to the grid holders facilitated loading of the rod bundles into the frame assemblies.

A sand-cast and machined stainless steel end-fitting with a cone-shaped crosspiece forming an adapting end provides a base on the frame assembly for positioning the element in the reactor core. The corners of the frame assembly consist of Zircaloy-2 angles which were formed from 0.081-in.-thick strip stock on a press break after resistance heating the stock to approximately 700°C. The angles were screwed to the stainless steel end fitting and resistance spot welded to 0.081-in.-thick Zircaloy-2 lifting plates at their free ends. A leaf spring formed from $\frac{1}{32}$-in.-thick Zircaloy-2 strip stock was resistance spot welded to each lifting plate to aid in stabilizing the position of each element in the reactor.

III. Irradiation Testing and Examination of Fuel*

A. Irradiation Testing of Prototype Fuel Element Samples

As soon as the U-5 w/o Zr-1.5 w/o Nb alloy was chosen as the reference fuel for the reactor, experiments were begun in order to evaluate the irradiation behavior of the alloy. Of particular interest were the dimensional stability of the alloy under irradiation and the manner in which the dimensional stability was affected by fabrication and heat treatment. Also of considerable interest, of course, was the ability of the alloy to retain its corrosion resistance when subjected to irradiation. Presented herewith are the results obtained in irradiation studies of the dimensional stability of the U-5 w/o Zr-1.5 w/o Nb alloy.

The irradiation specimens can be conveniently classified into various groups depending upon their fabrication and heat treatment. As will be shown, the irradiation behavior of the alloy is very dependent upon its fabrication and thermal history. Each group of specimens thus showed a characteristic response to irradiation. The groups will therefore be discussed separately and in the approximate chronological order in which they were irradiated and examined.

Results from as-fabricated specimens, which comprised the first group of irradiated specimens, are shown in Fig. VII-17 and 18, and data listed in Table VII-1. The two cast specimens, as expected, were much more stable than the highly oriented swaged specimen. The large scatter in the growth rates of the castings is unusual, although similar behavior has occasionally been noted in cast uranium-zirconium alloys.

Of greatest interest was the dimensional stability under irradiation of the alloy when given a prior heat treatment for corrosion resistance. The second group of irradiation specimens was made from this type of material. The heat treatment consisted of quenching the alloy from the gamma phase, followed in some cases by an aging treatment. All specimens, with the exception of a group that was restrained during irradiation, showed growth rates that were even higher than those obtained with as-fabricated material. Values of G_i, the growth coefficient, were near 300 microin./in. per fission/10^6 total atoms for the wrought specimens. Repeated gamma quenches steadily enhanced the growth rate. All the quenched specimens were found to have distorted severely under irradiation. The following conclusions can be drawn from the results on these specimens:

1) The high irradiation growth rate of the wrought alloy was further increased by quenching from the gamma phase to impart corrosion resistance.
2) The loss in corrosion resistance resulting from irradiation was not due to surface changes.

*J. Kittel and C. Reinke

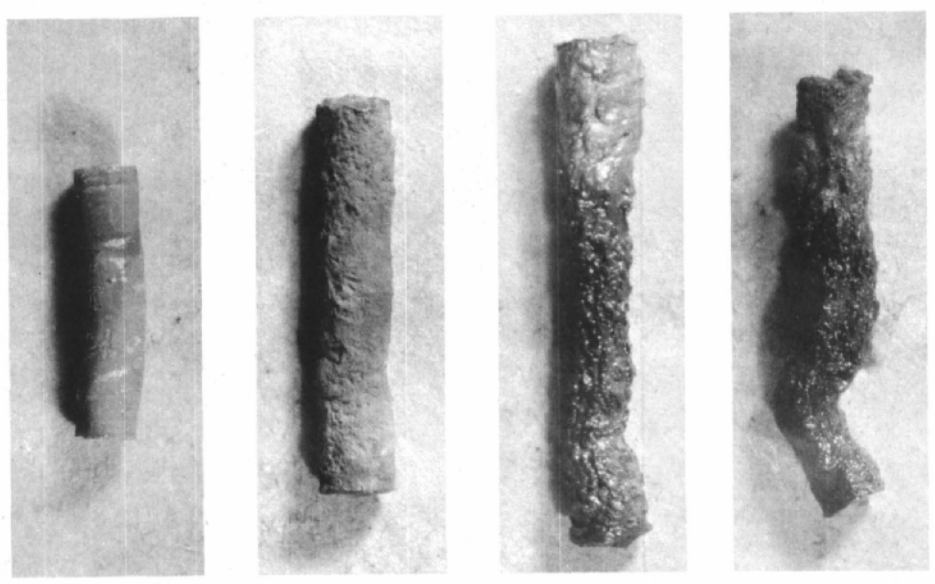

Specimen No.	AH-1-2	AF-1	AF-3	AF-5
Burnup, a/o	0.046	0.16	0.42	0.51
Irradiation Temp, °C	130	210	480	580

Typical Cast and Gamma-quenched Specimens after Irradiation

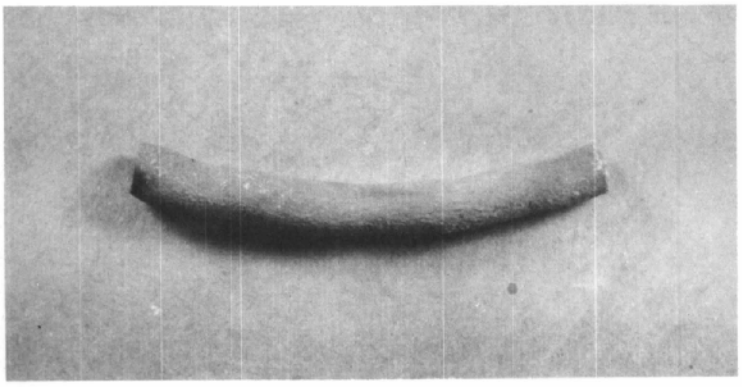

Specimen AB-36-2, Swaged and Gamma-quenched, after 0.071 a/o Burnup at 160°C

Fig. VII-17

Effects of Irradiation on Various Heat Treatment Samples of U-5 w/o Zr-1.5 w/o Nb.

Specimen AH-1-4, Swaged, Furnace Cooled, and Gamma Quenched, after 0.046 a/o Burnup at 130°C

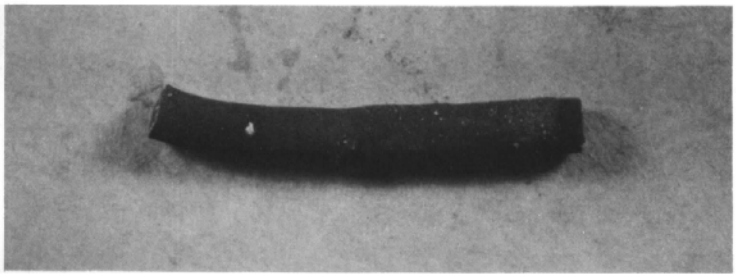

Specimen AH-4-3, Swaged, Gamma Quenched and Tempered for 24 Hours at 550°C Four Separate Times, Followed by Gamma Quenching, after 0.046 a/o Burnup at 130°C

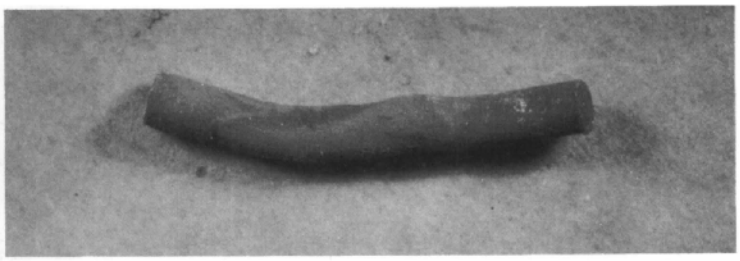

Specimen AH-2-5, Swaged, Isothermally Transformed for 24 Hours at 650°C Four Separate Times, Followed by Gamma Quenching, after 0.048 a/o Burnup at 130°C

Fig. VII-18

Irradiation Effects on Various Heat Treatment Samples of U-5 w/o Zr-1.5 w/o Nb

Table VII-1

EFFECTS OF IRRADIATION ON AS-FABRICATED SPECIMENS (Group 1)

Specimen No.	Fabrication	Burnup, w/o	Irradiation Temp, °C		Length Change, %	Growth Rate, G_i*	Diameter Change, %	Remarks
			Surface	Center				
AH-1-6	Cast	0.046	120	130	+1.16	+25	0.44	
AH-2-6	Cast	0.048	120	130	-0.02	-0.4	1.31	
AB-36-1	Swaged at 800°C	0.071	140	160	11.5	+11.5	-3.4	Slightly Warped

*G_i = microin./in. per fission/10^6 total atoms.

After the first results became available on the specimens in Group 2 that had been gamma quenched for corrosion resistance, irradiations were begun on a third group of specimens in an attempt to find a suitable heat treatment for dimensionally stabilizing wrought U-5 w/o Zr-1.5 w/o Nb alloy under irradiation. The selection of the various types of heat treatment for dimensional stabilization was largely based on earlier irradiation studies of uranium-zirconium alloys. In these experiments and in subsequent work the following gave a stable condition to U-2 w/o Zr alloys: (1) cooling at an optimum rate from the gamma phase, (2) quenching from the gamma phase and tempering in the $\alpha + \gamma_1$ region, and (3) isothermally transforming from gamma in either the $\alpha + \gamma_1$ region or in the upper temperature range of $\alpha + \delta$. Since in some respects the U-5 w/o Zr-1.5 w/o Nb and U-2 w/o Zr alloys appeared to respond similarly to heat treatment, the same three types of heat treatment listed above were explored for their effectiveness in stabilizing the ternary alloy. The following conclusions can be drawn from the Group 3 specimens:

1) U-5 w/o Zr-1.5 w/o Nb alloy can be stabilized against irradiation growth by several different heat treatments.

2) None of the dimensionally stabilizing heat treatments could be expected to confer a corrosion-resistant condition in the alloy.

3) The most effective stabilizing heat treatment consisted of heating the alloy into the gamma phase, followed by a 24-hr isothermal transformation to alpha at 650°C.

The successful attempts in stabilizing the U-Nb-Zr alloy, as described for the Group 3 specimens, led to preparation of a fourth group of specimens. Since the dimensionally stabilizing heat treatments were exactly opposite from those required for imparting the corrosion-resistant condition, the intent with this group was first to stabilize the wrought alloy against irradiation growth by suitable heat treatment and then to superimpose an additional heat treatment for conferring corrosion resistance in the material. Quenching the stabilized alloy resulted in irradiation growth rates as large as those obtained with quenching as-fabricated material

which had been given no intermediate stabilizing heat treatment. It was evident that quenching the stabilized material not only raised the growth rates to their formerly high levels in quenched as-fabricated material, but also caused severe irradiation-induced warping to reappear.

When irradiations were completed on the Group 4 specimens, a decision was required regarding the heat-treatment specification for the EBWR fuel plates, which were soon to be in production. Although the Group 4 specimens had indicated that simultaneous resistance to both irradiation growth and aqueous corrosion could not be imparted to the alloy with any combination of heat treatments known at that time, it had been decided in any case to use the U-5 w/o Zr-1.5 w/o Nb alloy for the EBWR fuel loading because of the ease with which the fuel alloy could be roll bonded to Zircaloy-2 cladding. Since either dimensional stability or corrosion resistance could be achieved in the fuel alloy, but not both, the choice of heat treatment was dictated by which condition was regarded as being the more essential to successful reactor operation. On this basis it was decided to heat treat the fuel alloy for dimensional stability. The decision to remove corrosion resistance as an essential requirement for the fuel was based primarily on two factors:

1) Even when the fuel was in the corrosion-resistance condition, irradiation largely destroyed the corrosion resistance by the time 0.1 a/o burnup had been achieved.

2) Fabrication by roll cladding consistently produced defect-free closures, so that it appeared that entire reliance could be placed on the cladding for preventing catastrophic corrosion failures.

Accordingly, a 24-hr isothermal transformation at 650°C was selected as the best heat treatment. Since the 650°C transformation temperature is approximately 10°C below the upper limit of the alpha-plus-gamma region, it could be expected that dimensional stability of the alloy might be markedly affected if transformation were performed in a region of higher-temperature because of, for example, inadequate control of furnace temperature. In order to provide for some latitude in furnace temperatures, as would be desirable for shop conditions, an isothermal transformation temperature of 640°C was specified for the EBWR fuel loading. The decision to heat treat the fuel for dimensional stability and to rely on the cladding for corrosion protection was wise. The EBWR fuel elements by mid-1959 had achieved a maximum of 0.39 a/o burnup with negligible dimensional changes and no failures due to corrosion or any other cause.

The specimens used in Groups 1 through 4 were round rolled, or swaged, to form cylindrical irradiation specimens. This shape was simplest to produce and served as a convenient specimen shape for studies of the basic behavior of the U-Zr-Nb alloy under irradiation. During these

experiments, however, it was recognized that the fuel for EBWR would be flat rolled and would have a texture considerably different from that produced in round-rolled or swaged material. The irradiation growth characteristics of flat-rolled material could, therefore, be expected to differ from those shown by the cylindrical specimens in Groups 1 through 4. An additional feature of the actual fuel plates, not represented by the cylindrical specimens, would be the presence of metallurgically bonded cladding. It could be assumed that the cladding would modify, in some fashion, the growth rate of unclad material. Irradiations were also made on plate specimens during the period when the cylindrical specimens in Groups 1 through 4 were being investigated.

The plate specimens comprising Group 5 were the first attempt to determine the irradiation growth tendency of clad plates. The dimensions of each plate were approximately 1.25 x 0.75 x 0.19 in. The plate size was necessarily this small in order to accommodate them in standard MTR-X basket capsules. Each of these miniature plates was clad with 0.015 in. of Zircaloy-2 which was roll bonded to the fuel on the flat side. Of the six specimens irradiated in Group 5, three had open ends so that only the edges and sides were clad. The remaining three specimens were also clad on the edges and sides, and were closed at the ends with welded plugs. Before irradiation, each specimen was heat treated for corrosion resistance by quenching from 850°C, followed by aging for 45 min at 425°C.

The effect of irradiation on the quenched alloy may be similar to that produced by overaging, which numerous tests have shown to result in a marked loss in corrosion resistance. One might conclude, therefore, that it would be undesirable to age the quenched alloy prior to irradiation to obtain a minimum corrosion rate, as this would hasten the onset of irradiation damage to corrosion resistance. Post-irradiation corrosion tests were performed on specimens with 0.021 and 0.079 a/o burnup, respectively. The cladding on each specimen was defected before corrosion testing with a hole of 0.125-in.-diameter. The specimen which was tested for 58 hr at 260°C showed no effects from the test. On the other hand, the other specimen which was tested for 66 hr at 290°C largely disintegrated during the test.

The miniature plates described above were useful in first showing that a substantial degree of restraint could be expected from roll-bonded Zircaloy-2 cladding. It was not possible to extrapolate accurately the results obtained to full-size EBWR plates. This was true because of the wide differences in fabrication history that necessarily existed between the miniature plates and the much larger 54-in. EBWR plates. In order to obtain information on the behavior of material rolled under EBWR plate-fabrication conditions, a sixth group of specimens was prepared by cutting 1.00 x 0.75-in. coupons from full-sized plates. The first six specimens were given a double heat treatment intended to provide both dimensional stability and corrosion resistance. Three of the six specimens were given a final quench from 725°C, which is near the lower temperature limit of

gamma equilibrium. The remaining three specimens were quenched from 850°C. Little difference was shown in the lengthwise growth coefficients that can be attributed to the difference in quenching temperatures. For each quenching temperature, a much greater dependence was shown on irradiation temperature (and possibly burnup). The lengthwise rate of growth diminished markedly with increasing irradiation temperature. For both quenching temperatures, the width of the specimens increased under irradiation at rates up to 5 times the rates of length increase. A difference in temperature dependence was noted, however. For the 725°C quenched material, the rate of width increase increased with irradiation temperature; for the 850°C quenched material, the rate of width increase decreased with increasing irradiation temperature. Both groups of specimens decreased in thickness under irradiation. Somewhat higher rates of thickness decrease were shown by specimens of the 725°C quenched material. For both groups the rate of thickness decrease seemed to be only randomly affected by irradiation temperature.

In order to determine more quantitatively the effectiveness of the cladding in reducing irradiation growth, irradiations were made on an additional seven specimens cut from a full-sized EBWR plate. The plate was quenched from 850°C prior to being sectioned for irradiation specimens. The plate was prepared with a 0.060-in.-thick cladding instead of the customary 0.020-in. thickness. One of the specimens was left with the full 0.060 in. of cladding. The cladding was partially removed by grinding from two other pairs of specimens to give cladding thicknesses of 0.034 and 0.004 in. The cladding was completely removed from a third pair of specimens, to determine the growth tendencies of unrestrained gamma-quenched fuel alloy. The following conclusions can be drawn from the results on the Group 6 specimens cut from quenched, full-sized EBWR plates.

1) Both width and length increases occurred under irradiation, with the width increases occurring at higher rates.

2) The rates of width and length change depended on both quenching and irradiation temperatures.

3) The thickness of the plates decreased under irradiation, but the rate of decrease appeared to be only randomly affected by quenching and irradiation temperatures.

4) Zircaloy-2 cladding thicknesses as small as 0.004 in. reduced irradiation growth of the fuel alloy, so that it could be expected that the 0.020-in.-thick cladding specifications for EBWR plates would aid materially in stabilizing the fuel elements against dimensional changes.

5) The corrosion resistance of the quenched alloy was destroyed by between 0.04 and 0.06 a/o burnup, with some indication that the loss in corrosion resistance might be the result of structural changes similar to overaging.

The following general conclusions could be reached from the aforementioned and subsequent irradiation investigations:

1) The most effective heat treatment for dimensionally stabilizing swaged or round-rolled U-5 w/o Zr-1.5 w/o Nb alloy consisted of a 24-hr isothermal transformation from the gamma phase at 650°C. This heat treatment was subsequently used as a basis for specifying the heat treatment to be given to the EBWR fuel plates.

2) The most effective heat treatment for dimensionally stabilizing flat-rolled material consisted of a 12% reduction in thickness by cold rolling, followed by a 24-hr isothermal transformation from the gamma phase at 655°C.

3) Swaged alloy could not be successfully heat treated to be both dimensionally stable and corrosion resistant.

4) Flat-rolled material could be made both dimensionally stable and corrosion resistant by first reducing the material in thickness 12% by cold rolling, then isothermally transforming the alloy from the gamma phase for 24 hr at 665°C, and finally quenching from 800°C.

5) Flat-rolled fuel alloy under irradiation generally increased in length and width and decreased in thickness.

B. Examination of Irradiated Core-1 Fuel Elements

The examination of fuel elements from a reactor provides useful information on their performance which could not be obtained in any other way, and corroborates and expands on the initial information which formed the basis for the choice of fuel for the reactor. With these facts in mind, the effects of in-pile operation and radiation damage on EBWR Core-1 fuel were determined.

During the course of an examination which covered the period from June 1958 to November 1959, two fuel elements were disassembled and sampled. They were fuel elements T-23 and ET-51, which were in the reactor for a period of 1 year and $2\frac{1}{3}$ years, respectively. The fuel plates in element T-23, which had a maximum burnup of 0.11 a/o, were composed of 0.170 in. of natural U-5 w/o Zr-1.5 w/o Nb alloy clad with 0.020 in. of Zircaloy-2. Element ET-51, which had a maximum burnup of 0.39 a/o, was identical with T-23, with the exception that the uranium used was 1.44% enriched instead of natural.

The two EBWR fuel elements were first examined visually through the windows of a hot cell. The elements appeared to be in good condition with no excess fuel plate warpage or swelling evident (see Fig. VII-19). The Zircaloy-2 side plates and stainless steel end fittings

were attached firmly; also, there was no indication of preferential corrosion at the spot weld or rivet areas. A considerable quantity of surface scale was observed on the fuel plates of both elements. In the element with the longest exposure (ET-51) extensive portions of this scale were not adherent. X-ray diffraction and spectrochemical analyses of the scale revealed aluminum as the major metallic constituent. Significant quantities of nickel and iron were present also. Based on these analyses, boehmite ($Al_2O_3 \cdot H_2O$) was one constituent of the scale. A variation in the thickness of the deposited scale resulted in a graduation in shading along the length of the plates.

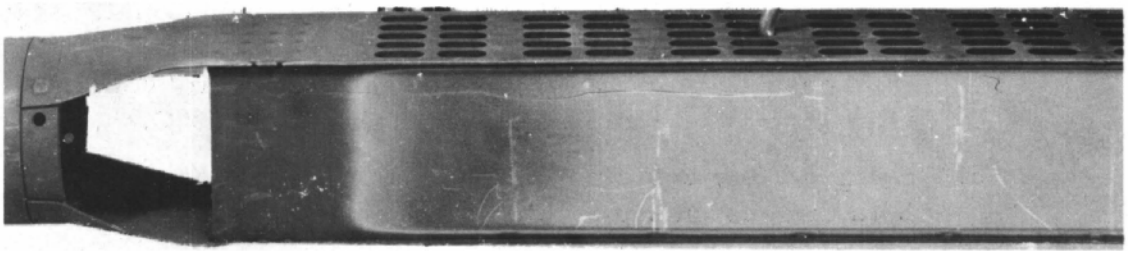

Lower End of EBWR Fuel Element T-23 in the As-received Condition

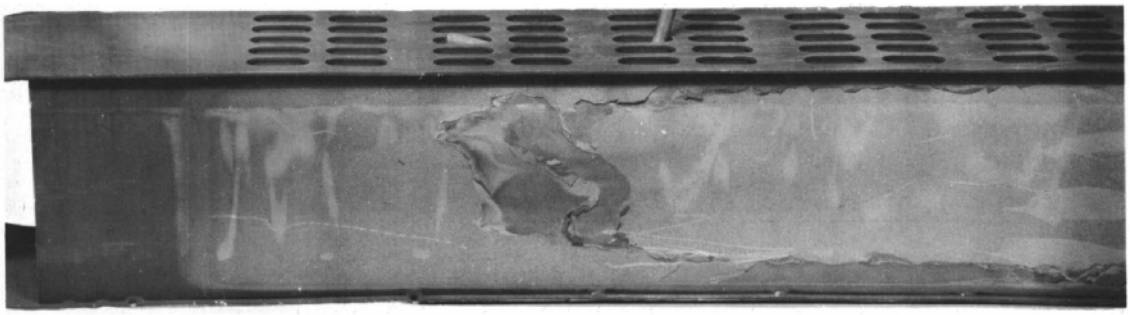

Lower End of EBWR Fuel Element ET-51 in the As-received Condition

Fig. VII-19

Crud Deposits on EBWR Fuel Plates

The fuel plates in elements T-23 and ET-51 exhibited good dimensional stability under EBWR reactor operating conditions. Preirradiation measurements of width were made at a minimum of three random locations along the length of each plate, excluding the last 6 in. at each end. On the basis of these measurements and the post-irradiation values, which were accurate to $\pm \frac{1}{32}$ in., there was no change in either the width or length of any of the plates checked. The thickness of a plate from fuel element T-23 increased by a consistent 0.004 to 0.005 in. maximum along the bottom half of the plate. This increase was due to the sum of any volume increase plus scale deposition during in-pile operation. It is significant to note that even with this increase the post-irradiation dimensions fell within the specifications for the unirradiated plate.

Thickness measurements on the plates from fuel element ET-51 included an unknown thickness of scale. The thickness is unknown because: (1) areas were present at which partial descaling occurred, and (2) the plates were wire-brushed prior to the ultrasonic examination which preceded the dimensional measurements. Measurements on scale which had spalled from the fuel plate surfaces indicated a thickness of about 0.005 in. It is estimated that the thickness of the plates in fuel element ET-51 increased by a consistent 0.010 to 0.015-in. maximum along the bottom half of each plate. Since 0.010 in. of this increase was attributed to surface scale deposit during operation, the remaining 0 to 0.005 in. was due to the volume increase accompanying the burnup of the uranium. On the basis of the 0.005-in. increase in thickness, if the length and width continue to remain constant, a volume increase of about 6 to 7% per a/o burnup can be expected due to burnup alone under normal EBWR operating conditions.

After separating the fuel elements into individual plates, the integrity of the core-to-clad bonds was determined by an ultrasonic inspection. An ultrasonic inspection consisted of a scan across the width of each plate and along its length. These two dimensional recordings of the irradiated plates when compared with preirradiation scans indicated that the cladding was firmly adherent to the core on all the plates tested. The initial scan of the plate from fuel element T-23 disclosed an area of poor ultrasonic transmission which coincided with a deposit of scale. The plate was removed from the scanner and wire brushed, after which it was scanned again. The second scan did not reveal any abnormalities. It is believed that the poor ultrasonic transmission observed in the first scan was due to a loosely adherent or porous scale deposit. The ultrasonic scan of each plate also gave an indication of the condition of the core. Since porosity or cracks would be observed as an area of poor ultrasonic transmission and since such areas were not found, it is believed that no large cracks were present in the fuel plate cores.

Samples were milled from the fuel plates of both elements with a slitting saw. Metallographic specimens were cut from these samples by electrical-discharge machining and cold mount using Hysol 6040 compound. Thin samples cut from the fuel plates in element ET-51 warped and cracked, suggesting a relieving of locked-in stresses and indicating that, after 0.39 a/o burnup, the fuel cores were in a brittle, highly stressed condition. The metallographic examination of 40 samples cut from various locations throughout fuel element ET-51 revealed cracks in fuel core, with the most extensive cracks occurring at areas adjacent to the side-plate spot welds. There is no doubt that samples from ET-51 were cracked during specimen preparation. However, it cannot be determined from the results whether microcracks did or did not exist in both fuel elements prior to the cutting operation.

Samples of irradiated fuel core were removed from the plates for corrosion tests in water at 260°C (500°F). The fuel alloy in EBWR was given a heat treatment for maximum dimensional stability rather than for improved corrosion resistance. Over the burnup range of 0.005 to 0.09 a/o, the results of the tests (see Table VII-2) indicate a marked improvement in the corrosion resistance of the fuel with irradiation. The tabulated rates are based on original exposed area. True rates would be higher, but the quoted rates are valid for purposes of comparison. At present there is no positive explanation for this improvement in corrosion resistance. Thermal spikes associated with the fission product atoms may influence in part the improvement in corrosion rates. The effect may be one of changing the structure from the dimensionally stable, isothermally transformed structure to the corrosion-resistant quenched gamma (see Figs. VII-20 and 21) with the effect of additional burnup being similar to overaging, which would lower the improved corrosion resistance. In support of this hypothesis, the hardness values obtained on the irradiated core are comparable to those obtained on unirradiated material by quenching from the gamma phase.

Table VII-2

CORROSION OF IRRADIATED U-5 W/O Zr-1.5 W/O Nb ALLOY IN WATER AT 500°F to 520°F AS A FUNCTION OF BURNUP

Burnup, a/o	Corrosion Rate, mg/(cm^2)(day)	Burnup, a/o	Corrosion Rate, mg/(cm^2)(day)
0.000	9470	0.024	1880
0.005	2500	0.088	1890
0.009	2780	0.11	5160
0.017	2310		

Samples were removed from both fuel elements for analyses of their hydrogen contents. Samples were taken from the edges and center of the plates along the plate length. The specimens from the edges of the plates were solid Zircaloy-2, while those from the center contained 0.170 in. of fuel core clad on two sides with 0.020 in. of Zircaloy-2. Results obtained with a plate from fuel element T-23 indicate a higher hydrogen concentration at the edge than at the center of the plate. The values ranged from 31 to 105 ppm at the edge of the plate, with an average value of 66 ppm and a standard deviation of ± 17. In comparison, the values at the center of the plate ranged from 11 to 21 ppm, with an average value of 14 ppm and a standard deviation of ± 3. Results obtained from the plates from fuel element ET-51 also indicated higher hydrogen concentrations at the edges than at the centers of the plates. The values ranged from 26 to 76 ppm at the edges of the plates, with an average value of 46 ppm and a standard deviation of ± 10 ppm. In comparison, the values at the centers of the plates ranged from 11 to 41 ppm, with an average value of 20 ppm and a standard deviation of ± 7 ppm.

(a)

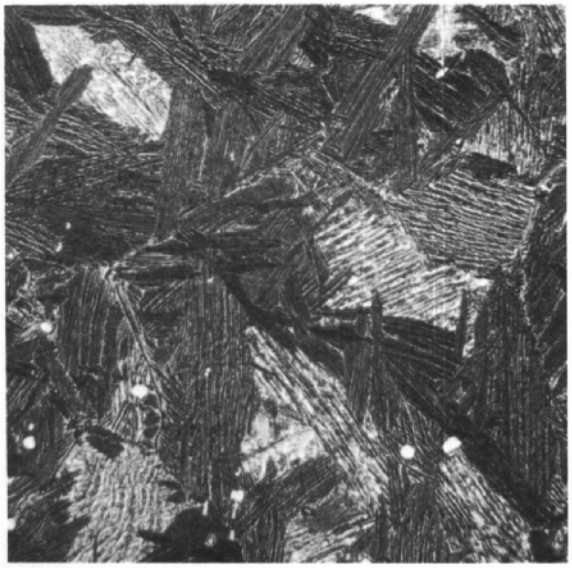

0.0 a/o

(b)

0.01 a/o

(c)

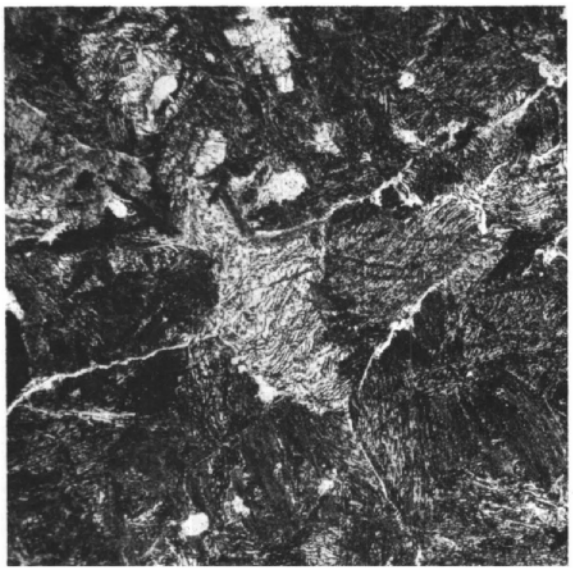

0.03 a/o

(d)

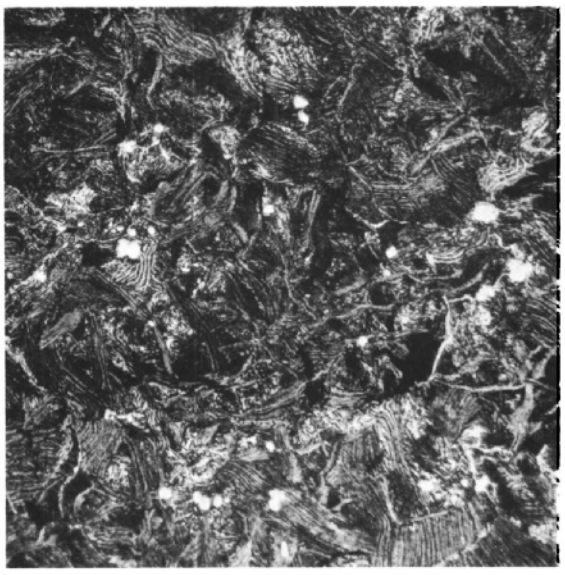

0.09 a/o

Fig. VII-20

Structure of U-5 w/o Zr-1.5 w/o Nb Core Alloy As a Function of Burnup

(e)

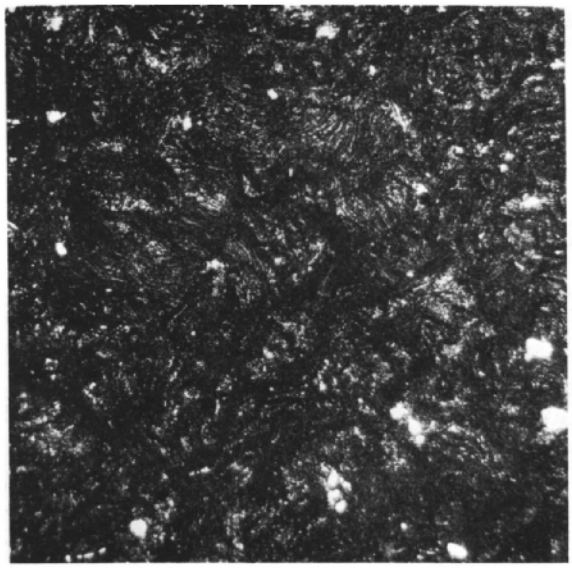

0.17 a/o

(f)

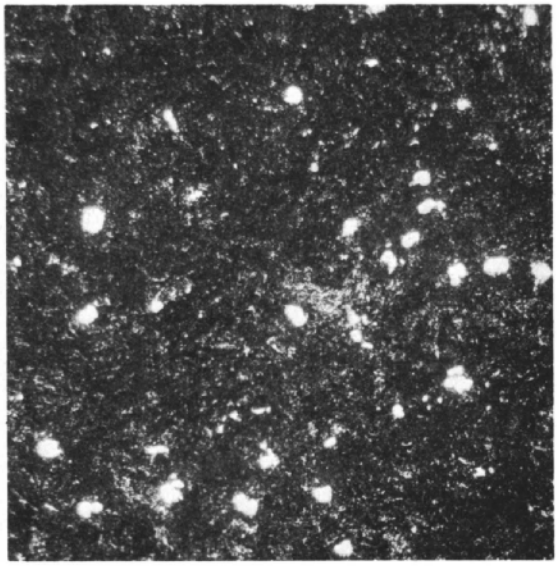

0.26 a/o

(g)

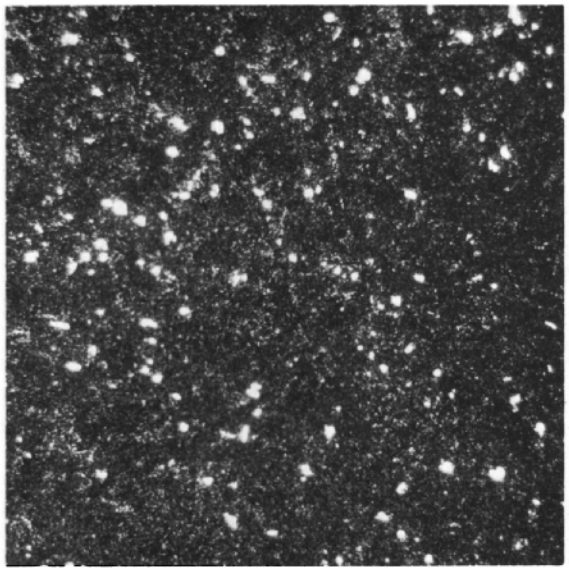

0.30 a/o

(h)

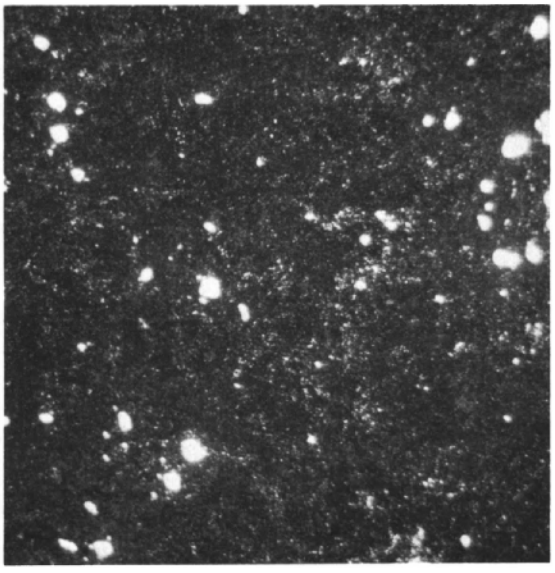

0.32 a/o

Fig. VII-21

Structure of U-5 w/o Zr-1.5 w/o Nb Core Alloy As a Function of Burnup

Samples ranging in length from 1 to 6 in. and having burnups ranging from 0.01 to 0.36 a/o were cut from the plates for postirradiation annealing studies. These specimens were clad on four sides with Zircaloy-2. An area of fuel, 0.170 in. by 3.31 in., was exposed at each end of the sample. The studies were conducted in electrically heated pots containing a heat-treating salt with the following composition: 39% K_2CO_3, 33% Na_2CO_3, and 28% Li_2CO_3. Results of this study are shown in Fig. VII-22.

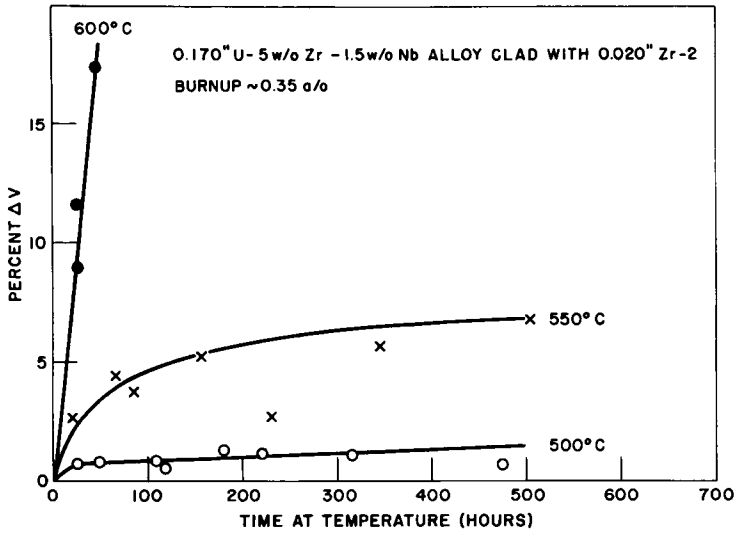

Fig. VII-22

Per cent Increase in Volume of Sections of U-5 w/o Zr-1.5 w/o Nb Alloy Fuel Plate Versus Annealing Time for Various Temperatures.
106-5009

Conclusions from these studies are:

1) EBWR fuel elements are generally in satisfactory condition after operation at central fuel temperatures up to at least 400°C and burnup of 0.4 a/o.

2) Volume increases of 6 to 7% ΔV per a/o burnup due to the burnup of uranium can be expected with EBWR fuel plates operated at fuel temperatures up to 400°C and 0.4 a/o burnup.

3) The hardness of the EBWR fuel core alloy has increased with increasing burnup up to 0.4 a/o. For burnups of 0.3 a/o to 0.4 a/o, Rockwell C values in the low to middle 50's, respectively, are to be expected.

4) Zircaloy-2 possesses considerable ductility after an integrated exposure of 1.6×10^{21} nvt fast at temperatures of 260 to 325°C. (500 to 617°F).

5) For burnups from 0.005 to 0.11 a/o, the corrosion resistance of the irradiated EBWR fuel alloy is superior to that of the unirradiated material.

6) Hydrogen is picked up by the EBWR fuel plates under reactor operating conditions with the probable formation of isolated areas of small amounts of zirconium hydride. The plates operate in demineralized water with a pH of 7 and a surface temperature of 250 to 325°C. (482 to 617°F).

7) Annealing studies on sections of fuel plate at 500 and 550°C (932 and 1022°F) indicated bulk volume increases of 1 to 2% and 5 to 10%, respectively, after 500 hr.

8) Annealing studies at 600°C (1112°F) on sections of fuel plate with 0.35 a/o burnup indicated a bulk volume increase of 17% after 45 hr.

SECTION VIII

WATER CHEMISTRY AND CORROSION

C. Breden
N. Grant
W. Knapp
S. Skladzien

NOTES AND EDITED DATA FROM LECTURES - June 30, 1961

SECTION VIII

WATER CHEMISTRY AND CORROSION

I. Water Chemistry*

A. Water Decomposition

The decomposition of the water coolant in the EBWR system is of considerable importance due to the effect on corrosion, heat transfer characteristics, moderator density, and other parameters. The basic reactions are summarized:

1)	$H_2O \rightarrow H + OH$	Produced by all types of ionizing radiations
2)	$H + OH \rightarrow H_2O$	Favored by γ or light-particle radiation
3)	$H + H \rightarrow H_2$	Favored by α or other heavy-particle radiation
4)	$OH + OH \rightarrow H_2O_2$	Favored by α or other heavy-particle radiation

Combining 1, 3, and 4 gives the forward reaction:

5) $2H_2O \rightarrow H_2 + H_2O_2$.

At temperatures above about 320°F,

6) $H_2O_2 \rightarrow H_2O + 1/2\ O_2$.

The back reaction results from a chain

7) $H + H_2O_2 \rightarrow H_2O + OH$

8) $OH + H_2 \rightarrow H_2O + H$

Therefore,

9) $H_2 + H_2O_2 \rightarrow 2H_2O$.

There are many factors which affect these reactions in a reactor system. For example, not only is the type of radiation important, but also the energy of the radiation. Even a fast electron normally lightly ionizing becomes densely ionizing as it slows down at the end of its track. Also, temperature is significant: temperature has little effect on the forward reaction but does influence the back reaction. Finally, impurities are

*C. Breden, W. Knapp, and S. Skaldzien

important. Iodides and bromides inhibit the back reactions and increase the net decomposition. Techniques have been studied to control the decomposition in reactor systems. Experience with the EBWR is discussed below.

Studies in EBWR indicated that normal steady-state levels of oxygen at 600 psig and 20 Mw were as follows:

Feedwater	0-5 ppb
Reactor Water	0.24 ppm
Steam	28 ppm

During the preliminary design stage it had been assumed, based on experience with pressurized water reactors, that there would be a negligible amount of radiolytic water dissociation (or water decomposition) and that as a result there would be very little oxygen in the water. This had been a large factor in justifying the use of conventional steam-plant materials. The BORAX experiments showed that boiling reactors have a relatively high oxygen content in the water due to their higher net rates of dissociation of water. The reason for this is, apparently, that the boiling process tends to strip gaseous decomposition products out of the reactor before they can recombine. This finding was the basis for the decision to line significant portions of the steam plant of EBWR with Kanigen nickel to protect it from the possible effect of the high oxygen content of the steam.

The first data on water decomposition in EBWR (see Table VIII-1) showed a rather wide spread from 45.7 to 66 cc/liter and averaged 55.1 cc gas/liter of condensed steam (uncorrected for H_2 and O_2 dissolved in the condensed steam). The average of the twelve analyses used gave 30.7% O_2,

Table VIII-1

EBWR WATER-DECOMPOSITION DATA AT A POWER LEVEL OF 20 Mw

Date	Time	Reactor Water Quality			Gas Yield, cc/liter[a]	Condensed-steam Gas Analysis			Air-ejector Gas Flow, cfm[b]	Air-ejector Gas Analysis		
		pH	Conductivity									
			Determined, ohms/cc	Recorded, μ mhos		O_2, %	H_2, %	Inert Gas, %		O_2, %	H_2, %	Inert Gas, %
12-23-56[c]	0115	7.0	180,000		50	22.7	47.0	30.3[d]		25.2	32.8	42.0
12-23-56[e]	2015	7.0	180,000		69	20.4	44.5	35.1[d]		22.6	27.2(?)	50.2
12-29-56[f]	2210	5.2	90,000		53	30.2	55.9	13.9		29.4	56.1	16.1
1-11-57[g]	1630	5.0(?)	410,000		47.5	29.7	68.6	1.7				
1-30-57	1715	7.05	900,000		66	31.0	63.4	5.6		30.4	53.9	15.7
2-11-57	1917	7.0	760,000		52.5	30.0	66.2	3.8		28.2	47.3	24.5
2-11-57	2330	7.0	600,000		46	29.2	62.4	8.4		28.9	44.6	26.5
2-12-57	1300	7.15	640,000		45.7	29.3	69.2	1.5				
2-12-57	2020	7.2		0.8	47.8	30.2	67.3	2.5		29.5	48.0	22.5
2-13-57	1030	7.1		0.9	58.5	31.6	66.6	1.8				
2-13-57	1920	7.08		0.9	55	30.0	66.0	4.0		29.9	47.5	22.6
2-14-57	1200	7.1		1.0	57.8	31.1	66.5	1.8		29.9	49.7	20.4
2-14-57	2110	7.02		1.0	63.3	32.5	67.5	0.0	1.2	29.7	51.8	18.5
2-18-57	1115	7.3		0.8	59.8	31.7	67.0	<1.3	1.0	30.5	56.0	13.5
2-20-57	1000	6.9		0.9	58.0	31.7	66.2	2.0	0.92	30.9	56.1	13.0
Average of samples of 1-11-57 through 2-20-57					55.1	30.7	66.4	2.9		29.7	50.5	19.7

[a] Not corrected for gases dissolved in the condensed steam.
[b] Not corrected for gas density; values reported are for air at 80°F in ft^3/min.
[c] This sample was steam, bypassed to the condenser.
[d] Values are high owing to transfer of sample or actual nitrogen in system.
[e] This sample was steam going to the turbine.
[f] Boric acid in the reactor water was 0.748 g/liter for this sample.
[g] Only 8.3 ppm boric acid was in the reactor water for this sample.

66.4% H_2, and 2.9% inerts. This decomposition was about three-fourths that obtained from BORAX-III, namely, 77 cc gas/liter analyzing 32% O_2, 60% H_2, and 8% inerts with water at pH 7.0. The pressure and temperature in EBWR was 600 psig and 488°F as compared with 300 psig and 420°F in BORAX. The results obtained December 29, 1956, are of interest because they indicate that the presence of 0.748 gm boric acid/liter of water (pH 5.2 resistivity 90,000 ohm-cm) had no significant effect on water decomposition. The decomposition, 53 cc total gas/liter of condensed steam at 20 Mwt, was very close to the 55.1-cc/liter average.

The next group of experiments on water decomposition was concerned with effects of power level and pressure. The data were obtained by measuring the total gas liberated from a known mass of steam. It is seen from Fig. VIII-1 that a plot of the decomposition rate as a function of reactor power indicates a linear relationship; further, at the same power level the higher pressure and temperature are associated with the lower net rate of water decomposition. The rate of oxygen production at 600 psig is 0.41 liter/min/Mwt and at 300 psig is 0.61 liter/min/Mwt. Assuming that 8 Mev of the total energy per fission is absorbed in water dissociation, the moles of hydrogen produced per 199 ev are 0.15 and 0.21, respectively. In subsequent EBWR water-decomposition experiments, the effect of gaseous and chemical additions to the reactor feedwater have been studied.

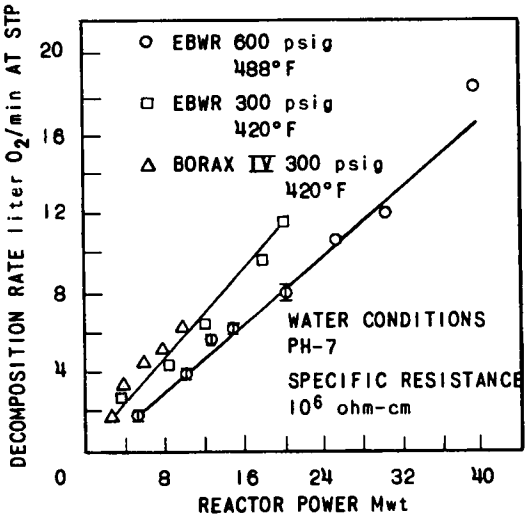

Fig. VIII-1
Reactor Power vs
Decomposition Rate
112-868

In BORAX-III, the addition of gaseous hydrogen to the reactor water was shown to have a marked effect in reducing net dissociation. The magnitude of the effect depended on the point of injection, i.e., when hydrogen was fed through the feedwater sparger, the reduction in net decomposition was greater than when it was injected through a drain line in the bottom of the reactor. This effect is believed to have been due to more complete solution of the hydrogen, better mixing, and possibly longer exposure time to flux affecting recombination when the hydrogen was injected with the feedwater. Reduction in net decomposition by hydrogen addition has been observed also in BORAX-IV.

In the EBWR experiments, hydrogen gas was metered into the reactor feedwater side stream from the purification system. After an equilibrating period of 10 min, samples of steam, condensate, and feedwater

were analyzed. Gas samples were analyzed for oxygen, hydrogen, and inerts, and the liquid samples for oxygen. Results are shown in Fig. VIII-2. Two conclusions reached from these experiments were:

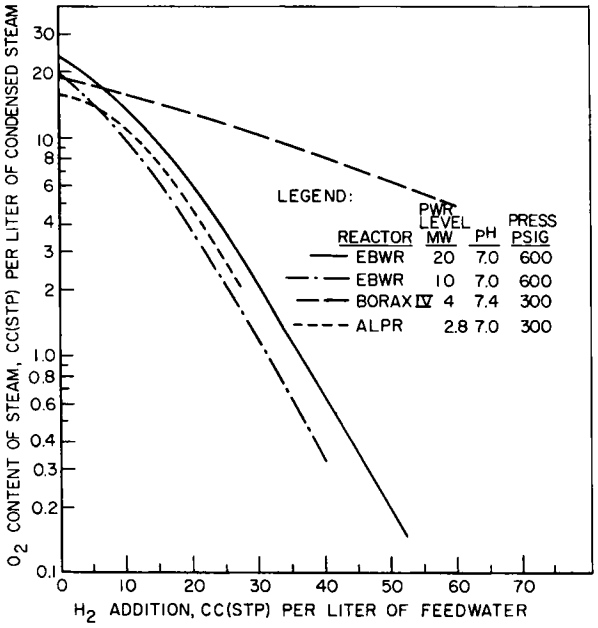

Fig. VIII-2
Effect of H_2 Addition on Water Decomposition
111-7514

1) The BORAX reactor requires much more added hydrogen to give a specific reduction in net decomposition than does EBWR or ALPR.

2) Although small amounts of hydrogen cause a sharp decrease in water decomposition, the effectiveness of additional amounts diminishes rapidly, and the data imply that it may be impractical to attempt reducing the oxygen content of the steam below $\frac{1}{2}$-1 ppm by this method.

The effect of added hydrogen in reducing radiolytic decomposition and lowering the oxygen content of the steam, and the reported breakdown of hydrazine (N_2H_4) under radiation to evolve hydrogen, suggested the use of hydrazine as a more convenient source of hydrogen for use with a boiling reactor than bottled gas. As a 35% water solution, it could be metered and injected easily by a positive-displacement feed pump.

The addition of about 3 ppm of hydrazine resulted in a sharp rise in conductivity of the water in the reactor and hotwell, and in activities measured at several points in the system. The rate of water decomposition decreased slightly and then increased to a value considerably above the initial rate. The pH of the hotwell increased slightly while that of the reactor decreased to a value of about 5.2. No hydrazine was detected in the reactor, and nitrate concentration increased from less than 0.1 to 0.8 ppm. The addition of 0.5 ppm ammonia produced similar results. The addition of nitrogen gas produced no noticeable changes in decomposition rate, reactor water conditions, or plant activities. It was concluded that hydrazine, ammonia, and nitrogen offered no promise in reducing water decomposition.

B. Nitrogen-16 in the EBWR System

Significant amounts of N^{16} have been found in the EBWR system as a result of the $O^{16}(n,p)N^{16}$ reaction. The isotope N^{16} decays with a 7.35-sec half-life to O^{16} by beta decay. Gamma radiations of

6.13, 7.13, and (in a negligible amount) 8.89 Mev are emitted. These gamma activities are by far the most energetic of all those emitted by activation products. The energy of gamma radiations determines the shielding thickness and density requirements. From its low cross section and short half-life, N^{16} would not seem to be such an ominous creature; but when O^{16} is present in such large quantities as it is in the H_2O coolant-moderator of a water reactor, it is regretful that the activation cross section is not many magnitudes lower than it is.

The short half-life of the isotope presents both advantages and disadvantages. For example, an advantage: if the transit time of N^{16} ions from the reactor is long enough, much of the N^{16} will have decayed out before it is spread throughout the auxiliary systems. This is the case to some degree in pressurized water reactors in which the water velocities are relatively low. The disadvantage of a short half-life is the consequential high specific activity of the isotope that is particularly appreciable during the first seconds after the formation of N^{16}.

Now to evaluate the "art of breeding and raising" N^{16} isotopes in a boiling water reactor: first, there is the marriage of high neutron flux in the core - including a considerable amount of fast neutrons in the process of being moderated - and a large O^{16} concentration. Soon there is N^{16} through the natural processes. It is uncertain as to what degree of activation occurs within the steam voids or in the water, but in any event the steam being simultaneously formed within the core strips volatile products from the reactor water and carries these into the auxiliary systems.

Surprisingly enough, only about 0.2% of the N^{16} formed in normal reactor operation is stripped into the steam phase. Further study reveals the reason for this. When initially formed, N^{16} must exist as a free radical. The probability of two N^{16} free radicals joining together is very small. Life is not that long. At the same time as O^{16} from an H_2O molecule is converted to the N^{16} free radical, a certain amount of the free radical H must be formed. Simultaneously, radiolytic decomposition of water is taking place and considerable amounts of highly reactive oxygen and hydrogen are produced.

At extremely low temperatures, free radicals can be preserved for limited lengths of time and studied, but at 489°F this is not the case. It is expected, then, that the nitrogen atom will combine readily with hydrogen and/or oxygen to give a cationic or anionic molecule. It is known that molecules of the ammonia class are readily volatile while those of the nitrate group have an affinity, particularly in an extremely dilute condition, for the water phase.

It was desirable to determine in EBWR the total production of N^{16}, the proportion which was stripped into the steam phase, and the factors contributing to the stripping process. Although the reactor was not

originally designed for experimental analytical work of this type, provisions were made for drawing samples from the core. (With the 100-Mw conversion, even better provision has been made for this type of work. The instrumentation nozzles are a great convenience as compared with previous methods.)

Water and steam samples were drawn continuously from the reactor vessel with sample transit times of the order of 10 to 30 sec. Steam samples were condensed in the process. These were immediately monitored by gamma-spectrum analysis instrumentation, that is, a sodium iodide scintillator coupled with a single-channel analyser. The analyser was adjusted to sum all gamma pulses with energies greater than 4.5 Mev.

In this work, which was done over two years ago, some of the sampling and analysis factors were not optimized. For instance, the scintillators used were of small size and not the most suitable for high-energy gamma-radiation analyses, so that the precision could possibly be improved.

Samples of both the water and condensed steam drawn from the reactor vessel were passed through anion or cation exchange resin beds, and the absorption was determined for each. It was determined that N^{16} was produced in the reactor in the following ionic forms: anionic ~90%; cationic ~10%; neutral ~0.5%. The stream contains practically all of the neutral species, only part of the cationic species, and none of the anionic species. It was found that only a small portion (0.2%) of the N^{16} formed in the reactor was carried over by the steam. This amount increased exponentially with an increase in power. The amount of cationic species stripped from the water increases almost proportionately with power, so that N^{16} concentrations in the reactor water are proportional to power and, in the steam, are proportional to the square of the power.

In order to evaluate the N^{16} distribution in EBWR further, various gases and some chemicals were added to the reactor system. Nitrogen and argon had no effect on N^{16} production or distribution. Hydrogen additions caused the N^{16} activity in the steam to increase tenfold. This is primarily due to a shift in the relative amounts of cationic and anionic species in the water from 12-88 to 55-45, respectively, above the core, and from 15-85 to 92-8 below the core. Hydrazine and ammonia were added and caused an increase in steam activity, although in the quantities used there was no significant effect on the ionic ratio in the water. Work will continue on the N^{16} problem in connection with higher powers and new EBWR reactor operating parameters, such as higher shroud and different feedwater-ring location.

One study using N^{16} that may be expanded is the study of the water-steam interface using N^{16} concentrations in the cooled, continuously flowing water samples as a tool. With a series of probes located below, through, and above this interface, it is possible to determine the character of this layer and to estimate frothing that may be occurring. Other methods are also being studied, but this application is at least an interesting one.

In the boiling water reactor, the ideal situation from the standpoint of shielding design would be the retention of all N^{16} within the reactor core, where the shielding is designed for fission radiation far in excess of any N^{16} radiation that would ever be encountered. Free radicals and nitrogen compounds being what they are, it is not conceivable that this will ever be totally accomplished or even partially accomplished in EBWR. It is interesting that N^{16} distributions can be changed with hydrogen addition. One can assume that the opposite effect might be obtained with a suitable oxidizing agent in a reactor specifically designed, material-wise, to allow the use of such an agent. It appears that N^{16} will continue to be the major activity in the auxiliary systems of the boiling water reactor, and all that can be done is to evaluate it for design data applicable to other reactor projects. Even though it is a major activity, it has not presented a hazard in EBWR that would hamper research work in the plant.

There are other activities formed in EBWR in a similar manner and as yet not fully evaluated. These include N^{17}, which is a delayed-neutron emitter with about a 4-sec half-life, N^{13} emitting 0.5-Mev gamma radiation with a 10-min half-life, and F^{18} which also emits 0.5-Mev gamma radiation with a 2-hr half-life. The neutron-emitting N^{17} is of importance in the operation of a water-moderated reactor. The other isotopes have no significant effect on plant operation or radiation activity levels.

C. Activities Carried by Reactor Water and Steam

There are two chief reasons for the great concern of reactor engineering people about activity levels in a reactor system like EBWR. The first obvious reason has to do with safety. The activity levels may have reached the point where it would be extremely hazardous to conduct maintenance operations on the various parts of the reactor system. The second reason concerns what might be termed the "inversion factor." The activity levels in the water depend considerably on the rates of corrosion and erosion of the reactor materials, and on the activation and transportation of these products to various parts of the system. So, in a sense, the activity level can be taken as a measure of the rate at which the system is changing from a reactor containing water to water containing a reactor.

Fortunately, conditions are not as bad as was originally anticipated. After 4 yr (8850 Mwd) of operation only minor contamination of the primary system components external to the reactor vessel has occurred. When the reactor is operating the major activity in the system is N^{16}. It originates from the reaction of a fast neutron (9-18 Mev) with O^{16} in the coolant water. Fortunately, 99.8% of this N^{16} activity remains in the water and only about 0.2% is carried out of the reactor vessel by the steam.

After the reactor has been shut down, accessibility to the plant or plant equipment is determined by the longer-lived nuclides present in

the system that result from activation of corrosion products. A typical analysis of the reactor water for these nuclides after the reactor had been operating for some time at 20 Mwt with the ion-exchange flow at 10 gal/min yielded the data shown in Table VIII-2. The Na^{24} originated primarily from Al^{27} in the dummy elements, which now have all been removed. In spite of this there is a considerable amount of scale on the fuel assemblies, and this scale, which is about 80% Al_2O_3, will continue to yield Na^{24} to the system for quite some time. Mn^{56} originates from the Fe^{56} due to corrosion of the steel. Co^{58} originates from Ni^{58} in the nickel-nickel phosphide plating in the main steam lines, and Co^{60} from Co^{59} present as an impurity in stainless steel.

Table VIII-2

PRINCIPAL LONG-LIVED RADIOACTIVE NUCLIDES PRESENT IN EBWR REACTOR WATER

Isotope	Half-life	Type of Decay	Decay Intensity in Reactor Water (d/m/ml x 10^4)
Na^{24}	15 hr	β	20
Mn^{56}	2.6 hr	β	6
Co^{58}	71 day	β-γ	0.4
Co^{60}	5.2 yr	β-γ	0.04
Others			0.02

An experiment was conducted to determine the carryover of corrosion activity by the steam. Through the use of Na^{24} as a tracer, it was found that about 0.02% of the Na^{24} activity in the reactor water was carried to the external system by the steam. Another experiment showed that the Na^{24} is in no way combined with or carried by any of the other corrosion products in the reactor water. The experiment involved obtaining a sample of reactor water and following the gross decay rate of a given volume of the sample. Then another portion of this same sample was passed through a filter (0.1 μ). The filtrate gave a decay curve typical of Na^{24} with little or no tailing. The decay curve of the residue showed that no Na^{24} was present. A gamma spectrum of the residue yielded mainly the characteristic peaks of Co^{58} and Co^{60}. These results would seem to indicate that a few improvements could be made in the system for water purification.

First, more emphasis might be placed on water cleanup by filtration. This would permit operating the cleanup system at a higher temperature. Now it is limited by the stability of the ion-exchange resin, and 170°F is probably the top temperature. Also, filter units having higher flow capacities could be used. Under these conditions the insoluble materials in the reactor water, both active and inactive, would be maintained at a lower level.

Among the elements present in trace amounts are:

Zr^{95}(63-d) from the Zircaloy cladding on the fuel assemblies.
Hf^{181}(46-d) from the control rods.
Cu^{64}(12.8-hr) probably from the baffle rings in the turbine.

During the time required to reduce the temperature of the reactor system so that maintenance operations can proceed, the Na^{24} and Mn^{56} decay to negligible levels leaving Co^{58} as the major source of activity present.

In addition to the corrosion product activity in EBWR, trace amounts of fission product activities can easily be found in water samples, and gaseous activities like Xe^{138} are continuously monitored in the stack gases. Their presence in the system is due to uranium contamination on the surfaces of the fuel assemblies. Several I^{131} determinations and rate measurements for Xe^{138} yielded values which correspond to a contamination of about 0.5 mg of U^{235}.

D. Fission Products in EBWR

The total production of the single fission-product isotope, xenon-138, from one gram of U^{235} in the high-flux zone of EBWR operating at 20-Mwt power has been calculated to be over 2500 c/day. Another isotope, krypton-88, would be produced at the rate of 170 c/day. Obviously, the total production of fission products from one gram of U^{235} is phenomenal. The curie refers to a certain number of disintegrations (3.7×10^{10} per sec) and is dependent on the decay rate of the individual fission product isotopes. Since the majority of these are relatively short lived and, to compound the felony, have several radioactive daughters, the production rate in curies is more astounding than would be the production rate as numbers of atoms.

It is this very problem which separates nuclear power plants from conventional plants and which has determined the necessity for a containment shell and all the other special precautions. The first line of defense against uncontrolled release of these fission products is the fuel-element cladding.

The present concern in EBWR, then, is in fission products that are present from diffusion through defects in the cladding or from "tramp" uranium in the reactor. There is concern with the potential release of this material from fuel-cladding defects of various kinds and magnitudes. There is equipment and controls for the day-to-day monitoring of background production of fission products. Scram procedures have been established, even automated, for more hazardous conditions. The source of the day-to-day fission products released within the reactor system is due to the above-mentioned diffusion phenomena. There is uncertainty how much of this may be via minute defects, such as hairline cracks, manufactured into the

assemblies and how much is due to true diffusion phenomena. The other source (commonly known as tramp uranium) is due perhaps to contamination of the fuel elements during fabrication and testing of the assemblies, or it may be due to a metallurgical contamination of uranium in the zirconium cladding of the elements or in the structural materials. In any event, the quantity of exposed uranium present is estimated at 35 mg. The observed fission products from these sources being discharged from the stack of EBWR, contain just less than 0.5 c/day with the reactor at 20 Mwt.

Fission products from this day-to-day source readily divide into three groups: those which are gaseous (at least during some phase of their decay chain), those which are water soluble and in ionic form, and those which are so highly chemically reactive as to plate out almost immediately after being formed. Because of the problems involved in studying this latter group, little is known or established. The first group includes the xenon and krypton isotopes. In the boiling reactor these are readily stripped into the steam phase. Since these generally decay with a short half-life, they deposit radioactive daughters throughout the auxiliary system. Fortunately, the daughters are soluble, so that no great accumulation has been found. The longer-lived isotopes are eventually carried through the steam condensor and are then stripped from the condensate, along with any air in-leakage and the hydrogen and oxygen from radiolytic decomposition by the air-ejector system. The noncondensable gases including the xenon and krypton are then discharged through the stack. Subsequent to being separated into the noncondensable gas phase, these radioactive elements continue to decay so that their daughter products are deposited in the stack or are discharged as particulate matter.

The water-soluble activities continue to circulate in the reactor water, controlled at some maximum value by the continuous cleanup. This amounts to a side stream of reactor water being drawn off at up to 10 gpm, cooled, and passed through filter ion-exchange beds. A 10-gpm side stream from a 3000- to 4000-gal operating system is not the best way to control the activities in the water, but it does a satisfactory job. The activity of the ion-exchange beds reaches relatively high values, not from the fission products, but from the activation products which have been absorbed.

The activity in the stack effluent is due to N^{16} and the fission gases. A stack monitor instrument is in use which through a simple continuous analog subtracting circuit subtracts the activity due to N^{16} from the total activity in the stack, reading out the difference as these fission gases.

The fission product activities cannot be detected in the reactor water or steam due to the presence of N^{16} and due to the relatively large amounts of sodium-24, manganese-56, and cobalt-58 without a chemical separation being performed. What appears to be relatively large amounts of radioactive materials to a radiochemist would normally not be

detectable by any other chemical method. So even if the purification side stream is relatively small, it is sufficient to hold the buildup of fission-product activities to a low value.

Whenever the purification system is down for a period of reactor operating time (60 hr, for example), the fission products do build up. For instance, Ba^{140} rose from 16 to 123 d/min/ml, and I^{131} rose from 5 to 50 d/min/ml. The other soluble fission products normally reported are Cs^{138}, Mo^{99} and Sr^{89}. These are misleading. For example, I^{131} is an 8-day half-life activity. Other isotopes of iodine that are present in the reactor water are a 21-hr, a 6.7-hr, a 2.4-hr and a 54-min isotope, all of which can be analyzed. The analysis is much more of a problem, however, because the spectrum becomes more complex as the time since sampling is decreased. For most fission product studies it is much simpler to draw a sample, allow it to decay (possibly 8-16 days in the case of I^{131}), separate, and analyze. A nice clean spectrum is obtained that does not include the shorter-lived components. The unfortunate consequence of this approach is that one is then studying only isotopes of no importance in the operating reactor. These are only the badly distorted fossils of the life that once existed. The shorter-lived isotopes have proportionately higher specific activities and hence contribute much more to the fission product activity of the operating system.

On the other hand, the gathering of specific information on soluble fission product activities directly from water samples meets with activation product problems, particularly N^{16}. One approach to the study of certain activities that has not been exploited in EBWR concerns the delayed-neutron-emitting halogen isotopes.

It was important to determine what the effect of a defective thorium, oxide-enriched uranium-oxide element was to the EBWR system. Two tests were conducted and have been reported in ANL-6022. Similar work had been done in other facilities on UO_2 elements. The purpose of using mixed fuel would be to evaluate the mixed fuel and to study the effects of a rupture on the reactor. For all practical purposes, EBWR was only a glorified irradiation facility. No similar work has been done, incidentally, with uranium alloy fuels such as constitute the major loading of EBWR.

In the first test, a small fuel specimen only 3 in. long was used. It contained a 10-mil hole through the stainless steel cladding at the center line. It was located within a thin, enriched element in the EBWR core in a position of highest flux. Tubes projecting into the vessel down to near the top of the core in several locations were used to determine if the ruptured specimen could be located by experimental methods. Results of these tests were all negative. During reactor operation, the fission product distribution in the reactor system was studied. An increase in activity by a factor

of about 2.5 was obtained in the stack effluent due to fission gases. After 5000 Mw hr of operation, this started to decrease to a value near normal operation, probably due to corrosion product plugging the defect hole. It was determined that only about 0.015% of the fission gases actually produced were being released through the defect to the reactor. The steady-state activity levels of the soluble fission products either did not increase at all, or, in the case of I^{131}, increased by various factors up to nearly 10.

The second study used a 48-in. specimen with a 20-mil hole near the top. No significant changes were detected, and the information obtained supported the findings of the first test. The conclusions were: (1) The main radioactive nuclides which escape from the defect are fission product gases. Radioiodines were released at a lower rate than with UO_2, as studies with other reactors reported. (2) The rate of release is controlled by a diffusion-type mechanism as demonstrated by appreciably lower concentrations of the short-lived isotopes being present than would be predicted. The release of fission products amounted to about 0.01% of those produced in the element. (3) With one small defect the major activities in the system continued to be from activation products such as N^{16}, Na^{24}, Mn^{56}, and Co^{58} rather than from fission products. (4) The release of fission products from a defect can be increased or decreased by changing position of a control rod located nearby.

There have been no major fuel ruptures within EBWR. BORAX-IV experienced a rupture of moderate proportions but actually had little difficulty. EBWR could benefit by better fission product-detection instrumentation, and particularly from a method for locating the defective element should a rupture occur. A more basic evaluation of the shorter-lived radionuclides in EBWR, even with uranium additions put directly into the water, could give knowledge of what might occur in the future. The fission products probably present one of the most interesting fields for study of any topic concerning the reactor and its chemistry. On the other hand, they present one of the most ticklish problems to the reactor design engineer, for it is because of fission product release that high-cost cladding and containment shells are necessary.

E. Chemical Control of EBWR

There are certain advantages in using chemical poisons as a control mechanism in reactor systems:

1) More compact and uniform fuel lattices can be designed if soluble poisons replace space-consuming control rods.

2) Heat transfer considerations limit the maximum power level of a reactor. Distortions in the flux near the control rods often cause hot spots which limit power from a given core configuration. A soluble poison shim would uniformly depress the flux and alleviate the hot-spot problem.

3) Akin to 2, fuel could be more economically used since uneven burnup is minimized.

4) Less complex and cheaper control rods can be used.

5) The excess reactivity required for high-power loadings and for fuel burnup can be easily accomplished with soluble poisons.

Factors determining the choice of a chemical poison are:

1) cost and availability;

2) solubility in H_2O;

3) corrosive effect;

4) negative temperature coefficient;

5) neutron-gamma reaction;

6) stability;

7) effect on scale formation;

8) effect on water decomposition; and

9) difficulty of cleanup.

A study of various poisons quickly reveals that almost all would be unsuitable for use as a soluble poison in EBWR. Boric acid, however, is particularly adaptable to this application. It is cheap, readily available in high purity, readily soluble in the range of interest in water, and it has no significantly active daughter resulting from neutron activation. It is stabile, noncorrosive, nonscale forming on the fuel plates, and does not significantly affect water decomposition in the range of interest. Aqueous solutions of boric acid can be maintained in a high-purity condition by circulating it through a boric acid-saturated, mixed ion-exchange resin column. The anionic nature of the borate radical prevents interference in cleanup of accumulated corrosion and activation products, nearly all of which are cationic. Boric acid appears to have a zero temperature coefficient and therefore does not deviate appreciably from the desired negative temperature coefficient property. In view of its adaptability for chemical control, boric acid is the logical choice for operation of EBWR at 100 Mw.

In order to attain the highest possible power, it is necessary for the control system used for operation of EBWR at 100 Mwt to provide more control than previously required. Additional reactivity must be provided to compensate for that lost from both increased voids and xenon concentrations at higher power levels. In view of the foregoing considerations, it was decided to use boric acid with EBWR Core 1A to provide sufficient range of reactivity control to insure cold shutdown margins and yet permit the possibility of reaching power levels approaching 100 Mwt.

Core 1A will be subcritical, cold, with 9 rods fully inserted without boric acid. It will be necessary, however, to use boric acid in order to provide a margin of safety at shutdown. Additional control is provided by boric acid to insure that the system can be held subcritical in case of maloperation of one of the control rods. Since such safety precautions are normally included in provisions of cold shutdown, Core 1A is said to provide cold 8-rod shutdown by the use of boric acid.

The original hazards report for EBWR (ANL-5781, p. 115) specified 7-rod cold shutdown, i.e., the system would be subcritical under all conditions with any 7 of the 9 rods inserted. The present specification is one of 8-rod shutdown to be obtained with the use of boric acid; 9 rods will be required for full shutdown in the absence of boric acid.

The presence of boric acid tends to make the various self-limiting reactivity coefficients less negative. It is not expected that the concentration would approach that at which the void coefficient becomes positive. It is always permissible to have boric acid in the system regardless of the reactor conditions. However, the boric acid concentration must be managed in a manner which at no time leaves the system without the prescribed shutdown requirements. Boric acid has been used as a chemical poison in EBWR when operating at 20 Mwt and at lower powers. The previous use of boric acid shows the expected results of lowering the reactivity in voids, decreasing the void and temperature coefficients, and also increasing the sensitivity of the reactor power to changes in water level resulting from loss of water due to insufficient makeup; that is, if the water level changes but the boric acid inventory in the system remains constant, the reactivity available for compensation by steam voids also changes.

In general, boric acid will be present whenever the reactor is cold and a core suitable for high-power operation is installed. Boron remains in the vessel during preheat, although its concentration will be reduced as the water expands. As the reactor is raised to operating temperature (on nuclear heat), boric acid will gradually be removed. In no case will the 9-rod shutdown criterion be violated. The experience to be gained by operating a power reactor with partial control by soluble poison is expected to be quite valuable. There are strong arguments to suggest that soluble poison control may become a widely used technique in water reactors.

The presence of the boric acid will somewhat alter the values of various reactivity coefficients. The one of most concern is the void coefficient, since boric acid will tend to reduce the magnitude of the negative void coefficient and, if present in sufficient concentration, even to reverse its sign and make the void coefficient positive. For the present system the void coefficient with 10 gm/gal (2.64 gm/liter) boric acid is still negative

with the reactor cold (and therefore at all other reactor conditions), even though substantially smaller in magnitude compared to the no boric acid case. Table VIII-3 illustrates the effect of boric acid concentration on the void coefficient. The void coefficient of the reactor will be measured at various boric acid concentrations as a part of the preliminary experimental program to guarantee that the void coefficient is negative at all concentrations to be used in the system.

Table VIII-3

EFFECT OF BORIC ACID ADDITION ON VOID COEFFICIENT

gm/gal	gm/liter	$\Delta k/\Delta v$
0	0	-0.12
5	1.32	-0.085
10	2.64	-0.045

The temperature coefficient will be only slightly affected by the presence of the boric acid. For the case of rods inserted, approximately 0.04 of reactivity is lost in going from the cold condition to the hot (no-void) condition with a roughly linear temperature dependence. The bulk of the effect is due to the increased worth of the rods at higher temperature. (The temperature coefficient of the core without rods is very much smaller.) Since the boric acid provides only a small part of the total absorption, it is relatively unimportant in effects on the temperature coefficient.

The presence of the boric acid should have a negligible effect on the stability of the system (what small effect it has should enhance stability). In general, at operating conditions very little of the boric acid will be present. The effect of the boric acid on the void coefficient becomes progressively less important as the system goes up in temperature and void content. What boric acid remains at operating condition should enhance stability by reducing the magnitude of the negative void coefficient.

The system for adding boric acid consists of a 100-gal mixing tank, a 200-gal storage tank, and 3 positive displacement-type pumps. The system is capable of adding boric acid when the reactor is at pressure, cold or hot. The solubility of boric acid varies from 102 gm/gal (27 gm/liter) at 32°F to 1550 gm/gal (402 gm/liter) at 212°F. At 68°F, the solubility is 197 gm/gal (52 gm/liter). In order to avoid the need for heating and insulating the entire boric acid-feed system and to reduce the possibility of crystallization in the pumps or lines, the concentration which will be used is 182 gm/gal (48 gm/liter). The solution of boric acid is accomplished by agitation with an electric mixer. Heat can be applied by use of an immersion heater to accelerate solution of boric acid in the mixing tank.

The 200-gal storage tank into which the contents of the mixing tank is dumped is connected directly to the inlet side of each of the three pumps for boric acid addition. The discharge sides of the pumps are connected to a $\frac{1}{2}$-in. pipe line which feeds through a check valve to the line leading to the 3-in. feedwater ring at a point just before this line enters

the reactor shielding. Branch lines from the outlet of these pumps lead to the condenser hotwell and to the line leading to the low-pressure boric acid-injection ring. This allows addition of boric acid to the hotwell when the reactor is not in operation and to the water used to fill the reactor for a hydrostatic test or for shielding when the top is removed.

The stock solution of boric acid will contain 182 gm H_3BO_3/gal (48 gm/liter). The volume of water in the reactor is 4000 gal (15,000 liters). At the maximum addition rate of $2\frac{7}{8}$ gpm (10.9 liters/min), a total of 520 gm/min can be added. For a final concentration of 6.25 gm/gal (1.65 gm/liters) in the reactor, 25.0 kg H_3BO_3 are required, which takes 48 min to add at the maximum pumping rate.

The existing purification system of EBWR has been modified to provide for boric acid control. The modified purification system consists of the original reactor cleanup ion-exchange units with the addition of two small ion-exchange units and revamped piping to these units. In the modified system, the two existing ion-exchange units, each with a capacity of 9 ft^3 of resin, are used for anion-exchange resin only. These units can be valved in series with either unit first, in parallel, or with either or both units by-passed. For the removal of boric acid from the reactor water, the two large anion-exchange units and the small unit containing standard resin will be operated in series. The anion resin in the larger units will remove the borate ions from the water and the small unit will "polish" the water by removing any remaining impurities so as to insure the return of neutral water to the reactor. The small units are referred to as high-flow rate polishing units. Good reactor management policy requires that the operators be able to determine the concentration of soluble poison in the reactor at any given time. This information is required to interpret changes in the behavior of the reactor system, and Table VIII-4 shows a list of typical data and management requirements. When the system is at atmospheric

Table VIII-4

REACTIVITY CONDITIONS AND BORIC ACID MANAGEMENT FOR EBWR CORE 1A

Power	Temperature	Control Rods	Concentration (gm/gal)	k_{eff}	Suggested Boric Acid Management
Zero	Cold	All in	0	0.995	Boric acid required for cold shutdown
Zero	Cold	8 in	0	1.025	
Zero	Cold	8 in	5	0.985	Boric acid shutdown concentration, 5 gm/gal.
Zero	Preheat to 325°F	All in	0	0.99	Boric acid still required at preheat conditions.
Zero	Preheat	8 in	0	1.022	
Zero	Preheat	8 in	5	0.98	At least 2 of 5 gm/gal can be safely removed at preheat conditions - more likely removal will occur while going to operating conditions.
Zero	Preheat	8 in	3	1.00	
Zero	Hot, no voids	All in	0	0.985	
Zero	Hot, no voids	8 in	0	1.020	
Initial full, no xenon	Hot, voids	All out	0	1.045	If all boric acid not removed when high power starts, it is OK since there is time until xenon builds in before all the reactivity is needed.
Equilibrium full, equilibrium xenon	Hot, voids	All out	0	1.01	

pressure with the reactor vessel open, water samples can be dipped directly from the vessel. Otherwise, all sampling or monitoring must be performed with water from the purification system, and circulation through this system is mandatory during sampling or monitoring operations. Two primary monitoring methods will be used. These are continuous monitoring of water flowing through a sample cell in the purification system, and bi-hourly determinations of poison content of the water in an apparatus designed for individual samples.

II. Corrosion*

A. Corrosion Design and Behavior

The EBWR is composed of many materials, all of which are subject to corrosion attack. A great deal of time and money has been spent on investigating the effects of this attack, and it is believed that for the most part the results are partially responsible for the successful operation of the reactor. What are the materials in this reactor which were of concern? The original core assemblies were made of uranium alloy and Zircaloy-2; the dummy assemblies of aluminum X-8001 or Type 304 stainless steel; the original control rods of Zircaloy-2, hafnium, 2% boron-304 stainless steel, and type 304 and 17-4 PH stainless steel; the other internal support parts primarily of 304 stainless steel; the pressure vessel of SA-212 Grade B boiler plate, clad with 304 stainless steel where surfaces are in contact with primary water or steam; most piping of 304 stainless steel; some Kanigen (electroless) nickel plate in the turbine casing and the inlet pipe to the turbine; the condenser tubes of aluminum duplex tubes, 6063 on the outside (steam) and 72-S on the inside (cooling heater). Some of these materials were evaluated by corrosion tests before and during the design work, while some were never tested separately but only observed at intervals after operation of the reactor had begun.

1. Uranium Alloy

Early emphasis was to find a uranium alloy that would be relatively corrosion resistant and physically stable during irradiation. The term "corrosion resistant" in this case indicated something that did not oxidize disastrously in high-temperature water as does unalloyed uranium, the latter having a corrosion rate of about 64,000 $mg/cm^2/day$ in 260°C (500°F) water. Incidentally, 50 mg/cm^2 of corrosion of uranium is approximately 1 mil of uniform penetration. Alloying agents consisted primarily of zirconium, niobium, tin, molybdenum, and silicon, individually and in various combinations. The maximum addition was usually 10% (by weight) of any element. From a corrosion standpoint there were several alloys more favorable than uranium-niobium-zirconium ternary. Two of these were straight U-Nb alloys, one 3%, the other 6%; another alloy was U-3.8 % Si,

*N. Grant and C. Breden

and yet another U-12% Mo. However, most of these other alloys had parasitic neutron-absorption characteristics and others presented fabrication problems. Thus, from an overall standpoint, the uranium-niobium-zirconium alloy soon appeared the most favorable. The best alloy combination for this ternary was found to be 5% Zr and $1\frac{1}{2}$% Nb. A proper combination of corrosion and heat treatment required a great deal of testing. Various heat treatments were tried:

a. 800°C (1472°F) for 4 hr; oil quench in vacuum.

b. 800°C (1472°F) for 1 hr; oil quench, alpha anneal at 600°C (1112°F) for 6 hr.

c. 800°C (1472°F) for 1 hr; furnace cool to 600°C (1112°F) anneal for 5 hr.

d. 800°C (1472°F) for 1 hr; furnace cool to 700°C (1292°F); oil quench in vacuum.

e. 800°C (1472°F) for 1 hr; vacuum cool to room temperature; alpha anneal at 260-343°C (500-650°F) for 6 hr.

Only heat treatment (a) (commonly called gamma quenching) proved to be a good method for these alloys. The effect of temperature on corrosion was also measured. The amounts of impurities such as carbon, nitrogen, and silicon were found to be important and had to be carefully controlled. Finally, results as low as of 6 mg/cm^2/day were achieved in 290°C water. Later, several experiments indicated that the corrosion-product hydrogen absorbed by the sample was the cause of sharply increased corrosion leading to disintegration.

Unfortunately, heat treatment (a) led to very poor dimensional stability under irradiation. It was found the best heat treatment for this alloy and for stability was heating at 800°C (1472°F), quench to 650°C (1200°F), hold for 23 hr, and air cool. This material had an unirradiated corrosion rate of 9500 mg/cm^2/day in 260°C (500°F) water, only better by a factor of 7 than that for unalloyed uranium. There was an indication of some improvement of corrosion rate after irradiation, but the results varied. Of the original and several other heat treatments tried, none could maintain low corrosion rate above 0.06 atom % burnup. With this new heat treatment, stability could be maintained to at least 0.14 atom % burnup. The decision had to be made: stability or corrosion resistance. It was for stability. Therefore, a cladding material was developed.

A fuel assembly was removed in 1958. It was separated into elements and an element sectioned. One section that had 0.26 atom % burnup was placed in an autoclave and exposed to water at 260°C. During the first 1.9 days, it corroded at 2500 mg/cm^2/day. After an additional 2.5 days, the sample was gone. An unirradiated sample, identical with the

previous one, was gone after 1.67 days. The test was repeated for verification, and the conclusion drawn that irradiation does decrease the corrosion rate of the uranium alloy. The rate of corrosion of the second unirradiated sample was 5940 mg/cm^2/day.

2. Zircaloy-2 Cladding

The choice was for Zircaloy-2 for the first core. Specifically, Zircaloy-2 is an alloy containing 1.5% tin, 0.12% iron, 0.10% chromium, and 0.05% nickel. Corrosion is less than 0.05 mg/cm^2/mo up to 315°C (600°F) water for tests conducted up to 3 yr. One phenomenon of the corrosion of this alloy was a breakaway type of corrosion. This is a sudden upward change in rate of corrosion. In 360°C (680°F) water it occurs after 120 days; in 400°C (750°F) steam (100 atm) it occurs after 50 days. The weight gain at breakaway is usually from 0.40 to 0.50 mg/cm^2 (1 mil of metal penetration is equal to about 16 mg/cm^2 weight gain).

There are a few factors that will affect the corrosion of this alloy. The presence of over 100 ppm nitrogen, or 5000 ppm oxygen, or 1500 ppm hydrogen will cause loss of corrosion resistance. Less than a total of 0.3% of iron, chromium, and nickel will greatly increase the corrosion. Proper surface preparation is one of the most important factors. Even the best machining and grinding techniques will not give a corrosion-resistant material. It is necessary to remove $1\frac{1}{2}$ to 3 mils of metal by pickling in a solution of 10 parts water, 9 parts HNO_3, and 1 part HF to insure a corrosion-resistant surface. Further, a good flush must be obtained so that no acid remains on the surface. However, the corrosion of the alloy is not affected by small additions of salts such as NaOH, $NaNO_3$, $Na_2Cr_2O_7$, KOH, and LiOH to the water.

Corrosion tests were made on the fuel plates, and in some cases intentional defects were made in the plates. Some tests were made on early experimental plates, but the only thing found was that there had to be a good bond between the core and the clad to prevent catastrophic swelling. One set of pre-manufacture plates was made by the roll-bonding technique, and these were tested at 288°C (550°F) for periods up to 6,622 hr. Heat treatments of the plates included that required to favor corrosion resistance in some, aging in others, and dimensional stability in others. None of these plates failed, with the exception of one that had an intentional defect.

A miniature plate was made in a manner identical with that used for the full-sized ones and placed in MTR. The bulk water temperature of the loop was 252°C, and the maximum heat flux was 95 w/cm^2 initially. The test has been run off and on for more than a year of operating time, and the burnup is approximately 1.4 atom %. The last examination indicated no significant changes. A measurement of thickness by means of a micrometer indicates a metal loss of approximately 1.4 mils per side.

In order to be certain that each fuel plate to go into EBWR would be satisfactory, they were all tested in an autoclave at 288°C (550°F) for periods from 9 to 15 days. Out of almost 1000 plates, 3 failed. The failures occurred in the first 3 days and were noted by a rise in autoclave pressure (due to hydrogen). The plates were manufactured into assemblies, and the assemblies then corrosion tested. There were no failures for 140 assemblies.

3. Hafnium Control Rods

If there is any material that is almost completely corrosion resistant in high-temperature water, it is hafnium. In addition, its corrosion is not affected by nitrogen content. Before the control rods were manufactured, a brief corrosion test was made on the crystal-bar stock purchased to make certain that the amount of impurities was not so great as to decrease its corrosion resistance.

4. Boron-Stainless Steel Control Rods

Using type 304 stainless steel as a base material, quantities of boron up to 10 w/o were added to obtain a poison material for the reactor. Alloys containing more than 3% B were deemed almost impossible to manufacture, since they take on properties similar to glass. In addition, they are very sensitive to oxygen content in the water in corrosion tests, and tend to pit and rust. Several corrosion tests were run on 1 to 2% alloys, and no unusual corrosion tendencies over type 304 stainless steel were noticed.

5. Aluminum Dummy Fuel

A great deal of work has been done to determine a good aluminum alloy for the EBWR and other reactors of this type. Several years ago the Metallurgy Division found the addition of 1% nickel to 1100 aluminum gave good corrosion resistance above 200°C (400°F). Thus a new alloy was born, first named M-388, later X8001 - both designations by Alcoa which was the first commercial manufacturer. The nominal composition of this alloy includes 1% Ni, 0.5% Fe, 0.17% Cu, and 0.17% Si. After preliminary tests had indicated no catastrophic corrosion up to 360°C (680°F), the decision was made to use this alloy for the EBWR fuel dummies.

There has been an extensive amount of testing on aluminum X8001 alloy. The results indicate that a large number of factors influence the corrosion of this alloy. The first factor is temperature. Test results indicate that on increase from 260°C (500°F) to 316°C (600°F) (other factors constant) the corrosion rate almost doubles. The velocity of water past the sample is another factor. Tests at 0, 7, 18 and 22 ft/sec indicate a very marked increase in corrosion with increased velocity.

Corrosion is affected also by the amount of aluminum surface area corroding per unit volume of circulating loop water. Figure VIII-3 shows that the higher this ratio, or the more aluminum area in any given system, the lower will be the corrosion. A big factor in corrosion of this alloy is the water condition. A pH level over 7 has very bad effects on X8001. Neutral water of high purity (resistance of over one megohm/cm^2) gives fairly good results. These can be improved slightly by lowering the pH slightly with nitric acid, or improved greatly by using phosphoric acid. However, lowering the pH too much, say below 4, results in sufficient loss of purity of the water as to cause localized attack of the metal. The best results can be obtained with phosphoric acid and a pH level of 5.0 to 5.5.

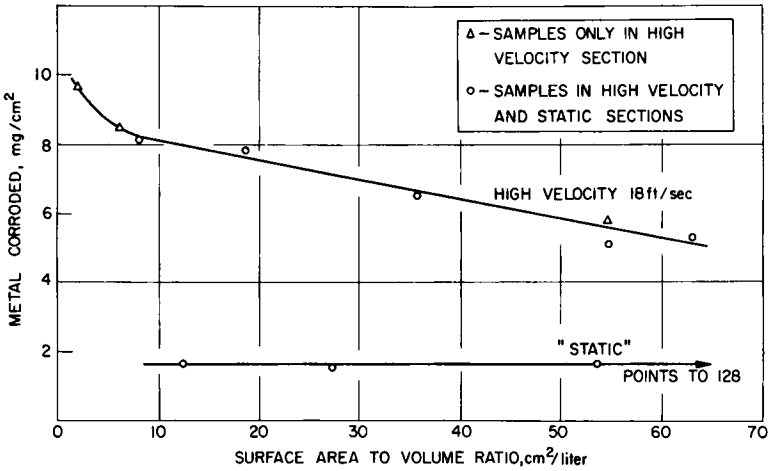

Fig. VIII-3

Effect of Ratio of Surface Area to Volume on the Corrosion of Aluminum Alloy X8001 - One Week at 260° C in Distilled Water
111-6558

Some of the variables investigated that did not affect the corrosion of this alloy were surface boiling, irradiation, and coupling with stainless steel (see ANL-6204). One exception was in the case of coupling: some galvanic attack was evident if the water quality was poor. The EBWR dummy elements described later are an example of this.

An illustration of how some of these variables affect the corrosion results for 5 tests is shown in Table VIII-5. The surface area-to-volume ratio was approximately 55 cm^2/liter for each test, and no irradiation was involved in any of them.

Table VIII-5

SUMMARY OF DYNAMIC CORROSION TESTS ON X8001 ALLOY

Test No.	Temp, °F	pH	Corrosion Rate, mils/yr			Weight Loss at 215 Days, mg/cm^2		
			18 fps	7 fps	Static	18 fps	7 fps	Static
I	500	7	6.3	1.9	-	38.0	18.8	-
II	500	5 to 6	4.2	2.5	-	26.2	18.8	-
III	600	5 to 6	8.1	5.6	-	62.0	40.0	-
IV	600	5.5 (H_3PO_4)	4.2	1.9	0.7	15.3	8.2	3.4
V	600	4.5 (H_3PO_4)	-	-	-	5.4*	-	2.4*

*169 days

In the meantime, one or two new aluminum alloys had been developed. The most important of these contains 1% Ni and 0.1% Ti in pure aluminum. This material is as good or better than X8001 in water and is even good in 400°C (750°F) steam. For strength purposes, powder metallurgy products of these alloys are being developed, but there are problems with corrosion resistance. This is due to the presence of some oxide in the powder. The oxide has a tendency to form stringers when the material is worked, and the water follows the path of these stringers and causes internal corrosion, thus swelling.

Returning to the dummy elements in EBWR, on two occasions one of these was removed for examination. The first time was in December 1957, at which time the reactor had operated the equivalent of approximately 6 months of power. The element had a red-grey oxide on the outside and a light grey oxide on the inside. This is what could be expected, since some deposition of iron in the oxide would be expected on the outer surfaces. There were pits on the aluminum, apparently initiated during the early days of the reactor when the vessel had low-purity water in it, and then continued during the early part of reactor operation. Figure VIII-4 shows the appearance of the surface at the time of examination.

Another dummy was removed in December of 1958 (after another 6 months of operation), and at this time there did not appear to be any increased corrosion of these pits. A section of the element was descaled and measured. This indicated approximately a 3-mil metal loss on each side of the plate.

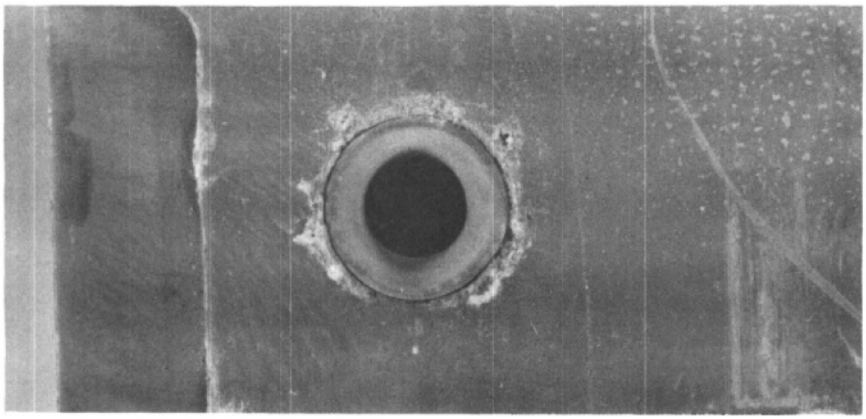

BACK - 4X

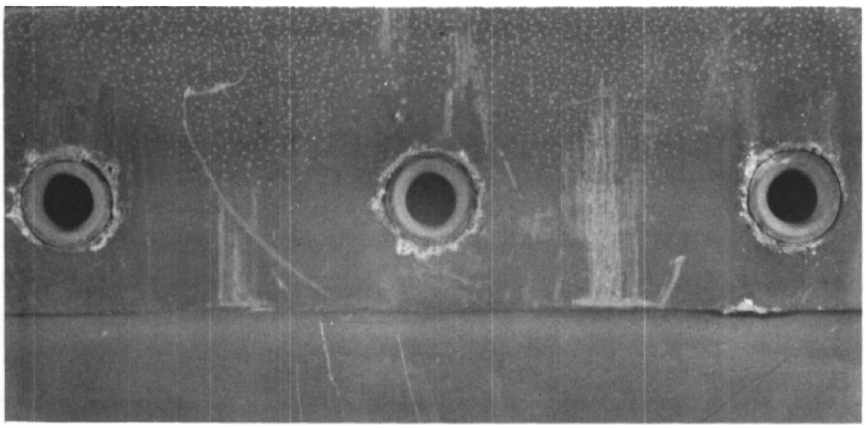

BACK - 2X

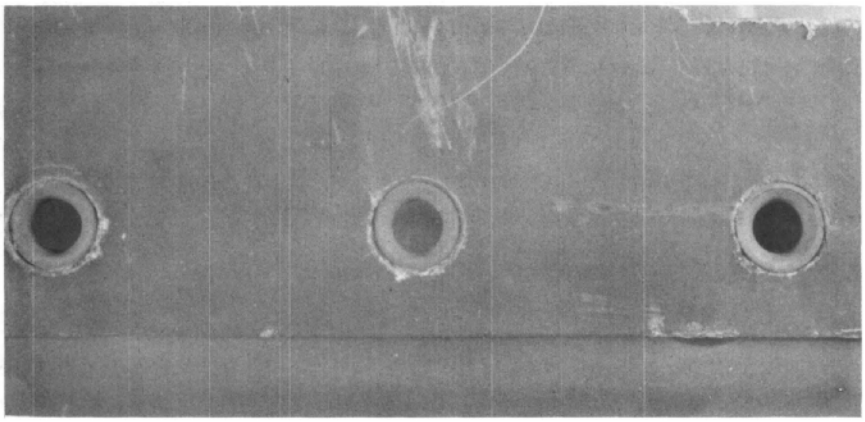

FRONT - 2X

Fig. VIII-4

Corrosion of Aluminum at Stainless Steel Rivets
in EBWR Dummy from Core Position K2
111-5924

6. Turbine and Steam-line Kanigen Coating

It had been intended to use a standard turbine coupled to the reactor since it was thought that the oxygen content of the steam would be no higher than in a standard power plant. During the construction of the reactor, however, results with BORAX-III indicated a much higher gas content due to dissociation. In order to prevent excessive corrosion of the turbine casing and piping leading to the turbine, the decision was made to Kanigen plate these items. Although these were large pieces of equipment to handle, the operation was completed in a satisfactory manner.

The turbine and piping was inspected in February of 1958, fourteen calendar months after startup. Two things were found in the piping. First, the areas that had been heat treated due to welding on the exterior of the pipe were harder and less corroded than the major portion of the pipe that was not heat treated. Second, there were a large number of microscopic cracks through the clad to the bare metal (see Fig. VIII-5). In the turbine, it was noted that the clad was gone entirely in some areas of high-velocity steam. Where there was relatively static steam, the clad appeared undisturbed to the naked eye. Even where the plate was gone, there did not appear to be any excessive corrosion taking place. Some of the low alloy steel had pitted, but in these places there was sufficient thickness of metal so that this caused no concern. Subsequent inspections have revealed no major changes from the original findings.

In the meantime, static and dynamic corrosion tests of Kanigen and electrically plated samples were started (plate thicknesses for Kanigen - 1, 3, and 5 mils;for electrically plated - 3, 8, and 13 mils). In the autoclave tests the Kanigen plate had good corrosion resistance at all three temperatures, 260°C (500°F), 316°C (600°F), and 360°C (680°F), in degassed and air-saturated water. The electrically plated samples behaved erratically in that they corroded relatively rapidly in 260°C and 360°C, air-saturated water, but did as well as Kanigen at the other conditions. In the dynamic test at 288°C (550°F) and a velocity of 25 fps, the Kanigen samples corroded at about 0.5 mil/yr up to 5000 hr, when they suddenly started to lose their plate on the leading edges. The electrically plated samples corroded at a rate of 1 to 1.5 mil/yr, but the plate was still intact at 5000 hr.

A corrosion-sample holder was placed at a flange of the steam line leaving the reactor. The materials placed here were those used to manufacture the turbine; in some cases samples were from the same lot of material used to manufacture the turbine part. The materials included structural steel (diaphragm web), 4140 steel (wheels), 13% chrome steel (buckets), 1% Cr-$\frac{1}{2}$% Mo steel (shaft), low carbon steel (diaphragm band), and 13% chrome nonhardening steel (nozzle element). The test was operated for three periods of 2,249 hr, 3,522 hr, and 778 hr, or a

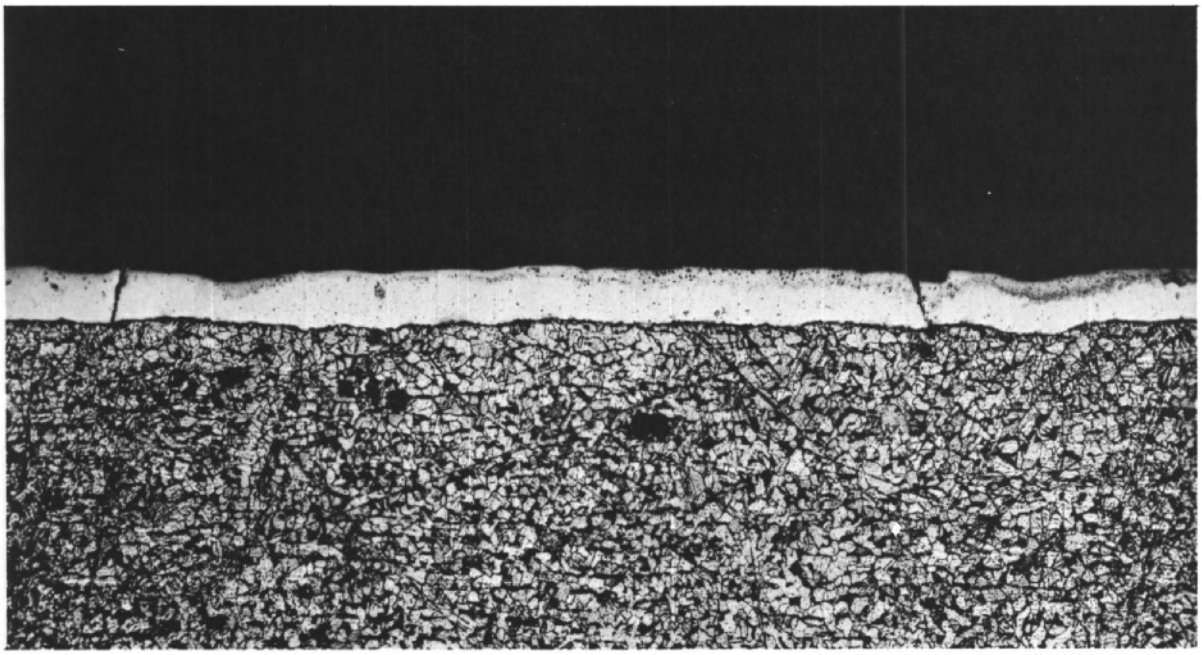

Nitol Etch Heat-Treated Kanigen 75X

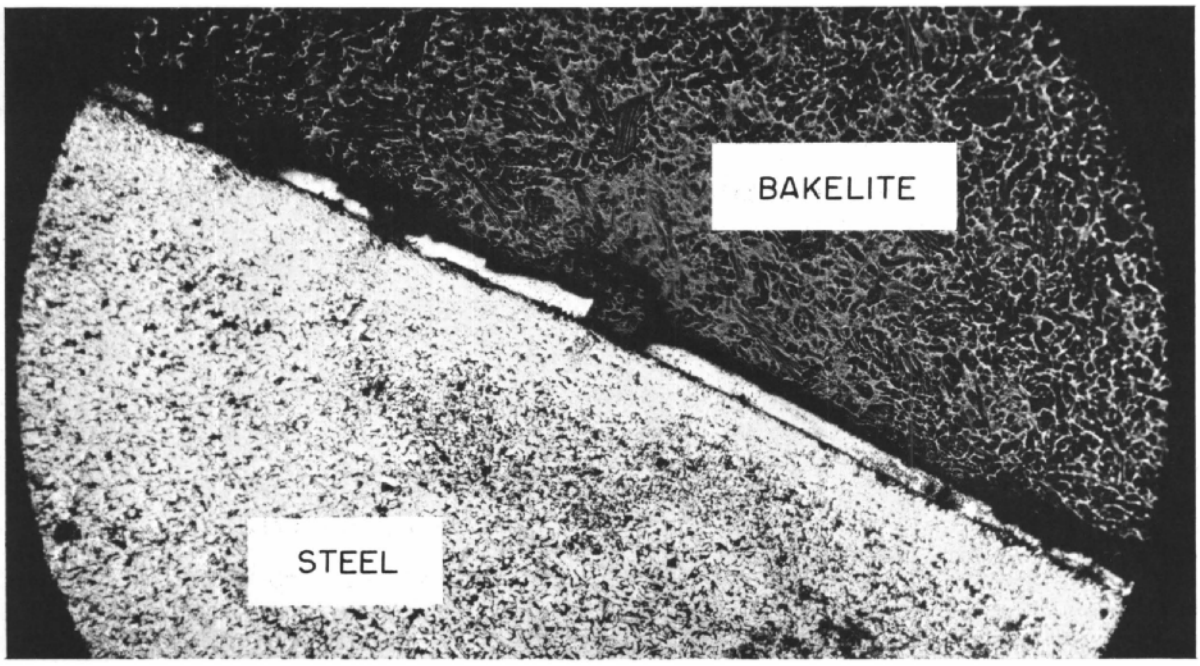

Nitol Etch Nonheat-Treated Kanigen 50X

Fig. VIII-5

Effect of Heat Treatment on the Corrosion and Erosion Resistance of Kanigen Coating

total of 6,569 hr. The activity of the samples was quite low. They were descaled and weight losses measured. During the first two periods the low carbon and structural steels corroded at a rate of about 0.1 mil/yr, the 4140 and 1% Cr-$\frac{1}{2}$% Mo steels at 0.01 to 0.04 mil/yr and the high chrome steels a negligible amount. However, between the second and third periods, the samples were flooded with water for about five weeks because of continued maintenance in the primary vessel. As a result, the low alloy steels all were pitted and exhibited a greatly increased corrosion. The 1% Cr-$\frac{1}{2}$% Mo alloy was the worst, as actual metal loss increased by a factor of 10. The high alloy steels were unaffected.

The need for continued corrosion testing of the samples in the vessel and steam line is almost self-explanatory. The less expensive materials for equipment and cladding are very important, and these are the types of material that are being tested in these facilities.

B. Investigations of Fuel-element Scale

The EBWR is the first high-temperature water reactor in which crud or scale formation on fuel elements has been a significant problem. Some conclusions from the results obtained during the first investigations of solids in the reactor water were:

1) Very little chromium was found in the insoluble particulate matter, as compared with aluminum, iron, and nickel. This suggests that most of the chromium corrosion product must be present in a soluble form.

2) Values obtained for aluminum, iron, and nickel from early samples were consistently lower than those at other sampling dates. Since this was the only group for which the pore size of the filter was recorded, there is a possibility that a filter of smaller pore size was used in the other surveys.

3) Significant amounts of crud pass through the prefilter and to a lesser extent through the ion exchanger.

4) A significant decontamination factor exists between reactor water and steam for particulate corrosion products.

5) The steam dryer alone does not seem to exert much of a decontaminating effect on suspended particulate matter.

6) The amount of suspended aluminum in the feedwater is less than that in the reactor water. None is removed by the feedwater filter, indicating that, if aluminum comes from the condenser, it is in a dissolved form.

7) The amount of insoluble nickel in the feedwater is less than that in the reactor water. Some is removed by the feedwater filter.

8) The amount of suspended iron in the feedwater is nearly as great as in the reactor water. Significant amounts are removed by the feedwater filter.

In 1959, a special device was developed to determine the amount of total solids (suspended and dissolved) in reactor water. The basic design allows water from any place in the primary system to be pumped into a weighed crucible in an autoclave which is operating at 100°F above the saturation temperature. The steam is condensed, expanded to atmospheric pressure, and the total water flow measured. By using various safety measures in the system, the experiment may be operated continuously with only occasional maintenance. After installation of the equipment, one run was made on reactor water before final shutdown for 100-Mw conversion. Evaporation of 107 liters of reactor water resulted in the collection of 7.7 mg, or a concentration of 0.07 ppm. Examination of the activity present by means of a 200-channel gamma-ray analyzer indicated Co^{58} and Co^{60} present in a ratio of about 10 to 1. The analysis is shown in Table VIII-6.

Table VIII-6

SOLIDS CONTENT OF EBWR WATER
(March 1959)

Element	Assumed Compound	Amount, mg		%	
		Element	Compound	Element	Compound
Al	$Al_2O_3 \cdot H_2O$	1.59	3.53	59	70
Fe	Fe_2O_3	0.68	0.97	25	19
Ni	NiO	0.43	0.54	16	11
Totals		2.70	5.04	100	100

During July 1957, one fuel element, which had been in the core for 1370 Mwd of operation, and two dummy elements were examined. At this time samples of the deposits on these elements were taken. Observations were made to determine the nature of the deposits (adherent or non-adherent), and samples were submitted for spectrographic and radiochemical analyses. Three samples were taken by underwater wiping with new cellulose sponges as follows:

1) external surface of end fuel plate of fuel element (upper portion);

2) external surface of dummy element; and

3) internal surface of dummy element.

All three deposits were nonadherent and readily removed by a single wipe of the sponge. The deposit on the fuel plates was reddish-brown in color, and a dark gray zirconium oxide film appeared intact when the deposit was wiped off. The deposit on the external surfaces of the dummy element was greenish-blue when observed in the reactor core; however, when the dummy was moved to the storage pit, the color was much lighter, and, finally, when the deposit was removed, it was a dirty white color. The appearance of both the external and internal surfaces of the dummy was not bright when the deposit was wiped off. This would be expected since the aluminum alloy would have formed an oxide layer before the crud or corrosion product layer had been deposited.

The deposits were very soft and flocculent in texture, and when washed off the sponge appeared to be very finely divided. An attempt was made to determine the particle size of the fuel-element deposit, but by the time the sample was photographed (in the electron microscope) the particles had agglomerated. Later, a sample of deposit from the external surface of the dummy element was prepared and an electron microscope photograph taken at 3100A. Most of the particles appeared to be less than 1.5 μ in diameter.

This deposit should be similar to that on the fuel element. The physical characteristics of the deposit on the dummy elements changed after drying. When additional samples were taken from the dummy elements recently, the deposit was very adherent and had to be scraped off. Two external surfaces had a dark reddish-brown color and the other two sides had a mottled appearance with light-colored dots, which probably were the corrosion products of the aluminum alloy. The amount of deposit on the fuel element could not be determined; however, those on the external and internal surfaces of the dummy element were determined.

Both the fuel-element deposit and the deposit from the external surface of the dummy fuel element consisted primarily of iron, nickel, and aluminum oxides in decreasing order of relative amounts present. The aluminum content of the deposit from the external surface of the aluminum dummy was higher than that from the Zircaloy-clad fuel, as would be expected. The nickel content of all the deposits was considerably higher than would be expected and is due to two factors:

1) In the insoluble corrosion products of stainless steel, the nickel content is much higher than the chromium content because chromium is more soluble.

2) The nickel pickup in the steam piping and turbine by the condensate must be quite high, as indicated by erosion of diaphragm nozzles.

The deposit from the internal surface of the dummy was quite different from the other two deposits. The low iron content might be expected since the water

in the dummies was stagnant and the deposit primarily due to the corrosion products of the aluminum alloy M-388. The high nickel content of this deposit is of significance in that the ratio of aluminum to nickel in the deposit is not the same as in the alloy (1% Ni-99% Al).

The amount of deposit present on the fuel elements was more than had been expected, since the quality of the reactor water has been maintained at less than one-micromho conductivity during most of the reactor operation. In view of results examined later, it should be noted that at this time the external surface films on fuel element and dummy appeared to be nonadherent. They were composed largely of oxides of iron, nickel, and aluminum, in relative amounts decreasing in that order. There was considerable speculation about having an accumulation of crud in the bottom of the reactor vessel. During the July shutdown, when the reactor was open, an attempt was made to determine whether there was a layer of loose deposit at the bottom. A probe (28 ft long) was put down through one of the outer dummy holes, and water was drawn up with a vacuum system. No deposit was drawn up. It could be that the probe, which was quite flexible ($\frac{1}{4}$-in. stainless steel tubing), did not get past some of the plates located below the grid support plate.

Examination of the EBWR core in January 1958, after about a year of operation, showed the presence of considerable scale on another fuel element. This was evident by the flaking off of the scale from it as the fuel element was lifted out of the core toward the surface of the water in the reactor for observation (see Fig. VIII-6). Large flakes of scale

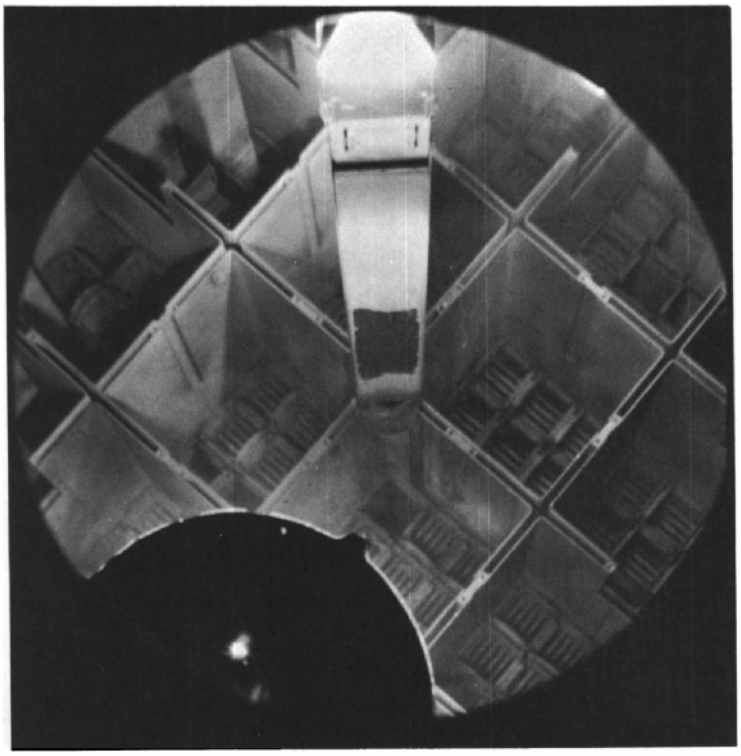

Fig. VIII-6

EBWR Central Fuel Element Showing Flaked Deposit Area Following Approximately 3600-Mwd Operation of Core
111-6082

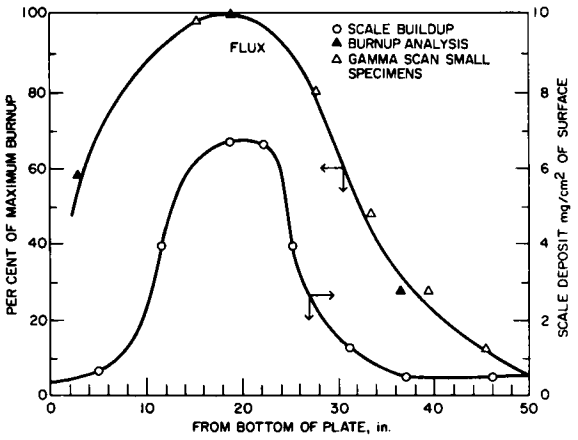

Fig. VIII-7

Relation between Scale Buildup and Burnup after Operation for About One Year

112-1180

could be seen floating away from the external plate, and a relatively large area (estimated to be about 40 in.^{2}) in the highest heat flux zone from which the scale had flaked away could be observed. X-ray analysis showed the scale to be at least 50% boehmite ($Al_2O_3 \cdot H_2O$). The X-ray diffraction pattern was identical with that observed from samples of the corrosion layer on the aluminum-nickel dummy fuel elements. Figure VIII-7 shows the correlation of measured deposition of scale with the fission product distribution (i.e., thermal-neutron flux).

The aluminum is believed to have come from corrosion of the aluminum-1% nickel dummy fuel elements - the nickel largely from the aluminum-1%nickel, from the stainless steel, and possibly from the Kanigen nickel plate on the turbine and piping. The iron is believed to have come from the stainless steel corrosion products. A list of the activities is shown in Table VIII-7.

Table VIII-7

ACTIVITIES IN EBWR FUEL-ELEMENT DEPOSIT

Nuclide	Half-life	Crud, d/(min)(mg)	Probable Nuclear Reaction
Co^{58}	71 d	1.43×10^7	Ni^{58} (n,p) Co^{58}
Co^{60}	5.3 yr	1.66×10^6	Co^{59} (n,γ) Co^{60} Ni^{60} (n,p) Co^{60}
Fe^{59}	45 d	2.43×10^5	Fe^{58} (n,γ) Fe^{59}
Mn^{54}	300 d	2.08×10^5	Fe^{54} (n,p) Mn^{54}

In January 1958, a fuel element was submitted to the Metallurgy Division for destructive examination. Preliminary findings indicated a rather nonadherent scale; however, no spalling was observed. Spectrographic analysis (factor-of-2 accuracy) indicated major constiuents as follows:

Aluminum	18%
Nickel	12%
Iron	6%

X-ray diffraction data indicated the scale was largely boehmite, and there was a second phase, resembling aluminum-silicon monohydrate, present.

In April 1959, another irradiated fuel element was examined by the Metallurgy Division. This element showed areas where scale had spalled off. In the course of cutting up the element, a considerable amount of scale flaked off. The thickness of the scale from the general zone of high heat flux was determined to be 0.0046 in. by measurement of photomicrographs of the scale in cross section. The thickness, as measured with a micrometer, was 0.005 in., based on several measurements. Due to surface roughness, these values are larger than those established from photomicrographs. The density of the scale, determined from weight measurements and volume calculation, was 2.5 gm/cm^3. Pieces of scale tested were found to be attracted by a magnet. X-ray diffraction measurements indicated the presence of boehmite and of a second, unidentified phase. This analysis is shown in Table VIII-8

Table VIII-8

ANALYSIS AND CALCULATED COMPOSITION OF EBWR FUEL ELEMENT SCALE

Element	Analysis (w/o)	Assumed Compound	X-ray Identification	Calculated (w/o)
Al	36.3	$Al_2O_3 \cdot H_2O$	Boehmite	80.6
Ni	10.6	NiO	Not identified	12.6
Fe	3.9	Fe_3O_4	Not identified	5.1
Si	0.8	SiO_2	Not identified	1.6
			Total:	99.9

When the core was removed in July 1959, for 100-Mw conversion, a large number of fuel elements showed the loss of patches of scale, and the water was murky due to the amount of suspended material stirred up or released by the removal operation. The loose crud was removed from the pressure vessel by flushing with water from a hose down through valves on control rod thimbles and recirculation nozzles provided for the occasion. A manifold system carried the slurry through a full-flow filter to a sump, and then to the retention tank. The filters were changed about a dozen times during the operation. No measurements were made, but an estimate was made that the amount was "less than a cubic foot."

The scale deposit on the EBWR fuel elements has a pronounced effect on the operating temperatures of the individual fuel plates. The maximum EBWR fuel centerline temperature is given as 767°F, based on a total heat generation rate of 100 Mw and a maximum heat flux of 485,000 Btu/hr-ft^2. The calculation of this temperature involves the assumption that there is no scale deposit on the surfaces of the fuel plates. It is apparent, therefore, that any additional thermal resistance present on the surface of the fuel plate will increase this centerline temperature by an amount essentially equal to the temperature drop through the added resistance, assuming no changes in heat flux or surface temperature. It was believed that, as fuel temperatures approached 900°F, growth of the uranium alloy may be observed. It became necessary to determine the thermal conductivity of the scale deposit in order to make a good estimation of the maximum fuel temperature that may be present under varying conditions of scale formation.

The highest fuel temperature attainable, 1692°F, was calculated by use of the most pessimistic values of scale thickness and thermal conductivity. Even the most optimistic calculation, considering the thinnest scale specimen recovered (0.004 in.) gives a temperature bordering on 900°F. If correct, then one would indeed expect growth problems to develop as the EBWR begins 100-Mw operation. The thermal conductivity of the EBWR scale measured by the comparative method appears to be independent of the choice of the contact-resistance model as reported in ANL-6136. This is probably due to the fact that the scale area in contact with the upper copper rod was only about 8% of the total area. Conceivably, if a smoother specimen were used, this percentage would be larger and the effect on the value of the thermal conductivity would be greater.

The scale which has deposited on the EBWR fuel plates has proven to be extremely adherent. Although the scale itself is very brittle, hammering on the fuel plate has had no observable effect on scale cracking or loosening. The only chemical means of removing the scale cannot be employed because it will attack the Zircaloy-2 cladding. It was felt that the extremely good bond between scale and cladding was somehow dependent upon the water of hydration of the boehmite ($Al_2O_3 \cdot H_2O$). If the water could be driven off, the scale might flake off or at least become loosened to the point where wire brushing might be effectively employed. On the basis of this theory, coupons from a fuel element were heated to 850°F in an inert atmosphere for 8 hr, after which time the scale did, in fact, curl and flake off. After the encouraging results with the fuel plate coupons, as shown on Fig. VIII-8, a program was set up to test this method of scale removal on a complete subassambly and eventually to employ this means on a production basis to descale all the fuel elements in the EBWR fuel-storage pit.

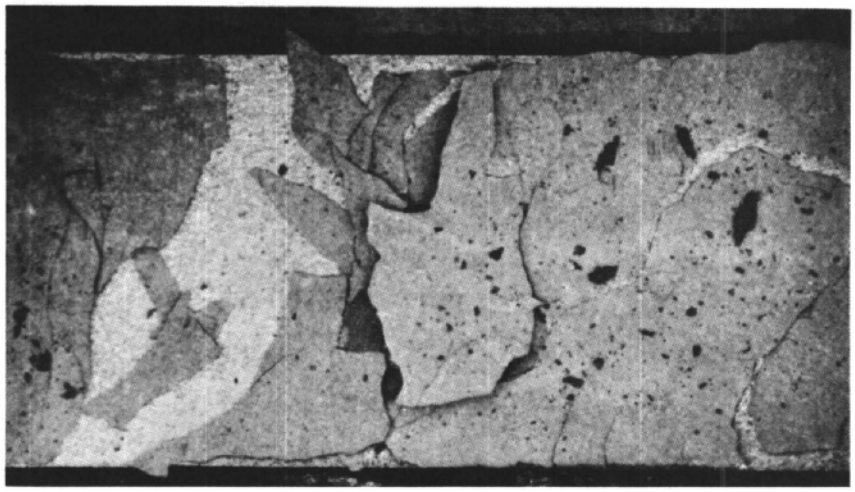

Fig. VIII-8
Coupon from Fuel Assembly ET-51 Heated 8 hr at 850°F in Argon
112-600

The most significant result of the descaling test was that the $\frac{1}{16}$-in.-thick Zircaloy-2 side plates buckled along their lengths between the spot welds on the fuel plates (see Fig. VIII-9). The buckling amounted to at least $\frac{1}{8}$ in. on each side. Even if this treatment had been successful in removing scale, the side-plate deformation would preclude subsequent use of the fuel element in the reactor because of insufficient clearances. One theory concerning the cause of the plate buckling considers that the fuel plate has a coefficient of thermal expansion greater than that of Zircaloy-2. As the fuel plates heat up and expand, they stress the side plates beyond the yield strength. Upon cooling, the greater shrinkage of fuel plate causes the side plates to buckle outward from the spot welds. Since the cladding is in compression at room temperature and since the predicted radiation growth has not materialized, it is quite possible that the cladding never becomes stressed beyond the yield strength. Thus, it maintains its integrity.

The EBWR fuel elements cannot be descaled by heating to 850°F because of side-plate deformation at this elevated temperature. Other means must be found to remove this tenacious scale. It has been shown that the scale can be removed by slurry honing the plates with an abrasive-water mixture (see ANL-6216).

It would be of interest to perform another series of tests on high-burnup fuel plates. It should not be difficult to construct an oven for heating individual fuel plates in which one could guarantee no oxygen contamination. By virtue of being able to measure the three dimensions before and after heating, one cannot only calculate the changes in gross and local volumes at varying temperatures and burnup, but can also determine the degree of residual anisotropy in the fuel plates.

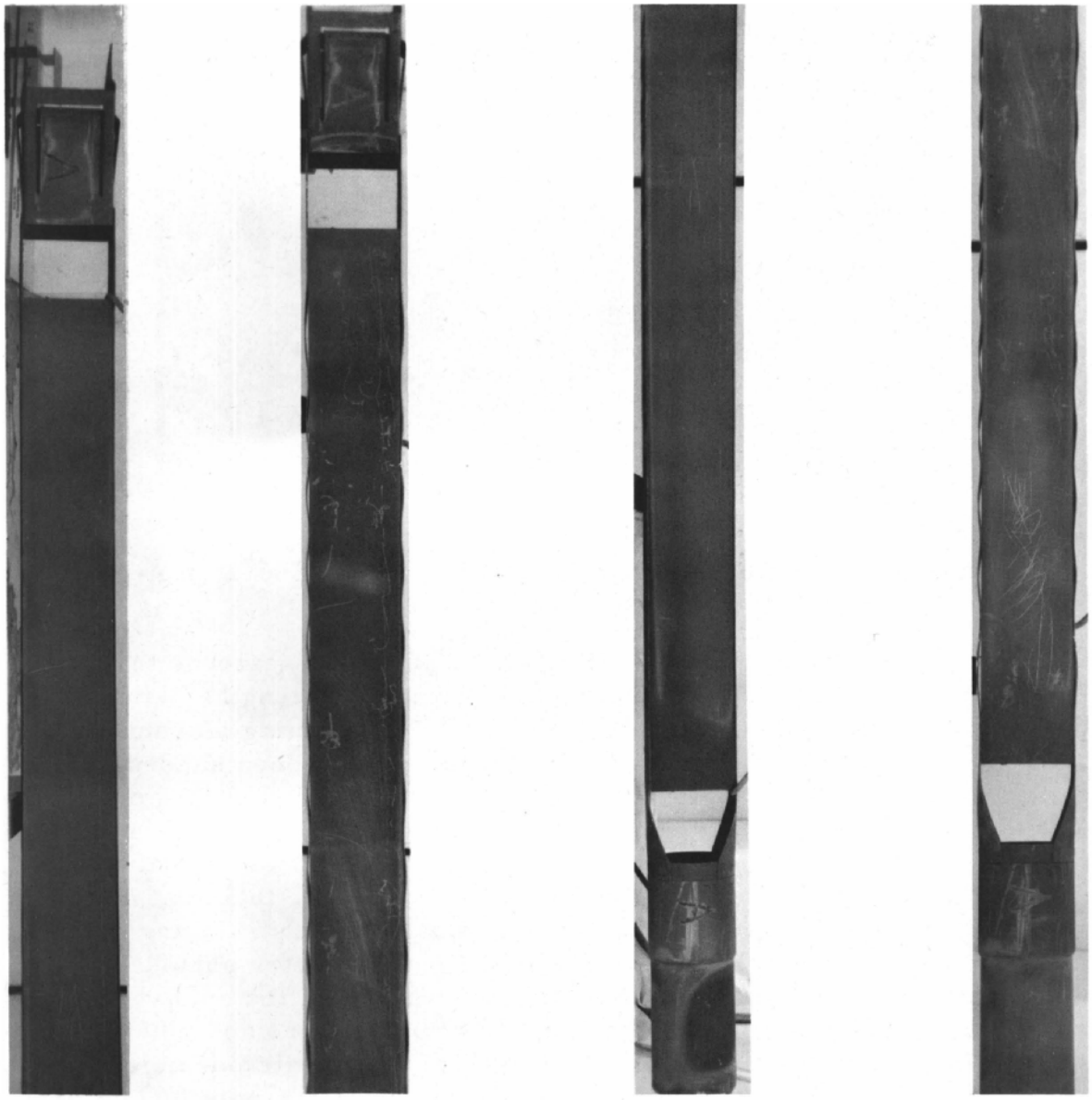

Fig. VIII-9

Fuel Plate "A" Before and After Heating for 25 hr at 850°F

SECTION IX

HEAT TRANSFER

P. Lottes
M. Petrick
G. Popper

NOTES AND EDITED DATA FROM LECTURES - July 5, 1961

SECTION IX

HEAT TRANSFER

I. Basic Concepts*

The process of boiling is defined as heat transfer with a change in phase from liquid to vapor. The means by which energy is transferred from a solid heat transfer surface to vapor is not easily understood. A few facts about the process have been determined by experiment. It is true that for an equilibrium condition a change in phase from liquid to vapor occurs at constant temperature. In forming a bubble of vapor, the liquid-vapor interface is supposed to remain at a constant temperature. In reality, the formation of a bubble takes place in a violent manner and may be considered as a minor underwater explosion.

In the first place, a force balance on a bubble shows that the vapor pressure inside the bubble is greater than the liquid pressure outside the bubble. The difference ΔP is related to the surface tension σ of the liquid and the bubble radius r, according to the equation $\Delta P = 2\,\sigma/r$. As r approaches zero, the required pressure difference approaches infinity. Since fluids have as one of their thermodynamic properties an increase in boiling point with pressure, it now becomes necessary to have a "superheated" liquid before boiling can occur. Assume, for example, that a bubble is present with radius "r." For an equilibrium condition without heat transfer, the bubble vapor temperature will be equal to the surrounding liquid temperature. Due to surface tension, the bubble pressure will be higher than the surrounding liquid pressure. For the bubble to exist at all, the vapor temperature must be equal to or higher than the saturation temperature corresponding to the bubble pressure. The liquid will, therefore, be at this same temperature and will be at a temperature higher than the saturation temperature corresponding to the liquid pressure. This state of the liquid is referred to as liquid superheat. The presence of liquid superheat has been demonstrated in the Laboratory.

The sudden explosive growth of bubbles in superheated liquid causes a very high turbulence level in the liquid. It is this turbulence or violent mixing and agitation of the liquid that accounts for the high rates of heat transfer. The effect of boiling from a heated solid surface is that the layers of liquid near the solid surface are disrupted by the mixing action of the bubbles. This in effect causes the bulk of the liquid to move in next to solid surface. The overall result is a very efficient scouring action of the liquid upon the surface, causing a high heat transfer coefficient. There are several types of boiling heat transfer to be considered. These types may be classified as follows (see Fig. IX-1):

1) Local boiling or surface boiling, as it is sometimes called, occurs when the hot solid surface is above the liquid saturation temperature while the liquid is below saturation temperature.

---

*P. Lottes

2) Net boiling or nucleate boiling occurs when the liquid is at or above saturation temperature.

3) Film boiling occurs when the hot surface is completely covered with a blanket of vapor, and the heat is transferred by conduction through and radiation across the vapor blanket.

4) Transition boiling is a combination of 2 and 3 above.

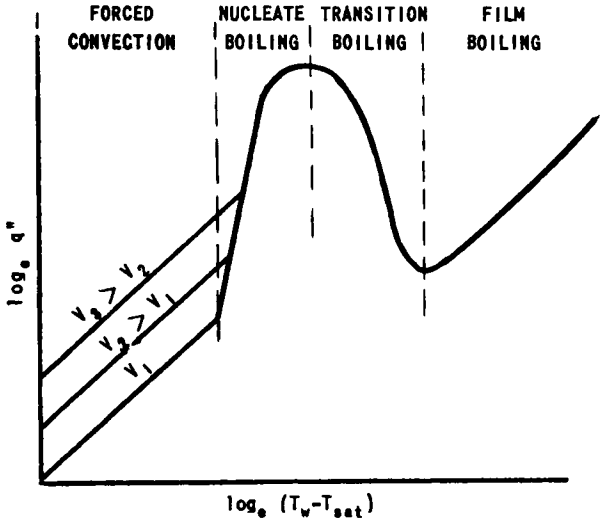

Fig. IX-1

Boiling Regions

Local boiling has the unique condition that there is no net formation of vapor. The bubbles may or may not leave the hot surface. If they do leave, they are very quickly condensed. Bubble lifetimes range from a few microseconds to several seconds, depending on the amount of subcooling in the liquid phase: the higher the subcooling, the shorter the lifetime. It is also worthy to note that the effect of velocity on boiling heat transfer is negligible, even though forced-convection heat transfer coefficients vary as the 0.8 power of the mass flow rate. The reason for the independence of boiling heat transfer coefficients from flow rate is due to the "turbulency promoter" action of the bubbles. The turbulence level is relatively unaffected by flow rate and, therefore, the heat transfer coefficient is relatively unaffected. It is also of interest to notice that (1) the temperature differences between surface and liquid are rather small for nucleate boiling and (2) rather large for film boiling. The part of the curve that has zero slope is the maximum point for nucleate boiling. It is this value which is of greatest concern to designers in the boiling field. In a boiling reactor, for example, this value is the maximum value that would occur just before the element jumps into film boiling. The onset of film boiling will cause the temperature of the solid surface to rise to the melting point of the material. This condition is referred to as "burnout."

One of the main problems in the design of natural-circulation, water-cooled, water-moderated boiling reactors is the prediction of the density of the boiling mixture for a given power level. The hydrodynamic analysis presented differs from the approach of early investigators in that the steam velocity relative to the water is considered.

The performance of a natural-circulation boiling channel must satisfy the following three equations. For the recirculating loop within the reactor,

$$\Sigma \Delta P = 0 \quad . \tag{1}$$

This equation states that the summation of pressure drops around the closed loop consisting of riser, downcomer, crossover pipes, fittings, etc., must be equal to zero for steady-state flow conditions. For the reactor core tubes or channels, the relations,

$$Q_t = W_t[(h_f - h_{in}) + xh_{fg}] = W_g[(h_f - h_0) + h_{fg}] \quad , \tag{2}$$

which represents a heat balance, and

$$\frac{W_g}{W_f} = \frac{xW_t}{(1-x)W_t} = \frac{\rho_g A_g V_g}{\rho_f A_f V_f} = \frac{\rho_g \alpha A_t V_g}{\rho_f (1-\alpha) A_t V_f}$$

$$x = \frac{1}{1 + (V_f/V_g)(\rho_f/\rho_g)(\alpha^{-1} - 1)} \quad , \tag{3}$$

which represents a mass balance at the exit of the average heated channel, must be satisfied. The general procedure in calculating performance is: a value of exit steam volume fraction is assumed; the flow equation (eq. 1) is solved; knowing the system pressure and velocity, the proper value of slip ratio is selected for use in (eq. 3) to obtain the steam quality; the power and subcooling are found by substituting known values of quality and feedwater inlet enthalpy into (eq. 2).

In a differential element of length in a constant flow area channel, it is assumed that the overall pressure drop may be written as a summation of each pressure drop component independently. This approximation may be written as

$$\int_0^L \left[\frac{d}{dL}(\Delta P_f) + \frac{d}{dL}(\Delta P_a) + \frac{d}{dL}(\Delta P_h)\right] dL = \Delta P_f + \Delta P_a + \Delta P_h \quad . \tag{4}$$

The total pressure drop within the channel is now approximated by a summation of the frictional, acceleration, and hydrostatic pressure drops of the mixture; the effect of the ratio of steam-to-water velocity on each of the three terms may be studied.

Slip ratio is defined as the ratio of local steam velocity to local water velocity. The relationship between power density, voids, quality, recirculation flow, pressure, and geometry for boiling systems is not yet

completely understood. At this time the best way to show the relationship appears to be in the form of slip ratio vs total mass velocity (or inlet water velocity). This correlation was originally developed from boiling tests at 150 and 250 psig. More recent tests show fair agreement with these earlier tests. From both of these experiments, slip ratio appears to be dependent on total mass velocity (or inlet water velocity) and system pressure - essentially independent of power density, quality, or steam volume fraction.

Tests at Argonne on the loop shown in Fig. IX-2 indicate the possibility of correlating two-phase friction multipliers as a function of steam volume fraction. This relationship is in a convenient form to use for two phase-flow calculations. The original purpose of these particular tests did not include the study of pressure drop. Pressure taps were installed as an afterthought after the first test section had been installed in the boiling facility. The exact values of friction-factor multipliers could not be calculated from the measured pressure drops, since these measured values included a two-phase exit loss plus two contractions and an expansion loss. An attempt was made to get a measure of the true static pressure at the exit by using a pitot-type instrument with the static tap placed at an angle of 35° from the direction of flow. Two-phase friction-pressure drop values for the test section were then obtained by subtracting calculated inlet, exit, and contraction losses, as well as acceleration and nonboiling friction losses, from the measured values.

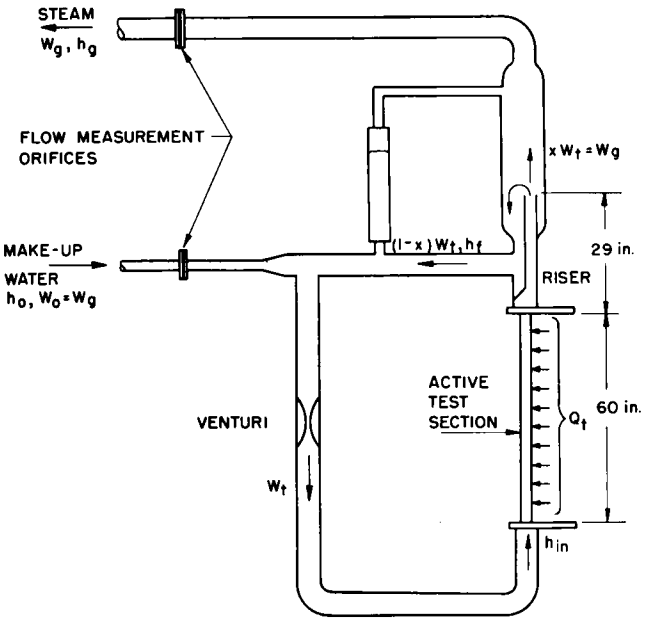

Fig. IX-2

Experimental Arrangement
111-4342

Calculations were made before the experiments were completed. Comparison of these predictions of performance with test results showed good agreement. The obtained data curve shown in Fig. IX-3 was believed to be too high because of the location and operation of the downstream pressure tap, as previously explained. Although the location of this curve is subject to question, its shape is significant. The form of this curve indicates for the range of variable covered: (1) that two-phase frictional pressure drop during boiling can be expressed in a convenient

form as a function of steam volume fraction for low values of quality and independent of system pressure, heat flux, slip ratio, and mass flow rate, and (2) that the two-phase frictional drop can be shown to be essentially due to the increased velocity of the liquid phase alone. If the friction multiplier is a function of steam volume fraction and independent of pressure and flow rate, then perhaps the frictional effect is primarily due to drag of the water phase along the wall. If so, then for small values of quality,

$$\overline{R}\,\frac{f_0\ \rho_f V_{in}^2}{2g}\left(\frac{L}{D}\right)=\frac{f_0\rho_f}{2gD}\int_0^L V_f^2\,dL=\frac{f_0\rho_f V_{in}^2}{2gD}\int_0^L\left(\frac{1}{1-\alpha}\right)^2 dL \quad . \quad (5)$$

From eqs. (2) and (3) it can be shown that, for (1 - x) very close to unity, for constant heat flux and constant slip ratio (V_g/V_f) along a steaming channel, the local liquid velocity, $\alpha/(1-\alpha)$, and $1/(1-\alpha)$ are all linear with length of channel, so that the above integral can be evaluated to give

$$\overline{R}=\frac{1}{3}\left[1+\left(\frac{1}{1-\alpha_e}\right)+\left(\frac{1}{1-\alpha_e}\right)^2\right] \quad . \quad (6)$$

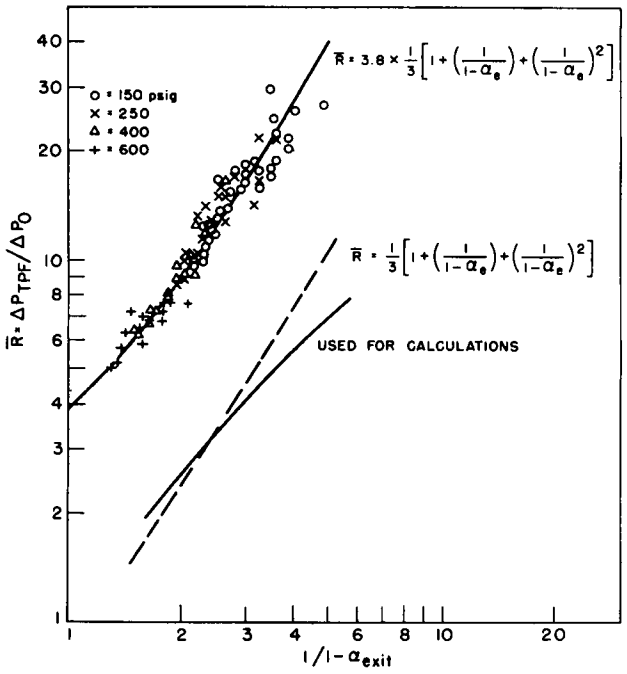

Fig. IX-3

Two-phase Boiling Friction Factors for a $\frac{1}{2}$ x 2 x 60-in. Vertical Heated Channel

111-3914

For any given ratio of steam to water velocity, the acceleration pressure drop may be evaluated. Martinelli and Nelson have shown that the acceleration pressure drop may be expressed as

$$\Delta P_a = r\ G^2/g_c \quad , \quad (7)$$

where

$$r = \left[\frac{(1-x)^2}{1-\alpha} + \frac{x^2}{\alpha}\left(\frac{\rho_f}{\rho_g}\right) - 1\right]\frac{1}{\rho_f} \quad . \tag{8}$$

Figures IX-4, 5, and 6 show r as a function of voids at various pressures.

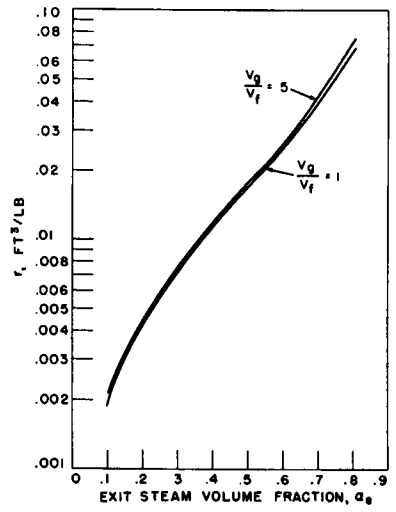

Fig. IX-4

Acceleration Multiplier "r" vs Exit Steam Volume Fraction for 25 psia

111-3690

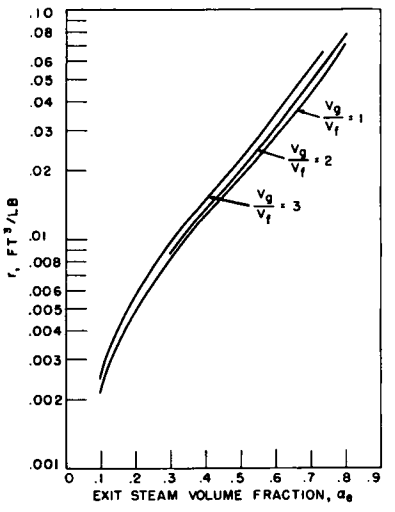

Fig. IX-5

Acceleration Multiplier "r" vs Exit Steam Volume Fraction for 600 psia

111-3684

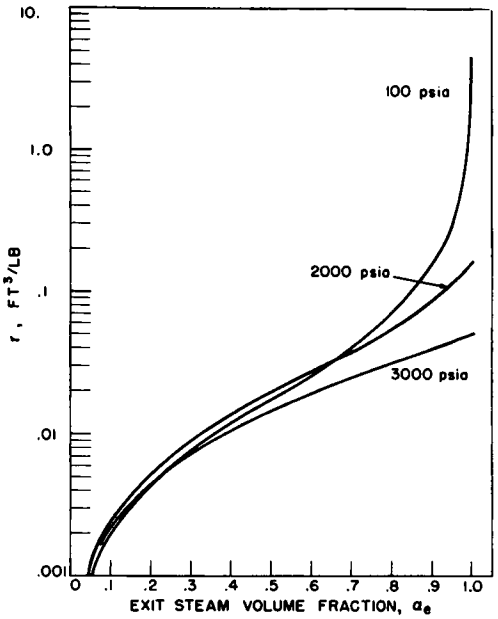

Fig. IX-6

Acceleration Multiplier "r" vs Exit Steam Volume Fraction for Slip Ratio of Unity

111-3682

The hydrostatic head may also be found as a function of pressure, slip ratio, and exit steam volume fraction. The following development is based upon the assumption that the slip ratio is constant along the channel, and the results are given in Figs. IX-7, 8, and 9.

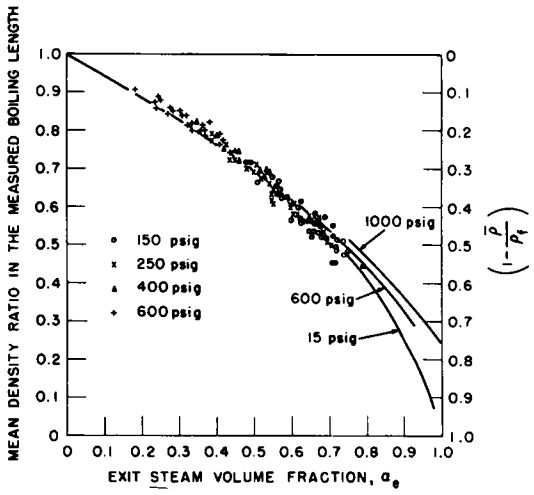

Fig. IX-7

Comparison of Calculated and Measured Mean Density Ratio for Constant Flux Distribution along the Length

111-3688

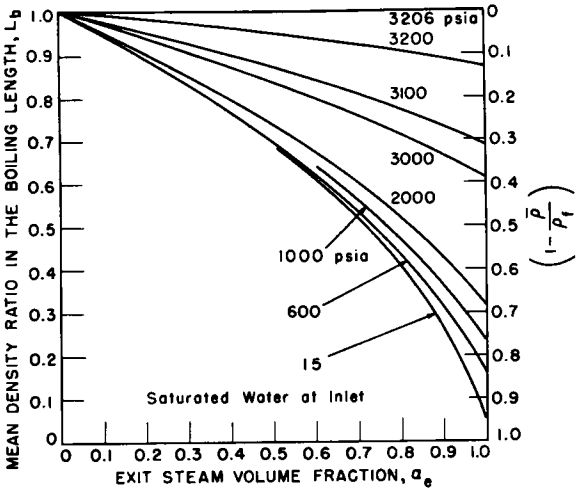

Fig. IX-8

Ratio of Mean Density in Vertical Boiling Channel to Liquid Density for Uniform Heat Generation and Slip Ratio of Unity

111-3691

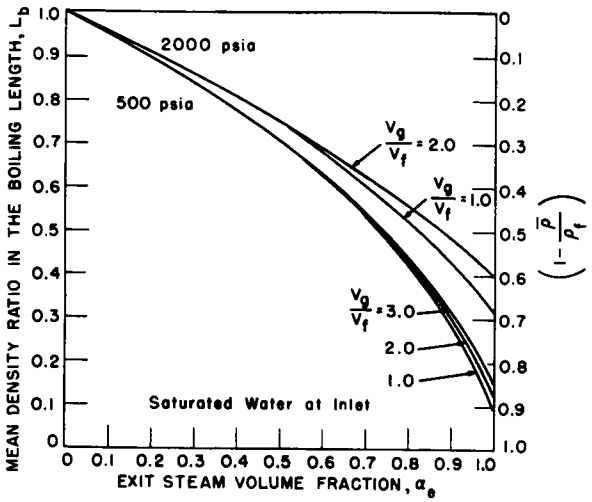

Fig. IX-9

Ratio of Mean Density in Vertical Boiling Channel to Liquid Density for Uniform Heat Generation with Pressures of 500 and 2000 psia and Slip Ratio from 1 to 3

111-3692

As one example, we assume constant heat flux along length. At any point L in the channel

$$\rho = \rho_f(1 - \alpha) + \rho_g\alpha \quad . \tag{9}$$

The average channel density is

$$\bar{\rho} = \frac{1}{L_t} \int_0^{L_t} \rho \, dL \quad . \tag{10}$$

For uniform longitudinal heat generation and constant pressure, steam quality varies linearly with length, so that eq. (10) may be written as

$$\bar{\rho} = \frac{1}{x_e} \int_0^{x_e} \rho \, dx \quad . \tag{11}$$

Combining eqs. (3), (9), and (11) and rearranging terms,

$$\frac{\bar{\rho}}{\rho_f} = 1 - \frac{1}{x_e} \left(1 - \frac{\rho_g}{\rho_f}\right) \int_0^{x_e} \frac{x \, dx}{(V_g/V_f)(\rho_g/\rho_f) + [1 - (V_g/V_f)(\rho_g/\rho_f)]x} \quad . \tag{12}$$

For constant slip ratio and pressure, the solution of eq. (12) is

$$\frac{\bar{\rho}}{\rho_f} = 1 - \frac{1 - (\rho_g/\rho_f)}{1 - \phi} \left\{ 1 - \left(\frac{1}{\alpha_e(1 - \phi)} - 1 \right) \log_e \left[1 + \left(\frac{1}{\alpha_e(1 - \phi)} - 1 \right)^{-1} \right] \right\} \quad , \tag{13}$$

where

$$\phi = \rho_g V_g / \rho_f V_f \quad .$$

The starting point in the solution is to assume a given value of exit steam volume fraction. Equations (1) and (4) are now combined and rearranged as follows:

$$\left(1 - \frac{\bar{\rho}}{\rho_f}\right) L_b = \frac{V_{in}^2}{2g_c} \left[\frac{f_0 L_0}{D_e} + \frac{\bar{R} f_0 L_b}{D_e} + 2r\rho_f + K \right] \tag{14}$$

where D_e is the equivalent diameter, f_0 the friction factor, and K the unaccounted-for losses in the loop.

Values of $(\bar{\rho}/\rho_f)$, r, and R are found for a given exit steam volume from plotted data. Values of f_0, K, and D_e are found by conventional methods. The exit loss for two-phase flow is questionable. No data or references have been found in the literature for two-phase form losses. It is assumed that the exit losses are due only to changes in flow area for the water phase. The exit losses for the steam phase were neglected.

Equation (14) may now be solved for V_{in}, the inlet velocity to the riser. This value of velocity is used to determine slip ratio. The value of slip ratio is used to solve eq. (3) for steam quality. Equation (2) may now be solved for power input or heat addition for any feedwater inlet enthalpy, h_0. The solution is then repeated for other assumed values of exit steam volume fraction.

The performance of a laboratory natural-circulation boiler system was calculated according to the described method. This boiler was composed of a 0.5-in. x 2-in. x 60-in. vertical channel uniformly heated, and the necessary piping to complete a natural-circulation loop. Steam was taken from the system, and makeup water was added to simulate typical reactor operation. The calculations were made before the experiments were completed. The assumed friction drop is therefore somewhat different than the measured value. The close agreement between measured and calculated performance, as shown in Figs. IX-10, 11, and 12, indicates that the method can be very useful, even with slight discrepancies in assumed values of friction drop. A discussion of additional Argonne experimental results correlating the steam volume fraction as a function of phase velocities is included in Nuclear Science and Engineering, Volume 7, No. 6, June 1960.

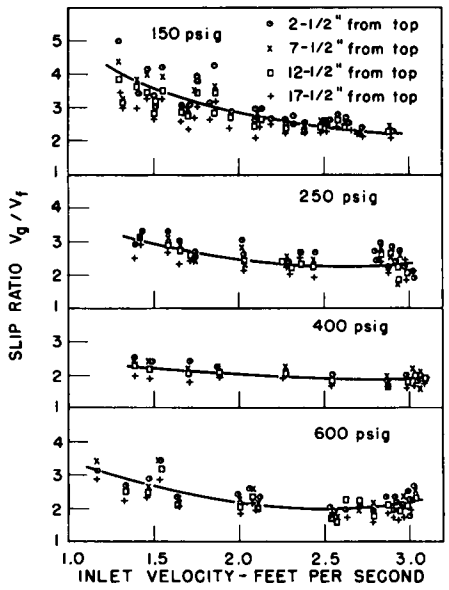

Fig. IX-10

Slip Ratio vs Velocity at Constant Pressure for $\frac{1}{2}$ x 2 x 60-in. Vertical Channel

111-3689

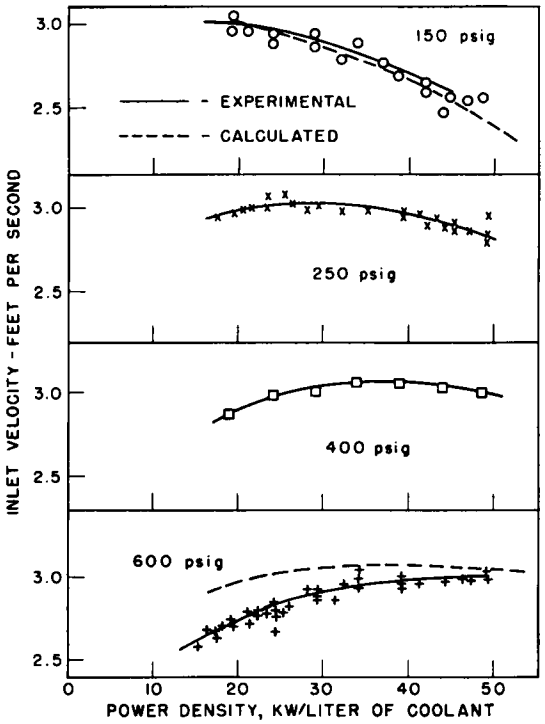

Fig. IX-11

Inlet Velocity vs Power Density for a $\frac{1}{2}$ x 2 x 60-in. Vertical Heated Channel

111-3685

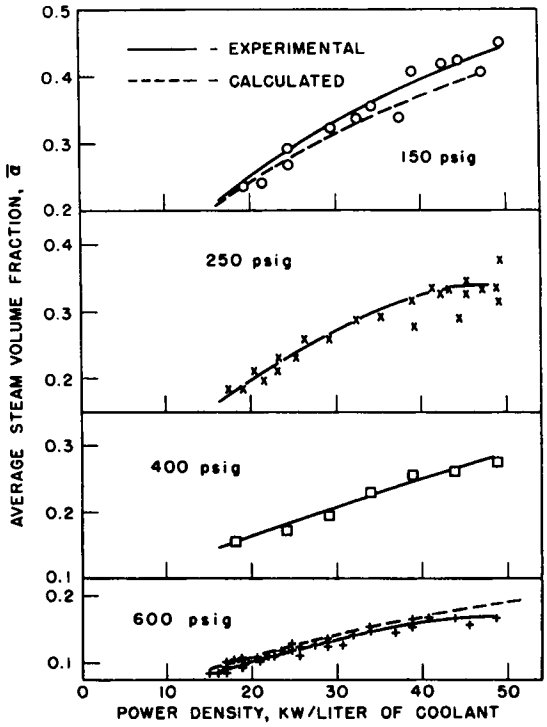

Fig. IX-12

Average Steam Volume Fraction vs Power Density for a $\frac{1}{2}$ x 2 x 60-in. Vertical Heated Channel

111-3683

The foregoing analysis of a basic, simple, natural-circulation system does not account for various riser-heated section geometries which tend to complicate the problems considerably, nor does it account for the effect of subcooling, which becomes increasingly important at higher pressures. A more general approach which considers such phenomena and which can be modified for application in a forced-circulation system is presented in ANL-6063. It should be pointed out that in this analysis the nonboiling region is treated as follows:

Since a large fraction of the nonboiling region may be in local boiling, the question immediately arises concerning the length of the local boiling region and the uncertainty in the distribution and magnitude of the local boiling voids. For the purpose of this analysis, it is tacitly assumed that the local boiling voids adhere to the wall and therefore do not decrease the density of the fluid. The acceleration pressure drop due to the pressure of local boiling voids will be neglected here and incorporated into a calculation of total void acceleration pressure drop in the boiling section.

The inception of local boiling, and hence the length of the local boiling region, can be estimated in the following manner. The wall temperature in the local boiling region is calculated by the Jens-Lottes equation:

$$\Delta T_{sat} = 60 \left(\frac{q}{10^6}\right)^{0.25} \Big/ e^{P/900} \quad , \tag{15}$$

and the value plotted on a temperature-length graph, as illustrated in Fig. IX-13.

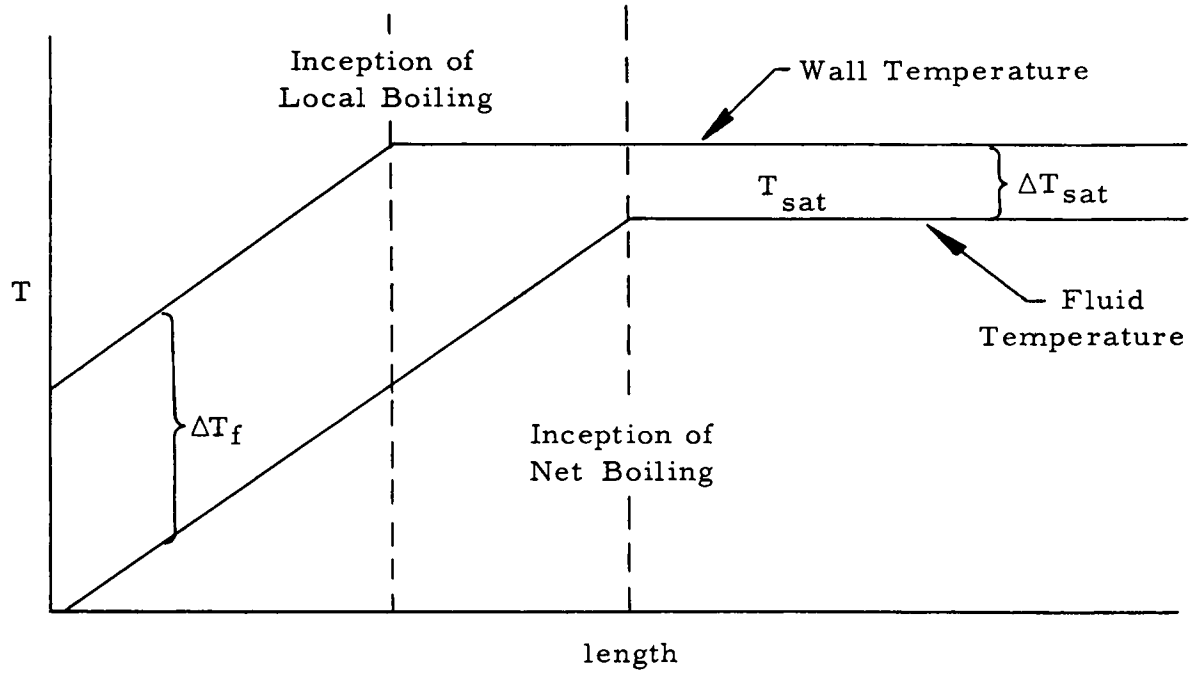

Fig. IX-13

Temperature-heated Surface Length Relationship for Boiling Heat Transfer

The wall temperature in the nonboiling region is then calculated by

$$T_w - T_f = q''/h \quad , \tag{16}$$

where h is given by the Colburn equation:

$$h = 0.023 \frac{k}{D} (Re)^{0.8} (Pr)^{0.4} \quad . \tag{17}$$

(Since Re depends on velocity, a trial-and-error procedure is necessary.) The temperature in the nonboiling region is also plotted vs the channel length, and the intersection of the two wall-temperature profiles is designated as the inception of local boiling. Having established the length of the local boiling region, the total pressure drop across the nonboiling region can be computed by the mathematical techniques presented in ANL-6063.

Two-phase Expansion Losses

When a flowing mixture of vapor and liquid suddenly expands due to a change in flow area, a static pressure change may be observed across the expansion. Most boiling reactors include regions where such expansions occur, and knowledge of the expected pressure changes is therefore necessary in order to calculate flow rates, pressure losses, etc. The need for information of this type is greater for natural-circulation boiling reactors,

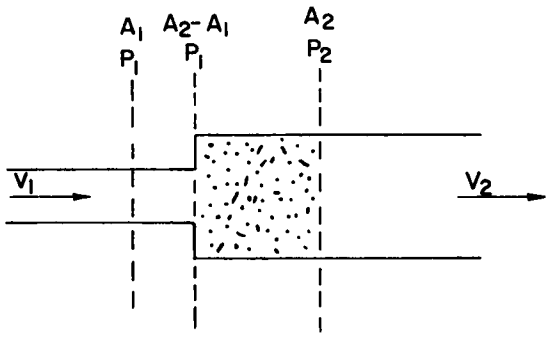

Fig. IX-14

Sudden Expansion of a Flowing Fluid
111-9155

since the pressure changes can be relatively large. For example, a pressure loss of one velocity head of the flowing liquid at the exit of a boiling reactor core might correspond to a number as high as 6 or 8 inlet velocity heads. Since the pressure losses are proportional to the square of the local liquid velocities, it is apparent that the regions of highest loss are the regions of highest void fraction and highest liquid velocity.

The momentum balance across the expansion shown in Fig. IX-14 can be represented as follows:

$$P_1A_1 + \frac{W_{f1}V_{f1}}{g} + \frac{W_{g1}V_{g1}}{g} = P_2A_2 + \frac{W_{f2}V_{f2}}{g} + \frac{W_{g2}V_{g2}}{g} \quad . \tag{18}$$

This assumes that the pressure P_1 upstream from the expansion also acts on the area A_2 just after the expansion. This is the same method as that applied to the sudden expansion of single-phase fluids. From materials balance and the continuity equations, it can be shown that

$$W_{f2} = W_{fi} = W_0(1-x) = \rho_f V_0 A_1(1-x) = \rho_f V_0 \sigma A_2(1-x) \tag{19}$$

and

$$W_{g2} - W_{gi} = xW_0 = \rho_f V_0 A_1 x = \rho_f V_0 \sigma A_2 x \quad , \tag{20}$$

where

$$V_{f1} = \frac{V_0(1-x)}{1-\alpha_1} \quad ; \tag{21}$$

$$V_{f2} = \frac{\sigma V_0(1-x)}{1-\alpha_2} \quad ; \tag{22}$$

$$V_{g_i} = V_0 \frac{x}{\alpha_1} \frac{\rho_f}{\rho_g} \tag{23}$$

$$V_{g2} = \sigma V_0 \frac{x}{\alpha_2} \frac{\rho_f}{\rho_g} \quad . \tag{24}$$

If equations 18, 19, and 20 are combined, the static pressure change is found to be

$$P_2 - P_1 = \frac{\rho_f V_0^2}{2g}(2\sigma)\left[x^2\left(\frac{\rho_f}{\rho_g}\right)\left(\frac{1}{\alpha_1} - \frac{\sigma}{\alpha_2}\right) + (1-x)^2\left(\frac{1}{1-\alpha_1} - \frac{\sigma}{1-\alpha_2}\right)\right] \quad . \quad (25)$$

Figure IX-15 shows the pressure recovery in terms of local liquid velocity head just before the expansion.

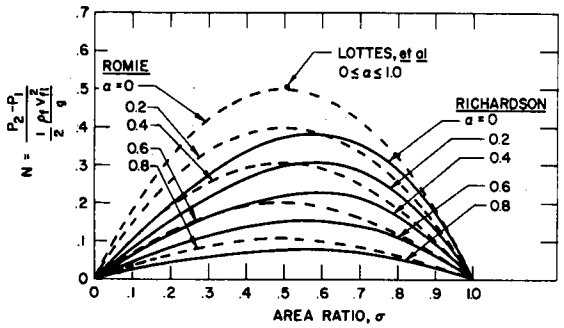

Fig. IX-15

Pressure Recovery for Sudden Expansion of Two-phase Flow
111-9154

II. 100-Mw Modification*

Experimental hydrodynamic investigations at the Laboratory have shown that the addition of a riser or chimney to the top of the reactor core will materially increase the rate of flow of coolant by natural recirculation and enhance the likelihood of achieving high power densities (see ANL-6063). The riser produces a greater head differential between the low-density steam-water mixture leaving the core and the water in the downcomer space. The resulting increased recirculation permits a greater rate of steam production for the same steam void fraction in the core. The latter is an important factor in reactor stability. Therefore, a riser has been installed in the pressure vessel. It is fabricated from Type 304 stainless steel ($\frac{1}{8}$ in. thick). The lower cylindrical portion is bolted to the core support plate using the studs originally provided for the forced-circulation shroud. The upper portion of the riser is conical to an elevation where the cross-sectional area is equal to the flow area of the core, at which point a transition to a cylinder is made. The conical reduction in core-effluent area effects a corresponding increase in downcomer area. This, in turn, reduces the downcomer flow velocity and enhances the disengagement of steam from the recirculating water. The upper conical portion of the riser is removable in order to permit access to the outer rows of fuel subassemblies for loading operations. Bayonet-type locking bolts hold the upper shroud in place.

*M. Petrick

In order to permit removal of the quantity of steam corresponding to 100-Mw operation, removal of the steam-collection ring and replacement of the present 6-in. steam-outlet nozzle with one of a larger size has been necessary. If the former arrangment had been allowed to remain, excessive steam velocity, pressure drop, and surface erosion would result.

A system of baffles fabricated from $\frac{1}{8}$- and $\frac{1}{16}$-in.-thick Type 304 stainless steel were installed in the top of the reactor vessel to assure collection of steam from the highest feasible point in the vessel. The system is made up of a box section welded to the steam outlet nozzle. The baffle system is designed to permit operation with the higher water level in the reactor and still provide a means of steam separation. A new 6-in. feedwater-inlet nozzle and distribution ring have been installed above the top of the conical section of the new core riser. The new arrangement will permit the larger feedwater flows required for 100-Mw operation without excessive pressure drop, and will provide for injection of the colder feedwater at the top of the downcomer, where it will be most effective in collapsing entrained steam bubbles in the recirculating water and in increasing the driving force for natural recirculation.

Figure IX-16 graphically illustrates the physical dimensions significant to the 100-Mwt core heat transfer and hydraulic analysis.

III. In-core Instrumentation*

To obtain more specific information about certain reactor parameters, two sets of instrumentation have recently been installed within the EBWR pressure vessel. One set is of the pressure-sensing type, with the exception of some thermocouples for measurements of fluid temperature and is installed at about a dozen different points throughout the pressure vessel (see Fig. IX-17). It will provide basic data on performance, carry-under of steam into the downcomer, true interface height, vapor holdup, downcomer velocities in the reactor, and the average steam voids in the riser.

Some experimental work with pressure-drop methods of measuring voids and with the particular type of pressure taps which are in the reactor has been previously done. These are of a "concentric water-cooled static pressure tap" design, and enable one to combine high- and low-pressure taps in a single, large tube. This greatly simplifies installation and operating problems. Individual tubes from the pairs of pressure taps are mounted inside a larger tube carrying cooling water from a central connector box. This box is mounted on the inside wall of the reactor vessel in the steam zone above the core (see Fig. IX-18). The pressure taps are separated from the cooling water tubes on the inside of the "connector box" and are led through the reactor vessel wall inside of a 2-in. pipe to a connector

*M. Petrick and G. Popper

	Area	D_e
Plate elements	0.0580 ft^2	0.0573 ft
Spike elements	0.0591 ft^2	0.0417 ft

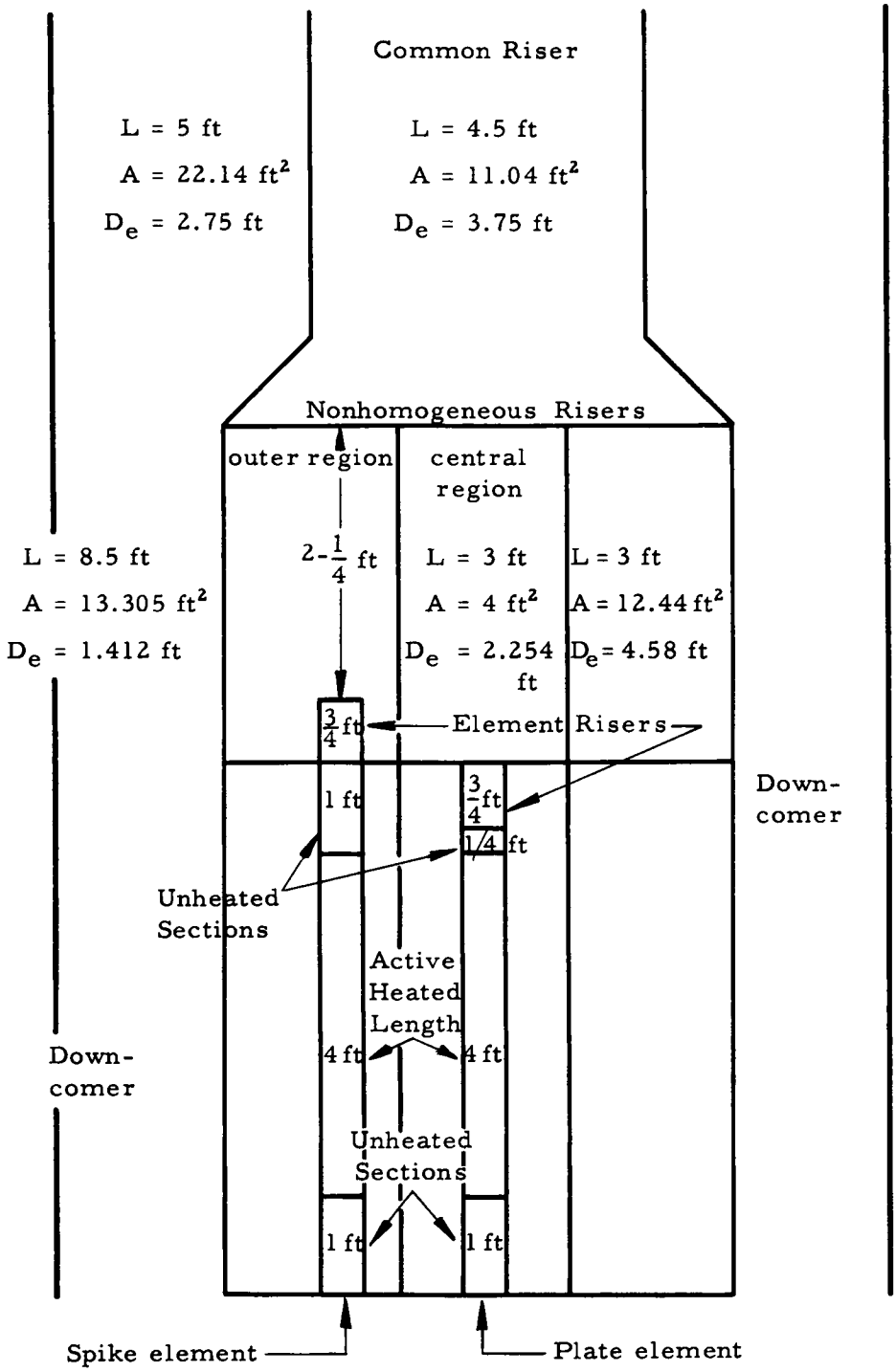

Fig. IX-16

Significant Heat Transfer and Hydraulics Physical Dimensions

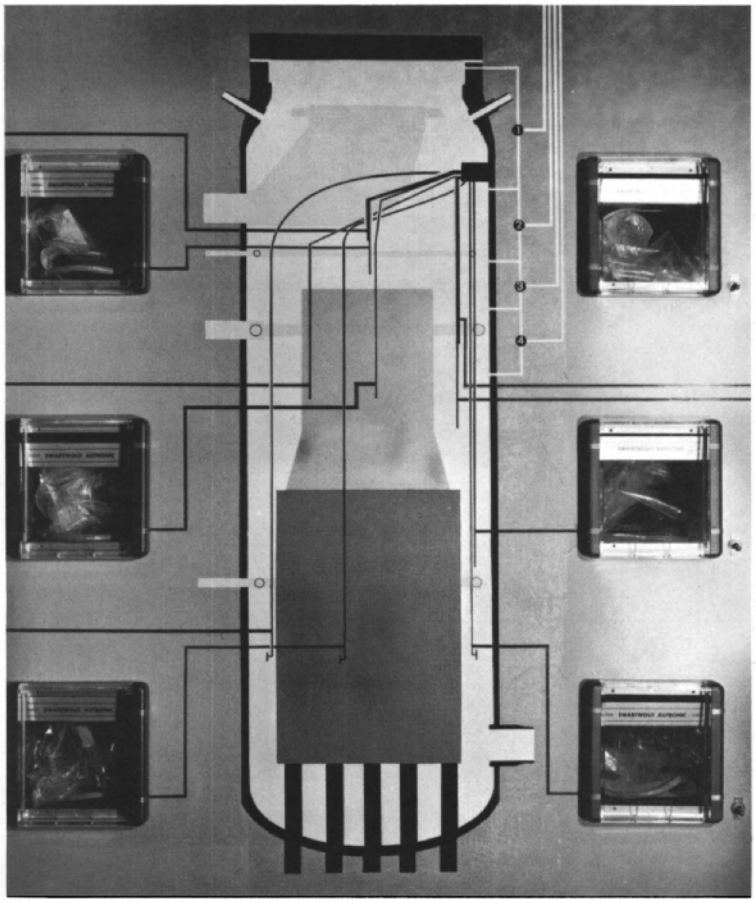

Fig. IX-17

Pictorial Data
Recording Board
111-9065

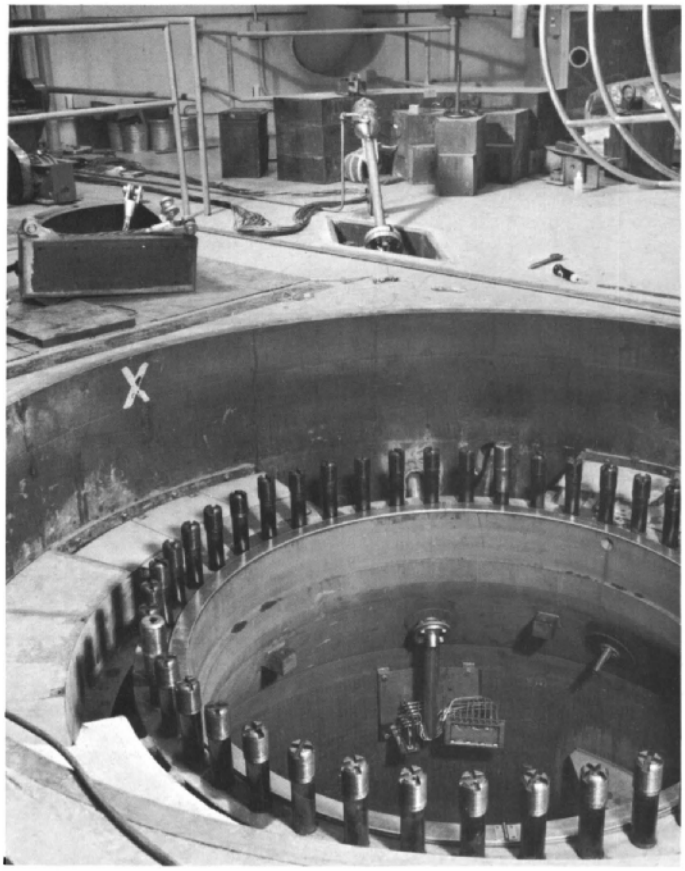

Fig. IX-18

Location of Central Connector Box in Pressure Vessel. (Note Connector Head in Background.)
111-9037

"head" (see Fig. IX-19). At this point, they are isolated from the reactor system and are led to differential-pressure transducers. The electrical signals from these transducers are then brought out of the reactor shell and fed into strip chart recorders mounted in the control room.

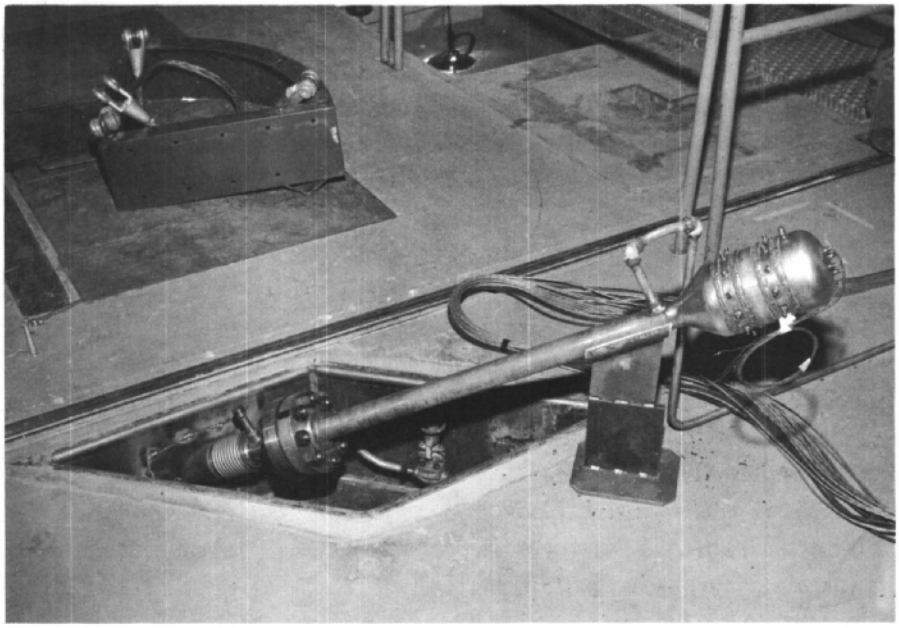

Fig. IX-19

Pressurized Connector Head
111-9034

The pressure taps must be cooled as they pass upward through the steam zone of the boiler vessel. If this precaution is not taken, the signal-transmitting medium inside the pressure tap, namely water, will reach the saturation temperature of the boiling system in which it is immersed. When this occurs, the saturated water in the pressure tap can flash to steam as soon as head pressure in the tap becomes less than the system pressure on the outside of the tube; this will destroy the differential pressure being read across the tap openings.

When this work was first begun in boiling test loops, it was believed the best approach would be one of splitting makeup water flow to the system and injecting a part of this water into the cooling jacket tube at a rather high rate. By doing this, one could maintain a low temperature in the jacket relative to the environmental system temperature. This portion of the makeup flow was then discharged from some convenient location near the end of the cooling jacket. The validity of this approach was disproven in the first test, when it became apparent that, in spite of the high rate of coolant flow, a severe axial temperature gradient was incurred along the tube. The inability to measure or calculate this gradient with any degree

of certainty resulted in large errors in average steam-volume fractions (voids) calculated from the pressure-drop measurements. A second approach, in which a very low rate of flow of coolant water was maintained, proved successful and highly reliable. With this method, the cooling water reached nearly the saturation temperature of the system shortly after its entrance into the cooling jacket and remained fairly constant in temperature throughout the run. The temperature drops through the walls of the concentric tubes and the cooling water layer are sufficient to maintain a slight subcooling up the entire length of the pressure tap, eliminating the flashing problem and the difficulties caused by large axial temperature gradients.

There are three instruments in the reactor downcomer to measure downcomer flow velocity. Two of these instruments are Stauschiebe tubes, small cylinders placed perpendicular to the flow direction with pressure taps on the upstream and downstream faces; the third is a conventional pitot tube. The Stauschiebe tubes require calibration to determine a flow coefficient. This coefficient will be checked in place against the flow values yielded by the pitot tube and compared to flow coefficients obtained on similar Stauschiebe tubes in an air-water loop. The velocity-measuring instruments are spaced circumferentially, about 120° apart, in the downcomer area around the core.

A set of pressure taps is installed in the downcomer along one of the Stauschiebe tubes. The taps span approximately 30 in. of downcomer length and will be used to determine the existence and magnitude of steam carryunder in that area. Thermocouples are mounted on the Stauschiebe and pitot tubes to measure the amount of subcooling at their location in the downcomer. By means of these thermocouples and others, a reactor inlet coolant temperature can be found.

Two more pressure taps have been installed at the same elevation and just below the elevation of the feedwater-return ring. With these taps, some information on the amount of steam carryunder, before and immediately after the jets of feedwater began to mix with recirculating water from the riser, will be obtained. The previously mentioned pressure taps will give the final steam-carryunder condition. Quenching of steam carryunder is expected in the downcomer below the feedwater ring. Two sets of pressure taps are located inside the riser and will be used to measure the average steam-volume fraction present in the riser. One set is placed at approximately the center of the riser; the other is near the edge. The riser itself is cylindrical. Two taps will be used in an attempt to measure the height of the water-steam interface; these are located above the riser in the center of the vessel.

The second set of instrumentation is mounted directly on a fuel subassembly; this instrumentation is designed to measure flow velocities, steam void fractions, and eventually heat flux and neutron flux. Power-distribution

measurements have been made in the EBWR fuel assemblies by means of a wire-activation technique. Curves of relative power as a function of fuel-element length are then plotted. To measure the steam void fractions in these same fuel assemblies, a second wire, which was cadmium covered, was inserted into the fuel channel alongside the bare wire. The bare wire then determines the total, whereas the cadmium-covered wire determines only the epithermal flux. From the cadmium ratio, which is the counting rate determined from the bare wire divided by the counting rate determined from the wire which was cadmium covered, one can calculate the void fraction. This method of measuring void fractions appears to have been successful. However, the only check on this technique is the very good comparison of the steam void fractions determined from the cadmium-ratio measurements to the steam void fractions predicted by performance calculations.

One of the instrumented fuel assemblies built for placement in the core of the EBWR (see Fig. IX-20) includes two neutron detectors, one of which is cadmium covered. These detectors should allow the determination of the neutron flux and the cadmium ratio at a specific point in the boiling channel under both static and dynamic reactor operating conditions. The in-core chambers will be placed in diagonally opposite corners of the assembly so that, when the fuel element is placed in the core, these chambers are in approximately the same neutron flux. It is not possible, however, to scan the entire fuel-element length as with the wires. Use of the neutron detectors will eliminate the need to change wires every time a flux or void measurement is needed, and the flux and void fractions under dynamic reactor operation may be studied.

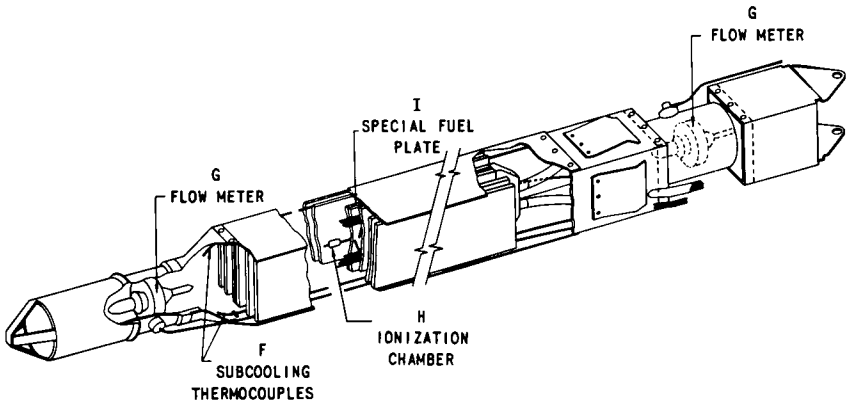

Fig. IX-20

Instrumented Subassembly for EBWR
112-1029

The instrumented fuel assembly has thermocouples that measure the centerline fuel temperature, which is directly proportional to power generation. The thermocouples that will be used to measure centerline

fuel temperature will be placed between two standard, thin, fuel plates. This is a sort of "sandwich" arrangement with a dead zone of clad on both sides of the thermocouples. Approximately 100 thermocouples spaced at $\frac{1}{2}$-in. intervals along the 4-ft fuel plate will eventually be installed. These thermocouples will allow measurements of power distribution. From the measurement of the centerline fuel temperature, one will also be able to calculate the heat flux at the plate surface, because the temperature drop between the surface of the plate and the water is small in the boiling region of the channel compared with the temperature drop through the fuel. One can, therefore, calculate an approximate film drop and find the surface temperature of the fuel plate. From these two temperatures, centerline and surface, the heat flux can be calculated.

Thermocouples placed at the inlet of the fuel assemblies and in the steam dome will be connected as thermopiles to measure the inlet subcooling. By measuring the inlet subcooling and by obtaining the feedwater flow rate and temperature and the system pressure, it is possible to calculate the rate of water circulation through the entire core. This calculation can be made, however, only when the steam entrainment in the downcomer is zero. The trouble encountered when measuring the inlet temperature directly is that this temperature ranges from only 2 to 10°F below the saturation temperature of the system. Therefore, if there is a relatively small error in determining the inlet temperature, the subcooling and hence the calculated recirculation rate will be considerably in error. With the instrumented assemblies, the inlet velocity will be measured directly by a turbine-type flowmeter, as shown in Fig. IX-21. A second turbine flowmeter (see Fig. IX-22) is placed at the exit of the fuel assembly to measure the exit liquid velocity. By measuring the inlet velocity and the exit liquid velocity, the steam void fraction at the exit of the assembly can be calculated. One of the requirements necessary to calculate the exit void fraction is that flow continuity through the element be assured.

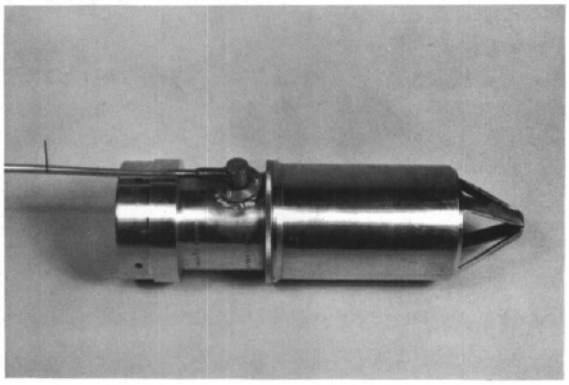

Fig. IX-21

Inlet Turbine Flowmeter
111-8798

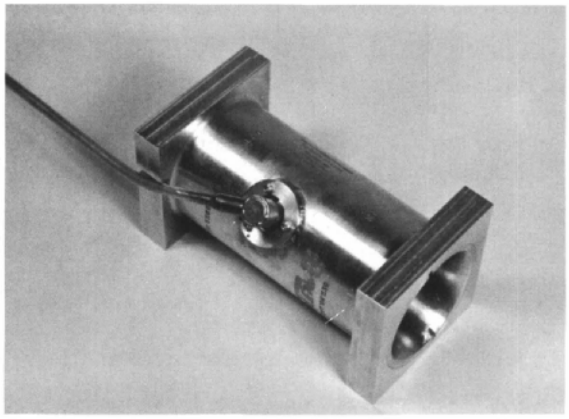

Fig. IX-22

Outlet Turbine Flowmeter
111-8797

To show that these flowmeters could be used to measure the void fraction successfully, an experimental out-of-pile flow system was built. The first experimental tests were conducted with a two-phase air-water mixture. The flow system was run to obtain void fractions ranging from 0.11 to 0.71. An inlet water velocity range of from 2 to 7 ft/sec was also covered. The void fraction was measured with a gamma-ray densitometer and simultaneously calculated from the two-flow measurements. The gamma-ray densitometer is considered the standard. The error plot of the void fractions obtained indicated an error of ± 10 per cent (see Fig. IX-23). These results were encouraging enough to proceed with similar tests in which the temperature and pressure conditions would duplicate those of the reactor, 486°F and 600 psig. The need for an instrument capable of displaying the void fraction directly became apparent while running the air-water tests. An electromechanical computer that would calculate the void fraction from the two velocity measurements was designed and built.

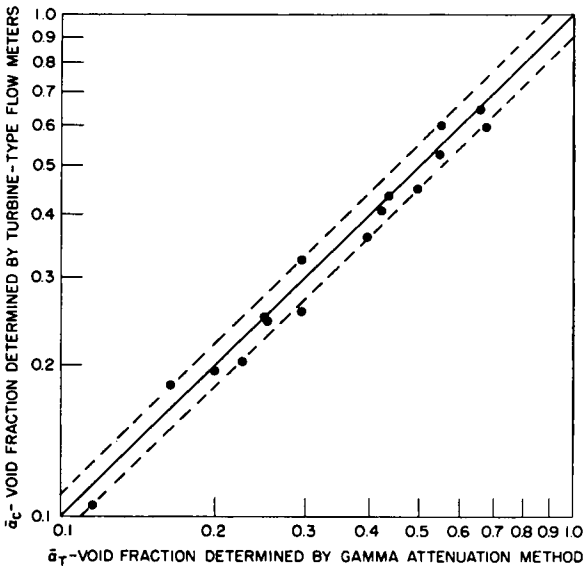

Fig. IX-23

Error Plot of Void Fractions from Air-water Tests

111-8793

A series of tests were run with a natural-circulation loop (see Fig. IX-24) to obtain void fractions ranging from 0.24 to 0.70. Because of the heat losses in the loop, the lowest void fraction that could be obtained and still hold system pressure was 0.24. Again, the void fractions compared to within ± 10 per cent in most cases (see Fig. IX-25), where $-\overline{\alpha}_T$ is the void fraction obtained from the densitometer and $-\overline{\alpha}_C$ is the void fraction calculated from the two velocity measurements. During these tests, the flow rate measured by the inlet turbine flowmeter was continuously compared with the flow rate measured by a calibrated Venturi meter. The accuracy of the turbine-type flowmeter was found to be within ± 1 per cent and repeatable to within ± 0.5 per cent. The void fractions obtained from the two velocity measurements were repeatable to within ± 2 per cent. Both flowmeters have been operating satisfactorily in this loop for over 350 hr.

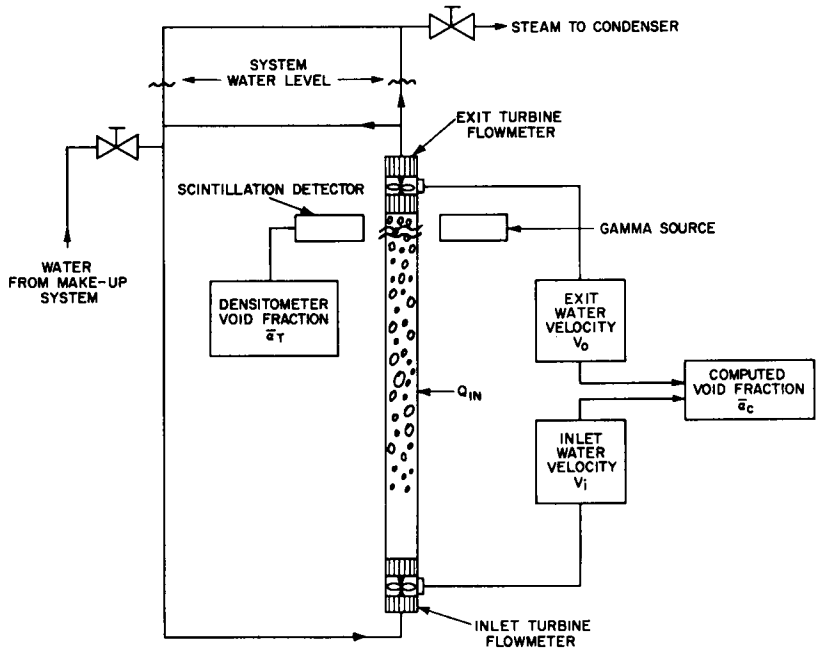

Fig. IX-24

Schematic of Natural-circulation Flow System
111-8789

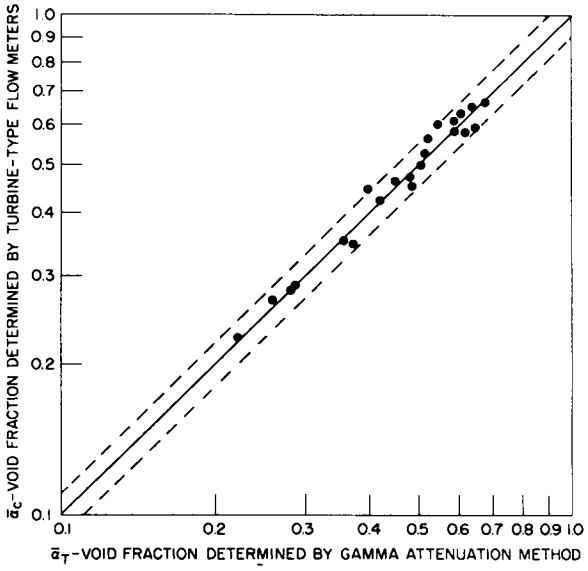

Fig. IX-25

Error Plot of Void Fractions
from Steam-water Tests
111-8794

To use the turbine-type flowmeters for an in-core application, several modifications were required. These modifications were made by the Potter Aeronautical Company. First, the relatively large standard high-temperature pickup coil had to be reduced in size so that the entire flowmeter and coil would be smaller than the outside dimensions of the fuel assembly. The electrical leads had to be an integral part of the coil assembly, so that the coil and leads would withstand the pressure and temperature in the reactor vessel, and lastly, the entire flowmeter had to be constructed of materials that would be compatible with the nuclear environment of the core. The redesigned pickup coil (see Fig. IX-26) is only 1 in. in height and affixes to the meter body by means of a flange. The coil is wound with ceramatemp-insulated wire manufactured by Hi-Temp Wires, Inc.

Two nickel wires enclosed in an inconel sheath and insulated by aluminum oxide are then welded to the ends of the coil. The sheath is welded to the coil assembly and the entire coil potted with Saureisen cement. A plug is then welded to the assembly to make it pressure tight.

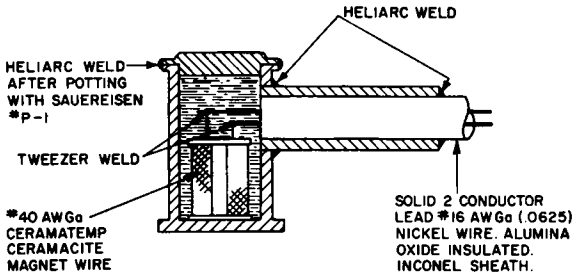

Fig. IX-26

Cutaway of Redesigned Potter High-temperature Pickup Coil 111-8791

IV. Future Experimental Work*

There are many possibilities for further experimental work with the EBWR system, both in-core and out-of-core. The entire field of in-core instrumentation is essentially in its infancy. There is a strong demand throughout the industry for development of in-core instrumentation techniques. Many problems still remain to be resolved. As an example, accurate devices for measuring low flow rates still remain to be developed. Other areas in which effort is needed are the development of techniques for readily adjusting the flow rates across a core, resolving the differences between horizontal and vertical two-phase systems, examining of the phenomena associated with two-phase downflow, quick detecting of fuel failures, extending data on two-phase friction factors for core geometries, exploring of bubble size and distributions in two-phase systems, etc.

One of the major problems in reactor design is the prediction of the maximum heat flux or "burnout" point. If boiling takes place on an electrically heated wire immersed in a pool of water and the temperature difference between the wire and the water is measured, the well-known convection (nucleate boiling) film-boiling curve will be obtained. Initially, the wire will be cooled only by convection currents in the water. As the heat input to the heater is increased, vapor bubbles will begin to grow on the heater surface and collapse as the bubble touches the main body of subcooled liquid. This is known as local or subcooled boiling and is characterized by a change in slope of the heat flux-temperature difference curve. As the water temperature increases to the saturation point, vapor bubbles will grow and detach themselves from the heater surface and "net" or "bulk" boiling will occur. Both types of boiling are known as "nucleate boiling." As the heat flux is increased, a vapor film will tend to form on the heater surface. The change in slope is defined as the departure from nucleate boiling. As the heat flux is further increased, a maximum heat flux (which is referred to as the "critical heat flux" or "burnout" point)

* M. Petrick

is reached. Since most heater materials will fail because of the sudden large temperature increase, characteristics of the same type are observed in flowing channels. As a result, the reactor designer must usually incorporate large factors of safety unless specific data for the geometrical arrangement and variables in question are available. Usually other factors, such as fuel-element temperature, limit the design heat flux.

It should be mentioned here for the sake of completeness that the standard methods of core analysis include the use of hot-channel factors and "uncertainty" factors. The factors arise from a number of conditions, such as the distribution of nuclear flux, flow distribution, and differences in fuel concentration. It should be remembered in connection with this that burnout will not necessarily occur at the channel exit or the point of maximum heat flux, but at some intermediate point, usually very close to the point at which the maximum surface temperature would occur if a single-phase system were considered. One of the most important design needs of burnout information is in the case of forced-circulation reactors, where the reactor must have adequate cooling during loss of flow transients.

Current design practice is not to allow the heat flux at any point in the reactor to exceed the "burnout" heat flux. Under certain conditions the attainment of the critical heat flux may not necessarily mean that the heating surface will melt, that is, the critical flux and "burnout" may not be synonymous. The temperature excursion of the fuel element will depend on the heat transfer that can be attained in film boiling. If heat transfer coefficients during transition and film boiling can be predicted, then the resulting temperature rise can be calculated. If this temperature rise is allowable, the critical point can be exceeded. This could be of importance in relaxing hot-channel factors, particularly during transient conditions in cases where the reactor is being shut down because of a loss-of-flow accident and heat fluxes are quite low. Very little work that is specifically applicable to boiling reactor design has been done. Considerable additional experimental work is needed before heat transfer coefficients in the film-boiling region can be estimated with accuracy.

In a reactor such as EBWR, where steam is withdrawn directly from the reactor vessel, a reactor power is ultimately reached where the problem of vapor-liquid separation becomes so acute that excessive moisture carryover and steam carryunder occur, adversely affecting reactor operation. The present trend of increasing the power and operating pressure of boiling water reactors has caused vapor-liquid separation to become one of the major problems in boiling water reactor plant engineering. Knowledge concerning the mechanism and various factors influencing the separation of steam from steam-water mixtures in reactor vessels or in separate steam drums is quite incomplete. As a result of lack of information, sizing of the reactor vessel and internals with any degree of confidence becomes difficult at best. The little information that has been reported has appeared in the English and Russian literature. However,

the experimental data obtained by different techniques are in some cases inconsistent, and the given equations do not predict correctly the fraction of moisture carried by the steam for certain ranges of steam loads and pressures. In a natural-circulation boiling water reactor of the EBWR type, the problem of vapor-liquid separation can be divided into the following parts: (1) liquid carryover in the effluent steam, (2) steam carryunder in the downcomer, (3) effectiveness of injection of liquid makeup water and the rapidity of steam quenching thereafter, and (4) transport of steam through stagnant steam-water mixtures (vapor holdup above core).

The problem of carryunder or entrainment of steam in the liquid in a natural vapor-separation system is a major one in either a natural- or forced-convection system. The entrainment of the steam in the liquid in the downcomer is, in general, a function of the downcomer velocity and system pressure. In a natural-circulation system, any entrainment that may occur in the downcomer adversely affects reactor operation, since the recirculation is reduced and this in turn lowers the reactor power. There is practically no information available that could be used for estimating the amount of carryunder that could be expected under normal reactor conditions. The carryunder problem in a forced-circulation system could be just as severe. In general, the velocities are somewhat greater in such a system, both in the core and the downcomer. The entrainment of the steam into the suction lines of the pump could decrease the NPSH to a point where pump cavitation problems could become serious, depending on the condition of the makeup water and point of injection. The seriousness of the steam-carryunder problem will be determined by the rapidity with which the entrained steam bubbles are quenched and, of course, by the amount of steam entrained. It is conceivable that the entrained steam bubbles are not collapsed immediately because of insufficient mixing in the downcomer; as a result, the steam would be carried a considerable distance before condensing. This will, to a large degree, be dependent on the mode of injection of makeup water. The makeup water-injection ring must be designed so that the makeup water is distributed evenly across and around the entire downcomer to insure fast, thorough mixing. Should substantial quantities of steam carryunder occur, the net driving head for natural circulation would be reduced. A reduction in net driving head would reduce the recirculation flow rate and increase the core steam-volume fraction.

In a closed reactor vessel, the mixture-vapor interface of a two-phase fluid depends upon the initial water level and upon the steam void content (power level in a reactor system). The voids that are formed in the reactor core and riser and entrained in the downcomer displace an equal volume of water, which causes an increase in the mixture height. The water level above the riser is further expanded by the vapor flowing through it, which creates a stagnant two-phase mixture or "bed." The final height of the two-phase mixture is a function of the superficial steam velocity (based on vessel diameter) and water content above the riser. Thus,

for a given initial water level at saturation (with no voids present), the expansion of the two-phase "bed" increases with increasing power because of the higher superficial steam velocity and the increased water content which was expelled from the region below the riser.

The height of the two-phase mixture cannot be obtained by purely analytical means. Recourse must be made to experimental data on vapor holdup through stagnant beds of water. Unfortunately, no data exist for flow of steam through stagnant water at 600 psi in large vessels. Calculations of the height of the vapor-mixture interface have been made for EBWR at 40 Mw and tend to explain the increase in carryover actually measured at that power level, since they show that the interface would have been very close to the steam ring at these powers. Additional data on the transport of vapors through low-velocity water at the higher pressures must be obtained before optimum vessel sizes can be chosen.

SECTION X

REACTOR PHYSICS

K. Almenas
R. Avery
H. Iskenderian
W. Lipinski
E. Pennington

NOTES AND EDITED DATA FROM LECTURES -
June 22 and 29 and July 7 and 10, 1961

SECTION X
REACTOR PHYSICS

I. Basic Theory*

A. General Approach

Basically, the approach to reactor physics calculations for the EBWR and similar reactor systems is the same as for nonboiling, water-moderated heterogeneous systems. There are, however, certain phenomena that demand special attention in analyzing the EBWR. Epithermal effects are important, necessitating 3-group analyses, while computers must be used to account for irregular geometrical configurations. Transport theory is needed for determination of the cell disadvantage factor; calculations of resonance escape probability are quite involved; and the temperature-dependent Doppler effect is significant.

The main problem in analyzing the power distribution in the core is the calculation of the local flux dependence on the distribution of steam voids. Cooperation between physicists and heat-transfer experts in the iteration procedures of the calculations is necessary in order to ensure consistency. The power distribution in boiling reactors tends to flatten radially, but in the axial direction the voids are always greater at the top, and one could say the power distribution "works against itself." It is necessary to have a small negative, operating void coefficient of reactivity without having a positive cold coefficient. Of course, boric acid injection will affect the coefficient and must be considered.

There are many areas of uncertainty which limit the prediction of the maximum power level of stable operation. It is difficult to know in advance (accurately) how steam voids and Doppler broadening will affect reactivity, and it is evident that a more basic study of even the relatively simple phenomenon of boiling is essential. Although a good deal of experimental work concerning transient reactor behavior with uranium metal fuel has been done, there have been almost no transient experiments using uranium oxides. The object of the entire EBWR experimental program is to develop confidence in analytical descriptions of boiling reactors. To this end, an extensive experimental program is planned in the approach to 100 Mw. Measurements will be made at 20-Mw increments, and successive extrapolations to higher powers will be made. In these calculations a new power-transfer function will be required because of plutonium buildup. The effect of the newly installed riser must be carefully considered.

Although the calculation of EBWR reactivity changes has up until now yielded quite good results, much work remains to be done. Much available data have been put aside without analysis because of personnel limitations. There are certain fields, such as fuel management that have been relatively untouched.

---

*K. Almenas, R. Avery, H. Iskenderian, and E. Pennington

B. Basic Statics Theory

By the principle of neutron conservation, neutron production minus absorption minus leakage equals the rate of change of the neutron population. It is assumed that scattering is isotropic except in heavy absorbers (e.g., fuel) and near the boundaries of heavy absorbers. These areas are treated by transport techniques (e.g., spherical harmonics), and equivalent cross sections are calculated. The entire reactor volume is then "homogenized," and the basic relation for the steady state becomes

$$-D\,\nabla^2\phi + \Sigma_a\phi = \epsilon\nu\Sigma_f\phi \quad . \tag{1}$$

The following energy groups are considered:

Fast	10 to 0.18 Mev
Epithermal	0.18 Mev to 0.625 ev
Thermal	0.625 to 0 ev

,

and the 3-group equations are:

$$-D_1\,\nabla^2\phi_1 + \Sigma_1\phi_1 - \epsilon\nu(\Sigma_{f2}\phi_2 + \Sigma_{f3}\phi_3) = 0 \tag{2}$$

$$-D_2\nabla^2\phi_2 + \Sigma_2\phi_2 - \Sigma_1\phi_1 = 0 \tag{3}$$

$$-D_3\nabla^2\phi_3 + \Sigma_3\phi_3 - \Sigma_{s\ell 2}\phi_2 = 0 \quad . \tag{4}$$

In these relations,

$\Sigma_1 = \Sigma_{s\ell 1}$ = Probability of a scattering collision that removes a neutron from the fast group (assume no absorptions)

$$\Sigma_2 = \sum_{a2}^{1/v} + \sum_{a2}^{\text{resonance}} + \Sigma_{s\ell 2}$$

$\Sigma_{s\ell 2}$ = Probability of a scattering collision that removes a neutron from the epithermal group.

$\Sigma_3 = \Sigma_{a3}$.

The following relation also holds for all three groups:

$$\nabla^2\phi + B^2\phi = 0 \quad . \tag{5}$$

Therefore,

$$D_1B^2\phi_1 + \Sigma_1\phi_1 - \epsilon\nu(\Sigma_{f2}\phi_2 + \Sigma_{f3}\phi_3) = 0 \tag{6}$$

$$D_2B^2\phi_2 + \Sigma_2\phi_2 - \Sigma_1\phi_1 = 0 \tag{7}$$

$$D_3B^2\phi_3 + \Sigma_3\phi_3 - \Sigma_{s\ell 2}\phi_2 = 0 \tag{8}$$

Now, defining

$$L_3^2 = \frac{D_3}{\Sigma_3} \quad ; \quad L_2^2 = \frac{D_2}{\Sigma_2} \quad ; \quad L_1^2 = \frac{D_1}{\Sigma_1} \quad , \tag{9}$$

and dividing through, the result is

$$(L_1^2B^2 + 1)\ \phi_1 - \frac{\epsilon\nu}{\Sigma_1}(\Sigma_{f2}\phi_2 + \Sigma_{f3}\phi_3) = 0 \quad ; \tag{10}$$

$$(L_2^2B^2 + 1)\ \phi_2 - \frac{\Sigma_1}{\Sigma_2}\phi_1 = 0 \quad ; \tag{11}$$

$$(L_3^2B^2 + 1)\ \phi_3 - \frac{\Sigma_{s\ell 2}}{\Sigma_{a3}}\phi_2 = 0 \quad . \tag{12}$$

Further, define

$$L_1^2 = \tau_1 \quad ; \quad L_2^2 = \tau_2 \quad ; \quad L_3^2 = \tau_3 = L^2 \quad . \tag{13}$$

By convention, $1 + L_1^2B^2$ is called the reciprocal of the nonleakage probability. Formerly, the first two energy groups had been lumped together but the importance of considering an epithermal group was demonstrated in the BORAX and subsequent experiments.

The initial EBWR 2-group calculations resulted in a 3.39% error in k_{eff}, which leads to a fuel-loading error of the order of magnitude of 2. Calculation uncertainties could be ascribed to the computation of the resonance escape probability (p) primarily, and to other parameters. For example, the following relations involving p were assumed:

$$k_{eff} = \frac{\epsilon p \eta f}{(1 + L^2B^2)(1 + \tau B^2)} \text{ (two-group model)} \tag{14}$$

$$p = e^{-f_r/(1-f_r)} \tag{15}$$

where

$$f_r = \frac{\text{resonance}}{\text{utilization}} = \frac{\Sigma_U^{res}}{\Sigma_U^{res} + \Sigma_{H_2O}^{res}} \tag{15a}$$

$$\frac{f_r}{1 - f_r} = \left(\frac{\Sigma_U^{res}}{\Sigma_{H_2O}^{res}}\right) \text{ or } p = \exp - \left(\frac{\Sigma_U^{res}}{\Sigma_{H_2O}^{res}}\right) \tag{16}$$

$$\Sigma_U^{res} = N^{238}\, \sigma_{res}^{238} \tag{17}$$

with

$$\sigma_{res}^{238} = \frac{\text{resonance}}{\text{integral}} = 7.5 \left(1 + \frac{3.4}{0.11 + \frac{M}{s}}\right) .$$

To agree with the experimental data, the value of the resonance integral has been multiplied by 1.209, and fast leakage described by $e^{\tau B^2}$ instead of $1 + e^{\tau B^2}$ as previously.

C. Basic Kinetics Theory

The presence of delayed neutrons has an important effect in determining the distribution of neutron flux in a nonstationary system. The essential features of this behavior are amply demonstrated by means of the one-velocity model. In this case, the appropriate time-dependent differential equations for the thermal flux and the concentration of precursors are

$$D\nabla^2\phi - \Sigma_a\phi + (1 - \beta)k_\infty\Sigma_a\phi + \sum_i^N \lambda_i C_i = \frac{1}{v}\frac{\partial\phi}{\partial t} \quad . \tag{18}$$

$$\frac{\partial C_i}{\partial t} = -\lambda_i C_i + \beta_i k_\infty \Sigma_a \phi \quad \text{with } i = 1,2,.....N \quad , \tag{19}$$

where

$$\phi = nV$$

$$\nabla^2\phi = -B^2\phi$$

$$\ell = \frac{1}{\Sigma_a V\left(1+\frac{DB^2}{\Sigma_a}\right)} = \frac{1}{\Sigma_a V(1+L^2B)}$$

$$\beta = \sum_i^N \beta_i$$

$$k = \frac{k_\infty}{1+L^2B^2} \quad .$$

Substitution of these expressions into equations (18) and (19) gives

$$\frac{\partial n}{\partial t} = [k(1-\beta)-1]\frac{n}{\ell} + \sum_i^N \lambda_i C_i \tag{20}$$

$$\frac{\partial C_i}{\partial t} = -\lambda_i C_i + \frac{k\beta_i n}{\ell} \quad . \tag{21}$$

For the case of a step increase in k (e.g., sudden withdrawal of a control rod), equations (20) and (21) are solved by Laplace Transform techniques as follows:

$$S\bar{n}(S) - n(o) = \frac{[k(1-\beta)-1]\bar{n}(S)}{\ell} + \sum_i^N \lambda_i \bar{C}_i(S) \tag{22}$$

$$S\bar{C}_i(S) - C_i(o) = -\lambda_i \bar{C}_i(S) + \frac{k\beta_i \bar{n}(S)}{\ell} \tag{23}$$

$$S\bar{n}(S) - n(o) = \frac{[k(1-\beta)-1]\bar{n}(S)}{\ell} + \sum_i^N \frac{\lambda_i}{S+\lambda_i}\left[C_i(o) + \frac{k\beta_i\bar{n}(S)}{\ell}\right] \tag{24}$$

$$\bar{n}(S) = \frac{\sum_i^N \frac{\lambda_i C_i(o)}{S+\lambda_i} + n(o)}{S - \frac{[k(1-\beta)-1]}{\ell} - \sum_i^N \frac{\lambda_i k\beta_i}{(S+\lambda_i)\ell}} \tag{25}$$

$$= \frac{n(o)\left[1+\frac{k}{\ell}\sum_i^N \frac{\beta_i}{S+\lambda_i}\right]}{S - \frac{[k(1-\beta)-1]}{\ell} - \frac{k}{\ell}\sum_i^N \frac{\beta_i\lambda_i}{S+\lambda_i}} \quad . \tag{25a}$$

Since

$$\mathcal{L}^{-1}\left(\frac{A(S)}{B(S)}\right) = \sum_{j}^{N} \frac{A(\lambda_j)}{B'(\lambda_j)} e^{\lambda_j t} \quad ,$$

where $B(\lambda_j) = 0$,

$$\frac{n(t)}{n(o)} = \sum_{j} \left(\frac{1 + \frac{k}{\ell} \sum_{i}^{N} \frac{\beta_i}{S_j + \lambda_i}}{1 + \frac{k}{\ell} \sum_{i}^{N} \frac{\beta_i \lambda_i}{(S_j + \lambda_i)^2}} \right) e^{S_j t} \quad , \tag{26}$$

where

$$k(1 - \beta) - 1 + k \sum_{i}^{N} \frac{\beta_i \lambda_i}{S_j + \lambda_i} = \ell S_j$$

or, substituting, the famous Inhour Equation is

$$\text{reactivity} = \rho = \frac{k - 1}{k} = \frac{\ell S_j + S_j \sum_{i}^{N} \frac{\beta_i}{S_j + \lambda_i}}{1 + \ell S_j} \quad . \tag{27}$$

For $k > 1$ there is one positive S_j and N negative S_j, whereas for $k < 1$ there are N + 1 negative S_j. Considering $k > 1$, after a time all $e^{S_j t} \to 0$ except the one corresponding to the positive S_j, which is now denoted by S. The asymptotic period is given by $T = 1/S$, and

$$\rho = \frac{\frac{\ell}{T} + \sum_{i}^{N} \frac{\beta_i}{1 + \lambda_i T}}{1 + \frac{\ell}{T}} \quad . \tag{28}$$

For small reactivities, i.e., large periods such that $T >> 1/\lambda_i$,

$$T \approx \frac{1}{\rho}\left(\ell + \sum_{i}^{N} \frac{\beta_i}{\lambda_i}\right) \approx \frac{1}{\rho} \sum_{i}^{N} \frac{\beta_i}{\lambda_i} \quad . \tag{29}$$

Thus, the period depends essentially on the delayed-neutron constants and is almost independent of the neutron lifetime. For small reactivities the delayed neutrons make the period much longer than it would be without them.

For large reactivities, i.e., small periods such that $T \ll 1/\lambda_i$,

$$T \approx \ell/k(\rho - \beta) \quad . \tag{30}$$

Thus, T depends strongly on ℓ. Note that this equation could be derived from equation (20) by ignoring

$$\sum_i^N \lambda_i C_i \quad .$$

Now, consider a ramp increase in k such that

$$k - 1 = \gamma t \quad .$$

For simplicity assume only one group of delayed neutrons; differentiate equation (20) and substitute for C_i in the result the value for C_i obtained from equation (21). Thus

$$\ddot{n} + \left\{ \lambda - \frac{[\gamma t(1 - \beta) - \beta]}{\ell} \right\} \dot{n} - \left(\frac{\gamma(1 - \beta)}{\ell} + \frac{\lambda \gamma t}{\ell} \right) n = 0 \tag{31}$$

Using a few approximations relating the constants, this can be solved analytically in some cases. Of course, it can always be solved exactly by numerical techniques.

Now, as a third model, consider a step increase in k with feedback proportional to energy and with no delayed neutrons (Fuchs method). The following relations obtain:

$$\frac{1}{P} \frac{dP}{dt} = \frac{k - 1}{\ell} = \frac{\delta k}{\ell} \tag{32}$$

$$k - 1 = \delta k = \delta k_0 - \alpha T \tag{33}$$

$$E = \int P dt = CT \quad , \tag{34}$$

where P is the power, E the energy, α the temperature coefficient, and C the heat capacity. Solutions of (32), (33), and (34) are:

$$P = P_0 \frac{4}{(1 + Y_0)^2} e^x \left[\frac{1}{1 + \left(\frac{1 - Y_0}{1 + Y_0} \right) e^x} \right]^2 \tag{35}$$

$$T = \frac{b}{\alpha}(1 - Y_0)\frac{(e^x - 1)}{\left[1 + \left(\frac{1 - Y_0}{1 + Y_0}\right)e^x\right]} \tag{36}$$

$$\delta k = b\left[\frac{1 - \left(\frac{1 - Y_0}{1 + Y_0}\right)e^x}{1 + \left(\frac{1 - Y_0}{1 + Y_0}\right)e^x}\right] , \tag{37}$$

with

$$Y_0 = \frac{\delta k_0}{b}\ b = \sqrt{\delta k_0^2 + \frac{2\alpha P_0 \ell}{C}}\ x = \frac{bt}{\ell} \quad . \tag{38}$$

Some interesting relations are shown in Table X-1.

Table X-1

RELATIONSHIPS AMONG PHYSICS VARIABLES

t	T	P	δk
0	0	P_0	δk_0
$\exp(bt_{max}/\ell) = \frac{1 + Y_0}{1 - Y_0}$	$\frac{\delta k_0}{\alpha}$	$P_0 + \frac{C\delta k_0^2}{2\alpha\ell} = P\ max$	0
$\exp(bt/\ell) = \left(\frac{1 + Y_0}{1 - Y_0}\right)^2$	$\frac{2\delta k_0}{\alpha}$	P_0	$-\delta k_0$
∞	$\frac{\delta k_0 + b}{\alpha}$	0	$-b$

Other models for a step increase in k of magnitude k_0 include:

Corben's Model $$P(t) = P_1 e^{\alpha t} - P_2 e^{2\alpha t} \tag{39}$$

with $P_2 << P_1$ and $\alpha = \frac{\delta k_0}{\ell}$

Quasistatic Model $$\frac{\ell \bar{E}}{E} = k_0 - b^n E^n \tag{40}$$

Long Delay Model $$\frac{\ell \ddot{E}}{\dot{E}} = k_0 - \left[bE_0 \exp\frac{k_0}{\ell}(t - \tau)\right]^n \quad . \tag{41}$$

II. Experimental Activities*

A. Measurements of Void Coefficient

Measurements of the void coefficient have been performed by inserting perforated styrofoam sheets in the water channels of the fuel elements. The styrofoam sheets were designed to simulate the changes in moderator density (voids) associated with the temperature and boiling characteristics of the reactor. The "temperature void" sheets (with uniform perforations) simulated a void volume proportional to the loss of water density due to temperature. The "boiling void" sheets (with nonuniform perforations) simulated a void volume proportional to the loss of nonuniform water density at full power. All void coefficients determined are defined as:

$$\frac{d\rho}{dV} = \frac{\text{change in reactivity, in \%}}{100 \times (\text{change in water volume in channels/the original water volume})} . \tag{42}$$

B. Temperature Coefficient

1. Factors Affecting Temperature Coefficient

The temperature coefficient for the EBWR Core 1A is difficult to determine because of the complex nature of the present core. The main complications are:

a. Three types of fuel elements are used.

b. Plutonium has built up in the older elements.

c. Boron-stainless steel poison plates are used in the spiked elements.

d. Boric acid is used to obtain a shutdown margin.

In order to describe the temperature coefficient analytically, some simplifying assumptions must be made. The two primary assumptions are: 1. the coefficient depends only on the spiked and the enriched elements; 2. the control rods are withdrawn completely from the core. Both assumptions are on the conservative side, since the presence of control rods and/or natural uranium fuel elements tend to make the coefficient more negative. A further assumption is that the coefficient can be divided into a prompt effect due to the temperature rise in the fuel, only, and an equilibrium effect due to the moderator temperature. The latter effect is more significant in any power variation, except the extremely short-period accidental rises, where both effects will influence the coefficient.

*K. Almenas

In determining the prompt temperature coefficient, 3 phenomena must be considered:

a. Doppler broadening of the U^{238} epithermal resonance-absorption peaks;

b. radial expansion of the fuel elements, resulting in a decrease of moderator density in the core and any poison dissolved therein; and

c. longitudinal expansion of the fuel elements, resulting in a decrease of fuel density (a negative reactivity effect) and elongation of the core (a positive reactivity effect).

2. Doppler Broadening

Recent experimental work in the field of resonance escape has shown that for U^{238} analytical approaches yield results accurate to within 10%. Thus, the empirical formulas used are now put on a theoretical foundation.

The fuel used in EBWR is a tertiary alloy of uranium, zirconium, and niobium. Thus, the scattering cross section per U^{238} atom is higher for the EBWR fuel than for pure U, for which most of the work on resonance escape probability has been concentrated. To apply the uranium metal data, a correlation is necessary. The parameter to be correlated is

$$\xi = \frac{\rho_U}{4N_U \sigma_U}\left(\frac{S}{M}\right) + \frac{\sigma_N}{\sigma_U} \quad , \tag{43}$$

where S/M is the surface-to-mass ratio and the subscript N refers to the alloying metal. We have

$$\xi(\text{U metal}) = 10.61 \left(\frac{S}{M}\right)_{\text{U metal}}$$

and

$$\xi(\text{EBWR alloy}) = 11.49\left(\frac{S}{M}\right)_{\text{EBWR alloy}} + 0.141 \quad .$$

The resonance integrals will be identical for identical ξ; therefore,

$$\left(\frac{S}{M}\right)_{\text{EBWR alloy}} = 0.923 \left(\frac{S}{M}\right)_{\text{U metal}} - 0.0123 \quad .$$

For the enriched thin (ET) elements (applying a self-shielding factor of 0.873), the effective resonance integral becomes

$$I_{eff} = 13.22\ (1 + 0.009\ \sqrt{T}) \quad . \tag{44}$$

The integral increases with increasing temperature, resulting in more resonance absorption and, thus, causing a reactivity decrease with temperature.

3. Expansion of Fuel

Assuming that the fuel expands linearly with temperature, all parameter changes resulting from expansion can be expressed as first-order functions of T.

The equilibrium temperature coefficient is much more complex and not susceptible to such a simplified analytical approach. To account for the changes in the ratio of hydrogen to fuel atoms, which determines the neutron spectrum, computer codes are used. Input data must be adjusted to account for heterogeneous reactor effects, since the codes used consider an infinite homogeneous region and compute cross sections on this basis.

4. Experimental Procedures

$$\text{Reactivity} = -\frac{1 - k_{eff}}{k_{eff}} \times 100 = \text{per cent} \quad . \tag{45}$$

To examine the behvaior of a reactor when $k_{eff} < 1$, we have

$$\text{neutron population} = N = \int_{\text{Volume of core}} \frac{S\ell^*}{1 - k_{eff}}\, dv \tag{46}$$

S = source strength (Sb-Be source for EBWR) .

ℓ^* = effective neutron lifetime.

Note that $N \to \infty$ as $k_{eff} \to 1$; thus, strictly speaking, a reactor having a source and operating at a steady power is always somewhat subcritical. The counting rate is proportional to N, the neutron population thus can be used to obtain an extrapolation to $N \to \infty$ as shown in Fig. X-1. When $1/CPM = 0$, the neutron population approaches ∞ and the reactor is critical.

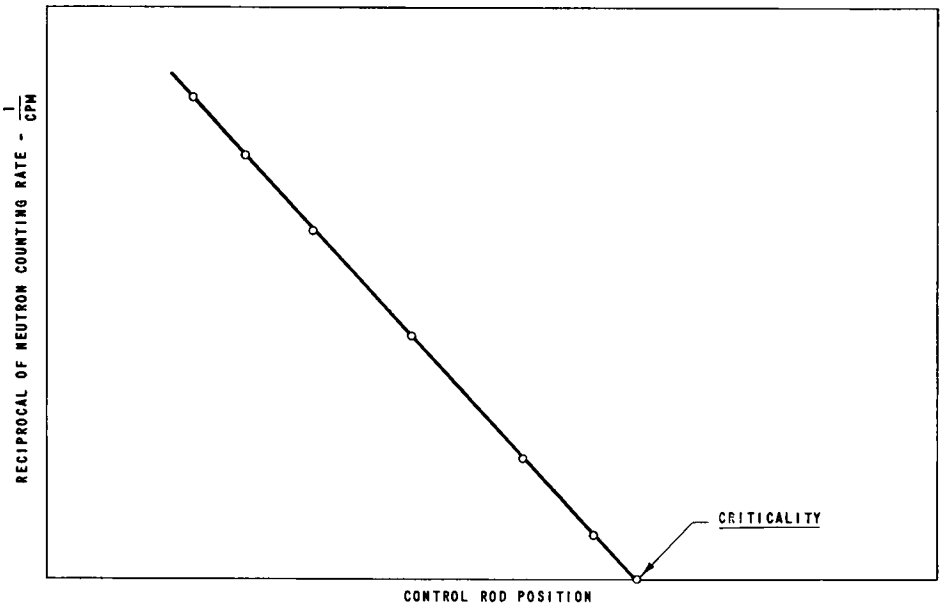

Fig. X-1

Sample Startup Plot of Rod Position vs
Reciprocal of Neutron Counting Rate

The power distribution in EBWR has been determined from measurements of gamma flux. The gamma flux was measured by inserting a small ion-chamber probe between the fuel plates of the fuel assemblies. The probe is essentially an ion chamber; a voltage of 600 v is impressed between the center wire of the coaxial cable and the outer casing. The 170 chamber ($3\frac{3}{8}$ in. long) is ionized by the gamma flux, and the resulting current is read on the Keithly micromicroammeter. By applying the probe sensitivity to the current read, the gamma flux can be directly calculated.

Three particular phenomena that have been under inspection are:

1) Vertical flux distribution of two typical fuel elements near the center of the core.

2) Difference in flux level between individual plates of fuel assemblies.

3) Horizontal flux distribution at various cross sections of the core, taken at the point of maximum vertical flux ($16\frac{1}{2}$ in. from bottom of fuel plate).

C. Reactivity Measurements

Small reactivity variations are usually measured by the positive-period method. The sequence of steps is as follows:

1) The reactor is brought to criticality, usually by removing control rods, and the position of the rods is noted.

2) The rods are reinserted (reactor now subcritical).

3) The change for which a reactivity worth is desired is performed (i.e., change in fuel position, change in temperature, etc.).

4) Rods are brought out to the position of step 1. Now, if the reactivity change of step 3 was positive, the reactor would be supercritical, and the reactivity worth of the change is determined by the resulting period. If the reactivity change is negative, the procedure has to be modified so that the reactor is supercritical during step 1 and, consequently, less supercritical during step 4. The reactivity worth of the change is then determined from the differences in the periods.

Reactivity measurements of reactors having strong stationary sources are performed under two power limitations. At low power the source contributes an appreciable and indefinitely known fraction of the total flux measured. At high power the source has less effect, but the reactivity measurements are adversely affected by heat. A way to minimize the source error is to take static and dynamic reactivity measurements at the same power level so that the source affects both of them equally. This assumption is correct if the spatial flux distribution is identical in both cases. If, however, gross rod movements are made so that the flux distribution is distorted, identical instrument readings do not necessarily correspond to identical power levels.

The kinetics equation after all the transients have died out is

$$\frac{dn(t)}{dt} = \frac{n(t)}{T} + S \quad , \tag{47}$$

where T is the asymptotic period and S the source strength (n/sec). If a plot of dn/dt versus $n_{(t)}$ is made, a straight line with a slope 1/T and an intercept S will result. At dn/dt = 0, denoting the prompt-neutron lifetime by ℓ^*,

$$S = -\frac{n(t)}{T} - \frac{n(t)\,k_{eff}}{\ell^*} = \frac{n(t)(1 - k_{eff})}{\ell^*} \quad . \tag{48}$$

Thus, S can be calculated. In order to evaluate S from positive periods, very long periods must be available, since sufficient time must be allowed for the transients to die out. For short periods, the power is carried too high above the source level.

III. 100-Mw Core Considerations*

A. New Core Loading

Experiments conducted in 1957 and 1958 affirmed that the reactor was capable of operation at power levels up to approximately 60 Mw. Control and heat-removal characteristics precluded any further increase in power level. Moreover, the reactivity of the operating core, Core 1, would not permit prolonged operation at total powers substantially above the design level. Therefore, to facilitate experiments at high power densities, the reactor core and system components are being modified. It is hoped that the modifications will allow the reactor to attain a power of 100 Mw.

The "spike" concept for attaining 100-Mw operation is predicated on:

1. a minimum amount of new fuel element construction; and
2. the maximum utilization of the existing Core 1 fuel elements.

The 28 spikes will be located in a square surrounding the central 36 four-ft-long fuel elements. The amount of reactivity produced by the U^{235} in the spiked region will be determined experimentally during prestartup operations. The positioning of the spikes in the core will cause the flux at the outer periphery to be raised and a degree of power flattening achieved.

B. Boric Acid System

In order to attain the highest possible power with the new loading, it is necessary for the EBWR control system to provide more control than had been previously required. This results from the additional reactivity lost from both increased voids and higher xenon concentrations at increased powers. It will be necessary to use boric acid for cold shutdown in EBWR Core 1A. It is expected that Core 1A will have 9-rod cold shutdown. It will be necessary to use boric acid in order to provide a margin of safety at shutdown as, for example, may be needed in the case of malfunction of one of the control rods. Since such safety precautions are normally included in provisions of cold shutdown, Core 1A is categorized as requiring boric acid for cold shutdown.

Core 1A has available a number of different fuel elements. In addition to the thin and thick enriched elements (the primary constituents of Core 1) and the thin and thick natural uranium elements, there are spike

*K. Almenas and H. Iskenderian

elements specifically fabricated for Core 1A. Additional flexibility is obtained by the use of boron-stainless steel strips which may be fastened to the sides of the spike elements. It is expected that an average of 1.5 boron-stainless steel strips per spike will be required for 100-Mw operation. Since some of the calculations may be conservative, 2 strips per spike will be used and will be removed only if necessary.

The capacity (maximum that might be needed under conservative assumptions) indicated for the boric acid system for Core 1A is 4 gm boric acid per gallon of cold water. The contributors to the quoted capacity of 4 gm/gal are as follows (1 gm/gal is worth about 1% reactivity):

1. shortage from 9-rod shutdown, ~1.5% (assuming that for one reason or another only 1 B-SS strip per spike is desirable);
2. shutdown subcriticality margin, ~2% (not required). One-rod withdrawal worth (to guarantee 8-rod shutdown) ~3.5%.

An added advantage resulting from the use of boric acid for cold shutdown is the operating experience in chemical control which will be gained. It is quite likely that future power reactors (and some already under design construction) may resort to such control for cold shutdown.

The presence of the boric acid will somewhat alter the values of various reactivity coefficients. The one of most concern is the void coefficient, since boric acid tends to reduce the magnitude of the negative void coefficient and, if present in sufficient concentration, can make the void coefficient positive. For the present system we find that the void coefficient with 5 gm/gal boric acid is still negative with the reactor cold (and, therefore, at all other reactor conditions), even though substantially smaller in magnitude compared to no boric acid:

$\Delta k/\Delta v = 0.12$	0 gm/gal
$\Delta k/\Delta v = 0.005$	5 gm/gal (1.33 gm/liter)(no control rod in)

The temperature coefficient is only slightly affected by the presence of the boric acid. For the case of all rods inserted, approximately 4% reactivity is lost in going from the cold condition to the hot (no-void) condition with a roughly linear temperature dependence. The bulk of the effect is due to the increased worth of the rods at higher temperature. (The temperature coefficient of the core without rods is very much smaller.) Since the boric acid leads to only a small part of the total absorption, it is relatively unimportant in effects on the temperature coefficient.

The presence of the boric acid should have a negligible effect on the stability of the system (what small effect it has should enhance stability). In general, at operating condition, very little (if any) of the boric acid will be present. The effect of the boric acid on the void coefficient becomes progressively less important as the system goes up in temperature and void content. What small boric acid remains at operating condition should enhance stability by reducing the magnitude of the negative void coefficient. Table X-2 lists the boric acid management required for Core 1A.

Table X-2

REACTIVITY OF CORE 1A UNDER VARIOUS OPERATING CONDITIONS

Reactor Condition	Reactivity k_{eff}	Suggested Boric Acid Management
Cold, all rods in, no boric acid	1	
Cold, 8 rods in, no boric acid	1.03	Boric acid required for cold shutdown
Cold, 8 rods in, 5 gm/gal	0.98	Normal boric acid shutdown concentration 5 gm/gal
Preheat, all rods in, no boric acid	0.98	Boric acid still required at preheat conditions
Preheat, 8 rods in, no boric acid	1.01	
Preheat, 8 rods in, 5 gm/gal	0.96	At least 2 of 5 gm/gal can be safely removed at preheat
Preheat, 8 rods in, 3 gm/gal	0.98	conditions; more likely removal will occur while going to operating conditions

IV. Reactor Stability*

A. Introduction

The following equations describe the kinetics of a zero-power reactor:

$$\frac{dn}{dt} = \frac{\delta k - \beta}{\ell^*} n + \sum_{i}^{6} \lambda_i C_i \quad ; \quad i = 1,2,3,....6 \quad ; \qquad (49)$$

*W. Lipinski

$$\frac{dC_i}{dt} = \frac{\beta_i}{\ell^*} n - \lambda_i C_i \quad . \tag{50}$$

Assume small oscillatory deviations and linearize equations (49) and (50); then take the Laplace Transform to obtain

$$\frac{\delta n(S)}{\delta k(S)} = \frac{n_0}{\ell^* S} \left[\frac{1}{1 + \sum_i^6 \frac{\beta_i}{\ell^*(S+\lambda_i)}} \right] \quad . \tag{51}$$

Define $S = \delta k(s)/\beta$ and rearrange to obtain

$$\frac{\left[\frac{\delta n(s)}{n_0}\right]}{\left[\frac{\delta k(S)}{\beta}\right]} = G(S) = \frac{\beta/\ell^*}{S\left[1 + \frac{1}{\ell^*}\sum_i^6 \frac{\beta_i}{s+\lambda_i}\right]} \quad , \tag{52}$$

where G(S) is the zero-power transfer function, defined as the amplitude and phase relation of the sinusoidal variation in flux or power output with respect to the sinusoidal reactivity input. Figure X-2 shows the analytical zero-power transfer function for EBWR as a solid line and the circles as the experimentally measured values.

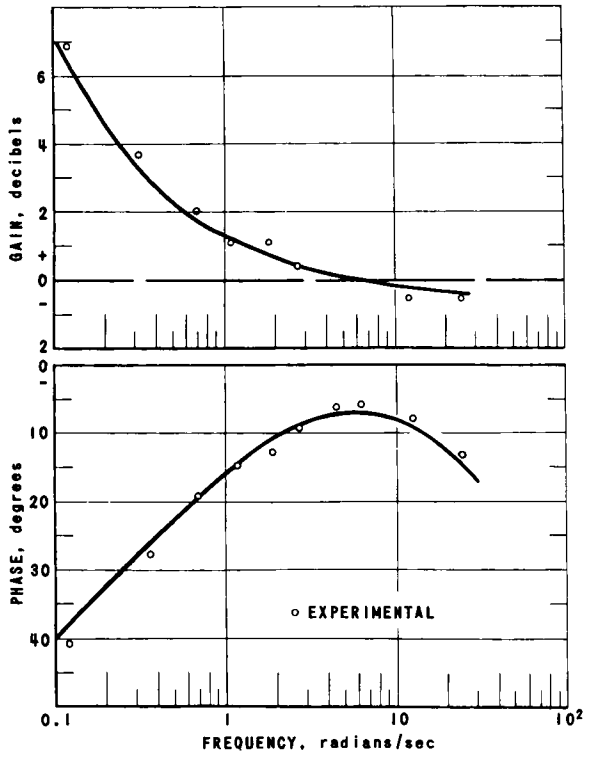

POWER, Mw	ZERO (6 kw)
PRESSURE, psi	150
BORON	NO
CENTER ROD, in.	13.6
8-ROD BANK, in.	14.5
STEAM BYPASS	MANUAL
PEAK REACTIVITY, % FOR 1-in. PEAK STROKE	0.087

Fig. X-2

Zero-power Frequency Response
111-6106

The power reactor transfer function is simply the zero-power function modified by power-to-reactivity feedback. The feedback schematic is shown in Fig. X-3.

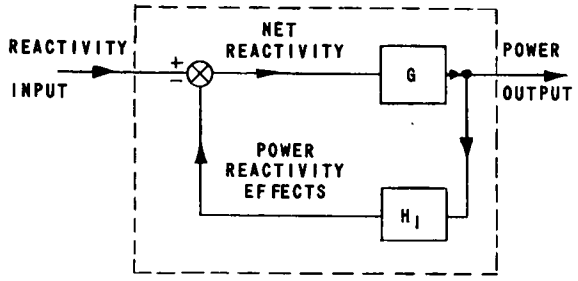

Fig. X-3

Schematic of Power-to-Reactivity Feedback
111-7627

Then,

$$P = \frac{G}{1 + GH} = \frac{\text{Flux Output}}{\text{Reactivity Input}} \tag{53}$$

where

P = Reactor power transfer function for the power parameters specified

G = Zero-power transfer function [Equation (4)]

H = Power-to-reactivity feedback.

Various well-known techniques can be employed to yield quantitative stability for the mode of operation it represents. Thus, P could be calculated and stability predicted if H were known. However, H is difficult to calculate quantitatively from thermodynamic data, and the nature of the direct-cycle concept makes specific measurement of H extremely difficult. Another method is to measure P and calculate H by means of the relation

$$G/P = 1 + GH$$

$$H = GH/G \tag{54}$$

Calculate GH by means of trends in H can be obtained and used to predict stability. The latter technique was used for EBWR.

B. Experimental Transfer Function

The power transfer function of EBWR was measured by applying a sinusoidal reactivity forcing function. A special rod drive was installed in place of the regular central rod drive, as shown in Fig. X-4. The drive consisted of a variable-displacement bell crank driven by a combination of mechanical and hydraulic transmissions to provide a

frequency range from 0.01 to 25 rad/sec, as shown in Fig. X-5. The hydraulic motor shown on the right-hand side of Fig. X-6 was operated only over a 10-to-1 speed range. The gears were changed to provide the ratios necessary for the overall 3.5-decade range. The reactivity amplitude was adjusted by means of the off-center setting on the bell crank shown in Fig. X-7. A spring was used to bias out the pressure forces and resonate with the inertia to reduce the horsepower requirements, as shown in Fig. X-8.

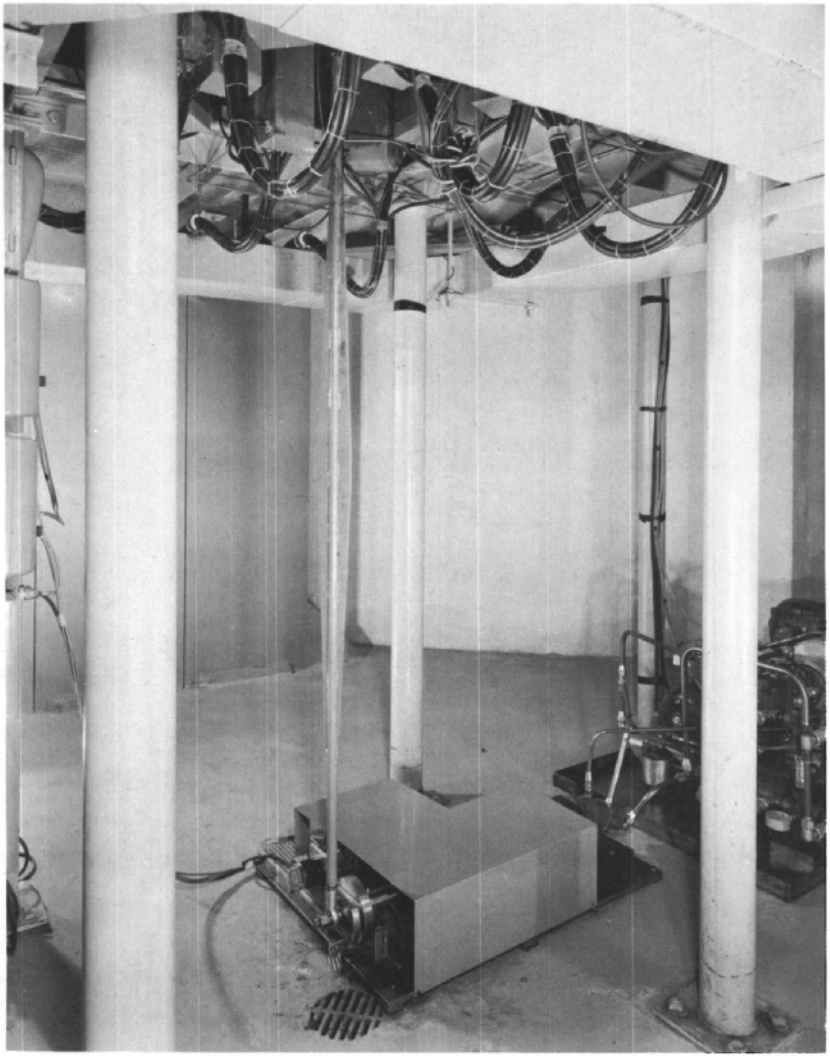

Fig. X-4

Sinusoidal Control Rod Oscillator Mechanism
111-5712

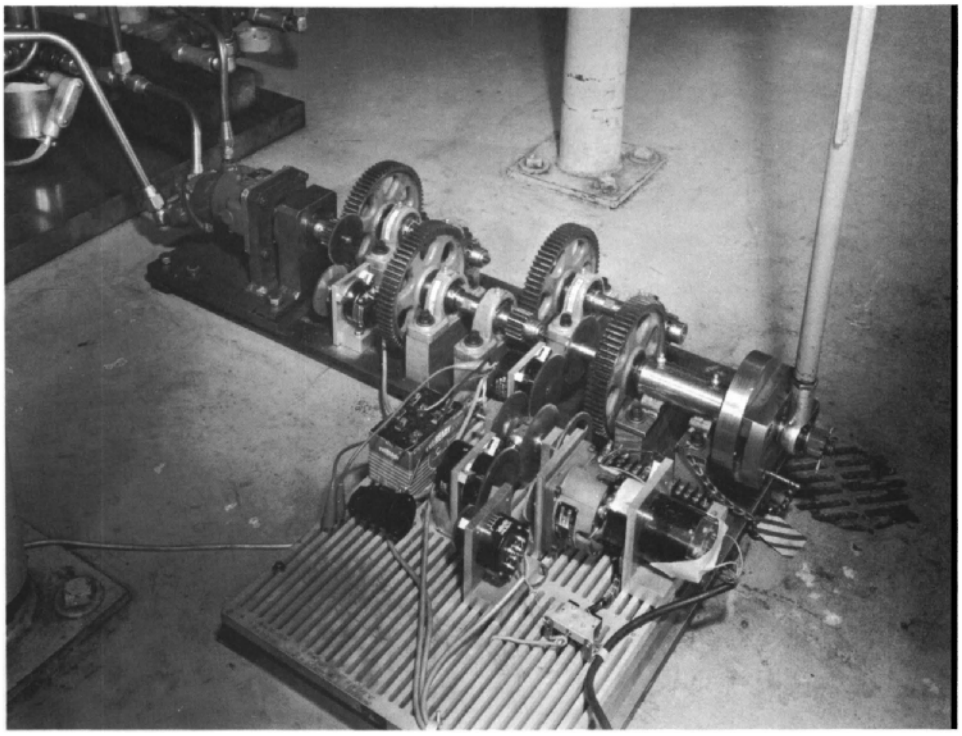

Fig. X-5

Oscillator Mechanism Gear Train
111-5702

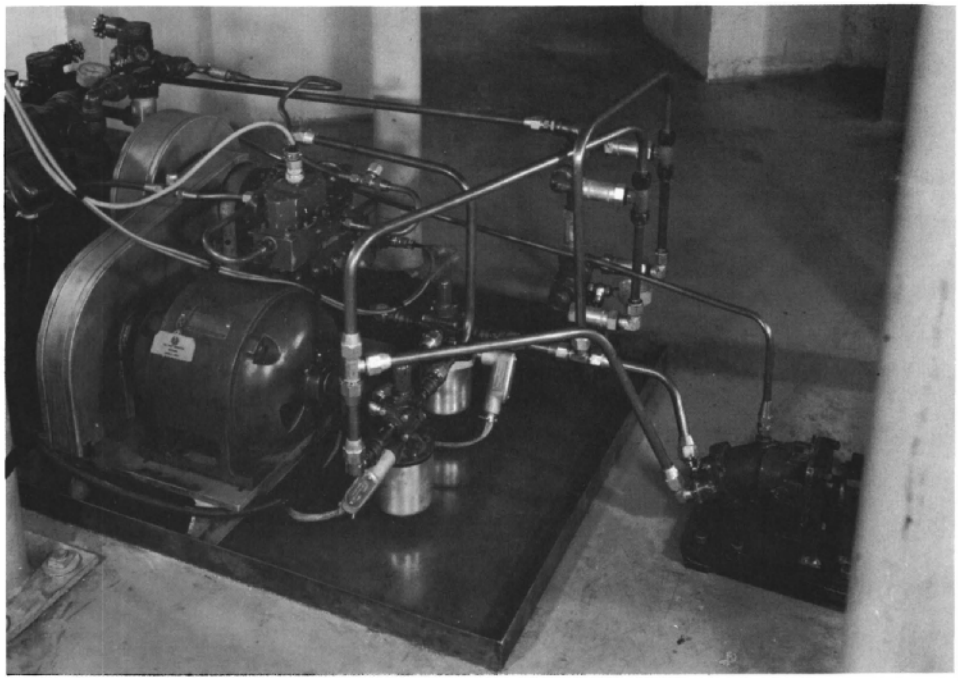

Fig. X-6

Hydraulic Motor
111-5705

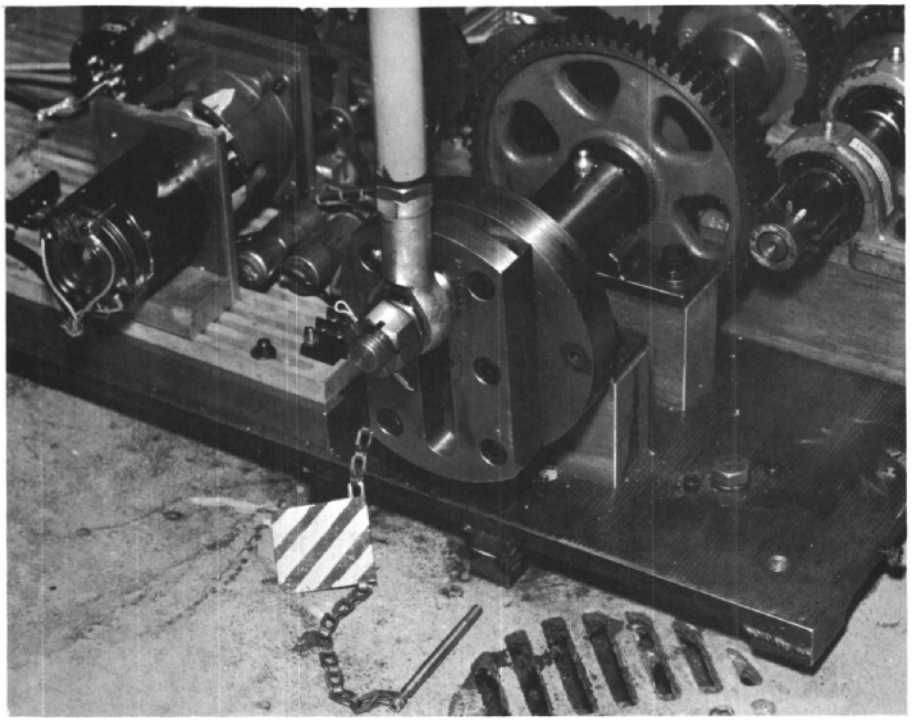

Fig. X-7

Oscillator Bell Crank
111-5691

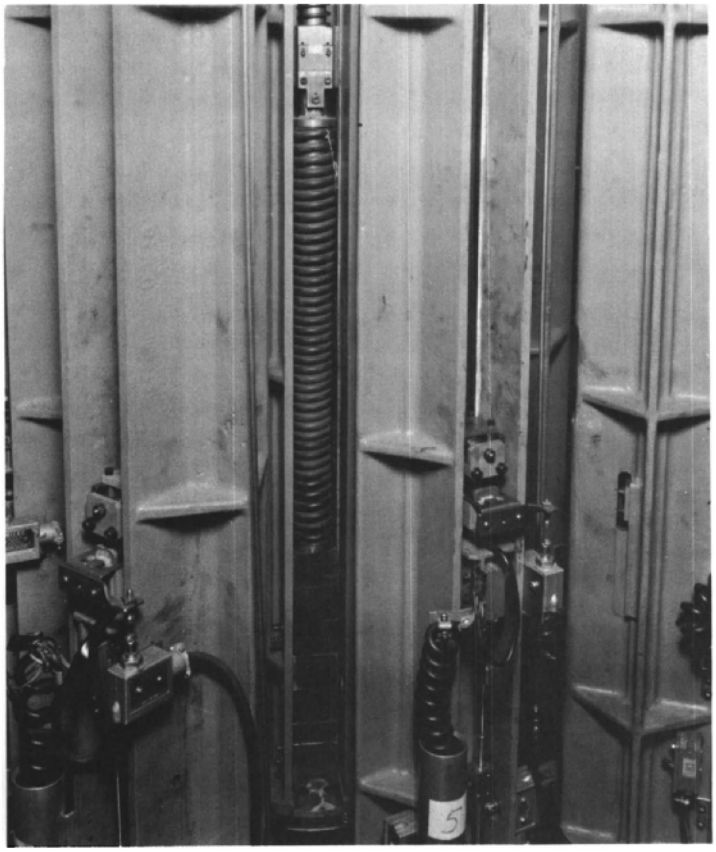

Fig. X-8

Oscillator Balance Spring
111-5703

A wave analyzer was used to measure the amplitude and phase shift of the reactor power transfer function. The analyzer operated by means of a correlation technique in which the variation of reactor flux output measured by an ionization chamber was multiplied by an amplifier gain which was correlated to the reactivity driving function in both amplitude and phase. The block diagram of the wave analyzer is shown in Fig. X-9. The schematic diagram of the correlator is shown in Fig. X-10. It is possible to select a correlation which reduces the fundamental component of the multiplied signal to zero, leaving only a small second harmonic plus any noise present in the original flux signal. The resistance R_2 is used to adjust the amplitude correlation by changing the feedback. The phase shift of "r" was adjusted by means of a mechanical differential, shown in Fig. X-11. The second harmonic and noise output of the analyzer was reduced by passing the analyzer output signal through a band-pass filter as shown in Fig. X-12. The data-output end of the analyzer is shown in Fig. X-13. The left-hand cabinet contained equipment associated with the hydraulic servo motor and the velocity controls. The cabinet on the right contained, from top to bottom: operational amplifier manifold, R_2 adjustment, phase dials, recorder, and band-pass filter. The amplitude of the reactor transfer function was determined from the R_2 setting as shown in Fig. X-14. Under ideal conditions, measurements have been made to better than $\pm 0.5\%$ in amplitude and $\pm 0.5°$ in phase; under a unity signal-to-noise ratio, the measurements were accurate to $\pm 5\%$ in amplitude and $\pm 2°$ in phase.

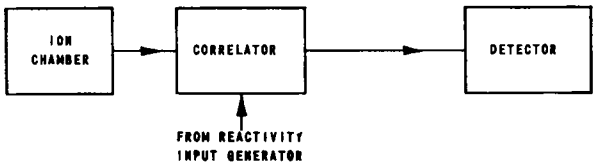

Fig. X-9

Block Diagram of Wave Analyzer
111-9092

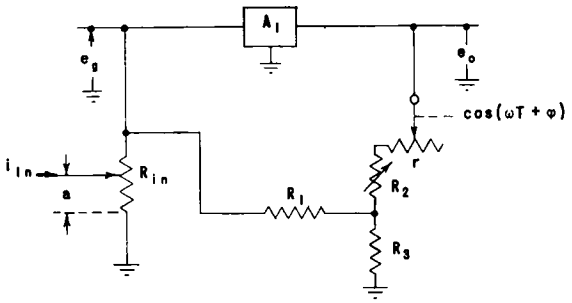

Fig. X-10

Schematic Diagram of Correlator
111-9093

Transfer functions were measured at different powers and pressures with and without automatic steam by-pass control. The data are presented in Table X-3 and Figs. X-15, 16, and 17.

The experimental P functions were determined with an accuracy of about ± 5 per cent in amplitude and $\pm 2°$ in phase (which was insufficient), so a means was developed for smoothing the data. The function GH was determined from the function 1 + GH by plotting 1 + GH on the log polar plane. With this plot, it was possible to draw a smooth curve through the experimental points to provide data smoothing. Variation in the normalizing

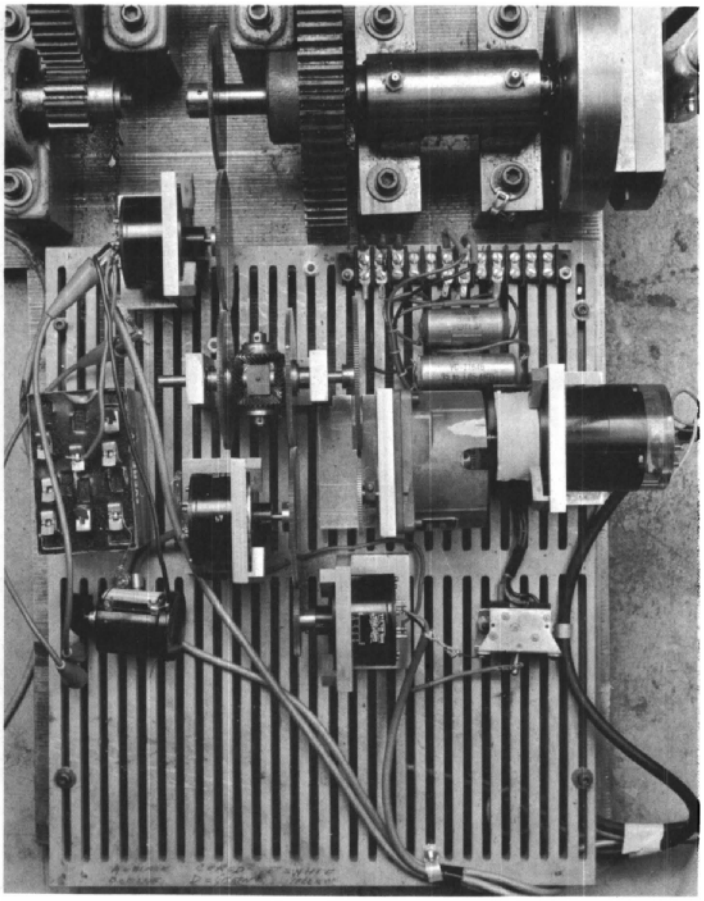

Fig. X-11

Wave Analyzer Components
111-5710

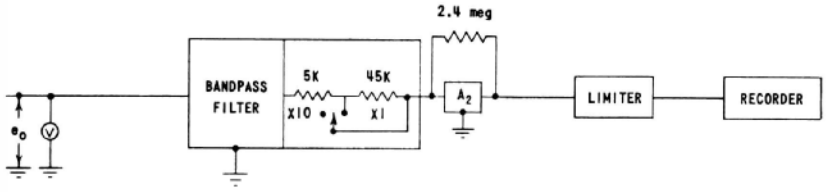

Fig. X-12

Schematic Diagram of Detector

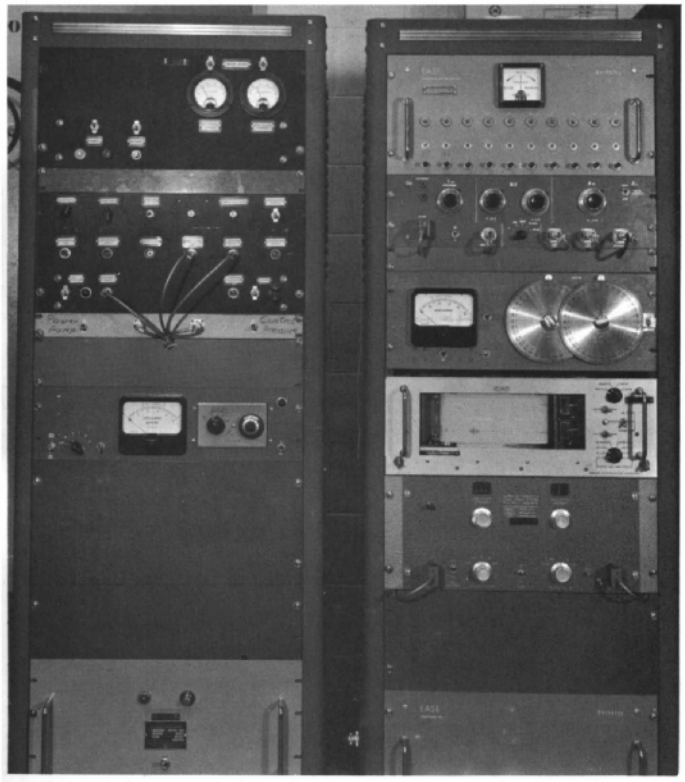

Fig. X-13

Analyzer Equipment
111-5701

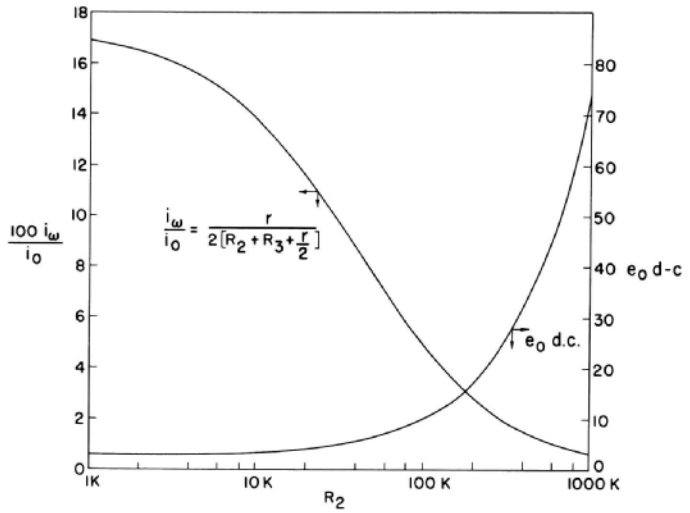

Fig. X-14

Correlator Calibration
111-9094

TABLE X-3
POWER FUNCTION MEASUREMENTS

TEST PARAMETERS (EQUILIBRIUM XENON EXCEPT TEST NO. 15)	TEST NUMBER													
	1	2	3	4	5	6	7	8	9	10	11	13	14	15
POWER, Mw	ZERO (6 kw)	5.4	9.7	20	20	5.7	5.2	5.2	5.1	20	20	20	33	50
PRESSURE, psig	150	550	550	550	550	550	310	300	130	300	550	310	550	600
BORON	NO	NO	NO	NO	YES	YES	YES	NO	NO	NO	NO	NO	NO	NO
CENTER ROD, in.	13.6	13.6	13.8	23.7	23.7	23.7	23.9	13.8	13.8	23.9	26.0	23.9	41.0	41.0
8-ROD BANK, in.	14.5	24.1	29.0	33.0	41.3	41.3	41.2	22.9	22.3	36.7	33.1	35.1	47.0	47.0
STEAM BYPASS	MANUAL	MANUAL	MANUAL	MANUAL	MANUAL	MANUAL	MANUAL	MANUAL	MANUAL	MANUAL	AUTOMATIC	AUTOMATIC	MANUAL	AUTOMATIC
PEAK REACTIVITY (%) FOR 1-inch PEAK STROKE	0.087	0.071	0.10	0.063	0.068	0.068	0.063	0.067	0.065	0.066	0.063	0.060	——	——

RATIO OF FLUX TO REACTIVITY AMPLITUDES AND RELATIVE PHASE OF FLUX TO REACTIVITY
Ratio is Given in Decibels (Zero Db. = 132) and Phase in Degrees

FREQUENCY, radians/sec	CALC.		EXPTL.		Db	Phase	Db	Phase	Db	Phase	Db	Phase	Db	Phase	Db	Phase	Db	Phase	Db	Phase	Db	Phase	Db	Phase	Db	Phase	Db	Phase	Db	Phase
	Db	Phase	Db	Phase																								
0.016	+15.8	-65	—	—	—	—	—	—	-3.6	0	-1.0	+2	+6.3	0	+6.2	-10	+2.3	-5	+0.2	0	-1.5	-5	-7.5	+9	-6.5	+17	-0.6	+10	—	—
0.032	+11.9	-53	—	—	—	—	—	—	-3.6	-10	-1.8	-12	+5.8	-15	+5.6	-16	+1.6	-12	-0.3	-8	-2.2	-12	-7.5	+11	-5.3	+16	-0.9	-6	—	—
0.063	+9.1	-44	—	—	—	—	—	—	-5.2	-17	-2.7	-13	+3.0	-20	+3.8	-20	+0.2	-15	0	-13	-3.5	-20	-5.0	—	-3.6	+10	-2.0	-18	—	—
0.126	+6.5	-37	+6.9	-41	-0.9	-19	-2.3	-17	-5.2	-14	-3.6	-15	+1.0	-23	+1.1	-22	-1.4	-18	-2.7	-18	-5.2	-22	-4.5	+5	-3.6	-6	-4.7	-20	—	—
0.252	+4.2	-30	—	—	—	—	—	—	—	—	—	—	—	—	—	—	—	—	—	—	—	—	-4.5	-10	-6.1	-16	—	—	—	—
0.314	+3.6	-28	+3.7	-28	-2.6	-15	-6.4	-13	-5.6	-12	-5.9	-12	-1.3	-17	-0.8	-16	-3.9	-13	-5.2	-14	-8.1	-14	-5.5	-6	-6.5	-16	-6.3	-20	—	—
0.63	+2.0	-20	+2.0	-18	-4.2	-4	-6.3	-7	-7.7	-6	-7.8	-5	-2.3	-3	-2.0	-1	-5.1	-1	-6.6	+2	-9.4	-2	-7.6	0	-7.5	-5	-10.7	-15	—	—
1.26	+1.0	-14	+1.1	-15	-5.0	+15	-5.9	+16	-7.4	+10	-7.4	+13	-2.3	+9	-1.3	+10	-6.8	+14	-5.4	+18	-9.4	+12	-8.1	+12	-9.2	+18	-10.7	-10	—	—
1.89	+0.7	-11	+0.5	-9	-2.9	+27	-4.8	+31	—	+24	-7.4	+28	-1.3	+20	-0.6	+16	-4.2	+27	-5.3	+28	-9.3	+23	-8.7	+20	-8.3	+25	—	—	—	—
2.52	+0.5	-9	—	—	—	—	—	—	—	—	—	—	—	—	—	—	—	—	—	—	—	—	—	—	—	—	-9.4	+35	—	—
3.14	+0.4	-8	+0.4	-8	+0.8	+30	-1.4	+43	-5.2	+46	-4.7	+50	+1.7	+16	+2.1	+16	-0.4	+36	-3.1	+46	-8.2	+45	-5.8	+51	-7.0	+47	—	—	—	—
4.4	+0.3	-8	+0.2	-6	+2.5	+16	+1.4	+33	-1.6	+58	-0.1	+57	+2.2	+5	+2.6	+6	-6.1	+29	+0.7	+43	-5.8	+65	-1.8	+55	-3.9	+64	—	—	—	—
5.0	+0.2	-7	—	—	—	—	—	—	—	—	—	—	—	—	—	—	—	—	—	—	—	—	—	—	—	—	-4.7	+75	—	—
6.28	+0.2	-7	0	-6	+2.5	+1	+3.2	+10	+3.7	+46	+3.4	+34	+1.6	-3	+1.9	-4	+2.6	+10	+3.4	+23	+1.0	+73	+2.8	+41	+2.4	+71	+2.1	+75	—	—
7.5	+0.1	-7	—	—	—	—	—	—	—	—	—	—	—	—	—	—	—	—	—	—	—	—	—	—	—	—	+6.4	+65	—	—
8.8	+0.1	-7	—	—	—	—	—	—	—	—	—	—	—	—	—	—	—	—	—	—	—	—	—	—	—	—	+8.1	+15	+6.6	+80
9.4	+0.1	-8	—	—	—	—	—	—	—	—	+3.6	+1	—	—	+0.7	-6	+1.3	-5	+1.4	-4	+6.7	+26	+4.3	+2	+6.6	—	+6.3	+8	+8.2	+90
10.7	+0.1	-8	—	—	—	—	—	—	—	—	—	—	—	—	—	—	—	—	—	—	—	—	—	—	—	—	—	—	+13.0	+10
11.0	+0.1	-8	—	—	—	—	—	—	—	—	—	—	—	—	—	—	—	—	—	—	—	—	—	—	—	—	+5.0	-7	—	—
11.6	0	-8	—	—	—	—	—	—	—	—	—	—	—	—	—	—	—	—	—	—	—	—	—	—	—	—	—	—	+12.3	0
12.6	0	-8	-0.5	-8	+0.6	-10	+0.1	-10	+1.3	-11	+2.0	-5	+0.2	-6	+0.1	-6	-0.8	-7	-0.4	-9	+4.0	-6	+2.0	-12	+3.9	-10	+2.1	-6	+4.8	-10
15.7	0	-10	—	—	—	—	—	—	—	—	—	—	—	—	—	—	—	—	—	—	+2.1	-9	+0.7	-15	—	—	—	—	—	—
18.8	-0.1	-11	—	—	—	—	—	—	—	—	—	—	—	—	—	—	—	—	—	—	+1.2	-9	+0.3	-17	—	—	+1.5	-9	+4.0	-20
25.1	-0.2	-13	-0.5	-13	-0.6	-16	-1.5	-17	-0.2	-19	-0.3	-11	-0.4	-14	-0.5	-14	-2.4	-16	-1.6	-15	+0.3	-12	—	—	—	—	+1.8	-10	-0.3	-15

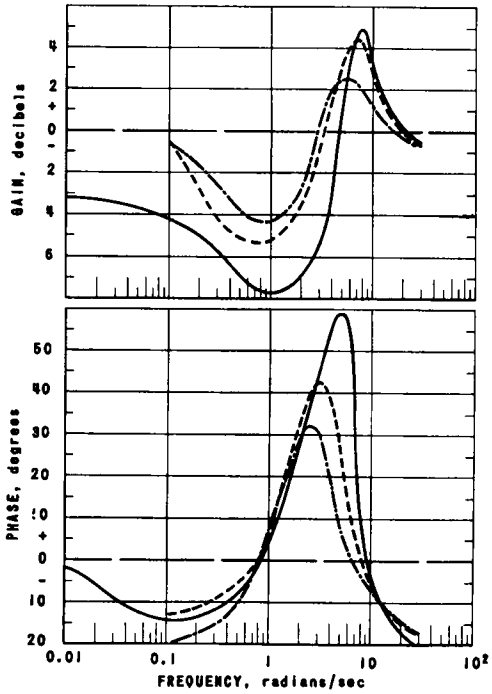

CURVE	—·—	- - - - -	———
POWER, mw	5.4	9.7	19.9
PRESSURE, psi	550	550	550
BORON	NO	NO	NO
CENTER ROD, in.	13.6	13.8	23.7
8-ROD BANK, in.	24.1	29.0	33.0
STEAM BYPASS	MANUAL	MANUAL	MANUAL
PEAK REACTIVITY, % FOR 1-in. PEAK STROKE	0.071	0.089	0.043

Fig. X-15

Effects of Power on Frequency Response
111-9088

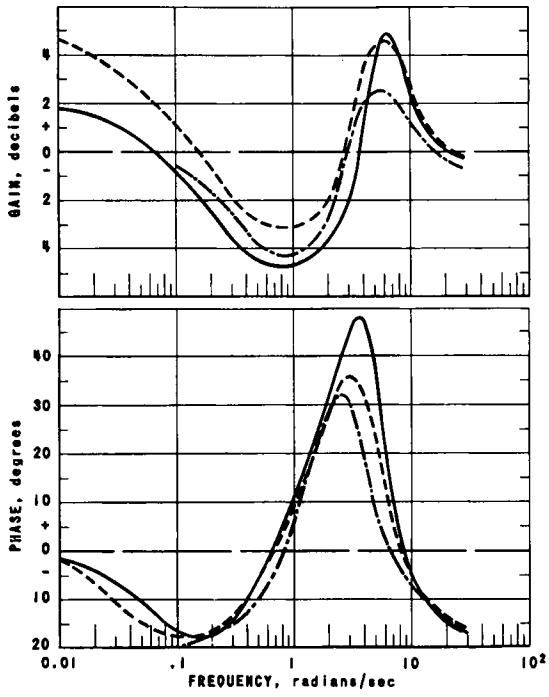

CURVE	—·—	- - - - -	———
POWER, mw	5.4	5.15	5.1
PRESSURE, psi	550	300	131.5
BORON	NO	NO	NO
CENTER ROD, in.	13.6	13.8	13.8
8-ROD BANK, in.	24.1	22.9	22.3
STEAM BYPASS	MANUAL	MANUAL	MANUAL
PEAK REACTIVITY, % FOR 1-in. PEAK STROKE	0.071	0.053	0.055

Fig. X-16

Effects of Pressure on Frequency Response
111-9089

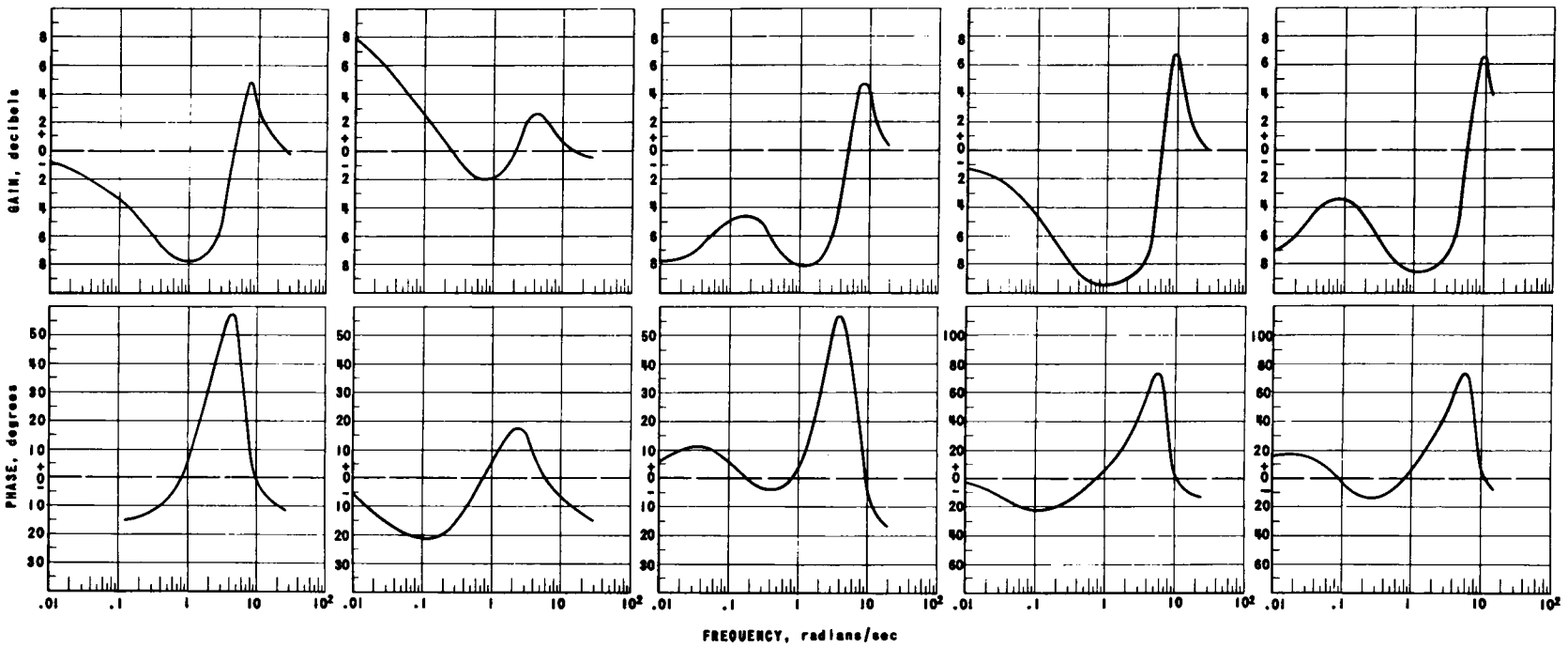

PARAMETERS	TEST NO. 5[a]	TEST NO. 7[a]	TEST NO. 11[b]	TEST NO. 10	TEST NO. 13[b]
POWER, mw	19.4	5.15	20.0	19.9	19.94
PRESSURE, psi	550	310	550	305	310
CENTER ROD, in.	23.7	23.9	24.0	23.9	23.9
8-ROD BANK, in.	41.3	41.2	33.1	34.7	35.1
PEAK REACTIVITY, % FOR 1-in. PEAK STROKE	0.048	0.043	0.043	0.046	0.040

a H_3BO_3 ADDED

b AUTOMATIC STEAM BYPASS

Fig. X-17

Effects of Multiple Parameter Variation on Frequency Response
111-9091

factor was accomplished by sliding the entire curve up or down along the (1 + GH) axis. The control rod worth in the presence of voids is unknown. Therefore, the absolute gain of the reactor power transfer function was assumed to be equal to the zero-power transfer function at ω = 25.1 rad/sec, by means of which it was possible to establish the initial absolute gain used in the 1 + GH plot. Figure X-18 shows a typical curve for 1 + GH. Table X-4 shows the tabulated values of the various experimental feedback transfer functions, H. Figures X-19, and 20 show the plots of these calculated points along with an analytical curve.

If the experimental measurements could be verified by an analytical derivation, then extrapolations could be made to predict reactor behavior at higher powers.

C. Analytical Model

Figure X-21 shows a preliminary model of a natural-circulation boiling water reactor plant in the form of a block diagram. The transfer-function measurements made with EBWR were performed with feedwater flow held constant, manual pressure control, and with the turbine off; therefore, that portion of the figure outside of the dashed section of Fig X-21 can be neglected in determining an analytical expression for the feedback transfer function from reactor power output to reactivity input. The resulting reactor model is shown in Fig. X-22 with appropriate transfer functions for the various elements. The temperature coefficient of reactivity is small compared with the reactivity effects due to power, flashing, and boundary voids. Figure X-23 in which the temperature feedback is neglected, shows the simplified reactor model with the resultant transfer function of the pressure minor loop. Figure X-24 shows the Bode plot of the pressure minor loop. If frequencies below 0.01 radian/sec are not considered, then the pressure minor loop may be approximated as shown in Fig. X-25. The transfer function H(s), from reactivity input to reactor power output, is given by the following equation:

where

$$H(s) = \frac{K_{\delta K}\left[n_0 v - \frac{\sigma}{\eta}(b+d)\right]\left\{1 + s\left[\frac{(n_0 v\gamma - \sigma d)\,T_r}{n_0 v\eta - \sigma(b+d)}\right]\right\}}{\left[1 + (sT_r\gamma/\eta)\right](1 + sT_h)(1 + sT_{pv})(1 + s\tau)} \qquad (55)$$

b	Boundary void coefficient, $(ft^3)(sec)/psi$	v	Power void coefficient, ft^3/Mw
d	Flashing void coefficient, $(ft^3)(sec)/psi$	$K_{\delta K}$	Void reactivity coefficient, dollars/ft^3
T_r	Recirculation time constant, sec	γ	Steam constant, lb/psi
s	Laplace operator	η	Steam constant, lb/psi
T_h	Heat transfer time constant, sec	σ	Steaming rate, lb/(sec)(Mw)
T_{pv}	Heat transfer time constant, sec	τ	Steam transit time constant, sec
n_0	Reactor power, Mw		

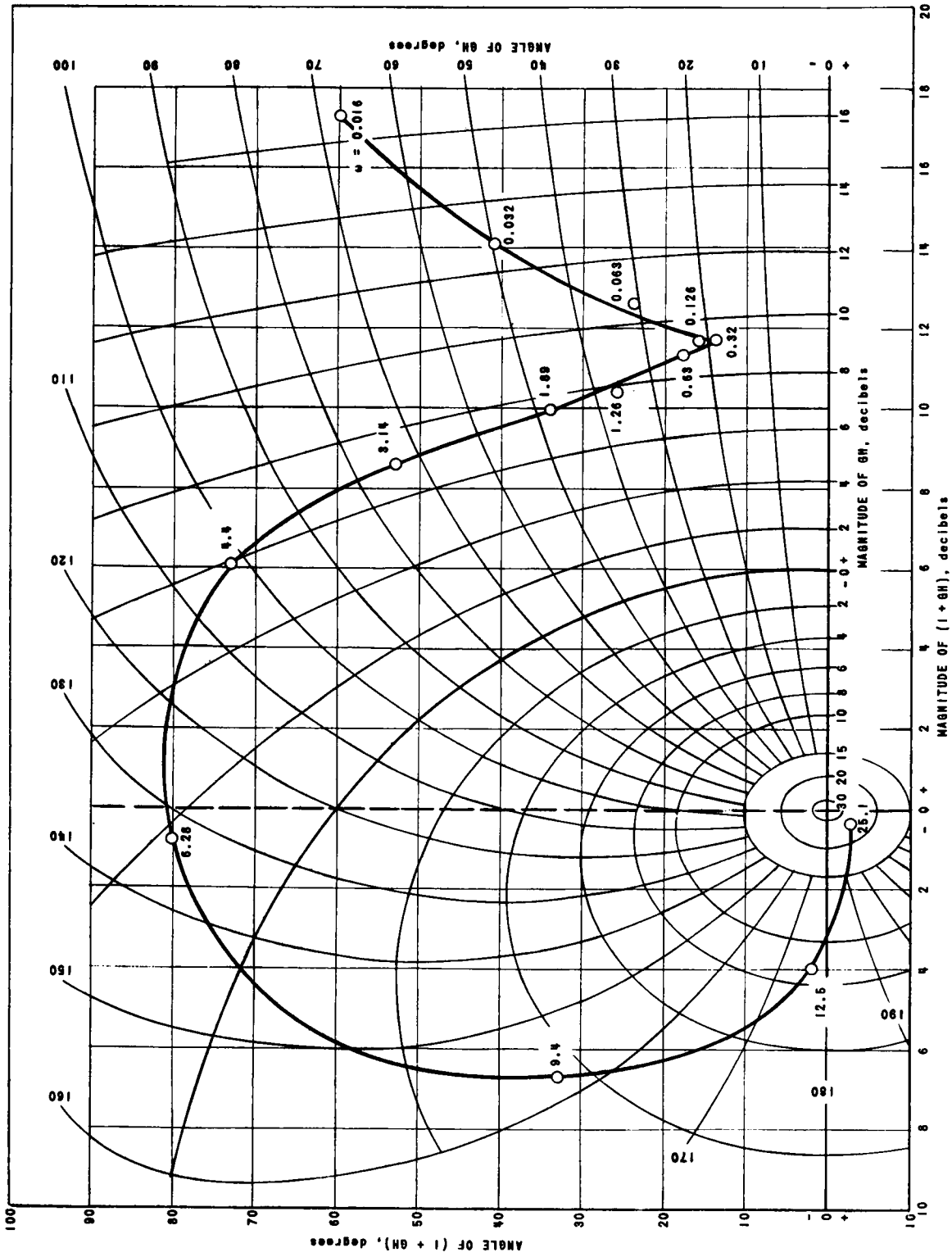

Fig. X-18

Determination of Experimental GH

111-7629

TABLE X-4

EXPERIMENTAL FEED-BACK FUNCTION DATA

TEST PARAMETERS (EQUILIBRIUM XENON EXCEPT TEST NO. 15)	TEST NUMBER										
	2	3	4	5	6	7	8	9	10	14	15
POWER, Mw	5.4	9.7	20	20	5.7	5.2	5.2	5.1	20	33	50
PRESSURE, psig	550	550	550	550	550	310	300	130	300	550	600
BORON	NO	NO	NO	YES	YES	YES	NO	NO	NO	NO	NO

RATIO OF REACTIVITY TO FLUX AMPLITUDES AND RELATIVE PHASE OF REACTIVITY TO FLUX

Ratio is Given in Decibels (Zero Db. = 0.00755) And Phase in Degrees

FREQUENCY, radians/sec.	Db	Phase	Db	Phase	Db	Phase	Db	Phase	Db	Phase	Db	Phase	Db	Phase	Db	Phase	Db	Phase	Db	Phase	Db	Phase
0.016	—	—	—	—	+2.4	-6	+0.5	-10	-7.6	-21	-7.6	-8	-3.4	-7	-0.8	-9	+1.0	-2	+0.1	-19	—	—
0.032	—	—	—	—	+2.0	+3	+0.4	+3	-7.8	-8	-7.5	-5	-3.3	-2	-1.1	-4	+1.0	+4	-0.4	-5	—	—
0.063	—	—	—	—	+1.9	+7	+0.7	+3	-7.6	0	-9.3	0	-3.2	+1	-0.8	-1	+1.6	+9	-0.4	+8.6	—	—
0.126	-3.4	+6	-1.1	+6	+2.7	+4	+0.9	+5	-7.0	+7	-7.0	+5	-2.5	+5	-0.6	+8	+3.7	+16	+0.7	+14	—	—
0.314	-2.8	+3	+1.9	+5	+3.1	+4	+2.6	+4	-5.5	+3	-6.6	-1	-0.5	+3	+1.6	+6	+6.5	+8	+4.4	+17	—	—
0.63	-1.0	-11	+2.3	-1	+4.6	0	+4.6	-2	-4.5	-21	-5.5	-17	+0.7	-13	+3.2	-15	+7.6	-1	+7.9	+15	—	—
1.26	-1.4	-42	+2.2	-36	+4.8	-23	+4.1	-28	-4.4	-64	-5.9	-55	+0.4	-38	+1.6	-41	+7.5	-21	+8.1	+0.4	—	—
1.89	-1.2	-67	+1.7	-61	+4.6	-42	+4.8	-48	-4.4	-72	-6.2	-75	+0.5	-60	+2.0	-55	+7.6	-36	+7.5	-23	—	—
3.14	-4.0	-105	-0.5	-94	+4.2	-75	+3.4	-84	-7.7	-114	-7.8	-116	-2.4	-99	+1.3	-87	+7.2	-65	+7.2	-67	—	—
4.4	-7.5	-126	-3.8	-113			+0.9	-114	-11.0	-134	-10.2	-138	-4.8	-116	-1.8	-110	+6.2	-94	+6.3	-97	—	—
6.28	-11.3	-151	-8.6	-139	-1.4	-130	-3.7	-129	-15.4	-153	-14.6	-160	-9.1	-135	-5.9	-131	+2.1	-127	+3.0	-136	—	—
8.8	—	—	—	—	—	—	—	—	—	—	—	—	—	—	—	—	—	—	—	—	-0.3	-147
9.4	—	—	—	—	-7.7	-160	-9.0	-155	—	—	—	—	-16.9	-160	-16.9	-149	-4.1	-158	-5.7	-160	0	-155
10.7	—	—	—	—	—	—	—	—	—	—	—	—	—	—	—	—	—	—	—	—	-2.2	-167
11.6	—	—	—	—	—	—	—	—	—	—	—	—	—	—	—	—	—	—	—	—	-2.4	-170
12.5	-23.4	-185	—	—	-16.9	-183	-12.9	-156	—	—	—	—	—	—	—	—	-8.1	-169	-9.5	-165	-7.4	-175
15.7	—	—	—	—	—	—	—	—	—	—	—	—	—	—	—	—	-12.2	-177	—	—	—	—
18.8	—	—	—	—	—	—	—	—	—	—	—	—	—	—	—	—	-16.2	-185	—	—	-7.9	-185
25.1	—	—	—	—	-25.1	-224	—	—	-31.8	-205	—	—	—	—	—	—	-23.1	-203	—	—	-25.9	-267

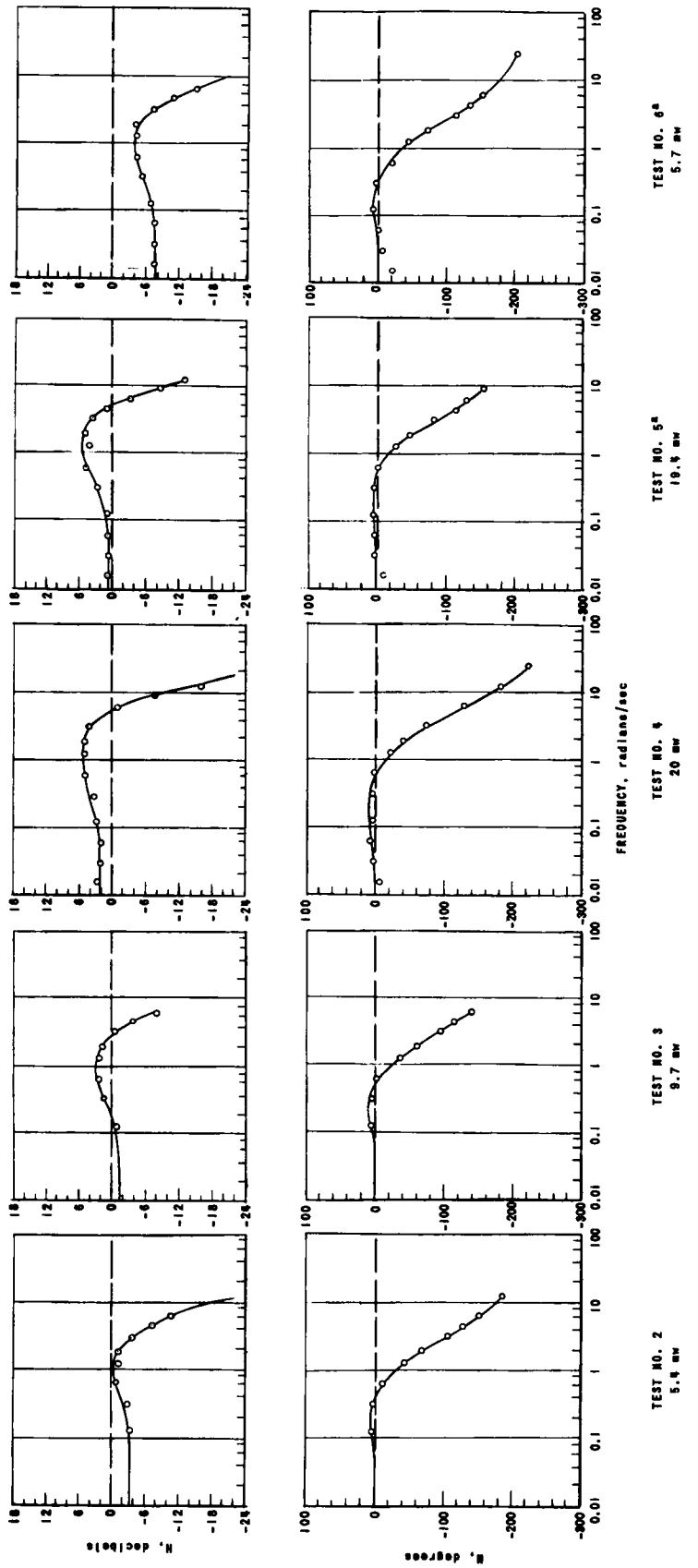

Fig. X-19

Power Effects on Feedback Function at 550 psi
111-7630

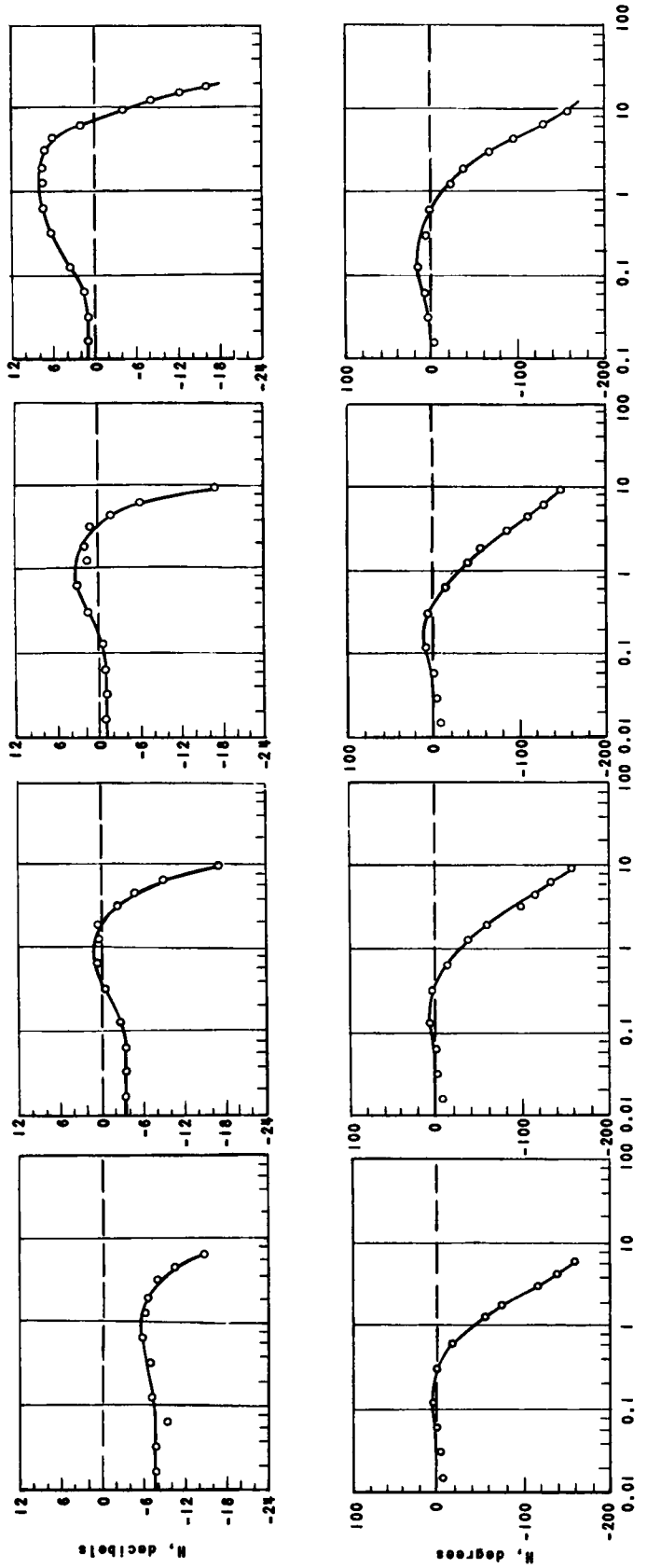

Fig. X-20
Pressure Effects on Feedback Function
111-7631

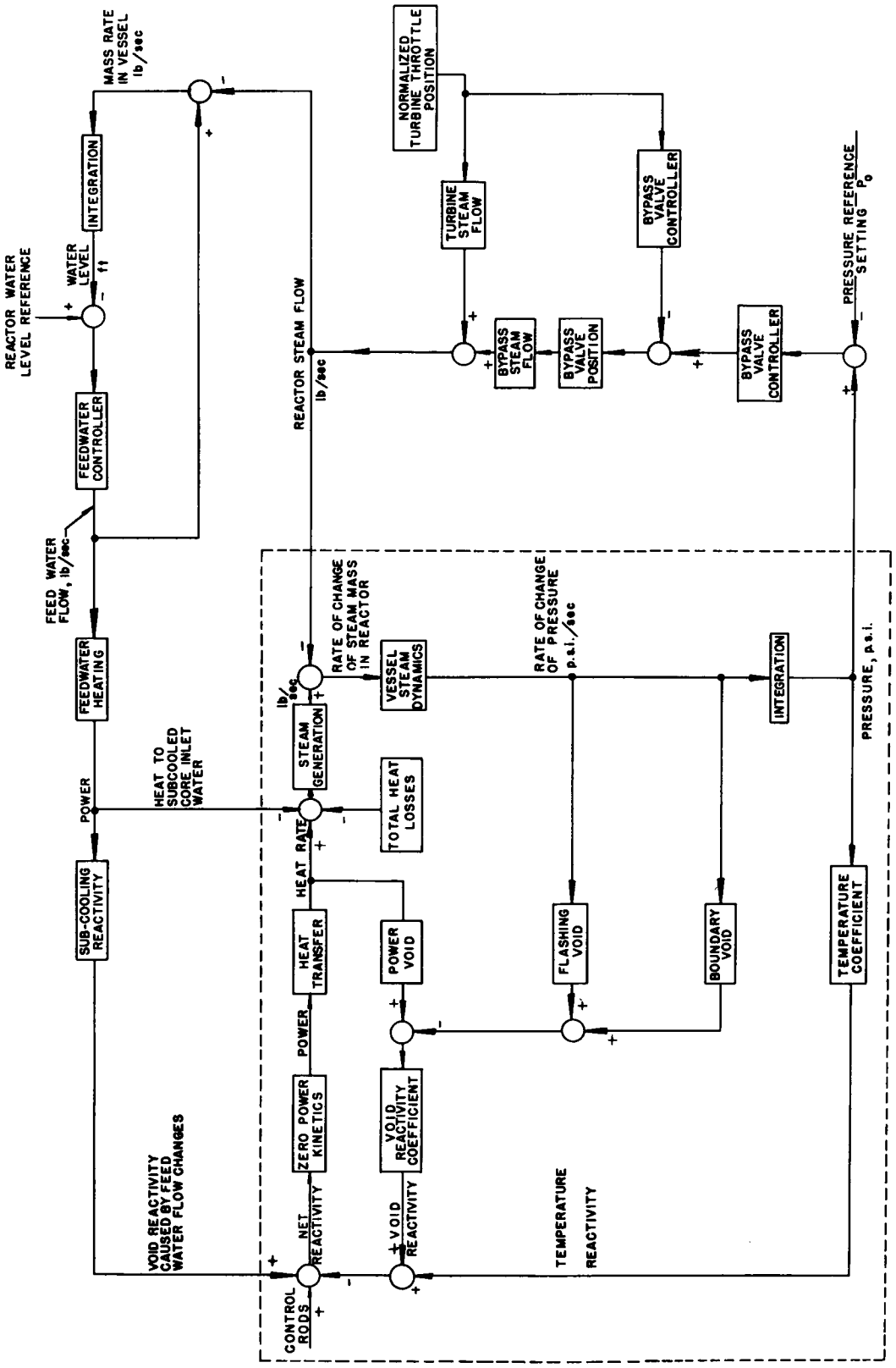

Fig. X-21

Plant Block Diagram of EBWR

111-7632

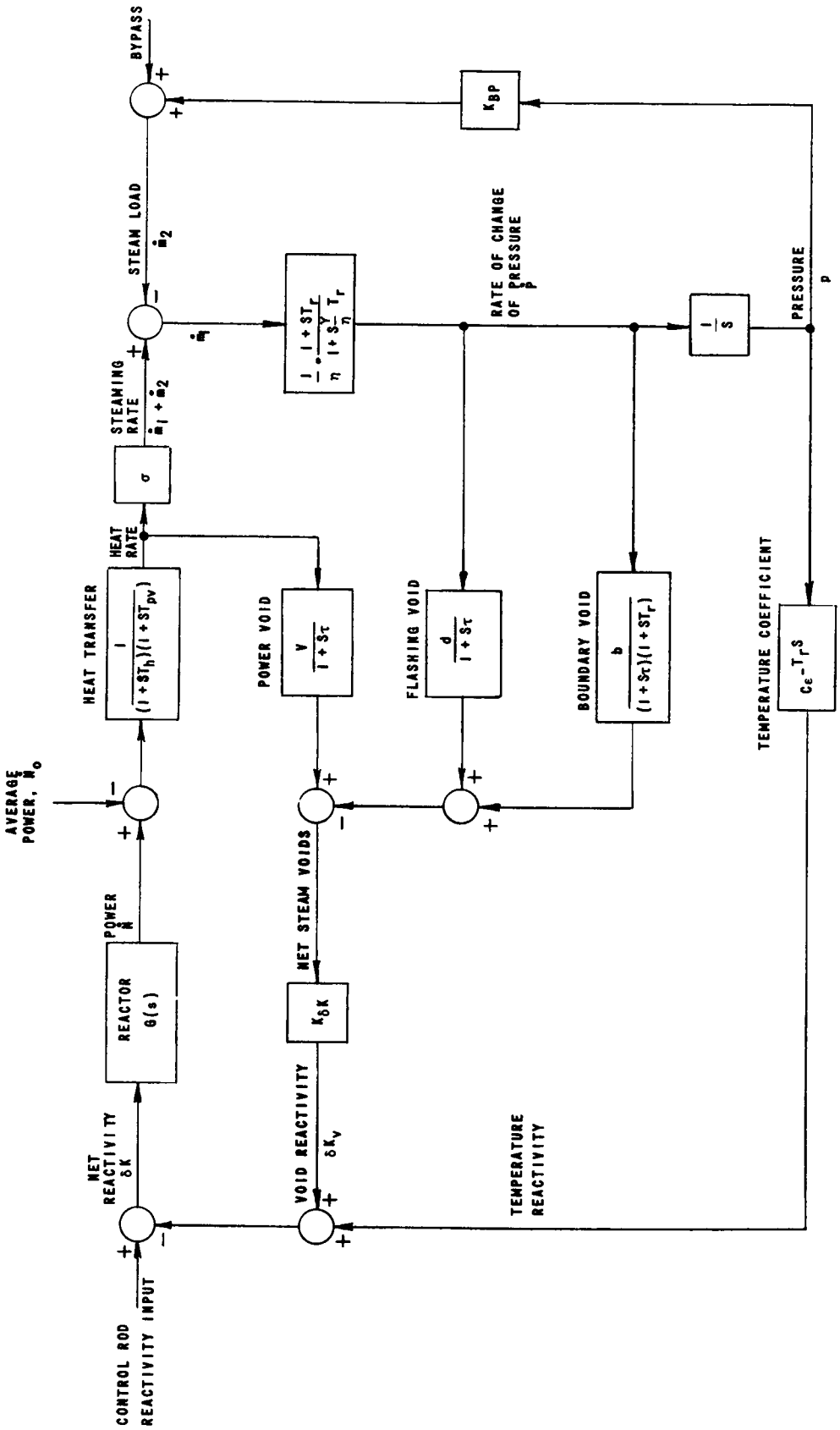

Fig. X-22
Linearized Incremental-signal Reactor Model
111-7633

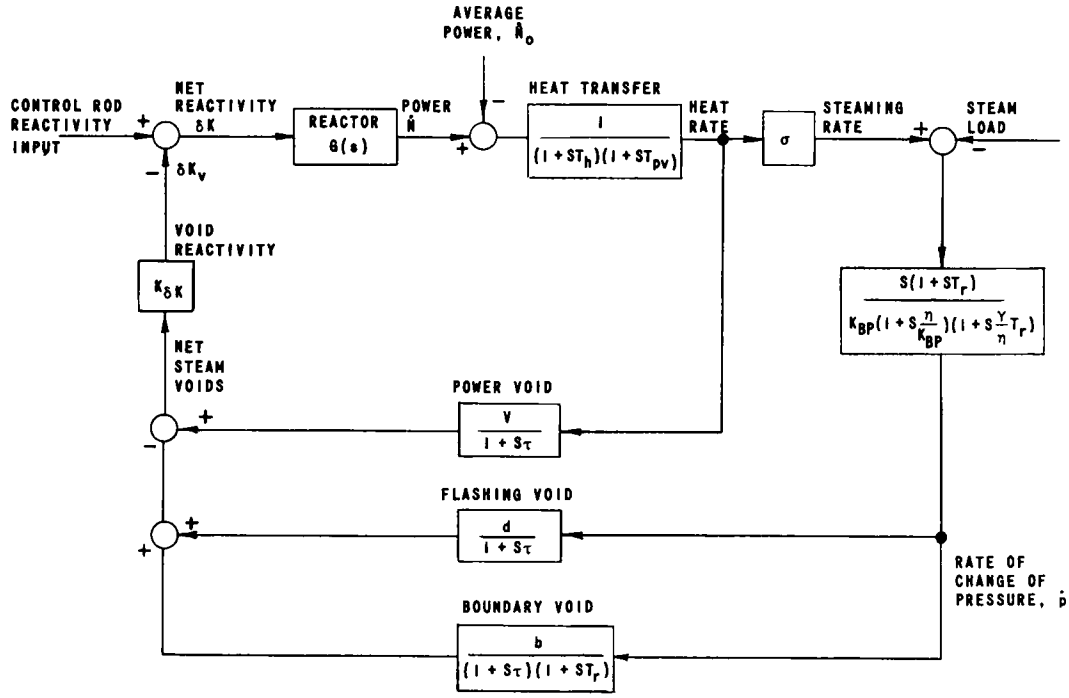

Fig. X-23

Reactor Model Without Temperature Feedback
111-7652

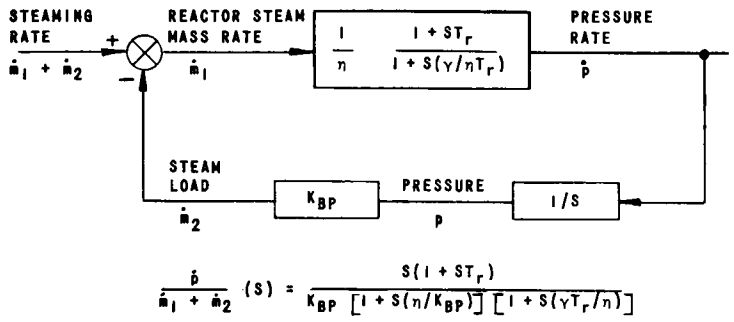

$$\frac{\dot{p}}{\dot{m}_1 + \dot{m}_2}(S) = \frac{S(1+ST_r)}{K_{BP}\left[1+S(\eta/K_{BP})\right]\left[1+S(\gamma T_r/\eta)\right]}$$

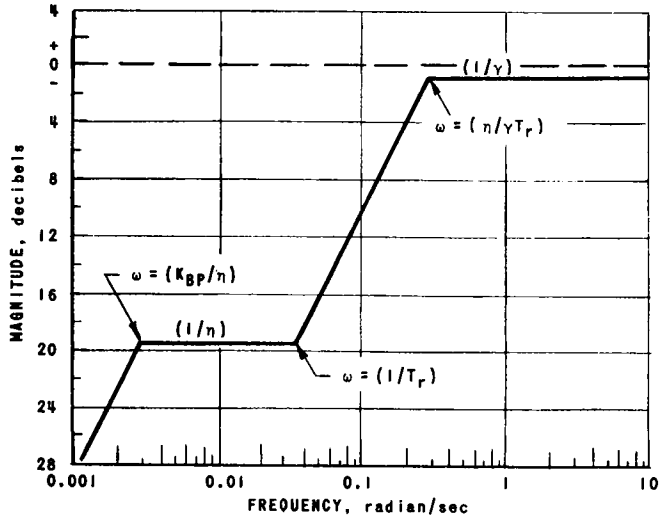

Fig. X-24

Pressure Rate Analysis
111-7634

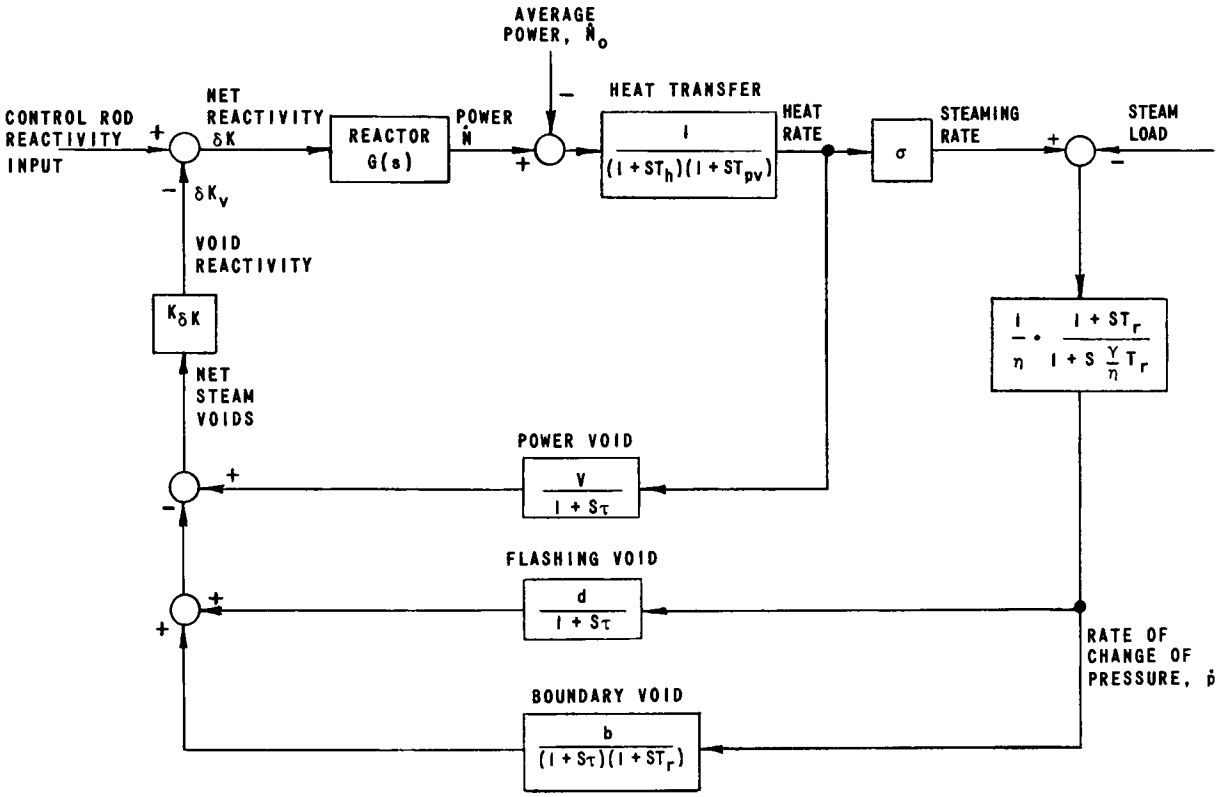

Fig. X-25

Simplified Reactor Model
111-7653

Figure X-26 shows the Bode diagram for equation (55). The shape of this diagram is interesting. Below 0.1 rad/sec the feedback gain is less than that due to the power void reactivity feedback, $K_{\delta K}V$, alone. The reduction is caused by the combined effects of void flashing, d, and void boundary, b, which are pressure dependent. Through the mid-frequency range near 1 rad/sec the feedback amplitude is again less than the power void reactivity feedback, $K_{\delta K}V$, and the reduction is determined by void flashing, d. All pressure effects are absent above about 1 rad/sec, and the reduction of the feedback amplitude at higher frequencies is a function of the time constants T_h and T_{pv} of fuel heat transfer and of the time constant τ for steam transit. For frequencies greater than $1/\tau$, the feedback amplitude falls off at 18 db/octave.

The power coefficients and time constants which describe the reactor can be determined by comparing the amplitude and phase of the experimental feedback transfer function (calculated from closed loop measurements) with the amplitude and phase of the analytic feedback transfer function described by equation (55).

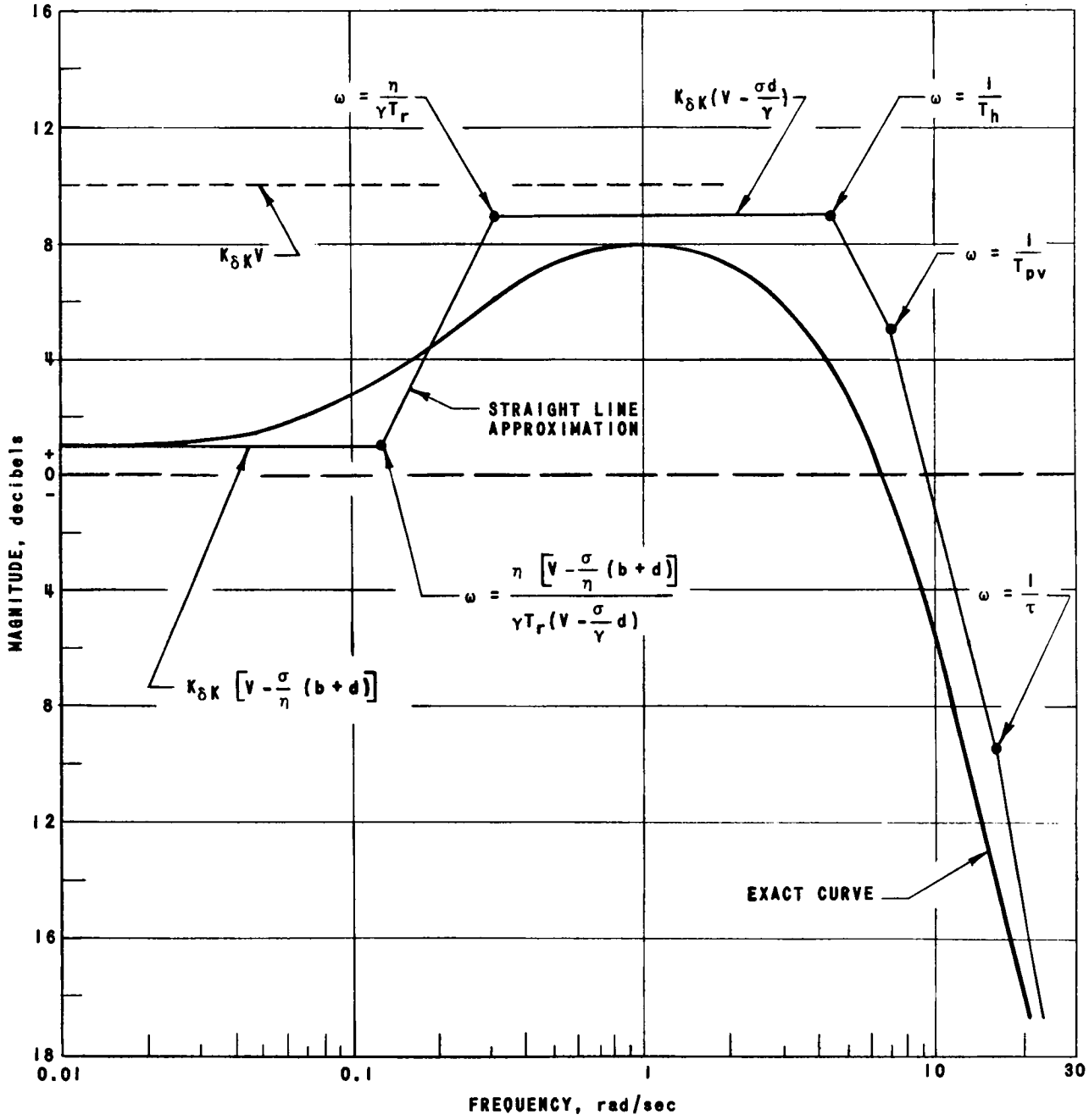

Fig. X-26

Analytic Bode Feedback Diagram
111-7656

Figure X-27 shows the analytic feedback response curves obtained by fitting the experimental data, represented by small circles for 20 Mw and 300 psi. The accuracy of the analytic feedback function is checked by calculating an analytic closed loop function and comparing it

with the experimental values as shown in Fig. X-27. Figures X-28, 29, and 30 show the analytic and feedback functions for 6 other tests. Table X-5 summarizes the calculated power coefficients and time constants. The data from Table X-4 have been plotted in Figs. X-31 and 32 with power as a variable and with pressure constant at 550 psi, and in Figs. X-33 and 34 with power constant and pressure as a variable.

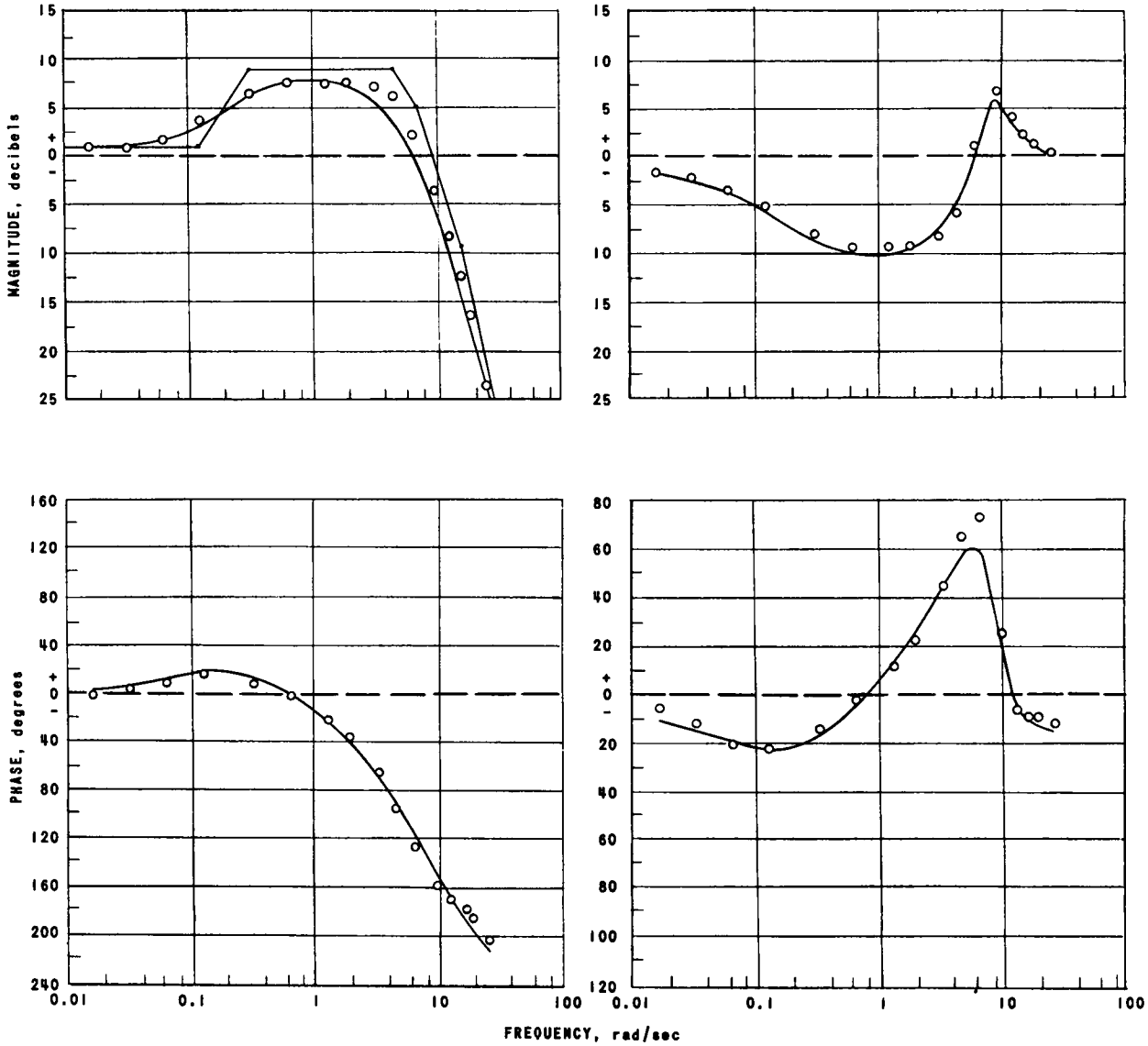

(a) FEEDBACK TRANSFER FUNCTION

$$H = \frac{1.135(1 + s/0.19)}{(1 + s/0.31)(1 + s/4.4)(1 + s/7)(1 + s/16)}$$

(b) POWER TRANSFER FUNCTION

Fig. X-27

Transfer Functions for 20 Mw, 300 psig
111-7635

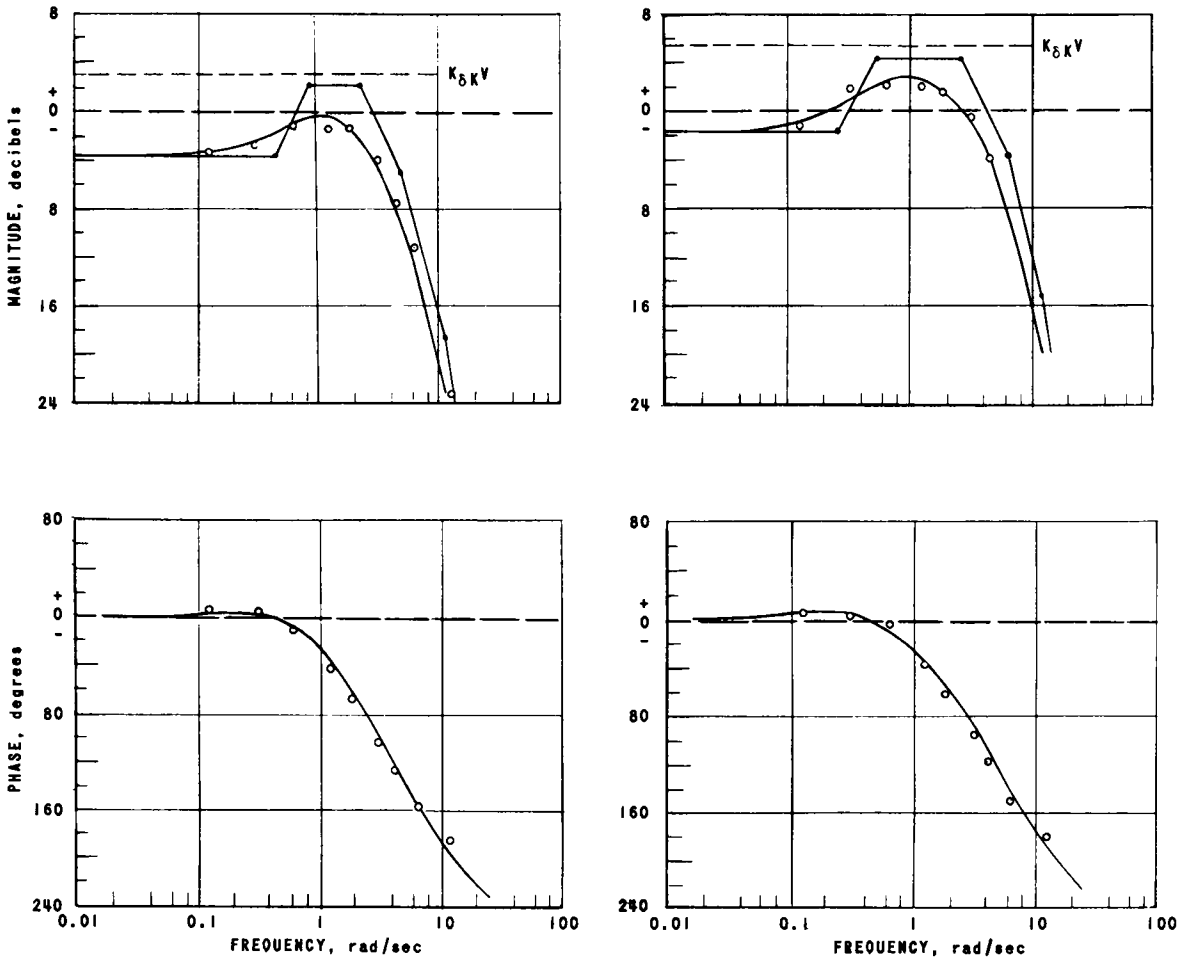

$$H(s) = \frac{0.66(1 + s/0.46)}{(1 + s/0.88)(1 + s/2.3)(1 + s/4.3)(1 + s/12)}$$

$$H(s) = \frac{0.83(1 + s/0.26)}{(1 + s/0.52)(1 + s/2.6)(1 + s/6.4)(1 + s/12)}$$

Fig. X-28

Analytic Feedback Functions for Tests 2 and 3
111-7649

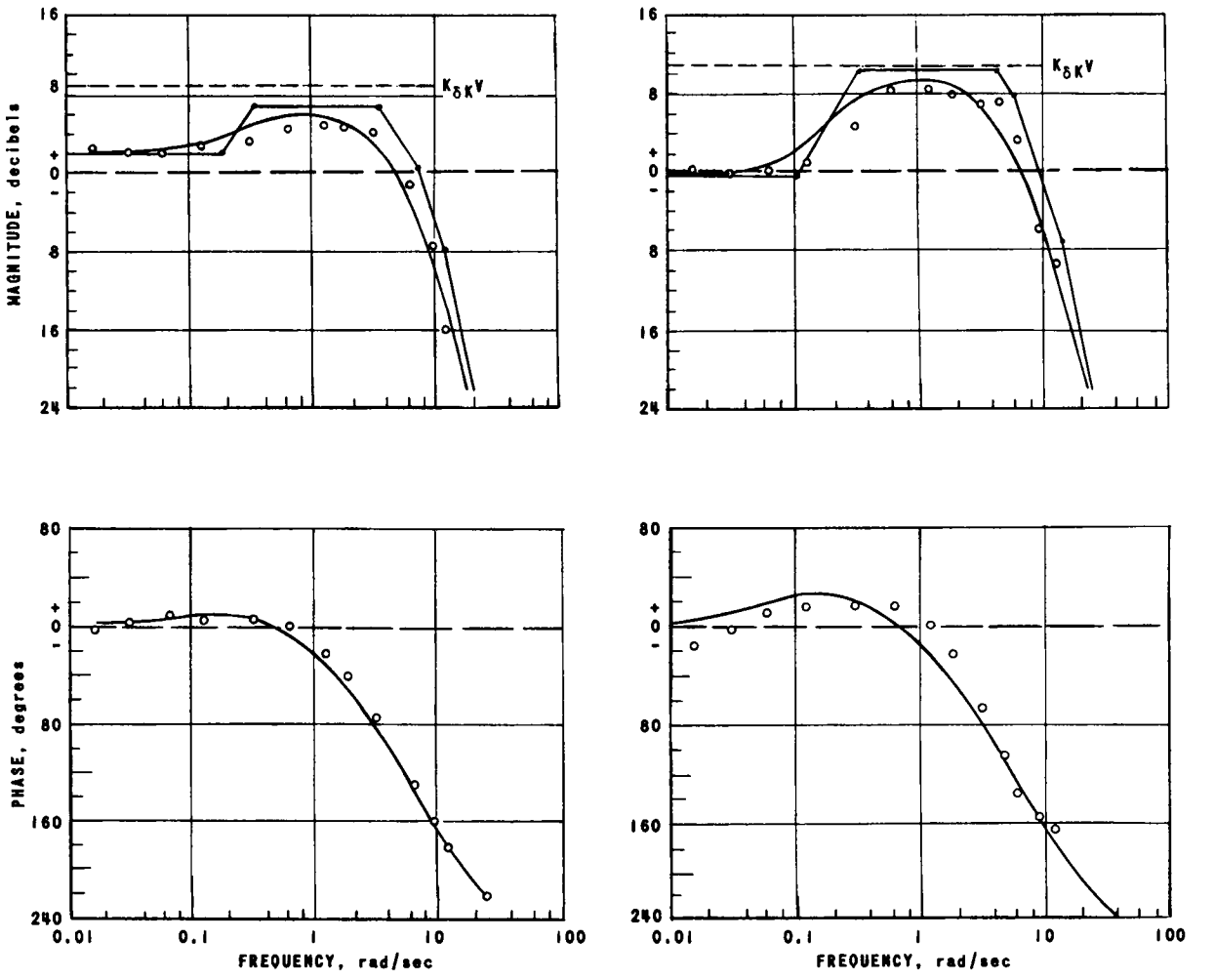

TEST NO. 4: 20 Mw, 550 psig

$$H(s) = \frac{1.26(1 + s/0.195)}{(1 + s/0.34)(1 + s/3.5)(1 + s/7)(1 + s/11.5)}$$

TEST NO. 14: 33 Mw, 550 psig

$$H(s) = \frac{0.94(1 + s/0.104)}{(1 + s/0.346)(1 + s/4.4)(1 + s/5.9)(1 + s/13.3)}$$

Fig. X-29

Analytic Feedback Functions for Tests 4 and 14
111-7636

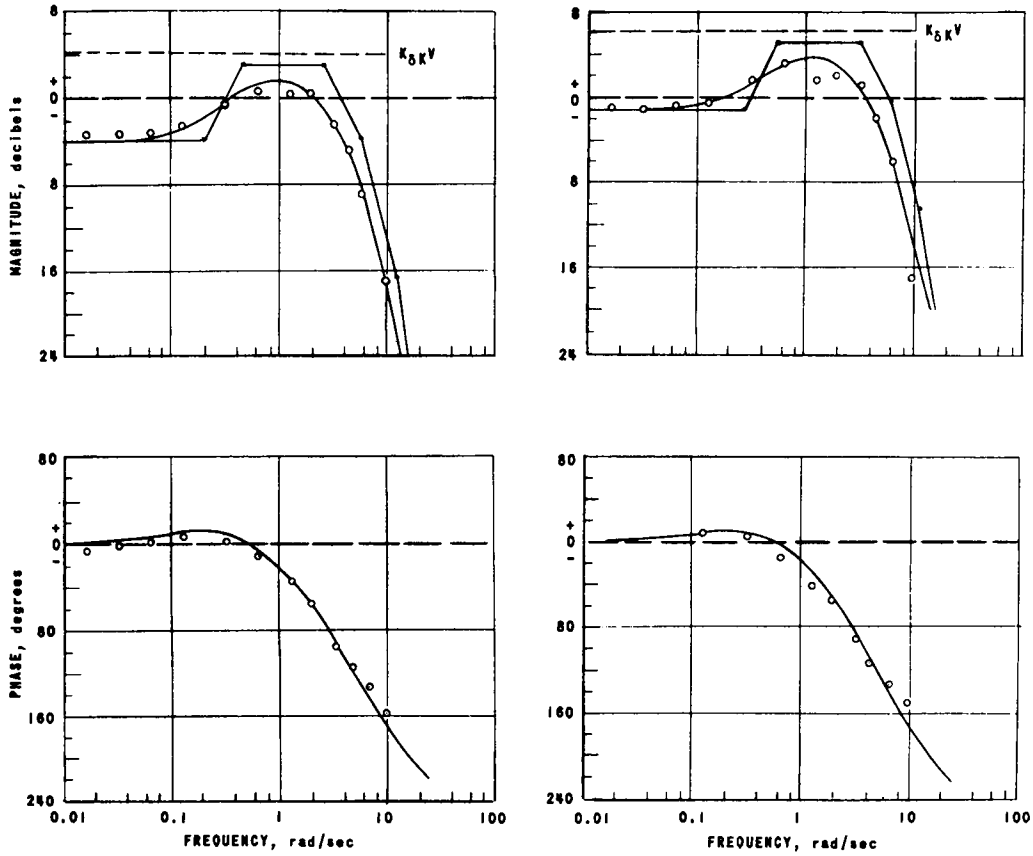

TEST NO. 8: 5.2 Mw, 300 psig

$$H(s) = \frac{0.68(1 + s/0.2)}{(1 + s/0.45)(1 + s/2.6)(1 + s/6)(1 + s/12)}$$

TEST NO. 9: 5.1 Mw, 130 psig

$$H(s) = \frac{0.87(1 + s/0.27)}{(1 + s/0.56)(1 + s/3.2)(1 + s/6)(1 + s/11)}$$

Fig. X-30

Analytic Feedback Functions for Tests 8 and 9
111-7637

Table X-5

COMPARISON OF PREDICTED AND EXPERIMENTAL FEEDBACK PARAMETERS

	40-Mw Extrapolation	33-Mw Test
Power-Mw	40	33
Pressure - psig	550	550
γ - lb/psi	1.05	1.05
η - lb/psi	6.53	6.53
σ - lb/sec	51.2	42
V - ft^3	2.6	2.1
b - ft^3 sec/psi	0.20	0.23
d - ft^3 sec/psi	0.004	0.007
T_h - sec	0.23	0.23
T_{pv} - sec	0.14	0.17
τ - sec	0.062	0.075
T_r - sec	28	18
$K_{\delta K}$ - \$/ft^3	1.4	1.6

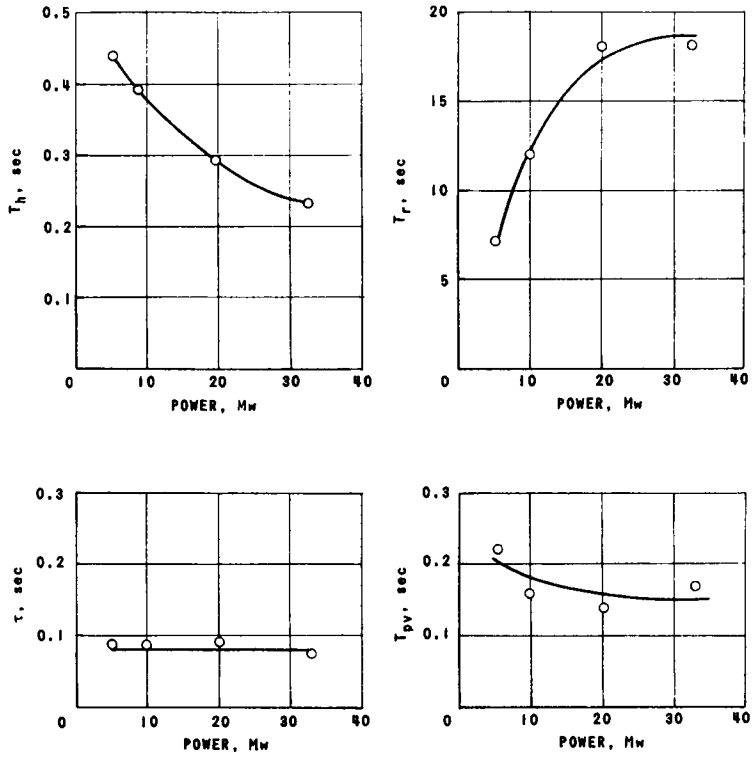

Fig. X-31

Variation of Power Coefficients with Power at 550 psig

111-7671

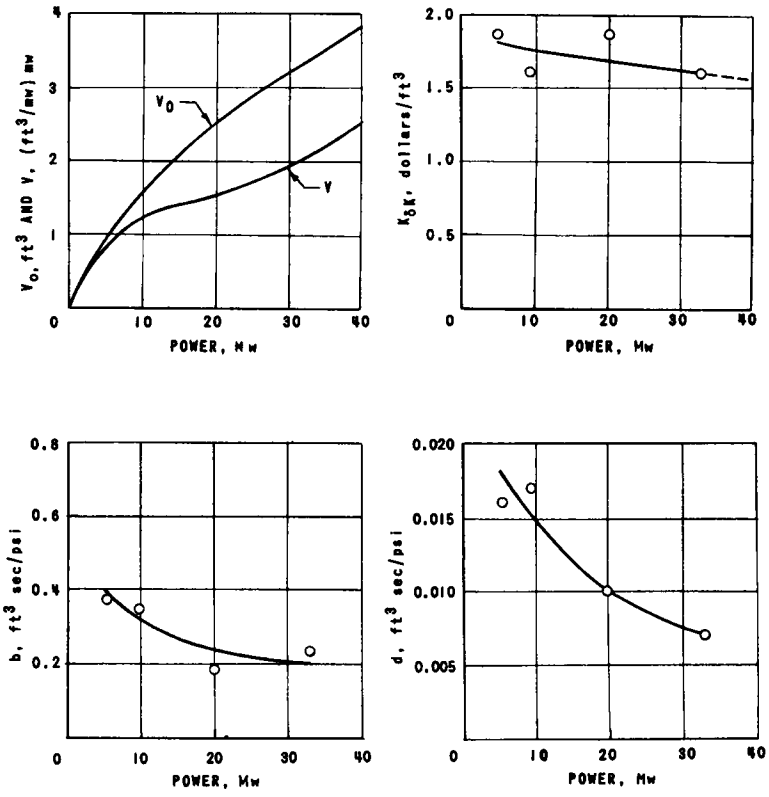

Fig. X-32

Variation of Time Constants with Power at 550 psig

111-7657

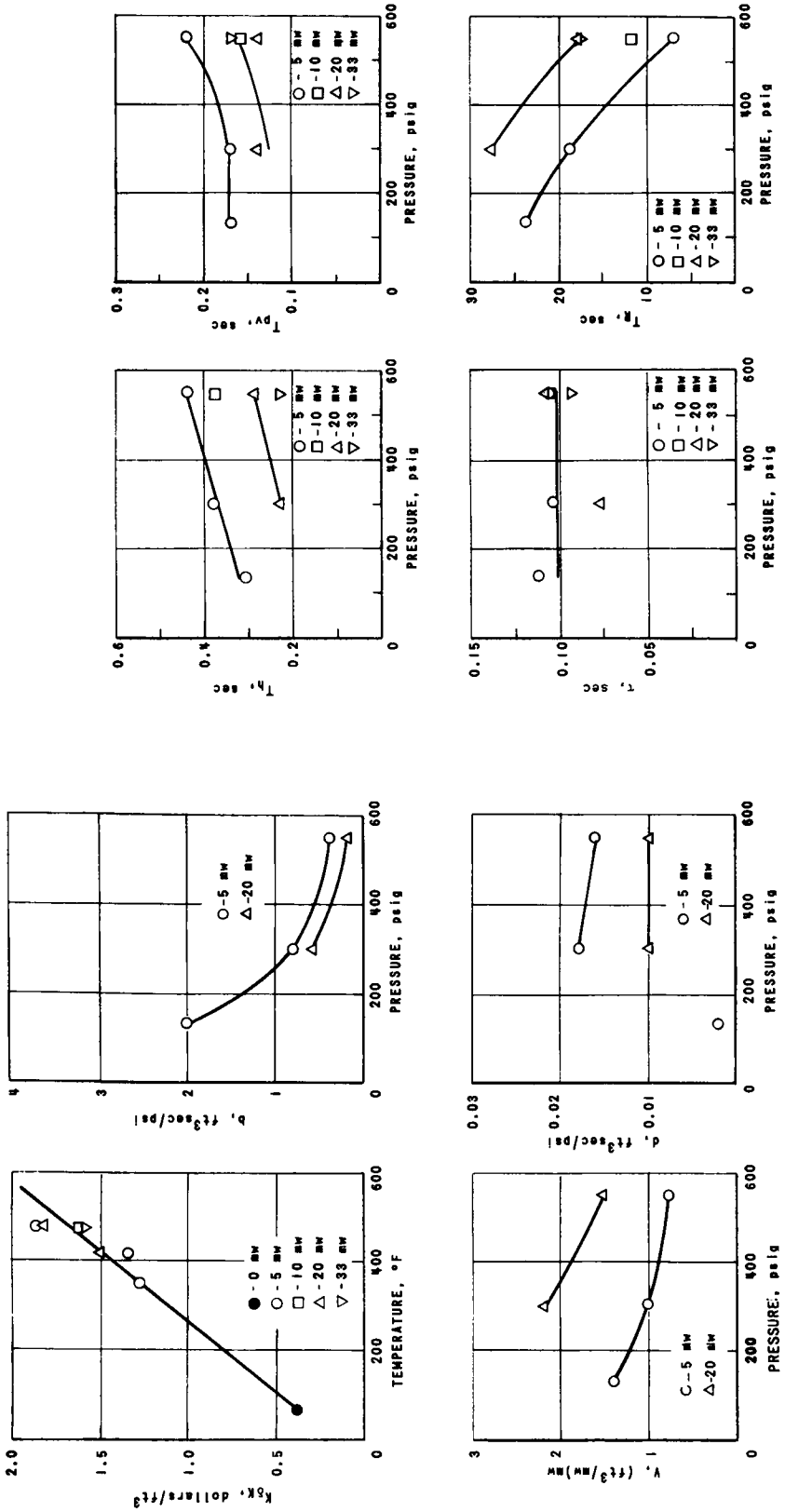

Fig. X-33

Variation of Power Coefficients with Pressure and Temperature
111-7650

Fig. X-34

Variation of Time Constants with Pressure
111-7651

D. Extrapolation to Higher Power

Reactor performance and stability may be predicted for power levels in excess of those for which dynamic measurements exist. A power transfer function may be calculated and stability determined by measuring the feedback function at low power and then extrapolating it to the desired power. The quantity $K_{\delta K}V$ is important to reactor stability because it determines the gain magnitude of the open loop transfer function. The value of $K_{\delta K}V$ may be obtained by measuring the void-reactivity vs power curve at lower powers and extrapolating it to the desired power, as shown in Fig. X-35.

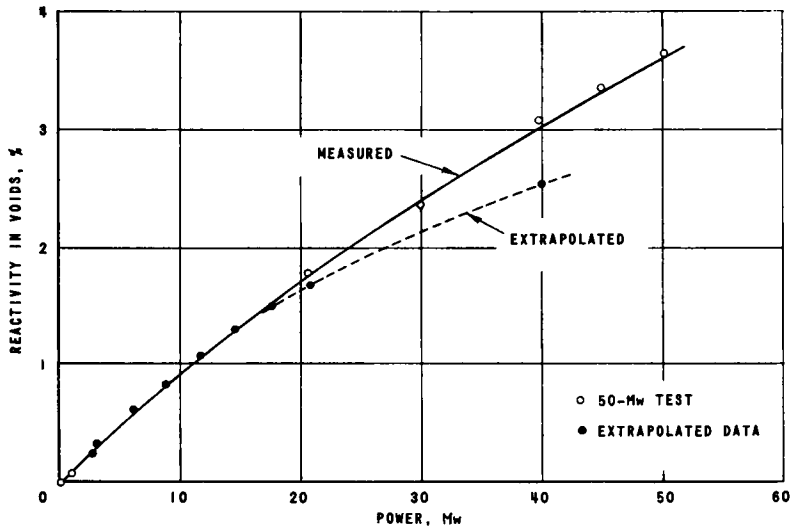

Fig. X-35

Reactivity in Voids as a Function of Power
111-7645

Reactor performance was extrapolated to 40 Mw, and experimental measurements were made at the maximum attainable power with equilibrium xenon for 33 Mw. Table X-6 shows the extrapolated 40-Mw

Table X-6

SUMMARY OF ANALYTIC FEEDBACK PARAMETERS

Parameter	Test Number					
	2	3	4	8	9	10
Mw	5.4	9.7	20	5.15	5.1	20
p - psi	550	550	550	300	130	300
γ - lb/psi	1.0	1.0	1.0	1.1	1.1	1.1
η - lb/psi	6.5	6.5	6.5	9.3	15	9.3
σ - lb/sec	6.9	12	26	6.0	5.5	23
V - $(ft^3/Mw)Mw$	0.77	1.2	1.5	1.0	1.4	2.2
b - ft^3sec/psi	0.38	0.34	0.19	0.80	2.0	0.57
d - ft^3sec/psi	0.016	0.017	0.010	0.018	0.002	0.010
T_h - sec	0.44	0.38	0.29	0.38	0.31	0.23
T_{pv} - sec	0.22	0.16	0.14	0.17	0.17	0.14
τ - sec	0.084	0.084	0.087	0.083	0.09	0.062
T_r - sec	7.1	12	18	19	24	28
$K_{\delta K}$ - \$/ft^3	1.9	1.6	1.8	1.3	1.3	1.5

feedback parameters as compared with the experimentally determined 33-Mw values. Figure X-36 shows the predicted 40-Mw curves and the measured 33-Mw points.

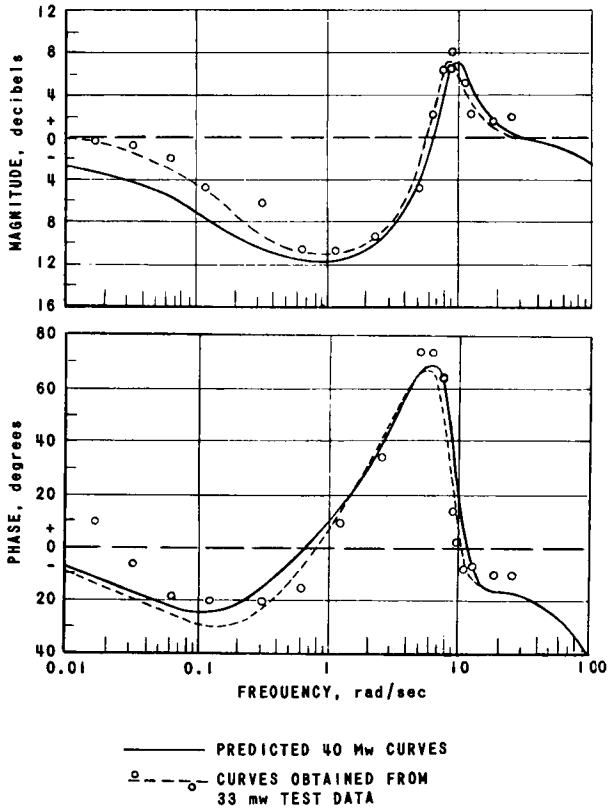

Fig. X-36

Predicted 40-Mw Power Transfer Function
111-7644

E. Investigation of Oscillation Threshold

The reactor would be stable for all values of open loop gain if no time lags were present in the reactivity feedback. In the actual case, there are several time lags associated with the feedback, which result in increased phase shift at higher frequencies. This is shown in Fig. X-37, which is a log polar plane plot of the frequency locus of the open loop transfer function GH for the 20-Mw, 550-psi experiment. The point of interest is the magnitude of the open loop gain when the open loop phase shift is -180°. As $|GH|$ becomes unity, the reactor closed loop gain will approach infinity and the reactor flux will oscillate spontaneously with no sinusoidal input reactivity at a frequency very nearly equal to the frequency at which the closed loop gain is infinite.

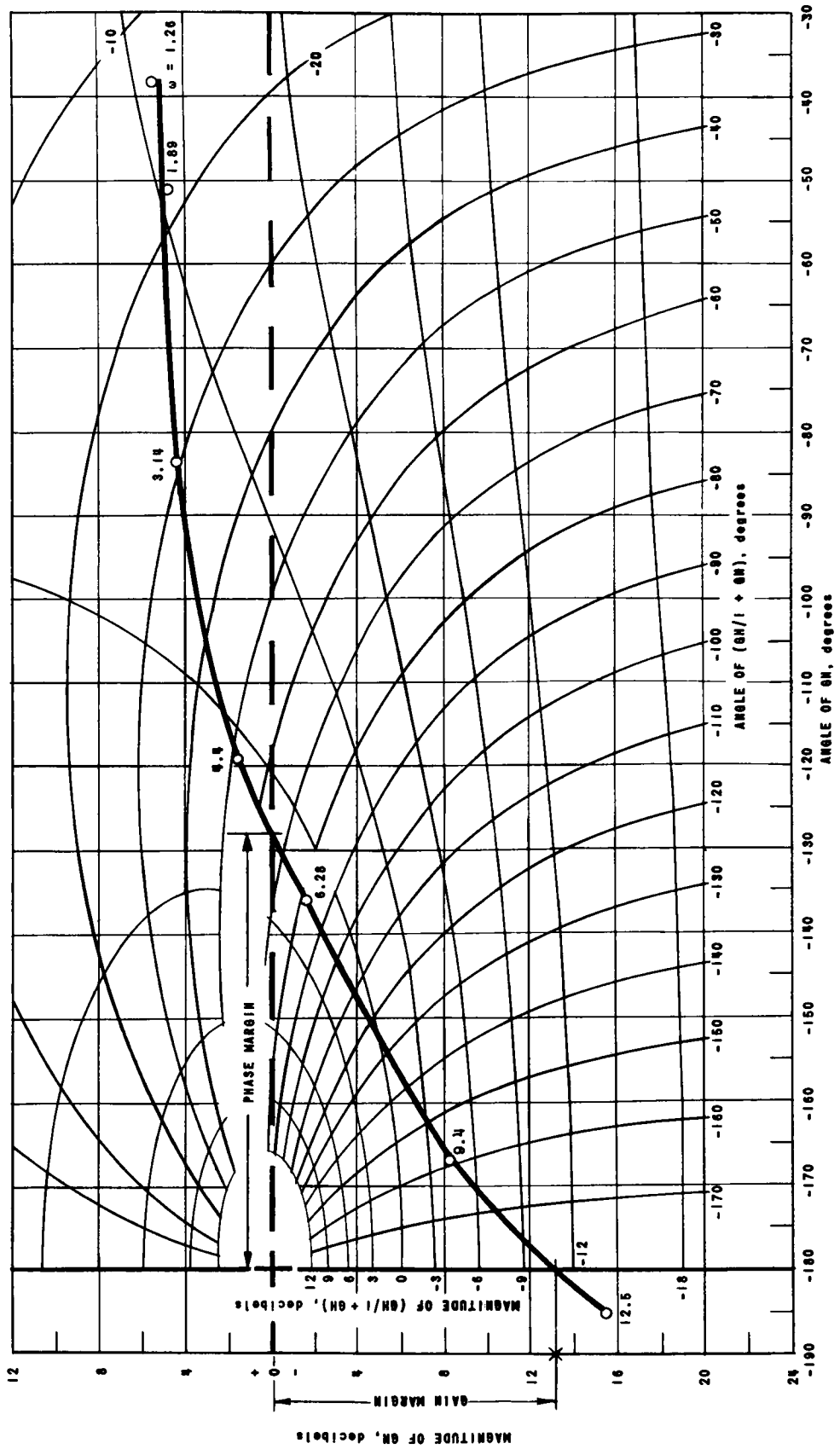

Fig. X-37

Open Loop Frequency Locus for 20 Mw and 550 psig

111-7642

Gain margin is a term used to designate stability quantitatively. It is defined as the increase in gain that will produce unity open loop gain at -180° phase shift. The phase margin is defined as the additional phase lag required to produce a total of -180° phase shift at unity open loop gain. It is convenient to plot the absolute magnitude of GH that exists at -180° rather than its reciprocal, which is the gain margin. This is shown in Fig. X-38, where oscillation will occur when the ordinate is unity or larger, as indicated by the region marked "unstable operation." Extrapolation of gain and phase shows that instability occurs at about 66 Mw.

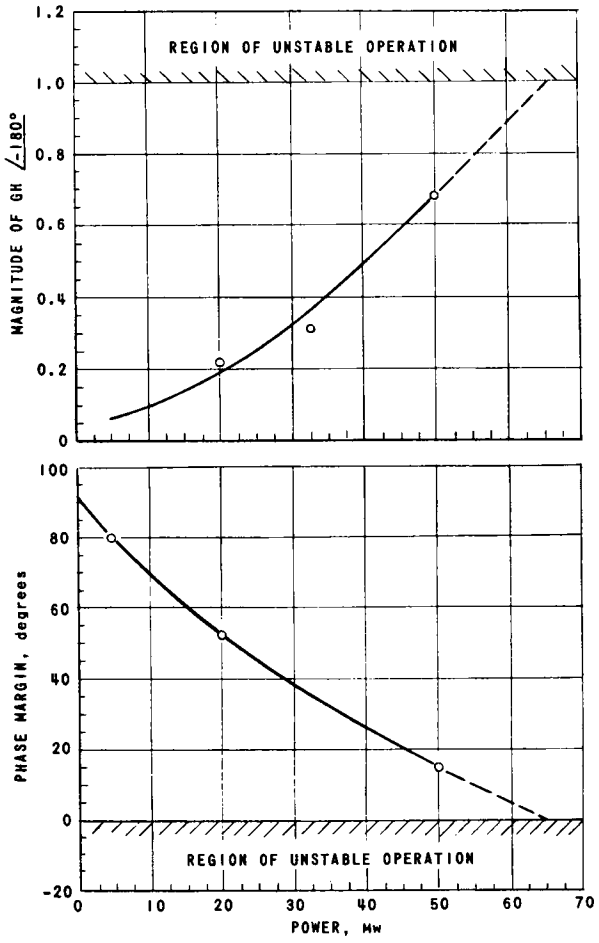

Fig. X-38

Reactor Gain and Phase
Stability Extrapolation
111-7641

A system exhibits resonance peaking in the frequency domain as the gain and phase margins approach unity and zero, respectively, and appears in the time domain as a decaying oscillatory response to a step input. For this reason, a series of step-reactivity flux responses were measured during the probing run to 50 Mw. Figure X-39 shows the flux response to reactivity step inputs at various power levels.

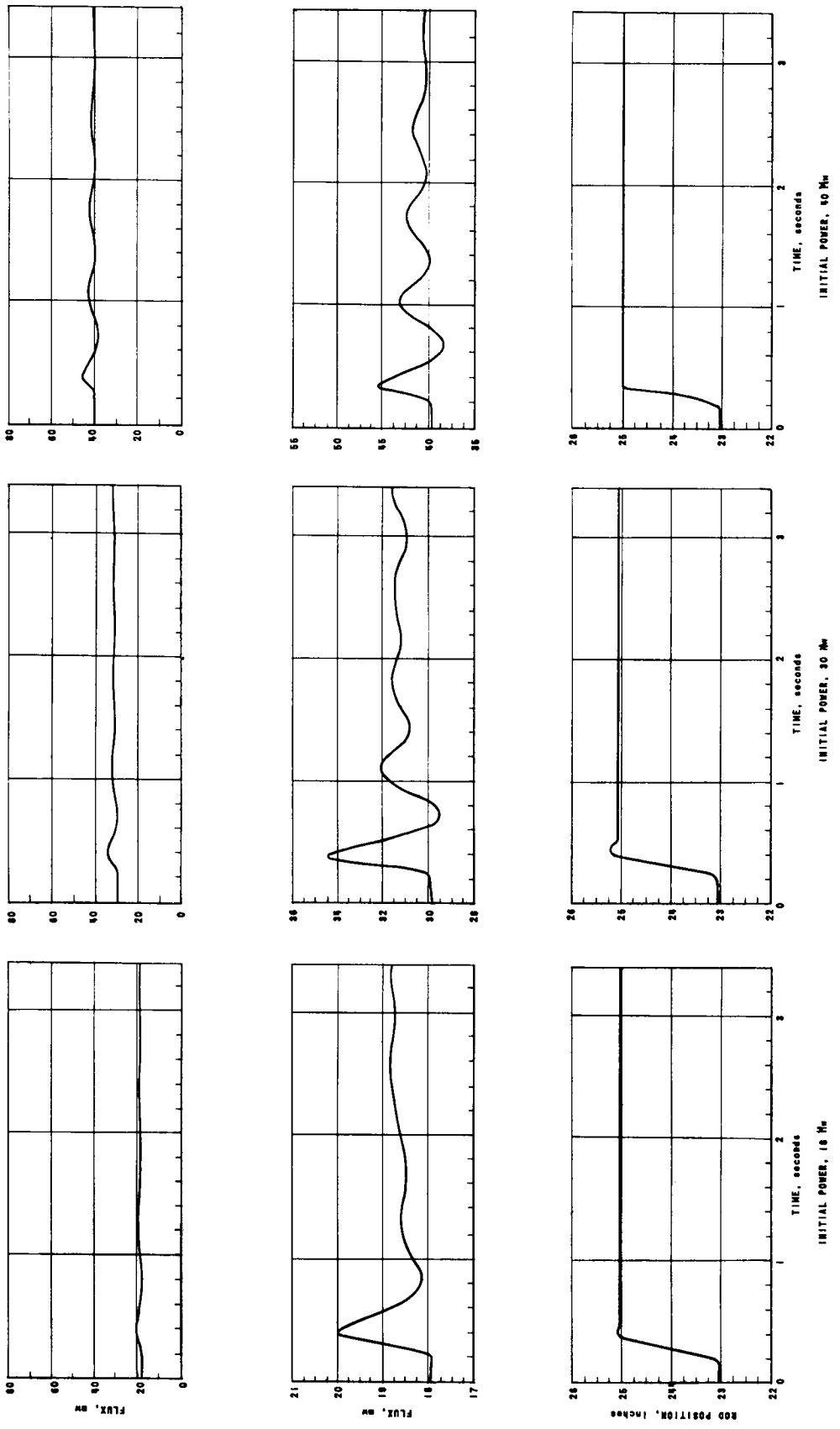

Fig. X-39

Flux Response to a Reactivity Step for Various Power Levels at 600 psig

111-7640

A transfer function was measured for operation at 50 Mw and 600 psi. Because of poor signal-to-noise ratio, only a few questionable points were obtained in the resonance region, as shown in Table X-3. Another high-power experiment was performed subsequently to the 50-Mw test to determine whether the reactor was stable up to the 66-Mw threshold. At 61.7 Mw, the capacity of the feedwater pump was reached. Power was increased in short bursts to an estimated 65 Mw with reactor water level falling slightly. The reactor remained stable and controllable.

F. 100-Mw Operation

The reactor core has been modified for 100-Mw operation. Therefore, a new series of transfer-function measurements will be made at lower powers and extrapolations made to predict reactor behavior at higher powers as part of the experimental approach to 100-Mw operation. Cross-correlation techniques which reject noise by modulation and integration will be used to improve the accuracy of the experimental measurements.

SECTION XI

REACTOR INSTRUMENTATION, CONTROL, AND SAFETY SYSTEMS

A. Hirsch
E. Martinec
J. Matousek

NOTES AND EDITED DATA FROM LECTURES -
July 11 and 12, 1961

SECTION XI

REACTOR INSTRUMENTATION, CONTROL, AND SAFETY SYSTEMS

I. EBWR Instrumentation*

A. Instruments

The parameters directly affecting the reactor such as flux level, control rod position, reactor pressure, and feedwater flow are available at the console. The parameters not directly affecting the reactor, such as plant temperatures, and turbine and generator parameters, are displayed in the control room but are not grouped close to the console (see Fig. XI-1).

Fig. XI-1

EBWR Console
201-1551

The nuclear instrumentation includes two BF_3 counters used during startup. Preamplifiers are located close to the instrument holes containing the BF_3 chambers (see Figs. XI-2 and 3). The output from the amplifier is registered on a scaler at the console. At the lower flux levels, a Keithley micromicroammeter is used in conjunction with a compensated ionization current chamber. As shown on the included Nuclear Instrumentation Range chart in Fig. XI-4, a Leeds and Northrup micromicroammeter, a log amplifier, and a battery-powered galvanometer are used for the higher flux levels. The log amplifier signal is fed to a periodmeter which will indicate and trip on set periods between 30 and 3 sec.

The three identical safety chains shown in Figs. XI-5 and 6 are used to shut down the reactor under abnormal conditions. The current from an uncompensated ionization-current chamber is used to activate a sensitive relay and to trip an electronic trip circuit. The electronic circuits are set to trip at 120 per cent of normal full power and the sensitive relays are set to trip at 125 per cent of normal full power. Tripping any

*A. Hirsch

two of the electronic circuits is required to shut down the reactor. If an electronic circuit fails, it can be repaired with the reactor in operation while the other two protect the reactor. Tripping of any one of the sensitive relays will shut down the reactor.

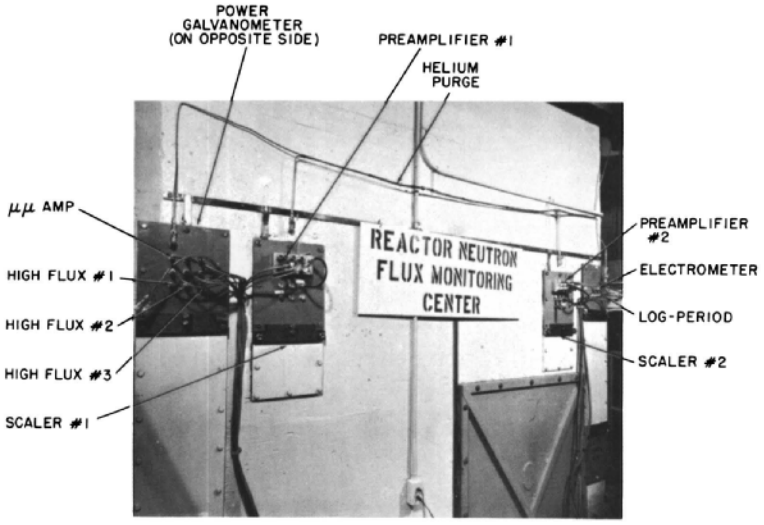

Fig. XI-2

EBWR Neutron Instrumentation Chamber Locations
111-5223

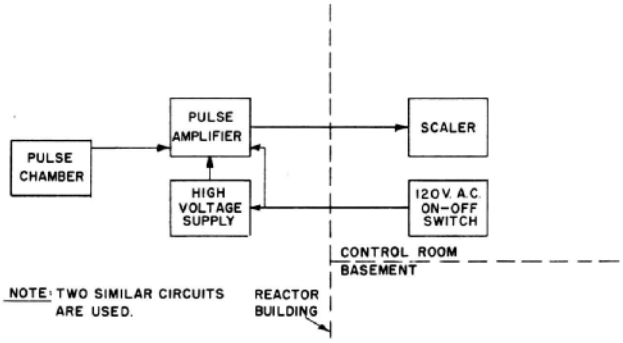

Fig. XI-3

BF_3 Counter Chain
RE-6-18997-A

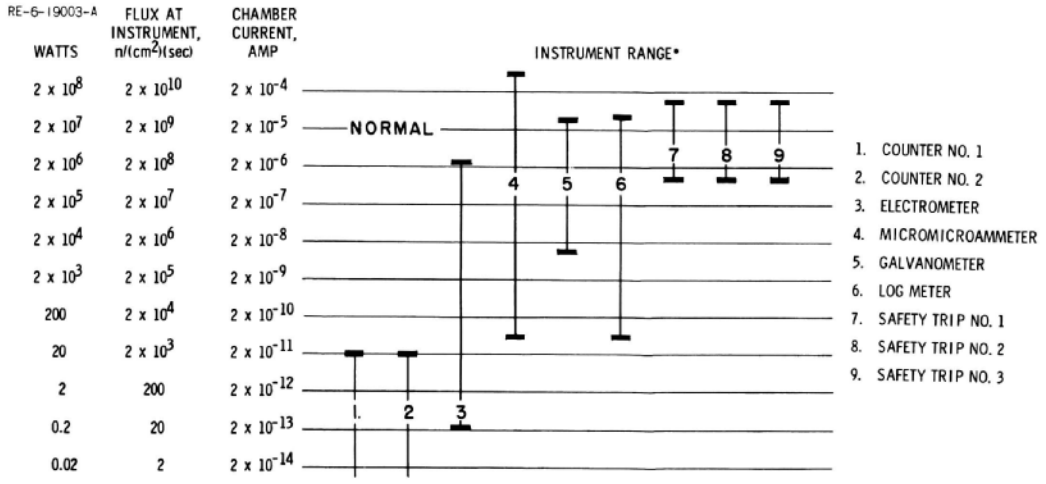

Fig. XI-4

Ranges of Nuclear Instrumentation
RE-6-19003-A

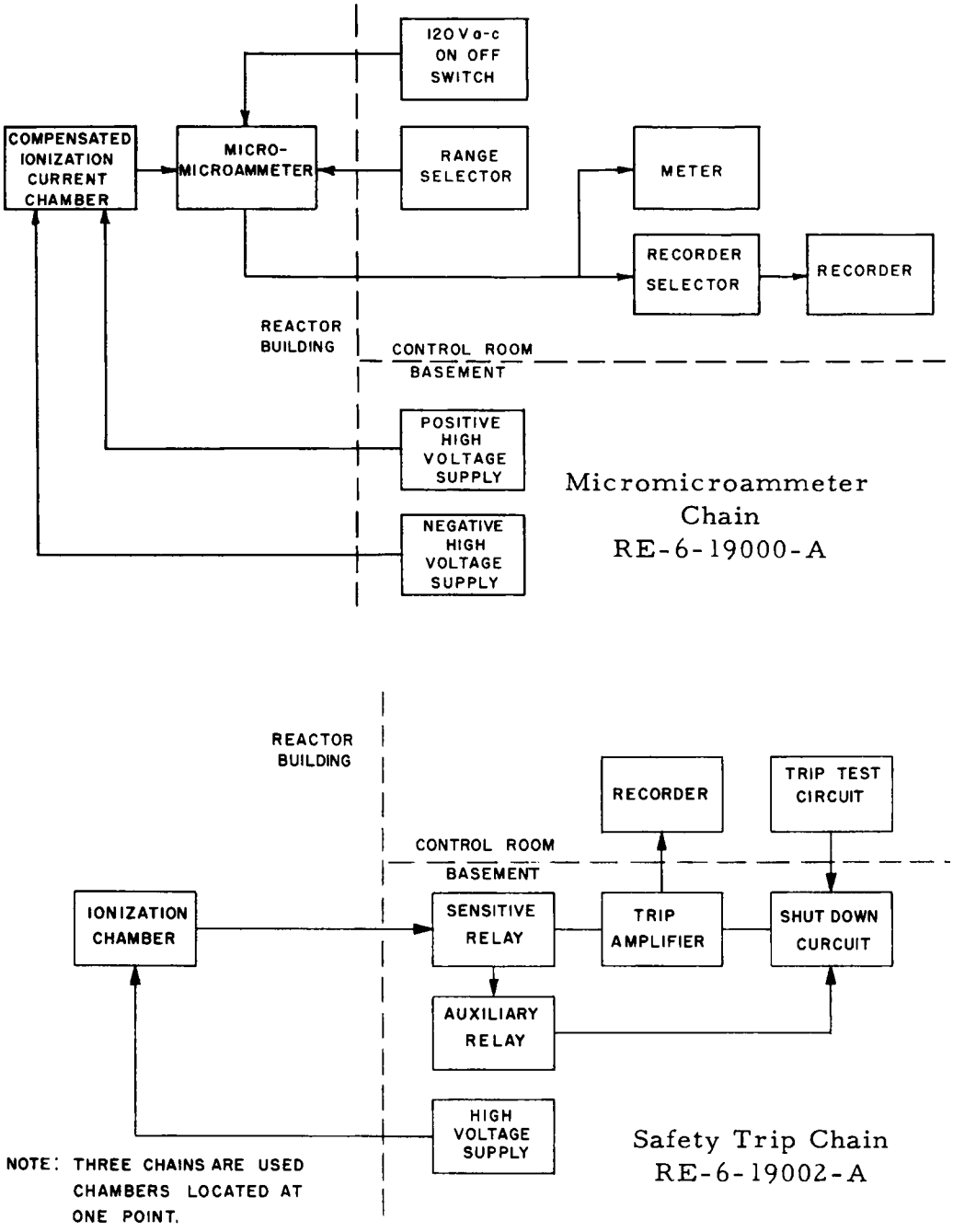

Fig. XI-5

Reactor Safety and Shutdown Chain #1

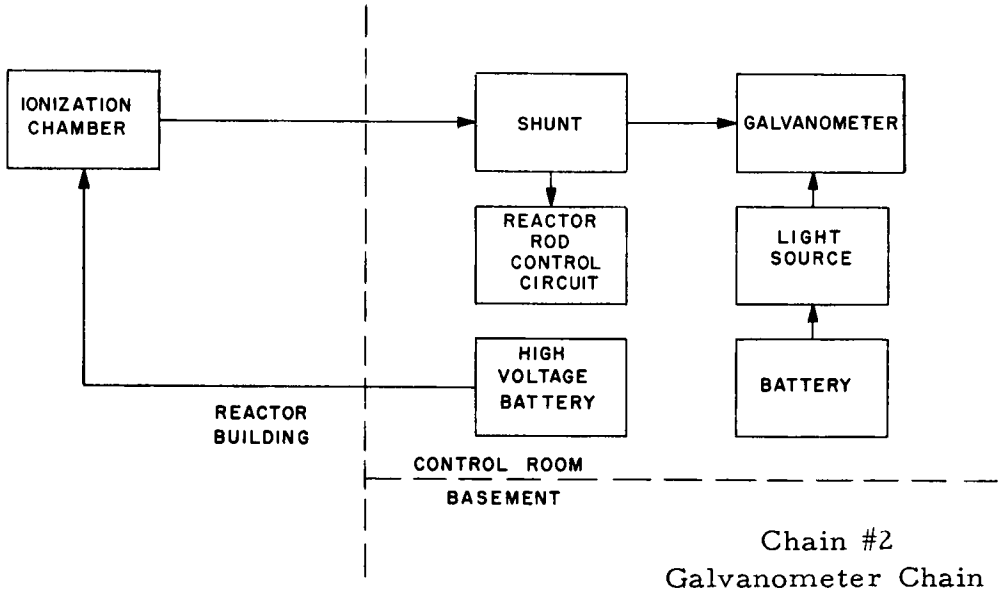

Chain #2
Galvanometer Chain
RE-6-18999-A

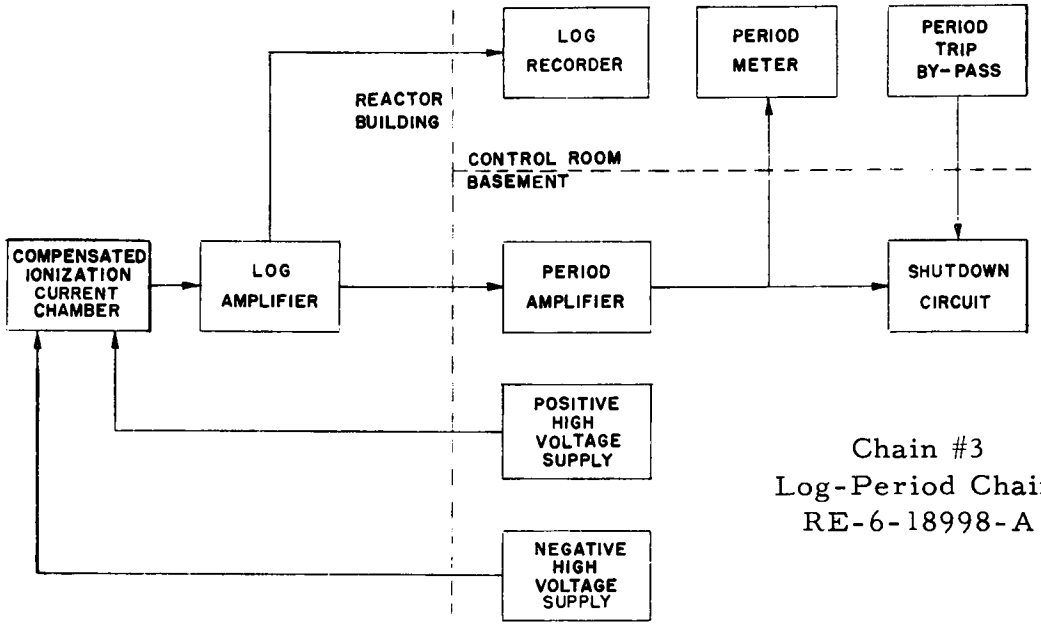

Chain #3
Log-Period Chain
RE-6-18998-A

Fig. XI-6

Shutdown Chains #2 and #3

A strip-chart linear-flux recorder is used to record the output of the Keithley micromicroammeter at low power levels and the output of the L & N micromicroammeter from intermediate to full power levels. It is calibrated linearly from 0 to 100, has a 3-sec pen speed, and has chart speeds of 2 in./min and 12 in./hr. The output of the log amplifier is recorded on a strip-chart recorder with a logarithmic scale calibration. This instrument also has a 3-sec pen speed and chart speeds of 2 in./min and 12 in./hr. The fast chart speeds are used during startup.

Selsyn position indicators at the console show the control rod positions (see Fig. XI-1). Control rods are moved one at a time. During normal operation, the rods are kept as nearly banked as possible. Prior to startup, the rods are put through a drop test to insure proper functioning. If the reactor is operating steadily, the rods are occasionally "exercised" in position.

All instrumentation of plant parameters is done by electrical transmission. Remote-controlled closed-circuit television is used to provide a direct indication of reactor water level from a sight glass and of main-line steam pressure from a tube-type gage. Plant temperatures are measured with either iron-constantan thermocouples or resistance-thermometer detectors. Reactor vessel temperatures are measured with chromel-alumel thermocouples. Water and steam flow are measured by applying the differential pressure across a flow nozzle to a differential pressure cell. Air flow is measured by using the beam-balance unit to determine the position of a plug inside a tapered-flow tube.

B. Reactor Startup

Under normal startup, the reactor is preheated with an external heat source until the pressure is approximately 100 psi. Reactor power is then used to increase pressure from 100 to 600 psi - the normal operating pressure. In a typical startup as shown on the recording in Fig. XI-7, the starting pressure was 130 psi. Control rods were pulled out of the core until a 30-sec period was obtained; the control rods were left in a fixed position. Reactor power increased exponentially starting from about 2 w. As the core temperature increases, the period is increased because of the negative temperature coefficient. Boiling takes place and a peak power of 640 kw is obtained. The erratic boiling process is associated with pressure-dependent flow instabilities and hydraulic effects in the core. The heat generated by the core increases the pressure and temperature. The increase in temperature reduces the excess reactivity and results in lower output. After 225 sec, the pressure and temperature have increased further and reactor power has decreased. The variations of neutron flux decrease with increase in pressure. After the flux has settled down to small variations, the control rods are withdrawn to increase reactor power. Once boiling has started, power output

is roughly proportional to control rod position. Reactor power is increased to 1 Mw and is held constant until the 600-psi operating pressure is reached. At this pressure, the automatic bypass valve and feedwater controls take over to hold reactor pressure and water level at the proper operating points. The control rods are further withdrawn until 60,000-lb/hr steam flow is obtained.

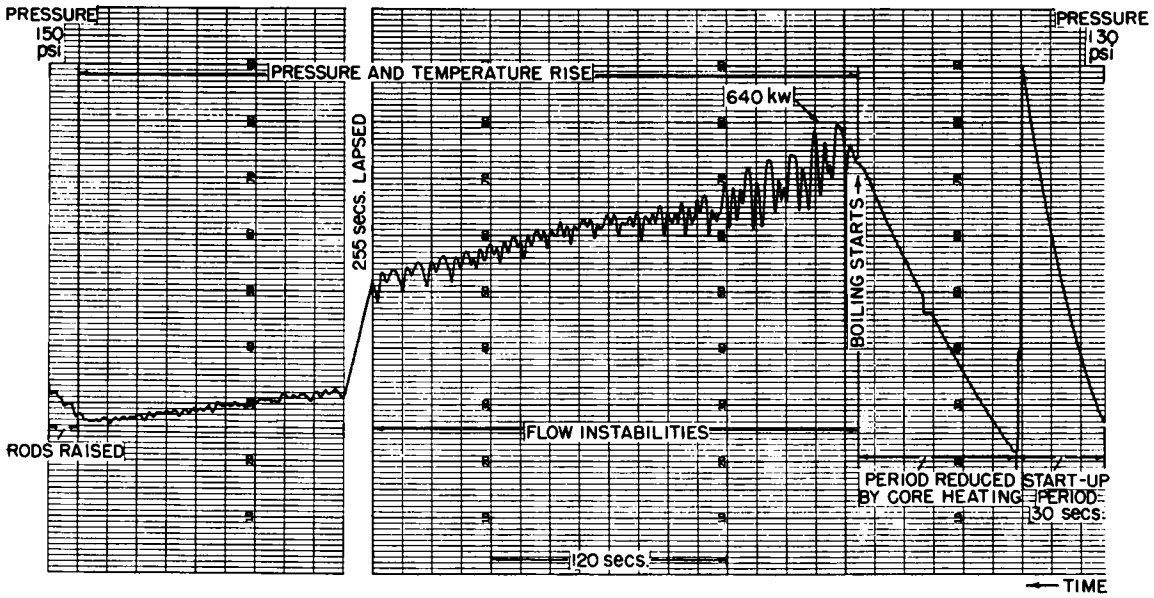

Fig. XI-7

Neutron Flux Recording for Typical Startup

II. Electrical Generation and Distribution System *

In the design of the electrical system of the EBWR Facility, consideration was given to the various fundamental and practical requirements, such as reliability, flexibility, continuity of power supply, control and instrumentation, maintenance, safety, and economy.

The EBWR Facility is arranged for parallel operation with the Utility Power System and consists of two main divisions, namely, the power plant area and the control area.

The power plant area is a cylindrical, gas-tight steel building which contains the reactor, the steam bypass system, the overpressure relief system, the 5,000-kw turbine-generator, the condenser, the feedwater system, the circulating-water system, the feedwater makeup system, the air-drying and fluid-recovery system, and various auxiliaries.

---

*A. Hirsch

The control area consists of a conventional masonry building in which general offices, laboratories, the plant control room, the 1,000-kva, 4160/480-v unit substation, and various electrical distribution and control equipment are housed. The 4,160-v metal-clad switchgear and 6,250-kva main-power transformer (together with the 862-kva reserve auxiliary power transformer) are located in the outdoor substation.

As indicated in the simplified line diagram (see Fig. XI-8), the output leads of the 5,000-kw generator are connected to the 4,160-v, 3-phase, 60-cycle bus of the outdoor unit substation switchgear through a 1,200-amp, 3 P.S.T. generator air-circuit breaker. The 4,160-v side of the 5,000/6,250-kva main-power transformer is connected to the 4,160-v bus of the outdoor unit substation switchgear through a 1,200-amp, 3 P.S.T. main transformer breaker. The 13.2-kv side of the main transformer is connected to the north bus section of the Laboratory Central Switching Station by means of the gang-operated disconnect switches in the EBWR outdoor substation, the overhead 13.2-kv EBWR pole line, and an oil-circuit breaker in the north bus section of Facility 544.

A 1,200-amp, 3 P.S.T. air-circuit breaker is included in the EBWR unit substation switchgear to feed the 1,000-kva main auxiliary power transformer.

For normal startup and operation of the EBWR Facility, the 4,160-v bus is energized from the north bus section of Facility 544. The EBWR auxiliaries are served by the 1,000-kva main auxiliary power transformer. When it is desired to place the generator in parallel operation with the Utility Power System by means of the governor control on the steam turbine, the load on the generator can be adjusted to take: first, the EBWR Facility auxiliaries load, and, second, the Laboratory load.

As a precaution against delivery of power from the EBWR generator to the Utility Power System, suitable reverse power relaying is installed in the Laboratory main-transformer station (Facility 543) which provides alarm and indicating-light signals in the EBWR control room when the power from the Utility Power System to the Laboratory decreases to a value of approximately 200 kw. When this condition occurs, it will be necessary for the operator in the EBWR control room to decrease the output of the generator.

To provide power supply for the various auxiliary drives in the event of loss of the 13-kv EBWR pole line circuit to Facility 544 (when the generator is not operating) and/or loss of the 1,000-kva main auxiliary transformer circuit, a 862-kva reserve auxiliary transformer is incorporated in the design to furnish power to the 480-v, 3-phase, 60-cycle bus

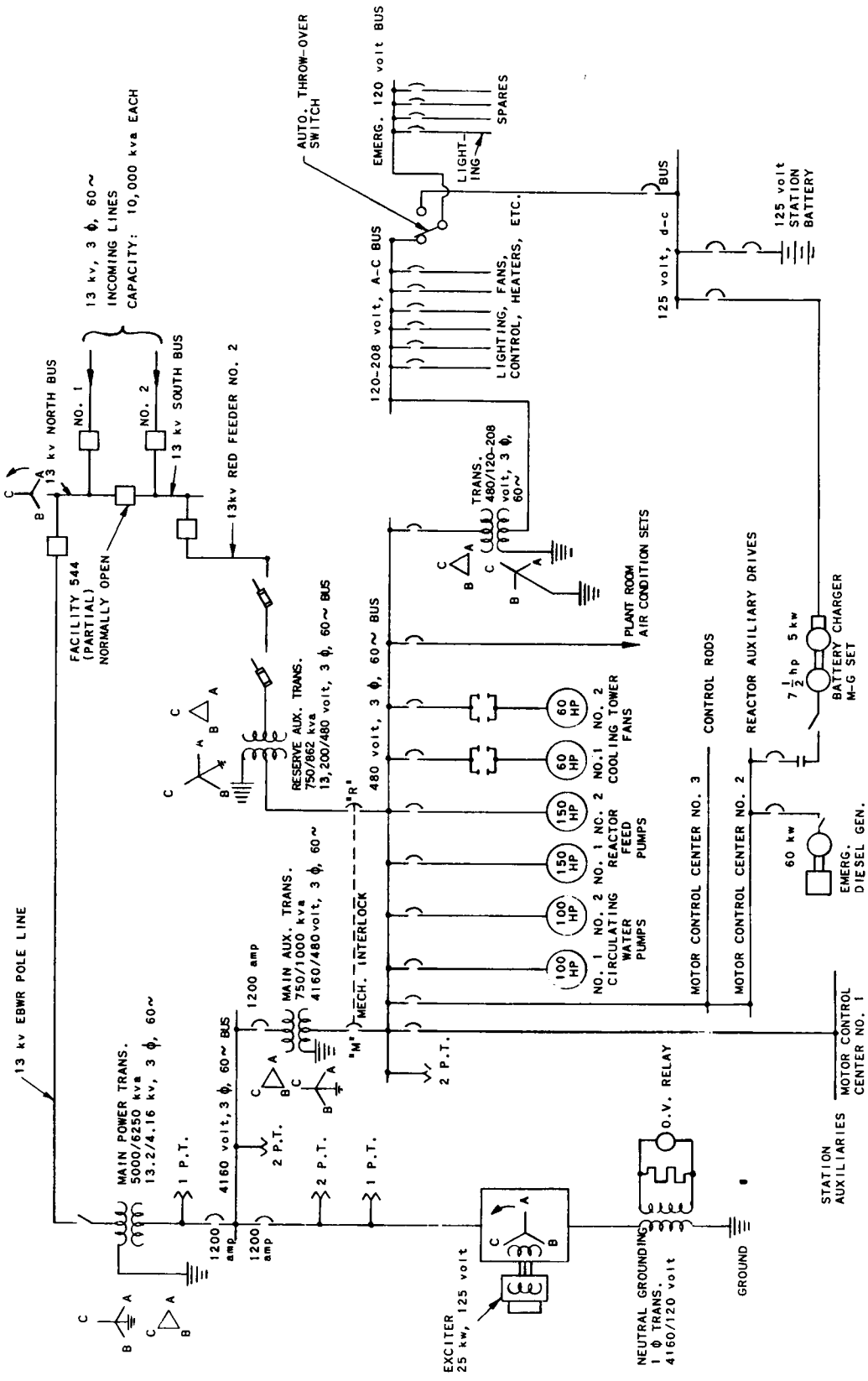

Fig. XI-8

Simplified Line Diagram of EBWR Electrical System

RE-8-17047-B

via the south bus section of Facility 544, as indicated in Fig. XI-8. In normal operation, the 480-v bus is fed from the 1,000-kva main auxiliary power transformer as previously described. Loss of voltage on the 480-v bus initiates the operation of undervoltage relays on the 480-v bus to effect the automatic tripping of the circuit breaker (designated "M" in Fig. XI-8). After a time delay of approximately 1.5 sec, it causes the circuit breaker designated "R" to close, thus restoring power to the 480-v bus. A selector switch is included on the electrical-auxiliaries control panel under the control room to select either the main or reserve auxiliary power supply as desired. Automatic transfer is provided in either case.

To provide emergency power supply for the reactor control rod drives and such auxiliaries as the reactivity blowers and heaters, the makeup-air Freon compressor, recovery-system Freon compressor, cooling-water pumps, and shield-cooling circulating pumps, an automatic starting diesel-generator set (60-kw, 480-v, 3-phase, 60-cycle, 0.8 power factor) is incorporated in the design. The control is arranged for the initiation of automatic starting of the diesel-generator set following loss of voltage on Motor Control Center No. 2 after the time required for the restoration of voltage on the 480-v switchgear bus via air-circuit breakers "M" and "R" as described above. The automatic starting of the diesel generator set begins after approximately 4 sec of sustained loss of voltage and restores voltage to Motor Control Centers Nos. 2 and 3 within approximately 15 sec.

To provide continuity of emergency lighting, an automatic throw-over switch is included in the ac/dc Distribution Cubicle to transfer the emergency lighting circuits to the 125-v, dc bus. This transfer takes place immediately upon loss of voltage on the 120-208-v, ac bus, but returns automatically to the ac bus position with restoration of power on the same bus.

In the event of sustained loss of 480-v supply from the main and reserve auxiliary transformers (in which case the emergency diesel-generator set will be operating), it will be necessary to restart the 5-kw battery-charger M-G set on Motor Control Center No. 2 and to close the generator air-circuit breaker (which will have opened due to reverse current flow) in order to relieve the station battery of its load.

III. Operational Control of Reactors*

A. General Theory of Reactor Control

For a particular system the reactor power is proportional to the average flux, whereas the relation for a unit volume is

*J. Matousek

$$P\left(\frac{w}{cm^3}\right) = \frac{F}{c}\left(\frac{\text{fissions/sec-cm}^3}{\text{fissions/w-sec}}\right) = \frac{\phi\Sigma_f}{c} \quad .$$

For the entire reactor the power generally can be expressed in terms of the average flux and the volume of the system containing fissionable material as follows:

$$P_{total} = \overline{\phi}\Sigma_f V_f/c \quad .$$

In the foregoing,

P = power in w/cm^3

F = fissions/sec-cm^3

c = constant of equivalence ($\sim 10^{10}$ fissions per w-sec)

ϕ = flux (number/cm^2-sec = nv)

$\overline{\phi}$ = average flux

Σ_f = macroscopic fission cross section (cm^{-1})

V_f = total volume of system containing fissionable material (cm^3).

These relationships suggest that in order to increase the power of a particular system it is necessary to increase the flux, since the other terms are fixed by design. During steady-state operation, the flux is constant and the effective multiplication constant (k_{eff}) is equal to one. More specifically, k_{eff} is equal to the infinite multiplication constant minus the losses. The point is that, in steady-state operation, the number of neutrons formed after each generation or cycle is maintained essentially equal to the preceding generation as closely as control will permit.

In order to increase flux it is necessary to increase k_{eff} so that the number of neutrons increase in succeeding generations until the new power is reached. This must be done slowly and under controlled conditions; otherwise, the neutrons would multiply too rapidly and the flux increase could not be contained by the system. Increases or decreases in k_{eff} are designated by δk, which is defined as $\delta k = k_{eff} - 1$ and referred to as "excess reactivity." It is the "excess reactivity" that is of prime importance in the design of reactors and the associated controls. Therefore, the following discussion about reactor control will consider changes in δk as produced by either inherent or external controls and the consequent effect on the fission and thermodynamic processes. It should be emphasized at this point that the discussion will not include the problems or controls necessary for startup or shutdown, both of which represent separate control loops in themselves.

The two processes common to the external and inherent disturbances are represented by the boxes shown in the Reactor Control System diagram (see Fig. XI-9). Beginning with the fission process, reactivity input (δk) to the process is shown, which represents the sum of the reactivity changes produced by external and inherent disturbances. The fission process supplies power to the thermodynamic process, this being shown by the arrow between the two processes. Load demands and disturbances on the thermodynamic process are also represented. The extraneous disturbances which make a demand on the thermodynamic process are such items as loss of coolant flow, malfunctioning of equipment and controls, and inadvertent opening of valves. The input to the fission process is in the form of the resultant reactivity change. The reactivity changes produced by both external and inherent feedback are summed in the box to the left of the fission process. The external disturbances include items such as xenon buildup, samarium, burnup, and changes in control rod position. The inherent disturbances causing reactivity changes are produced by feedback due to fuel temperature, moderator temperature, pressure, voids, and density changes.

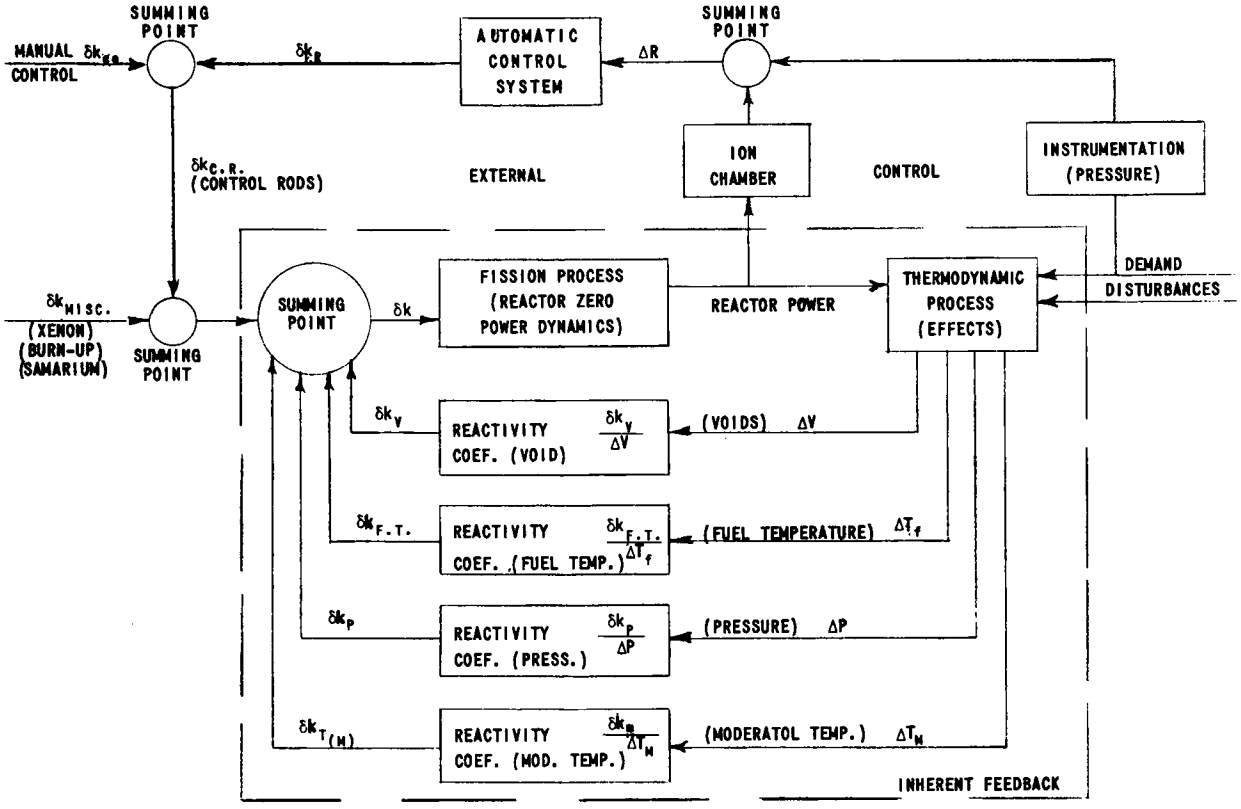

Fig. XI-9

Schematic of Reactor Control System

Inherent feedback is dependent upon changes in the thermodynamic process, and the latter is dependent upon reactor power and load demand. Effects on the thermodynamic process caused by changes in reactor power and demand are designated by the symbols ΔV, ΔT_f, ΔP, and ΔT_m.

The blocks shown as reactivity coefficient denote the inherent relation between the change in reactivity and the change in the particular thermodynamic variable. Each reactor has a characteristic reactivity coefficient for each thermodynamic variable, and the coefficient is fixed by the nature of the system or by design. The reactivity changes in the inherent feedback loop are shown combined with any reactivity changes caused by external control. If the reactor possesses a reactivity coefficient that produces a reactivity change of correct sign for a change in one of the thermodynamic variables, an inherent control system results.

External systems are essentially artificial reactivity coefficients introduced to the fission process. They can be either manual or automatic, both methods being shown in the schematic diagram. For automatic control, instrumentation is required to measure reactor output (neutron flux) and demand (pressure). Instruments for both of these measurements are shown, and the sum of the signals is represented by ΔR. The signal ΔR is applied to the automatic control system. The automatic control system is analogous to a reactivity coefficient, since it converts the ΔR to a change in reactivity by the movement of control rods. For illustrative and comparative purposes, different philosophies of control have been selected:

1) direct cycle with steam bypass (EBWR);
2) dual cycle (Dresden);
3) direct cycle with automatic control rod positioning (ALPR); and
4) pressurized water systems.

B. EBWR Control System

Remedial action to load disturbances generally can be classified as either preventive or corrective. In the case of EBWR, the former method is employed, since an attempt is made to isolate the reactor and prevent load disturbances from being reflected back to the reactor. This method avoids the inherent characteristic of a direct-cycle system in which changes in load produce a reactivity change in the wrong direction. For example, if the load decreases considerably in a direct-cycle boiling water reactor system, the resultant pressure increase causes a decrease in voids, which, in turn, produces an increase in reactivity - this inherent feedback being directly opposite to the desired effect. In a direct-cycle

boiling water reactor, inherent control or self-regulation is not available for load changes, and some means must be employed either to compensate for or to avoid the problem. This is accomplished by incorporating an automatic steam-bypass valve whose function is to maintain a constant steam flow. In this way the load demand on the reactor remains constant despite variations in turbine-generator demands. Figure XI-10 shows a diagram of the EBWR system utilized for the operation of the 20-Mw system.

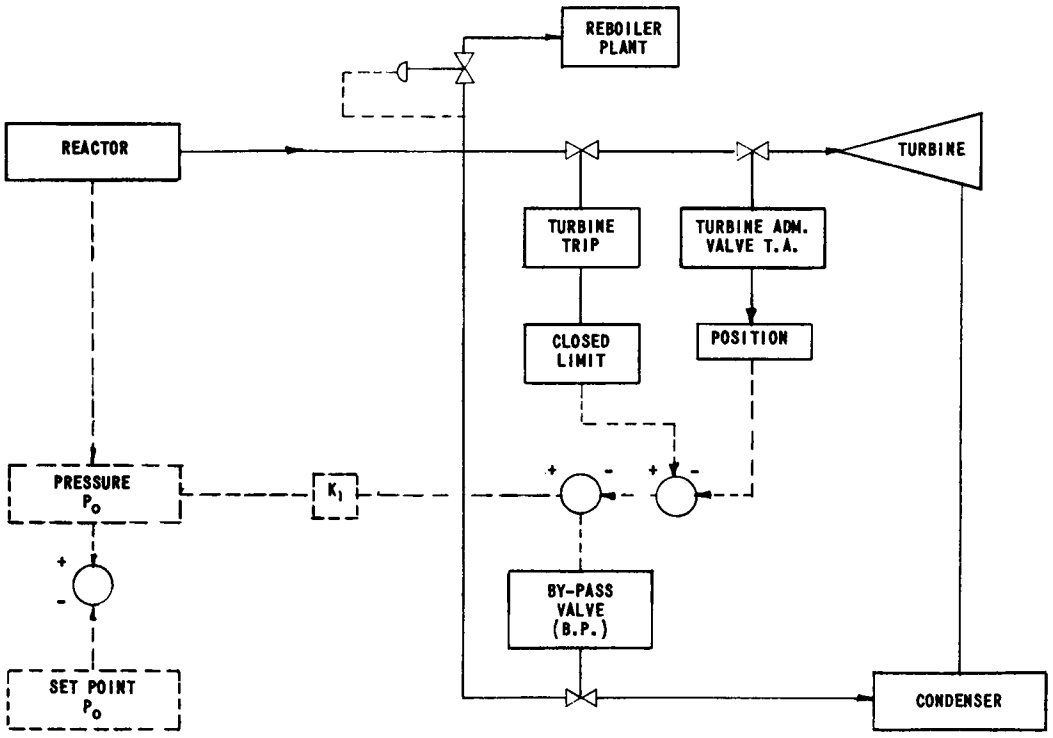

Fig. XI-10

Schematic EBWR Control

The EBWR operates at a constant power level determined by the setting of the control rods. The automatic external control loop shown in the Schematic of Reactor Control System is not utilized and feedback is prevented - power output being determined by manual control rod positioning and with steam from the reactor made to flow either to the turbine or through a bypass directly to the condenser. The bypass valve is hydraulically operated and is positioned by a hydraulic control system in which steam pressure is the main control parameter. The reactor steam pressure P is compared with a mechanically set pressure P_0. The bypass valve operates proportionally to the difference $P - P_0$ by design of the valve-operator mechanism. A desired pressure P can be obtained by remotely adjusting P_0 through an electrical-drive unit. The steam load will then match the reactor power at any desired pressure P. Operation

of the bypass valve can be visualized by assuming that at the initial condition $P = P_0 = 600$ psig (the reactor is at zero power with no steam flow) and the turbine admission valve is closed. Under these conditions, the bypass valve is closed. As soon as steam is generated (or steaming rate increased), $P - P_0$ becomes greater than zero and the difference is applied as a signal to the bypass valve. The bypass valve begins to open until the steam flow through the valve is equal to the steaming rate for the particular value of $P - P_0$. The proportional band is adjustable in the controller by means of a mechanical linkage and has been set at a value of 25 psi for 20-Mw steam load of 60,600 lb/hr. This means that for each pressure differential of 1 psi for $P - P_0$, the rate of steam flow is approximately 2400 lb/hr. Therefore, it is necessary for the operator to decrease P_0 progressively as steaming rate increases in order that the high-pressure trip does not shut down the reactor. The final P_0 setting is approximately 585 psig. The valve has been sized to be about one-half open for steam flow at 20 Mw.

After the desired steaming rate is established through the bypass valve, the turbine is started by opening the turbine trip valve; the steam to the turbine is then controlled by the turbine admission valve. The turbine admission valve is positioned by the turbine governor. A cam attached to the operating lever on the admission valve is calibrated to give a signal proportional to the turbine-steam flow. With the turbine running, reactor power output must be equal to the turbine plus bypass steam load. A hydraulic link between the turbine admission valve and bypass valve makes the sum of the valve openings proportional to the set pressure difference $P - P_0$ and can be expressed by the following equation:

$$K(P - P_0) = \text{S.B.} + \text{T.A.} = \text{reactor power} \quad ,$$

where

P = reactor pressure
P_0 = reference set pressure
S.B. = bypass valve position
T.A. = turbine admission valve position
K = proportionality constant.

During operation, 5% of the total reactor steam output is bypassed directly to the condenser. Therefore, reactor power is not affected by load changes provided no increase in turbine load is greater than 5%. If the increase in load is greater than the buffer offered by the 5% bypass, the reactor power is increased by withdrawing control rods manually. Sudden loss of generator power causes the trip-throttle valve to close. The closed position of the turbine-trip valve cancels the position signal of the admission valve, and the full $P - P_0$ signal is applied to open the bypass valve, which then assumes the full load.

During 100-Mw operation, when the reboiler plant is on stream, reactor pressure regulation will be taken over by the new steam-pressure regulating valve and the bypass will normally be closed. No change has been made in the bypass valve during the revision of EBWR for 100-Mw operation, and it will be used in the same way as before for startup and operation of the 20-Mw plant. The bypass control system for the original 20-Mw plant and the new pressure regulator to the reboilers act independently of each other.

Prior to the startup of the reboiler plant, approximately 30,000 lb/hr of steam in excess of that required by the turbine are bypassed to the condenser. This steam flow is then available to the reboiler plant when pressure regulation is taken away from the bypass valve and assumed by the new pressure regulator. The new pressure-regulator control consists of a proportional controller with automatic reset. Reactor pressure control is transferred by lowering the reference setting (P_0) of the new regulator from an elevated value to 600 psig. As a result, the steam bypass valve will accept less and less steam until finally it approaches full closure. Thereafter, the P_0 setting of the bypass control is set slightly above 600 psig. When this is completed, the transfer is accomplished. Reactor power increases are then made by withdrawing control rods.

In case of a pressure rise at a rate greater than the new pressure regulator can handle, the bypass valve will open as soon as reactor pressure reaches its P_0 setting and will aid in maintaining pressure. As reset action compensates for the new load on the pressure regulator, the bypass valve will close again and will remain in a standby condition. The method of control adopted for the reboiler plant is similar in philosophy to that for the original plant; for example, inherent feedback is prevented. Should a change in reactor output be required, it is accomplished by the manual operation of control rods.

C. Control Systems of Other Reactors

In the direct cycle, steam is generated in the reactor and sent directly to the turbine. Although the cycle is very simple, it has some disadvantages for a power reactor. The continuous dumping of steam through the bypass valve does not represent economy of operation. Also, for large central stations it is desirable to incorporate inherent control (self-regulation).

A pressurized water reactor system (in which secondary steam for the turbine is generated in a heat exchanger) is a good example of inherent control obtainable in an indirect cycle. If load is increased, steam flow to the turbine increases; thus, steam pressure and temperature of the secondary system decrease. As a result, the primary fluid

temperature is decreased on leaving the heat exchanger and entering the core. In terms of the first schematic, ΔT_m becomes negative as the load increases. Since the reactor has a negative temperature coefficient, $\delta k_{T(m)}$ becomes positive and reactor power increases as load increases. The increase in reactor power causes an increase in T_m by driving ΔT_m positive. Thus, the system is self-regulating and equilibrium is reached at a new power level; if the inherent feedback is large enough, external control can be eliminated or minimized.

In order to retain some of the good features of a direct cycle and still possess correct reactor response to load demand, the Dresden Plant utilizes a dual cycle which is a modification of the direct cycle (see Fig. XI-11). Essentially, primary steam is supplied directly to the turbine along with secondary steam obtained from heat exchangers. To accomplish this, the mixture of steam and water from the reactor is sent to a separating drum from which the steam flows directly to the turbine. The saturated water flows from the drum through heat exchangers where secondary steam at a lower pressure is generated. The secondary steam is admitted to the lower stages of the turbine. Since the ratio of primary water to primary steam leaving the reactor is approximately 16 to 1, the temperature of the primary water leaving the heat exchanger essentially controls the temperature of the feedwater to the core.

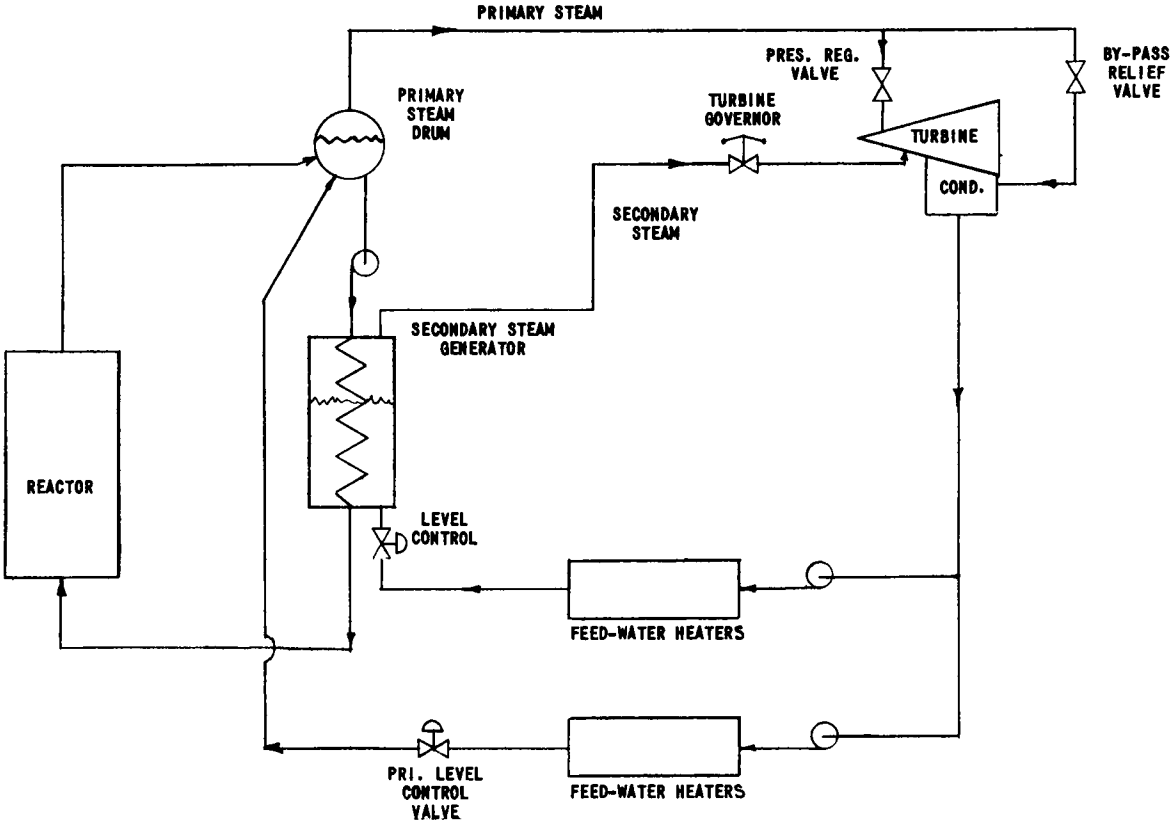

Fig. XI-11

Dresden Flow Diagram

The Dresden Plant is controlled by means of a turbine-speed governor and pressure regulator. The pressure regulator attempts to hold constant pressure on the reactor to prevent reactivity changes. Primary steam is admitted to the turbine in sufficient quantity to hold set pressure. However, a steam bypass valve is incorporated in the system in the event that the turbine cannot accommodate the primary steam. The turbine-speed governor controls the secondary steam to the turbine to complete the total turbine requirements and control reactor-inlet water subcooling. Inherent control is obtained in the following manner for an increase in load demand.

As the load on the turbine is increased, the speed governor signals for more secondary steam to the turbine. As a result, the secondary steam pressure will drop and cause a greater ΔT over the heat exchanger, which increases the heat transfer. The increase in heat transfer rate decreases the temperature of the primary fluid leaving the heat exchanger and entering the reactor. Because of the increase in subcooling, boiling occurs at a higher level in the core and the effective reactivity associated with the voids is diminished. This means that the reactivity δk becomes positive and the core flux increases. Consequently, core power output increases, and primary steam and steam voids build up. The increase in voids increases the neutron leakage because of the decrease in moderator in the boiling section. The increase in neutron leakage reduces, and finally cancels, the positive reactivity introduced by the increase in subcooling. An inherent feedback control of reactivity is obtained and self-regulation is the result. In this way, a new power level is reached without repositioning the control rods.

The increase in the steaming rate will cause an increase in reactor pressure and the primary admission valves will open more - thereby increasing the flow of primary steam. By this process of self-regulation, the reactor will reach a new power level sufficient to produce the correct primary and secondary steam flow for the new load. If the generator load decreases, the process is repeated except that regulation is in the reverse direction. It is said that by means of the inherent-control operation, about 40 to 100% of full load is possible without changing control rod position. Greater changes are handled by manual positioning of control rods or by bypassing steam to the condenser.

The initial boiling water reactor plants were designed to take advantage of the self-regulating feature of the reactor core to movement of control rods. The total steam load was manually or automatically adjusted to equal reactor power in order to maintain constant reactor pressure. In EBWR, the turbine steam load is determined by generator output, and a steam bypass to the condenser is incorporated to keep reactor steam load constant. However, the continuous dumping of steam is not economical and manual adjustment of control rods is necessary for increases in

load in excess of the small amount of steam usually dumped by the bypass. A reactor is operated most economically when reactor power is adjusted to equal load demand with no bypass steam. This can be accomplished if advantage is taken of the feature that reactor pressure provides a direct indication of the balance between reactor power and steam load. For example, any differential between steam load and reactor power manifests itself as a change in pressure. Therefore, a method for controlling reactor power in a boiling reactor by moving control rods in proportion to a pressure error is possible and, in fact, was designed for ALPR at the Idaho site during January 1959.

As an example, consider a decrease in load demand. Reactor pressure will increase, voids will decrease, and reactivity will increase. Reactor power will increase since this is characteristic of boiling water reactors. The change in reactor pressure will be sensed and control rods will be automatically moved downward to compensate for the decrease in load. Under steady-state conditions, the rate of change of pressure is zero, and reactor power is equal to steam load. Since a proportional controller is used for control rod position, no movement of rods will occur unless the reactor pressure is changing. Since the controller output signal is proportional to the error, control rod position is proportional to, and fixed by, the pressure error. The pressure error and rod-position relation, of course, is not fixed, since it is contingent upon the reactor power and load. Various loads will require manual resetting of the pressure reference in order to maintain reactor pressure within required limits.

IV. Accident and Emergency Analysis*

A. Shutdown Cooling

Immediately after EBWR shutdown, the core decay heat is approximately 6 per cent of the full operating power prior to shutdown. Hence, after 100-Mw operation the decay heat at shutdown is 6 Mw. The decay heat from the core decreases to about 3 Mw after 5 min and to 1 Mw after 7 hr. Normally, decay heat is removed by boiling for the first 3 hr, and the steam generated is discharged to the condenser until the reactor water reaches about 263°F. Thereafter, the reactor water is circulated through the secondary cooler of the Reactor Water Purification system and returned to the reactor. If sufficient cooling is unavailable in the Reactor Water Purification system secondary cooler, the secondary cooler in the standby Reactor Water Purification system can also be utilized. Should the steam bypass valve become inoperative, the 4 x 8-in. steam-powered pressure regulator will automatically admit steam to the condenser and limit reactor pressure to 640 psig until the decay heat decreases sufficiently to allow the reactor pressure to drop. In the event of a power failure, the normal shutdown system cannot be used and the emergency cooler

*E. Martinec

is utilized to dissipate decay heat. Operation of the emergency cooler can be initiated from the control room. Loss of instrument air or 125-v dc power automatically turns on the emergency cooler.

B. Reactor Vessel Rupture

In the event of a major vessel-nozzle rupture, a limited amount of cooling is available to the core if complete loss of water does not occur and if the break is above the core. Introduction of the cooling water is either automatically or manually initiated. When both reactor level and pressure fall below preset limits, the system is automatically actuated. Since the new riser will interrupt the spray and prevent efficient cooling of the core, whatever cooling is obtained from the spray ring will be accomplished by the addition of water to the downcomer area. Should a major vessel-nozzle rupture occur at the bottom of the vessel, all the water will be lost from the reactor vessel. Under these conditions no cooling is available and, because of the new riser, the spray ring will have limited usefulness.

A major rupture of the reactor vessel resulting in a loss of water and exposure of the core may result in melting of the fuel elements. The high temperatures reached in the fuel plates can cause the zirconium clad to oxidize (exposing the hot uranium fuel), and fission products can be released to the atmosphere. For a major rupture, measures must be incorporated into the plant other than confining the fission gases and products to the vapor-containment vessel. A minor rupture of the vessel cannot result in loss of all water from the vessel, since provisions have been incorporated to replace water. If the rupture occurs above the top of the core, flashing caused by the pressure drop will provide cooling and prevent overheating of the fuel elements. When the reactor pressure and level drop to a preset point, water from the 15,000-gal overhead tank will be injected automatically. The core can also be flooded manually by water from the Laboratory main. If the rupture occurs below the core, the operator can reduce pressure in the reactor by opening either the steam bypass valve or the reactor pressure-control valve and dump the steam to the condenser or reboilers. As in the previous case, low levels of reactor water and pressure will automatically cause injection of water from the overhead tank.

C. Power Failure

Following loss of power to the magnetic clutch, the control rods drop to a position of maximum shutdown in less than 1.5 sec (fail-safe operation). Flow of water to the Emergency Cooler is automatic on loss of 125-v dc power or instrument air. Water from the overhead storage tank can be admitted to the Emergency Cooler upon signal from the control room.

In case of loss of power from the utility lines, the reactor is automatically shut down and the turbine-generator is tripped off. The reactor steam pressure-regulating valve to the primary reboilers closes automatically upon a loss of reactor control power. The steam bypass valve bypasses steam to the main condenser and prevents reactor pressure from rising above approximately 610 psig. Continued operation of the turbine bypass system is assured through the use of an oil-accumulator tank. Since the circulating-water pumps are without power, the flow of cooling water to the condenser is obtained by natural convection. The natural circulation is obtained by the automatic opening of a bypass valve which allows water to flow directly to the storage basin of the cooling tower. Unless this bypassing is accomplished, the height of the cooling-tower risers would prevent circulation. The ventilation openings in the containment building are closed automatically on power failure. All primary system lines penetrating the containment shell are isolated automatically on power failure.

D. Pump Failure

Safety provisions for failure of the circulating-water pumps, turbo-generator system-feedwater pumps, cooling-water pumps, shield-cooling pumps, and reactor purification pumps are adequately described in ANL-5607. If the primary feedwater pumps in the reboiler system fail because of power interruption, an electrical interlock will automatically shut down the reactor. Reactor shutdown causes automatic closure of the steam regulator, and admission of steam to the primary reboiler is interrupted. Failure of the reactor feedwater pumps to supply feedwater even though electrical power is available will result in a decrease in reactor water level; low water level will initiate reactor shutdown. Should the deaerator water level drop to a preset low level, a low-level pump-cutoff switch will automatically cut the power to the primary feedwater pumps - resulting in automatic reactor shutdown. A failure of an intermediate pump or decrease in flow of intermediate feedwater will cause the pressure in the reactor to rise, since low level will decrease the heat-removal capacity of the reboilers. As a result, the steam bypass valve will begin to open between 602 and 610 psig to maintain pressure in the reactor. The operator will have to start the standby, intermediate feedwater pump in order to resume normal operation. If the standby pump fails to start or flow is not resumed, one of the following actions will occur:

1) Reactor overpressure interlock will initiate reactor shutdown at 630 psig.

2) Primary reboiler shell low-level alarm will warn the operator that water is being boiled away with little or no makeup.

E. Control Valve Failures

The steam system is designed without any valves which can close suddenly other than the present turbine trip-throttle valve and the pressure control-trip valve. For 20-Mw operation without the reboilers, experience indicates that one of the following three events will occur because of sudden closure of the turbine trip-throttle valve:

1) The reactor will be shut down by the turbine-trip interlock.

2) If the turbine-trip interlock is bypassed with a key switch, the bypass valve will open fully. The reactor will continue operating without sensing the interchange if the pressure does not increase beyond 600 psig.

3) Should the bypass valve fail to make the interchange in case (2), control rods will be inserted by one or two shutdown interlocks: high flux and/or overpressure. EBWR has been shut down by the high-flux interlock when the power rate of increase was approximately 1 Mw/sec. This corresponded to a rate of increase of pressure of about 3 psi/sec.

At less than 100-Mw reactor operation with the reboilers accepting steam and the turbine-trip interlock bypassed, sudden closure of the trubine-trip valve will cause a pressure-control valve to open to maintain reactor pressure at 600 psig. The additional steam will be directed to the primary reboilers. Since the secondary reboiler is normally base loaded, the added heat load will be dissipated in the air-cooled heat exchangers. Once the design heat-removal capacity of the primary reboilers is reached, reactor pressure will rise and the steam bypass valve will open and dump steam to the condenser. Should the primary reboilers be operating at peak capacity (100 Mw) at the time of the incident, reactor pressure will rise immediately. Since the primary reboilers cannot handle the entire load of 100 Mw at a reactor pressure of 600 psig, the steam bypass valve will open and maintain reactor pressure slightly above 600 psig by dumping steam to the condenser. Actually, the transfer of 100 Mw of heat to the intermediate system requires a primary condensing pressure of approximately 635 psig. The steam bypass will eventually take up the majority of the load with a small part of the load going to the reboilers because of a slightly higher condensing pressure.

The steam bypass valve is normally closed during operation of the new reboiler plant since it is set to open slightly above reactor pressure. Therefore, the steam bypass valve will not compensate for the above failure incident to the turbine-admission valve until the reactor

pressure rises sufficiently to open the valve. A failure resulting in full closure of the steam bypass valve or failure to open when required will not affect the operation of the turbine-admission valve, which will continue to function in accordance with demand. Any changes in reactor pressure occurring, thereafter, must be fully compensated for by the pressure-control valve or else the pressure will continue to rise. If reactor pressure exceeds 630 psig because of a subsequent incident, the control rods will automatically drop and the reactor shut down.

F. Control Rod Failure

Since there are nine control rods whose combined strength at operating conditions is sufficiently greater than the maximum amount of excess reactivity they are required to control, failure of one, or even two, rods does not necessarily create a dangerous situation. However, should a rod failure occur, reactivity can be reduced by the injection of boric acid from the high-pressure system. In event a control rod does not fall in by gravity force alone, the overriding clutch feature of the mechanism may be used to help drive the rod into the down position.

G. Excessive Pressure

If the pressure exceeds 630 psig, the reactor is shut down automatically by an overpressure shutdown interlock. If the pressure increases to 640 psig, the 4 x 8-in. steam-powered back-pressure regulator opens and dumps steam to the condenser. Further increases in pressure will trip safety valves set to open at 700, 725, 750, and 775 psig. These safety valves also dump steam into the condenser. Opening of any of the relief valves will automatically shut down the reactor, since the control rods are electrically interlocked with the valves. If the condenser pressure exceeds 20 psig (which may result if all steam valves open), two rupture disks in the condenser are sized to burst and discharge steam into the vapor-containment building. Consequent release of radioactivity will automatically initiate closing of the ventilating valves in the building.

H. Reactor Water Level

Control rods cannot be withdrawn if the water level in the reactor is too low or too high. The rods will be inserted automatically if the water level exceeds preset limits during operation. The rods cannot be withdrawn if the reactor water temperature is below 325°F. Hence, excess reactivity cannot be added to a cold reactor even if the water level safety trip is inoperable.

I. Water Leaks from the External System

The dominant radioactivity in the steam circuit is due to fast-neutron irradiation of O^{16} to form N^{16}. Since the molecular density of steam

is very low compared with that of water, the amount of N^{16} will also be correspondingly low. The short half-life (7.4 sec) of N^{16} prevents accumulation of this activity in the vicinity of a leak. Even if all of the water in the system should flash down to atmospheric pressure, the integrated exposure from the N^{16} will not pose a serious hazard to operating personnel in the building.

Development of leaks in condenser tubes will permit leakage of circulating water into the primary fluid in the condenser. An increase in electrical conductivity of condensate or of reactor water will be the first indication of major leakage in the condenser. Water-level indicators would eventually show an increase in primary water inventory. With evidence of a leak, the operator can isolate the half of the condenser involved by closing butterfly valves in the inlet and outlet circulating water lines. The water boxes and tubes on the leaking side can then be drained to a tank in the basement of the Power Plant Area. The remaining half of the condenser can still condense the turbine exhaust and/or bypassed steam although at a slightly higher back pressure. The operator can open the valve admitting spray water into the bypass desuperheater to prevent damage to the condenser because of high thermal gradients. Condenser tubes have failed in the present condenser by erosion because of steam deflecting off the condenser bracing. The above sequence was followed for locating and plugging the faulty tubes; thereafter, circulating water was restored to both halves of the condenser. The entire operation took place without reducing reactor power from its 20-Mw level.

If a leak or tube break occurs in the primary reboiler or drain cooler, radioactive fluid will enter the 350-psig intermediate system. This system will be monitored constantly for radiation; if radioactivity is detected, a leak or tube failure would be suspected. Further verification of a leak can be made by observing whether or not there are changes in inventory in both the primary and intermediate systems. By isolating the affected unit, operation can be continued in the parallel unit under reduced power. The same analysis applies to the primary subcooler, except that the cooling-tower water leaving the unit is monitored.

J. Startup Accidents

The existing antimony-beryllium neutron source, previously irradiated to saturation and maintained at full strength by operation of the EBWR, will be used in the new core. The period meter will be set to release control rods at periods of less than 5 sec and will be used in all the reactor startups. It is not desirable to use the period-trip meter at full power because short-period variations of the neutron flux are liable to shut down the reactor accidently.

The control rods cannot be withdrawn unless the flux-indicating galvanometer is on its most sensitive scale and the water temperature is 325°F or above. The rate of addition of reactivity by rod withdrawal is limited to approximately 0.01% per second. At this rate of addition of reactivity, the water will begin to boil as soon as the fuel plates reach a temperature just slightly higher than the boiling point of the water, and the negative steam void and temperature coefficients will automatically compensate for the reactivity added by rod withdrawal during startup. Experience with EBWR has shown that the safety procedures employed during startup are adequate.

K. Failure of Steam System

A failure of the main steam system may occur by:

1) rupture of the steam piping, steam dryer, or a valve upstream of any control mechanisms;

2) rupture of the steam piping or valves downstream of the control mechanism, the turbine or condenser casing, a reboiler, or tubes in the reboiler; and

3) internal mechanical failure of turbine valves or control mechanism.

Rupture of the main steam piping or steam dryer upstream of the shutoff valves on the primary reboiler will permit the steam to escape into the gas-tight building. In case of a wholesale failure, the rate of steam flow will be sufficient to reduce the reactor power instantaneously because of flashing. If the operator has not already inserted the rods, they will be inserted automatically:

1) when the general level of radioactivity in the building rises above a predetermined level;

2) when the water level in the reactor drops; or

3) when the water temperature drops to 325°F.

The effect on the reactor of a failure of the condenser or turbine casing or other elements downstream of the control mechanisms would be similar.

In the event that the EBWR turbine shaft or casing should fail, the reinforced concrete lining of the steel shell will prevent puncture of the shell by flying fragments. The failure of the turbine will either trip the throttle valve or completely open the governor valves, depending on the sequence and nature of the failure. Tripping the throttle valve will shut off steam to the turbine and reactor pressure will be maintained. Control rods will be inserted into the reactor because of:

1) high radioactivity in the building;

2) low water level in the reactor;

3) loss of vacuum in the condenser; or

4) action of the operators.

Opening of the governor valves will increase the flow of steam from the reactor and, in addition to the shutdown signals just mentioned, will reduce power in the reactor temporarily because of flashing in the core. The reactor after being shut down will be cooled by one of the cooling systems previously described, since the condenser will be inoperative.

In the event that a tube rupture occurs in either the primary reboilers or drain coolers, control rod insertion may be automatically initiated by the low water level in the deaerator, which will cut off the reactor feedwater pump and result in reactor shutdown. If a tube rupture is detected before any of the interlocks operate, the operator can initiate reactor shutdown.

A $\frac{5}{8}$-in. tube rupture in one of the primary drain coolers will result in a flow of approximately 250 gpm of primary fluid (at 482°F and a differential pressure of 210 psi) into the intermediate system. The amount of primary fluid entering the intermediate system is based on flow from two nozzles, since this would be the case for a complete rupture. The calculated flow is assumed to be 82% of the theoretical discharge from a long nozzle running full and without flashing prior to discharge. A change in inventory will occur in the flash tank, since liquid level is controlled in all the remaining vessels of the intermediate system. The change in inventory will be equal to the primary system leakage. For a single tube rupture, the leakage is less than one-half of the total intermediate feedwater rate. A rise in reboiler level will cause a valve on the line to the affected cooler to close partially and decrease the intermediate feedwater rate by the amount of leakage. Hence, the reboiler associated with the leaking drain cooler is still fed an equivalent amount of feedwater as prior to the rupture. Discounting the small amount of flashing, the feed to the affected reboiler is saturated and the steam generated still remains essentially as before. Therefore, for a single tube rupture the inventory increase in the flash tank will be approximately 209 gpm based on a temperature of 278°F. With the 1000-gal flash tank normally operated at one-half of its volume capacity, the elapsed time between rupture and complete filling is approximately 2.5 min.

As the primary system is being depleted by an amount equal to the leakage, an inventory change will occur in the deaerator, since it is the only vessel in the primary circuit where water level is not normally controlled. During operation, 1000 gal are stored in the deaerator; thus,

the stored water will be depleted in about 5 min for a single tube rupture. Low water level in the deaerator will result in pump cutoff, which in turn will initiate reactor shutdown. In the event the pump interlock fails, reactor level will begin to drop approximately 5 min after drain cooler-tube rupture. In approximately 7.25 min after a single drain cooler-tube rupture, reactor low water level will initiate reactor shutdown, this being based on a 2-ft (575-gal) drop in water level which will result in uncovering of the top shroud. Rate of inventory change in the deaerator is directly proportional to leakage; rate of change of inventory in the flash tank is directly proportional to leakage up to, but not exceeding, the intermediate feedwater rate to the one bank of the drain coolers affected.

A $\frac{3}{4}$-in. tube rupture in one of the primary reboilers will result in a maximum possible steam flow of approximately 210 lb/min into the intermediate system. Although the pressure drop across the rupture is 210 psig, the calculated flow is based on critical flow; the actual flow will be slightly less. Since negligible leakage will occur from the direction of the water box, the amount of primary steam escaping to the intermediate system is based on flow from a single nozzle. Steam leakage in the reboiler will cause the associated valve to close partially. As a result, the flash tank will fill up at a rate equal to the leakage and the deaerator level will decrease by a like amount. Changes in inventory are not as great for ruptures involving steam as for ruptures involving water. It is not expected that the intermediate steam pressure will rise because of one reboiler-tube rupture. Other than radioactive carryover, the main difficulty is the change in flash tank inventory; however, safety valves have been provided on the flash tank to relieve pressure.

SECTION XII

OPERATIONS, HAZARDS AND CONTAINMENT

A. Heineman
D. Rossin
E. Wimunc

NOTES AND EDITED DATA FROM LECTURES - July 13 and 14, 1961

SECTION XII

OPERATIONS, HAZARDS AND CONTAINMENT

I. Operational Aspects and Emergency Procedures*

A. Operation

During the design and construction of the EBWR, the three Project Engineers responsible for Instrumentation and Controls, Building and Reactor Components, and Power Plant and Associated Equipment reported directly to the Project Manager. Each of the three groups was responsible for the design, approval, field inspection, final checkout of the equipment, and for writing the operating procedures for the respective area. These procedures were compiled and, in November 1956, were published in the Operating Manual, which served as the textbook during on-the-job training of the operators. The staff personnel involved in power equipment and instrumentation development became the logical candidates for operating supervisors. The five senior operators initially assigned to EBWR had experience with CP-2, CP-3, and CP-5.

There were no critical experiments run prior to the actual loading of EBWR, which began November 26, 1956. Nineteen subcritical tests were made until criticality was reached on December 1, 1956, with 81 fuel assemblies in the vessel. Three weeks of intensive experimentation followed to arrive at a final loading which would provide the most practical void vs reactivity effect and give the proper amount of excess reactivity to overcome fission product poisons. On December 23, 1956, the first power run was made. At that time, the reactor was operated by staff members having experience with the BORAX projects. Within a few months the plant was turned over to the Reactor Operations Division for routine operation around the clock.

A group consisting of the Project Manager, Project Engineers, Group Leaders, and the Reactor Operations Division Director met weekly to develop the early experiments to be run. However, a number of the original staff members have left Argonne, and a precise routine for conducting tests has been established. The Project Manager approves the written requests of experimentalists or, if necessary, can refer the requests to a Project Group which, in turn, renders a decision or seeks advice from the Reactor Safety Review Committee.

Failures in EBWR performance to date have been due almost entirely to defects in the mechanical equipment purchased. For example, there has been condenser-tube failure, turbine-blade failure, and feedwater pump-bearing failure.

---

*E. A. Wimunc

While there is always a concern about radiation levels near a reactor, there has been no problem during operation of EBWR. The areas inside the containment shell have been found to be areas of low background, and personnel have been able to work for 8 hr without receiving any appreciable exposure. Higher-radiation areas have included the control rod drive room, the reactor steamline to the drier due to N^{16}, and the purification filters. At Argonne a special department effectively handles the problems of radioactive waste.

During fuel-loading operations, five men work over the reactor while one remains in the control room and a Health Physics representative monitors the area. Under the "cocked rod" philosophy, the control rods are positioned at ~25% of the cold critical rod setting used during the previous fuel loading. Hence, unexpected rises in fission rates can be subdued by a reactor scram. In preparation for 100-Mw loading, all fuel elements were removed and transferred to a storage pit. The racks in the fuel-storage well include poisons, and the pit is monitored to assure there will be no critical concentrations. Handling of the spike elements requires the utmost care to insure there will be no accumulation of a critical mass outside the reactor.

The reactor operating rules are spelled out in the Operations Manual and Hazards Report. The Operations Manual is revised periodically in order to keep it up to date.

IMPORTANT DATES IN EBWR HISTORY

May 27, 1955	Construction started.
December 1, 1956	First critical achieved.
December 23, 1956	Construction completed, and first power produced.
December 28, 1956	First achievement of design power level of 20,000 kw.
December 29, 1956	First generation of electricity at the rated power level.
February 9, 1957	EBWR is dedicated and put "on the line" as the nation's first reactor to produce large-scale daily quantities of useful power. EBWR has been producing 5,000 kw of electricity, which supplies most of Argonne's daily power needs.
December 2, 1957	Doubling of the operating power level from 20,000 to 40,000 kw with no change in the number or arrangement of fuel elements within the core.

December 23, 1957	More than doubling the operating power level from 20,000 to 50,000 kw with no change in the number or arrangement of fuel elements within the core.
March 20, 1958	More than tripling the operating power level of EBWR from 20,000 kw to 61,700 kw with no change in the number of fuel elements within the core. The three increases have opened the door to substantial reductions in the cost of producing nuclear power.

B. Emergency Procedures

The term emergency procedure carries the connotation of action which is vigorous and prompt. Yet this action should be carefully considered and planned so that it will not enhance the seriousness of the emergency and so that "the cure may be worse than the ailment." In the case of nuclear plant and reactor emergencies, the presence or possibility of release of radioactive materials in various forms or states which may be toxic or otherwise injurious to people at the site of the emergency or in the surrounding area is a consideration of major importance in determining the appropriate action. Other considerations are damage to valuable parts of the nuclear installation and extended loss of operating time as a result of employing improper emergency procedures.

Since action should be prompt, the emergency procedure should be as direct and uncomplicated as possible. In general, this would involve manipulation of selected control devices, use of designated emergency equipment, evacuation of certain areas, retreat to established shelter areas, and consultation on further action to be taken. The emergency procedure for a nuclear installation should thus chiefly differ only in detail from the normal close down of operation when the plant or reactor installation is to be left remotely attended. This means mainly omission of time-consuming steps and unnecessary entrances into doubtful or unsafe areas, along with a minimum of added steps.

In the case of the EBWR nuclear installation, the emergency procedure is to be initiated and carried out by the Chief Reactor Operator or Shift Supervisor and the other reactor operators under his supervision when the occasion calls for it. All operators are expected to be familiar and practiced in the normal shutdown procedures. They are also expected to be well versed in this Emergency Procedure so they thoroughly know the steps in their proper order.

In the event of an emergency condition, a shutdown of the EBWR is to be executed with the following changes and additions from a normal

shutdown procedure. Examples of emergency conditions would include a reactor incident (runaway, etc.), major steam or reactor coolant release, explosion, fire or notification of an Air Raid Red Alert.

Exceptions from Normal Shutdown for Emergencies:

1) Shutdown with the "Plant Shutdown" pushbutton will close air inlet and exhaust valves, site steam valve, instrument air to Reboiler Building solenoid valve, and Reactor Steam to Reboiler Building valve. In addition, this will produce a reactor scram. (The shutdown is not to be delayed by decreasing the generator output, as is normally done.)

2) Immediately make an announcement over the "P.A." system to evacuate the plant. Repeat the announcement three times. An operator designated by the Shift Supervisor will now check the Plant Sign-in sheet to ascertain that the evacuation is complete.

3) (a) 20-Mw Operation
Shut down the turbine plant feedwater pump.

(b) 100-Mw Operation
Shut down the reboiler plant feedwater pump and turbine plant feedwater pump.

4) Eliminate those normal shutdown procedures which require entrance into the containment shell until a proper survey of the situation can be accomplished.

5) Do not close the steam stop valve to the turbine. Close the Primary Reboiler Steam Stop valve. Close the reboiler plant feedwater-regulating valve. Close the two motor-operated shut-off valves in the Reboiler Condensate return lines. Shut off the fans for the air-cooled heat exchangers and shut down the intermediate feedwater pump.

6) If all nine control rods do not return to their Full In positions, energize the "Control Boric Acid" system to inject boron solution into the reactor vessel.

7) Should the reactor power level begin to increase after the control rods have been inserted, the High-pressure Boric Acid system pushbutton should be depressed to inject boron solution into the reactor vessel.

Additions to Normal Shutdown Procedure:

1) Notify a designated supervisor of the emergency by use of the P.A. system or phone, and dial 13 to report name, location, nature of emergency, and request the type of assistance required.

2) In the event of an Air Raid Red Alert, a warning or maximum of one-hour notice announced by a 3-min warbling signal over the public address system. Evacuate to the air raid shelter after (a) emergency shutdown, (b) turning off lights, and (c) closing windows. Turn off ventilating equipment in the service basement where the air raid shelter is located. Air Raid Yellow Alert, as announced by a 3-min steady signal over the P.A. system, will allow time for normal shutdown.

3) In the event of a fire, sound fire siren.

4) Open manual valve to building spray system if type of emergency will cause a rise in plant enclosure pressure to 4 psig.

5) If conditions warrant, it may be necessary to evacuate the service building.

In any emergency, reactor operators will wear "Scott Air Paks" inside the air-lock area until it can be established that there is no danger from air-borne radioactivity. Additional action will be based upon analysis and diagnosis of the emergency by Laboratory experts, which include the Reactor Supervisor, the Division Director, representatives from the Industrial Hygiene and Safety Division, the Fire Protection department, and other divisions of the Laboratory. Practice Air Raid and Evacuation Drills do not require the reactor and plant to be shut down. Two operators must remain in the control room during such practice drills.

II. Safety and Hazards*

The AEC has established a definite routine for the review of safety procedures. The Advisory Committee for Reactor Safety (ACRS), a statutory body reporting directly to the Commissioners, is the highest level AEC safety review group. It is composed of about 50% university representatives and 50% industrial and national laboratory representatives, and usually meets monthly or bimonthly. In view of the number of safety reports submitted to the AEC, a permanent organization, the Reactor Hazards Evaluation Branch (RHEB), was set up. Until recently, it initially reviewed Hazards Reports and other material, and submitted to ACRS only the more difficult questions. Often safety reports were initially routed through local AEC operations offices which could usually resolve the minor problems. Since the SL-1 accident and the Fermi reactor decision by the Supreme Court, the AEC has been drastically reorganized. To prevent internal pressures from being applied on safety review bodies, the Licensing and Regulations Division is no longer tied to the Reactor Development Division but reports directly to the Commissioners.

Within Argonne Laboratory there is a local review committee which must approve every paper concerning safety before it is forwarded to the AEC.

---

*A. D. Rossin

Project Managers can always call on the committee for advice. Once a Hazards Report is approved, it becomes the "bible." Any deviation from the procedures established therein must be approved by the AEC. Professional reputation, as well as the possibility of future licensing and contractual difficulties with the AEC (rather than legal sanctions), ensure compliance with the Hazards Report. Thus far, Hazards Reports have defied codification, although there has been a move toward codification. It should contain a description of the site and equipment, important elements of operating procedures, and an analysis of possible hazards, including a "maximum credible accident" which occasionally assumes conditions beyond the realm of realistic thinking.

A possible hazard concerns malfunctions which could lead to fuel-element failure and release of fission products. What could cause failure of a fuel element? Corrosion or sudden excursion. What could cause an excursion? Sudden control rod withdrawal or dropping fuel elements during loading. A step-by-step analysis is carried out, examining the cause and effect of each accident considered.

The shutdown requirements for EBWR are stated in the new Hazards Report, ANL-5781-Add. (Rev.), now being reviewed by the Atomic Energy Commission. While this report refers to the forthcoming high-power experiments, which will use the Core 1A loading, the requirements are currently in effect. Reactivity worths for the 20-spike loading now in the reactor can be inferred from the "Analysis of Core 1A" (see ANL-6305). Shutdown margin must be sufficient that the reactor will be subcritical with any single control rod fully withdrawn. When the revised addendum is approved, this requirement may be satisfied with the addition of boric acid poison to the system. In that event an additional rule applies: the reactor must be able to remain subcritical with all nine rods fully inserted and no boric acid in the reactor vessel.

During the current shutdown, all the drawings of the electrical system are being checked against the actual circuits and brought up to date. The operating Manual for EBWR presents detailed descriptions and references for operation and maintenance of the system. This new revision is in preliminary form and necessary changes will be added by memoranda to the working copies used by the operating staff. During the current period of modifications and experimental work, the organization and lines of responsibility are established by the Project Manager with the approval of the Division Director. A test procedure is written, reviewed, approved, and circulated to all persons concerned (including Shift Supervisors) before any experiment can be performed. A memorandum is issued to all Shift Supervisors prior to any core changes describing their extent and their significance. The Project Manager is designated by the Division Director and has primary responsibility for all activities which take place at EBWR.

III. EBWR Containment*

A. General

Containment for a nuclear reactor comprises a basic gas-tight vessel, whose integrity must be maintained in the event of the most disastrous incident assumable under operating conditions and the means by which this integrity is maintained. The problem therefore resolves itself into two definite phases. The basic problem, the containment vessel, will be discussed first; and the prevention of destruction of the integrity of the vessel will be taken up later.

B. Containment Vessel

The design of a containment vessel for a reactor system must result from consideration of many factors. Among these factors are economics and space requirements, possible external pressure as affected by anticipated operation of vacuum relief valves, and possible internal pressure which might result from system rupture caused by component failure, a primary pressure excursion, or a violent fuel-coolant chemical reaction with attendant complete release of coolant largely in the vapor state and possible further energy release by ignition of gases resulting from a fuel-coolant reaction.

The containment vessel for the EBWR was designed to house the reactor proper, the spent-fuel storage well, and the steam power plant and its related auxiliaries. Cooling water for the main condenser and auxiliaries enters and leaves the shell through welded openings in a separate closed circuit, so that the cooling tower could be located outside and operated in the conventional manner. Since all design parameters are interdependent, when one is varied all others may be affected; selection of dimensions, volume, and configuration become a rather difficult compromise. For EBWR the size and configuration were based largely upon economic and space considerations. A cylinder, 80 ft in diameter, with a hemispherical top head and hemi-ellipsoidal bottom head and having a total height of 119 ft, was chosen. The total net volume of the building is about 400,000 ft^3. Details of the containment shell construction are shown in Fig. XII-1.

Experimental work at Argonne National Laboratory and by others, although insufficient in scope to be conclusive, had indicated early in the design of EBWR the possibility that a portion of the component metals of the core in the reactor might react violently with water, provided the metal was at a temperature above its melting point. In most experiments, a fine dispersion was also required for reaction. Since it is inconceivable that more than a small percentage of the core metal might reach these conditions of temperature and dispersion at a given moment, designing for a 25 per cent reaction was adjudged to be sufficiently conservative. To

---

*A. Heineman

contain the volume of steam and gas which would be released in a 25 per cent core metal-water reaction with attendant rupture of the primary water-steam system, the containment shell was designed for an internal pressure of 15 psig. In calculating this design pressure, consideration was given to the circumstances under which the hydrogen displaced by the metal is released. This release necessarily takes place in a steam atmosphere, and the mixture of steam and hydrogen escapes through the breach in the primary system. This would effectively blanket the hydrogen as it diffuses with the building air contents. At worst, if ignition temperatures are encountered by the hydrogen, it would burn in small, spasmodic bursts with correspondingly slight shock-wave effects. The energy released by ignition of all hydrogen in such bursts is included in the calculation, even though their occurrence is quite remote. If now such burning occurs during diffusion, the danger of a hydrogen explosion is eliminated at equilibrium by reduction of the hydrogen concentration below the inflammable range.

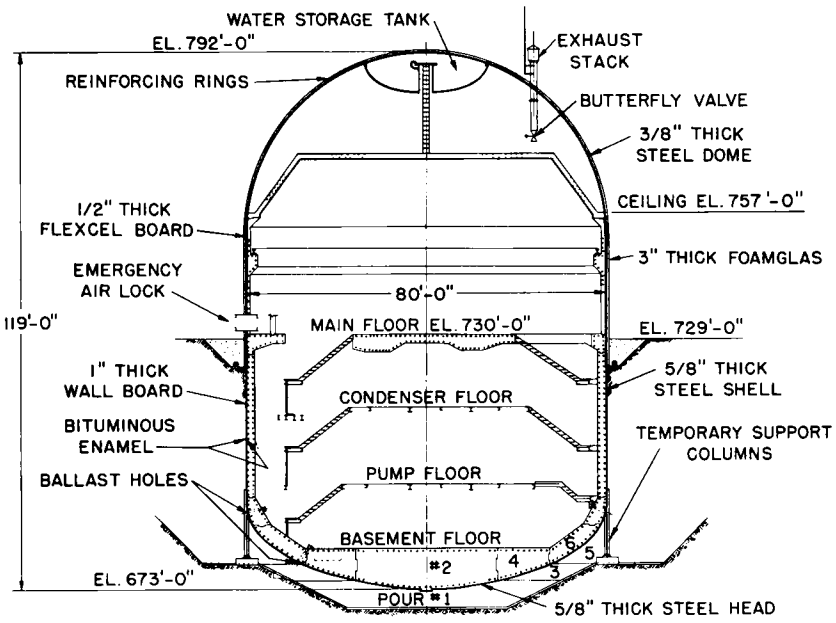

Fig. XII-1

EBWR Containment Shell
111-4846

The present core (Mark IA, with oxide fuel) has only a small amount of additional metal as compared with the 20-Mw cores, so that the foregoing applies very closely to the existing, current conditions. In case that a 100-Mw core is installed in the future with metallic fuel, the amount of metal would be roughly doubled over that contained in the 20-Mw cores. The containment capability would be reduced to approximately that of a 13 per cent metal-water reaction.

The cylindrical portion and bottom head of the shell are of $\frac{5}{8}$-in.-thick steel plate, and the top head is of $\frac{3}{8}$-in. plate. The design conforms with the requirements of the ASME Pressure Vessel Code Section VIII for welded construction. The rules in this section of the code which apply to nonradiographed, nonstress-relieved vessels were also followed for control of quality of materials, fabrication, welding, and inspection, as well as the pressure-strength test. However, it was not required that the code stamp be affixed to the vessel. The material selected for all pressure-stressed members conforms with the ASTM-A-201, Grade B, Firebox quality specifications and was produced in accordance with the ASTM-A-300 specifications with V-notch Charpy test at -50°F for specimens taken in the rolled direction. We were aware that the Charpy tests are not necessarily a good criterion for ductility when materials are stressed biaxially. Up to the present time, however, there have been no other criteria developed which are recognized in the United States as standard practice. In addition, spot-test radiographs were made of approximately 10 per cent of the total length of the welded seams. A large proportion of these were made at weld junctures since improper fusion is most likely to occur at these points. Wherever faults were shown, they were traced to their vanishing points and if necessary, cut out and rewelded, and new radiographs taken.

For construction and test purposes, the shell was supported on temporary columns attached to the lower end of the cylindrical portion. The excavation provided about 4 ft of minimum clearance under the bottom head for access for welding, radiographing, and testing for leaks. As described farther on, the space below the bottom head was filled with bulk concrete out to the radius of the cylindrical portion of the shell and up to about 2 ft below the tops of the columns. After a sufficient curing period, a section of each column was cut out above the concrete, thus transferring the entire load of the shell and power plant to the concrete slab underneath. Cutting of the columns eliminated the possibility of damage to the shell in case of differential settlement between column footings and the slab. Prior to testing, all welding on the steel shell was completed with the following exceptions: the personnel access and emergency escape air locks and their reinforcing had not been installed; the permanent freight door and its reinforcing had not been installed; the temporary closure for the ballast openings in the bottom head were left in place for future permanent welding; holes through the shell for the cable pans and temporary closures for all other penetrations were not cut out and were left for future permanent closure; and the large temporary access openings were not cut out and were left for future permanent closure. We do not recommend testing prior to installation of large components, such as airlocks and freight door. These items were not completed in time for the test, and in the interest of expedition, the test was conducted as described.

It is worth mentioning at this point that with the ballast openings in the bottom head closed and the welding complete, it was necessary to have a man on hand 24 hr/day and 7 days/week as a precaution in case of heavy

rains which might flood the excavation to a point where flotation of the vessel would occur. This might happen if the accumulation rate exceeded the capacity of the temporary pumping equipment, or in case of pump or power failure. In such a case, a ballast opening would have to be cut out.

C. Containment Vessel Pressure Test

The pre-acceptance tests on the Power Plant steel shell were made in the following sequence: (1) The shell was pressurized by four portable compressors to approximately 10 psig. (2) A gate valve in the temporary inlet line was closed and the compressors stopped. (3) All welds in the shell were painted with a thick soap solution and observed for bubbles or dry flaking, which would indicate air leaks. No leaks were found by this method. (4) The pressure was increased to 18.75 psig (25 per cent over the design pressure) for the pressure strength test. (5) The valve was then opened to depressurize the shell preparatory to the leakage-rate test. (6) The temporary manhole in the side wall of the shell was opened and the following equipment was installed:

a) Ten thermocouples were wedged against the inside surface of the shell.

b) Eight resistance-thermometer elements were suspended in the air space.

c) Three dew-point cells of the high-level alarm type for determining the approximate relative humidity of the contained air were placed in the air space.

d) Six blowers were placed at various locations inside the shell. The total capacity of these blowers (9,700 cfm) was sufficient to recirculate the entire building contents (497,500 ft^3) in a little less than one hour. The amount of air motion produced by the blowers proved sufficient to reduce stratification to a tolerable degree during periods when reliable readings could be obtained.

Figure XII-2 shows the location of the instrumentation and blowers in the containment shell. Thermocouple readings were made in the conventional manner by means of a manually adjusted potentiometer and calibration table. Resistance-thermometer readings were made by means of a calibrated Wheatstone Bridge with all elements and their leads calibrated in connection with the bridge. Alarm signals from the dew-point cells were received by their own commercial instruments. Pressure readings were made with a mercury manometer, and readings from a mercury barometer were added to those from the manometer to obtain total absolute pressure. The manhole cover was replaced, the shell was again pressurized to approximately 15 psig, and the valve closed. Temperature and pressure readings were taken over a period of eight days at approximately

2-hr intervals. Readings were converted (by means of Boyle's and Charles' laws) to terms of volume of dry air at standard temperature and pressure within the building, taking into account the variations in building volume by metal expansion and contraction, and the variation of water (or ice) vapor pressure with temperature.

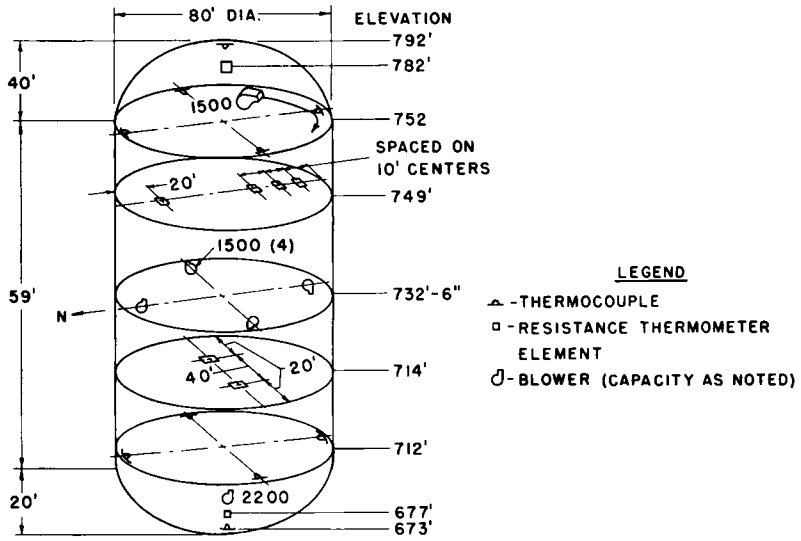

Fig. XII-2

Location of Instrumentation and Blowers
for EBWR Steel Shell Leakage-rate Test
111-4839

In determining what might be considered as reliable readings during the leakage-rate test, several factors were taken into consideration. All erratic readings (except one) occurred at times when the shell temperature was very high or else when the shell temperature was changing rapidly. Both of these conditions might be expected to give unreliable results for the following reasons:

1) When the temperature is very high, the moisture in the air is not saturated; thus, since the relative-humidity instruments gave only approximate indications, water vapor pressure could not be corrected for. If saturation were assumed, an overcorrection would result.

2) When the temperature is changing rapidly, there can be no assurance that the arithmetical average from the several resistance-thermometer elements is indicative of the true average air temperature.

It was decided, therefore, that only those readings which complied with the following limitations would be considered reliable:

1) No readings were considered valid when the average shell-metal temperature was higher than 50°F.

2) No readings were considered valid when the average shell-metal temperature differed by more than 4°F from the temperature read 2 hr before or after the reading in question.

Calculated volumes of dry air are shown plotted against time in Fig. XII-3 only for those readings which satisfied the above limitations. The specified maximum allowable leakage rate was 500 ft^3 of air at STP per 24 hr.

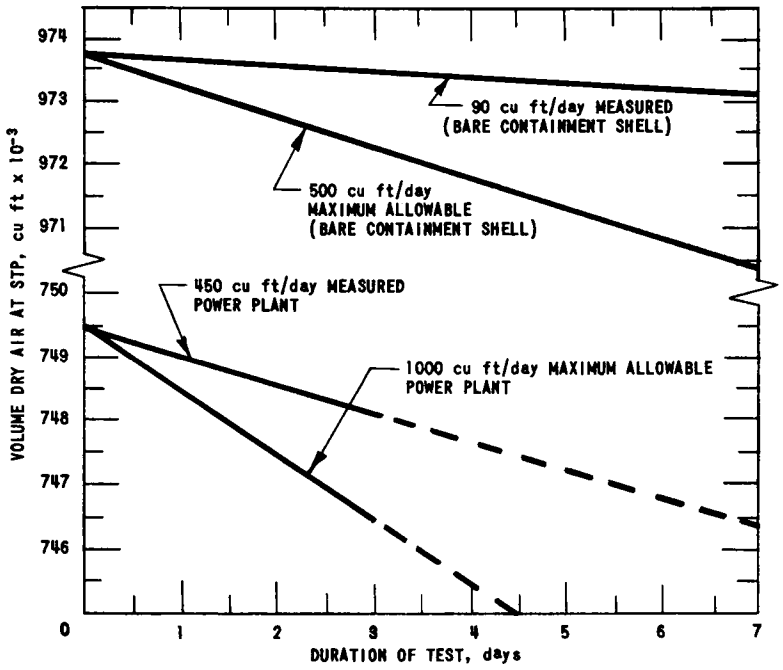

Fig. XII-3

EBWR Containment Leakage-rate Data
RE-7-35391-A

The specifications further stated that a second soap solution test might be omitted provided the indicated leakage rate was less than 100 ft^3 per 24-hr period. Inasmuch as the actual leakage rate was less than 500 ft^3 and might be interpreted as somewhat less than 100 ft^3 per 24 hr, the second soap test was terminated when about one-half complete in order to permit subsequent construction to proceed. (Since the time of the test, a curve fitted by the least-squares method shows a rate slightly less than 100 ft^3/day.)

One of the safety features incorporated in the design of the power plant building is a general sprinkler system by means of which all

areas in the plant may be sprayed with water. This sprinkler system would be used in the case of an accident which liberated radioactive gases or steam within the building and would serve to hold down or reduce pressure, temperature, and contamination of the atmosphere in the building. To insure infallibility of water supply, a 15,000-gal storage tank is provided under the top dome of the building shell. This tank is supported by the top dome structure which consists of $\frac{3}{8}$-in.-thick plates with light reinforcing rings which are located in the area immediately surrounding the tank within a radius of 21 ft 4 in. The radius of the tank shell where it attaches to the dome is 13 ft 8 in.

Since the power plant building is constructed approximately one-half below grade, there was danger of flotation of the shell during construction in case of heavy rains. At all times, except during the pressure and leak tests, ballast holes in the bottom head were left open. The lower set of holes were left open until the first two inside concrete pours were completed. These lower holes were then closed and permanently welded. The upper holes are about 24 in. below the tangent line of the bottom head and are equipped with short pipes which extend inward beyond the inner face of the concrete. These holes were left open until all concrete was poured inside the building, at which time they were permanently welded closed. Concrete pours and backfilling were sequenced to minimize distortion of the shell. No. 1 pour was made outside, under the bottom head, and contacted the head to a radius of 16 ft 6 in. from center line of building. No. 2 pour was made inside up to basement floor elevation and out to radius 16 ft 6 in. No. 3 pour was outside to radius 27 ft and No. 4 pour was inside to this same radius, and so on. The pouring sequence is indicated in Fig. XII-1.

Corrosion protection of the shell below grade, both inside and outside, was provided by applying two coats of bituminous enamel. To protect this enamel from abrasion on the outside during backfilling operations, commercial insulating board, 1 in. thick, was applied over the enamel and left permanently in place. Above grade the shell was painted on the inside with one field coat of bituminous enamel over the shop coat and $\frac{1}{2}$-in.-thick commercial insulating board was applied prior to pouring the concrete liner. The entire outside of the shell above an elevation 5 ft below grade was insulated with 3 in. of Foamglas impaled over studs which are welded to the shell. The joints between blocks were filled with mastic by "buttering" the edges before placing. A coat of mastic was then applied over the Foamglas and one ply of Glasfab cloth was pressed into the mastic on the cylindrical portion. On the top dome, another coat of mastic and a second ply of Glasfab were applied. A final coat of mastic was then applied over the entire insulated surface. The insulated surface was finished with two coats of aluminum paint.

Permanent access means for personnel through the building shell is provided by means of an air lock. The outer shell of the air lock, shown in Fig. XII-4, is cylindrical (approximately 10 ft in dia by 7 ft long).

The ends are closed by flat bulkheads with stiffeners attached to peripheral members consisting of curved 12-in.-diameter pipe. In each bulkhead there is a 3-ft x 7-ft clear opening hinged door which seals against a rubber gasket by means of a mechanical latching mechanism. The latching mechanism is geared to a valve which equalizes the pressures on either side of the bulkhead before unlatching. The latching mechanisms are interlocked so that neither can be operated unless the other is in the completely closed and latched position. A clutch is provided in the interlocking mechanism so that the interlock may be overridden by operation of a lever at the outside station of the outer door only. This lever is kept locked and would be used only when the reactor is shut down and it is desired that both air-lock doors be open at once.

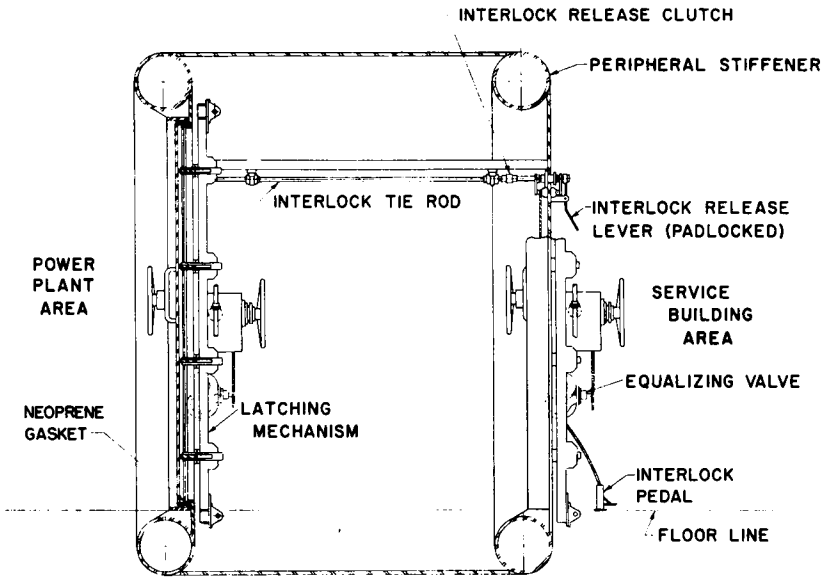

Fig. XII-4

Main Air Lock
111-4798

Permanent emergency escape and access means for personnel are provided in the form of an emergency air lock (see Fig. XII-5). The outer shell of the emergency air lock is cylindrical and approximately 4 ft in diameter by 6 ft long. The ends are closed by flat bulkheads, in each of which there is a 30-in.-diameter round door which seals against a rubber gasket by means of a mechanical latching mechanism. The latching mechanism is linked to a valve which equalizes the pressures on either side of the bulkhead before unlatching. The latching mechanisms are interlocked so that before the valve for one door opens, the other door latches and its valve closes. The valve for the first door then opens and the door is unlatched. For emergency access to the power plant, the outer door may be

opened by its outside operator. The lever inside the back is normally rendered inoperative for access to the inside by a padlock which holds a pin out of engagement with the operating shaft. The padlock may be unlocked and removed. With the operating lever in the fully latched position for the inner door, the pin may be engaged with the shaft. The lever may then be used to latch the outer door and close its valve, and then to open the valve for the inner door and unlatch the inner door.

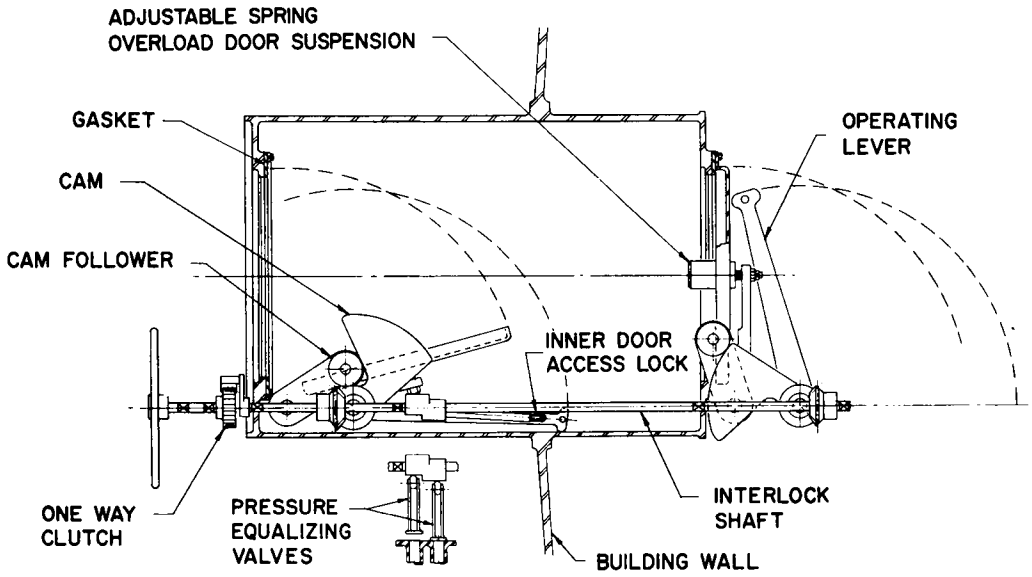

Fig. XII-5

Schematic of Emergency
Air-lock Doors for EBWR
111-4840

The steel shell of the power plant building is designed to withstand a maximum negative pressure of 0.5 psi. To prevent negative pressures exceeding this amount, two vacuum breaker valves are provided. These are 6-in. spring-loaded, single-port relief regulators with soft composition disks for tight shutoff. Each valve has a capacity of 100 cfm. They are set to open at 0.25 psi and have full relief at 0.50 psi. There is no relief valve for excessive positive pressure.

The power plant building is ventilated, heated, and air conditioned by means of four packaged units. Two of these units are located on the main floor near the outside wall, spaced at about 60° apart near the north centerline. They draw recirculating air from immediately below the main floor and discharge into the main floor area. One of these units also draws in fresh air from the outside, normally about 3000 cfm, which is mixed with the recirculating air through adjustable dampers. The other two units are located on the pump floor (Elev. 696 ft) near the outside wall,

spaced at about 30° on either side of the south centerline of the building. They draw recirculating air through vertical ducts which lead down from openings through the main floor; these units discharge into the pump-floor area. The air displaced by the fresh air drawn in through the air intake by the unit on the main floor is discharged through an exhaust stack. This stack exhausts from a point above the ceiling slab, and thence through the roof of the building.

To prevent outleakage of radioactive gases or dust, both the air-intake duct and the exhaust stack are equipped with automatic, tight, shutoff dampers. These dampers are weight operated and are held open by solenoid-actuated latches which release upon de-energizing to allow the dampers to swing shut. The dampers are actuated by radioactivity-monitoring instruments which are adjusted to act at a predetermined maximum activity level of the air leaving the power plant building through the stack. The dampers, therefore, close in case of accidents which cause high radioactivity in the building or power interruption.

There are various other permanent penetrations through the building shell for water, steam, air, and electric cables and control leads, etc., as shown in Fig. XII-6. Pipelines were welded directly to the shell where they passed through. Sizes of 2 in. and under were welded without reinforcement, whereas lines larger than 2 in. were reinforced in accordance with ASME Code requirements. Control leads were brought through Amphenol "spark plug" type connectors which were mounted in Micarta phenolformaldehyde-laminate disks. The connectors are sealed individually with gaskets and threaded collars, inside and outside, and with a sealing cement. The Micarta disks are sealed with gaskets and pipe flanges bolted to the reinforcing rings around the openings in the shell. The generator cables were led through pipe sleeves welded through the shell. The space between the cables and the sleeves was filled with a transformer compound and the outer ends were blocked by filling a box built around the sleeves with Epoxy resin. The ends of the cables were sealed by dipping in a rubber sealing cement to prevent internal leakage through the cables. All other electrical and thermocouple leads were run through cable troughs. The troughs were then blocked by filling with hard setting sealing compound, and the ends of the troughs were then filled with soft compound and a final layer of Epoxy resin to restrain the soft compound. The ends of all cables were sealed by dipping in rubber sealing cement.

For access during construction, two large temporary openings were cut through the shell. One of these openings was located to give access at the main floor elevation. This opening was approximately 12 ft wide by 18 ft high to accommodate the largest subassembly component, the condenser. The other temporary opening (5 ft wide x 10 ft high) was located approximately midway between grade level and the extreme bottom of the shell. A short bridge from the service building footing excavation provided

access to this opening. In fact, this was the only access for construction until backfilling was completed to provide a ramp to the larger opening above. After these openings had served their purpose, the sections of plate which were cut out were replaced and the openings welded closed.

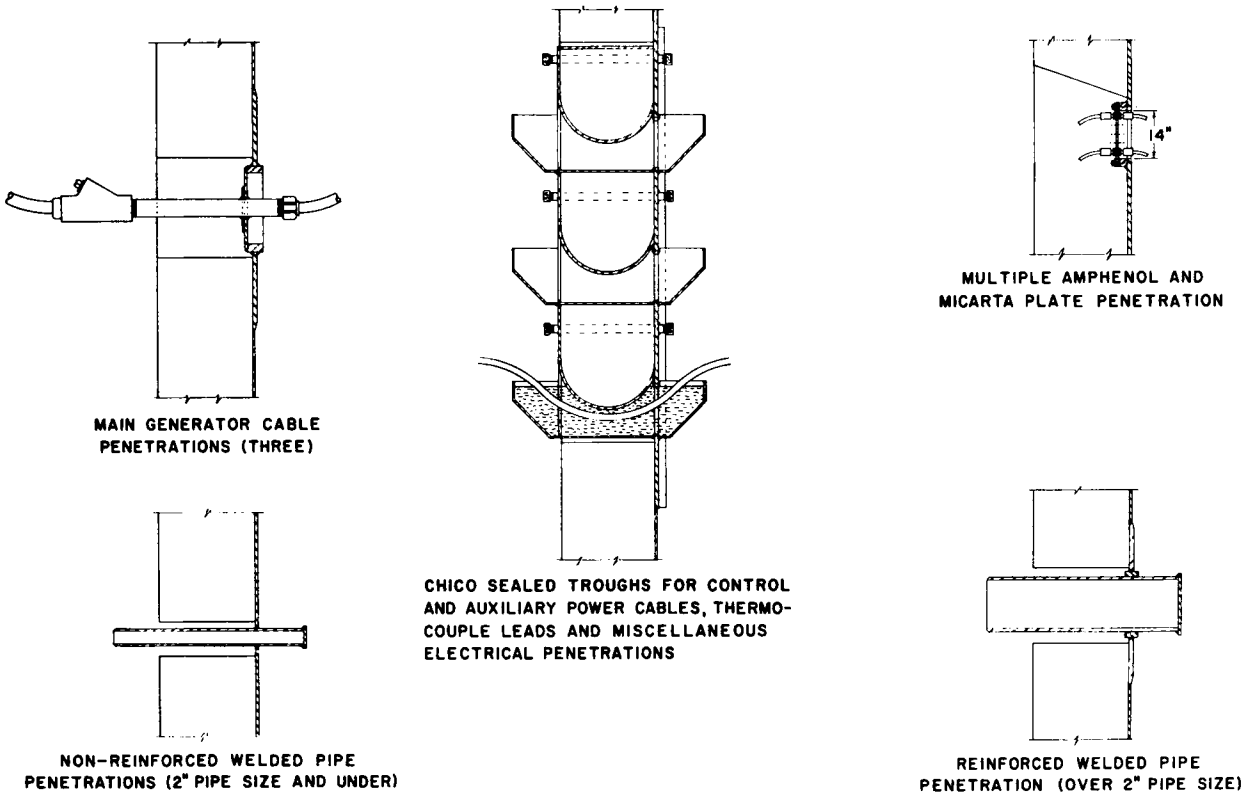

Fig. XII-6

Power Plant Shell Penetrations
111-5151

After all construction work had been completed and power plant components and piping, reactor and shield, wiring and instrumentation were complete and the plant ready to operate, a final pressure test and a leakage-rate test were conducted. Instrumentation for the leakage test was somewhat similar to that for the previous, bare-shell test. However, it differed in a few important points. The shell-metal temperature was not measured, since most of its area was buried, or lined with concrete, or insulated, rendering it difficult of access, but also relatively insensible to expected temperature effects. The air temperature was measured with thermocouples instead of resistance-thermometer elements. The pressure was monitored by means of a single absolute manometer (tall barometer) with a scale long enough to read the total absolute pressure. A description of this barometer and how it functions is given at the end of this paper. The instrumentation was set up, the air conditioning was turned on for circulation, and the shell was pressurized to 15 psig. All new welds were tested

for leaks with soap solution, and all cable penetrations, air-lock shafts and gaskets, etc., were tested by the same method. All detectable leaks were repaired where possible or reduced to a negligible amount before measurements for the rate test were started. From this final test could be seen the vast improvement in accuracy of the data as compared with the previous test and a leakage rate of approximately 450 ft^3 per 24 hr. The allowable leakage as prescribed in the specifications for the completed building is 1000 ft^3 per 24 hr ($\frac{1}{4}$ of one per cent of net building volume). Based on these results the building was found acceptable for operation of the reactor (see Fig. XII-3).

The above figure for allowable leakage is a rather arbitrary one. In the first place, a measurable amount had to be chosen. Measurements of this sort for a vessel of this magnitude are difficult. For example, an error in pressure reading of 0.15 mm Hg or an error in temperature reading of 0.045°F, is equivalent to about 100 ft^3 of leakage. The figure chosen was believed to be about as small as could reasonably be detected with credence. However, it seems reasonable that a rate of $\frac{1}{4}$ of one per cent should be acceptable from the standpoint of safety. Normally, the sprinkler system could be turned on to reduce the pressure within a few minutes to a value representing the added volume of noncondensables released by a metal-water reaction. This is a small fraction of the total rise which is largely due to steam. The leakage rate would be much smaller than the stated allowable and it would continuously diminish as leakage progressed. At worst, the sprinkler system might fail and it would require a few days for the steam to condense. However, the leakage during this period would average about one-half the initial amount and would be of the order of one per cent of plant volume if it required as long as eight days for the steam to condense. From this time on the conditions would be about the same as in the previous case after cooling.

There have been subsequent leakage-rate tests about once a year. Each of these tests has shown a leakage rate of less than 1000 ft^3 per 24 hr.

D. Prevention of Destruction of Containment Integrity

In order to formulate design parameters for missile containment to prevent destruction of the integrity of the air-tight shell, the physical arrangement of the several main components of the power plant was established as follows: The reactor vessel was located completely below the main operating floor with its top closure flange 24 in. below the finished floor line. The turbine and generator, of course, were located on the operating floor, with the condenser suspended immediately below the floor. All other components of the steam plant and cooling system were placed below the operating floor.

Calculations for a 25 per cent metal-water reaction in the reactor indicated a total energy release of 2.18×10^6 Btu. Inasmuch as there were insufficient data from which to establish a probable time of release of the energy from this type of reaction, the ultraconservative assumption was made that the release would be of the order of a TNT explosion. This information was turned over to the Armour Research Foundation, who made a study to determine the forces which might be developed, their areas of application, and the sequence in which they would be applied. The results obtained from this study are shown in Table XII-1.

Table XII-1

DYNAMIC LOADING AND LOADING SEQUENCE FOR INTERNAL EXPLOSION EBWR REACTOR VESSEL

Area	Shock Wave Pressure, atm	Arrival Time, msec	Duration, msec	Damage
Vessel Wall below Water Level	40,700	+1	2	Rupture
Bottom Head	13,800	+1	2	Rupture
Vessel Wall above Water Level	260	Varies	6	Upper portion remains intact
Vessel Cover	260	+5	6	Remains intact
Lower Portion of Biological Shield	-	-	-	Reduced to rubble
Bottom Shield Plug	-	-	10	Reduced to rubble

The following conclusions were drawn from this analysis:

1) The upper portion of the vessel and the vessel-cover and bolting would not fail. This conclusion is based on the indicated low intensity of the shock wave above the water line, and, although the equivalent pressure is about 3800 psi, when credit is taken for the high strain rate involved with its dynamic load factor, that the equivalent static stresses are well below the ultimate strength of the materials involved.

2) The lower portion of the vessel would fail by fragmentation caused by the shock wave, and the biological shield surrounding the lower part of, and underneath, the vessel would be reduced to rubble for a distance of about 10 to 12 ft from the center of the explosion source.

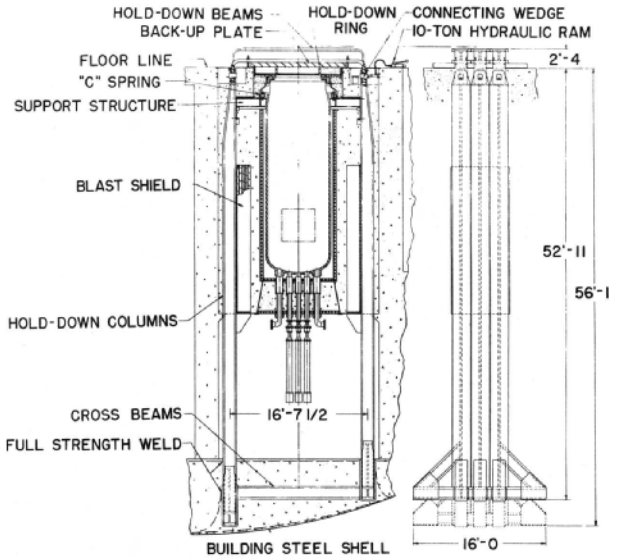

Fig. XII-7

EBWR Pressure Vessel Holddown and Blast Suppression Structure Details
111-4851

Consequently, a conical shield plug, about 8 ft 6 in. in diameter at the top and 10 ft at the bottom, was constructed below the reactor vessel, as shown in Fig. XII-7. This plug has a weak section around its periphery, so that early failure to start pressure relief would occur as soon as possible. This plug and the surrounding concrete shielding extend only 4 ft below the reactor and, according to the above conclusions, would all be reduced to rubble and blown downward into the subreactor room. Large openings are provided from the subreactor room to vent the vessel contents, which would thus be rapidly dissipated throughout the power plant. The basement floor slab is about 8 ft thick in this area and is heavily reinforced. This slab would easily stop the flying rubble and vessel fragments, and prevent shell penetration.

The biological shield which surrounds the vessel is octagonal, 25 ft from face to face outside. According to the Armour conclusions, the formation of rubble would stop short of the outside faces. However, sections of piping leading outward from the reactor vessel and removable concrete block shielding in tunnels through which these pipes are led are possible missiles which might be launched by an explosion. To protect the gas-tight shell from damage by such missiles, a 24-in.-thick concrete liner was formed against the inside in all areas below the main floor. Two conical sections of concrete approximate the contour of the bottom head of the shell down to the basement slab and maintain a minimum thickness of 24 in.

To protect against damage to the air-tight shell in case of turbine-rotor disintegration, it was necessary to determine the thickness of concrete or steel required to contain the most dangerous fragment which might emerge through the turbine casing. Assumptions based on the literature were used in making an analysis of the turbine rotor disintegration which occurred at Ridgeland Avenue Power Station near Chicago and to draw an analogy with EBWR. The findings in this analysis closely approximated the actual circumstances, and it was concluded that the values used are sufficiently reliable to use as a basis for an analysis of a hypothetical

rotor disintegration in the EBWR turbine. This analysis indicated that the most dangerous fragment which might emerge through the turbine casing is one-half of the heaviest wheel at a velocity of about 212 fps. This analysis also indicated that a 12-in. thickness of concrete or $1\frac{1}{4}$ in. of mild steel plate would contain this fragment.

Above the main floor, therefore, for a height of approximately 26 ft, the shell has a 12-in.-thick reinforced concrete liner. The ceiling slab at this height completes the concrete envelope. This slab has a $\frac{3}{8}$-in.-thick steel plate on the underside and is 12 in. thick. Intermediate support for the ceiling slab is provided by trusses spaced on 25-ft centers and equidistant from the centerline of the building. The portion of the ceiling slab between these trusses is elevated to the level of the top chord members of the trusses, and the trusses are embedded in 1-ft-thick walls of concrete with $\frac{3}{8}$-in. steel liners.

This configuration results in approximately 12 ft additional head room in the central 25 ft straddling the North-South centerline of the building. Nine openings (4 ft 6 in. in diameter) and a ladder hatchway provide venting through the ceiling slab. These openings have protecting slabs above them which overlap the openings sufficiently for missile shielding. There is no concrete liner for the shell above the ceiling slab.

Whenever openings occur in the concrete envelope, other provision is made for missile shielding: 1-ft-thick concrete walls protect the main air lock and emergency air lock, $1\frac{1}{4}$-in.-thick steel plates protect the freight door and the large temporary opening. A doorway through the concrete wall in front of the main air lock is closed by means of a $1\frac{1}{4}$-in.-thick plate, also. These plates are either removable or hinged depending on their size and/or frequency of use.

The remaining major problem is that of restraining the potentially large missile formed by the upper portion of the reactor vessel which, according to the Armour conclusions, would remain intact. The upward force on this section induced by the shock wave was calculated at 21,000,000 lb. The force is applied rapidly and for a very short interval, which implies high strain rate with accompanying low dynamic-load factor.

The system developed for restraining the upper portion of the reactor vessel has been termed the "hold-down" structure. Many configurations for this system were evolved, but they fell into two categories. One type employs columns spaced uniformly around the vessel, or a cylindrical shell, and a radial beam system, or a platen, spanning the top of the vessel. The other type employs parallel beams spanning the top of the vessel with columns clustered at either end.

Armour's analysis showed that any such structure within the biological shield would be subjected to lateral forces large enough to destroy

it, unless specific means were provided to protect the structure from these forces. The solution was a "blast shield." The necessity for a blast shield definitely indicated a preference for a hold-down structure consisting of parallel beams and clustered hold-down columns, since the area of protection was thus minimized. On this basis the final design was selected, namely, three parallel hold-down beams and two clusters of three hold-down columns at opposite sides of the reactor vessel. Figure XII-8 shows a cutaway view of upper hold-down structure arrangement.

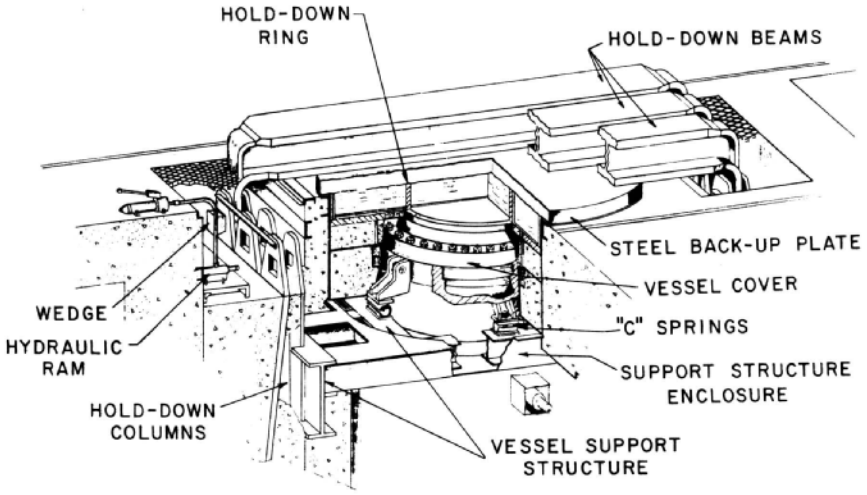

Fig. XII-8

Upper Vessel Structural Arrangement
111-4845

Armour conducted a series of compression tests to determine the optimum constituents of the blast shields. The final design comprises alternate layers of 3 in. of redwood and 1 in. of steel plate, repeated three times; and then alternate layers of 3 in. of Celotex and 1 in. of steel plate repeated twice as we advance away from the explosion source. The average density of this blast shield plus the steel columns is very nearly equivalent to the heavy concrete which is displaced thereby; thus, the effectiveness of the biological shield is not seriously affected. Armour calculations indicate that the intensity of the shock wave is decreased by approximately a factor of two through each layer of the softer material by conversion of a portion of the shock energy to heat energy. The residual material velocity is transformed into shock energy at each steel plate layer and the process is then repeated through the successive layers. By introducing five such steps, the resultant shock-wave pressure on the hold-down columns is reduced to a value which the columns can sustain. The upward force on the columns which occurs several milliseconds later can thus be restrained.

A biological shield was also required above the pressure vessel. A convenient design was evolved using a steel ring and a structural steel backup plate (6 in. thick) to transmit the upward force from the pressure vessel cover through the ring and the plate to the bottom flanges of the hold-down beams. The backup plate serves as a biological and missile shield, and distributes the upward force over a wide area on each of the three hold-down beams. The space below the plate within and around the steel ring is enclosed with lighter structural steel plate and filled to a depth of $11\frac{1}{2}$ in. with water to provide a hydrogenous biological shield.

In order to anchor the ends of the horizontal hold-down beams, the two sets of three parallel columns extend downward into the floor of the control rod room below the reactor. The concrete floor is not affected by the shock waves from a possible explosion. The shock-wave energy would be dissipated by passage through the various media from the reactor core and the air in the control rod room.

To develop the required anchoring force, the columns are welded to 16-ft-long horizontal anchor beams. These anchor beams are buried as deeply as possible in the concrete control rod room floor. Reinforcing rods are welded to the anchor beams so that failure of the concrete would be in shear along planes 45° from vertical beginning at the edges of the lower anchor-beam flanges. Failure strength in these planes exceeds that of the six columns.

The outboard anchor beam cannot be buried as deep as the inboard anchor beam because the bottom of the building is hemi-ellipsoidal. Two cross beams are used as compression members to keep the outboard anchor beam from moving inward and out from under the mass of concrete below the fuel-storage well.

To facilitate easy access to the pressure vessel cover, wedges are used to connect the horizontal hold-down beams to the vertical columns. Wells have been provided around the upper ends of the columns to accommodate a portable hydraulic ram to force the wedges horizontally into and out of position. The use of wedges also provides some vertical adjustment to allow for buildup of tolerances on the various parts being assembled. Four jack screws are provided in the bottom flange of each hold-down beam so that the bottom of the beam can be brought down to just contact the 6-in.-thick top shield backup plate. This minimizes impact loading of the hold-down structure due to spaces between components. The weight of the beam and the wedging force are resisted by the jack screws which bear on steel channels imbedded flush with the surface of the main floor concrete.

The three horizontal hold-down beams can be removed separately; their individual weights are less than the building crane limitation of 20 tons. The top shielding tank and integral backup plate must also be removed to gain access to the pressure vessel cover, and the weight was kept below the maximum allowable crane load.

E. Absolute Manometer

Pressure measurements beyond the accuracy of commercially available equipment were required. An instrument was needed which could be read to the required accuracy by any of several operators. A description of the manometers evolved follows:

These manometers are designed for pressures up to 70 in. Hg abs for the EBWR tests and 90 in. Hg abs for the EBR-II tests. For ease of filling, the top, or closed, end is sealed by means of a stop cock. Below the stop cock a glass capillary tube bent into a goose-neck is fused to the top of the main tube and the lower end of the stop cock. By pressurizing the mercury reservoir with argon or nitrogen, the mercury is forced up through the capillary and stop cock until it partially fills a small glass reservoir above the stop cock. The stop cock is then closed and sealed, and the gas pressure released slowly from the mercury reservoir.

The height of the mercury column is measured by means of a stainless steel rod cut accurately to a length about 12 in. short of the expected average pressure. Shorter rods cut accurately to length are used to extend this length to locate a sliding platform which clamps in place at 2-in. intervals. A micrometer height gage is clamped to this platform, and a reading sight is supported by this height gage by an accurately machined bracket. The height gage reads from 0 to 4 in.

A reading slot in the sight is accurately located, and consists of a wide portion at the center and very thin portions at the sides. The meniscus is thus able to eclipse most of the aperture suddenly as its crest reaches the top of the slot (the tops of the three portions of the slot are coincident). A small calibrated light bulb shines through the slot, and the intensity of the beam is sensed by a photoelectric cell at the opposite side. The signal from this cell is registered on a sensitive galvanometer which indicates the sudden near eclipse of the beam by a rapid fall of the pointer and gives a high precision reading of the meniscus level.

To zero the lower end of the measuring rod, a sharp point is formed at its lower end. A low-voltage circuit induced through the reservoir wall and the rod, via an indicating red light bulb, is made or opened as the sharp point touches or leaves the surface of the mercury. The usual adjustable plunger immersed in the mercury is used to raise or lower the surface until the red light flickers out by gently tapping on the reservoir.

These reading and zeroing means produce high accuracy and are repeatable to very close limits by almost any operator. Thus the human element is virtually eliminated from pressure measurement.

In considering types of pressure-measuring devices and their availability, differential manometers of the bidensity-biliquid type were discussed. However, the accuracy of this type of micromanometer depends on accurate dimensional tolerances which are difficult to achieve and maintain. Aneroid-type absolute instruments are available, but none was found which had an acceptable freedom from hysteresis errors.

SELECTED READING LIST

SELECTED READING LIST

SECTION I - Introduction

5th Nuclear Power Report, Electrical World (May 1960), p. 63.

SECTION II - History and Development of the EBWR

W. H. Zinn et al., Transient and Steady State Characteristics of a Boiling Reactor. The BORAX Experiments, ANL-5211 (1953).

J. R. Dietrich, Experimental Investigation of the Self-limitation of Power during Reactivity Transients in a Subcooled, Water-moderated Reactor. BORAX-I Experiments, ANL-5323 (1954).

The Experimental Boiling Water Reactor (EBWR), ANL-5607 (May 1957).

Reactors on the Line EBWR, Nucleonics, 15 (July 1957).

Cost of Containment Features for Boiling Water Reactors for ANL, Lemont, Illinois, AECU-4109 (Oct 1957).

J. W. Weil, Boiling Water Reactor Stability, GER-1468 (1957).

B. S. Maxon, O. A. Schulze, and J. A. Thie, Reactivity Transients and Steady-state Operation of a Thoria-Urania-fueled Direct-cycle Light Water-Boiling Reactor (BORAX-IV), ANL-5733 (Feb 1959).

SECTION III - Experimental and Support Study Facilities at ANL

R. E. Macherey et al., Manufacture of Fuel Plates for the Experimental Boiling Water Reactor, ANL-5629 (June 1957).

J. A. Thie, EBWR Physics Experiments, ANL-5711 (July 1957).

J. W. Harrer, Starting Up EBWR, Nucleonics 15, 60 (July 1957).

J. N. Young, Design and Performance Characteristics of Magnetic Jack-type Control Rod Drive, ANL-5768 (Dec 1957).

J. M. Harrer et al., Performance Evaluation of Direct Cycle Boiling Water Nuclear Power Plants Based on Recent EBWR and BORAX Data (F,S), Proc. Second UN Int'l. Conf. on Peaceful Uses of Atomic Energy, Geneva, Switzerland, 9, 264 (1958).

H. Etherington, editor, Nuclear Engineering Handbook, McGraw Hill Book Co., Inc., New York (1958).

R. J. Schiltz, J. H. Monaweck, and E. S. Sowa, EBR-II Fuel Irradiation Facilities, ANL-5940 (Nov 1958).

W. C. Redman, Critical Facilities for Reactor Design, Nucleonics, 16, 40 (Dec 1958).

R. D. Carlson, In-pile Loop Study of UO_2-NaK Slurry, Nuclear Science and Engineering, 7, 508-513 (June 1960).

J. H. Monaweck and E. S. Sowa, Summary Report on Irradiation of Prototype EBR-II Fuel Elements, ANL-6010 (Sept 1960).

C. E. Dickerman, E. S. Sowa, and D. Okrent, Fast Reactor Safety Studies in TREAT - A Status Report, Nucleonics, 19, 114 (April 1961).

C. E. Dickerman et al., Studies of Fast Reactor Fuel Element Behavior under Transient Heating to Failure. I. Initial Experiments on Metallic Samples in the Absence of Coolant, ANL-6334 (Aug 1961).

SECTION IV - EBWR System and Material and Components Design

A. Smaardyk, Summary of Shaft Seal Tests for High-temperature, High-pressure Water Application, ANL-5220 (April 1954).

The Experimental Boiling Water Reactor (EBWR), ANL-5607 (May 1957).

Welding of Stainless Steel which Contains More than One Per Cent Boron, Minutes of the Seventh Annual Atomic Energy Commission Welding Conference, Held in Chicago, Ill., TID-7562 (Nov. 1957) p. 15.

N. Balai, T. L. Kettles, and R. E. Bailey, Reactor Pressure Vessel Design for Nuclear Applications, ASTM-STP 233 (June 1958), p. 63. Symposium Effects on Materials - Vol. 3.

J. M. Harrer and E. A. Wimunc, EBWR Turbine Blade Failure, ANL-5941 (Nov 1958).

R. J. Gariboldi and D. R. Jacobson, Operation Tests of EBWR Vapor Recovery System, ANL-6189 (Aug 1960).

V. M. Kolba, EBWR Test Reports, ANL-6229 (Nov 1960).

T. Kettles, Modifying EBWR Vessel for 100 Mw(th) Operation, Nucleonics, 19, 50 (Aug 1961).

SECTION V - EBWR Shielding

M. Grotenhuis and J. W. Butler, Experimental Boiling Water Reactor (EBWR) Shield Design, ANL-5544 (Aug 1956).

The Experimental Boiling Water Reactor (EBWR), ANL-5607 (May 1957).

Reactor Physics Constants, ANL-5800 (1958).

M. Grotenhuis, Lecture Notes on Reactor Shielding, ANL-6000 (Mar 1959).

V. M. Kolba, EBWR Test Reports, ANL-6229 (Nov 1960).

V. C. Hall, Jr., and R. H. Leyse, Radiation Levels in EBWR, Nucleonics, 19, 80 (March 1961).

SECTION VI - EBWR Control Rods and Control Rod Drives

Reactor Engineering Division Quarterly Report (for) October 1, 1954 through December 31, 1954, ANL-5371 (Jan 1955).

Reactor Engineering Division Quarterly Report on the Power Reactor Program (for) January 1, 1955 through March 31, 1955, ANL-5461 (April 1955).

Reactor Engineering Division Quarterly Report (for) July, August, September 1955. Section II, ANL-5511 (Jan 1956).

Reactor Engineering Division Quarterly Report (for) October, November, December 1955. Section I, ANL-5561 (April 1956).

Reactor Engineering Division Quarterly Report (for) January, February, March 1956. Section I, ANL-5571 (July 1956).

Reactor Engineering Division Quarterly Report (for) April, May, June 1956. Section II, ANL-5601 (Dec 1956).

The Experimental Boiling Water Reactor (EBWR), ANL-5607 (May 1957).

C. F. Bullinger and W. J. Kann, Control Rod Drive Mechanism on the EBWR, Nuclear Science and Engineering, 3, 379-86 (April 1958).

N. Balai, Materials, Fabrication and Performance of the EBWR Control Rods, Nuclear Science and Engineering, 4, 429-38 (1958).

SECTION VII - EBWR Fuel Design and Behavior

A. E. Dwight, Allotropic Transformations in Titanium, Zirconium, and Uranium Alloys, ANL-5091 (Sept 1953).

The Experimental Boiling Water Reactor (EBWR), ANL-5607 (May 1957).

Papers Presented at the Technical Briefing Session Held at Argonne National Laboratory, May 27-28, 1957, Boiling Water Reactor Program, TID-7535.

R. E. Macherey et al., Manufacture of Fuel Plates for the Experimental Boiling Water Reactor, ANL-5629 (June 1957).

C. H. Bean, R. E. Macherey, and J. R. Lindgren, Roll Cladding Uranium-Zirconium-Niobium Alloys with Zircaloy-2 for Plate-type Fuel Elements, ANL-5628 (Feb. 1958).

R. E. Macherey, Fabrication of the Uranium-base Fuel Plates and Assemblies for the Experimental Boiling Water Reactor, Proc. Second UN Int'l. Conf. on Peaceful Uses of Atomic Energy, Geneva, Switzerland, 6, 443 (1958).

Progress in Nuclear Energy, Series V, Vol. 2, Metallurgy and Fuels (Pergamon Press: 1959).

R. F. S. Robertson, Tests of Defected Thoria-Urania Fuel Specimens in EBWR, ANL-6022 (May 1960).

J. H. Kittel, Effects of Irradiation on the EBWR Fuel Alloy Uranium-5 w/o Zirconium-1.5 w/o Niobium, ANL-5639 (July 1960).

C. F. Reinke and R. Carlander, Examination of Irradiated EBWR Core-1 Fuel Elements, ANL-6091 (July 1960).

I. Charak, Removal of EBWR Fuel Element Scale by Slurry Honing, ANL-6216 (Sept 1960).

C. R. Breden, I. Charak, and R. H. Leyse, Water Chemistry and Fuel Element Scale in EBWR, ANL-6136 (Nov 1960).

V. M. Kolba, EBWR Test Reports, ANL-6229 (Nov. 1960).

SECTION VIII - EBWR Water Chemistry and Corrosion

J. R. Humphreys, E. K. Abers, and Y. Solomon, Decomposition and Recombination in Irradiated Static Water Systems at High Temperatures, ANL-5004 (March 1953).

C. R. Breden and A. Abers, Corrosion and Stability Tests on Chemical Poisons in High-temperature Water, ANL-5147 (Sept 1953).

A. E. Dwight and A. H. Roebuck, Preliminary Report on Corrosion of Low-Uranium, Zirconium-base Alloys, ANL-5196 (Oct 1953).

C. Wohlberg and F. W. Kleimola, Factors which Affect Formation and Deposition of Transport Corrosion Products in Hight-temperature Recirculating Water Loops, ANL-5195 (Dec 1953).

K. Anderson, Nitrided Stainless Steels for High-temperature Water Service, ANL-5192 (March 1954).

C. R. Breden, W. S. Brown, and M. Sivetz, Soluble Poisons in Reactor Control, ANL-5244 (Nov 1955).

D. J. DePaul, Corrosion and Wear Handbook for Water Cooled Reactors, TID-7006 (March 1957).

The Experimental Boiling Water Reactor (EBWR), ANL-5607 (May 1957).

J. H. Kittel et al., Effects of Irradiation on Some Corrosion-resistant Fuel Alloys, Nuclear Science and Engineering, 2, 431-449 (July 1957).

S. Greenberg and J. E. Draley, Effects of Irradiation on Corrosion Resistance of Some High Uranium Alloys, Nuclear Science and Engineering, 3, 19-28 (Jan 1958).

R. E. Bailey, Irradiation Effects on Zirconium-clad Uranium-Zirconium Fuel Plates, ANL-5825 (Feb. 1958).

S. Greenberg, Corrosion of Irradiated Uranium Alloys, Nuclear Science and Engineering, 6, 159 (Aug 1959).

R. F. S. Robertson and V. C. Hall, Jr., Fuel Defect Test - BORAX-IV, ANL-5862 (Oct 1959).

C. R. Breden and N. R. Grant, Summary of Corrosion Investigations on High-temperature Aluminum Alloys. Feb. 1955 - Oct. 1956, ANL-5546 (Feb 1960).

R. F. S. Robertson, Tests of Defected Thoria-Urania Fuel Specimens in EBWR, ANL-6022 (May 1960).

I. Charak, Removal of EBWR Fuel Element Scale by Slurry Honing, ANL-6216 (Sept 1960).

G. C. K. Yeh and N. Zuber, On the Problem of Liquid Entrainment, ANL-6244 (Oct 1960).

C. R. Breden, I. Charak, and R. H. Leyse, Water Chemistry and Fuel Element Scale in EBWR, ANL-6136 (Nov 1960).

V. M. Kolba, EBWR Test Reports, ANL-6229 (Nov 1960).

N. R. Grant, Summary of Corrosion Investigations of High-temperature Aluminum Alloys, Oct. 1957 to Dec. 1959, ANL-6204 (Sept 1961).

V. C. Hall and R. H. Leyse, Radiation Levels in EBWR, Nucleonics, 19, 80 (March 1961).

R. L. Mittl and M. Theys, N^{16} Concentration in EBWR, Nucleonics, 19, 81 (March 1961).

SECTION IX - EBWR Heat Transfer and Hydraulics

J. F. Marchaterre, The Effect of Pressure on Boiling Density in Multiple Rectangular Channels, ANL-5522 (Feb 1956).

C. D. Alstad et al., The Transient Behavior of Single-phase Natural Circulation Water Loop Systems, ANL-5409 (March 1956).

W. H. Cook, Boiling Density in Vertical Rectangular Multichannel Sections with Natural Circulation, ANL-5621 (Nov 1956).

P. A. Lottes and W. S. Flinn, A Method of Analysis of Natural Circulation Boiling Systems, Nuclear Science and Engineering, 1, 461 (June 1956).

The Experimental Boiling Water Reactor (EBWR), ANL-5607 (May 1957).

P. A. Lottes, M. Petrick, and J. F. Marchaterre, Lecture Notes on Heat Extraction from Boiling Water Power Reactors, ANL-6063 (Oct 1959).

E. A. Wimunc and J. M. Harrer, Hazards Evaluation Report Associated with the Operation of EBWR at 100 Mw, ANL-5781 (Add.) (Dec 1959).

J. F. Marchaterre et al., Natural and Forced-circulation Boiling Studies, ANL-5735 (May 1960).

J. B. Heineman, An Experimental Investigation of Heat Transfer to Superheated Steam in Round and Rectangular Channels, ANL-6213 (Sept 1960).

V. M. Kolba, EBWR Test Reports, ANL-6229 (Nov 1960).

J. F. Marchaterre and M. Petrick, The Prediction of Steam Volume Fractions in Boiling Systems, Nuclear Science and Engineering, 7, 525 (1960).

Proceedings of the Power Reactor In-core Instrumentation Meeting, Washington, D.C., April 28-29, 1960, Division of Reactor Development, AEC, TID-7598 (March 1961).

P. A. Lottes, Expansion Losses in Two-phase Flow, Nuclear Science and Engineering, 9, 26 (Jan 1961).

SECTION X - EBWR Reactor Physics and Reactor Stability

S. Glasstone and M. Edlund, The Elements of Nuclear Reactor Theory, D. Van Nostrand Co., Inc., New York (1952).

H. P. Iskenderian, 20-Mw D_2O-Moderated Experimental Boiling Water Reactor Design Studies, ANL-5685 (Feb 1957).

J. A. DeShong, Jr., Styrofoam Simulation of Boiling and Temperature Effects in the EBWR Cold Critical Experiments, ANL-5697 (March 1957).

M. W. Rosenthal and R. L. Miller, An Experimental Study of Transient Boiling, ORNL-2294 (May 1957).

The Experimental Boiling Water Reactor (EBWR), ANL-5607 (May 1957).

J. A. DeShong, Jr., and E. S. Beckjord, Frequency Response Measurements of the EBWR Automatic Steam By-pass Valve Control System, ANL-5726 (June 1957).

J. A. Thie, EBWR Physics Experiments, ANL-5711 (July 1957).

J. A. DeShong, Jr., Power Transfer Functions of the EBWR Obtained Using a Sinusoidal Reactivity Driving Function, ANL-5798 (Jan 1958).

E. S. Beckjord, Dynamic Analysis of Natural Circulation Boiling Water Power Reactors, ANL-5799 (March 1958).

J. A. DeShong, Jr., and W. C. Lipinski, Analyses of Experimental Power-Reactivity Feedback Transfer Functions for a Natural Circulation Boiling Water Reactor, ANL-5850 (July 1958).

Reactor Physics Constants, ANL-5800 (1958).

J. A. Thie, Dynamic Behavior of Boiling Reactors, ANL-5849 (May 1959).

E. A. Wimunc and J. M. Harrer, Hazards Evaluation Report Associated with the Operation of EBWR at 100 Mw, ANL-5781 (Add.) (Dec 1959).

A. Z. Akcasu, Theoretical Feedback Analysis in Boiling Water Reactors, ANL-6221 (Oct 1960).

V. M. Kolba, EBWR Test Reports, ANL-6229 (Nov 1960).

R. Meghreblian and D. Holmes, Reactor Analysis, McGraw-Hill Book Co., Inc., New York (1960).

R. Avery et al., EBWR Core 1A Physics Analysis, ANL-6305 (Feb 1961).

R. Avery and C. N. Kelber, Physics Analysis of Proposals for EBWR Core 2, ANL-6306 (April 1961).

J. A. Thie, Burnup Experience in EBWR, Nucleonics, 19, 60 (May 1961).

SECTION XI - EBWR Instrumentation, Control and Safety Systems

Instrumentation of the EBWR Power Plant, Papers Presented at the Technical Briefing Session Held at Argonne National Laboratory, May 27-28, 1957. TID-7535 (Boiling Water Reactor Program).

M. A. Schultz et al., Power Reactor Control, Nucleonics, 16, 61 (May 1958).

W. C. Lipinski, A. Hirsch, and C. A. Pesce, Automatic Control of Boiling Water Reactors, Presented at the AIEE Summer and Pacific General Meeting and Air Transportation Conference, Seattle, Washington, Paper No. CP 59-928 (June 1959).

R. G. Lorraine, A Review of Boiling Water Reactors for Atomic Power Generation, GER-1287.

The Experimental Boiling Water Reactor (EBWR), ANL-5607 (Revised) (1962).

SECTION XII - EBWR Operations, Hazards and Containment

F. B. Porzel, Design Evaluation of BER (Boiling Experimental Reactor) in Regard to Internal Explosions, ANL-5651 (Jan 1957).

The Experimental Boiling Water Reactor (EBWR), ANL-5607 (May 1957).

Containment for the EBWR, Second Nuclear Engineering and Science Conference, ASME, Paper No. 57-NESC-90 (1957).

J. M. Harrer, Review of Boiling Water Reactor Performance, Fifth International Congress and Exhibition of Electronics and Atomic Energy, Rome, Italy, June 16-30, 1958, (U.S. Papers), TID-7557, p. 5.

A. H. Heineman and L. W. Fromm, Containment for the EBWR (F,S), Proc. Second UN Int'l Conf. on Peaceful Uses of Atomic Energy, Geneva, Switzerland, 11, 139 (1958).

R. F. S. Robertson and V. C. Hall, Jr., Fuel Defect Test - BORAX-IV, ANL-5862 (Oct 1959).

E. A. Wimunc and J. M. Harrer, Hazards Evaluation Report Associated with the Operation of EBWR at 100 Mw, ANL-5781 (Add.) (Dec 1959).

APPENDIX A

EXPERIMENTAL BOILING WATER REACTOR PARAMETERS

E. Wimunc

General

1. Reactor Type

   Slightly enriched uranium (1.44%) plate type and UO_2 (>90%) + ZrO_2 + CaO cylindrical pellet-spike fuel, light water-moderated and cooled, boiling water.

2. Number of Reactors in Plant

   1

3. Rated Output per Reactor

   Gross heat: 100 Mw (80 Mw for process steam, 20 Mw for turbine steam)
   Gross electricity: 5 Mw
   Net electricity: 4.5 Mw
   Self consumption: 10% of gross electrical output

4. Net Efficiency

   22.5% (electrical generation)
   ~70% (process steam generation)

5. Location

   Argonne, Illinois

6. Owner

   Owned by USAEC

7. Operating Authority

   Operated by Argonne National Laboratory

8. Designer

   Argonne National Laboratory

9. Main Contractors

   USAEC and Sargent & Lundy

10. Present Status

In operation at 20-Mw power level

11. Construction Schedule

	20 Mw (Orig.)	100 Mw (Revision)
Start of construction	May 1955	October 1959
Reactor critical - for 20 Mw	December 1956	April 1960
for 100 Mw	-	-
Full-power operation - for 20 Mw	December 1956	January 1962
for 100 Mw	-	-

Reactor Physics

12. Mean Neutron Energy in the Core

0.053 ev

13. Mean Lifetime of Prompt Neutrons

7.4×10^{-5} sec

14. Neutron Flux

Average thermal flux = 3×10^{13} nv
(Max/Avg) thermal flux = 2.67
Average fast flux = 1.15×10^{14} nv
(Max/Avg) fast flux = 1.91

15. Core Parameters

	Cold	Hot (20% Void)
ϵ	1.030	1.035
p	0.86	0.80
ηf	1.38	1.42
k_∞	1.208	1.174
k_{eff}	1.125	1.045 (No Xe)
L^2	4	6
τ	44	74
$1 + L^2B^2$	1.006	1.009
$1 + \tau B^2$	1.067	1.1132

16. Conversion Ratio

0.65 initial

17. Excess Reactivity, Δk, to Compensate for*

Temperature and voids	7%
Xe and Sm at rated power	3%
Burnup	1%

18. Maximum Excess Reactivity Built in

Cold 11%

19. Fuel Element: (Plates and Rods)

Plate Type: 6 plates per fuel assembly (thick and thin plates, enriched and natural)

Meat Dimensions:

thick - 51.0 x 3.31 x 0.241 in.
thin - 51.0 x 3.31 x 0.172 in.

Overall Dimensions:

thick - 54 x 3.625 x 0.280 in.
thin - 54 x 3.625 x 0.212 in.

Enrichment

natural - 0.72 a/o U^{235}
enriched - 1.44 a/o U^{235}

Meat Composition: 93.5 w/o U-5.0 w/o Zircaloy-2-1.5 w/o Nb

Rod Type: 49 pellet-type fuel rods per fuel assembly (uniform - diameter rods, highly enriched)

Meat Dimensions: 0.321 in. dia x 47.5 in. length
Overall Dimension: 0.375 in. dia. x 51.0 in. length
Enrichment: 0.93 a/o U^{235}
Meat Composition: 9 w/o UO_2-82.4 w/o Zr-8.1 w/o CaO, $\leq$ 0.5 w/o Al_2O_3 & SiO_2

20. Cladding

Plate Type: 0.020-in.-thick Zircaloy-clad, roll bonded
Rod Type: 0.375 in. OD x 0.025 in. wall thickness, Zircaloy-2 tube

21. Fuel Assembly

Plate Type:

Overall Dimensions: 3.75 x 3.75 x 79.625 in.
Side-plate Material: Zircaloy-2 - 0.0625 in. thick

*Preoperation calculated value.

21. Fuel Assembly (Cont'd.)

Rod Type:

Overall Dimensions: 3.875 x 3.875 x 89.25 in.

Side-plate Material: one to three side plates contain 1.1% boron-stainless steel 304 burnable poison strips - 0.0625 in. thick

22. Shape and Dimensions

Right cylindrical, 60 in. dia, 51 in. high

23. Number of Channels and Subassemblies

148 channels, 147 subassemblies (104 enriched-plate elements, 11 natural-plate elements, 32 enriched-spike elements) 1 source

24. Lattice

Square, 4.00-in. pitch

25. Critical Mass, Cold Unpoisoned

47.13 kg U^{235}

26. Core Loading at Rated Power

Fissionable material - 107 kg U^{235} + Pu
Fertile material - 5300 kg U^{238}

27. Average Specific Power in Fuel

930 kw/kg

28. Average Power Density of Core

48 kw/liter

29. Total Fuel Inventory per Reactor

107 kg of U^{235} in core
11.2 kg of U^{235} in storage

30. Burnup Expectancy at End of Life

1600 Mwd/metric ton

31. Total Amount of Fuel Reprocessed per Year per Reactor

None as yet

32. Fuel-loading and -unloading System

After shutdown, top shield tank and pressure vessel cover removed. Carrier assembly plug indexed and rotated into position. Fuel is grappled and raised into coffin and lowered through a shielded chute into water-filled storage pit close to reactor.

33. Irradiated Fuel Storage

Underwater, in fuel-storage tank adjacent to reactor shield, capacity for 148 elements, plus 33 spike assembly rack.

34. Expected Downtime due to Refueling and Interval between Refueling

Downtime for refueling: 100 hr
(Interval between refueling unknown)

35. Moderator and Coolant in Operating Primary Circuit

~32,000 lb H_2O
(486°F - 600 psig)

36. Blanket Gas

Steam

Core Heat Transfer

37. Heat Transfer Area

19.3 ft^2 per spike element
16.3 ft^2 per plate element
2,492 ft^2 total

38. Heat Flux on the Fuel Element Surface - Btu/hr-ft^2*

Central thin enriched zone -	avg	= 225,471
	max	= 344,838
Spike zone	avg	= 147,219
	max	= 245,365
Outer thin enriched zone	avg	= 184,356
	max	= 283,828
Thick enriched zone	avg	= 118,041
	max	= 172,419

*Preoperation calculated value.

39. Film Temperature Drop, Design*

18°F (avg)

40. Fuel Element Temperatures, Design*

Maximum fuel centerline temperature	
thin enriched element	724°F
thick enriched element	767°F
rod element (spike)	4500°F
Maximum cladding temperature	514°F

41. Coolant Flow Area

Thin enriched-plate element	7.94 $in.^2$
Rod element spike	9.60 $in.^2$
Total fuel zone	1220 $in.^2$

42. Channel Inlet Velocity of the Coolant (avg)*

6.3 fps

43. Heat Transfer Coefficient*

Central thin enriched zone	10,470 $Btu/(hr)(ft^2)(°F)$
Spike zone	7,742 $Btu/(hr)(ft^2)(°F)$

44. Coolant Mass Flow Rate*

~11.9 x 10^6 lb/hr

45. Coolant Temperature*

Feedwater	120°F
Inlet to core	477°F
Outlet	489°F

46. Coolant Pressure

600 psig

47. Hot Channel Factors*

Overall: 3.1

*Preoperation calculated value.

48. Provision for Shutdown Heat Removal

After blowdown of reactor to condenser to a temperature of ~110°C, the 3 liter/sec passed through the secondary cooler of one purification loop is used to cool the reactor coolant to ~120°F.

Reflector and Shielding

49. Reflector

Light Water Thickness: 12 in.

50. Shielding

Side	Thermal shield - 1 in. borated stainless steel Gamma shield - 3 in. lead Biological shield - 60 in. heavy concrete and 36 in. ordinary concrete
Bottom	2.5 in. steel, 3 in. lead, 48 in. ordinary concrete, and 36 in. water
Top	108 in. water and 15.75 in. steel
Cooling	Water circulated in horizontal coils imbedded in lead brick shield; avg temp rise of 10°F

51. Radiation Level Outside Shielding

20-Mw Power Level: Reactor top, 1 mr/hr; Turbine casing, 4 mr/hr; subreactor room, 10 mr/hr; control room - none.

100-Mw Power Level: not obtained as yet.

Control

52. Control, Safety, and
53. Regulating Rods

Nine control rods, of cruciform shape (10.0 in. x 10.0 in.), composed of 2 w/o boron-stainless steel, 0.250 in. thick. Lengths: absorber 58 in.; follower 36.5 in. (of Zircaloy 2); total 94.5 in.

Rod Spacing: 12.75 x 12.75 in.

Total Worth: ~14% $\Delta k/k$

Rod Withdrawal Speed: 28 in./min

Travel: 60 in.

54. Other Control Features

High negative temperature coefficient; boric acid addition for cold shutdown reactivity control

55. Maximum Rate of Reactivity Addition

0.037% $\Delta k/sec$

56. Scram Time and Type of Mechanism

1 sec for 48-in. drop

Free fall drop of rod into core by its own weight. Dashpot retards last 4 in. of fall.

57. Sensitivity of Automatic Control

Manual control of regulating rods

58. Temperature Coefficients*

Fuel: 1.0×10^{-5} $k_{ex}/°F$; Moderator: 1.06×10^{-4} $k_{ex}/°F$.

59. Burnable Poison

0.0625-in. thick, 1 w/o boron-stainless steel strips on sides of spike fuel assemblies; total reactivity worth: $5\% \pm 1.5\%$ $\Delta k/k$.

60. Other Safety Shutdown Provisions*

Boric acid solution under high pressure can be injected to control ~8.1% Δk. Additional boric acid can be pumped into the reactor.

61. Instrumentation

Nuclear: three electronic high-flux trip circuits and instruments; reactor period meter.

Temperature: temperature interlock to prevent control rod withdrawal below 325°F.

Pressure: steam bypass control system; maintain constant reactor pressure at 600 psig.

*Preoperation calculated value

Reactor Vessel

62. Form, Material, and Dimension

Cylindrical vessel of carbon steel, 2.375-in.-thick, lined with 0.100-in. stainless steel-304; 84 in. in inside diameter; 23-ft height; closure diameter: 64 in. (metal temp: 650°F, max design).

63. Working, Design, and Test Pressures

Working Pressure:	600 psig
Design Pressure:	800 psig
Test Pressure:	1200 psig

Fluid Flow

64. Heat Exchangers*

7 heat exchangers in one primary system loop, 2 reboiler type and 5 water-to-water type; stainless steel Type 304 tubing in all exchangers; 80-Mw thermal capacity with additional 20 Mw to turbine-generator plant. Steam flow rate is 60,500 lb/hr to the turbine and 244,500 lb/hr to the reboiler plant.

65. Primary Coolant Purification

Purification by two parallel loops (one as standby) having prefilters, afterfilters, pumps, two anion exchange units, and two mixed-bed units (one saturated with borate ion for boric acid control system). Continuous flow of 6-10 gpm is maintained.

66. Primary Coolant Decomposition and Recombination*

Decomposition: 2.67 lb/hr at 20 Mw.
Recombination by using a platinized alumina pellet bed.

67. Primary Coolant Losses*

Losses: ~19 lb/day.

68. Safety Features of Cooling System

Emergency cooler - drier for removal of decay heat. Emergency diesel set for power failure. Spray system with 15,000-gal tank for vessel rupture releasing steam. Safety valves release steam to condenser during system overpressure.

*Preoperation calculated value

69. Provision for Detecting Fuel-element Rupture

Continuous monitoring system using NaI(Th) crystal and a pair of counting-rate circuits installed at the air ejector. Any abnormal release of Xe due to fuel-element failure will be detected at once by a fission product monitor at air ejectors.

Reactor Overall Dimensions and Containment

70. Reactor Overall Dimensions with Shielding

25-ft concrete octagon

71. Containment Type and Material

Steel shell with hemispherical top, elliptical bottom, and concrete wall cell.

72. Dimensions

Shell: 0.625 in. thick on side and bottom; 0.375 in. thick on top. Inside diameter: 80 ft; inside height: 119 ft; net free volume: ~400,000 ft^3. Lined with 24 in. of concrete below and 12 in. above grade. Reboiler Building: Butler-type building with concrete cell of ~7920-ft^3 volume, 12-in.-thick walls in the room housing the reboilers.

73. Pressure

Shell design pressure: internal, 15 psig; external, 0.5 psig. Max allowable leak rate at 15 psig: 1000 ft^3/24 hr.

74. Surroundings

Open country, thinly populated. Population density within 1.5-mile radius: approximately 150 persons/sq. mile.

75. Turbine

One multistage impulse type, 5-Mw capacity (6.25-Mw capability), 3600 rpm, 560 psi at 481°F and 2.5 in. Hg at exhaust.

76. Generator

One synchronous generator, 6,250 kva at 0.8 pf, 3-phase, 4160-v, 60-cycle, 3600-rpm.

Cost Estimate

77. Total Capital Investment in Reactor, Plant, and First Fuel Loading but Excluding Research and Development

Reactor System	$ 1,953,000
First Fuel Loading	1,523,000
Power Plant	1,971,000
Building, Facilities, and Architect-Engineer	705,000
Total for 20-Mw Plant (excluding research and development)	$ 6,152,000
Process Steam Plant	$ 1,643,000
Revisions to 20-Mw Plant	383,000
Spike Fuel	400,000
Total for 100-Mw Plant	$ 8,578,000

78. Capital Cost per kw Installed

$85.78/kw(t) (this is based on reactor thermal output because of generation of both steam and electrical power.)

79. Availability of Load Factor

Indeterminable because of experimental nature of reactor.

80. Average Production per Year

Indeterminable

81. Expected Lifetime of the Plant

25 years

82. Rate of Annual Fixed Charges

14% interest rate

83. Staff

1 - Reactor Operations Manager
1 - Project Manager
1 - Reactor Supervisor
1 - Reactor Co-Ordinator
1 - Health Physicist
4 - Reactor Operators per shift
2 - Maintenance
1 - Receptionist
- Research and Engineering Staff which varies from time to time

APPENDIX B

CHARACTERISTICS OF HEAT DISSIPATION SYSTEM (100 Mw)

E. Martinec

1. Operating Conditions per Primary Reboiler Unit

Reboiler tube surface		4000 sq ft
Heat Exchanged, max		111 x 10^6 Btu/hr (32.5 Mw)
Quantity of primary steam to tube side		150,000 lb/hr (max)
Tube-side pressure -	operating	560 psig
	design	800 psig
	test	1500 psig
Tube-side temperature -	operating	482°F (both steam inlet and condensate outlet)
	design	520°F
Quantity of intermediate steam leaving shell side		140,500 lb/hr (max)
Shell-side pressure -	operating	350 psig
	design	400 psig
	test	600 psig
Shell-side temperature -	operating	435.7°F (both water inlet and steam outlet)
	design	448°F
Steam quality leaving shell dry pipe		~98%
Fouling Factor		0.0005
Shell-side water capacity at normal operating conditions		1925 gal
Weights -	Dry	31,500 lb
	Operating	47,500 lb
	Flooded	59,500 lb

2. Materials of Construction of Primary Reboiler Unit

Shell	ASTM-A-212 Grade B Firebox Quality Steel
Shell Weld Stubs	ASTM-A-105 Grade 1 Forged Steel
Channel	ASTM-A-212 Grade B Firebox Quality Steel with $\frac{3}{16}$-in.-thick (min), arc-deposited AISI 304 cladding on inside surface.

2. Materials of Construction of Primary Reboiler Unit (Cont'd.)

Channel Weld Stubs	ASTM-A-240 Type AISI 304
Tube Sheet	ASTM-A-212 Grade B Firebox Quality Steel with $\frac{3}{16}$-in.-thick (min), arc-deposited AISI 304 cladding on tube side.
Channel Partition Rib and Cover	ASTM-A-240 Type AISI 304
Tubes	ASTM-A-249 Type AISI 304 L
Shell Handholes and Weld Couplings	Steel

3. Operating Conditions per Primary Drain Cooler Unit

Drain Cooler Tube Surface	1080 sq ft
Heat Exchanged - Maximum	35.4×10^6 Btu/hr (10.4 Mw)
Quantity of primary steam condensate to tube side	132,200 lb/hr
Tube-side pressure - operating	560 psig
design	800 psig
test	1500 psig
Tube-side Temperature - operating - inlet	482°F
outlet	231°F
design	520°F
Quantity of intermediate feedwater to shell side	123,500 lb/hr
Shell-side pressure - operating	350 psig
design	400 psig
test	600 psig
Shell-side temperature - operating - inlet	160°F
outlet	435.7°F
design	448°F
Fouling Factor	0.0007
Weights - dry	10,000 lb
flooded	14,200 lb

4. Materials of Construction of Primary Drain Cooler Unit

Shell	ASTM-A-106 Grade B
Shell Nozzles	ASTM-A-106 Grade B or ASTM-A-53 Grade B Seamless Steel
Shell Head	ASTM-A-234 Grade WPB Seamless Steel
Channel	ASTM-A-240 Type AISI 304
Channel Nozzles	ASTM-A-312 Type AISI 304
Tube Sheet	ASTM-A-182 Type AISI 304 - Forged
Channel Partition Rib	Type AISI 304
Tubes	ASTM-A-213 Type AISI 304
Shell Handholes and Weld Couplings	Carbon Steel
Shell Longitudinal Baffle	Carbon Steel Plate

5. Operating Conditions of Primary Subcooler

Subcooler tube surface		1943 sq ft
Heat Exchanged - Maximum		17.25×10^6 Btu/hr (5.05 Mw)
Quantity of primary condensate to shell side		235,570 lb/hr
Shell-side pressure -	operating	10 psia
	design	100 psig
	test	195 psig
Shell-side temperature -	operating -	
	inlet	193.2°F
	outlet	120°F
	design	338°F
Quantity of cooling water to tube side		495,000 lb/hr
Tube-side pressure -	operating	50 psig
	design	100 psig
	test	150 psig
Tube-side temperature -	operating -	
	inlet	95°F
	outlet	129.8°F
	design	338°F
Fouling Factor		0.0022
Weights -	dry	8500 lb
	flooded	15,500 lb

6. Deaerator Design Specifications

Capacity	300,000 lb/hr
Design Pressure	100 psig and full vacuum at 100°F
Design Temperature	338°F
Empty Weight	10,000 lb
Operating Weight	21,000 lb
Flooded Weight	30,000 lb
Water-storage Volume	1,000 gal
Shell:	
Material	304 SS ASTM-A-240S
Thickness	$\frac{3}{8}$ in.
Outside	59 in.
Plate Length	13 ft
Overall length including heads	14 ft 9 in.
Heads:	
Material	304 SS ASTM-A-240S
Thickness	$\frac{3}{8}$ in.
Trays:	
Number	18 tray cubes
Size	Each cube 15 x 15 x 15 in.
Total Area	405 sq ft
Total Effective Surface	5400 sq ft
Thickness	17 gage
Material	304 SS ASTM-A-240S

7. Primary Feedwater Pump Operating Characteristics

Capacity	645 gpm at 320°F
Shut-off Head	2200 ft
Head (total dynamic)	2021 ft not including friction losses
Suction Head	221 ft
Developed Head	1800 ft
NPSH Required	30 ft
Design Pressure	900 psig
Design Temperature	320°F
Motor Horsepower, Rated	350 hp
Motor Voltage (3-phase, 60-cycle)	4000 v
Motor Speed	3550 rpm
Weights:	
Total (pump and motor)	7170 lb
Pump and baseplate	3350 lb
Motor	3820 lb

8. Primary Feedwater Pump Construction Materials

Casing	11-13% chrome
Shaft	11-13% chrome HT
Shaft Sleeves	11-13% chrome
Impeller	11-13% chrome
Casing Wear Ring	11-13% chrome (nitrided)
Impeller Wear Ring	11-13% chrome (stellited)
Packing Gland	11-13% chrome
Suction Nozzle Size	6-in. Schedule 40
Discharge Nozzle Size	3-in. Schedule 80

9. Feedwater Filter Design Specifications

Capacity	180 gpm at 120°F
Dry Weight	1900 lb
Shell:	
Material	ASTM-A-312 Type 304 SS
Thickness	$\frac{5}{8}$ in.
Outside Diameter	$19\frac{1}{4}$ in.
Overall length including heads	68 in.
Heads:	
Material	ASTM-A-312 Type 304 SS
Thickness	$\frac{5}{8}$ in.
Filter Elements:	
Number	75
Size	$2\frac{3}{4}$-in. diameter x $9\frac{3}{4}$ in.
Material	Cotton Thread
Pressure Drop	5 psi
Minimum particle size	2μ

10. Operating Conditions of Intermediate Feedwater Pumps

a. Performance

Capacity	600 gpm
Shutoff Head	1152 ft
Total Dynamic Head	1050 ft
Differential Head	1038 ft
NPBH Required	12 ft
Efficiency at Rated Capacity	66%
Design Temperature	260°F
Brake Horsepower	220

10. Operating Conditions of Intermediate Feedwater Pumps (Cont'd.)

b. Motor

Rated Horsepower	250
rpm	3570

c. Weight, Pump 2000 lb

Base Plate	800 lb
Motor	2500 lb
Total	5300 lb

11. Materials of Construction of Intermediate Feedwater Pumps

Casing	Carbon Steel
Shaft, Shaft Sleeve, Impeller, Casing and Impeller Wearing Ring	11-15% Chrome Steel
Packing Gland	11-15% Chrome Bronze Bushed
Suction Nozzle	6-in. raised face
Discharge Nozzle	4-in. raised face

12. Operating Conditions of Secondary Reboiler

Reboiler tube surface	9340 sq ft
Heat Exchanged	$19^3 \times 10^6$ Btu/hr (56.6 Mw)
Quantity of intermediate steam to tube side	241,000 lb/hr
Tube-side pressure - operating	310 psig
design	400 psig
test	600 psig
Tube-side temperature - operating	424.7°F (both steam inlet and condensate outlet)
design	448°F
Quantity of secondary steam leaving shell side	227,000 lb/hr
Shell-side pressure - operating	200 psig
design	250 psig
Shell-side temperature - operating - inlet	376.5°F
outlet	388°F
design	406°F

12. Operating Conditions of Secondary Reboiler (Cont'd.)

Steam quality leaving reboiler after steam separators	99.75%
Fouling Factor	0.0005
Shell-side water capacity at normal operating conditions	2,525 gal
Weights - Dry	45,900 lb
Operating	54,000 lb
Flooded	64,500 lb
Heat-up Rate - Normal	20°F/min
Maximum	30°F/min

13. Materials of Construction for Secondary Reboiler Unit

Shell	ASTM-A-212 Grade B Firebox Quality
Channel	ASTM-A-212 Grade B Firebox Quality
Shell and Channel Flanges	ASTM-A-105 Grade 2 (0.30% max carbon)
Shell and Channel Nozzles	ASTM-A-106 Grade B
Shell Steam Outlet Nozzles	ASTM-A-105 Grade 2 (0.30% max carbon)
Relief Valve Flanges	ASTM-A-105 Grade 1 (0.35% max carbon)
Shell and Channel Flanges	ASTM-A-111 Grade 1 (0.35% max carbon)
Tubes	ASTM-B-111 80-20 Cupro-nickel, Type A annealed
Tube Sheet	ASTM-A-212 Grade B Firebox Quality

14. Operating Conditions of Secondary Drain Cooler

Drain Cooler Tube Surface	1349 sq ft
Heat Exchanged - Maximum	34.4×10^6 Btu/hr (10 Mw)
Quantity of intermediate steam condensate to tube side	241,000 lb/hr
Tube-side pressure - operating	310 psig
design	400 psig
test	600 psig

14. Operating Conditions of Secondary Drain Cooler (Cont'd.)

Tube-side temperature - operating -		
	inlet	424.7°F
	outlet	289.8°F
	design	448°F
Quantity of secondary system condensate to shell side		227,000 lb/hr
Shell-side pressure - operating		200 psig
	design	250 psig
	test	375 psig
Shell-side temperature - operating -		
	inlet	230°F
	outlet	376.5°F
	design	406°F
Fouling Factor		0.0005
Weight - dry		7200 lb
	flooded	10,000 lb

15. Secondary Drain Cooler Materials of Construction

Shell	ASTM-A-106 Grade B Seamless
Shell Head	ASTM-A-234 Grade WPB
Channel Shell and Cover	ASTM-A-212 Grade B Firebox Quality
Flanges	ASTM-A-181 Grade 2 0.30% max carbon
Nozzle Necks	ASTM-A-106 Grade B
Nozzle Flanges	ASTM-A-181 Grade 1 0.35% max carbon
Tube Sheet	ASTM-A-212 Grade B Firebox Quality
Baffles and Impingement Plate	ASTM-A-283 Grade D

16. Air-cooled Steam Condenser Design Features

Heat Exchanger	
Number of sections	8
Surface per section, sq ft	16,941
Total surface, sq ft	135,528
Design pressure, psig	400
Design temperature, °F	448

16. Air-cooled Steam Condenser Design Features (Cont'd.)

Intermediate Coolant	
Flow, lb/hr	245,400
Operating pressure, psig	310
Temperature in, °F	424.7
Temperature out, °F	424.7
Pressure drop, psi	negligible
Heat exchanged, Btu/hr	196.5×10^6
Passes	1
Tubes	
Total number	736
Material	Admiralty SB-11.1 Type C
Size and gage	1-in. OD x 16 BWG
Pitch, in.	$2\frac{5}{8} \times 2\frac{11}{32}$
Layers	4
Length, in.	$359\frac{1}{2}$
Headers	Steel
Fins	
Material	Aluminum Type 1100-0
Number, per in.	11
Diameter, in.	$2\frac{1}{4}$
Thickness, in.	0.016
Type Bonding	Mechanical
Design	Grooved
Air	
Flow, lb/hr	3.4×10^6
Temperature in, °F	95
Temperature out, °F	336
Fan Assemblies	
Fans - Hartzell Propeller Fan Company	
Number of fans	
Variable pitch	1
Fixed pitch	3
Number of blades	6
Blade diameters, ft	12
Blade material	Plastic
rpm	292
Horsepower per fan	28.4

16. Air-cooled Steam Condenser Design Features (Cont'd.)

Gears	
Philadelphia Gear Corporation - model	3415 CT
AGMA Rating	40
Electric drive - 3-phase	
Allis-Chalmers model	TEFC
Horsepower	30
rpm	1750
Voltage	480 v
Frequency, cps	60

17. Air-cooled Drain Cooler Design Features

Heat Exchanger	
Number of sections	2
Surface per section, sq ft	16,941; 8,102
Total surface, sq ft	25,043
Design pressure, psig	400
Design temperature, °F	448
Intermediate Coolant	
Flow, lb/hr	245,400
Operating pressure, psig	310
Temperature in, °F	424.7
Temperature out, °F	291.7
Pressure drop, psi	16.7
Heat exchanged, Btu/hr	34.6×10^6
Passes	4
Tubes	
Total number	136
Material	Admiralty SB-11.1 Type C
Size and gage	1-in. OD x 16 BWG
Pitch, in.	$2\frac{5}{8} \times 2\frac{11}{32}$
Layers	4
Length, in.	$359\frac{1}{2}$
Headers	Steel
Fins	
Material	Aluminum Type 1100-0
Number, per in.	11
Diameter, in.	$2\frac{1}{4}$
Thickness, in.	0.016
Type Bonding	Mechanical
Design	Grooved

17. Air-cooled Drain Cooler Design Features (Cont'd.)

Air	
Flow, lb/hr	0.72×10^6
Temperature in, °F	95
Temperature out, °F	295
Fan Assemblies	
Fans - Hartzell Propeller Fan Company	
Number of fans	
Variable pitch	1
Fixed pitch	2
Number of blades	6
Blade diameters, ft	7
Blade material	Aluminum
rpm	500
Horsepower per fan	9.45
Gears	
Philadelphia Gear Corporation - model	3405 CT
AGMA Rating	20
Electric drive - 3-phase	
Allis-Chalmers model	TEFC
Horsepower	10
rpm	1750
Voltage	480 v
Frequency, cps	60

18. Air-cooled Flash Condenser Design Features

Heat Exchanger	
Number of sections	1
Surface per section, sq ft	5,410
Total surface, sq ft	5,410
Design pressure, psig	100
Design temperature, °F	338
Intermediate Coolant	
Flow, lb/hr	4,930
Operating pressure, psig	19.8
Temperature in, °F	258.5
Temperature out, °F	258.5
Pressure drop, psi	negligible
Heat exchanged, Btu/hr	4.64×10^6
Passes	1

18. Air-cooled Flash Condenser Design Features (Cont'd.)

Tubes	
Total number	46
Material	Admiralty SB-1111 Type C
Size and gage	1-in. OD x 18 BWG
Pitch, in.	$2\frac{5}{8}$ x $2\frac{11}{32}$
Layers	2
Length, in.	360
Headers	Steel
Fins	
Material	Aluminum Type 1100-0
Number, per in.	11
Diameter, in,	$2\frac{1}{4}$
Thickness, in.	0.016
Type Bonding	Mechanical
Design	Marley
Air	
Flow, lb/hr	0.6×10^6
Temperature in, °F	95
Temperature out, °F	127
Fan Assemblies	
Fans - Hartzell Propeller Fan Company	
Number of fans	
Variable pitch	1
Fixed pitch	2
Number of blades	4
Blade diameters, ft	7
Blade material	Aluminum
rpm	500
Horsepower per fan	4.5
Gears	
Philadelphia Gear Corporation - model	3405 CT
AGMA Rating	
Electric drive - 3-phase	
Allis-Chalmers model	TEFC
Horsepower	5
rpm	1750
Voltage	480 v
Frequency, cps	60

19. Air-cooled Subcooler Design Features

Heat Exchanger	
Number of sections	2
Surface per section, sq ft	25,780
Total surface, sq ft	51,560
Design pressure, psig	100
Design temperature, °F	338
Intermediate Coolant	
Flow, lb/hr	246,600
Operating pressure, psig	19.8
Temperature in, °F	258.5
Temperature out, °F	160
Pressure drop, psi	4.2
Heat exchanged, Btu/hr	24.5×10^6
Passes	4
Tubes	
Total number	280
Material	Admiralty SB-11.1 Type C
Size and gage	1-in. OD x 18 BWG
Pitch, in.	$2\frac{5}{8} \times 2\frac{11}{32}$
Layers	4
Length, in.	360
Headers	Steel
Fins	
Material	Aluminum Type 1100-0
Number, per in.	11
Diameter, in.	$2\frac{1}{4}$
Thickness, in.	0.016
Type Bonding	Mechanical
Design	Marley
Air	
Flow, lb/hr	1.2×10^6
Temperature in, °F	95
Temperature out, °F	180
Fan Assemblies	
Fans - Hartzell Propeller Fan Company	
Number of fans	
Variable pitch	1
Fixed pitch	1
Number of blades	4
Blade diameters, ft	12
Blade material	Plastic
rpm	292
Horsepower per fan	13.3

19. Air-cooled Subcooler Design Features (Cont'd.)

Gears	
Philadelphia Gear Corporation - model	3415 CT
AGMA Rating	31
Electric drive - 3-phase	
Allis-Chalmers model	TEFC
Horsepower	15
rpm	1750
Voltage	480 v
Frequency, cps	60

LEGAL NOTICE

Price $5.00 . *Available from the Office of Technical Services, Department of Commerce, Washington 25, D.C.*